40300

National Library of Canada / Bibliothèque nationale du Canada

CANADIAN THESES ON MICROFICHE / THÈSES CANADIENNES SUR MICROFICHE

NAME OF AUTHOR/*NOM DE L'AUTEUR* Karl Schumann

TITLE OF THESIS/*TITRE DE LA THÈSE* Geology of the Watchams Bay area, eastern end of the Cape Smith Belt, New Quebec

UNIVERSITY/*UNIVERSITÉ* University of Alberta

DEGREE FOR WHICH THESIS WAS PRESENTED/ *GRADE POUR LEQUEL CETTE THÈSE FUT PRÉSENTÉE* Ph D

YEAR THIS DEGREE CONFERRED/*ANNÉE D'OBTENTION DE CE GRADE* 1978

NAME OF SUPERVISOR/*NOM DU DIRECTEUR DE THÈSE* R.A. BURWASH

Permission is hereby granted to the NATIONAL LIBRARY OF CANADA to microfilm this thesis and to lend or sell copies of the film.

The author reserves other publication rights, and neither the thesis nor extensive extracts from it may be printed or otherwise reproduced without the author's written permission.

L'autorisation est, par la présente, accordée à la BIBLIOTHÈQUE NATIONALE DU CANADA de microfilmer cette thèse et de prêter ou de vendre des exemplaires du film.

L'auteur se réserve les autres droits de publication; ni la thèse ni de longs extraits de celle-ci ne doivent être imprimés ou autrement reproduits sans l'autorisation écrite de l'auteur.

DATED/*DATÉ* Aug 22 / 78 SIGNED/*SIGNÉ* [signature]

PERMANENT ADDRESS/*RÉSIDENCE FIXÉ* 4578 Patricia Avenue
Montréal, Quebec

NL-91 (3-74)

NOTICE

The quality of this microfiche is heavily dependent upon the quality of the original thesis submitted for microfilming. Every effort has been made to ensure the highest quality of reproduction possible.

If pages are missing, contact the university which granted the degree.

Some pages may have indistinct print especially if the original pages were typed with a poor typewriter ribbon or if the university sent us a poor photocopy.

Previously copyrighted materials (journal articles, published tests, etc.) are not filmed.

Reproduction in full or in part of this film is governed by the Canadian Copyright Act, R.S.C. 1970, c. C-30. Please read the authorization forms which accompany this thesis.

THIS DISSERTATION
HAS BEEN MICROFILMED
EXACTLY AS RECEIVED

AVIS

La qualité de cette microfiche dépend grandement de la qualité de la thèse soumise au microfilmage. Nous avons tout fait pour assurer une qualité supérieure de reproduction.

S'il manque des pages, veuillez communiquer avec l'université qui a conféré le grade.

La qualité d'impression de certaines pages peut laisser à désirer, surtout si les pages originales ont été dactylographiées à l'aide d'un ruban usé ou si l'université nous a fait parvenir une photocopie de mauvaise qualité.

Les documents qui font déjà l'objet d'un droit d'auteur (articles de revue, examens publiés, etc.) ne sont pas microfilmés.

La reproduction, même partielle, de ce microfilm est soumise à la Loi canadienne sur le droit d'auteur, SRC 1970, c. C-30. Veuillez prendre connaissance des formules d'autorisation qui accompagnent cette thèse.

LA THÈSE A ÉTÉ
MICROFILMÉE TELLE QUE
NOUS L'AVONS REÇUE

THE UNIVERSITY OF ALBERTA

GEOLOGY OF THE WAKEHAM BAY AREA, EASTERN END OF THE CAPE SMITH BELT, NEW QUEBEC

by

Karl SCHIMANN

A THESIS

SUBMITTED TO THE FACULTY OF GRADUATE STUDIES AND RESEARCH

IN PARTIAL FULFILMENT OF THE REQUIREMENTS FOR THE DEGREE

OF Doctor of Philosophy

DEPARTMENT OF GEOLOGY

EDMONTON, ALBERTA

FALL, 1978

THE UNIVERSITY OF ALBERTA

FACULTY OF GRADUATE STUDIES AND RESEARCH

The undersigned certify that they have read, and recommend to the Faculty of Graduate Studies and Research, for acceptance, a thesis entitled

"Geology of the Wakeham Bay area, eastern end of the Cape Smith Belt New Quebec"

submitted by Karl SCHIMANN

in partial fulfilment of the requirements for the degree of Doctor of Philosophy (Geology).

R A Burwash
.....
Supervisor

.....

.....

R. J. Lambert
.....

.....
External Examiner

DATE August 16, 1978

ABSTRACT

The Wakeham Bay area is situated in the northern part of the Ungava Peninsula. It encompasses the eastern end of the Cape Smith Belt and straddles the boundary between the Churchill and the Superior Provinces. By its location and the presence of a complete stratigraphic sequence, it is a key area in which to study the evolution of the Cape Smith Belt, as part of the Circum-Ungava Geosyncline, and its relation to the Archean basement. The Aphebian stratigraphic sequence is transgressive on this basement which had previously been intruded by earlier Aphebian dykes. It begins with coastal to shallow marine, detrital and chemical, iron-rich deposits (Iron Group) and continues with stable platform sediments (Pelitic Group). Volcanic activity, the beginning of which can be observed locally in the Iron Group, becomes significant in the third unit, the Volcano-Sedimentary Group; this unit consists of pelites, a carbonate horizon, tuffs, flows and some sills, and ends with arkosic sandstones and grits. The Lower and Upper Volcanic Group, composed of 80% volcanic rocks and 20% immature detrital sediments, testify to the increasing instability in the geosyncline. Although the stratigraphic sequence can be observed essentially anywhere from the basement upward, a eugeosynclinal domain may be distinguished from a miogeoclinal domain, which occupies the southern third of the area. In the eugeosynclinal domain the lower three groups are much

reduced in thickness; locally the Iron Group, sometimes also the Pelitic Group, are absent. The volcanic rocks are mostly massive and pillowed basalt flows with minor pyroclastics and numerous gabbro sills, chemically akin to oceanic tholeiites. Ultramafic sills occur mainly in the Upper Volcanic Group which is also characterized by the presence of komatiites (ultramafic extrusives). Minor calc-alkaline tuffs occur in the upper part of the sequence.

During the Hudsonian Orogeny, differential vertical movements of rigid basement blocks, along three main directions (E-W, NW-SE, NE-SW), resulted in three phases of folding in the overlying cover. The chronology of these phases varies from place to place. Only the E-W phase has affected the whole of the Aphebian sequence. In the western part of the area a weak N-S phase may be recognized. Penetrative deformation of the basement occurred only in the more highly metamorphosed part of the area.

The whole of the Aphebian sequence in the area studied has been regionally metamorphosed to greenschist and amphibolite facies. The increase in metamorphic grade across the region from South to North, and West to East is recognized in the metapelites by the succession: biotite, almandine, staurolite, kyanite, and in the metabasites by the change from the assemblage: albite + actinolite + epidote + chlorite to the assemblage: plagioclase + hornblende, with the coexistence over a broad range of actinolite and hornblende and the gradual up-grade decrease in the amount of

epidote and chlorite present. The order of appearance shows the metamorphism to be of an intermediate P/T, Barrovian, type. It also shows that the P/T ratio was lower in the South than in the North, where the Aphebian sequence was thicker. Use of the b_0 of potassic white micas confirms this. A biotite-garnet geothermometer was developed to quantify the metamorphic zonation. Together with the plagioclase-garnet-Al_2SiO_5-quartz thermometer-barometer, it yielded maximum (610°C, 7.25Kb) and minimum (500°C, P unknown) metamorphic conditions. The quantified metamorphic zonation revealed a distinct basement effect ("effet de socle") which is interpreted as the expression of a disequilibrium in the heat flow during metamorphism. This zonation is used also to study the compositional changes with temperature of electron microprobe analysed metamorphic minerals. A compositional gap is recognized in the plagioclase between An_7 and An_{15-20}, and in the calciferous amphibole between actinolite and hornblende.

Age determinations by the whole-rock Rb-Sr isochron method showed the basement gneisses to be at least 2900 m.y. old, and the Aphebian volcanism 2150-2200 m.y., compared with approximately 1850 m.y. in the Belchers Islands and the Labrador Trough. Despite lithostratigraphic similarities with these other parts of the Circum-Ungava Geosyncline, differences in tectonic style and the presence of komatiites, concur with the geochronological results to mark the Cape Smith Belt as an older segment of the Circum-

Ungava Geosyncline; it may be akin to the Thompson Belt.

The inadequacy of plate tectonic models, in particular that of continental collision and suture, to explain the Hudsonian Orogeny in the Wakeham Bay area, is demonstrated. The following model for the evolution of the Cape Smith Belt, as part of the Circum-Ungava Geosyncline, is proposed. During the period 2200-2150 m.y., a linear zone of mantle diapirism under an early Archean basement, which may be part of the North Atlantic Craton of Greenland, Labrador, and Scotland, caused vertical faulting, subsidence, and volcanism; this resulted in the 3 to 15 km thick, mainly marine, volcano-sedimentary sequence now visible. This activity must have continued on later, continuously or discontinuously, for another 15-18 km of volcanics and sediments is required to account for the present metamorphic grade; and at 1750-1650 m.y., it culminated as the Hudsonian Orogeny which has produced the main deformation, metamorphism, and uplift.

ACKNOWLEDGEMENTS

Dr E. Dimroth introduced me to the Circum-Ungava Geosyncline and so, initiated this study. The field work was supported by the Quebec Department of Natural Resources, for which I thank Dr R. Bergeron and Dr A.F. Laurin.

Completion of the thesis was made possible by Ecole Polytechnique and Centennial College in Montreal, who provided computer terminals for the editing of the text.

I would also like to express my gratitude to all those who have helped in the realisation of this work:

Dr R.A. Burwash for his guidance.

Dr R. St-J. Lambert for his interest in the petrological aspects of this work.

Dr D.G.W. Smith for introducing me to the electron microprobe, but also for enlighthening discussions.

Dr H. Baadsgaard for his teaching in isotope geology and the use of mass-spectrometers, as well as for performing some of the isotopic analyses.

Dr H.A.K. Charlesworth for his help in the processing and interpretation of structural data.

Dr C. Scarfe for the use of the experimental petrology laboratory.

And more generally, the academic staff of the Department of Geology, for their help, advice, and patience during my stay

at the University.

Last, but not least, I would like to thank Dr C. Gold for his help dealing with computer and other mathematical matters.

TABLE OF CONTENTS

LIST OF TABLES

LIST OF FIGURES

LIST OF PHOTOGRAPHIC PLATES

CHAPTER I

INTRODUCTION

1. SCOPE and PURPOSE of this WORK

The Wakeham Bay area is a part of the Canadian Shield at the boundary between the Churchill and the Superior Provinces. It encompasses the eastern termination of the Cape Smith Belt (a part of the Circum-Ungava Geosyncline) and consists of Aphebian supracrustal rocks and Archean basement rocks. The Wakeham Bay area occupies a key position in the Circum-Ungava Geosyncline, because the basement-cover relations are well exposed, a complete cross-section of the Belt is available, and the area is situated at a major change in trend of the Geosyncline. It thus offers the opportunity to study the evolution of an Aphebian fold belt, through sedimentation, volcanism, deformation, and metamorphism, and its relations to the Archean basement, as well as the effect of the Hudsonian Orogeny on this basement.

The aim of the present work is to study the various aspects of the geology of the area in order to unravel its history from Archean to Quaternary times from the view point of the evolution of the Canadian Shield. Within this framework, the investigation of the Hudsonian metamorphism is emphasized and leads to an ancillary study: the development of a geothermometer. Another ancillary study leads to a new method for rapid chemical analysis of rock samples.

The Wakeham Bay area includes the part of New-Quebec situated between latitudes 61°15'N and 61°45'N, and longitudes 73°W and the coast of Hudson Strait, i.e. approximately longitude 71°30'W. It embraces about 3400 km² of which some 1400 km² are Aphebian rocks, the remainder being the Archean basement (Fig. 1).

Mapping of the area was initiated by the Quebec Department of Natural Resources because of its economic potential; the nickel-copper deposits of New Quebec Raglan Mines Ltd (16 million tons averaging 2.58% Ni and 0.71% Cu: Canadian Mines Handbook 1977-78) occur in Aphebian rocks which extend into the Wakeham Bay area. The Aphebian rocks which form the eastern termination of the Cape Smith Belt (Churchill Province) were the main target.

Mapping, initially a three year programme, began in 1971, continued in 1972, but was discontinued in 1973 following a change in policy at the Quebec Department of Natural Resources. By that time some 1900 km², including more than 3/4 of the Aphebian rocks, had been mapped; a por-

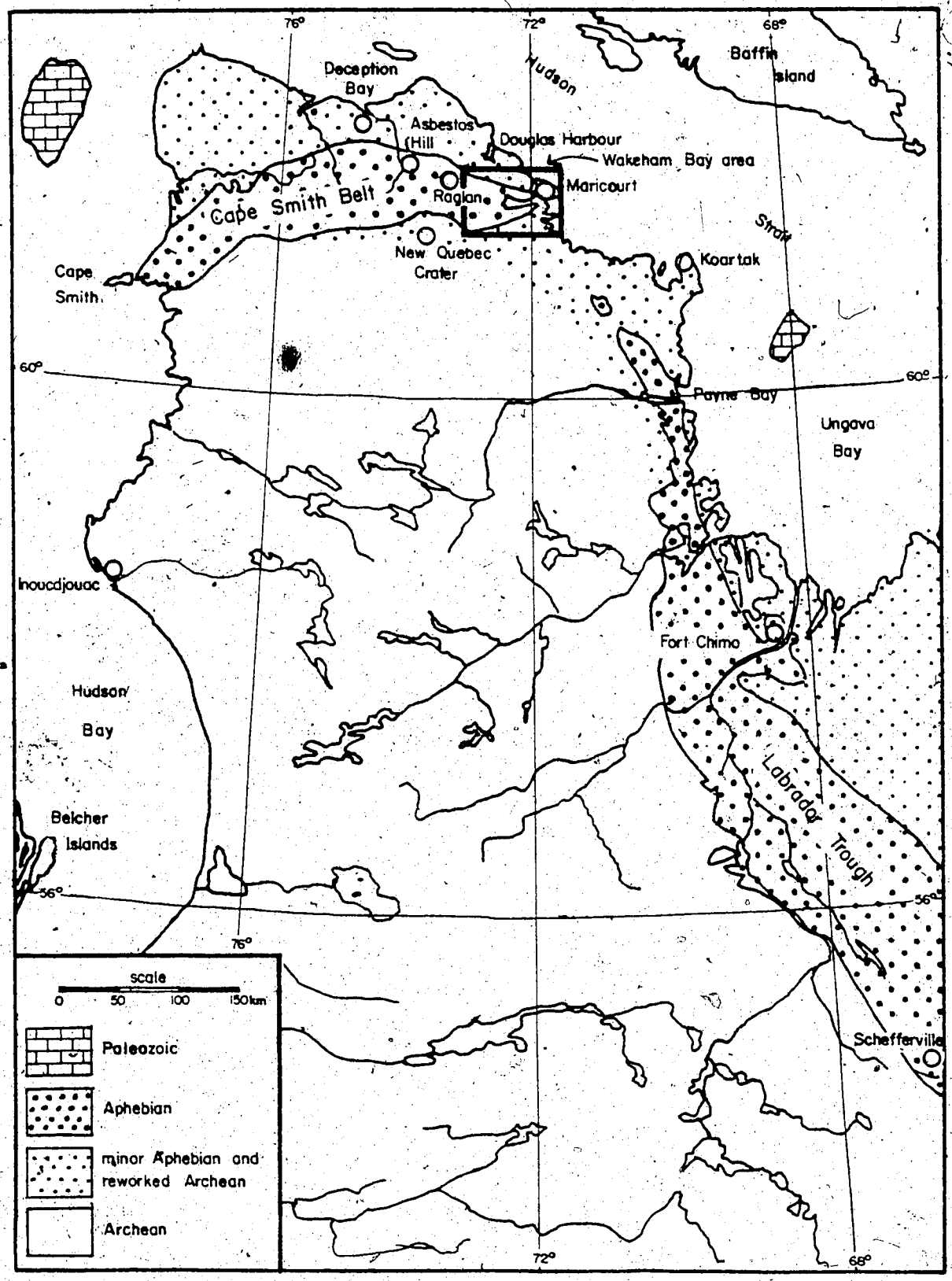

Figure 1. Location map of the Wakeham Bay area.

tion across the Belt in the central part and the one in the SE quarter of the area remain unmapped. As a result some of the stratigraphic and structural relations are not as clear as could be desired and the metamorphic zonation had to be extrapolated, from the western to the eastern map area, to produce a comprehensive model.

2. PREVIOUS WORK

The Wakeham Bay area per se had not been mapped previously, except at reconnaissance scale or locally by mining companies during exploration in the late 1950's and early 1960's. A good summary of early exploration of the Ungava Peninsula is given in Stevenson (1968).

The Cape Smith Belt was explored for sulphides in the early 1930's (Airth, 1933; Gunning, 1933). The central part of the Belt was mapped by the Quebec Department of Natural Resources (Beall, 1959, 1960; Bergeron, 1957, 1959; De Montigny, 1959; Gélinas, 1962; Gold, 1962). Kretz (1960) made a reconnaissance map of the northern part of the Ungava Peninsula. Stevenson (1968) mapped the area south of 61°N.[1]

---

[1] The area north of 61°N was mapped in 1973 (Taylor, 1974).

3. CLIMATE

The area has an arctic climate with strong marine influence. Summers are cool, wet, and windy with average maximum daily temperature of 10°C in July and August. The plateau is cooler than the coast and low-lying valleys. A few days reach 25 to 30°C. Precipitation although not abundant is frequent; fog is common in summer, mainly near the coast, and may become a problem in the use of helicopters.

The snow cover has sufficiently decreased, to start field work, by the end of June along the coast, and in the second half of July on the plateau. The ice break-up starts in early July along the coast, but ice remains till the end of July on lakes, at altitudes above 500 m. On these lakes ice starts to form again in the second half of September.

4. VEGETATION and WILDLIFE

The area lies some 300 km north of the tree line. Vegetation is sparse and consists of lichens, moss and herbaceous plants. A few shrubs, mainly alder, are to be found on protected slopes and in low-lying valleys.

Wildlife is not very abundant. Mammals consist of lemmings, bears and foxes on land, seals and belugas in the

coastal waters; polar bears are occasionally seen. Caribou are absent from the area now and can only be found 50 to 100 km to the south; however, the occasional antler encountered on the plateau testifies to their past presence. Canada geese, several species of ducks, and hawks, ptarmigans, snow owls, gulls, terns and loons, as well as numerous smaller birds were sighted. Lakes and rivers contain trout and arctic char. Mosquitoes and black flies are of little concern, except during the warmest summer days in wind protected areas.

5. PHYSIOGRAPHY

The Wakeham Bay area is situated along the Hudson Strait in the northeast of the Ungava Peninsula. It is at the junction of the Larch Plateau, the Povungnituk Hills, and the Sugluk Plateau physiographic regions of the Canadian Shield (Bostock, 1970).

The Larch Plateau rises slowly from an altitude of about 1000 feet in the central part of the Ungava Peninsula to about 1900 feet in the map area. The Sugluk Plateau continues this peneplaned surface at an altitude of 1900 feet to the Hudson Strait. In the two plateaux, underlain mainly by Archean granitic and gneissic basement rocks, the relief is subdued, consisting of low-rolling hills, with an irregu-

lar drainage and numerous lakes. The only interruption in the landscape of the Larch Plateau is the New Quebec Crater, rising some 400 feet above the peneplain.

In the western part of area, the east-west trending Povungnituk Hills underlain by Aphebian sedimentary and volcanic rocks, cut across the peneplain in two ridges, Monts Lune[1] and Mont Giraffe-Mont Umiak, separated by the Wakeham River valley. The Vicenza River valley forms a broad, low-lying area between Mont Giraffe-Mont Umiak and the slightly higher Larch Plateau to the south. The highest point of the area, and of the Ungava Peninsula, at 2275 feet, is located in the Monts Lune north of Lac Felix. In the Povungnituk Hills, the relief is more pronounced, consisting mostly of parallel ridges (cuestas) of gabbro sills or thick basalt flows. These ridges generally trend north-northwest. Drainage is structure-controlled and tends towards a trellis pattern. Lakes are less abundant than on the plateau and are smaller.

East of 72°25' to 72°30'W, where the belt of Aphebian rocks is split into two narrow branches and is of higher metamorphic grade, the distinction between the two physiographic types (basement rocks and supracrustal rocks) is less pronounced. Along the coast of Hudson Strait the Sugluk Plateau ends in high cliffs. This line of cliffs may be related to a fault structure as it is parallel to one of

---

[1] for place names, see Figures 1 and 16

the major lineament directions of the area (see Chapter on structure). The height of these cliffs decreases from about 1500 feet near Douglas Harbour to essentially nil at Cape Prince of Wales; at the mouth of Wakeham Bay they are still 500 to 1000 feet high. At Joy Bay, the ground rises gently westwards from sea level to 1000 feet within about 10 km.

In the first 10 to 20 km from the coast the relief is pronounced; the highlands have been dissected by glacial and fluvial erosion. Deep glacial valleys with hanging valleys and cirques, some with a tarn, are characteristic of the cliff-bordered coast. Some of the larger valleys are submerged forming deep fjords (Douglas Harbour, Wakeham Bay), others are already emerged (Ippijuaq, the lower Vicenza River valley).

The map area is composed of two main drainage basins: Wakeham River and Vicenza River. In addition, a few smaller rivers drain the area south of Wakeham Bay into Joy Bay.

The lower parts of the valleys of the Wakeham River and Vicenza River are typical U-shaped glacial valleys, the bottom of which rises to no more than 500 feet above sea level. The median part of the Vicenza River valley is a deeply incised V-shaped fluvial channel. The Wakeham River Canyon (median part of the Wakeham River valley) appears as a U-shaped glacial valley (possibly overprinting an earlier fluvial valley), undercut by a V-shaped fluvial channel. The upper parts of both the Vicenza River and the

Wakeham River valleys are fluvial valleys. Most of the tributaries to those two rivers, both in their upper and lower part, flow in fluvial valleys. A U-shaped glacial valley joins the east-west part of the lower Wakeham River valley through Lac Ruban to Joy Bay.

6. ACCESS

Access to the area is either by boat or by aircraft. During the months of July to September, several boats service the settlements along Ungava Bay and Hudson Strait. Maricourt (population about 200) is situated on Wakeham Bay.

Regular air service is available to Fort Chimo and Asbestos Hill or Deception Bay from Montreal(Fig. 1). Semi-regular flights out of a fixed-wing aircraft base in Fort Chimo bring mail and small supplies to the other settlements, except during freeze-up and break-up.

7. FIELD WORK

In addition to topographic maps at a scale of 1:50,000 and 1:250,000, air photos were available at a scale of about 1:30,000. Air photo interpretation was used to define the traverses to be done, on the basis of outrop availability and the complexity of the geology. Traverses on foot were run across the structural trend at an average spacing of 1.5 km. In addition, marker horizons and contacts were traced either on-foot or with the helicopter.

In 1971 the crew consisted, including the author, of 3 geologists, 3 field assistants, and a helicopter pilot; a helicopter engineer was occasionally present. The helicopter was a Hiller 12E (Skyrotors Ltd). The material (camping gear etc...) as well as the fuel and oil for the helicopter were shipped to the base camp in Douglas Harbour just after the break-up (end of July). The personnel was flown into Douglas Harbour using the air strip at Raglan. The helicopter was used mainly to set up fly-camps and bring in supplies. However, its prolonged unavailability (mechanical problems) made it neccessary at the end of August to use back-packing to move a fly-camp and complete a 3-day traverse, in order to obtain at least one complete cross-section of the Aphebian belt. Field work lasted from July 25 to September 1st.

In 1972 the crew consisted, including the author, of 3 geologists, 3 field assistants, one cook, a helicopter

pilot, and an engineer. Two Inuits were hired as field assistant for a short period to increase the number of mapping crews. The helicopter was a Bell 47G3 (Héli Voyageur Ltd). In the early spring, gas and oil caches for the helicopter were made on the plateau with a ski-equipped aircraft. The personnel and material were flown into Maricourt before break-up, with additional supplies shipped later in the summer. Buildings made available by the New Quebec School Board were used as base camp for one month; the area near the coast was mapped during that time. By July 24, the snow cover on the plateau had sufficiently decreased, and a second base camp was set up on Wakeham River, south of Felix Lake. Crews were flown out of the base camps with the helicopter and either walked back or were picked up at the end of the daily traverse. Field work lasted from June 24 till August 26.

CHAPTER II

GENERAL GEOLOGY AND STRATIGRAPHY

The Wakeham Bay area covers the eastern end of the Cape Smith Belt (Douglas, 1970). It consists of a gneissic basement of Archean age overlain by Aphebian sediments and volcanics. Two groups of diabase dykes are present, an early Aphebian one and a late Hadrynian one.

The Archean rocks south of the fold belt are part of the Superior Province; the Aphebian rocks of the fold belt and the reworked Archean basement north of it are part of the Churchill Province.

The Aphebian rocks form a synclinorium with a shallow westerly plunge. East of 72°30'W this synclinorium divides itself into a north branch, which ends NE of Maricourt, and a south branch, which ends west of Joy Bay. Several small basins of Aphebian sediments occur, one north of Ippijuaq, the others west and south of Whitley Bay (Fig. 2).

This synclinorium can be considered as a

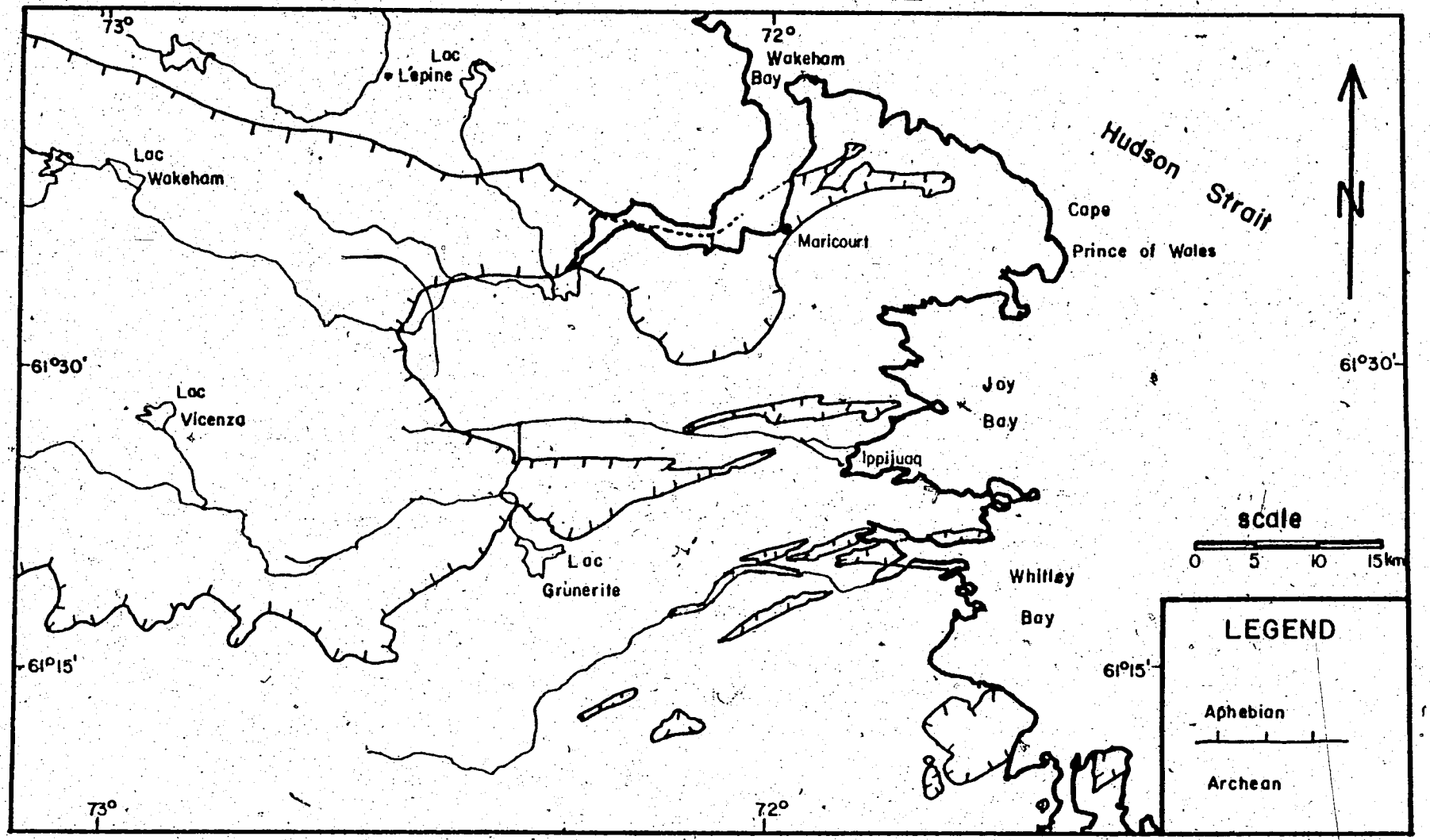

Fig. 2. The eastern end of the Cape Smith Belt (Wakeham Bay area): limits of the main part of the Aphebian geosyncline and of the outlying basins. Geology by the author (1971 and 1972) and by Taylor (1974).

geosyncline[1] and will be designated as such hereinafter. It consists of a eugeosynclinal domain in the north, containing mostly volcanic and immature sedimentary rocks, and a miogeoclinal domain in the south, containing mostly more mature sediments and only minor volcanic rocks. The miogeoclinal domain forms only a narrow margin in the western map area, but it may have extended much further south as witnessed by the small outlying basins mapped by Taylor (1974), and as postulated by Dimroth (1970).

The geology of the Wakeham Bay area is shown in 11 maps (Fig. 3-13; Fig. 14 is an index to the maps and Table 1 is the legend) and a series of tectonic profiles (Fig. 15). Table 2 shows the lithostratigraphic units mapped in the Wakeham Bay area.

The oldest unit consists of Archean gneiss with minor amphibolite and paragneisses; no stratigraphic subdivision could be made within the Archean in the map area. It is cut by a group of diabase dykes that are overlain by the Aphebian sediments and volcanic rocks, and deformed by the Hudsonian Orogeny. The Archean rocks and early Aphebian diabases are separated by an angular unconformity from the Aphebian sedimentary and volcanic rocks.

A cross-section through the geosyncline in the

---

[1] "a mobile downwarping of the crust of the Earth, either elongate or basin-like, measured in scores of kilometers, which is subsiding as sedimentary and volcanic rocks accumulate to thicknesses of thousands of meters." (Gary et al., 1972)

Table 2. Lithostratigraphic units of the Wakeham Bay area.

Quaternary	Glacial and post-glacial unconsolidated deposits
.....	angular unconformity .....
Late Hadrynian	Diabase dykes
.....	intrusive contact .....
	Upper Volcanic Group: flow and pillow-basalts, pyroclastics, detrital sediments, ultramafic flows, peridotite to gabbro sills
	Lower Volcanic Group: flow and pillow basalts, pyroclastics, detrital sediments, gabbro sills
Aphebian	Volcano-Sedimentary Group: volcanogenic tuffs, minor basalt flows, pelites, sandstones, dolomite, ultramafic flows or sills, gabbro sills
	Pelitic Group: pelitic to psammitic schists, minor chlorite-schists and graphitic schists.
	Iron Group: oxide-, silicate-, and carbonate-iron formation, pelites, sandstones
.....	angular unconformity .....
Early Aphebian	Diabase dykes
.....	intrusive contact .....
Archean	Granitic to granodioritic gneisses, amphibolites, paragneisses, diabase dykes or sills.

western map area shows no angular unconformity within the Aphebian rocks, neither can the observed succession be directly correlated with the Povungnituk and Chukotat Groups

of Bergeron (1957). Consequently the Aphebian stratigraphic succession shown in table 2 was defined, based on observations along a N-S section between 72°40'W and 72°45'W, from the southern contact with the Archean to the central part of the Monts Lune. This section can be considered as the type locality or area of these informal stratigraphic units.

The Aphebian stratigraphy consists of two sedimentary units at the base (Iron Group and Pelitic Group) and two mainly volcanic units at the top (Lower and Upper Volcanic Group) separated by the Volcano-Sedimentary Group of mixed volcanics and sediments.

The Aphebian rocks and the Archean rocks are cut by a second group of diabase dykes of late Hadrynian age. These dykes, the Aphebian sediments and volcanics, the early Aphebian diabases dykes, and the Archean rocks are all separated by an angular unconformity from the Quaternary glacial and post-glacial unconsolidated deposits.

CHAPTER III

STRUCTURE

1. INTRODUCTION

The general trend for the Archean foliation in the northern part of the Ungava Peninsula is northerly, but in the Wakeham Bay area it changes to NE and ENE; the Aphebian rocks trend EW on average.

Within the area mapped, the depth of erosion of the belt increases eastwards, i.e. the grade of metamorphism increases, deformation becomes more plastic, and the Archean rocks become more penetratively deformed by the Hudsonian Orogeny, together with the Aphebian rocks.

The Archean trend south of the belt varies from north in the West to ENE in the East. North of the belt the trend varies from about NS, NW of the Monts Lune, to EW, east of there; it is also EW in the Archean block south of the lower Wakeham Valley. In the peninsula between Wakeham Bay and Joy Bay, the trend of the Archean rocks is EW.

The Aphebian rocks have an ESE to EW trend; local variations exist, mostly around the southern and eastern edge of the belt.

The area may be subdivided into a western part (W of 72°32') and an eastern part (E of 72°20'); the belt was not mapped in detail between the two parts.

2. LARGE SCALE LINEAMENTS

On the topographic maps and the air photos several large scale lineaments may be seen. These can be grouped into three main trends; they are: EW, NNE to NE, NW (Fig. 16).

In the first group the most prominent ones are the lower Ippijuaq Valley, the lower Wakeham Valley, the central part of Wakeham Bay. In the second group are the eastern and western parts of Wakeham Bay, the upper part of Ippijuaq Valley, part of Wakeham Valley (from the first to the second bend inland) and possibly Douglas Harbour (a fjord north of Fig. 16). The main glacial trend in the area is parallel to this group of lineaments and enhances it. The third group consists of lineaments parallel to the coast of Hudson Strait: one along Stupart Creek, one through the village of Maricourt and several north of Wakeham Bay; they do not occur further inland.

The first two groups seem to occur essentially in Archean rocks, whereas the third group occurs equally in Archean and in Aphebian rocks. This third group is also parallel to numerous tension joints (calcite or quartz filled) that are best observed on Ford Point.

These lineaments probably represent jointing and/or faulting. Faults have been observed along lineaments of the first and third group, but none parallel to the second group.

3. ARCHEAN ROCKS

The Kenoran Orogeny metamorphosed and deformed the Archean rocks, producing high-grade gneisses and amphibolites with a good foliation (gneissosity), the trend of which varies as described above. In the western part of the area, only a narrow strip of Archean rocks was included in the mapping, along the Archean-Aphebian contact. The monotonous quartzo-feldspathic gneisses observed there did not disclose any folding. In the eastern part of the area, layers of amphibolite and of paragneisses illustrate the Kenoran folding overprinted by the Hudsonian folding. The Kenoran fold axes seem to have a shallow to intermediate easterly plunge (see geological maps).

The Hudsonian Orogeny has affected the Archean

rocks differently in the east and in the west. In the west, little, if any, penetrative deformation (schistosity or foliation) was observed that appears related to the Hudsonian Orogeny, except locally within the first metre from the contact (Fig. 17) . The stress release was confined to narrow shear zones. However, slivers of Archean gneisses occur locally in anticlinal position in hectometric to decametric faulted folds of Aphebian rocks (see Fig. 18). In the east, at least within the peninsula between Wakeham Bay and Joy Bay, the Archean rocks are penetratively deformed and folded together with the Aphebian rocks and will be included in their discussion below. The contact between the Archean and the Aphebian rocks appears structurally concordant; no fault was observed along it, and in several places there occurs a layer, 5 to 50 cm thick, of what seems to represent a metamorphosed regolith (paleosol?), both along the northern and along the southern contact. The northern contact is steep, vertical to 70S; the southern contact is sub-horizontal in the west and its dip steepens eastward to about 45N by 72°25'W, and to about 70N by 71°55'W.

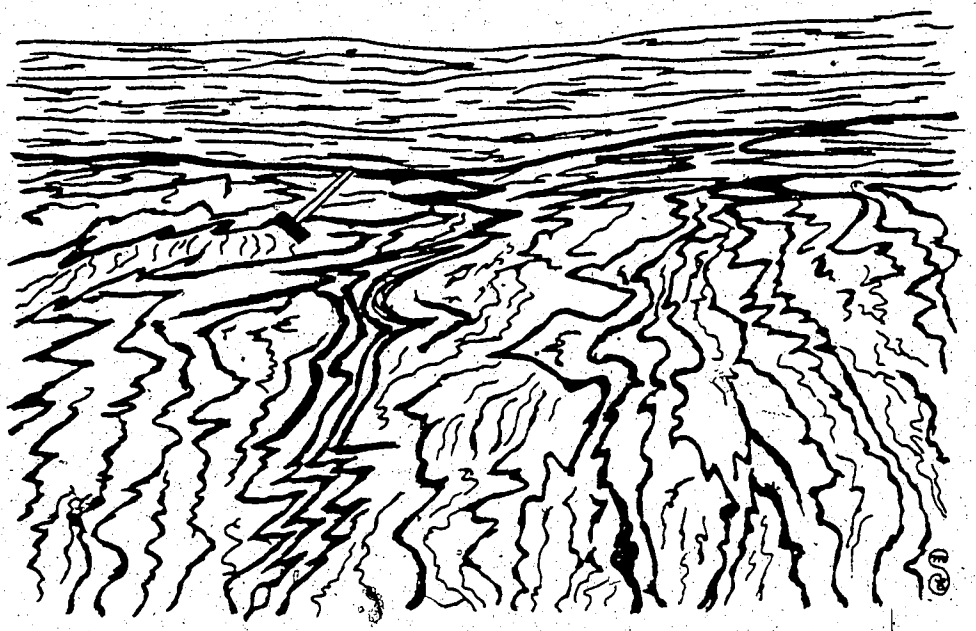

Figure 17. Contact of Archean gneisses and Aphebian mica-schists on the north shore of Wakeham Bay; sketch after a photograph.
Note that the Kenoran foliation in the gneisses is strongly affected by the Hudsonian deformation only within the first 2-3 metres from the contact.

4. APHEBIAN ROCKS

A GENERAL DESCRIPTION and METHOD of STUDY

The Aphebian rocks consist of diabase dykes and of supracrustal rocks (Iron Group, Pelitic Group, Volcano-Sedimentary Group, Lower and Upper Volcanic Group). The diabase dykes intruded the Archean rocks only and behaved during the Hudsonian Orogeny like the Archean rocks. In the West they are retrogressed but undeformed; in the East they are retrogressed and deformed (folded and faulted).

The Aphebian supracrustal rocks have been folded and faulted, during the Hudsonian Orogeny, throughout the belt. The tectonic style of the Aphebian rocks varies markedly in response to changes in metamorphic grade, total thickness of the stratigraphic sequence, as well as the thickness, competence, and homogeneity of the individual lithologic units. The observed folding varies from simple (one phase) to complex (multiphase) folding; up to four phases of folding have been observed. The complexity of the folding tends to increase with the metamorphic grade, i.e. from west to east. It also changes with the stratigraphy, i.e. the base of the sequence, composed of thinly bedded, varied sediments, is more complexly folded than the higher parts of the sequence, composed of thick units of basic volcanics and sills.

West of 72°30'W, the Aphebian belt consists of one large, very asymmetric synclinal structure, the axis of which runs parallel to and about 4 km south of the northern limit of the belt. The north limb dips steeply southward; on the south limb, dips vary from shallow in the south to intermediate in the north. East of 72°30'W, the belt splits into two synclines. The one south of the Ippijuaq Valley is prolonged by several isolated basins near the coast of Hudson Strait; the one north narrows and ends in the peninsula east of Maricourt (Fig. 2).

The structural data (foliation, lineation etc...) gathered in the field have been compiled and grouped into areal domains. Equal area projections of measurements made in each domain were prepared by computer and hand-contoured. The orientation of the eigenvectors and their eigenvalues were also computed for each population. The computer programmes were made available by H.A.K. Charlesworth. A description of the technique is given in Charlesworth et al. (1976) and Cruden (1968).

The spatial distribution of a set of structural measurements may be visualized as an ellipsoid with its longest axis corresponding to the maximum of the distribution of measurements and its shortest axis to the minimum. The eigenvectors correspond to the three axes of the ellipsoid and the eigenvalue are a measure of their length. Three main types of distribution may be recognized in terms of eigenvalues:

1- one large and two small eigenvalues: a distribution with one maximum;

2- one small and two large eigenvalues: a great circle distribution;

3- equal or nearly equal eigenvalues: uniform distribution.

In the case of cylindrical folding, the poles to the folded plane are distributed along a great circle and the fold-axis is parallel to the eigenvector associated with the smallest eigenvalue, perpendicular to the great circle.

The number of structural measurements available was not sufficient to do a detailed structural analysis of all the major folds; hence the mapped area was subdivided according to variations in local trend and rock type in order to obtain domains which were as homogeneous as possible. These are used to illustrate the regional variations in tectonic style. From there, an attempt is made to elucidate the mechanisms and causes of the Hudsonian deformation. This will be integrated with other structural observations into a model of the tectonic evolution of the Wakeham Bay area as part of the Cape Smith Belt. Figure 18 shows the various domains with pi diagrams of the foliation of each domain.

B WESTERN MAP AREA

Domains 1 to 6 occupy the northern part of the western map area; they are separated from the rest of it by a sub-vertical fault, which forms a distinct EW lineament. These domains show relatively simple pi diagrams (Fig. 19) in accordance with the thickness and competence of the Upper and Lower Volcanic Groups which predominate here. They have either a type 1 distribution (domains 1, 3, and 6) or a type 2 distribution (domains 2, 4, and 5). The trend of the axial part of the geosyncline (278/7) is defined by a combination pi diagram of domains 3, 4, 5, and 6 (Fig. 20).

In domain 1, two faulted folds have been mapped (Fig. 21). Fold 1, at the Archean contact, is a small syncline in the Pelitic and Volcano-Sedimentary Groups, open to the east, with a sliver of Archean gneisses in the faulted anticline. Fold 2 is a large syncline in the Lower Volcanic Group, open to the west; its south limb is faulted off. This fold is only the nose of a larger syncline mapped west of the area by Gold (1962). The axes of these two folds cannot be deduced from the available foliation measurements; but the axis of the larger syncline is probably parallel to the 270/43 direction of minor fold axes (Fig. 19). The axis of fold 1 must plunge in a south-easterly direction and this fold corresponds thus to a different phase of folding than fold 2.

In domain 3, several small folds, one faulted,

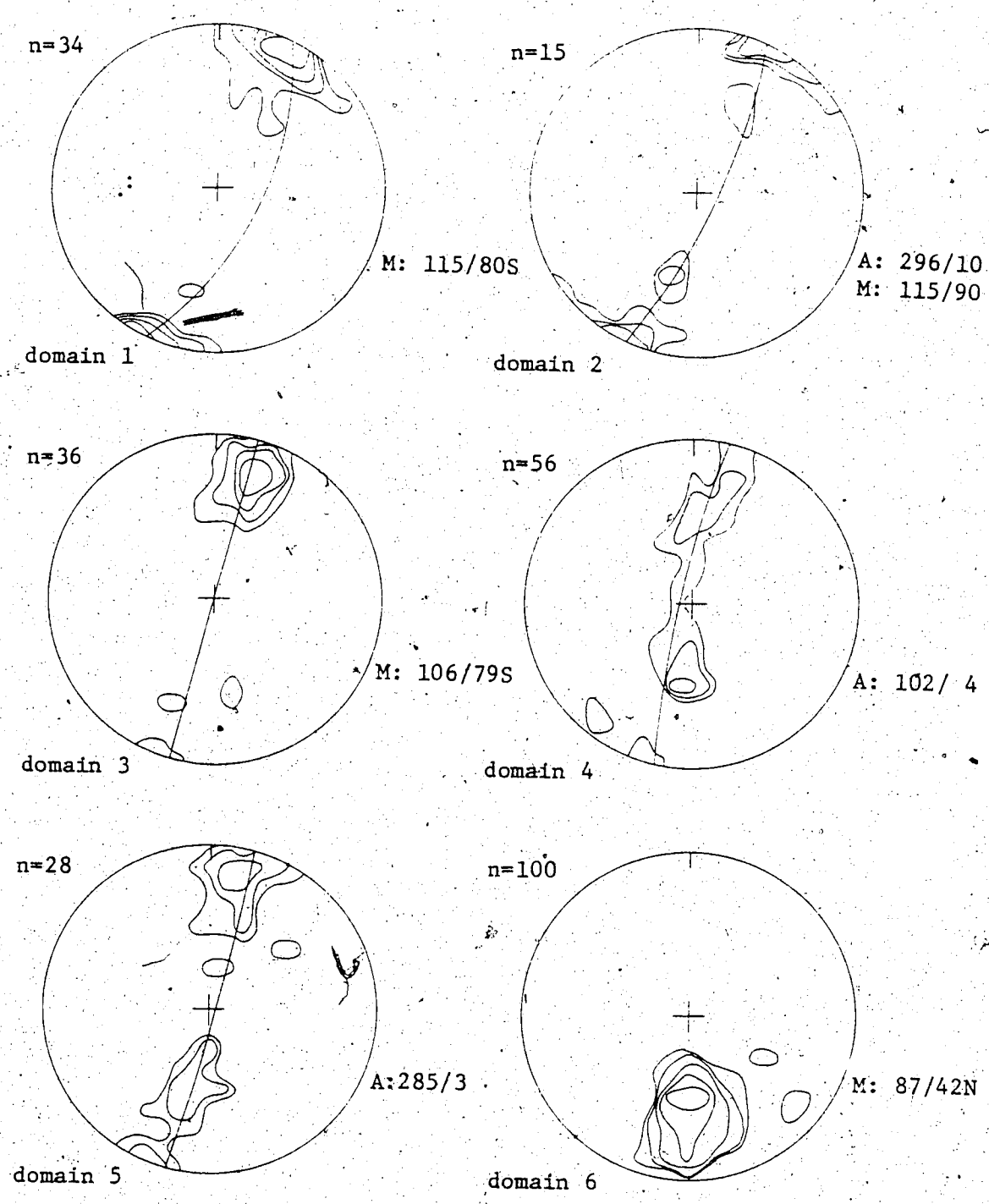

Fig. 19. Equal-area lower hemisphere projection. The contoured data corresponds to foliations. Contours are at 5,10,20% for $n<20$; at 2,5, 10% for $20<n<50$; at 1,2,5,10% for $n>50$. The orientation of axes to great circles (A) and maxima of contoured data (M) are marked on the left of the diagrams.

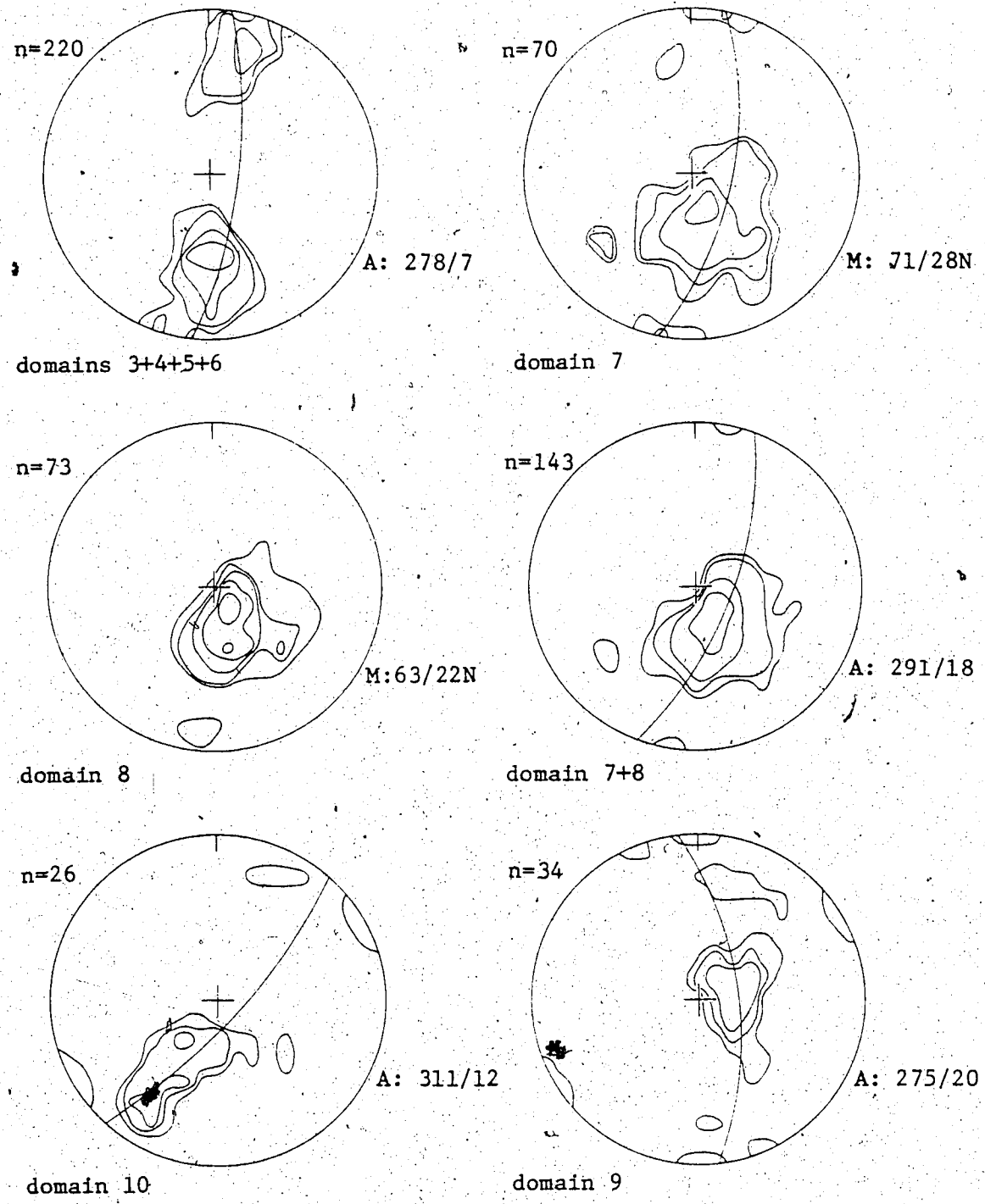

Fig. 20. Equal-area lower hemisphere projection. The contoured data corresponds to foliations. Contours are at 5,10,20% for $n<20$; at 2,5, 10% for $20<n<50$; at 1,2,5 10% for $n>50$. The orientation of axes to great circles (A) and maxima of contoured data (M) are marked on the left of the diagrams.

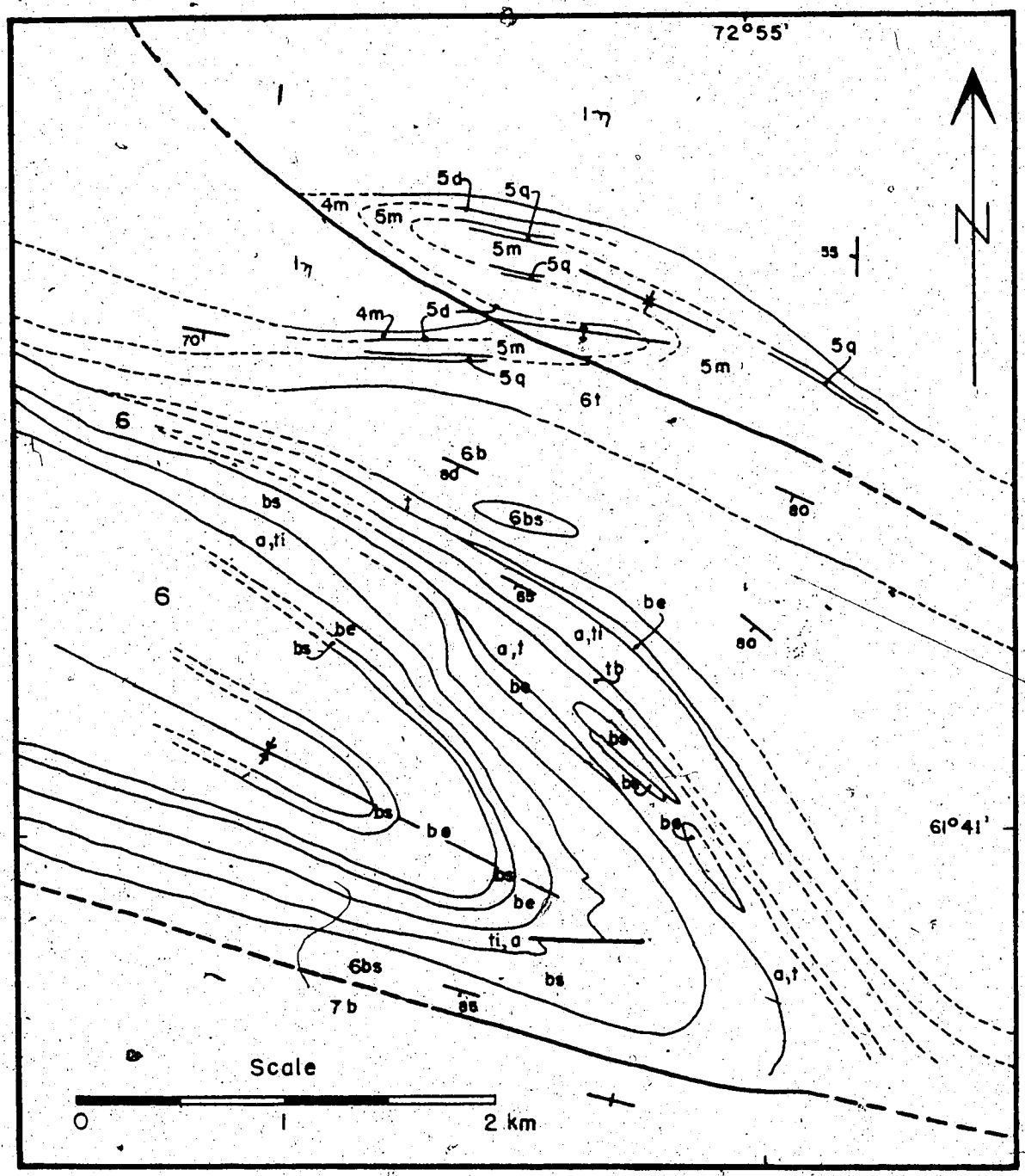

Fig. 21. Folds in domain I (legend in table I.).

occur below the Lower Volcanic Group; they are of the same type (E plunging axes) as fold 1 in domain 1. The minor fold axes recorded form two groups, one plunging SW, one plunging E. This last one should correspond to the folds mapped in the rocks below the Lower Volcanic Group.

Domain 2 is situated to the south of domain 1 and is separated from it by a fault. No folding was observed in this domain; but numerous shear zones and one fault were observed, sub-parallel to the trend of the rocks. These may represent tight vertical faulted folds. This domain corresponds to the axial zone of the geosyncline at this longitude.

The pi diagrams of domains 4 and 5 show a great circle distribution with a shallow easterly dip for domain 4 and a shallow westerly dip for domain 5, illustrating the axial culmination that occurs in the central part of the Monts Lune at the limit between these two domains.

No folding or faulting was observed in domain 6.

Domain 9 consists of the Iron Group, the Pelitic Group and the Volcano-Sedimentary Group in the Wakeham River Valley. The pelites and tuffs are complexly folded. The pi diagram (Fig. 20) shows a great circle distribution with some lateral spreading suggestive of refolding. A diagram of linear features (minor fold axis, mineral lineations etc...) shows a variety of subhorizontal directions with a maximum to the WNW (Fig. 22).

Domains 7, 8, 10, 11 and 12 constitute the remain-

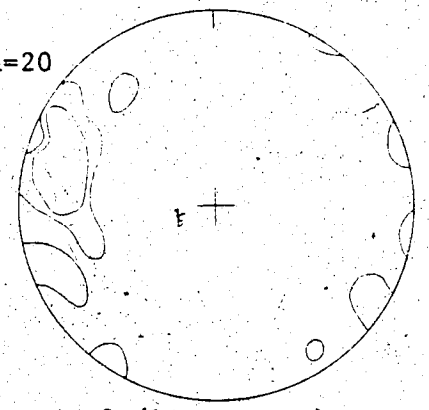

domain 9 (lineations)

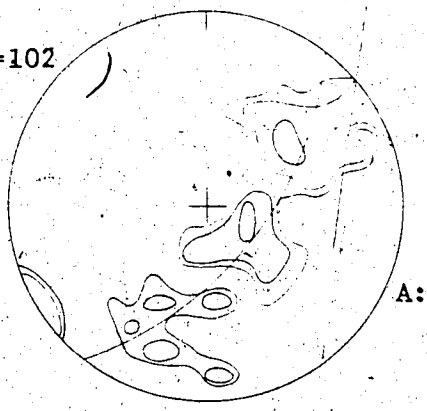

A: 308/24

domain 13

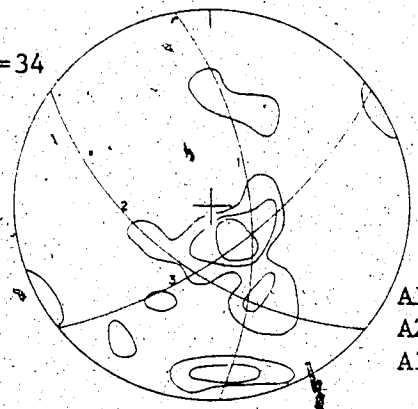

A1: 265/16
A2: 53/28
A3: 320/20

domain 11

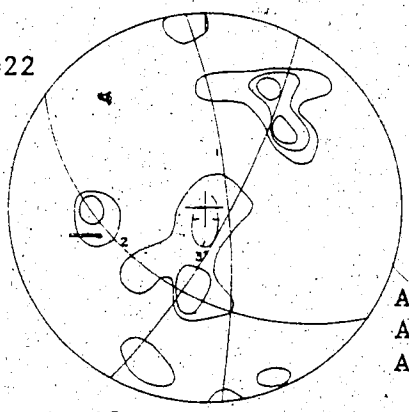

A1:265/10
A2: 36/36
A3: 308/24

domain 12

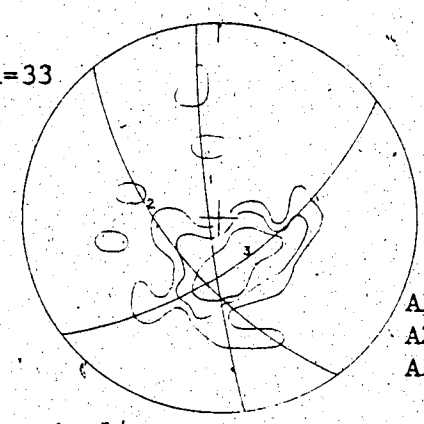

A1: 82/ 4
A2: 51/22
A3: 322/20

domain 14

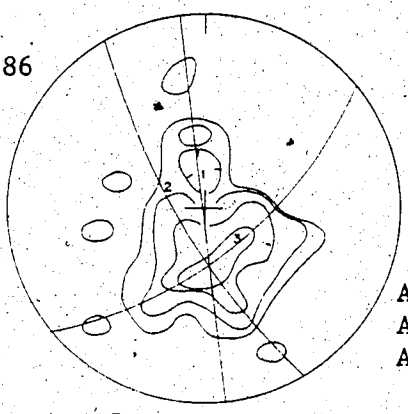

A1: 83/ 0
A2: 60/12
A3: 320/20

domain 15

Fig. 22. Equal-area lower hemisphere projection. The contoured data corresponds to foliations, except where noted otherwise. Contours are at 5,10,20% for $n<20$; at 2,5,10% for $20<n<50$; at 1,2,5,10% for $n>50$. The orientation of axes to great circles (A) and maxima of contoured data (M) are marked on the left of the diagrams.

der of the Lower Volcanic Group in the western area. In this group of domains, the Lower Volcanic Group is folded into a broad, open anticlinal-synclinal pair. The anticlinal axial zone is located more or less along the Wakeham River and faulted in a NW-SE direction along the river, below Mont Ptarmigan. The axial zone of the syncline is more difficult to define because it is a very open, broad fold. The nose of this fold constitutes domain 12 and is faulted off along the northern limit of domain 11. It is underlined by the topography of Mont Umiak and because of this is clearly visible on the geological map; the same phenomenon occurs again on the east slopes of Mont Ptarmigan were the syncline, slightly less open SE of the fault along the river, is clearly underlined by the topography. The pi diagrams of domains 7, 8, and 10 (Fig. 20) show simple type 1 or type 2 distributions. In domains 7 and 8, the directions are similar to those of domains 1 to 6, but in domain 10 the trend has changed to NW-SE.

The pi diagrams for domains 11 and 12 (Fig. 22) are more complex and akin to those of domains 14 and 15 with which they will be discussed below.

South of the Lower Volcanic Group we come into the Volcano-Sedimentary Group with, from west to east, domains 13, 14, and 15. Folding was observed, and mapped, in the field throughout this zone.

In domain 13, an anticline-syncline pair was mapped in the NW corner; the anticline is almost entirely

covered by Quaternary deposits NW of Lac Vicenza, but is quite visible west of 73°00'W in the area mapped by Gold (1962). This fold affects rocks of the Volcano-Sedimentary Group as well as rocks from the base of the Lower Volcanic Group. Further east as well, minor folding was mapped, overlapping the limits of these two units along the boundary of domains 10 and 13. The pi diagram of domain 13 (Fig. 22) shows a great circle distribution with an axis at 308/24.

In domain 15 the Volcano-Sedimentary Group, below the synclinal fold those of domain 12, is strongly folded into what appears to be a series of recumbent folds, probably with thrust faults paralleling some of the axial planes. The geological map shows only partly the complexity of this domain.

The pi diagram for domains 11, 12, 14, and 15 (Fig. 22) do not show clear great circle distributions. But a plot of linear structures for domains 14 and 15 (where a sufficient number of measures of fold axes, crenulations and mineral lineations was available) shows four maxima at 80/0, 40/10, 5/20, 310/15 (Fig. 23) . Taking this into account, it follows that the distribution of poles to foliations for these four domains may be explained by a combination of 3 great circle distributions with axes near 3 of the 4 maxima of the diagram of linear structures:

-domain 11: 265/16, 53/28, 320;/20

-domain 12: 265/10, 36/36, 308/24;

-domain 14: 82/4, 51/22, 322/20;

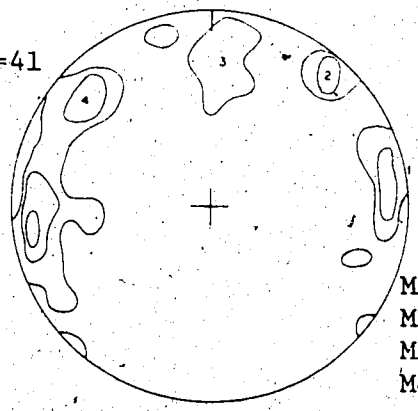

domains 14+15 (lineations)

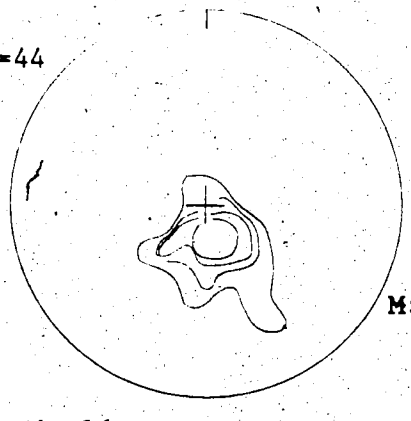

domain 16

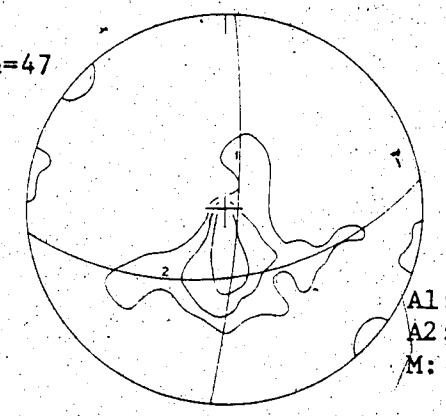

domain 17

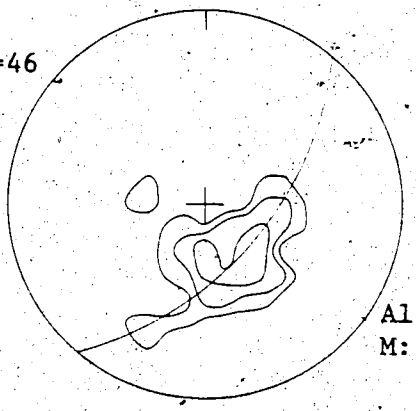

domain 18

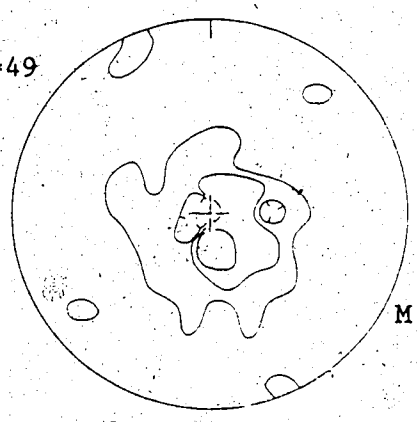

domain 19

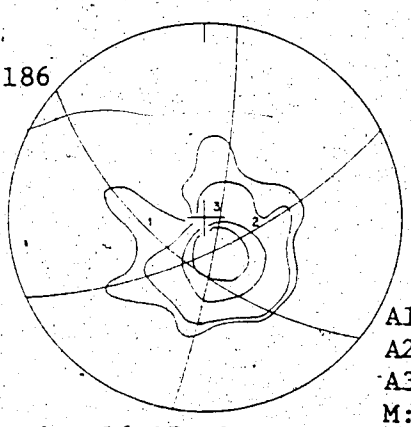

domains 16+17+18+19

Fig. 23. Equal-area lower hemisphere projection. The contoured data corresponds to foliations, except where noted otherwise. Contours are at 5,10,20% for $n<20$; at 2,5,10% for $20<n<50$; at 1,2,5,10% for $n>50$. The orientation of axes to great cicles (A) and maxima of contoured data (M) are marked on the left of the diagrams.

-domain 15: 83/0, 60/12, 320/20.

From this one may conclude that the rocks in domains 11, 12, 14 and 15 have been subjected to four phases of folding, one of which consists only of a broad warping, an undulation (as observed in the field), and is represented by a few NS linear structures. The EW phase consists of recumbent, almost isoclinal folds. The NE and NW phases both consist of more open folds with axial planes dipping respectively to the NW and NE.

Further south, we come into the Pelitic Group (domain 16) and the Iron Group (domains 17, 18, and 19). This area is complexly folded, at least at small scale; no major folds have been mapped. But this folding does not show on the pi diagrams which show only single maxima (Fig. 23); only domain 17 shows a distribution that might be attributed to the superposition of 2 great circles with axes at 274/5 and 350/30. A good representation of the complexity of the folding is shown by a diagram of minor fold axes for the area, in which one may recognize the following maxima (all with shallow plunges): 0, 30-50, 300-320, and 250-260. The mineral lineations, not included in this diagram, are trending north with a shallow plunge. A diagram of poles to axial planes, for the same area, shows one maximum (subhorizontal) and a great circle with an axis at 302/16, possibly another with an axis at 66/6.

The pattern in this group of domains (16, 17, 18,

and 19) presents a similarity to that of domains 11, 12, 14, and 15. And from this, one may attempt to establish a chronology of deformation, valid at least for the southern part of the western area, and based on the following observations:

1- Four phases of folding may be recognized, based on the distribution of planar and linear structures.

2- In the field, three types of folds have been observed: recumbent, sub-isoclinal; inclined, open; vertical, very open.

3- The mineral lineations, at least in the southern most domains, trend north with a shallow plunge.

4- The crystallization of the metamorphic minerals appears syntectonic to late tectonic.

5- A diagram of axial planes shows refolding around a NW axis, possibly also around a NE axis.

The chronology should therefore be:

F1: recumbent, sub-isoclinal folds with sub-horizontal EW axes.

F2 and F3: inclined, open folds; fold axes have a shallow plunge to the NW and to the NE respectively, the axial plane have an intermediate northeasterly and northwesterly dip.

F4: vertical, very open folds; the axes have a

shallow northerly plunge.

The relative ages of F2 and F3 cannot be determined at this point.

C EASTERN MAP AREA

Domains 20 to 23 contain mainly rocks of the Lower and Upper Volcanic Groups and show relatively simple structures. By contrast, domains 24, 25, 29, 30, and 31 which contain a larger proportion of rocks of the lower groups, where the Upper Volcanic Group is absent and the Lower Volcanic Group thinner, and where, in particular in domain 30 and 31, the metamorphic grade is higher, show complex fold structures. The complexity of these structures can only be partially shown on the geological maps.

Domains 20 and 21 consist of a large syncline with a shallow westerly plunging axis. A series of nearly vertical folds, one of which contains a sliver of Archean rocks, was observed on the east wall of the Wakeham Valley, near the outlet of the River (see inset in Fig. 18). In the SE corner of domain 21, just north of Lac Ruban, the lower part of the Aphebian section, including the contact with the Archean, is folded into an open anticline.

The pi diagram for domain 21 (Fig. 24) shows a broad maximum that can be explained by the superposition of

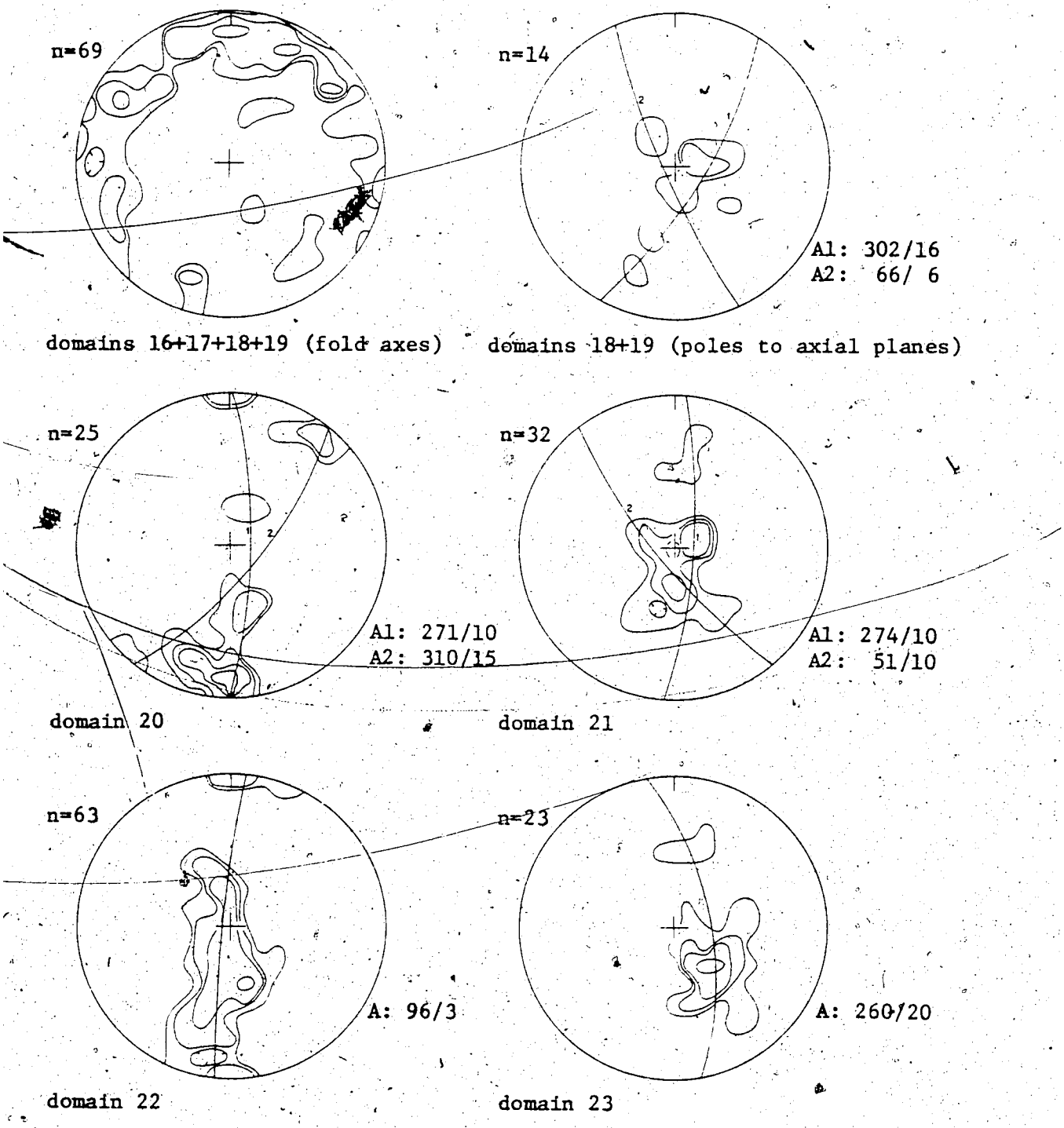

Fig. 24. Equal-area lower hemisphere projection. The contoured data corresponds to foliations, except where noted otherwise. Contours are at 5,10,20% for n<20; at 2,5,10% for 20< n<50; at 1,2,5,10% for n>50. The orientation of axes to great circles (A) and maxima of contoured data (M) are marked on the left of the diagrams.

a great circle with axis at 274/10 (general trend of the geosyncline) and one with axis at 51/10 (the open anticline north of the Lac Ruban).

In domains 22 and 23 the Upper Volcanic Group rocks form an EW elongated basin. Some minor folding was mapped in the sediments and tuffs at the base of this basin. The pi diagram for domains 22 and 23 (Fig. 24) show great circle distributions with axis plunging respectively E and W, in accordance with the basin structure.

Domains 24 and 25 consist of rocks of the Iron Group, the Pelitic Group, and the Volcano-Sedimentary Group, and some of the Lower Volcanic Group. Two large fold structures were mapped in these domains. Fold 1 is a long, isoclinal recumbent, EW syncline, closed at both ends, with several minor anticlines. Its core consists of rocks of the Lower Volcanic Group, separated from the main body of Lower Volcanic Group rocks to the north. Its axis is essentially horizontal, EW in domain 24, changing to SW-NE in domain 25. It is refolded into an open fold with a N to NW axis. Fold 2 occurs in the Iron Group and the Pelitic Group. It is marked by a layer of iron formation and is similar in shape to the first fold, but slightly more open and not as long. The northern half of domain 25 appeared complexly folded, but outcrop conditions precluded any accurate mapping of these structures. They do not appear on the pi diagram (Fig. 25) either.

Domain 26 corresponds to a small EW elongated

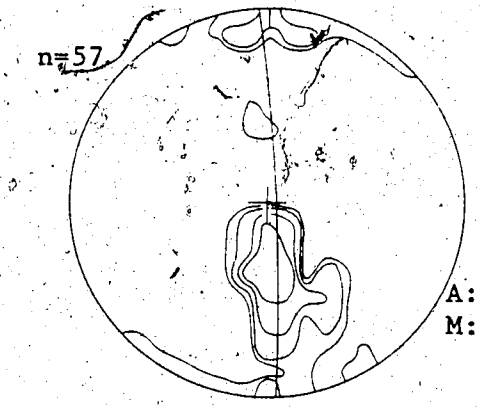

A: 267/ 3
M: 83/39N

domain 24

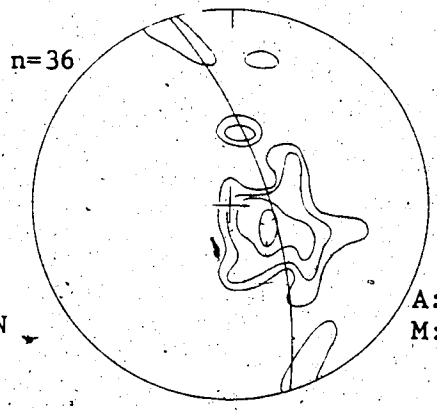

A: 251/17
M: 24/23W

domain 25

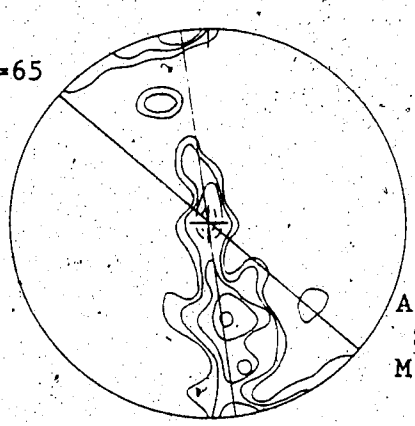

A: EW/0 to
SW-NE/0
M: -76/43N

domain 26

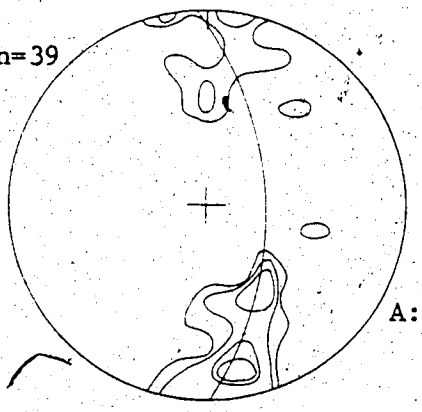

A: 267/25

domain 27

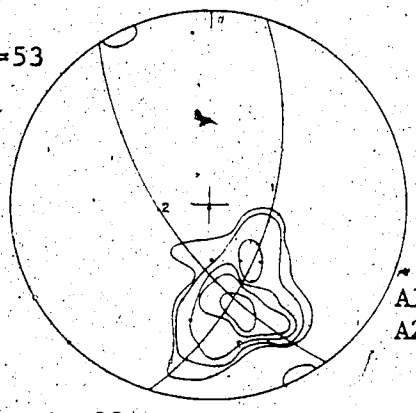

A1: 286/25
A2: 55/20

domain 28

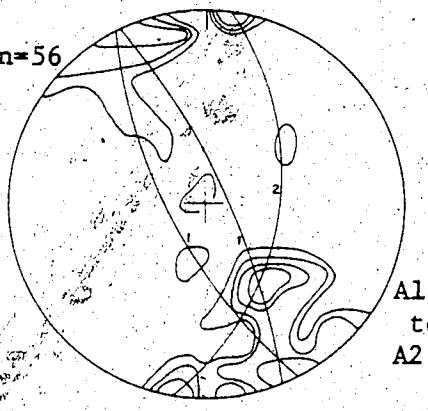

A1: 246/ 9
to 63/15
A2: 278/30

domain 29

Fig. 25. Equal-area lower hemisphere projection. The contoured data corresponds to foliations. Contours are at 5,10,20% for $n < 20$; at 2,5, 19% for $20 < n < 50$; at 1,2,5,10% for $n > 50$. The orientation of axes to great circles (A) and maxima of contoured data (M) are marked on the left of the diagrams.

basin of Iron Group and Pelitic Group rocks within Archean gneisses and amphibolites. The contact with the Archean traces several folds (see geological map). The pi diagram for domain 26 (Fig. 25) shows a great circle distribution with a horizontal axis varying from nearly EW to SW-NE and a maximum corresponding to an average trend of 76/43N.

Domains 27 and 28 are the Archean rocks between the Ippijuaq and the Qikirtaalualuk lineaments (27: western half; 28: eastern half). The trend of the Archean rocks in these domains is EW like that of the Aphebian rocks; but this is probably more a coincidence than a result of the Hudsonian deformation, as this trend remains unchanged further to the SW, outside of the main zone of Hudsonian deformation. Indeed folded amphibolite layers mapped in domain 28, north of domain 26, are discordant with the Hudsonian structure; an anticline in the Archean underlies a minor synclinal refolding of the Aphebian basin (see geological map and cross-section). The pi diagram for domain 27 (Fig. 25) shows a simple great circle distribution, but the pi diagram for domain 28 (Fig. 25) shows a maximum that could be considered as made up of a great circle with axis at 286/25 and one with axis at 55/20, corresponding to the folding illustrated by the amphibolite layers.

In the rest of the area (domains 29 to 35), the Archean rocks have reacted to the Hudsonian deformation by folding in the same manner as the Aphebian rocks which form a syncline trending SW in the western part of domain 29;

further east it splits into a NE trending branch, the end of which forms a complex fold-structure (Qialik Structure), and an east trending branch which ends a few miles further east. Domains 29 and 30 correspond respectively to the SW and to the W trending parts of the syncline.

Domain 31 consists of the Archean rocks north of the syncline, including the Qialik Structure. This structure contains the end of the north branch of the syncline, folded together with the Archean rocks. In the Qialik Structure, the NE trending syncline of Aphebian rocks is refolded:

1- by an EW syncline, to form an EW elongated basin;

2- by an anticline with a shallow easterly plunge, to form a crescentic antiformal basin.

A small flat-lying outlier occupies the centre of the crescent. Amphibolite layers within the Archean aid in illustrating this structure and, more generally, the EW phase of folding.

The pi diagrams for domains 29, 30, and 31 show rather complex distributions that may be explained by the superposition of three trends: EW, NW-SE, NE-SW. The pi diagram for domain 31 (Fig. 26) is slightly more complex than those of domains 29 and 30 (Fig. 25); it consists of two great circles with different patterns of scattering. The first shows more scatter in the foliations with steep dips than in those with shallow dips, resulting in an axis of variable direction (from 310/20 to 73/20); this may be ex-

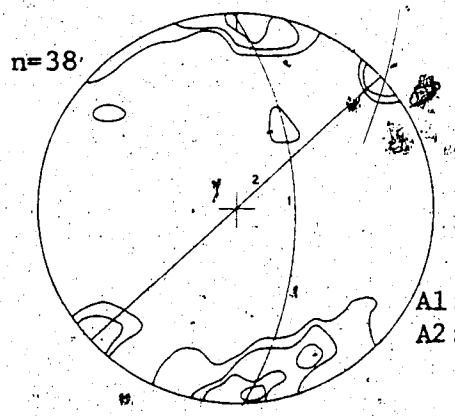

domain 30

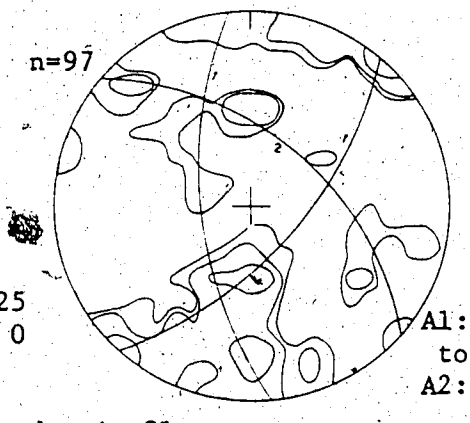

domain 31

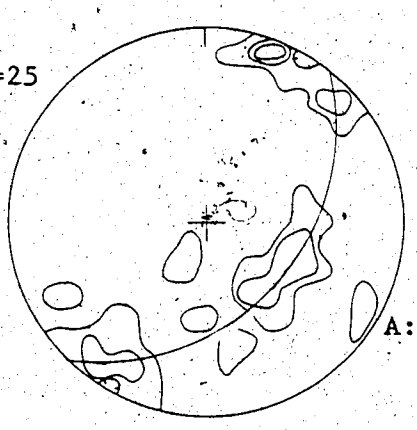

domain 34

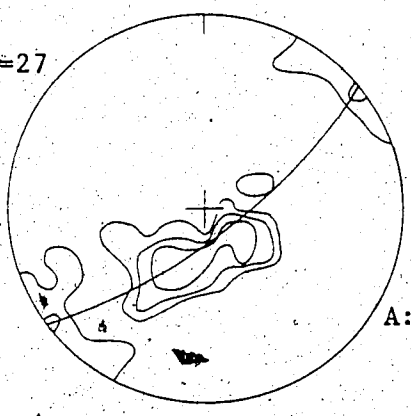

domain 35

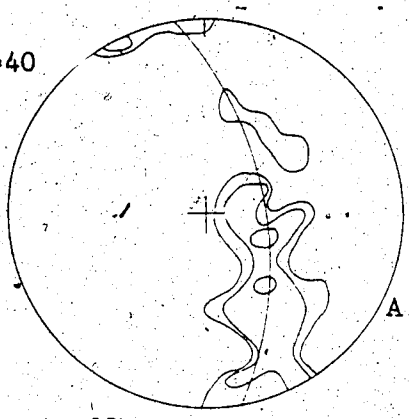

domain 32

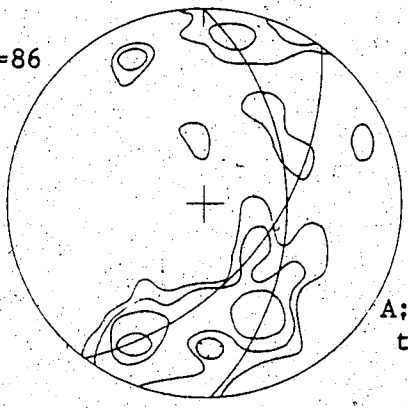

domain 33

Fig. 26. Equal-area lower hemisphere projection. The contoured data corresponds to foliations. Contours are at 5,10,20% for $n<20$; at 2,5, 10% for $20<n<50$; at 1,2 5,10% for $n>50$. The orientation of axes to great circles (A) and maxima of contoured data (M) are marked on the left of the diagrams.

plained by a change in trend from the western to the eastern part of the domain. The second shows more scatter in the foliations with intermediate to shallow dips than in those with steep dips, giving an axis at 218/0-40; this scatter appears to be the result of refolding along a shallow plunging axis which trends more or less perpendicular to the refolded one, and which could for example be the axis of the first great circle. The pi diagram for domain 31 illustrates thus clearly the chronology of deformation that resulted in the Qialik Structure:

1- folding along a SW trending axis;

2- refolding along an E trending axis.

A small refold of the Archean-Aphebian contact near the eastern end of the geosyncline (domain 30) is probably akin to the Qialik Structure.

Domains 34 and 35 consist of Archean rocks, east of the end of the north branch of the geosyncline, in which this structure is illustrated by four major horizons of basic rocks. Two of these, amphibolites, are typical refolded folds; the Kenoran (?) fold axes trend E to ENE and the plunge seems moderate. The two other layers appear to have been folded only once, by the Hudsonian deformation; one of these is clearly a diabase sill (or NW dipping dyke) with a relict ophitic texture; it is probably of early Aphebian age, of the same group as the diabase dykes observed elsewhere in the area, cutting Archean rocks and

overlain by the Aphebian supracrustal rocks; the other layer, however, is an amphibolite similar to the two refolded ones, i.e. metamorphosed during the Archean; it may correspond to a late- to post-tectonic sill. The pi diagrams for domains 34 and 35 (Fig. 26) show only the effect of the Hudsonian deformation, with a NW-SE trend. The scatter of points in the diagram for domain 34, as well as the relatively steep dip of the axes suggest that a certain amount of control of the Hudsonian structures by preexisting Kenoran structures, has taken place.

Domain 32 and 33 are the Archean rocks between the Qikirtaalualuk lineament and the main Aphebian syncline. In domain 32 the foliations in the gneisses suggest an anticline-syncline pair, more or less parallel to the contact with the Aphebian rocks. The pi diagram (Fig. 26) shows a great circle with axis similar to that of the adjacent domain 25. In domain 33, the pattern of foliations suggests folding, but the absence of marker horizons hindered the mapping of any fold. The pi diagram (Fig. 26) shows a great circle with an axis between 270/35 and 350/30, reflecting a change in trend within this domain similar to the change in trend from domain 30 to domains 34 and 35.

In the eastern map area, three phases of deformation may be recognized: EW, NW-SE, and NE-SW. The NS phase, observed in the western map area, appears to be absent. The chronology of the phases is also different from the western map area; the EW phase is still the major phase of deforma-

tion, but it is later, at least locally, than the NE-SW phase and contemporaneous with the NW-SE phase.

5. DISCUSSION

In the Wakeham Bay region two major periods of deformation can be recognized. The first, related to the Kenoran Orogeny, affected the Archean rocks only; it was a penetrative deformation producing a foliation, folding and, probably faulting. The second, related to the Hudsonian Orogeny, affected both the Archean rocks and the Aphebian rocks, albeit in a different manner.

In the Aphebian rocks, the tectonic style varies in response to changes in competence and thickness of the lithologic units, and to changes in metamorphic grade.

Where the Hudsonian metamorphic grade was low to medium, the Archean rocks reacted as an indurated basement i.e., the Hudsonian metamorphism was not penetrative and movement was concentrated along faults and narrow shear zones. But where the Hudsonian metamorphism was of higher grade, the accompanying deformation affected the Archean rocks penetratively and folded them in the same manner as the Aphebian rocks. In the Aphebian rocks the change in style with metamorphic grade is not so great; faulted folds are more common in the low metamorphic grade parts; the

upper portions of the stratigraphic section (the thick sequence of sills and flows) are characterized by large open folds, whereas, the lower portions (more thinly bedded sediments and tuffs) by more appressed, smaller folds.

The topographic maps and the aerial photographs show three systems of large-scale lineaments: EW, NW-SE, NE-SW. These lineaments are visible mainly in the Archean rocks; but some transgress into the Aphebian rocks. Faults have been observed along some of them. These lineaments show no changes in direction with changes in topography; this suggests that they are high angle features.

In the western map area four phases of deformation have been observed in the Aphebian rocks, corresponding to fold axes trending EW, NW-SE, NE-SW, and NS. This last phase is very weak and produced only a few very open folds. The chronology is EW, NW-SE and NE-SW, NS. In the eastern map area the NS phase is absent and the chronology is, at least locally, NE-SW, EW and NW-SE.

The continuity of the Aphebian stratigraphy around the basin and the absence of any break in the structural trend of the Archean rocks suggest that the Aphebian rocks were deposited on a continuous Archean basement, i.e. on a continuous continental crust.

Examination of various NS cross-sections through the Aphebian geosyncline (Fig. 15) shows that little, if any, crustal shortening has taken place during the Hudsonian Orogeny. The folding of the Lower and Upper Volcanic Groups,

which form the bulk of the Aphebian rocks, can be explained as well in terms of differential vertical movements (subsidence of the axial part of the basin), as in terms of horizontal movements (compression).

The various points discussed above:

1- relatively plastic folding of the Aphebian rocks over a basement undergoing brittle deformation,

2- changes in the relative chronology of the phases of Hudsonian folding from one part of the area to another, as well as lateral changes, within one structure, from one folding direction to another,

3- coincidence of the directions of Hudsonian folding with those of the major lineaments in the Archean basement,

4- lack of crustal shortening,

suggest that the Hudsonian deformation in this area was the result of differential vertical movements of rigid blocks of Archean basement along three systems of faults and shear zones. These movements occurred more or less concurrently along each of the three directions, controlling not only the folding of the supracrustal rocks but also the initial subsidence. The pattern of folding observed now is the result of the dominance of one phase over the others at different times in different parts of the area. In the area mapped the EW (to WNW-ESE) phase is the major phase of deformation, the only one that is of sufficient amplitude to affect the whole stratigraphic sequence. The other two phases are rapidly

attenuated upwards and affect only the lower three stratigraphic units, except in the East were the stratigraphic section is thinner and the deformation (and metamorphism) more intense.

6. CONCLUSIONS

The following model of structural evolution is proposed for the eastern end of the Cape Smith Belt during the Aphebian:

1- erosion of an Archean basement;

2- regional tensional regime resulting in the intrusion of numerous northwesterly trending diabase dykes;

3- subsidence and sedimentation, first, mature fine psammitic and pelitic rocks with iron formation, then, with gradual increase in volcanic activity, a change to more immature sediments;

4- extrusion of basic volcanics rocks accompanied by numerous sills and interlayered with minor immature detrital sediments;

5- deformation, folding, of the Aphebian rocks by intensification of the vertical movements, accompanied by metamorphism; the Archean basement is faulted along three major directions ('tectonique cassante') and the Aphebian, less rigid, is folded in response ('tectonique souple').

In the western and central part of the area, the thick competent mass of the Lower and Upper Volcanic Groups deform along the EW direction as very open folds, occasionally faulted. This movement compresses against the basement the less competent underlying sediments and tuffs into isoclinal recumbent folds; later movements, of lesser amplitude, refold these isoclinal folds into more open folds, trending NW or NE. A late phase produces some minor NS warps. In the eastern part of the area (east of Maricourt) which corresponds to a deeper crustal level, the three phases of folding are about equivalent in intensity and, locally, the NE trending phase is the earliest one. Because the portion of the geosyncline exposed here corresponds to its axial (deepest) zone, little or no differential movement took place between the two Volcanic Groups and the basement, and, consequently, no isoclinal folding in the intervening sediments and tuffs.

CHAPTER IV

LITHOLOGY

1. ARCHEAN

The Archean rocks consist mainly of light grey to pink, granitic to granodioritic, medium- to coarse-grained gneisses; a well developed foliation is present, as well as banding, parallel to foliation, that may correspond to an original bedding. They are composed of quartz, microcline, oligoclase or andesine, biotite and/or hornblende; apatite, zircon, opaques, secondary muscovite, chlorite, calcite, scapolite, and epidote may be present.

The gneisses are interlayered with minor amphibolite which may occasionally be sufficiently thick and continuous to form mappable units and, as such, useful marker horizons. They are composed of plagioclase (andesine to bytownite), olive-green hornblende, ilmenite, apatite, allanite; garnet, diopside, biotite, quartz may be present; secondary minerals such as green hornblende, chlorite, epi-

dote, calcite, scapolite, sphene, are generally present as well.

Paragneisses occur in the peninsula NE of Maricourt; along the shore of Wakeham Bay one can observe: grey banded dioritic to granodioritic gneisses interlayered with amphibolite, some of which are garnet and sulphide-bearing (rusty alteration); biotite, muscovite, diopside-rich gneiss or schist; sulphide-bearing hornblende, garnet, graphite gneiss; rusty gneiss with segregation of quartz-garnet-apatite-calcite. In the central part of the peninsula one can observe: biotite-rich grey banded gneiss, biotite-plagioclase-cummingtonite rock, garnet-amphibolite, diopside-amphibolite, kyanite-garnet-muscovite-biotite gneiss (386-391) (3 digit numbers are laboratory number of thin sectioned samples listed in Appendix IV).

The quartzo-feldspathic gneisses are migmatitized (incipient anatexis); but granitic pegmatites are common only in the area north and east of Stupart Bay.

Some of the larger, more continuous amphibolite horizons, in the peninsula northeast of Maricourt, appear to have been metamorphosed but not deformed by the Kenoran Orogeny; they may be late Archean dykes and sills.

2. EARLY APHEBIAN and LATE HADRYNIAN

Two groups of diabase dykes occur in the area. The first cuts the Archean rocks, is overlain by Aphebian sediments and volcanic rocks, and is locally deformed by the Hudsonian Orogeny. These dykes have a NW-SE or a NE-SW trend. Lowdon (1963) reports 7 isotopic ages (K-Ar) on similar dykes from an area south of the present map area. They range from 1995 to 2675 million years. The 2675 m.y. age is probably too high as these dykes cut Archean rocks with an age of about 2500 m.y. The average of the 6 other ages is 2149 m.y. This must be considered as a minimum age because some samples are from near the boundary of the Churchill Province and may have been affected by the Hudsonian thermal event and all show distinct deuteric(?) alteration which may have caused loss of ^{40}Ar. Moreover, Gates and Hurley (1973) have shown that K-Ar ages of diabase dykes are generally 100 to 200 m.y. younger than the age obtained by Rb-Sr mineral or whole-rock isochrons. An early Aphebian age can thus be attributed to this group of diabase dykes (2250-2350 m.y.).

Of the second group of diabase dykes, only one was observed, cross-cutting Iron Group rocks in the western map area. This diabase appears completely unmetamorphosed in thin section, barring some serpentinization of the olivine, whereas diabases of the first group always show the effects of the Hudsonian metamorphism. Isotopic dating (K-Ar) of similar dykes west of the present map area gives ages of

507±85 and 534±74 m.y. (Fahrig; 1967, 1968). Fahrig et al. (1971) consider these dykes to be part of the Franklin diabase which has an average age of 675 m.y., i.e. late Hadrynian. They trend NE-SW in the general area (Taylor, 1971). The localization of diabase dykes is shown in figure 27.

3. APHEBIAN

An angular unconformity separates the Archean and lower Aphebian rocks from the Aphebian sediments and volcanic rocks. This unconformity is visible in several localities in the map area, for example on Wakeham Bay and at the lower end of the Wakeham River Canyon. In several places a layer of a few centimetres to a few decimetres of a garnet- and biotite-rich rock occurs at the unconformity and is interpreted to be a paleosoil. In one thin section it is possible to recognize polycrystalline grains of quartz and feldspar in a matrix of biotite, garnet, muscovite and finer quartz and feldspar. In the Wakeham River Canyon, for example, 3 to 4 m of vertically foliated, white to light-grey (leached?) quartzo-feldspathic Archean gneiss is overlain by about 1 m of garnet-bearing, quartzo-feldspathic gneiss tightly folded and foliated parallel to the unconformity, i.e. nearly horizontal, followed by about 1 m of garnet- and

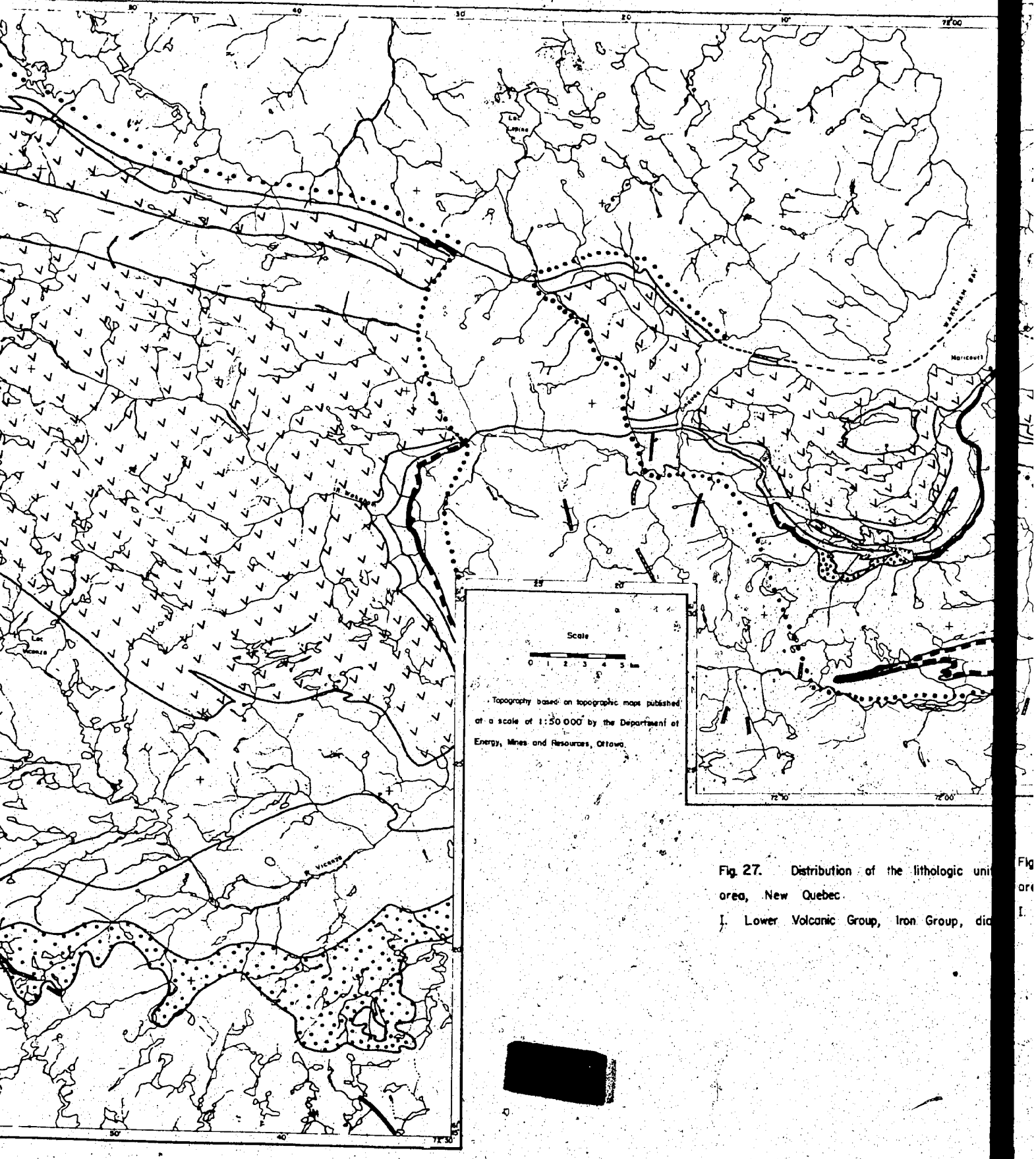

Fig. 27. Distribution of the lithologic uni
area, New Quebec.
I. Lower Volcanic Group, Iron Group, dia

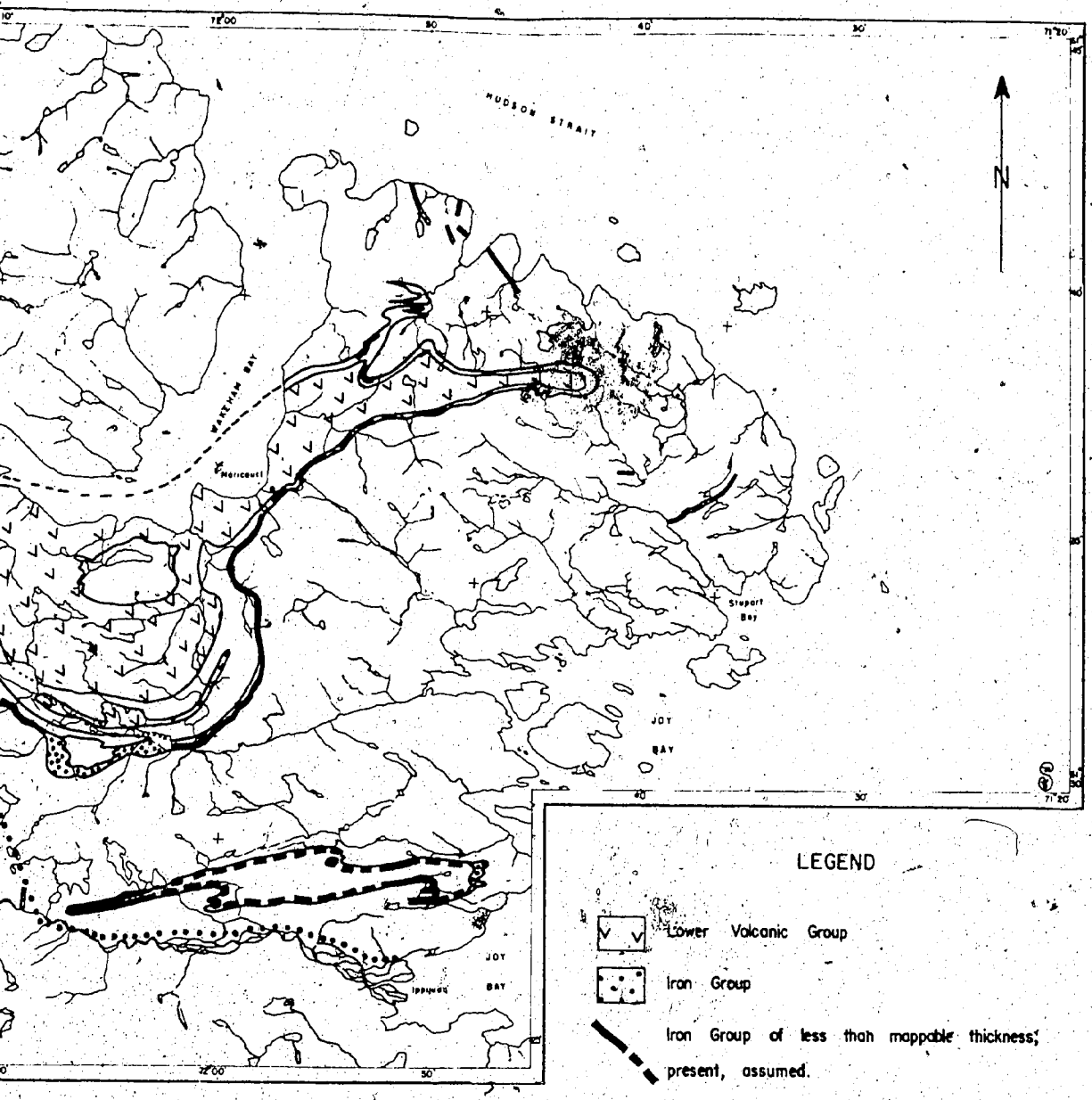

Distribution of the lithologic units of the Wakeham Bay
v. Quebec.

Volcanic Group, Iron Group, diabase dykes.

biotite-rich rock, followed by about 20 m of grunerite-garnet iron formation.

The unconformity can be overlain by rocks of the Iron Group or the Pelitic Group, occasionally the Volcano-Sedimentary Group.

A IRON GROUP

This group is best represented in the southern part of the western map area, in particular near Mont Table. It consists of:

- iron-rich rocks (iron formation);
- sandstone;
- pelites: mica-schist, chloritic mica-schist;
- dark green chlorite-schist.

The <u>iron-rich rocks</u> are very variable in composition; they are a mixture (in almost all proportions) of:

- quartz;
- oxides: hematite, magnetite;
- carbonates: calcite, dolomite, siderite and intermediate compositions, more or less manganiferous;
- silicates: grunerite ≅ stilpnomelane > garnet ≅ chlorite > biotite ≅ plagioclase.

Minor amounts of iron sulphides can be present. Some typical

compositions are, however, more common: quartz-rich, carbonate-rich, and silicate-rich.

Quartz-rich members are generally fine-grained, evenly thinly bedded and laminated, dark bluish to brownish grey; they contain a few percent of iron oxides, some stilpnomelane and some brown to yellow grunerite in fine radiating needles in the bedding planes. Zircon is often present. They contain oxide-rich interlayers, either as a thin-bedded, very fine-grained massive dark bluish grey rock containing up to 70-80% iron oxides, or as a medium-bedded coarser, gritty, quartz-iron oxide rock containing up to 40-50% iron oxides; neither of these last two is abundant.

The carbonate-rich member is medium- to thick-bedded with coarse, rather irregular, laminations; it weathers chocolate-brown when almost pure carbonate and quartz, lighter brown as the proportion of grunerite increases, or darker brown as the proportion of stilpnomelane increases; garnet, minor iron-oxides and chlorite can also be present.

The silicate-rich member is dark brownish to greenish grey, medium- to thick-bedded, with rather coarse laminations; it is composed of quartz, grunerite, stilpnomelane, chlorite, garnet, iron oxides and carbonates in varying amounts; round grains of carbonates often give a spotted aspect to the rock.

The sandstones are white to light buff, medium- to to thick-bedded (sometimes thin-bedded); they occur within the lower half or lower third of the Iron Group; they con-

sist of up to 90% quartz, with plagioclase, muscovite, biotite, chlorite, sometimes microcline. Just above the unconformity occurs locally a light green, chlorite-bearing, medium-bedded sandstone, up to 1 m thick, in which may occur poekilitic garnets forming large, light pink blotches.

The pelites are light to mediumgrey to greenish grey mica-schists; bedding and laminations are only occasionally recognizable because small scale folding and crenulation as well as metamorphic segregation into quartz-rich and mica-rich laminae obliterate sedimentary structures; only the more sandy beds can be easily recognized. They are composed of quartz (± plagioclase), muscovite and/or biotite and/or chlorite (± garnet); zircon, apatite, iron oxides, graphite, tourmaline, sphene are common accessories; carbonate, epidote, actinolite may be present in minor amounts.

The chlorite-schist is dark green, irregularly medium- to thin-bedded, composed of fine-grained quartz with up to 50% iron-rich chlorite, commonly with garnet. It is often found at the base of the sequence, above or below the green sandstone as well as higher up in the Iron Group. It is not known whether this rock represents a peculiar facies of the iron formation, or whether it represents interlayers of volcanogenic material.

Stratigraphic relations within the Iron Group have not been elucidated because of the complexity of the structure in the type area. The following generalisations only can be made:

- the proportion of mica-schist increases upwards;
- the proportion of sandstone increases downwards;
- among the iron-rich rocks, the silicate-carbonate member is more abundant in the upper half, the quartz-oxide member in the lower half of the Iron Group;
- the dark-green chlorite-schist is found mostly in the lower two-thirds of the Iron Group.

The last occurrence of iron-rich rock (generally a silicate-carbonate member) is taken as the upper limit of the Iron Group, its boundary with the overlying Pelitic Group. The distribution of the Iron Group is shown in figure 24.

The maximum thickness of the Iron Group is difficult to estimate because of the complexity of the structure in the type area; it is probably less than 500 m and may be no more than 200 m. It thins rapidly west and east of the type area. It occurs along the north branch of the geosyncline and around the Ippijuaq basin but only in thin horizons, often of unmappable thickness. In most of these occurrences, it consists of the silicate-rich member (grunerite-garnet-quartz ± magnetite, stilpnomelane, carbonate). A few thin layers of the oxide-rich member occur at the western end of the Ippijuaq basin. The thin-bedded quartz-rich member represents the Iron Group at the eastern end of the Ippijuaq basin and at one locality on the northern contact in the western map area; there, a thin, evenly-bedded

carbonate-bearing sandstone of light reddish brown colour, occurring right at the contact with the Archean, may represent the Iron Group.

The Iron Group occurs along most, but not all of the southern contact of the geosyncline; it is notably absent at Qinguaq and from there to Lac Ruban. The Iron Group is absent from the northern contact, except in two localities; this appears to be a real feature and not the result of a lack of exposure, as the northern contact is well exposed in several localities both in the eastern and in the western map area.

B PELITIC GROUP

This group consists mostly of pelites similar to those of the Iron Group (see description, above). In addition it contains small layers of quartzose schists to thin-bedded sandstones; chlorite-rich greenschists and graphitic blackschists are also present in minor amounts. Bedding is easily recognizable only where those different compositions are present.

This unit is fairly uniform and it could not subdivided within the western map area. In certain parts of the eastern map area (Ippijuaq basin), it is possible to distinguish a lower, heterogenous member with more abundant garnet mica-schists and graphitic blackschists from an upper homo-

geneous member composed of grey biotite-muscovite schist.

The Pelitic Group overlies the Iron Group or, directly, the unconformity. Its upper limit is defined by th base of the Volcano-Sedimentary Group, i.e. the first occurrence, upwards, of a significant volcanogenic tuff or of a dolomite horizon. The Pelitic Group grades into the underlying Iron Group and into the overlying Volcano-Sedimentary Group, both of which contain a significant proportion of pelitic schist. In the type area the thickness of the Pelitic Group can be estimated at 500-1000 m.

The distribution of the Pelitic Group is shown in figure 28. It occurs, in varying thickness, practically everywhere along the southern and the northern contact of the geosyncline. Along parts of the northern limits of the geosyncline it is very thin or absent.

C VOLCANO-SEDIMENTARY GROUP

This group is heterogeneous. It consists of the following lithologies:

- pelites;
- dolomites;
- sandstones;
- volcanogenic tuffs;
- ultramafic rocks;
- basic flows and sills.

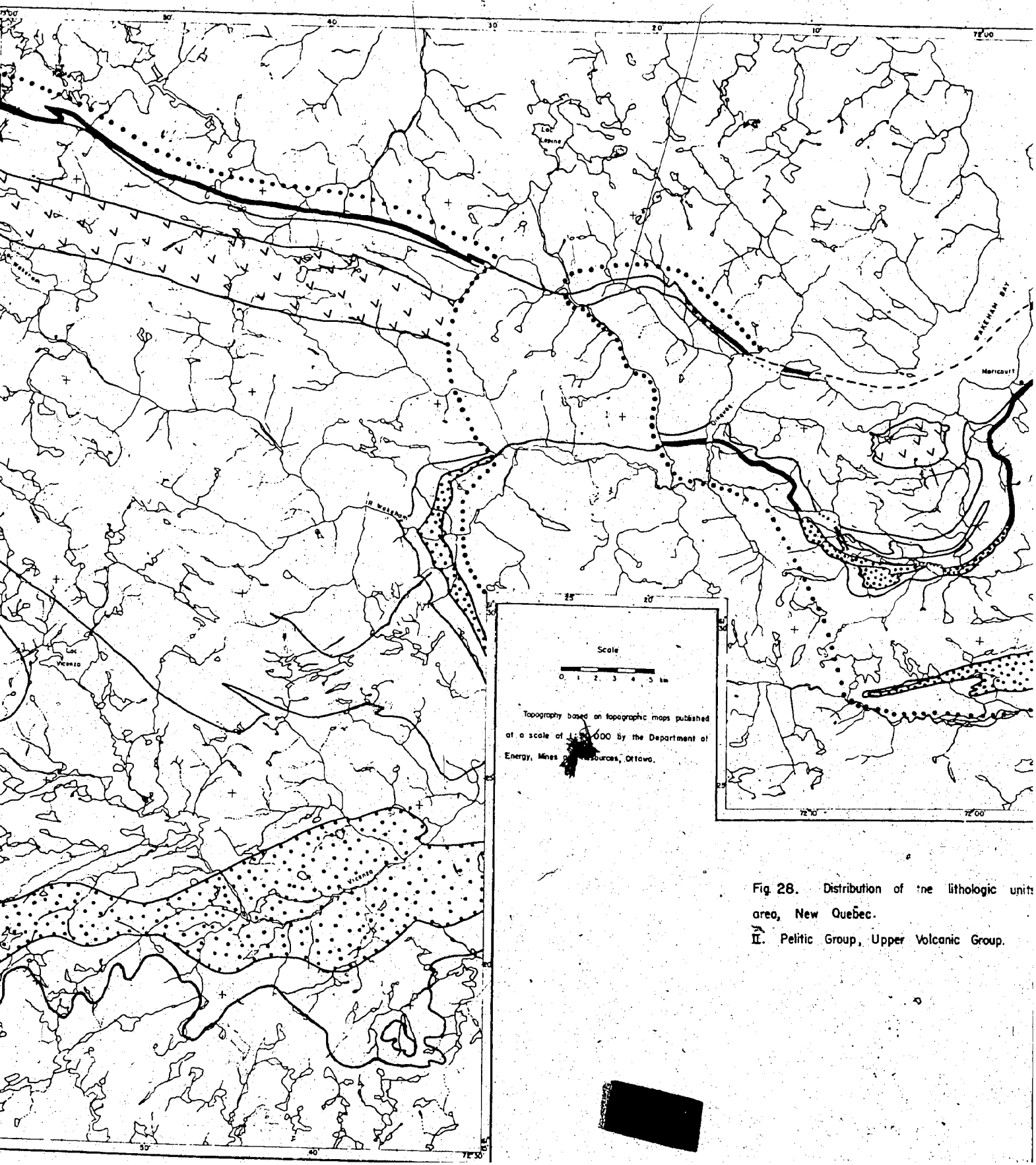

Fig. 28. Distribution of the lithologic units area, New Quebec.
II. Pelitic Group, Upper Volcanic Group.

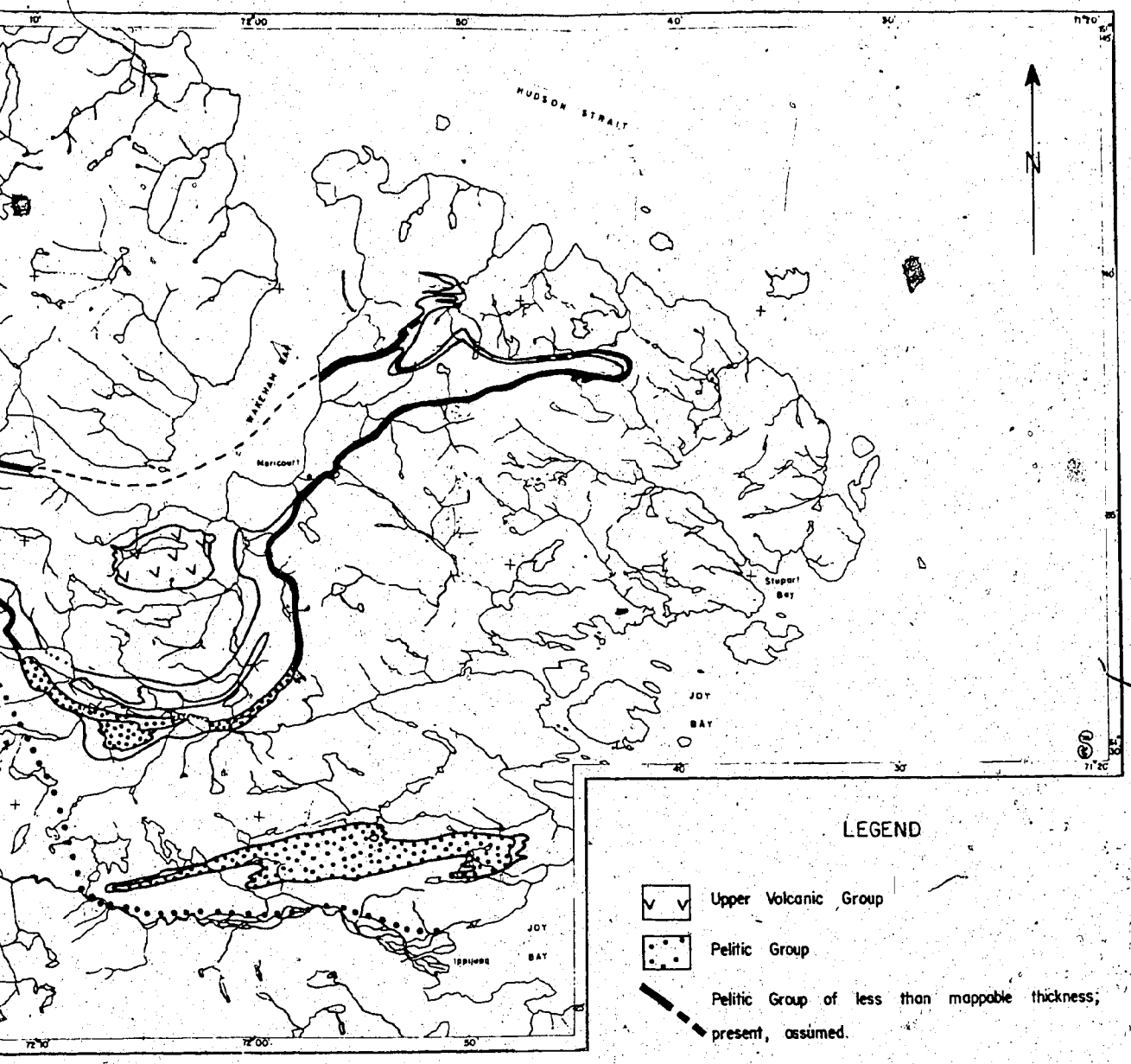

28. Distribution of the lithologic units of the Wakeham Bay , New Quebec.

Pelitic Group, Upper Volcanic Group.

The pelites are similar to those in the Pelitic Group, but graphitic, pyritic schists and garnet mica-schists are more common. The pelites grade on one hand into more quartzose compositions (psammoschists), on the other hand, with increasing admixion of volcanogenic material, into green, more chlorite-actinolite-carbonate-epidote-rich, schists; silvery green talc-schists are also present.

The sandstones are thin- to medium- to coarse-bedded, white to buff. They contain significant amounts of muscovite and feldspar, minor biotite, chlorite and carbonate are common. Medium- to thick-bedded arkosic grits are also present. At the western limit of the map area, the uppermost horizon of sandstone consists of a very thick-bedded breccia: angular fragments up to 1 m of orange brown dolomite in a matrix of light grey sandstone. This breccia grades into massive dolomite with a network of quartz veinlets.

The dolomite is generally massive, thick-bedded, fine-grained, buff to grey on fresh surface, buff to chocolate-brown on altered surface. Locally it is thin- to medium-bedded, schistose, siliceous or micaceous. It is 1 to 3 m thick, rarely more. A smaller, (0.5-1 m) massive, siliceous dolomite is locally present below the main horizon. Minor grey massive dolomite horizons are found, in beds of 0.5-1 m, associated with, and grading into carbonate nodule-rich basic volcanogenic tuffs. Contrary to the main dolomite horizon, which is a consistent marker, these are of small

lateral extent.

The volcanogenic tuffs consist of medium to thick-bedded, generally massive quartz-albite-chlorite greenschists containing varying amounts of tremolite-actinolite, carbonate, epidote. One occurrence of felsic tuff about 1 m thick was found; it consists of quartz, plagioclase, muscovite, minor biotite and zircon and 5% each of galena and sphalerite (454). Several occurrences of a dark olive-green to black, finely laminated silicate iron formation were observed, each about 0.5-1 m thick; They consist mainly of stilpnomelane, grunerite and minor sulphides (272, 452). Both are associated to volcanogenic tuff horizons and could be exhalites.

The ultramafic rocks occur as lenses, isolated or in groups, up to 50 m long; they are accompanied by minor horizons of basic and ultramafic tuffs (397). They are carbonatized to varying degrees and most are soapstones. Their brown alteration surface is very characteristic and they form little knolls in the landscape. In the less deformed ones the original (igneous) texture is still recognizable and it may be estimated that they contained about 70% olivine. These ultramafic lenses are always found stratigraphically just below the dolomite horizon, except at one locality near Rivière Lépine.

The basic volcanics occur as massive basaltic flows and gabbroic sills. The sills are generally a few tens of metres thick, rarely over 50 m. The flows are thinner and

less abundant. No pillow-basalt has been observed. Minor agglomerates, consisting of centimetric fragments of metabasalt in a chloritic groundmass, have been observed.

The base of this unit is defined as the first upward occurrence of a significant volcanogenic tuff or the dolomite horizon. In the type area, the dolomite occurs a few tens of metres above the first tuff. This limit is not very accurate and can be subjective, but was found to be the most practical; east of the type area the unit is thinner and mostly sedimentary and the dolomite horizon is the main marker. The top of the unit is the major (and last) sandstone horizon; it is thick bedded and gritty in part.

Within the Volcano-Sedimentary Group the sediments show the following succession, from base to top: pelites, dolomite, pelites, increasingly psammitic pelites, thin-bedded sandstones, thick-bedded sandstones; and the igneous rocks the following succession: basic to intermediate tuffs with minor gabbro sills, ultramafics, mostly gabbro sills with minor tuffs and basalt flows. In the type area, the sediments (excluding tuffs) form about 40% of this unit. The proportion of sills and basalt increases west of the type area, and decreases east of it. In the eastern map area volcanic material occurs only associated to the ultramafic lenses. The distribution of the Volcano-Sedimentary Group is shown on figure 29.

In the type area this unit is 1000-1500 m thick. It thickens westward and thins eastward. In the Wakeham

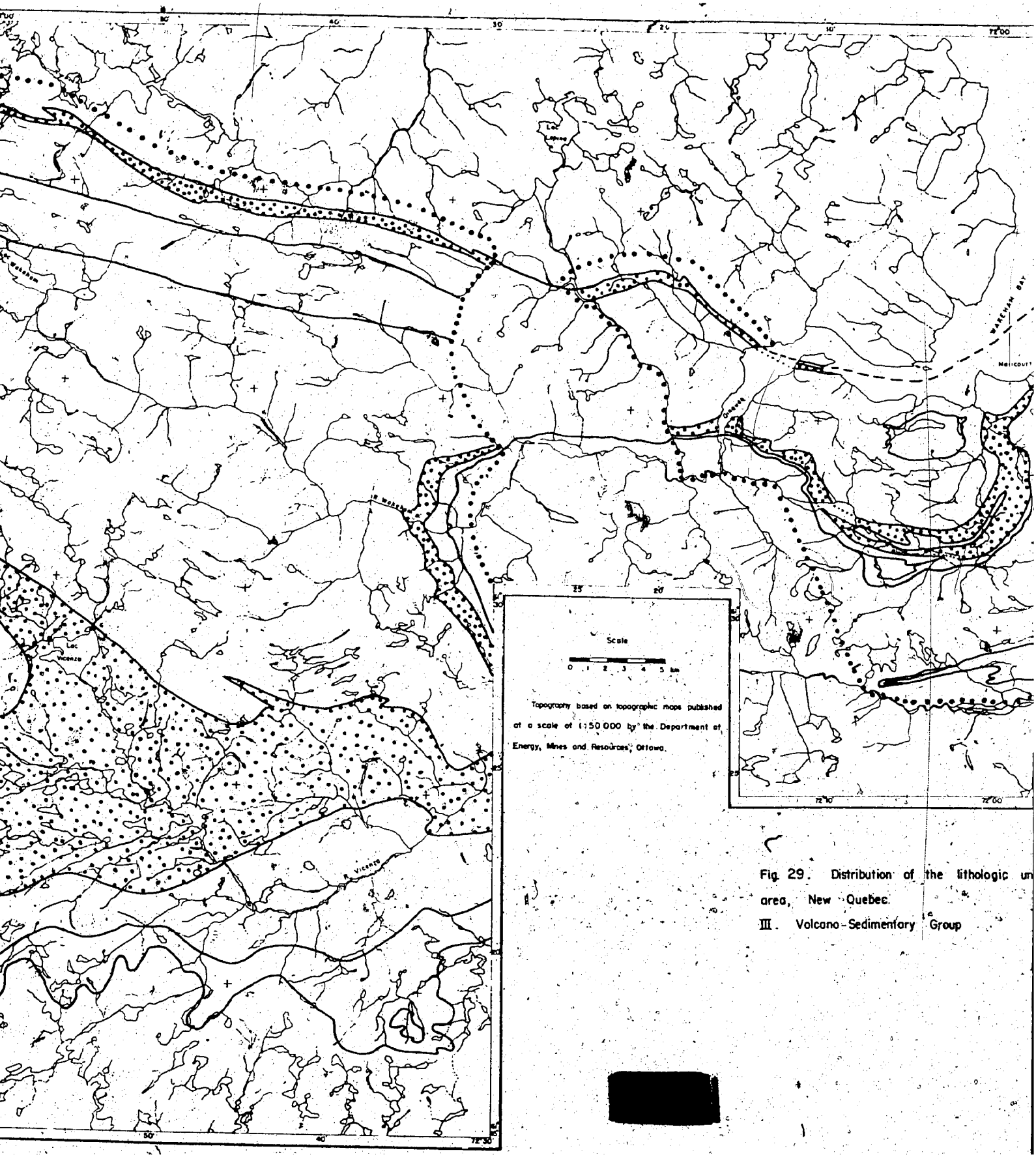

Fig. 29. Distribution of the lithologic un
area, New Quebec.
III. Volcano-Sedimentary Group

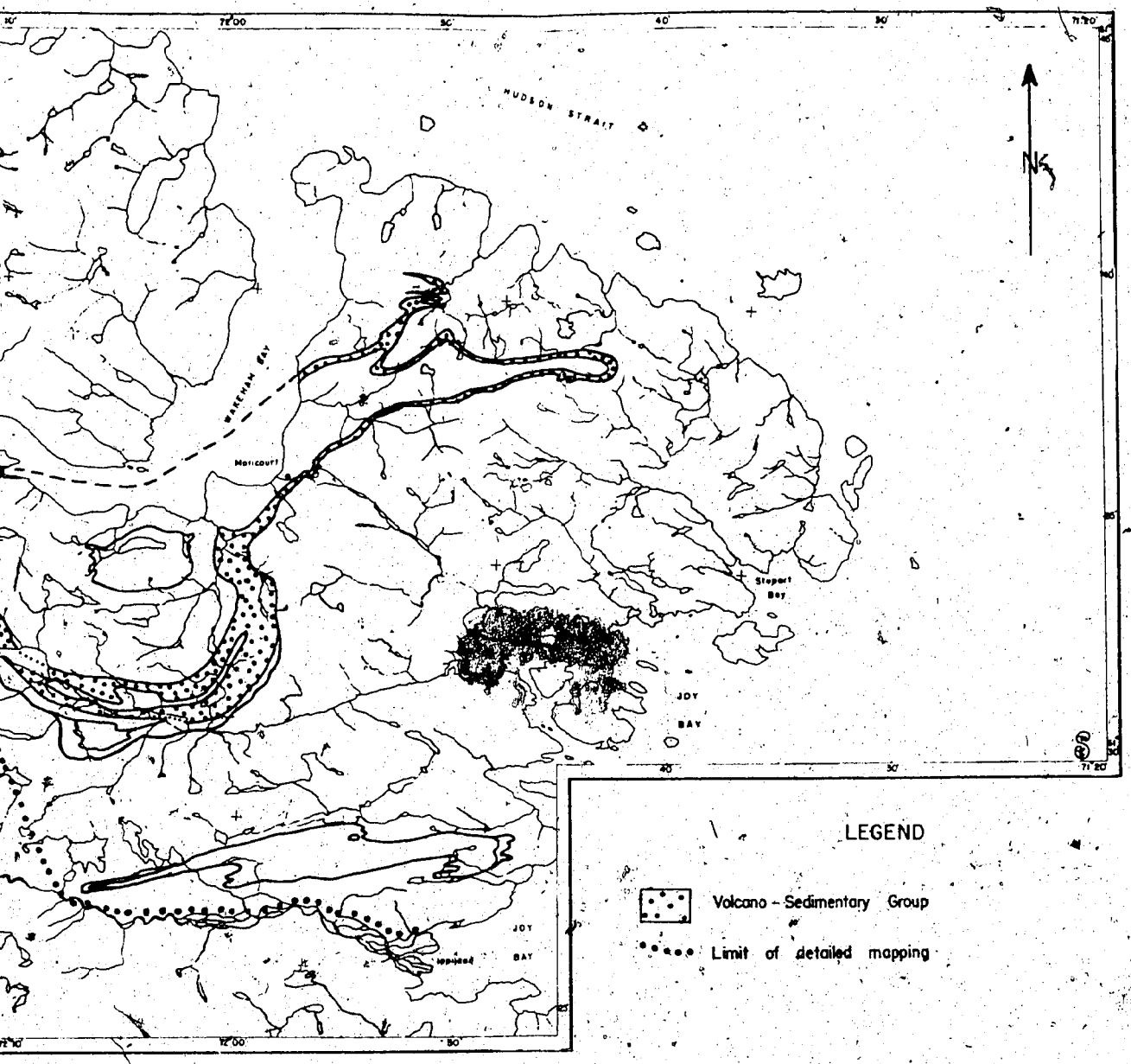

Distribution of the lithologic units of the Wakeham Bay
ew Quebec.
cano-Sedimentary Group

River Canyon, it is no more than 500 m thick, and probably less. It is very thin and may be absent along the southern contact near Maricourt. Where the Pelitic Group is absent it rests directly on the Archean gneisses. The dolomite horizon can be represented by no more than a few tens of centimetres of calcsilicate rock, for example at the northern contact, on the shore, north of Maricourt. Neither the Volcano-Sedimentary Group nor any of the units above it occur in the Ippijuaq basin.

D LOWER VOLCANIC GROUP

This very thick group consists of the following lithologies:

- pelites;
- sandstones;
- grauwackes;
- basic flows and pillow-lavas;
- basic to intermediate volcanoclastic rocks: tuffs, agglomerate;
- basic to locally ultramafic sills.

The sediments form no more than 10-20% of this group; they are merely intercalations between the volcanic rocks. These sediments are mostly pelites, argillites to siltstones grading into grauwackes. Unlike those of the

lower units they are often not mica-schists sensu stricto, but contain appreciable amounts of chlorite, epidote, actinolite. They are grey to black, finely laminated, often carbonaceous and sulphide-bearing, schists. Grauwackes and sandstones are found in the thicker occurrences. The grauwackes a[illegible]m to coarse-bedded, black to dark-green. The sandstones [illegible] thin- to medium-bedded, white to buff and often contain significant amounts of feldspar and mica (mostly muscovite). Small discontinuous horizons of grey weathering dolomite have been observed in [illegible] localities.

The volcanic rocks consist mostly of basaltic (massive, pillowed, and pahoehoe) flows and gabbro sills. The massive flows vary in thickness, but are rarely more than 10-20 m thick. The basic sills are a little thicker on average and some can be up to 100 m thick. The distinction between the thinner gabbro sills and the thicker massive basalt flows is difficult in the field. Criteria such as the presence of hornfels at the contact, of gravity differentiation within one layer, of a recognizable coarse ophitic or sub-ophitic texture, cross-cutting relationships, flow-surface structures etc.. are most often lacking and it was necessary to resort to more subjective criteria based on the author's experience in the Labrador Trough where similar rock types are thicker, less metamorphosed and better characterized; the criteria used were the colour of the alteration surface on the outcrop and the shape of the outcrops and blocks. The sills are darker, almost black, and form

more angular, less rounded outcrops and blocks; the result is a harder aspect. The basalts are more green than black. Although these criteria are subjective, they proved to be effective when compared with the results of the thin section study.

Pillows and pahoehoe flows constitute half to two-thirds of the basalts. Where it could be observed, the pahoehoe flows suggested a flow direction from north to south.

Volcanogenic tuffs (chlorite-actinolite schists) and agglomerates (centimetric basalt fragments in a chloritic matrix) are present in minor amounts, probaly no more than 10-20% of the basic rocks. Felsic to intermediate tuffs occur in the northwest corner of the map area.

The thicker gabbroic sills may have an ultramafic base and be dioritic near the top. Two thick (up to 300 m) sills of peridotite and pyroxenite occur at Lac Giraffe, associated with a gabbro sill.

The Lower Volcanic Group is the major lithologic unit in the Wakeham Bay area and constitutes more than 3/4 of the Aphebian stratigraphic sequence. Its thickness is estimated to be about 13 km, barring repetition and thickening due to faulting and/or folding. East of 72°30'W, it thins to less than 3 km. Its distribution is shown on figure 27.

E UPPER VOLCANIC GROUP

This group is composed of lithologies similar to those of the Lower Volcanic Group, i.e. volcanic rocks with minor intercalated sediments.

The base of the Upper Volcanic Group is constituted by a thicker than average horizon of sediments: pelitic schists, grauwacke, sandstone, tuffs. This is followed by thick (150-300 m), differentiated sills of pyroxenite to gabbro and peridotite to pyroxenite. These sills are separated by thin interlayers of sediments.

Above are found:

- pillow basalts and flows of picrite[1];
- agglomerates and tuffs of basic to acid composition;
- small sills or flows of essentially undifferentiated ultramafic rocks;
- thinner sills of gabbro;
- interlayers of grauwacke and pelitic schists.

The major sills of gabbro grade from a pyroxenitic base (lower quarter) to a dioritic top (upper quarter); near the upper contact they are again gabbroic. The large ultramafic sills (there is only one in the type area) are composed of pyroxenite with a peridotitic core that pinches out

---

[1] field term used for a rock more mafic than basalt, without being an ultramafic rock.

along strike.

The picrite flows appear to be related and to grade into the small ultramafic flows. There appears to be a complex transition from basaltic flows with a picritic base to picritic flows with an ultramafic base to ultramafic flows. The ultramafic flows are lenticular in shape; they are either massive or with columnar jointing (hexagonal). In one case, an ultramafic flow with columnar jointing was observed to grade laterally to a massive ultramafic rock which in turn graded upward into a picrite with a fractured upper-surface (cooling cracks of a flow surface). The thickness of the ultramafic plus picrite mass is 80-100 m, the columnar part not more than 20 m.

In the same area a cyclical succession was observed (from top to bottom):

- pillow-basalt and basaltic breccia;
- picrite, massive with fractured upper surface;
- massive to columnar ultramafic rock over a thin zone of volcanic breccia.

Three such cycles were observed in the Monts Lune; the thickness of each cycle is of the order of 20-40 m.

In the central part of the Monts Lune are one or more horizons of sulphide-bearing acid to intermediate tuffs that produce extensive gossans. A horizon of what appears to be a sulphide-rich exhalite occurs within sediments and tuffs between the major sills on the north flank of the

Monts Lune. Up to 1-2 m of massive to banded sulphides were observed. This horizon is fairly continuous and the gossan it produces can be observed for over 10 km along strike.

In the type area the Upper Volcanic Group reaches a thickness of 1.5-2 km in the south limb of the syncline. Its distribution is shown in figure 28. The Upper Volcanic Group extends from the western border of the map area (73°00'W) eastward to about 72°25'W. In addition, the thick differentiated sills of peridotite, pyroxenite, and gabbro that occur in the hills south of Wakeham Bay can be considered part of the Upper Volcanic Group. The base of this outlier shows little sediments but rather 10-20 m of basic to intermediate to acid tuffs. The acid tuff, composed of quartz, plagioclase, muscovite, biotite, is sulphide-bearing and weathers bright yellow to orange.

West of the Monts Lune, the Upper Volcanic Group is much sheared by vertical faults and only the south limb of the syncline appears to be present.

Within the Upper Volcanic Group, it is possible to recognize (at least in the type area) the following stratigraphic succession:

- sediments;
- major (thick) sills;
- pillow-basalt, picrite and ultramafic flows;
- pillow-basalts;
- pillow-basalts and thinner gabbro sills.

In this succession some of the pillow-basalts may be pahoehoe flows.

4. QUATERNARY: SURFICIAL GEOLOGY

A GLACIAL DEPOSITS and GLACIATION

The Wakeham Bay area was covered until about 8000 years ago by ice (Prest, 1970). The effects of glaciation are visible both in the physiography of the area and in the type and distribution of Quaternary deposits found therein. The glaciation is largely responsible for the present physiographic aspect of the region, and the presence of abundant and unweathered outcrops. Glacial erosion has enhanced certain lineaments and subdued others; and it is important to take this into account in the structural interpretation (see Chapter III).

The flow of ice, as shown by linear features (fluting, drumlinoids, crag-and-tail hills, striae), was towards the coast, i.e. to the northeast and north-northeast, locally to the east. No early east-southeast directions, as seen by Currie (1966) to the southwest of the map area, were observed, but ground observations of glacial features were cursary and such a direction may have been missed.

The whole area is covered more or less continuously by glacial till (ground moraine). The thickness of the till and the proportion of ground it covers decreases towards the coast. It covers about 50% of the (relatively flat) highlands and less than 10 to 20% of the first 15 to 20 km from the coast, where the relief is more pronounced and erosion more active; till remains there mostly on the valley floors and the flatter hilltops. Although it may have been thinner here than further inland, the former widespread presence of till is indicated by the numerous perched glacial boulders still remaining. Inland, the till has a thickness of 1-3 m, somewhat more in low-lying parts and valleys. It is composed of clay, sand, boulder etc... Even in areas underlain by Aphebian rocks, a significant proportion of the coarser fraction of the till is composed of Archean derived material (gneiss, granite, high-grade amphibolite); this is understandable if one considers the higher strength of these rocks, compared to many of the Aphebian rocks, and the proximity of the Archean basement to most of the Aphebian underlain area.

figure 30 shows the distribution of a certain number of glacial features and deposits in the map area.

Lateral moraines, probably associated with late stage glacial tongues, occur in the lower Wakeham River valley and in the lower Vicenza River valley. The major portion of these moraines has been washed away by the Vicenza and the Wakeham River or, rather, by their periglacial

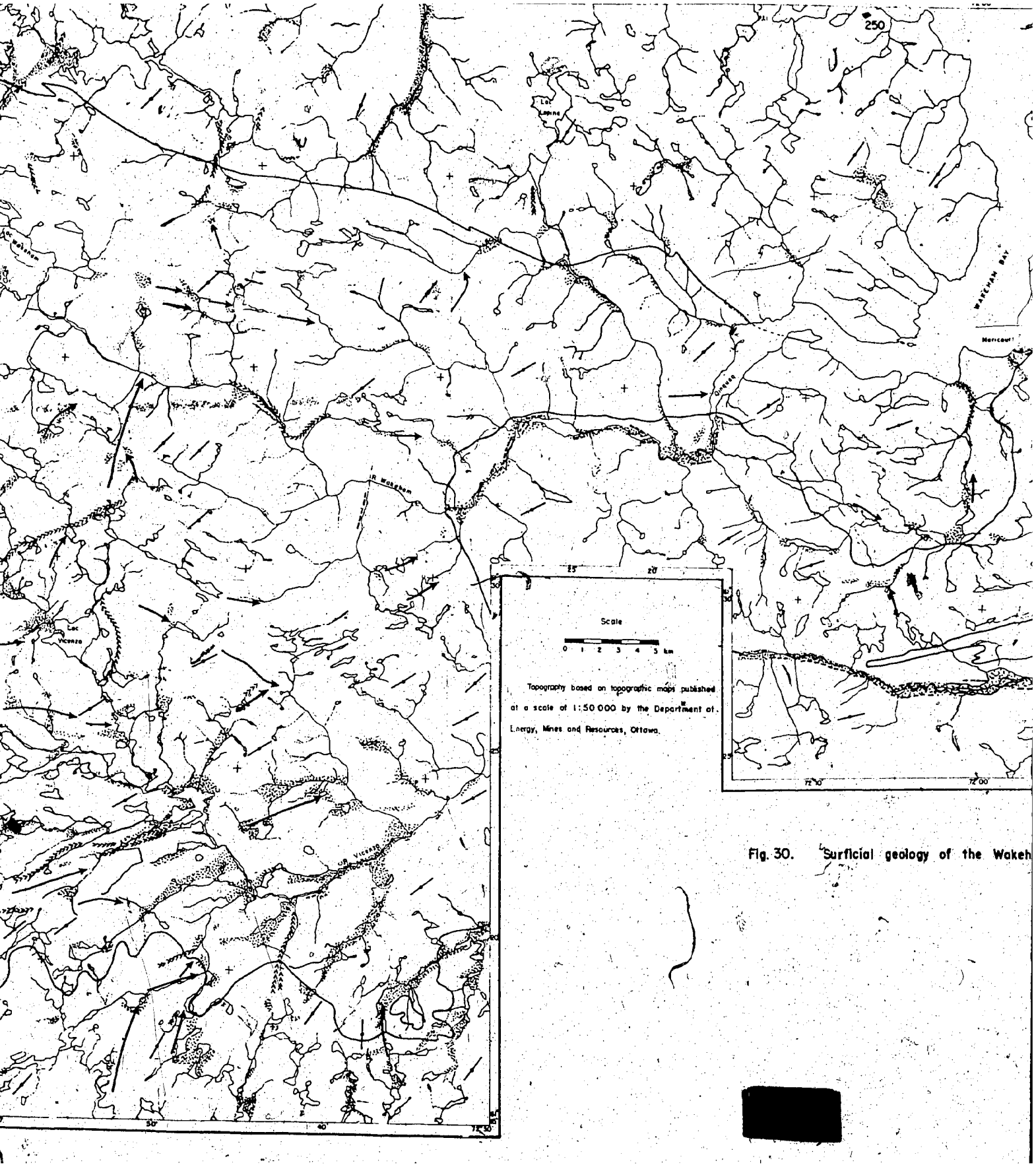

Fig. 30. Surficial geology of the Wakeh

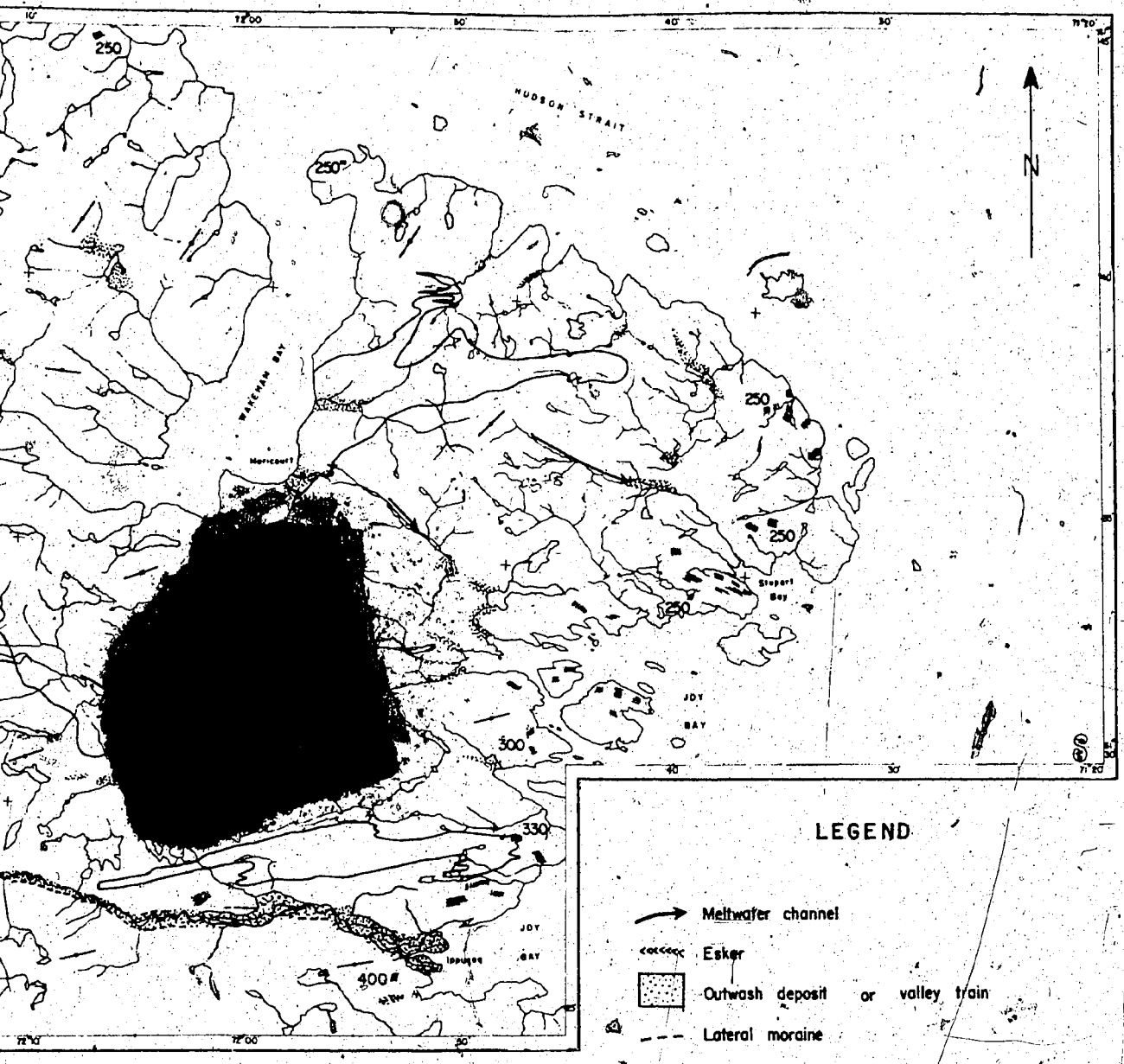

Surficial geology of the Wakeham Bay area, New Quebec

LEGEND

- Meltwater channel
- Esker
- Outwash deposit or valley train
- Lateral moraine
- Glacial lineation
- 250 Raised marine beaches; number indicates maximum altitude (obtained by comparing air photographs and 1:50,000 topographic maps).

Geology by K. Schimann, 1977, from air photograph interpretation and ground observations.

forerunners. In the southwest corner of the map area, some of what was indicated as outwash deposits in figure 30 could include some hummocky moraine.

B GLACIO-FLUVIAL DEPOSITS and FEATURES

In the western part of the map area, eskers, meltwater channels and outwash deposits are numerous; outwash deposits are particularly abundant in the South. The meltwater channels consist either of deep V-shaped gullies, some of which are dry now, or of strips of ground, a few tens to a few hundreds of metres wide, washed clean of till, except for the odd big boulder. Most of the outwash deposits can be correlated to a meltwater channel or to an esker. Many of the meltwater channels and eskers are oriented north to northeast, i.e. more or less parallel to the general trend of glacial flow, but at angle to the present trend of the drainage, which is structure-controlled.

The upper Vicenza River valley shows many east trending meltwater channels and trains of outwash deposits. Some of these are probably part of the outflow of the glacial lakes, that formed west of the map area in the headwaters of the Povungnituk River (Prest, 1970; Prest et al., 1967). Parallel to those meltwater channels and trains of outwash deposits, are a few eskers, suggesting that in the later stages of glaciation the ice was following the upper

Vicenza River valley.

Northeast of Lac Vicenza and in the Lac Felix area, a few deep gullies, located on, and parallel to the slopes, may be hillside channels, formed by glacial-margin streams, along the northern edge of the ice sheet or of an ice tongue following the upper Wakeham River valley or the upper Vicenza River valley.

In the eastern part of the map area, most of the fluvio-glacial deposits that may have existed have been eroded and features like meltwater channels are difficult to recognize. Only some valley train deposits are still visible.

No features related to glacial lakes have been observed within the map area, with the exception of a few terraces around Lac Wakeham, some 30-50 feet above the present level, that may reprsent the former level of this lake. Over most of the map area, the combination of topography and line of glacial retreat was not conducive to the formation of such lakes.

C LINEAR FEATURES

Drumlins, fluted surfaces, and crag-and-tail hills are uncommon in Aphebian underlain areas; they are somewhat more common in Archean underlain areas, or, maybe, only more conspicuous because of the less strongly oriented nature of

the rocks. In the eastern part of the map area they have, for the most part, been obliterated by the removal of the till.

D RAISED BEACHES

Remnants of raised marine beaches can be seen along the coast. They are rare on the steeper cliffs north-west of Wakeham Bay, but common around Joy Bay and Whitley Bay. The height above the present sea level of the highest beaches was estimated by comparing the air photographs and the 1:50,000 topographic maps. Their height above sea level increases from about 250 feet near the mouth of Wakeham Bay to about 400 feet near the outlet of the Vicenza River. Prest et al. (1967) show the "approximate elevation of the marine limit" to be 405 feet at Douglas Harbour and south-east of Whitley Bay.

E POST-GLACIAL FEATURES

The Wakeham Bay area is now at the limit of the continuous and discontinuous permafrost zones (Flint, 1971; p 270). The main effects of the permafrost are frost-wedging (and shattering) and solifluction.

A significant portion of the flat or gently slo-

ping ground not covered by glacial deposits is covered by felsenmeer. The size of the blocks is related to the fissility and spacing of joints, of the rocks. Except for massive gabbro sills, the Aphebian rocks produce small- to moderate-sized blocks; the Archean gneisses, however, often produce felsenmeer with blocks of 5 to 20 m^3, making not only the recording of structural data difficult, but also the walking. Ice-wedge polygons are often present on outwash sediment terraces. Patterned ground and frost-boils are generally present on flat-lying till. On gentle slopes, they grade into lobate forms.

Solifluction appears to be the main mass-wasting process in the area and its effectiveness in denudating hill-tops is quite visible. Frost-wedging combines with solifluction to mantle the lower half of the steeper slopes with a mixture of till and local material.

CHAPTER V

MINERALOGY

Several techniques were used to study the mineral composition of the various rock types of the area: macroscopic examination; microscopic examination, both in transmitted and reflected light; X-ray diffraction (powder patterns); electron microprobe analysis, both qualitative and quantitative. The mineral composition of thin sectioned samples and mineral analyses are listed in Appendix IV. The change in assemblages, as related to metamorphism will be discussed in the chapter on metamorphism.

1. TEKTOSILICATES

Quartz is present in most lithologies with the exception of some of the metabasites, ultramafic and calc-silicate-carbonate rocks, and iron formation. Quartz is mostly recrystallized metamorphic. In the more quartzose metasediments, some quartz may be primary (detrital). Occasionally quartz 'phenocrysts' may be recognized in metagabbro by the hexagonal shape of the grains and the presence in them of carbon dioxide-rich fluid inclusions.

K-feldspar is commonly present, as microline, in the Archean gneisses. In the Aphebian rocks it is much less common. It has been observed as detrital grains in conglomerates and sandstones of the Volcano-Sedimentary Group and in felsic tuffs, where it is also probably pre-metamorphic. In the eastern map area, microcline occurs in mica-schists, in a marble, and in an ultramafic rock as a metamorphic mineral. It occurs also in a pegmatitic phase in the upper part of a large gabbro sill.

Plagioclase is an almost ubiquitous mineral. The An content of the plagioclase has been determined in a number of thin sections by optical methods or with the electron microprobe (see Appendix IV). was done on part of these only.

In some conglomerates and sandstones the plagioclase is primary (detrital); elsewhere it is metamorphic. Its composition varies with grade from albite to andesine

and the potassium content is low. In Archean amphibolites that have been significantly affected by the Hudsonian metamorphism, zoning may be observed (calcic cores, sodic rims).

Potassium is present in equivalent to 0.5-1% Or molecule and shows no correlation with the An content. Fe is present in similar amounts; some of it may be due to the presence of impurities in the excited volume. The partition of Fe into Fe^{3+} and Fe^{2+} in the structural formulae is artificial and reflects probably more analytical error than actual oxidation state. Trace amount of Cr, Ni, Ti, and Co may be present; Ba is below the detection limit. Figure 31 shows the distribution of An content of the plagioclases. The gap between An_7 and An_{11} can be related to the peristerite solvus which will be discussed further in the chapter on metamorphism.

Scapolite occurs in the higher metamorphic grade part of the eastern map area. It has a composition of dipyre (optical determination). It was observed in calc-silicate rocks, both Archean and Aphebian, in Archean amphibolites and gneisses, and in a meta-diabase. All of these occurrences are in a restricted area (15 x 15 km) and near a sequence of Archean paragneisses. The formation of scapolite can be related to the Hudsonian event, by isochemical metamorphism in the calcareous schists, by metasomatism (introduction of Cl and CO_2 rich fluids) in the other rock types.

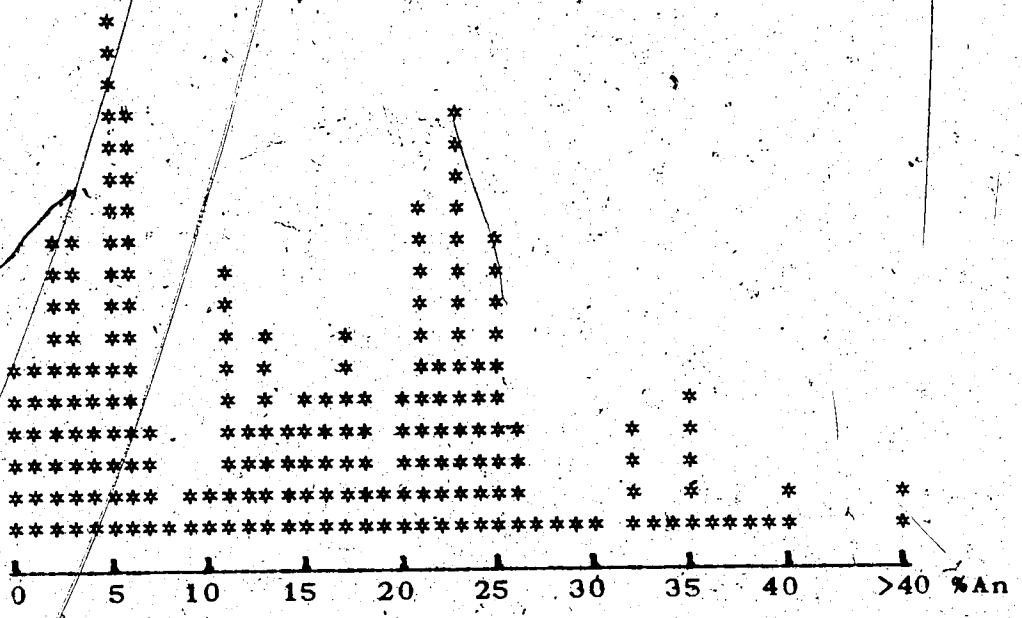

Figure 31. Histogram of An content of plagioclases.

2. PHYLLOSILICATES

Micas are common both in Archean gneisses and in Aphebian metasediments (which are mostly mica-schists). Biotite, phlogopite, muscovite, and paragonite were observed.

Biotites have been analysed, mostly in mica-schists where they coexist with garnet (see section on geothermometry). Biotite compositions can be represented in terms of the four end-members: annite, phlogopite, sidero-

phyllite, eastonite. Figure 32 shows that the $Al^{(4)}$ [1] is intermediate and nearly constant, the variance being expressed by the Fe/Mg ratio. The TiO_2 content is also variable, from 0.5-5.0%. Of the other minor elements, NiO, CoO, CaO, BaO, Na_2O, and CuO are occasionally present in the 0-0.5% range.

Phlogopite has been observed in a few samples of marble and calcareous rocks from the eastern map area.

Paragonite was observed in one sample of carbonate rich tuff, where it coexists with muscovite. They are intimately intergrown. Both were analysed; the paragonite contains about 9% muscovite molecule; the muscovite analysis shows a very low K content that could be attributed to replacement by hydronium. It is therefore not really possible to use this muscovite-paragonite pair as a thermometer.

Muscovite is present in Aphebian metasediments up to the highest grade. In the Archean gneisses it is commonly present but as a secondary mineral, apparently related to the Hudsonian metamorphism. The b_0 value was determined in a number of low-grade muscovites, the range is 8.991-9.040Å (the average, 9.020Å). The b_0 value is dependent in part on the Na/(Na + K) ratio but mainly on the content of Fe and Mg, i.e. a phengite will have a high b_0 (higher than about 9.025). The low-grade muscovites are thus close to phengites

---

[1] $Al^{(4)}$ and $Al^{(6)}$ are used respectively for tetracoordinated and hexacoordinated aluminium.

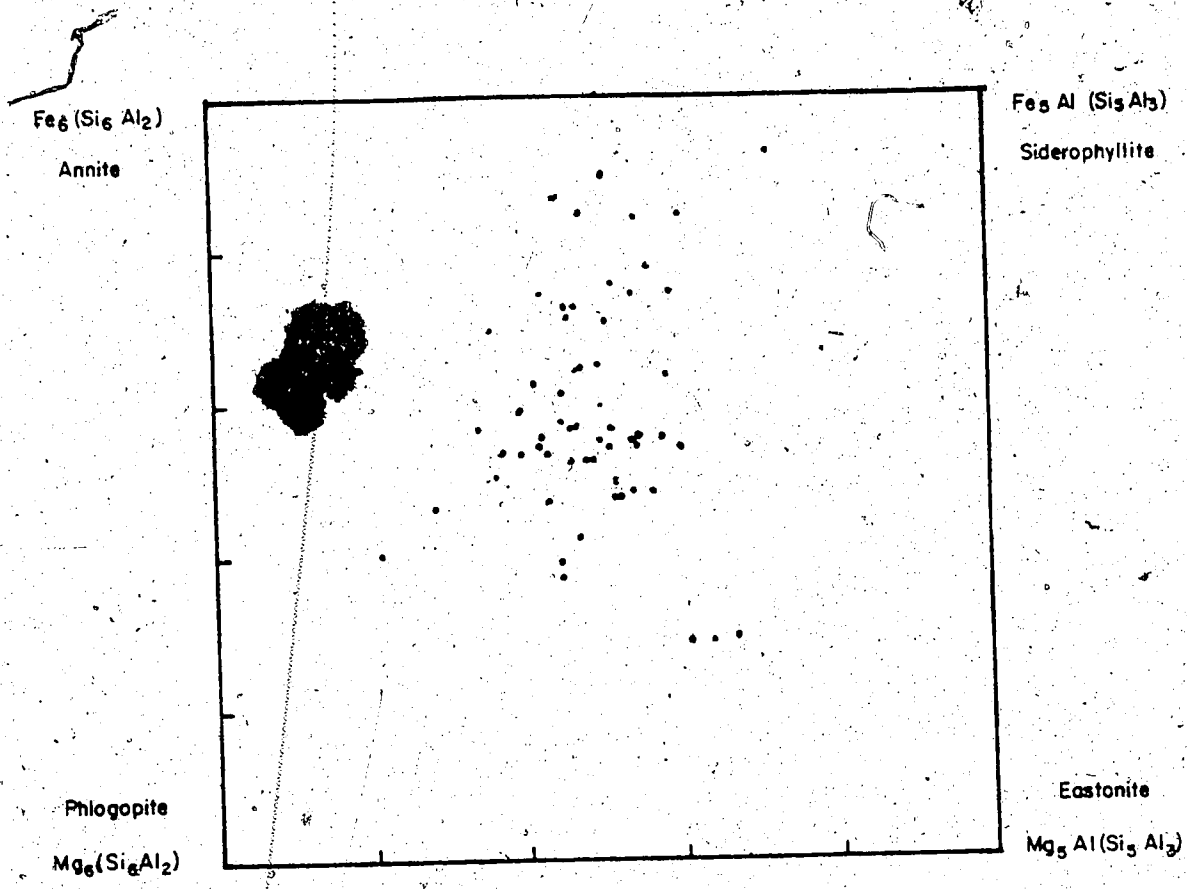

Figure 32. Composition of biotites.

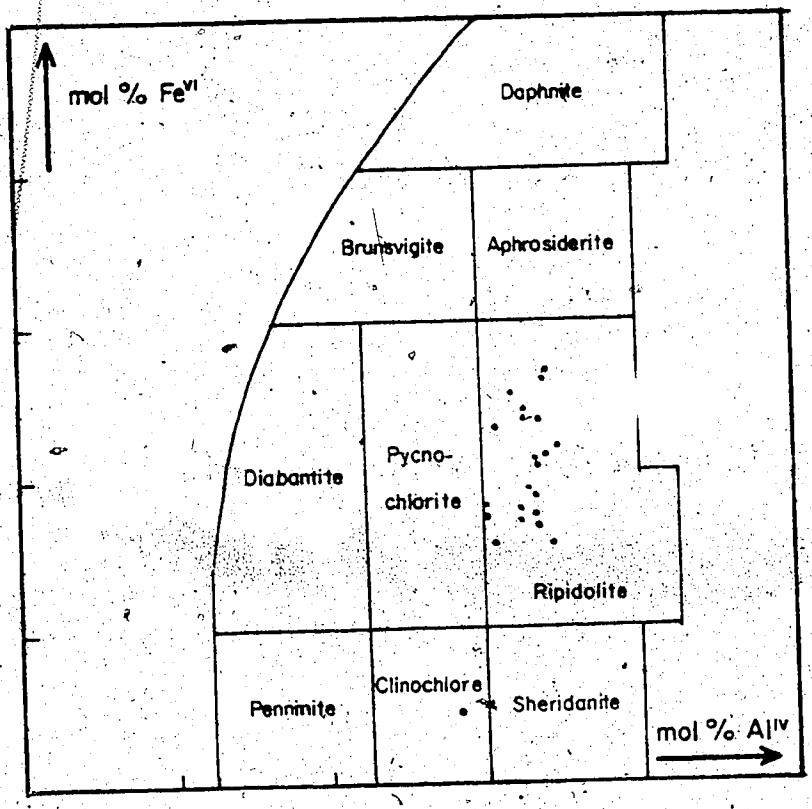

Figure 33. Composition of chlorites; classification after Tröger (1967).

on average.

Chlorites are a common and often abundant constituent of metabasites and ultramafic and pelitic rocks at low metamorphic grade. They persist into higher grade, although in lesser amounts.

Chlorites from metabasites and from one ultramafic rock were analysed (see Appendix IV). Their composition is plotted in Figure 33. Assuming they are all orthochlorites, they all fall in the ripidolite field, except the one from the ultramafic rock which is a clinochlore. Here again, as with biotite, the main variance is in the Fe/Mg ratio. Of the minor elements, Mn is the most common (0.2% MnO), Ca and Ni are present in most analyses, and Ti, Cr, and Co are occasionally present.

Serpentine is a common constituent of ultramafic rocks at low metamorphic grade. It occurs often as a pseudomorph of olivine, sometimes pyroxene; occasionally relics of these minerals are present. One analysis of serpentine has been made, which it is very low in silica; Mn, Co and Ni are the only minor elements detected.

Talc was observed in a few ultramafic rocks of low to medium metamorphic grade.

Stilpnomelane is a common and sometimes major, constituent of the iron formation. It is seen in thin section as yellowish brown to orange brown, sometimes greenish, biotite-like grains, with a distinct parting perpendicular to elongation. It also occurs in a few low-grade metabasites

that appear more iron-rich than average.

3. INOSILICATES

A PYROXENES

Orthopyroxene relics occur in a few ultramafic rocks, generally in the thicker sills, not only at low but also at high metamorphic grades.

Clinopyroxene is more widespread. It occurs together with orthopyroxene in ultramafic sills, where there appear to be both primary and metamorphic clinopyroxenes. It occurs also in marble, amphibolites, and gneisses as clearly metamorphic diopside, and its presence is in line with the parageneses in surrounding rocks. It is not very common, probably because metamorphic conditions were near the diopside-in isograd and its growth is restricted to the most favorable rock compositions. It occurs as a primary igneous mineral together with olivine in a diabase dyke of Hadrynian age which is probably the only unmetamorphosed rock in the area.

In some ultramafic sills, which also contain primary olivine and orthopyroxene, two clinopyroxenes occur, that can be distinguished by their habit: one is distinctly

metamorphic and consists of small rounded grains around the other, which appears as large poecilitic grains including partially to completely serpentinized olivine. An analysis of the second type (300) plots distinctly outside the field of metamorphic clinopyroxenes of Dobretsov (1968) (Fig. 34). In the Ca-Mg-Fe triangle, it plots near the magnesian end of the "normal magmatic trend" of Hess (1949) in accordance with the ultramafic composition of the host rock (Fig. 34). We have thus a magmatic clinopyroxene (endiopside) and a metamorphic clinopyroxene (probably a diopside) at low metamorphic grade. This occurrence can be compared with that in spilites where the commonly present clinopyroxenes have a composition intermediate between the "normal magmatic trend" and the diopside-hedenbergite join (see, for example Smith, 1970, or Lidiak, 1965).

B AMPHIBOLES

Orthoamphiboles have been observed in medium-grade ultramafic rocks and some metabasites and in high-grade gneisses. An orthoamphibole has also been observed in a low-grade metabasalt rich in iron sulphides. This is believed to be a sulphurized basalt (MacRae, 1974): sulphur metasomatism that may have been accompanied by locally higher temperature resulted in a silicate phase abnormally rich in magnesium. A gedrite was analysed in a medium-grade metabasite. It is Al-

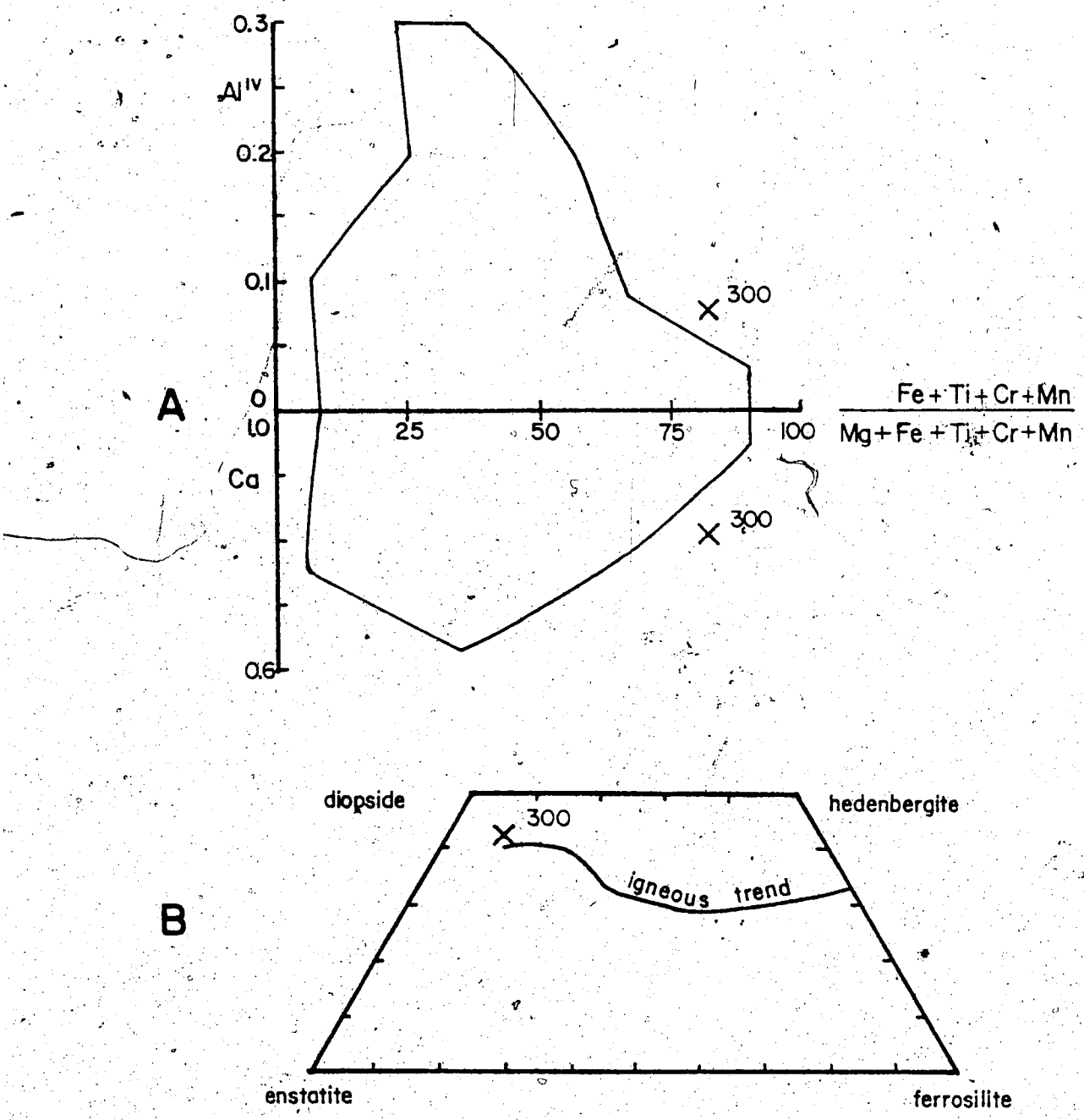

Figure 34. Clinopyroxene from sample 300 compared to:
A the field of metamorphic clinopyroxenes (after Dobretsov, 1967),
B the trend of igneous clinopyroxenes (after Hess, 1949).

rich with an intermediate Fe/Mg ratio, but is abnormally high in sodium; this cannot be accounted for by contamination with plagioclase (the Ca is very low). The sodium is higher than in the coexisting hornblende.

Grunerite is a major constituent of many iron formation samples and it may be concentrated as a fibrous shear-zone filling.

Cummingtonite occurs in high-grade (Archean) calc-silicate rich and magnesian gneisses, in a few medium-grade metabasites, and in a low-grade ultramafic sill base.

Calciferous amphiboles are major constituents of metabasites of all metamorphic grades. They are also present in metasediments, ultramafic rocks, and gneisses. Tremolite occurs in carbonate and/or calc-silicate-rich rocks at low to high metamorphic grade, in some low-grade ultramafic rocks, and in hornfels. Actinolite occurs in low-grade metabasites and metasediments. Hornblendes in low- to high-grade metabasites and in medium- to high-grade metasediments. A number of analyses of actinolites and hornblendes were made (Appendix IV).

Amphiboles, especially calciferous amphiboles, have a complex crystal-chemistry. Several cations can substitute in each of several sites:

Sites	Cations
A_{0-1}	K, Na
X_2	Ca, Na, Fe^{2+}, Mg, Mn, (K)
Y_5	Fe^{2+}, Mg, Mn, Al, Fe^{3+}, Ti

Z_8 Si, Al, (Ti)

Because of this complexity, calciferous amphibole analyses are difficult to represent in two-dimensional space and discussions of their crystal-chemistry are fraught with this problem. The best representation would be based on principal component analysis. A study was made by Saxena et al. (1970) using this method; however, their findings are of little use here because the work is based on analyses including Fe^{3+} as well as Fe^{2+}, and OH, and because the analyses are from diverse geological environments, both igneous and metamorphic.

A classical representation is that of Hallimond (1943) which is based on the four major end-members of metamorphic calciferous amphiboles; tremolite (Tr), tschermakite (Ts), edenite (Ed), and pargasite (Pa). In Figure 35, the amphiboles analysed form two distinct groups, with two distinct, but nearly parallel trends: the actinolite group on a line between Tr_{100} and Pa_{40}-Ts_{60}; the hornblende group on a less distinct alignment between Tr_{90}-Ed_{10} and Pa_{60}-Ts_{40}. This diagram represents the two major substitutions:

$$SiMg \leftrightarrow Al^{(4)}Al^{(6)} \quad \text{and} \quad Si \leftrightarrow NaAl^{(4)})\text{-M}$$

Another substitution, Fe <-> Mg is shown in Figure 36; here again two groups can be recognized.

In the low-grade metabasites actinolite and hornblende coexist. Hornblende occurs both as rims around the actinolite grains and as patchy intergrowths; the contact

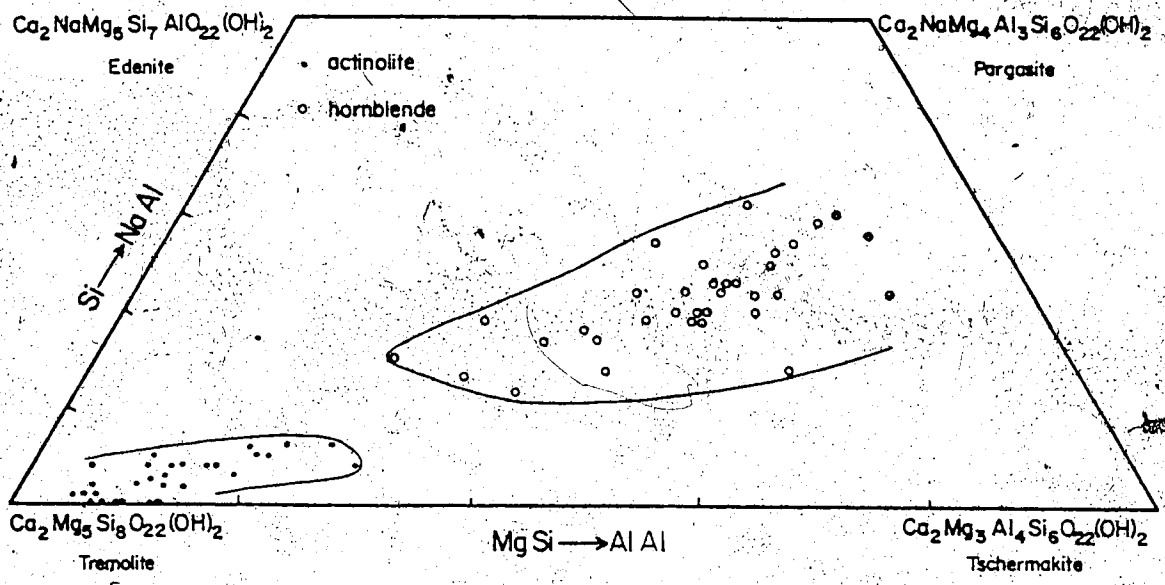

Figure 35. Calciferous amphiboles in the Hallimond triangle.
Note: compositional gap.

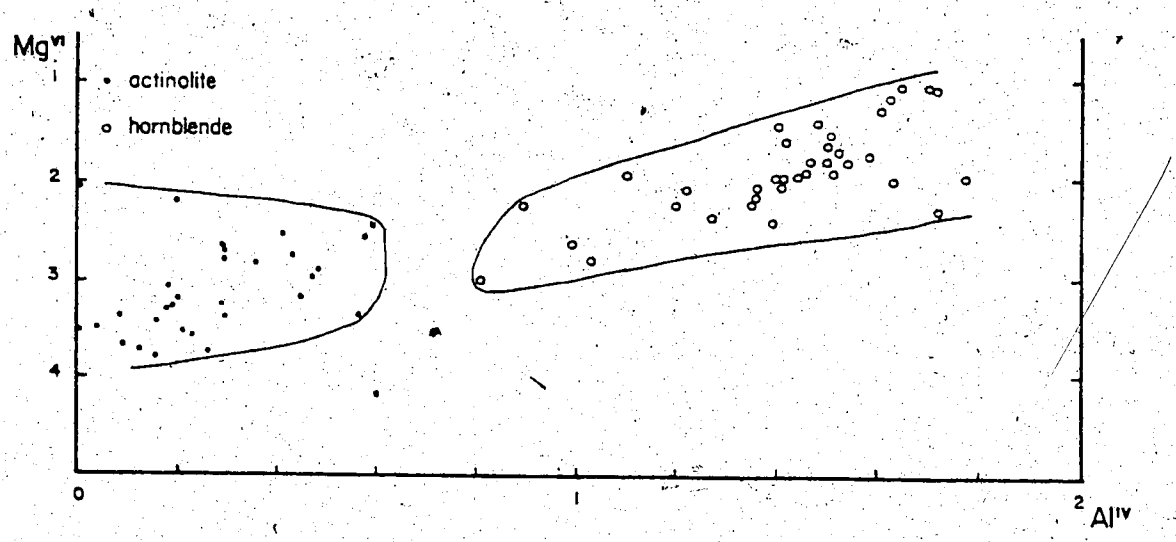

Figure 36. Calciferous amphiboles in a Mg-Al^{IV} diagram.
Note: compositional gap.

between the two phases is generally, although not always, sharp. No lamellar intergrowths, suggestive of exsolution, have been observed. The hornblende appears younger. Similar occurrences have been described by several authors (Lacroix, 1939; Miyashiro, 1958; Shido, 1958; Shido and Miyashiro, 1959; Klein, 1969; Cooper and Lovering, 1970; Graham, 1974), and ascribed to a miscibility gap or to non-attainment of equilibrium in a reaction involving a change in the composition of the calciferous amphibole phase.

Graham (1974) compiled amphibole analyses from various regions and discussed the miscibility gap problem, attributing the gap to incomplete chemical equilibration. His diagrams show that using certain representations a gap becomes apparent in amphibole composition from some regions (Haast, Shikoku, Dalradian) but not from others (Abukuma, Aracena). The absence of gap in some representation cannot be construed to mean that there is none, for it is sufficient to see a gap in one representation to prove the existence of a compositonal gap. In fact the existence of a miscibility gap should be studied not in a diagram of compositonal variable A versus compositional variable B, but rather in a diagram of a physical variable (T, P, etc...) versus a chemical variable (Fe, Al, Mg etc...). Indeed in Graham's diagrams the amphibole analyses showing no compositional gap come from regions with a low P/T metamorphic regime whereas those with a gap come from regions with a medium to high P/T metamorphic regime, like the Wakeham Bay area.

In actinolite, of the minor elements, MnO is always present in the 0.1-0.3% range; V, Cr, Ni are also commonly present (0-0.1, 0-0.3, and 0-0.1 wt% oxide range respectively); Ti, Co, and Ba are occasionally present.

In hornblende, Mn is slightly higher; TiO_2 is almost always present in the 0.1-0.6% range; there is no significant change in V, Cr, Co, Ni, Ba.

Kaersutite: a kaersutite-rich hornblende has been observed in several samples from ultramafic to gabbroic sills. It is distinctly pleochroic, orange brown to light brown, and occurs as poecilitic grains including the olivine relics and/or serpentine pseudomorphs. It is generally rimmed by pale green to colourless tremolite-actinolite with the same optical orientation. It is not as Ti- and K-rich as most kaersutites, and the Mg/(Mg+Fe) ratio is higher (0.8) suggesting that the grain analysed may already have retrogressed somewhat.

4. CYCLOSILICATES

Tourmaline is the only mineral of this group observed in the area. It is a common accessory ($\leq$ 1%) in pelitic to psammitic schists as well as in a few calcareous rocks; one occurrence in a biotite-rich amphibolite indicates a possible sedimentary source for this rock.

5. SOROSILICATES

Epidote group minerals are an abundant constituent of most low-grade metabasites and some of the impure pelitic schists. Their abundance in metabasites decreases with increasing metamorphic grade; but some persist at high-grade. The most common is a clinozoisite-epidote solid solution; but zoisite occurs also, generally together with epidote, in low-grade metabasites. Both the α and the β optical orientations were observed.

Analyses of epidotes give a range in composition from 12 to 72 mol.% $Ca_2Al_2FeSi_3O_{12}(OH)$. In the thin sections studied epidotes are most often unzoned, or only zoned over a small range, judging from the birefringence; both normal (Fe-rich core) and inverse zoning were observed, the former being more common. The miscibility gap proposed by Strens (1965) and described recently (Raith, 1976) in a high P/T metamorphic domain, is not a prominent feature of the epidotes of the area. It seems that their position in a temperature-composition field is in most cases outside of the domain of immiscibility (Fig. 37). In three samples twin analyses were carried out; only one shows two distinct compositions agreeing with the miscibility gap of Raith; the other two pairs have similar compositions. Of the minor elements, V and Cr are almost always present (respectively, 0.23 and 0.15 wt%. oxide on average). Ti and Mn are generally present, but in smaller amounts.

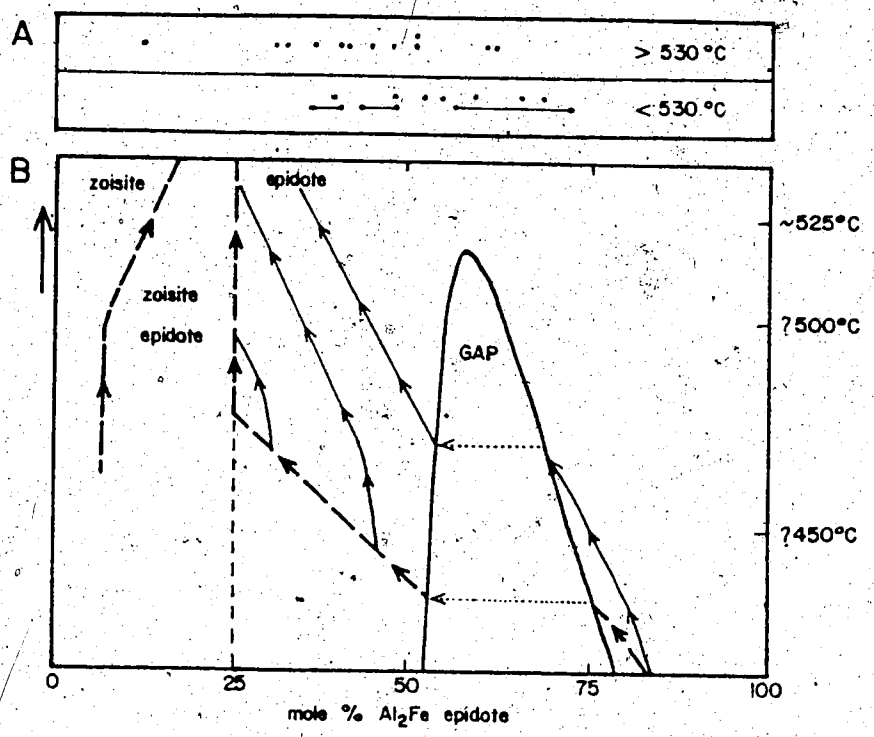

Figure 37. A histograms of epidote compositions,
B T-X diagram of epidotes in reduced sulphide-bearing metabasite assemblages, after Raith (1976) and Abraham et al. (1974). Bold arrows indicate the change in composition during prograde crystallization, light arrows the changes due to diffusional homogenization.

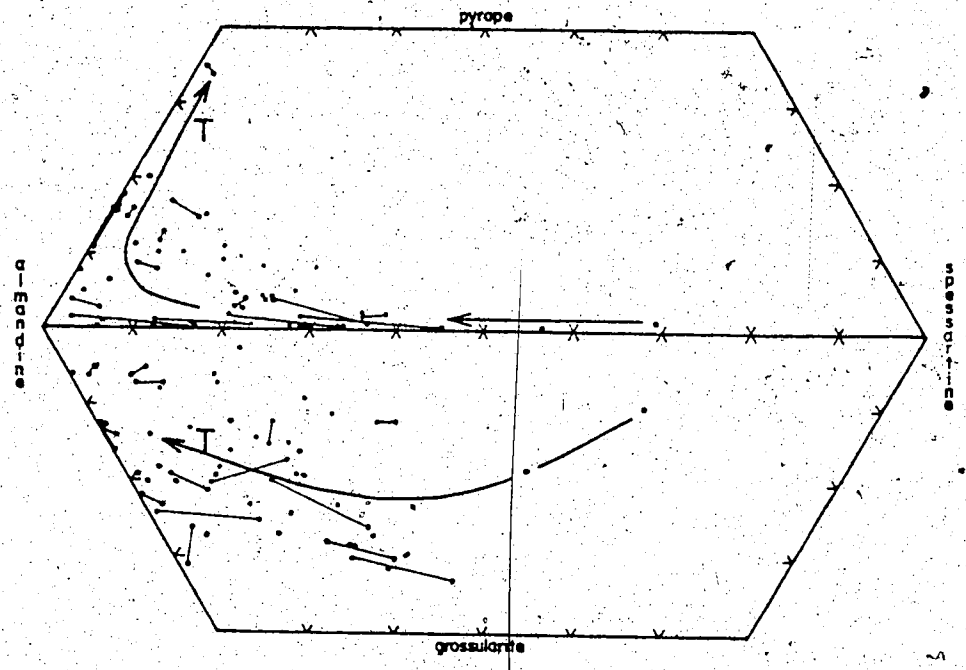

Figure 38. Composition of garnets in term of end-members. Arrows indicate prograde change in composition.

Allanite, a rare-earth enriched epidote, is a common accessory in higher grade metabasites; it becomes conspicuous at about the grade where epidote becomes less abundant. It occurs also in pelitic schists and some gneisses, in one of which it reaches 4%. Part of what is classified as MRAD (a radioactive accessory mineral) in the sample description of Appendix IV is probably allanite.

6. NESOSILICATES

Olivine occurs as partially serpentinized relics in some of the thicker sills and in one unmetamorphosed (Hadrynian) dyke. In the sills, it forms small (0.3-1 mm) euhedral grains, floating in large poecilitic amphibolitised pyroxenes. One analysis gives a composition of Fo_{84} with minor amounts of Ca, Ni, Mn.

Kyanite is the only aluminosilicate observed in the area. It occurs in three outcrops of reactivated basement gneisses NE of Maricourt. In two cases it is dispersed throughout the rock in centimetric grains, with an alignment approximately parallel to the local axial direction of the Hudsonian folding. In the third case it occurs as a 'vein-filling' with muscovite, some 10 cm wide and 1-2 m long.

Staurolite occurs in two localities, in pelitic schists with muscovite, biotite, and garnet, at medium meta-

morphic grade. Analyses made show that both have an almost identical composition with Mg/(Mg+Fe) = 0.16; they contain about 0.5% TiO_2 and 1-1.5% ZnO.

Zircon is a common accessory of metapelites and metapsammites, where it is easily recognized by its pleochroic halo in chlorites and biotites; it is also found in gneisses, iron formation, and some amphibolites. It was observed in a sample from the base of an ultramafic sill, but is generally absent from ultramafic rocks and metabasites.

Sphene is found as an accessory in almost all metabasites and most metapelites. It is less abundant at medium to high than at low metamorphic grade, due to the presence of an other Ti-mineral, ilmenite, at the higher grade.

Garnet is found in pelitic rocks and some iron formations, metabasites, and gneisses. It is not very abundant, either because of a lack of rocks of adequate composition or because of the P/T regime of metamorphism. Numerous analyses were made and the changes in composition with increase in temperature are discussed in the section on geothermometry.

The garnets are all pyralspites and almandine-rich (Fig. 38). Some of the low-grade garnets have from 10 to 27% MnO. Ni is the only minor element frequently present.

7. CARBONATES

Calcite is the most common carbonate. It occurs in metabasites, ultramafic rocks, pelitic and psammitic schists, iron formation, marble and calc-schists. In iron formation ankerite and/or dolomite have also been observed with calcite. Calcite may show exsolution phases.

Analyses have been made of some of the calcites and their exsolved phase. Figure 39 shows these analyses in a Ca-Mg-Fe(Fe+Mn) triangle. One of the two phases is always a Ca-rich carbonate or pure calcite, whereas the other (less abundant) contains from 5 to 30-40 at% of Fe and/or Mg. Coexisting carbonates can be used as thermometers, here, to measure the temperature of exsolution.

A diagram presented by Barron (1974) combines data from Harker et al. (1955) and Rosenberg (1967), and can be used to estimate temperature of formation of calcite coexisting with ankerite or dolomite. The composition of calcites coexisting with dolomite-ankerite should be on or near the lines joining equivalent temperatures in the two sets of data. We can see that exsolution took place at about 500°C for samples 514 and 448 and about 450°C for 479. These temperatures can be used as a minimum for the crystallization of the initial phase.

A small amount of Ni is also present in most carbonate analyses.

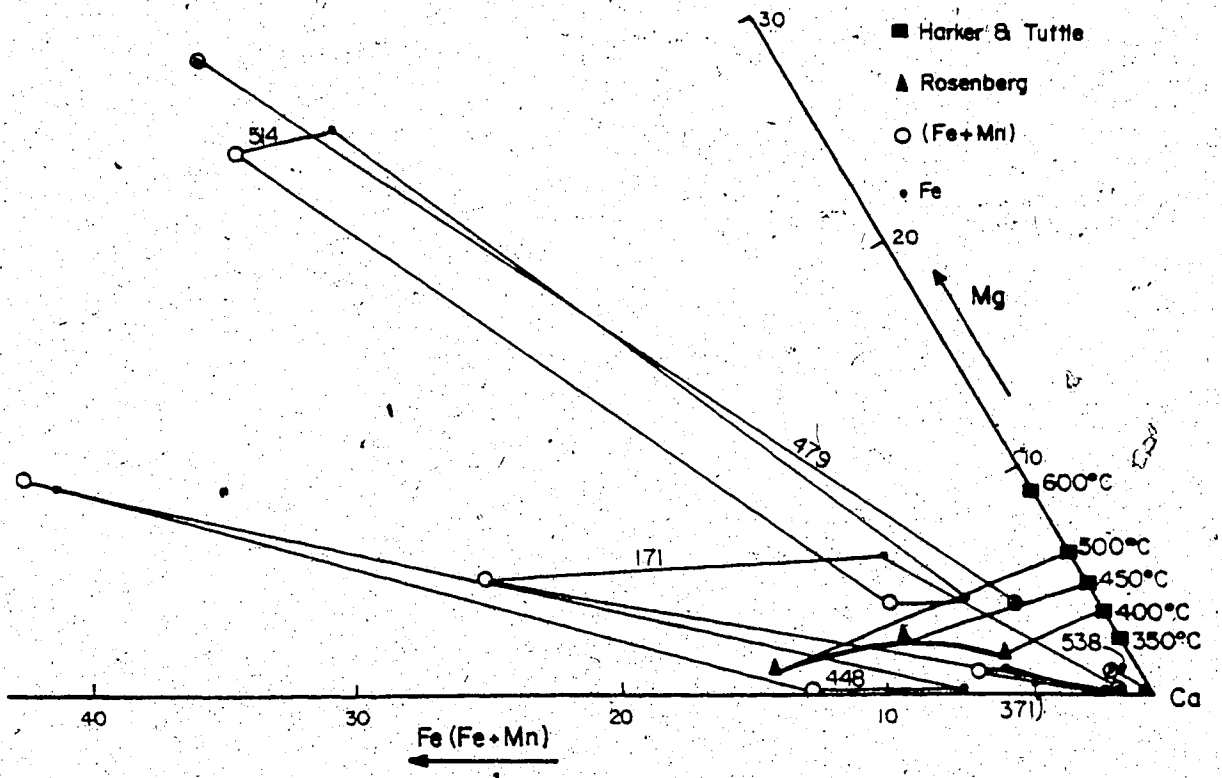

Figure 39. Carbonate host-exolution pairs in relation to experimental data on coexisting carbonates.

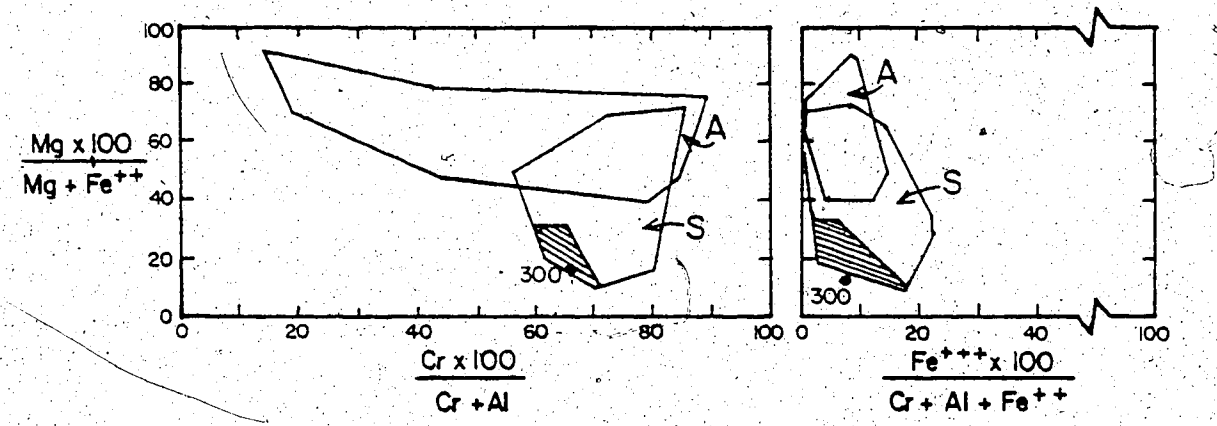

Figure 40. Chromite from sample 300 compared to the fields of chromites from alpine-type peridotite bodies (A) and stratiform complexes (S). The hatched area corresponds to disseminated chromites from the Bushveld complex (after Irvine, 1967).

8. OXIDES

Opaque minerals are present in most thin sections. They could be identified in the polished sections.

Ilmenite, because of its characteristic habit, could be extrapolated from the polished sections to the thin sections and recognized in some pelitic schists and in most higher grade metabasites. A series of ilmenites from metabasites and ultramafic rocks were analysed. They contain no hematite in solid solution (Ti=2.00), but are relatively rich in MnO (0.5-3%). Up to 0.5% MgO may be present, as well as some NiO. Some Si and Ca is present in most analyses; they may be part of the ilmenite lattice.

Rutile is present in only 3% of the thin sections studied but in a variety of rock types: low- to high-grade metabasite, pelitic schists, calc-schists, hornfels, ultramafic rocks.

Magnetite is present in most serpentinized ultramafic rocks as small cubes disseminated throughout the serpentine phase; it is the major oxide in iron formation and can be observed in some metabasites and pelitic schists, either alone or with ilmenite or with rutile (rutile + magnetite in place of ilmenite).

Hematite has been identified in only two samples of amphibolites (coexisting with ilmenite) and in a kyanite-bearing gneiss. It is also present in the more oxide-rich iron formation, together with magnetite.

Spinels have been identified in ultramafic rocks and in one high-grade iron-rich rock. In this case (573) it is an iron-rich hercynite-spinel solid solution with some Fe^{3+} and minor amounts of V, Co, Mn, Cr, Zn. A similar spinel was also observed in an ultramafic rock of the same metamorphic grade.

Primary igneous spinels are preserved in some of the ultramafic sills. In one sample (300) two spinels were observed and analysed; both appear primary. One is a chromite, the other a magnesium-rich hercynite-spinel solid solution. Comparison of the chromite composition with those compiled by Irvine (1967) shows that it is similar to disseminated chromite of the Bushveld complex, but different from other chromites, mainly in its very low Mg content (Fig. 40).

According to Irvine (1967, p.653) "natural spinels intermediate between chromite and spinel are especially common, thus this series would appear to be relatively stable". The coexistence here of two spinels suggests either that, under certain conditions, a miscibility gap exists between the $(Mg,Fe)Cr_2O_4$ and the $(Mg,Fe)Al_2O_4$ spinel series, or that the two spinels represent two stages in the differentiation of the sill.

Uraninite was observed in a high metamorphic grade rock rich in iron (573) that is probably an exhalite. A qualitative check on the electron microprobe show it to be composed of U and Pb with little or no Th, i.e. it is a low-

temperature uraninite.

9. SULPHIDES

Small amounts of sulphides are present in most rocks of the area. But they could only be identified in polished sections.

Pyrrhotite is the more common iron sulphide in metabasites, metasediments and ultramafic rocks. Pyrrhotite and pyrite may be major constituents (>10%) of some iron formation, both the sedimentary type (unit 3) and the exhalite type (units 5 and 7), and of some pelitic schists (metamorphosed black shale probably). The exhalite beds of unit 7 may contain more than 70% of pyrrhotite and minor pyrite.

Chalcopyrite accompanies pyrrhotite. The pyrrhotite/chalcopyrite ratio is 5-10 in most rocks; but in the major sills at the base of unit 7 the ratio decreases to 1-5.

Pentlandite, sometimes with chalcopyrite, has been observed as flamme-like exsolutions in pyrrhotites of about 10 polished sections of low-grade metabasalt, metagabbro, and ultramafic rocks. A qualitative microprobe check on specimen 300 yields Co:Fe:Ni = 10:40:50. These sulphide grains are believed to be of primary igneous origin.

Sphalerite and galena (about 5% each) occur in a

felsic tuff of unit 5 disseminated throughout the rock. A second occurrence of galena, in a quartz-calcite vein, was found in the vicinity.

10. MISCELLANEOUS MINERALS

Apatite was identified as an accessory in a variety of rock types. It is probably more common than shown in the sample description (Appendix IV), as it could have been missed in a number of sections amongst clusters of small grains of epidote.

Graphite was identified in a few sections of pelitic and carbonate-rich schists. The fine opaque dust commonly seen in low-grade pelitic schists may also be graphite in part.

Prehnite occurs in a few low-grade metabasites in vein-filling with calcite. It appears to be related to late stage shearing and retrogression. Three analyses show that, in addition to Si, Al, and Ca, it contains minor amounts of Fe, Cr, V, Ba, and Ti.

CHAPTER VI

METAMORPHIC PETROLOGY

1. INTRODUCTION

All Archean and Aphebian rocks in the Wakeham Bay area have been metamorphosed to some extent. The Archean rocks suffered metamorphism during the Kenoran Orogeny; the Hudsonian Orogeny metamorphosed the Aphebian rocks and the Archean rocks to the north and east of the Cape Smith Belt. The Archean rocks to the south suffered little more than heating sufficient to readjust mica K-Ar ages; some of the observed muscovitisation and chloritisation may also be related to the Hudsonian event, especially where it is related to schistosity developed along NE trending 'shear zones' that cut through Archean gneisses and early Aphebian diabase dykes.

The Archean rocks are mostly quartzo-feldspathic gneisses and amphibolites with minor paragneisses. Where it has not be destroyed by the Hudsonian metamorphism, the as-

semblage in the amphibolites is andesine-olive-green hornblende; the gneisses show signs of migmatisation, of incipient anatexis. One may therefore assume that the Kenoran metamorphism reached upper amphibolite facies, probably above the breakdown of muscovite (with quartz) as the muscovite that can be seen now appears secondary.

Only the Hudsonian metamorphism will be considered below.

The Aphebian rocks are divided into metapelites, mafic, ultramafic and calcareous rocks, and iron formation. Only the pelitic and mafic rocks are widely distributed. The ultramafic rocks can be observed at low-, medium-, and high-grade[1], but are less widely distributed. Iron formation occurs in abundance only at low-grade, in the southwestern part of the area. The opaque minerals will be discussed in a separate section.

The mineral assemblages are supplemented by geothermometry and geobarometry to describe the regional variations of metamorphic conditions during the Hudsonian event.

---

[1] low-, medium-, high-grade refer respectively to conditions equivalent to greenschist (biotite and garnet zones), low-amphibolite (staurolite zone), and mid-amphibolite facies (near aluminium-silicate triple point).

2. ASSEMBLAGES

A PELITIC ROCKS

The pelitic rocks are rarely very mature, aluminous rocks; often their composition is transitional to that of metabasites, i.e. equivalent to a grauwacke, rather than a shale; consequently, indicator minerals like aluminium-silicates and staurolite are rare, and garnet, although common, is not abundant.

On the basis of the observed assemblages, the pelites can be subdivided as follows:

biotite zone

- quartz + muscovite + biotite + chlorite ± albite ± opaque
- quartz + muscovite + chlorite ± albite ± opaque
- quartz + muscovite + biotite ± albite ± opaque ± epidote
- quartz + muscovite + biotite + chlorite + garnet (spessartite-rich pyralspite)

garnet zone

- quartz + muscovite + biotite + garnet (almandine-rich pyralspite) ± plagioclase ± opaque
- quartz + muscovite + chlorite + biotite ± plagioclase ± opaque
- quartz + muscovite + biotite ± plagioclase ± opaque

equivalent to staurolite zone

- quartz + muscovite + chlorite + biotite + garnet + staurolite ± plagioclase ± opaque
- quartz + muscovite + chlorite + biotite + staurolite ± plagioclase ± opaque
- quartz + muscovite + chlorite + biotite + garnet ± plagioclase ± opaque
- quartz + muscovite + biotite + garnet ± plagioclase ± opaque
- quartz + muscovite + chlorite + biotite ± plagioclase ± opaque
- quartz + muscovite + biotite ± plagioclase ± opaque

equivalent to kyanite zone

- quartz + muscovite + biotite + garnet + kyanite ± plagioclase ± opaque
- quartz + muscovite + biotite + garnet ± plagioclase ± opaque
- quartz + muscovite + biotite ± plagioclase ± opaque
- quartz + muscovite + biotite + chlorite ± plagioclase ± opaque.

The garnet zone is delimited by a garnet-in isograd based on the distribution of pyralspite garnet with less than 9%MnO. But the occurrences of staurolite and kyanite were not sufficiently numerous to define isograds.

The few occurrences of K-feldspar are considered

as non-metamorphic: relict sedimentary, in metasandstones and metaconglomerate, or igneous, in some metatuffs, or related to the Kenoran event in incompletely retrograded Archean gneisses. Stilpnomelane is absent. This absence of stilpnomelane and K-feldspar could be used to define minimum P-T conditions (Nitsch, 1970) for the biotite zone. The low-grade muscovites are significantly phengitic; they are discussed in the section on geobarometry.

B IRON FORMATION

Most iron formation assemblages are equivalent to the biotite zone of pelitic assemblages. The observed assemblages are:

<u>biotite zone</u>

- quartz + stilpnomelane + grunerite + carbonate ± magnetite ± biotite and/or chlorite
- quartz + stilpnomelane + carbonate ± magnetite ± biotite ± chlorite
- quartz + garnet + biotite + chlorite + magnetite ± carbonate
- quartz + grunerite + garnet + magnetite + carbonate ± biotite ± chlorite
- quartz + grunerite + magnetite + carbonate
- quartz + magnetite + hematite
- grunerite + stilpnomelane + chlorite + opaque + carbonate

Three samples came from higher grade; they have the assemblages:

garnet zone

- quartz + grunerite + garnet + biotite + magnetite + carbonate

equivalent to staurolite zone

- quartz + grunerite + magnetite + carbonate

equivalent to kyanite zone

- quartz + garnet + hercynite + biotite + hornblende + ilmenite

This last assemblage is in what appears to be an iron-rich exhalite. Magnetite is the common iron oxide; hematite is rare except in very oxide-rich rocks; the chlorite is of variable composition, but is often iron-rich; the carbonate is a manganese- and iron-bearing calcite, that often coexists with ankerite and possibly siderite. Garnet and stilpnomelane seem to be mutually exclusive, stilpnomelane being a lower grade mineral. At higher grade stilpnomelane disappears, replaced by grunerite + garnet (+ quartz).

Comparison with the zonation of James (1955) shows that the first group of assemblages does correspond to upper biotite zone. Some differences may be noted: the overlap of stilpnomelane and grunerite appears broader here; similarly chlorite extends higher, and garnet lower, to overlap.

C ULTRAMAFIC and CALCAREOUS ROCKS

Ultramafic rocks, because of their occurrence as thick sills (at least in part), are particularly prone to have metastable assemblages, including igneous minerals and some indicating conditions higher than those indicated by nearby assemblages in metapelites and metabasites.

Low-grade assemblages

- tremolite
- tremolite + talc
- tremolite + talc + carbonate
- tremolite + carbonate
- talc + calcite + dolomite or siderite
- diopside + serpentine + (olivine, enstatite)[1]
- diopside + serpentine + tremolite ± carbonate + (olivine, enstatite)
- tremolite + diopside + (olivine)
- tremolite + diopside ± carbonate
- tremolite + serpentine + talc + carbonate
- tremolite + serpentine ± carbonate

Medium-grade assemblages

- anthophyllite[2] + talc + calcite ± dolomite or siderite
- tremolite + carbonate

---

[1] in parenthesis: igneous relics
[2] an orthorhombic amphibole of the anthophyllite group.

- tremolite + talc
- tremolite + biotite

High-grade assemblages

+ tremolite + anthophyllite + enstatite + carbonate
- tremolite + anthophyllite + carbonate
- tremolite + carbonate
- anthophyllite + calcite + dolomite or siderite
- anthophyllite + carbonate + hercynite + epidote

Opaque minerals (iron oxides and/or sulphides) are additional phases in all assemblages. Chlorite is present in all low-grade assemblages and in some of the medium- and high-grade assemblages. The carbonate is calcite or ankeritic calcite unless otherwise indicated. The common but not ubiquitous presence of carbonates suggests that HCO_3^- was present in varying amounts in the fluid phase during the initial alteration (metamorphism) of the ultramafic rocks. The large number of assemblages observed, especially at low-grade, may thus be explained by the variability of the fluid phase as well as by the presence of significant amounts of Al and Fe in the rocks. Serpentine is present only at low-grade, as is diopside, in H_2O and CO_2 deficient assemblages. Tremolite is present from low- to high-grade, talc at low- and medium-grade.

The three groups of assemblages (low-, medium-, and high-grade) correspond fairly well to the sequence of

metamorphic reactions presented by Evans and Trommsdorff (1970). The major differences are the absence of forsterite and the presence of carbonates in the Wakeham Bay area. Indeed Winkler (1974) shows that in the system $CaO-MgO-SiO_2-H_2O-CO_2$ at 5 kb, forsterite is first formed at temperatures in excess of 640°C if the fluid phase contains more than 10% CO_2, i.e. in excess of the highest temperature estimated for the Hudsonian metamorphism in this area (see below). A high proportion of CO_2 in the fluid phase can also be invoked to explain the presence (apparently in equilibrium) of enstatite in the high-grade assemblages: low $P(H_2O)$ decreased the upper stability of a hydrous phase sufficiently to stabilize enstatite.

Calcareous rocks are not abundant and most samples collected are very impure: they contain significant though variable amounts of Fe, Al, and K.

Low-grade assemblages

- quartz + biotite + calcite + opaque
- quartz + plagioclase + chlorite + calcite ± dolomite ± biotite ± amphibole ± opaque

the amphibole is a very pale hornblende or actinolite.

Medium-grade assemblages

- quartz + microcline + phlogopite + chlorite + calcite + dolomite + actinolite + opaque
- quartz + plagioclase + biotite + calcite and/or dolomite

+ actinolite + rutile and/or sphene ± chlorite ± opaque

- quartz + plagioclase + biotite + chlorite + epidote + calcite and/or dolomite + rutile + opaque ± tremolite

- quartz + chlorite + tremolite + sulphide + rutile

This group is characterized by the presence of rutile (in 5 out of 8 samples), a relatively rare mineral in other rocks.

High-grade assemblages

- quartz (?) + scapolite + phlogopite + chlorite + dolomite + tremolite + talc + graphite

- quartz + cummingtonite + diopside + pale hornblende + opaque

- scapolite + plagioclase + phlogopite + calcite + diopside + opaque

- quartz + plagioclase + phlogopite + chlorite + tremolite + calcite + opaque

The last two are in Archean rocks and may be relict assemblages from the Kenoran event.

Comparison of these assemblages with those described by Thompson (1973) in impure calcareous rocks, shows some similarities; he recognized 4 zones:

1- biotite + calcite;

2- Ca-amphibole;

3- Ca-amphibole + microline;

4- diopside + microline.

Here microline is rare and chlorite is an additional phase

in most assemblages. The low-grade assemblages correspond approximately to zone 1, medium-grade to zone 3, and high-grade to zone 4.

D MAFIC ROCKS

Metabasites are the most abundant rocks in the area and occur in the whole range of metamorphic conditions; gradual changes in mineral compositions are best observed in metabasites.

Low-grade assemblage

- albite + actinclite + chlorite + epidote + sphene ± quartz ± biotite ± calcite ± sulphides

High-grade assemblage

- plagioclase + green hornblende + ilmenite ± quartz ± clinopyroxene ± garnet ± biotite ± sulphides

Between the two, various assemblages can be observed, resulting from the following reactions and gradual changes:

1- actinolite -> actinolite + blue-green hornblende -> green hornblende;

2- albite -> oligoclase -> andesine;

3- sphene -> ilmenite ± sphene;

4- chlorite becomes more magnesian then disappears;

5- epidote becomes less abundant, but persits sporadically

at high-grade; where it is absent it is replaced by a 'residual epidote' (allanite), containing the rare-earths, Th, and U that cannot be accomodated in the lattice of the remaining minerals.

6- calcite, the usual carbonate, tends to disappear at higher grade;

7- clinopyroxene appears at high grade.

The transition albite -> oligoclase is used to delineate the boundary between greenschist and amphibolite facies; it coincides approximately with the changes 'actinolite + hornblende -> hornblende' and 'sphene -> ilmenite ± sphene'. Chlorite, however, is common up to the transition 'oligoclase -> andesine'. Garnet occurs sporadically throughout the amphibolite facies, being more abundant at high grade, and one occurrence is observed in the greenschist facies. The presence of garnet seems to be strongly dependent on the Fe/Mg ratio of the rock. Stilpnomelane was observed in a few low-grade metabasites, cummingtonite in a few medium- to high-grade metabasites. The presence of neither could be correlated with a change in the other minerals.

E OPAQUE MINERALS

The opaque minerals were determined in a series of polished sections; ilmenite was recognized by its habit (large tabular poecilitic grains) in many medium- to high-grade metabasite thin sections. Rutile and sphene will also be considered here.),P In low-grade metabasites sulphides, pyrrhotite (sometimes pyrite) and chalcopyrite are the common opaque minerals and sphene is the titanium-bearing mineral. With increasing grade, sphene is replaced by ilmenite, but may persist in high-grade rocks, and the iron-sulphides decrease in abundance; chalcopyrite persists. Magnetite and hematite were rarely observed in metabasites.

In metapelites a fine opaque dust is often present at low-grade which is taken to be magnetite and/or graphite; distinct graphite was recognized in only a few rocks. Ilmenite was recognized in a few medium- to high-grade metapelites. The sulphides behave as in the metabasites.

Rutile has been observed in a variety of rocks. No clear relation appears between the presence of rutile and metamorphic grade, oxidation state, or the presence of other minerals.

The observed assemblages in a $FeO-TiO_2-Fe_2O_3$ system are:

- rutile + ilmenite (+ quartz ± sphene ± carbonate)
- rutile + magnetite (+ quartz ± sphene ± carbonate)
- rutile + ilmenite + magnetite (+ quartz ± sphene + car-

bonate)

- ilmenite + magnetite (+ quartz ± sphene ± carbonate)

In a TiO_2-CaO-CO_2 system they are:

- rutile + sphene + calcite (+ quartz ± magnetite)
- rutile + sphene (+ quartz ± magnetite ± ilmenite)
- rutile + calcite (+ quartz ± magnetite ± ilmenite)
- sphene + calcite (+ quartz ± magnetite ± ilmenite)

The following reactions have been considered:

rutile + calcite + quartz -> sphene + CO_2

rutile + magnetite + quartz -> rutile + ilmenite
or ilmenite,
or ilmenite + magnetite
(depending on the Ti/Fe ratio).

Both are prograde reactions; the equilibrium moves to the right with increasing temperature (Hunt and Kerrick, 1977; Mielke and Schreyer, 1972), or decrease in $P(CO_2)$ (first equation) or in $P(O_2)$ (second equation). The assemblages above are thus not diagnostic of temperature but of combinations of T, $P(CO_2)$, and $P(O_2)$ that can change rapidly over relatively short distances. Most rutile occurrences, however, are at medium- to high-grade.

The assemblages of oxides and sulphide minerals can be compared with those described by Banno and Kanehira

(1961). These assemblages correspond to higher $P(O_2)$ and $P(S)$: hematite and pyrite are common in all basic schists, and pyrrhotite and pyrite persist into the amphibolite facies; but as here, ilmenite and rutile appear above the oligoclase isograd.

3. METAMORPHIC CONDITIONS

A GEOTHERMOMETRY

1/ Introduction

The distribution of Fe and Mg between coexisting garnet and biotite may be used to estimate the temperature of crystallization, assuming equilibrium (Perchuk, 1967; Saxena, 1969; Thompson, 1976). The Fe-Mg exchange reaction for garnet-biotite pairs may be written:

(1) $Fe_3Al_2Si_3O_{12} + KMg_3AlSi_3O_{10}(OH)_2$

$\longleftrightarrow Mg_3Al_2Si_3O_{12} + KFe_3AlSi_3O_{12}(OH)_2$

and the distribution coefficient:

(2) $$KD = b(Fe/Mg)/g(Fe/Mg)$$ [1]

Assuming ideal solution and constant pressure, we may write:

(3) $$KD = \exp(-G/RT)$$

where T is temperature in degrees Kelvin, G the free energy, andR the gas constant.

Perchuk (1967) calibrated the garnet-biotite geothermometer, by comparison with previously defined geothermometers. Several authors (Kretz, 1959; Frost, 1962; Albee, 1965; Sen and Chakraborty, 1968) had observed that KD is influenced not only by temperature, but also by the substitution of other elements in both garnet and biotite.

Saxena (1969) attempted to define and quantify these relations using a multivariate regression method. He found that gFe, gMn, gCa, bFe, bTi, $bAl^{(4)}$, and $bAl^{(6)}$ ($Al^{(4)}$ and $Al^{(6)}$ denote respectively tetrahedrally and octahedrally coordinated Al) correlate significantly with KD, and defined equations, relating KD to these variables, one for low-grade metamorphism and one for high-grade metamorphism. He then used principal component analysis to define a function to replace KD, a function which into account the effect on KD of the cations mentionned above. This function,

---

[1] The prefixes b and g refer to biotite and garnet respectively and will be used as such out through this chapter.

the first transformed variable of the principal component analysis, is:

(4) $$\text{'Transformed KD'} = 0.5013KD - 0.4420gXFe - 0.3474gMn + 0.0865gCa + 0.1506bXFe - 0.0333bAl^{(4)} - 0.3165bAl^{(6)} + 0.5488bTi$$

The atomic proportions correspond to structural formulae based on 22 oxygens for biotite and 12 oxygens for garnet. XFe corresponds to (Fe/Fe+Mg). Saxena then proposed, as a possible geothermometer, a plot of transformed KD versus $1/T^{\circ}K$ of the averages of 3 groups of analyses of garnet-biotite pairs from different metamorphic grade (Fig. 41).

The following criticisms of his approach may be made:

1- intensive variables other than temperature have not been considered;

2- there is no direct evidence that the first transformed variable (transformed KD) should be a better measure of temperature than KD.

It may also be observed that the temperatures used in Figure 41 for the different groups of analyses could be modified in the light of more recent estimations of metamorphic temperature (see for example Winkler, 1974).

Thompson (1976) presented a plot of ln KD versus 1/T for a series of garnet-biotite pairs for which tempera-

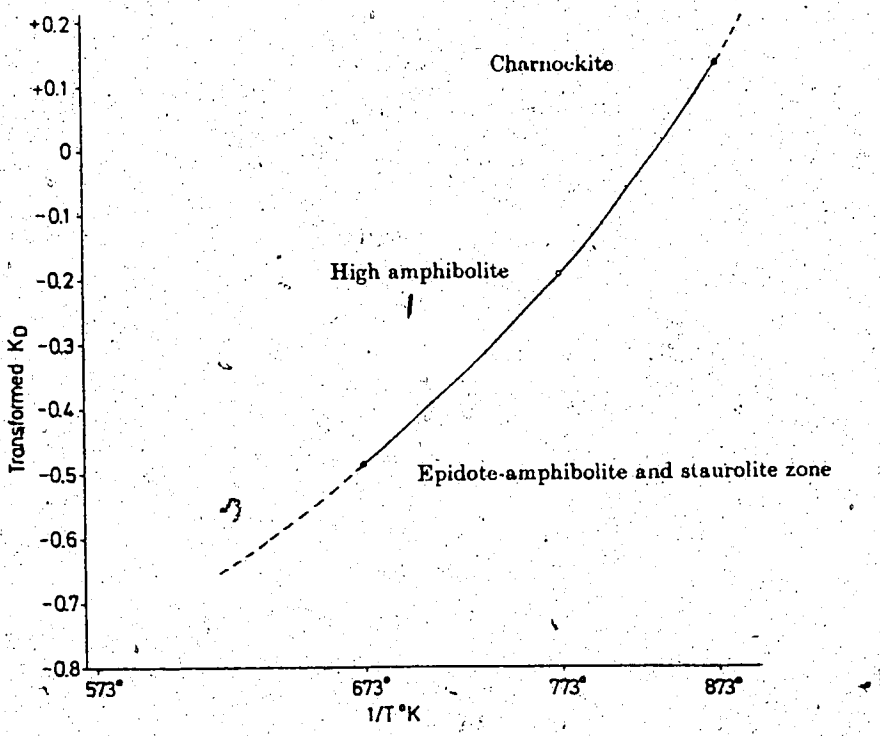

Fig. 41. Biotite-garnet geothermometer of Saxena(1969).

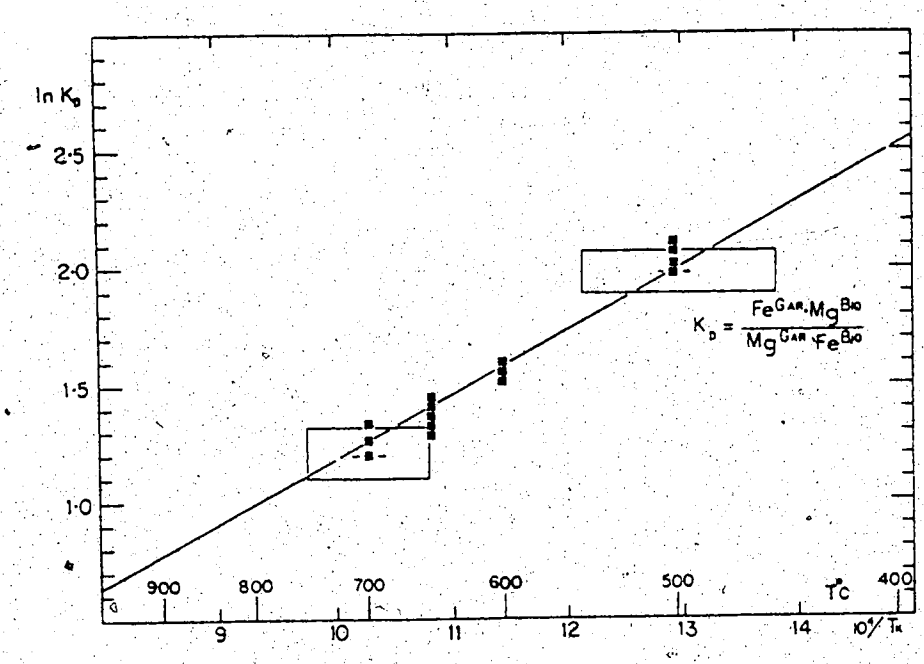

Fig. 42. Biotite-garnet geothermometer of Thompson(1976).

ture had been estimated independently from other mineral assemblages (Fig. 42). He remarks that KD "determined for garnet-biotite pairs from high-grade metamorphic rocks shows systematic displacements with increasing Ti in biotite".

2/ Statement of the problem

The problem is to find a relation between a physical parameter, temperature, and a series of chemical parameters, KD, bFe, bMg, gFe, bMg (and eventually other ions present in biotite and garnet). The chemical compositions of coexisting biotites and garnets are not, however, a function of T alone, but also of the chemical composition of the rock and of other physical parameters: P(s), $P(H_2O)$, $P(O_2)$, possibly also $P(CO_2)$.

$P(O_2)$ is known to affect the stability of biotite (Wones and Eugster, 1965) and that of garnet (Hsu, 1968). Atherton (1965) showed that $P(O_2)$, as expressed by the ratio $Fe^{3+}/Fe^{3+}+Fe^{2+}$ of the rock, strongly affects the amount of Mn in the garnet and the ratio Fe/Mg in both the garnet and the biotite.

$P(H_2O)$ affects the stability of biotite, as shown by Wones and Eugster (1965) and by the absence of biotite in the dryer parts of the granulite facies.

P(s) does have an effect on the stability of garnet (and biotite) as witnessed by the change in the relative order of appearance of garnet and biotite (and hornblende and plagioclase) in different metamorphic terrains

(Turner, 1968). Perchuk (1967) has calculated that for his geothermometer, based on KD alone, a pressure variation of +30 kb is equivalent to a temperature variation of -100°. The effect of pressure (favoring Mg in garnet over biotite) is small in the restricted system considered by Perchuk. But pressure may have a more pronounced effect on Ca or Mn in the garnet as the cell volume change is larger from almandine to spessartine and grossular, than between almandine and pyrope. A change in Ca and Mn of the garnet would indirectly have an additional effect on the change of KD with pressure. To conclude, it may be stated that for a garnet-biotite pair:

(5) $KD(Fe-Mg) = f[T, P(O_2), P(H_2O), P(s), C_1, C_2]$

Where C_1 and C_2 represent the chemical composition of the rock, and of the garnet and biotite, respectively.

3/ Proposed solution

In order to find a relation between the temperature of crystallization and the composition of garnet and biotite the number of parameters on the right-hand side of equation 5 must be reduced.

For regionally metamorphosed rocks of greenschist and amphibolite facies, one may assume that $P(H_2O) = P(s)$; although this assumption is invalid for the granulite facies, it is probable that $P(H_2O)$ is sufficiently close to

P(s) not to have too great an effect on the present problem for rocks from the hornblende-granulite sub-facies, as witnessed by the common occurrence of biotite in rocks from this sub-facies.

The effect of $P(O_2)$ can be neglected if one considers only rocks buffered by one system; for example by considering only graphite-bearing metapelites. In practice, one may include as well rocks free of graphite but with ilmenite and/or magnetite (free of hematite). In the case of coexisting ilmenite and magnetite, the ilmenite should have a low hematite-content.

The effect of P(s) may in first approximation be neglected because its effect on KD is small compared to those of temperature and because the effect of pressure and temperature are additive (Perchuk, 1967; Albee, 1965). Also, during regional metamorphism, pressure in general increases proportionally to temperature, albeit at a different rate in different areas.

In order to reduce variations due to the composition of the rocks, only pelitic or semi-pelitic compositions, with little or no carbonates, calcic amphiboles or epidotes should be considered, so that the garnet remains restricted to a pyralspite composition.

At this point equation (5) is reduced to:

(6) $$KD(Fe\text{-}Mg) = f(T,C)$$

where C represents the chemical composition of the coexisting biotite and garnet.

Equation 3 shows that in a simple chemical system, the relation between KD and T is of the type:

(7) $$KD = \exp(A/T)$$

In a more complex chemical system we have, by combining 7 and 6:

(8) $$KD = \exp(A/T) + C_1 + C_2 + \ldots$$

Where $C_1 + C_2 + \ldots$ represents the various chemical parameters of the coexisting garnet and biotite that bear a relation to KD and/or T. And we may write:

(9) $$\exp(A/T) = KD + C_1 + C_2 \ldots$$

To find a useful expression of equation 9, the following steps were taken:

1- gather from the geological literature as many analyses as possible of coexisting garnets and biotites.

2- estimate a temperature of crystallization on the basis of the description of the samples and of the geology of the area, using, whenever possible, already existing thermometers;

3- define the chemical parameters (of garnet and biotite)

that have an effect on KD or are influenced by temperature;

4- calculate a numeric expression of equation 9 using multivariate analysis.

4/ Data base

Table 3 lists the source of the analysed garnet-biotite pairs, as well as the temperature range estimated for each group of analyses.

Structural formulae were calculated where necessary, taking a base of 22 oxygens for biotite and 24 oxygens for garnets. A computer file was created containing for each analysed pair, the following variables: f(T), a function of temperature (see below); KD, $bAl^{(4)}$, $bAl^{(6)}$, bTi, bMn, bNa, bFe, bMg, bK, bFe^{3+}, b(K+Na), bXFe (XFe = Fe/Fe+Mg), gFe, gMg, gCa, gMn, gTi, gXFe, the ratio $Fe^{3+}/(Fe^{3+}+Fe^{2+})$ for the rock, $Va^{(6)}$[1], and "Transformed KD". Some of these variables (like the oxidation ratio of the rock or Fe^{3+} of biotite) were available for only part of the garnet-biotite pairs. The OH of biotites was not included because water analyses are often unreliable and because the proportion of electron microprobe analysed minerals is increasing, and will probably be even greater in the future. F(T) is a function of temperature, of the form $Aexp(-B/T^{\circ}K)$; the constants A and B

---

[1] octahedral vacancy in biotite

Table 3. Source of the garnet-biotite pairs

	Authors	Analyses	Estimated temperature (°C)
1	Hietanen (1969)	7	525-630
2	Atherton (1968)	12	510-575
3	Hounslow and Moore (1967)	7	550-590
4	Wynne-Edwards and Hay (1963)	5	675
5	Engel and Engel (1960)	9	600-675
6	Lambert (1959)	6	525-575
7	Chinner (1960)	2	600
8	Phinney (1963)	23	500-600
9	Dallmeyer (1974)	15	675-700
10	Sen and Chakraborty (1968)	18	550-620
11	Kretz (1959)	16	650-675
12	Fleming (1973)	7	600
13	Lyons and Morse (1970)	3	550
14	Albee (1965)	1	550
15	Green (1963)	3	575-600
16	Goulet (1971)	1	700
17	Reinhardt (1968)	12	675
18	Dahl (1969)	18	700

Metamorphic grade of the areas studied by the above authors.

1 zones: garnet, staurolite, staurolite-kyanite, kyanite, kyanite-sillimanite, sillimanite-muscovite.
2 garnet isograd to staurolite-kyanite zone
3 staurolite-almandine zone to near the sillimanite zone
4 limit between upper amphibolite and granulite facies
5 sillimanite-K-feldspar zone
6 garnet zone
7 near sillimanite isograd
8 zones: garnet, staurolite, staurolite-kyanite, kyanite.
9 hornblende-granulite facies (retrogressive effects in some samples)
10 zones: garnet(?), staurolite, sillimanite
11 sillimanite-K-feldspar zone
12 andalusite-staurolite zone
13 staurolite zone
14 kyanite zone
15 staurolite and sillimanite zone
16 hornblende-granulite facies
17 limit between upper-amphibolite and granulite facies
18 limit between upper-amphibolite and granulite facies.

were chosen to yield an f(T) in a convenient scale.

(10) $$f(T) = 1000\exp(-1000/T)$$

for example, 274 corresponds to 500°C and 358 to 700°C. The other variables were multiplied by 100, except XFe and KD, which were multiplied by 1000. The result was a matrix of 165 rows (garnet-biotite pairs) by 22 columns with all numbers between 0 and 999. This upscaling does not change the proportions of the chemical variables but provides for easier data handling. The temperature estimates were based on Winkler (1974). The following scale was used:

'isograd' garnet in	500°
'isograd' staurolite in	530°
'isograd' kyanite in	540-550°
'isograd' sillimanite in	600-625°
'isograd' muscovite out	650-675°
'isograd' hypersthene in	675-700°.

In addition, temperatures indicated by the authors were used when they were based on adequate experimental work. Where possible an attempt has been made to use other geothermometers, for example K-feldspar-plagioclase. Where maps of sample locations were available, temperatures were interpolated between 'isograds'.

5/ Multivariate analysis

The data were processed using a multiple linear regression programme made available to the Department of Geology of the University of Alberta by J.C. Davis. The result of multiple linear regression is an equation of the type:

$$Y = a_0 + a_1X_1 + a_2X_2 + \ldots \quad (11)$$

relating a dependent variable Y to several independent variables X. Listing of the programme (RMULT) and description of the method involved can be found in Davis (1973). The input was modified to adapt it to the data file and to be able to choose any combination of variables. The programme prints out a matrix of correlation coefficients and various regression statistics. These were used to examine the relations between the various parameters in order to keep only significant variables in the regression equation. The correlation coefficients in Table 4 express variations among the chemical variables induced by changes of physical parameters (T,P etc...) and chemical parameters, essentially the availability of the various chemical elements, i.e. the composition of the rock. Two elements may show correlation because there is:

1- substitution of one for the other:

- negative correlation if they are both major elements;

Table 4. Correlation coefficients of the various chemical parameters of biotite and garnet.

		f(T)	KD	B Al(4)	I Al(6)	O Ti	T Fe+3	I Mn	T Na	E K	K+Na	Fe	Mg	XFe	G XFe	A Fe	R Mg	N Ca	B Mn	T Ti	OX.R.	Va(6)
	TKD	+.844	+.701	-.027	-.678	+.921	-.446	-.210	-.178	+.444	+.019	+.152	+.122	+.016	-.696	+.008	+.729	-.160	-.556	-.090	-.287	+.068
	Va(6)	+.016	+.202	-.437	+.132	+.172	+.086	+.024	+.499	-.073	-.070	.286	-.403	+.120	-.082	-.012	+.071	-.194	+.024	+.402	-.151	
	OX.R.	-.207	-.164	-.072	+.278	-.322	+.180	-.077	-.039	-.203	+.035	-.365	+.250	-.358	-.015	-.310	-.071	+.302	+.103	-.024		
G	Ti	-.201	+.028	-.126	+.239	-.057	+.119	+.036	+.614	+.078	+.236	-.036	-.334	+.198	+.119	-.085	-.150	+.023	-.084			
A	Mn	-.372	-.436	+.030	+.113	-.340	+.029	+.343	+.076	-.261	-.126	-.066	+.065	-.092	+.368	-.420	-.451	+.211				
R	Ca	-.345	-.306	-.151	-.021	-.243	-.091	+.084	+.008	-.243	+.037	+.172	+.077	+.027	+.311	-.508	-.401					
N	Mg	+.807	+.754	-.065	-.285	+.666	-.248	-.193	-.198	+.430	-.044	-.040	+.352	-.402	-.982	-.097						
E	Fe	+.081	-.041	+.218	+.045	-.012	+.078	-.170	-.075	+.030	+.004	+.302	-.295	+.341	+.247							
T	XFe	-.776	-.744	+.089	+.266	-.636	+.252	+.157	+.152	-.410	+.028	+.454	-.388	+.454								
B	XFe	-.144	+.202	+.048	+.205	+.101	-.035	+.026	+.182	+.035	+.081	+.836	-.902									
I	Mg	+.238	-.260	+.097	-.465	-.001	-.210	-.032	-.348	+.032	-.057	-.529										
O	Fe	-.017	+.033	+.232	-.183	+.169	-.299	-.026	-.091	+.069	+.058											
T	K+Na	-.020	+.018	+.055	-.046	-.085	+.246	+.076	+.332	+.378												
I	X	+.553	+.420	+.247	-.242	+.392	-.107	-.016	-.163													
T	Na	-.233	-.018	-.170	+.292	-.092	+.097	+.059														
E	Mn	-.166	-.107	+.033	+.071	-.149	+.117															
	Fe+3	-.461	-.168	+.031	+.346	-.551																
	Ti	+.624	+.691	-.037	-.564																	
	Al(6)	-.538	-.052	-.139																		
	Al(4)	+.145	-.056																			
	KD	+.703																				

TKD= Transformed KD of Saxena(1969)

Va = octahedral vacancy of biotite

OX.R.= oxydation ratio of the rock: $Fe^{+3}/Fe^{+3}+Fe^{+2}$

- positive correlation if one is a major and the other a trace element accompanying the first one;

2- parallel increase or decrease if both react similarly to an external cause;

3- fortuitous parallel variations (may be due to an unrecognized external cause).

In the present case the two main factors are temperature and rock composition. However, because the population comes from a rather narrow range of rock compositions, temperature can be assumed to be the major cause of substitutions.

F(T) shows correlation with $+bTi$[1] , $+gMg$, $-gXFe$, $+KD$, $+bK$, $-bAl^{(6)}$, $-bFe^{3+}$, $-gMn$, $-gCa$, $-bMg$, $-bXFe$ (by order of decreasing R^2[2]). The main effects of an increase in temperature are thus an increase in Ti of biotite and Mg of garnet (resulting in a lower gXFe). Fe, Mg, and XFe of biotite show poor correlation with f(T), Mg in garnet does not replace Fe (R(gFe-gMg) small), but rather takes the place of Ca and Mn. Ca and Mn appear to act sympathetically in garnet:

$$R(gMg\text{-}gCa) \cong R(gMg\text{-}gMn)$$

$$R(gFe\text{-}gCa) \cong R(gFe\text{-}gMn)$$

$$R(f(T)\text{-}gCa) \cong R(f(t)\text{-}gMn)$$

$$R(KD\text{-}gCa) \cong R(KD\text{-}gMn)$$

---

[1] + or - are for positive or negative correlation.
[2] correlation coefficient.

The R(f(T)-gMn) for this population is rather small. The reason is that very few of the garnets are from very low grade, i.e. very few contain the very large proportion of spessartine molecule commonly found in the first appearing garnet in progressive metamorphism and as a result the range of Mn is small.

Ti of biotite increases with temperature, by replacing $Al^{(6)}$ and Fe^{3+} (negative correlation) in the octahedral site; concomitantly, K increases; to conserve a balance of charge $Va^{(6)}$ should decrease but $Va^{(6)}$ shows negative correlation with bFe and bMg, and little correlation with $bAl^{(6)}$, bTi, and bFe^{3+}. This suggests that $Va^{(6)}$ is independent of the type of trivalent octahedral cation and changes in response to the excess charge caused by the sum of trivalent octahedral cations. The negative correlation $Va^{(6)}$-$Al^{(4)}$ suggests that excess charge in biotite is reduced by an increase in $Va^{(6)}$ or $Al^{(4)}$. The reason for the positive correlation bNa-$Va^{(6)}$ is not clear. F(T) also shows small negative correlation with gTi and O.X.R. (oxidation ratio of the rock); the first is probably not significant, but the second corresponds to observations made by others that with increasing metamorphic grade the oxidation ratio of the rock tends to decrease (Engel and Engel, 1962; Best and Weiss, 1964; Hörmann and Raith, 1973). The small R(f(T)-bNa) is probably not significant.

KD shows correlation with +gMg, -gXFe, +f(T), +bTi, +bK, -gMn, -gCa, -bMg, +bXFe (by order of decreasing

R).

The good correlation of gMg and gXFe with KD and f(T) shows that gMg is the major factor in the change of KD with temperature; bMg and bXFe show rather poor correlation with KD as with f(T). The high R(KD-bTi) and R(KD-bK) result from the similar effects of temperature on KD, bTi, and bK. The good correlation of KD with gCa and gMn result from the fact that changes in KD are due to changes in gMg, itself replacing gCa and gMn.

Some other correlation coefficients are of interest, although they have little bearing on f(T). OX.R. correlates negatively with Fe of both biotite and garnet, i.e. an increase in the oxidation ratio of the rock results in biotites with less Fe; this corresponds to the observations of Chinner (1960). In biotite Fe is replaced by Mg, in garnet by Ca: positive correlation of OX.R. with gCa and bMg. OX.R. correlates with -bTi, $+Al^{(6)}$, -bK; these are probably parallel changes related to temperature. Various good correlations are seen between biotite parameters and garnet parameters; they can be attributed to temperature caused parallel changes. An exception is R(bMn-gMn). Because R(f(T)-bMn) is small, this correlation probably illustrates the availability of Mn from the rock.

The relationship of KD with the various chemical variables discussed above is quite different from the ones found by Saxena (1969, Table 2) where KD correlates with:

at low grade, -gXFe, +bXFe, +gMn, $+bAl^{(6)}$, +gMn (by

order of decreasing R).

at high grade, $-gXFe$, $+bXFe$, $-bTi$, $-gCa$, $-bAl^{(4)}$, $-bAl^{(6)}$.

These differences, which are quite marked considering that half of the garnet-biotite pairs used here were also used by Saxena, are due to the fact that Saxena calculates the correlation coefficients for sub-populations corresponding to narrow ranges of metamorphic grade, whereas here the population encompasses the major part of the regional metamorphic domain. This illustrates the fact that the variance of KD is caused by changes in metamorphic grade and by compositional variables. At this point, it is possible to say that an equation expressing f(T) as a function of the composition of coexisting garnet and biotite should include at least: bTi, gMg, $gXFe$, KD, bK, $bAl^{(6)}$, bFe^{3+}, gMn, gCa. Because of the impossibility, in practice, of determining the ferric/ferrous ratio with the electron microprobe, Fe^{3+} will be excluded, and total Fe only considered, as an approximation of Fe^{2+}.

Regression equations were calculated using the programme RMULT, for the above set of variables, as well as various other combinations. The equations were evaluated by the 'standard deviation of the estimated Y', i.e. the deviation of the f(T) calculated by the equation from the f(T) of the data file. At this stage, the temperature estimated previously for each garnet-biotite pair was reexamined with the

help of a computer plot of calculated f(T) versus estimated f(T). The temperature of pairs showing a systematic departure from the estimated f(T) for the various regression equations was reajusted within the limits of the temperature scale given above, where reasonably possible, or the pair excluded from further calculations, where no reason could be found for the departure. Two groups were excluded (Dahl's and Reinhardt's) to keep a balanced distribution over the total range in temperature. The result was a population of 125 garnet-biotite pairs that yielded the equation:

$$(12)\quad f(T) = 399.647 + 72.7KD - 8.23bAl^{(6)} + 54.82bTi + 12.94bFe + 4.49bMg + 24.01bK + 22.38gFe - 26.23gMg + 4.38gCa + 12.42gMn - 80.76bXFe - 264.9gXFe$$

with a standard deviation of the calculated f(T) of 6.89(16°) for the population of 125 pairs, and 12.0(21°) when equation 9 is used to calculate f(T) for the total population of 165 pairs. By comparison, an equation calculated using all the variables yields a standard deviation of 6.48(15°); a decrease in ±1° for an increase from 12 to 19 independent variables.

A regression of f(T) versus transf. KD of Saxena (1969) yields the equation:

$$(13)\quad f(T)/1000 = 0.3516 + 0.0881\text{Transf. KD}$$

with a standard deviation of the calculated f(T) of 12.23 (29°) for a population of 125 pairs. Note that this equation is not a numeric expression of Figure 7 of Saxena (1969) (Fig. 41), the temperature calibration being quite different from the one used in the present study.

A regression of f(T) versus bTi, the variable that shows the highest correlation with f(T) (after transf. KD), yields the equation:

(14) $$f(T) = 281.53 + 123.34bTi$$

with a standard deviation of the calculated f(T) of 12.94 (30°).

6/ Discussion and conclusions

An attempt will now be made to estimate the value of equation 12 as a geothermometer. First the causes for the deviation of the calculated f(T) from the estimated f(T) will be examined. They are:

1- poor estimate of the equilibrium temperature of a garnet-biotite pair;

2- poor analyses;

3- zoned garnets or biotites;

4- rock composition outside the range specified in 3/;

5- $P(O_2)$ outside the range specified in 3/;

6- bad choice of variables for equation 12.

1- Temperature estimate

The temperature scale presented in 4/. above is probably accurate, although this may be subjective, but it is not very precise. The error on the temperature, corresponding to the garnet isograd for example, is on the order of 30°; so is that of the triple point of the aluminium silicates. The muscovite out isograd is strongly dependent on the local $P(H_2O)$. Above this isograd there are no good temperature markers, except maybe the iron-titanium oxides geothermometer for which no information is available in any of the source studies.

2- Quality of analyses

Examination of the analyses recast into structural formulae reveals that a large number show a marked departure from the theoretical formula. These discrepancies are more easily recognized in garnet where they may attributed, to a certain extent, to minute inclusions (analyses by methods other than microprobe). In certain cases (Kretz, 1959), it was necessary to recalculate the Fe, Mg, Ca, and Mn of garnet to a total of 6. Whereas such discrepancies are not all too important when studying the relations within one population (assuming a systematic analytical error) or when using only element ratio, it may increase markedly the variance of a complex parameter calculated with the structural formulae from a sum of populations.

3- Zoning

Regional metamorphic garnets are often zoned. Many studies have been made on the subject (see for example Atherton, 1968; Cooper, 1972; Tracy et al., 1976; and references therein). By comparison with the prograde chemical changes in garnet, one may distinguish normal zoning when Mn and Ca decrease and Fe and Mg increase from core to edge, from reverse zoning when these changes are reversed. Zoning in garnets is particularly marked at low to intermediate grade, where it is generally normal; high grade garnet tend to be unzoned, except for a narrow fringe of reverse zoning (Tracy et al, 1976).

Little is known about zoning in biotite. Colour zoning of metamorphic biotite is rarely seen in thin section. The intensity of the brown colour of biotite is related (Tröger, 1959) to its content in Ti, which we have seen is a good indicator of temperature. Biotite can thus be considered as mostly unzoned. Tracy et al. (1976) state that for Mg and Fe "biotite was found to be essentially homogeneous within individual specimens, except in Zone VI where biotite immediately adjacent to garnet is more magnesian than elsewhere in the rock..., due to local retrograde exchange." Zone VI corresponds to their highest metamorphic grade (sillimanite + K-feldspar + cordierite).

The zoning of garnet will introduce an error in the derivation of equation 12 as most analyses used are of garnet separates and not all those done by electron micro-

probe give the location of the analysed points.

4- Rock composition

Only few of the garnet-biotite pairs used to define equation 12 come from rocks with epidote, hornblende or calcite. This should therefore not add too much to the standard deviation of f(T) calculated from the population of 125 pairs; it adds, however, to that calculated for the total population of 165 pairs.

5- Oxygen pressure

We have seen in 2/. above that $P(O_2)$ affects the stability of biotite and of garnet. The analyses compiled are in general of medium oxygen pressure, corresponding to coexisting ilmenite-magnetite. Consideration of the correlation coefficients showed that $P(O_2)$, as represented by the oxidation ratio of the rock, had a similar effect on garnet and biotite. Indeed two garnet-biotite pairs from the same metamorphic grade, but different oxide assemblages, one with ilmenite-magnetite (OX.R.=13.7%), one with magnetite-hematite (OX.R.=74.8%), show a difference in temperature of less than 10° as calculated with equation 12. Oxygen preesure is, therefore, not a major cause of variance of the calculated f(T).

6- Choice of variables

The choice of variables for equation 12 may not be optimal and as such add to the variance of the calculated f(T). But whether the choice is optimal or not can only be determined when most or all of the variance, due to factors discussed in 1 to 5 above, has been eliminated.

The adequacy of equation 12 as a geothermometer is difficult to test. The standard deviation of the calculated f(T) gives only the quality of the fit of the equation to the data base, and its value as a test rests on the accuracy and precision of the temperature estimates of the data base.

Comparison of the temperature calculated with equation 12 can be made with other garnet-biotite geothermometers or geothermometers based on other coexisting minerals and applicable to the temperature domain considered, example plagioclase-K-feldspar, iron-titanium oxides, garnet-cordierite, paragonite-muscovite, etc...

Comparison could be made with the plagioclase-K-feldspar for the garnet-biotite pairs of Engel and Engel (1962). It yields temperatures of 520-600°C after Barth (1956) (given by Engel and Engel), or 580-670°C using Figure 3 (5 Kb) Stormer (1975). These ranges were obtained by averaging the temperatures of groups of samples from the lowest and highest grade. The variance, however, is great; temperatures vary by 40-50° within each group. By contrast, using equation 12, the range per group is only 25° (if a

hornblende bearing sample is excluded); the total range is 625-685°C.

Comparison of the temperatures obtained from the vari garnet-biotite geothermometers (Perchuk, 1967; Saxe 969; Thompson, 1976) and equation 12, can only be used to estimate the relative precision, as expressed by the standard deviation of the calculated temperatures of groups of pairs from the same metamorphic grade. The accuracy is determined by the temperature scale used in calibrating the geothermometer: the temperature scales of Perchuk and Thompson are similar to the one used here, that used by Saxena 100-150°C lower. For groups of garnet-biotite pairs from the same source and the same metamorphic grade, the Saxena geothermometer shows standard deviations greater by a factor of 1 to 2 than those obtained from equation 12; the geothermometers based on KD alone (Perchuk's and Thompson's) show standard deviations greater by a factor of 1 to 8 than those obtained with equation 12. It is seen from this that temperatures obtained using equation 12 are more precise than those obtained using other garnet-biotite geothermometers. Their accuracy is that of the temperature scale given in 4/. above.

Equation 12 is therefore proposed as a garnet-biotite geothermometer. It is applicable to rocks of pelitic to semi-pelitic composition with little or no carbonates, calcic amphibole or epidote, over the whole range of coexistence of garnet and biotite (approx. 475-700°C). It is not

very sensitive to changes in $P(O_2)$; the effects of a change in P(s) are not known; but they should be small (see 2/. above). The garnets and biotites should be analysed preferably using a microprobe and by locating the analysis points near the edge of garnets, if possible near a biotite grain, for metamorphic grades up to 600-650°C; further inside the garnet and on biotites not too near a garnet at higher grade. The precision to be expected is ±10-20°.

It is believed that this geothermometer will be of use to students of metamorphism who, in this age of computers and hand-held electronic calculators, will not be deterred by the apparent complexity of equation 12. In cases where a more approximate estimation of temperature is sufficient, equation 14 can be used which requires only the knowledge of titanium in biotite coexisting with garnet and should have a precision of ±30°.

B GEOBAROMETRY

1/ The b_0 value of potassic white micas

a/ Introduction

Sassi and Scolari (1974) showed that the b_0 cell dimensions of potassic white micas can be used as a barometric indicator in low-grade metamorphism. They devised an empirical scale of b_0 values characterizing the various

baric types, from low pressure (for ex.: Bosost) to glaucophanitic metamorphism (for ex.: Sanbagawa) (Table 5). Their method is based on the following observations:

1- the b_0 spacing of the potassic white micas may be used to estimate their phengite (or celadonite) content (Cipriani et al, 1968);

2- at low metamorphic grade, the phengite content of the potassic white micas increases with increasing pressure of formation, other conditions (temperature, rock composition etc...) being equal (Cipriani et al., 1974; Ernst, 1963; Velde, 1965 and 1967).

In order to gain insight on the baric type of metamorphism of the Wakeham Bay region, a suite of samples from the western map area, as well as 5 samples from the lowest grade part of the eastern map area, were chosen and the b_0 value of the potassic white micas measured.

b/ Description of the samples

Sassi and Scolari (1974) state that the specimens used should, as far as possible be:

1- isochemical and of pelitic composition (phyllites and quartz-phyllites of Fritsch et al., 1967); very quartz-rich rocks, chlorite-rich rocks and rocks in which K-feldspar occurs as an essential component give high b_0 values; carbonate-bearing rocks give low b_0 values;

2- of low metamorphic grade (chlorite or biotite zone): the

Table 5. Empirical scale of the b_0 values of potassic white micas in low-grade metamorphism of pelitic schists (from Sassi and Scolari, 1974).

Facies series	1	2	3	4	5	6
Mean b 3° (Å)	≅8.990	≅8.995	≅9.010	9.020-9.025	≅9.035	≅9.055

1 Low pressure metamorphism (and+cord) without chlorite zone (for ex.: Bosost).
2 Low pressure metamorphism (and+cord) with chlorite zone (for ex.: Hercynian metamorphism in Eastern Alps).
3 Low-intermediate pressure metamorphism (and) with the chl->bio->alm sequence in the greenschist facies (for ex.: New Hampshire).
4 Typical Barrovian metamorphism (Dalradian metamorphism in Scotland).
5 Barrovian-type metamorphism, with simultaneous first appearance of biotite and almandine (for ex.: Otago).
6 Glaucophanitic greenschist facies (for ex.: Sanbagawa).

phengite content of the potassic white micas decreases with increasing temperature (Lambert, 1959; Velde, 1965 and 1967; Ciprani et al., 1974);

3- lacking in paragonite, pyrophyllite and margarite.

The samples used in the present study do not conform very strictly to the first condition because true phyllites are common only in a narrow zone in the southern part of the western region; as a result many specimens are quartz- or chlorite-rich or carbonate-bearing. Only a few contain K-feldspar as an essential component (retrogressed basement gneisses).

The samples are from the greenschist facies, equivalent to biotite or garnet zone; chlorite is still an essential constituent of the associated metabasites. A few

samples from the amphibolite facies have been measured, but the results are excluded from the cumulative curves. Paragonite was found in one sample which was excluded from Table 5.

c/ Methodology

The rock samples were saw-cut perpendicular to schistosity into 2-4 mm thick slices. The X-ray diffraction analyses were done with a Phillips apparatus, using Cu Kα radiation, a curved crystal monochromator and 1° divergence and receiving slits. A time constant of 4 seconds was used with a scanning speed of 1° 2θ/mn and a chart speed of 1 cm/mn. A range of 59 to 63° of 2θ was scanned (5 times per sample), in order to measure the (060) peak of the potassic white mica using the (211) peak of quartz in the rock as an internal standard. At the same time the possible occurrence of paragonite, margarite, or pyrophyllite could be verified ((060) peak at 62.5, 62.8-63.0, and 62.3° 2θ respectively). The sample was oriented with the schistosity either parallel or perpendicular to the slits of the diffractometer depending on the relative amounts of quartz and white mica present in the rock; it was observed that the mica peak tended to be higher and the quartz peak lower in the perpendicular position, probably as a result of preferential orientation of both of these minerals within the schistosity plane. Occasionally the biotite and/or chlorite (060) peak interfered with the (211) peak of quartz necessitating the re-

course to the (112) or the (203) peak of quartz.

The standard deviation of the b_0 measurements varied from 0.001 to 0.008Å in most cases it was between 0.002 and 0.004Å. The (060) peak of the white mica was generally broad, suggesting a certain variation in the composition of the white mica within a given sample.

d/ Results and discussion

The measured b_0 values are plotted on a map of the Wakeham Bay area (Fig. 43) and listed on Table 6.

A rather large spread of b_0 values have been measured (9.005 to 9.040Å). Despite this variability of the results, one may recognize a southern domain with lower b_0 values and a central to northern domain with higher b_0 values. A few very high values occur, however, in the South and a few very low ones in the North. The southern high values correspond to retrogressed basement gneisses; the northern low values correspond to samples from the amphibolite facies. Those values were thus discarded.

A cumulative freqency plot of all b_0 values on normal probability scale (Fig. 44) illustrates the presence of two populations; two straight lines fit the data better than one single straight line. Taking the limit between the Pelitic Group and the Volcano-Sedimentary Group as a boundary one may split the data into two populations, each fitting a straight line (Fig. 44). A Student's t-test on the means of the two populations shows them to be different at

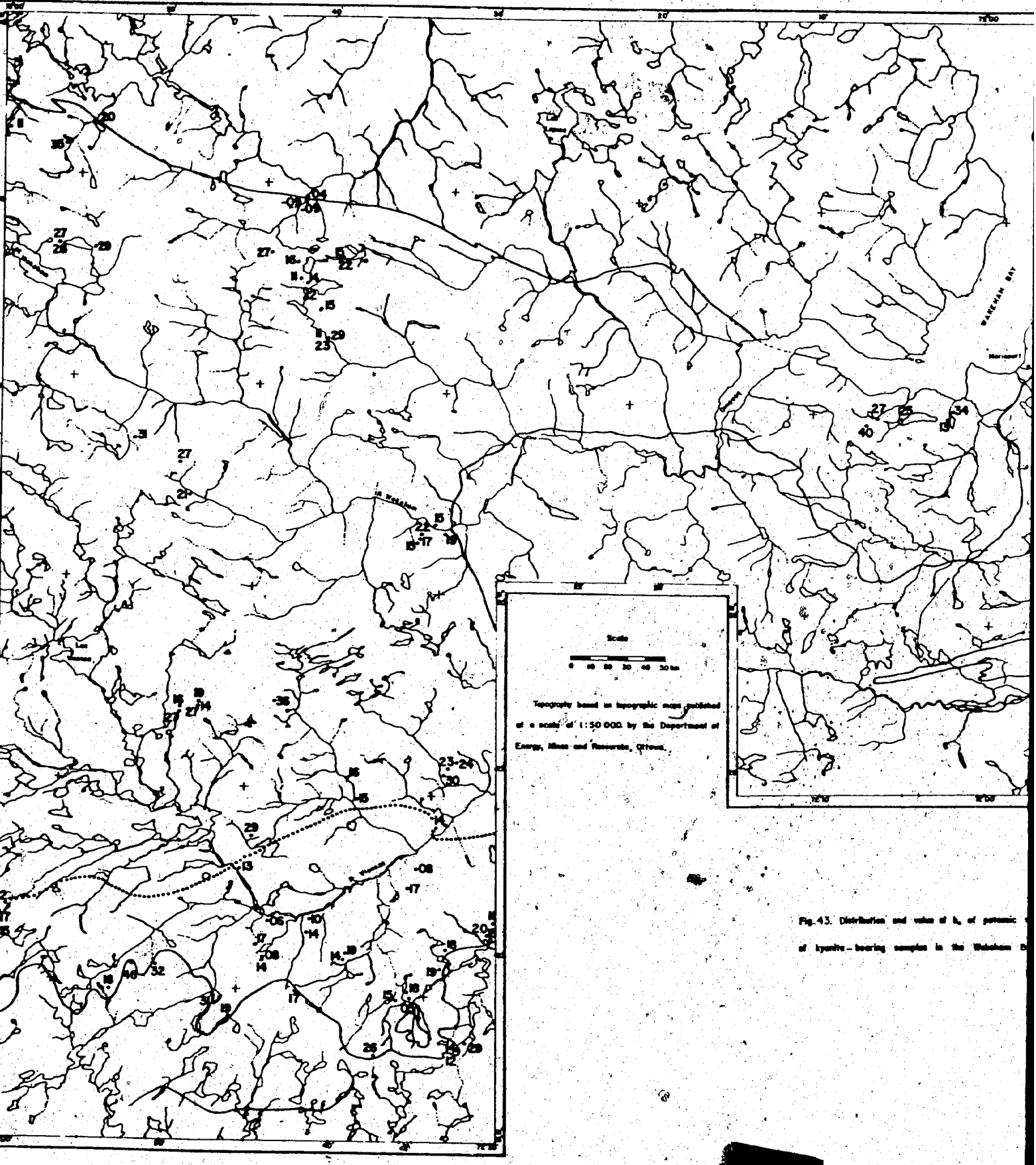

Fig. 43. Distribution and value of k_2 of potassic
of kyanite-bearing samples in the Wakeham

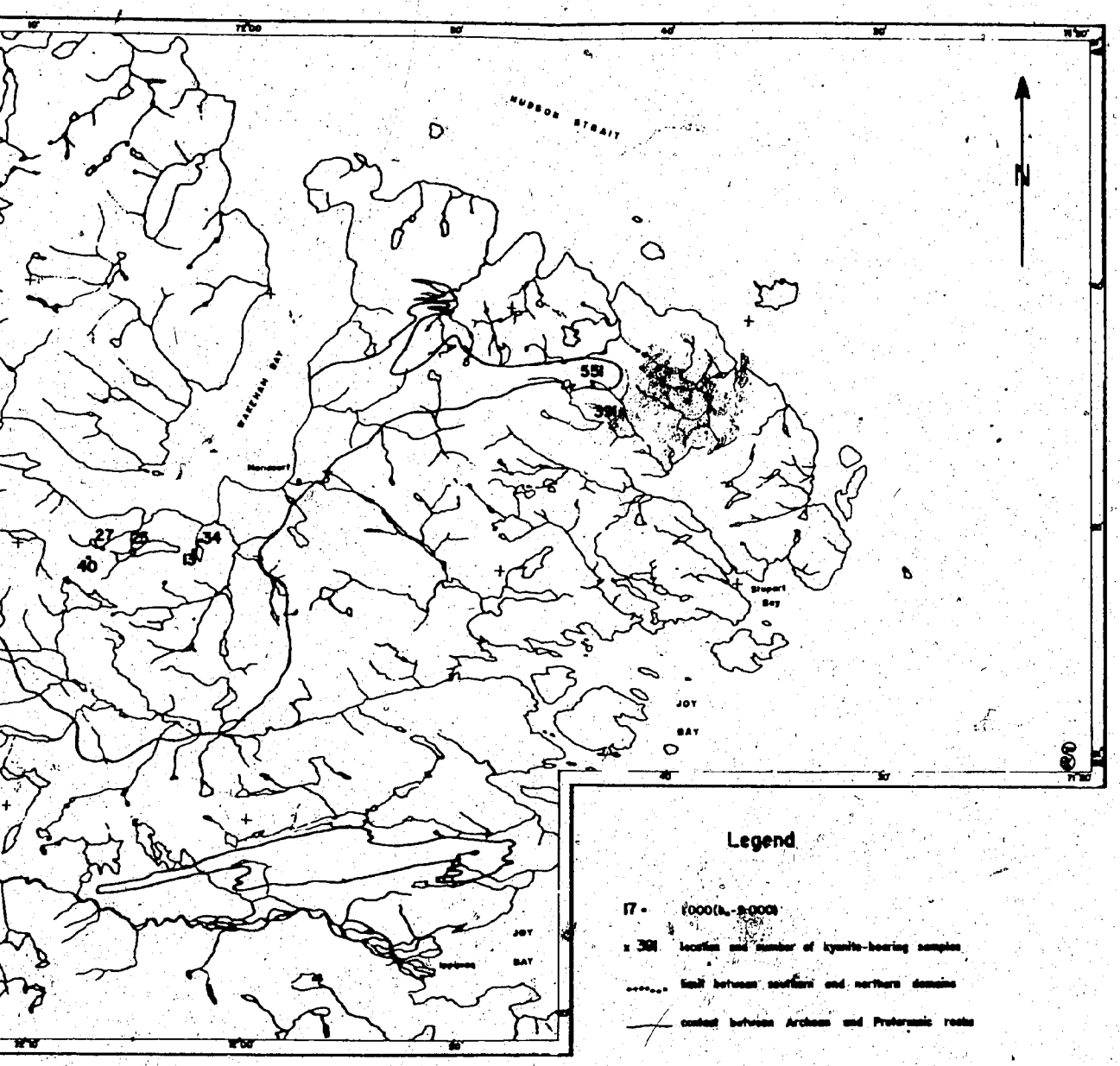

Fig. 43. Distribution and value of b_0 of potassic white micas and location of kyanite-bearing samples in the Wakeham Bay region.

Table 6. Location of samples and b_0 value of the potassic white micas.

Lab. No	Field No	Coordinates		b_0 (Å)	T6	Remarks
...	C19-2	155	110	9.032		basement gneiss
...	C19-7	142	109	9.046		basement gneiss
...	C19-10	131	95	9.018		
564	H1-9C	317	74	9.014		
89	H2-10	319	75	9.012		
91	H2-2	321	79	9.029		basement gneiss
...	H4-9B	335	129	9.018		
...	H4-9C	335	129	9.020		
...	H4-10B	336	134	9.011		
...	H4-17C	313	124	9.018		
...	H4-20	308	114	9.019		
98	H5-28A	254	206	9.016		
102	H5-33	259	106	9.015		
151	M2-9	290	156	9.017		
153	M2-13	294	161	9.008		
172	P9-18	69	111	9.015		
...	P9-24	69	128	9.017		
...	P9-26	72	135	9.012		
...	R3-6	197	86	9.019		
...	R3-13	189	98	9.031		basement gneiss
...	S1-3	255	80	9.026		
227	S2-1-2	291	98	9.005		
237	S2-1-14	291	98	9.018		
...	S2-3-1	295	100	9.015		
241	S4-13A	258	117	9.014		
242	S4-14A	263	123	9.019		
246	S4-22A	238	137	9.010		
247	S4-25B	234	128	9.014		
...	S7-5A	307	184	9.014		
...	S68-1A	232	100	9.017		basement gneiss
...	S68-7A	209	111	9.008		
449	S68-7C	209	111	9.014		
...	S68-9A	207	120	9.017		
...	S68-11A	216	132	9.006		
450	S68-14C	196	160	9.013		
454	S70-5	207	178	9.029		
...	C22-3B	160	360	9.027		
...	C27-8A	224	450	9.014		
...	C27-8B	224	450	9.012		
...	C28-2B	205	470	9.027		
...	C29-6A	242	464	9.015		
...	C29-6C	242	464	9.022		

Table 6. Cont'd.

107	H11-7P	291	325	9.015	
109	H11-9E	291	326	9.017	
112	H11-10D	292	327	9.022	
118	H12-6B	296	334	9.015	in amphibolite facies
...	H12-10D	303	332	9.019	in amphibolite facies
80	R6-3	105	525	9.020	in amphibolite facies
...	R8-4	107	464	9.029	
552	R9-6	60	527	9.011	in amphibolite facies
...	R11-1K	145	440	9.037	
...	R12-2B	164	234	9.027	
...	R12-3	163	235	9.016	
...	R12-4	168	238	9.027	
188	R12-5A	167	238	9.019	
...	R12-5B	168	238	9.014	
221	R22-2D	218	342	9.022	
255	S6-14	315	216	9.024	
257	S6-15	309	215	9.023	
258	S6-16	308	211	9.030	
274	S9-2D	213	244	9.036	
288	S14-17B	236	424	9.011	
291	S14-17E	236	424	9.029	
292	S14-17F	236	424	9.023	
296	S14-22A	231	439	9.015	
320	S15-4E	218	443	9.011	
333	S15-6C	217	461	9.016	
336	S16-1A	221	492	9.004	basement gneiss (amphibolite facies)
342	S16-1H	221	492	8.991	in amphibolite facies
348	S16-2B	220	491	8.991	in amphibolite facies
...	S69-10	135	370	9.031	
458	S72-2A	163	346	9.021	
472	S73-9A	90	514	9.035	
...	S74-5B	90	466	9.028	
...	S74-5C	90	466	9.027	
...	S53-9D	548	408	9.027	
382	S53-11E	547	400	9.025	
...	S60-1A	528	395	9.040	
...	S62-5A	574	400	9.013	
...	S62-7B	575	405	9.034	

the 99.95% level of significance (t=4.76).

This variation from south to north in the mean b_0 could be attributed to one of the following:

1- systematic difference in sample chemistry;

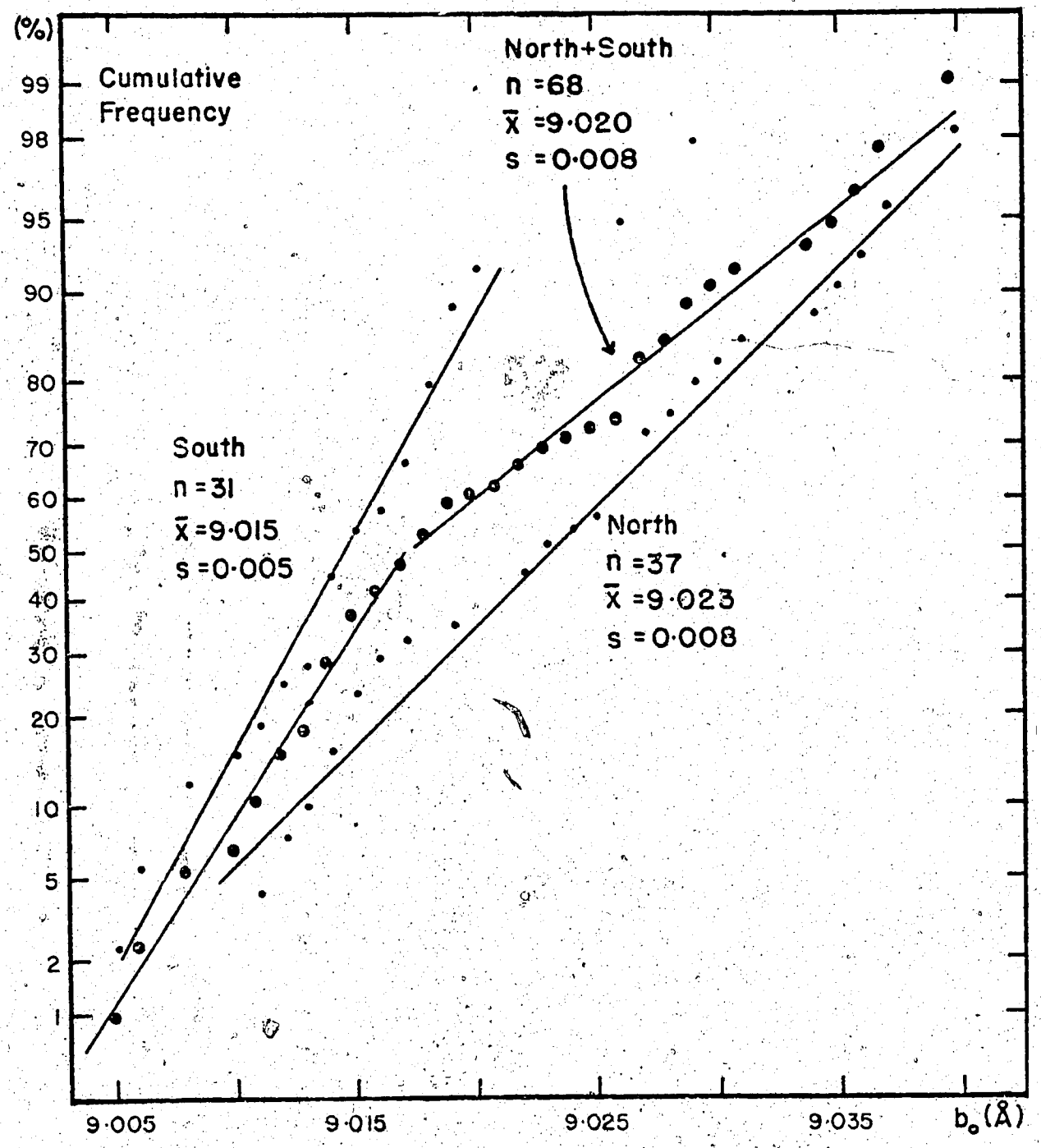

Fig. 44. Cumulative frequency curves of potassic white micas of the Wakeham region, illustrating the presence of two populations.

2- difference in metamorphic temperature;

3- difference in metamorphic pressure.

Whereas most samples from the southern domain are closer to phyllites than those in the northern domain, it remains that many are relatively quartz-rich and several are chlorite-rich, but still have low b_0 values. Furthermore, more samples from the northern domain tend to have carbonates and epidote than those from the southern domain. The difference in rock chemistry does not appear to be sufficient to account for a systematic difference in mean b_0, but may account for the scatter in values, particularly in the north.

Temperature differences between the two domains are small, and would rather favor a decrease in the b_0 values of the northern domain.

One must therefore conclude that this difference in mean b_0 is due to a slight difference in metamorphic pressure. The significance of this difference is not clear; but one may note that the boundary between the two domains corresponds approximately to the limit between what can be considered as a eugeosynclinal domain in the North, with a thick sequence of basic volcanics, and mostly immature sediments and a miogeoclinal domain in the South with a thin sequence of mostly mature sediments.

Figure 45 and Table 7 compare the b_0 values of the Wakeham Bay area with those of classical metamorphic areas.

Table 7. Summary of b_0 values of potassic white micas, compared with those of classical metamorphic area. (After Sassi and Scolari, 1974).

Population	Number of Samples	Mean b_0(Å)	Standard deviation
1. Bosost	132	8.994	0.009
2. Ryoke	46	9.013	0.006
3. N. New Hampshire	17	9.011	0.010
4. Eastern Alps	100	9.038	0.008
5. Otago	35	9.039	0.005
6. Sanbagawa	34	9.054	0.006
7. Daday-Ballidag	46	9.056	0.007
8. Wakeham Bay			
a. South	31	9.015	0.005
b. North	37	9.023	0.008
c. South + North	68	9.020	0.008
d. retrogressed gneisses	5	9.031	0.010
e. amphibolite facies	7	9.007	0.012

The mean b_0 of the southern domain is close to that of the Ryoke area, whereas the mean b_0 of the northern domain and that of all samples fall in the realm of typical Barrovian metamorphism on the empirical scale proposed by Sassi and Scolari (1974) (Table 5).

It is interesting to note that most of the cumulative frequency curves in Figure 45 reveal the presence of two or even three populations, i.e. of variations in the P/T regime within the areas considered. Such a variation in the P/T regime has recently been described in the Scottish Caledonides (Fettes et al., 1976).

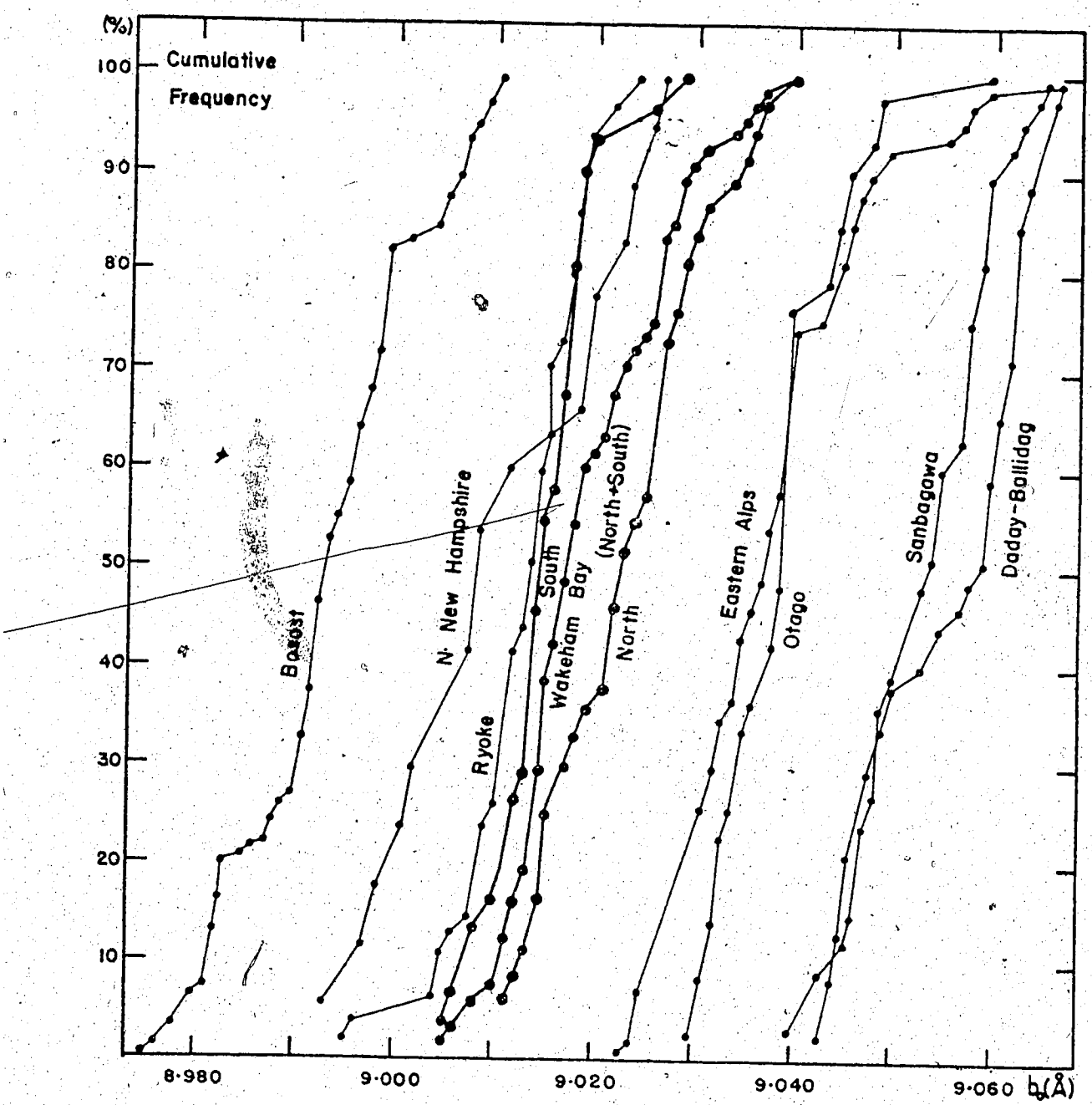

Fig. 45. Cumulative frequency curves of b_0 values of potassic white micas of the Wakeham Bay region, compared to those of classical metamorphic areas (after Sassi and Scolari, 1974). Note: the "Eastern Alps" curve corresponds to the Alpine metamorphism in the eastern Alps.

e/ Conclusions

The use of the b_0 value of the potassic white micas as a barometric indicator shows that the Wakeham Bay area has undergone an intermediate pressure metamorphism similar to what has been called Barrovian metamorphism, but that P/T was higher in the northern and central parts of the belt, consisting of a thick sequence of basic volcanics and mostly immature sediments, than in the southern part of the belt, consisting of a thin sequence of mostly mature sediments.

2/ The plagioclase-garnet-Al_2SiO_5-quartz assemblage

Ghent (1976) presented a geobarometer-geothermometer using the reaction:

(1) $3CaAl_2Si_2O_8 = Ca_3Al_2Si_3O_{12} + 2Al_2SiO_5 + SiO_2$

3anorthite = grossular + 2Al-silicate + quartz

The equilibrium for the reaction with kyanite can be described by equation (1b) of Ghent(1976):

(2) $0 = -3272/T + 8.3969 - 0.3448(P-1)/T$

where T is the temperature in degrees Kelvin and P is the pressure in bars.

For the assemblage plagioclase-garnet-kyanite-quartz, where only kyanite and quartz can be considered as

pure phases, terms for activity of anorthite solid solution in plagioclase (a_2) and activity of grossular solid solution in garnet (a_1) have to be added:

(3) $$0 = -3272/T + 8.3969 - 0.3448(P-1)/T + \log a_1 - 3\log a_2$$

where $a_1 = X_1^3 \cdot \gamma_1^3$ and $a_2 = X_2 \cdot \gamma_2$

X_1 = mole fraction of grossular

γ_1 = activity coefficient of grossular

X_2 = mole fraction of anorthite

γ_2 = activity coefficient of anorthite

The activity coefficient can be calculated (Ghent, 1976) by:

(4) $$\ln \gamma = (1-X_1)^2 W/RT$$

where W for an almandine grossular mixture is near 1 Kcal/mole (Ganguly and Kennedy, 1974). The activity coefficient for anorthite is 1.276 for the range $An_{0-63.8}$ (Orville, 1972). Table 8 gives the compositions and calculated pressures for two samples for which temperatures had been obtained independently using the garnet-biotite geothermometer (see also Fig. 46).

The two samples are located about 1.5 Km apart in the field; even assuming the present surface vertical at the time of metamorphism, this distance could account at most for a difference in pressure of 1/2 Kb. Similarly the dif-

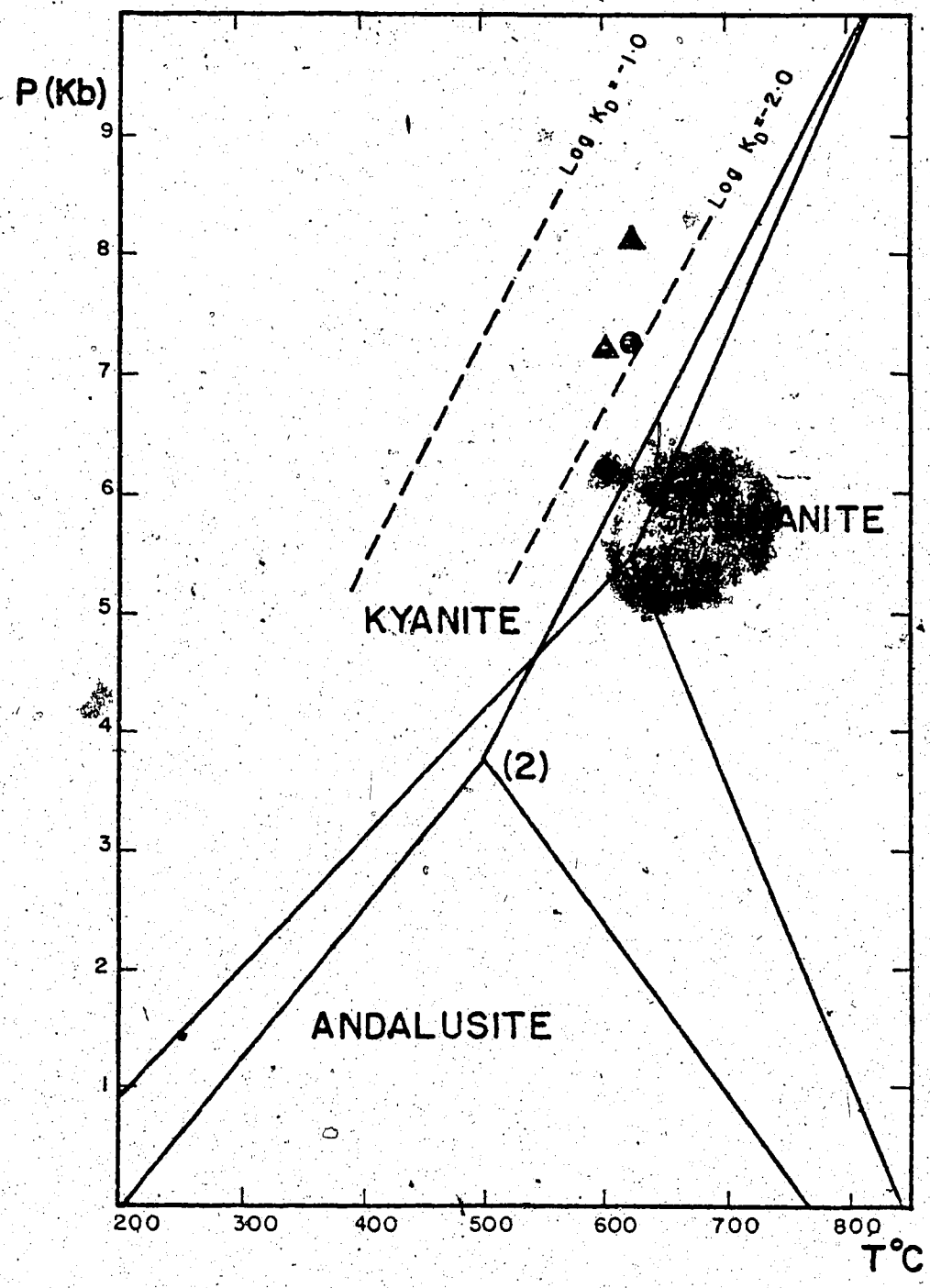

Fig. 46. Pressure-temperature diagram showing Al_2SiO_5 phase relationships, (1) after Richardson et al. (1969) and (2) after Holdaway (1971). P-T curves for log KD = -1.0 and -2.0 calculated from equation (1b) of Ghent (1976), using an ideal solution model.

P-T relations of two samples of the eastern Wakeham Bay region are plotted as circles, ideal solid solution, and triangles, non-ideal solid solution.

Table 8. Composition of garnet and plagioclase in kyanite-bearing samples, and calculated pressure.

Sample number	391	551
Temperature from biotite-garnet	896°K	874°K
Mole fraction of anorthite in plagioclase	0.26	0.25
Mole fraction of grossular in garnet	0.058	0.046
Mole fraction of almandine in garnet	0.722	0.781
Mole fraction of pyrope in garnet	0.161	0.154
Mole fraction of spessartine in garnet	0.060	0.019
Log KD	-1.955	-2.206
Activity coefficient of grossular in garnet	-1.646	-1.732
Pressure calculated assuming:		
1. Ideal solid solution	7.22 Kb	6.20 Kb
2. Non-ideal solid solution	8.12 Kb	7.25 Kb

ference in temperature (38°) would produce a gradient in temperature of 25°C/Km. This again assumes the present surface to have been nearly vertical at the time of metamorphism which is not supported by the structural relations of the area. One has to conclude from this that the calculated temperature difference is too large, resulting in too large a difference in calculated pressure. Recalculating the pressures using an average temperature of 885°K reduces the differences to about 1/2 Kb.

The conclusion is that at a temperature of 610°C, the metamorphic pressure was 7 Kb, possibly 8 Kb.

C TEMPERATURE ZONATION

The garnet-biotite thermometer described above is applied to the Wakeham Bay area. The garnets and biotites from all samples of pelitic and semi-pelitic rocks were analysed. The temperatures obtained are listed in Appendix IV and shown on Figure 47. The garnet-biotite-bearing samples tend to cluster in certain areas. From these clusters one can see that in a restricted area, the temperatures obtained vary little, if one excepts the odd sample; indeed, because of the paucicity of garnet-bearing samples, those analysed do not always conform strictly to the restrictions specified in the section on geothermometry and as a result some of the temperatures obtained are clearly out-of-line.

A series of isotherms were interpolated from these data, supplemented by the distribution patterns of minerals (mainly plagioclase) and field observations (degree of crystallinity, etc...). In addition to isotherms, a garnet isograd is traced, based on the presence in metapelites of garnet with less than 9 wt% MnO (about 1.2 Mn in the structural formula).

Two observations can be made at this point:

1- the isotherms tend to parallel (at least in the westerm map area) the Aphebian-Archean contact;

2- the garnet isograd may not be isothermal i.e. it may correspond to a higher temperature in the South than in the North.

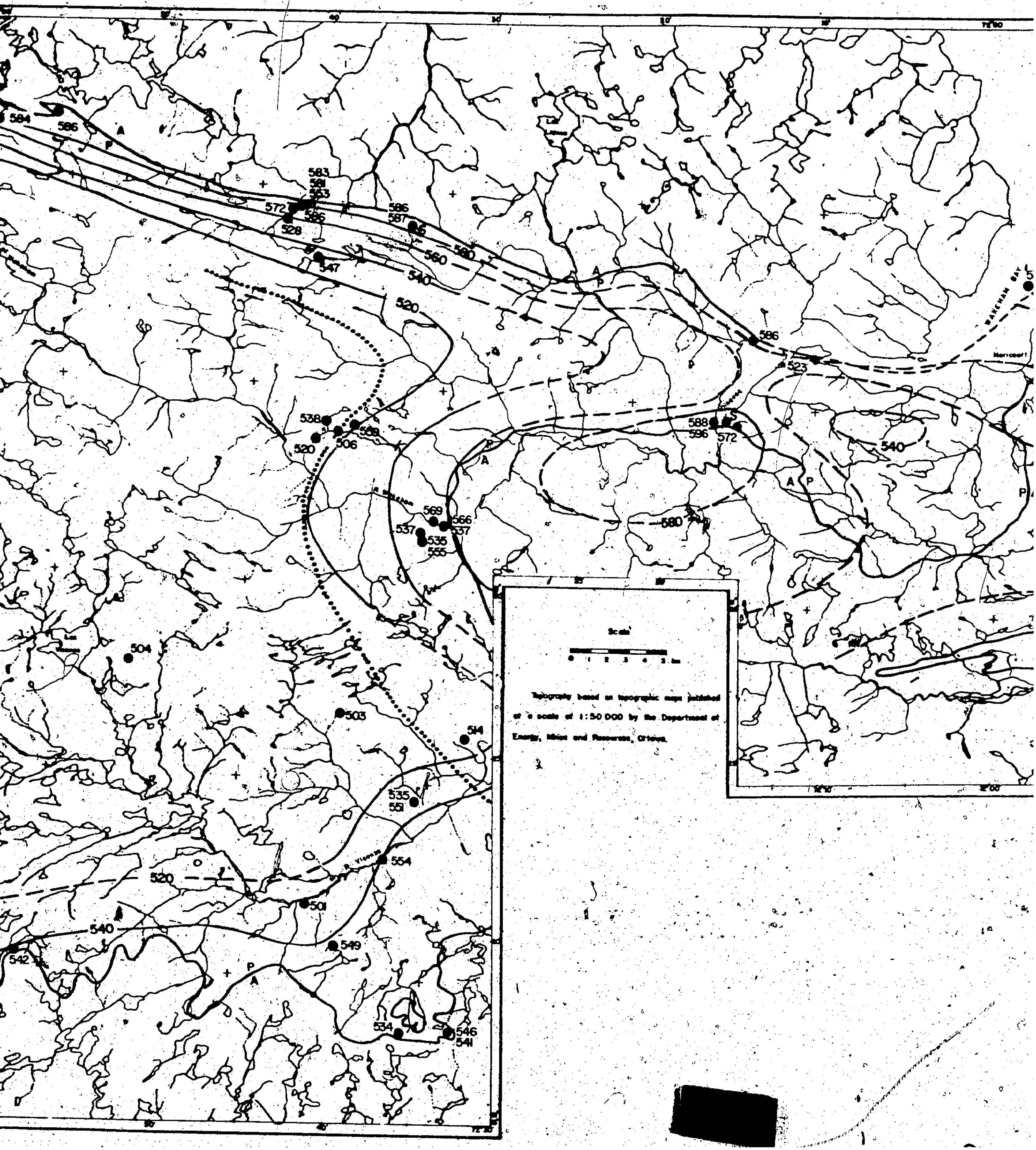

584
586
A
P
583
581
563
572
528
585
586
587
580
560
547
540
520
586
523
538
589
506
520
588
596
572
540
A
P
P
A
569
566
537
537
535
555
580
504
503
514
535
551
554
520
501
540
549
542
P
A
534
546
541
Scale
0 1 2 3 4 5 km
Topography based on topographic maps published at a scale of 1:50 000 by the Department of Energy, Mines and Resources, Ottawa.

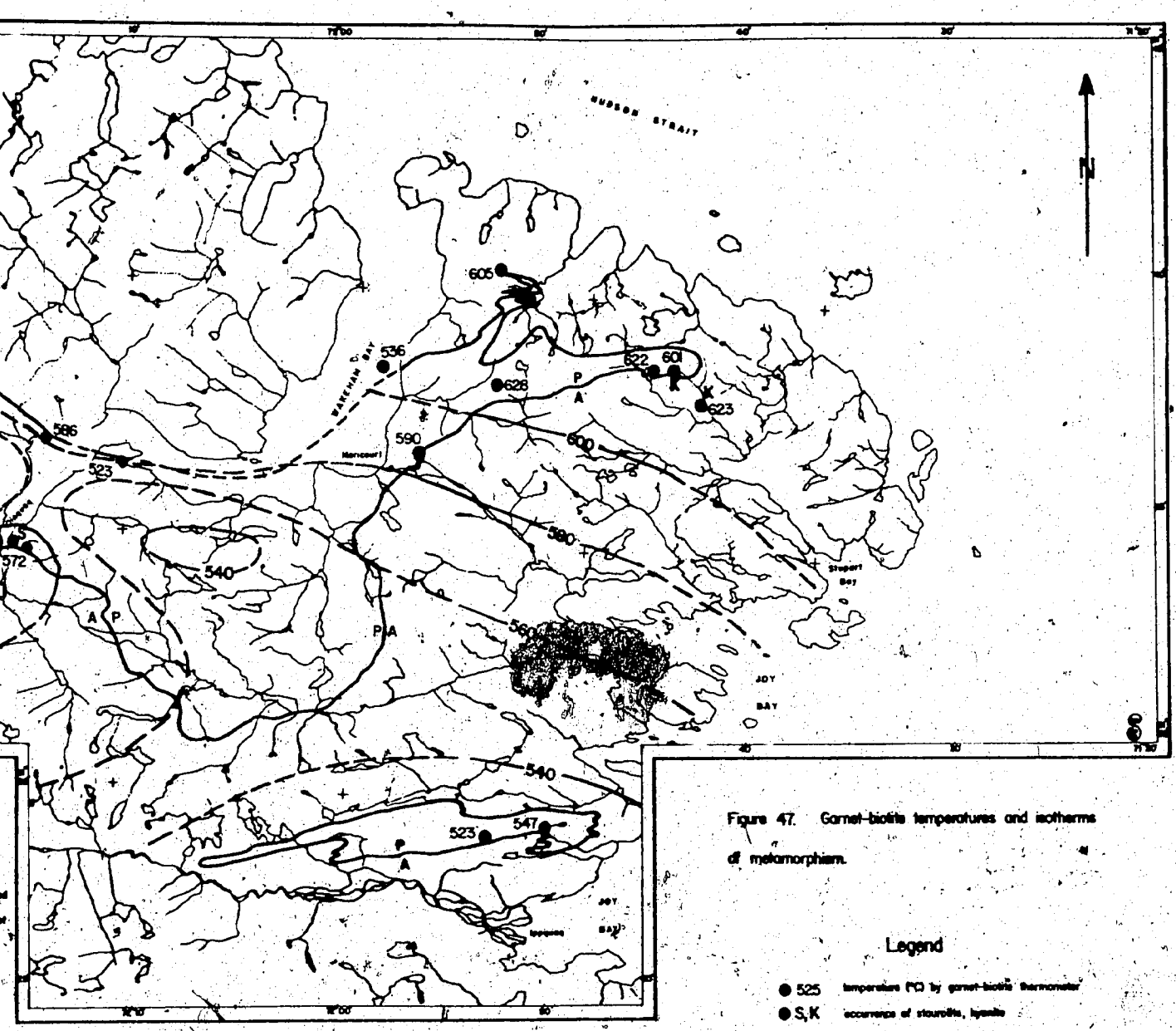

Figure 47. Garnet-biotite temperatures and isotherms of metamorphism.

Legend

- ● 525 temperature (°C) by garnet-biotite thermometer
- ● S,K occurrence of staurolite, kyanite
- garnet isograd
- 525 isotherm
- A/P contact between Archean and Aphebian rocks

4. VARIATIONS in MINERAL COMPOSITIONS with TEMPERATURE

An attempt is made to correlate the thermal zonation (Fig. 47) not only with the distribution of minerals but also with variations in their composition.

A PLAGIOCLASES

The An content of the plagioclases was determined in some 150 samples of metabasites. In these samples the plagioclases are generally small, interstitial grains with no visible twinning or cleavage. The An content was determined:

1- with the U-stage by measuring the optic axial angle in law-grade samples where the plagioclose can be assumed to be in the range An_{0-25} and no ambiguity arises in 2V versus An;

2- by fully quantitative energy dispersive microprobe analysis (Smith and Gold, 1976);

3- by rapid energy dispersive analysis (see Appendix II).

The results are presented in Appendix IV, together with the temperature estimated from the garnet-biotite thermometer.

The An content of plagioclases has been used for metamorphic zonation (see for example Wenk and Keller, 1969, in the Alps). The plagioclase in amphibolites varies there

from albite in the greenschist facies to labradorite in the upper amphibolite facies.

The distribution of An content of plagioclases for the Wakeham Bay area is shown in Figure 48 together with the oligoclase isograd. This isograd corresponds to a temperature of about [illegible]°C (Compare with Figure 47). An andesine isograd was [illegible]aced, but it would correspond about to the 580°C isotherm. Very few plagioclases have a labradorite composition; they occur in the eastern most part of the area, above 600°C (in Figure 48 they are group[illegible]th andesine).

It has been observed in many areas that the composition of plagioclase in metamorphic rocks jumps from albite to calcic oligoclase near the greenschist-amphibolite facies boundary (see for example Brown, 1962; Crawford, 1966, and references therein). This jump has been attributed to the existence of a solvus, the peristerite solvus. Noting that this jump in composition is not observed in regions of low P/T metamorphic regime, Brown (1962) proposed a T-P-X diagram in which the peristerite solvus plunges beneath a plagioclase breakdown surface at low pressure.

Crawford (1966) made a detailed study of plagioclase compositions in semi-pelitic schists from Vermont (U.S.A.) and New-Zealand, along traverses across the biotite and garnet zones. She concluded that an asymmetric peristerite solvus is present with a top at An_5 and 450-490°C. The metamorphism of both areas is of the intermediate P/T

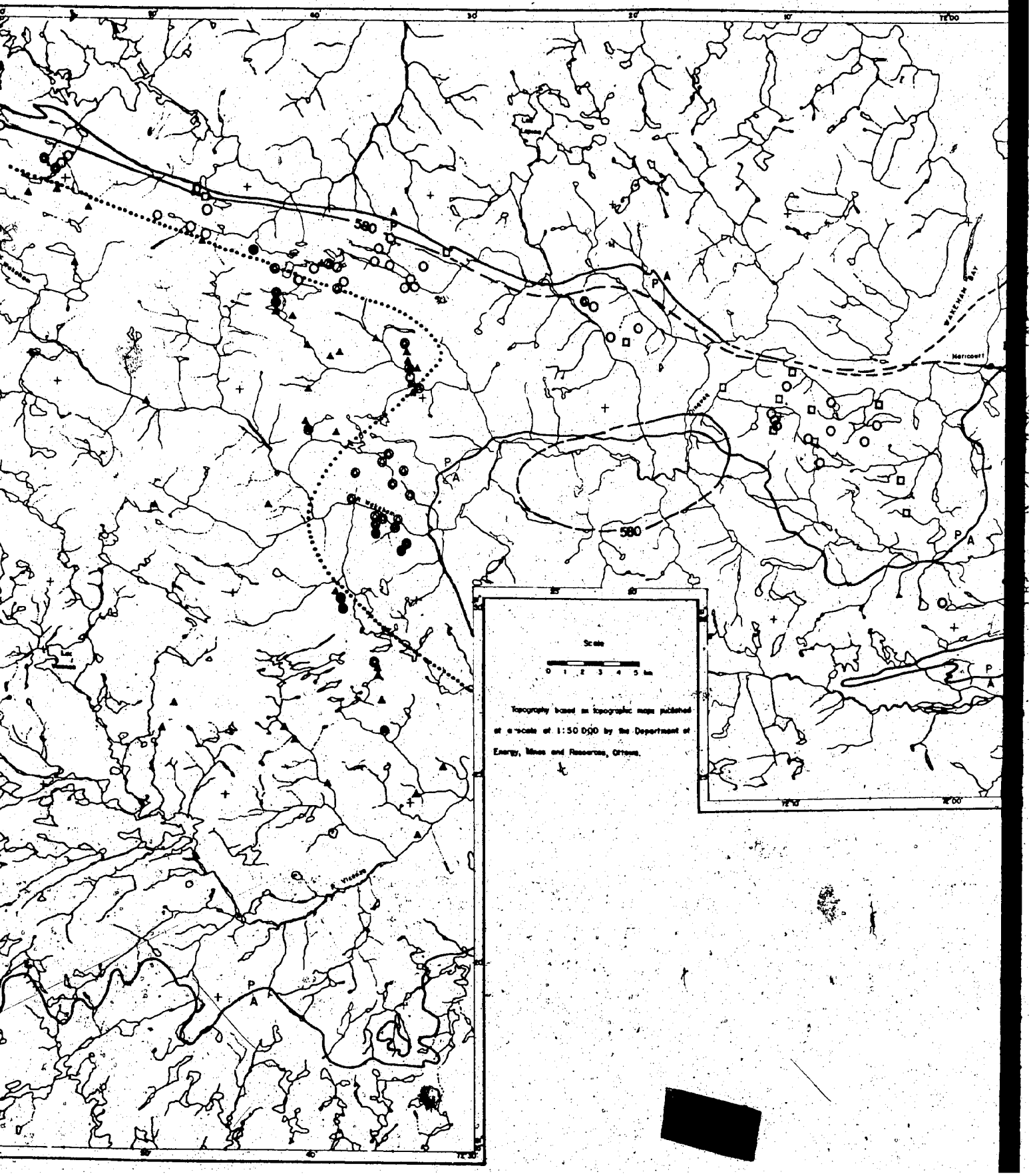
580
580
Scale
0 1 2 3 4 5 km
Topography based on topographic maps published at a scale of 1:50 000 by the Department of Energy, Mines and Resources, Ottawa.

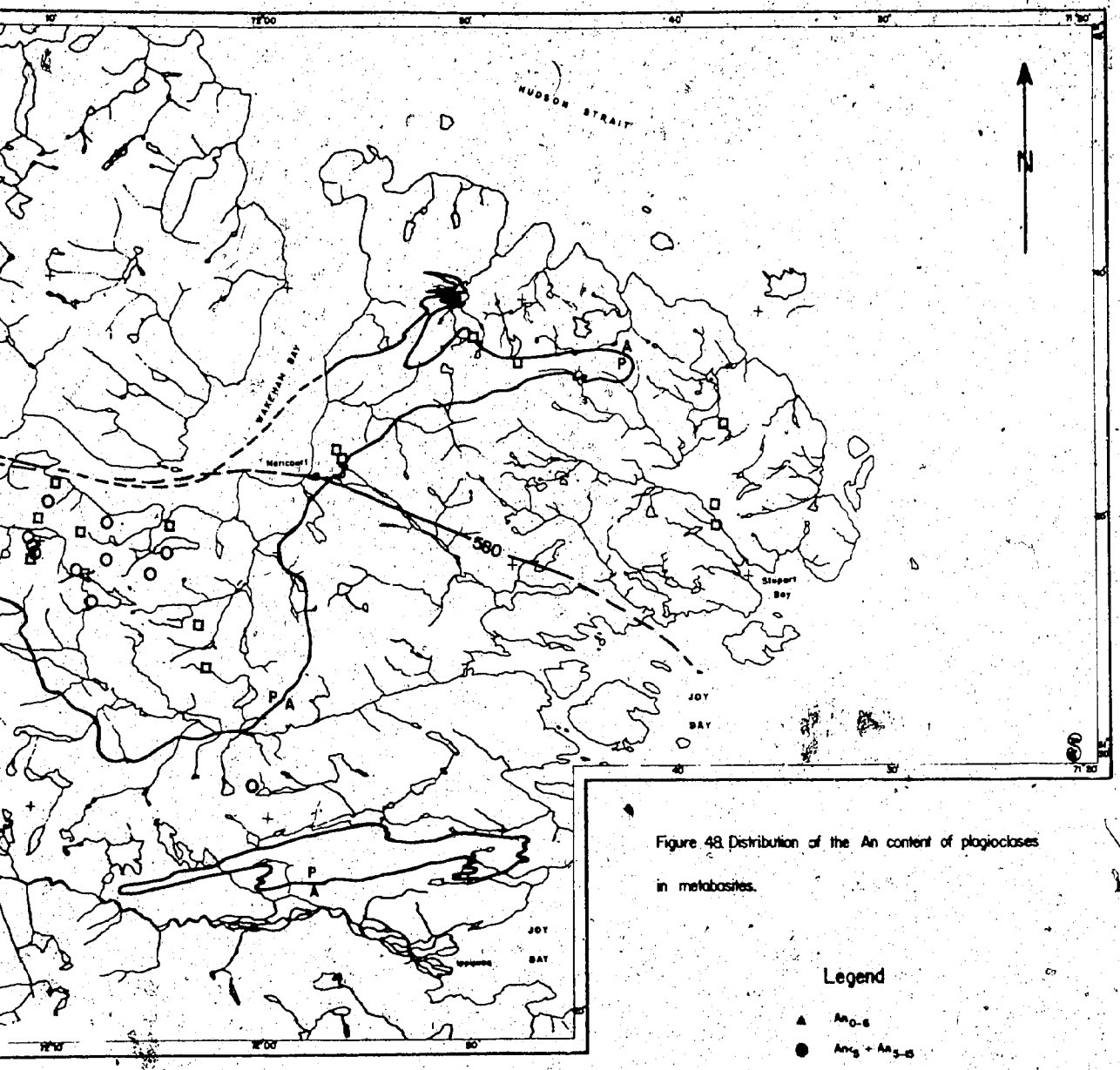

Figure 48 Distribution of the An content of plagioclases in metabasites.

Legend

- ▲ An_{0-5}
- ● $An_{5} + An_{5-15}$
- ◉ $An_{>17} + An_{>17}$
- ○ An_{20-30}
- ▣ $An_{>30}$
- oligoclase isograde
- 580 — 580°C isotherm
- A/P — contact between Archean and Aphebian rocks

type. Her conclusions thus are in line with Brown's model.

In metabasites, equilibrium with other phases, including fluid phases, controls the bulk plagioclase composition; the position of this composition with regards to the peristerite solvus (in a T-P-X volume) controls the presence of one or two plagioclase phases, their composition, and the relative amounts of these two phases. Figure 49 shows the analysed plagioclases in T-X diagrams. In Figure 49A, a solvus can be recognized; this is not as easy in Figure 49B where a number of analyses fall within the 'solvus'. Although some of these may be due to analytical errors, it is believed that they represent mainly metastable compositions. The area having an intermediate P/T metamorphic regime (see section in geobarometry), it is not unreasonable to assume a solvus. Figure 49C illustrates the change in plagioclase bulk compositions with increasing metamorphic grade: starting with an albite composition, it evolves along paths as shown, either above the solvus or through the solvus; depending on the chemical parameters of the system (bulk composition, fluid phase composition, etc...) the plagioclase bulk composition shows a more or less rapid increase in An content with grade. The path followed will control the composition of coexisting plagioclases and the temperature at which they will be observed.

This solvus is somewhat different from the one proposed by Crawford (1966), it is less asymmetric and further from the albite side, and its top is some 50-100°C hi-

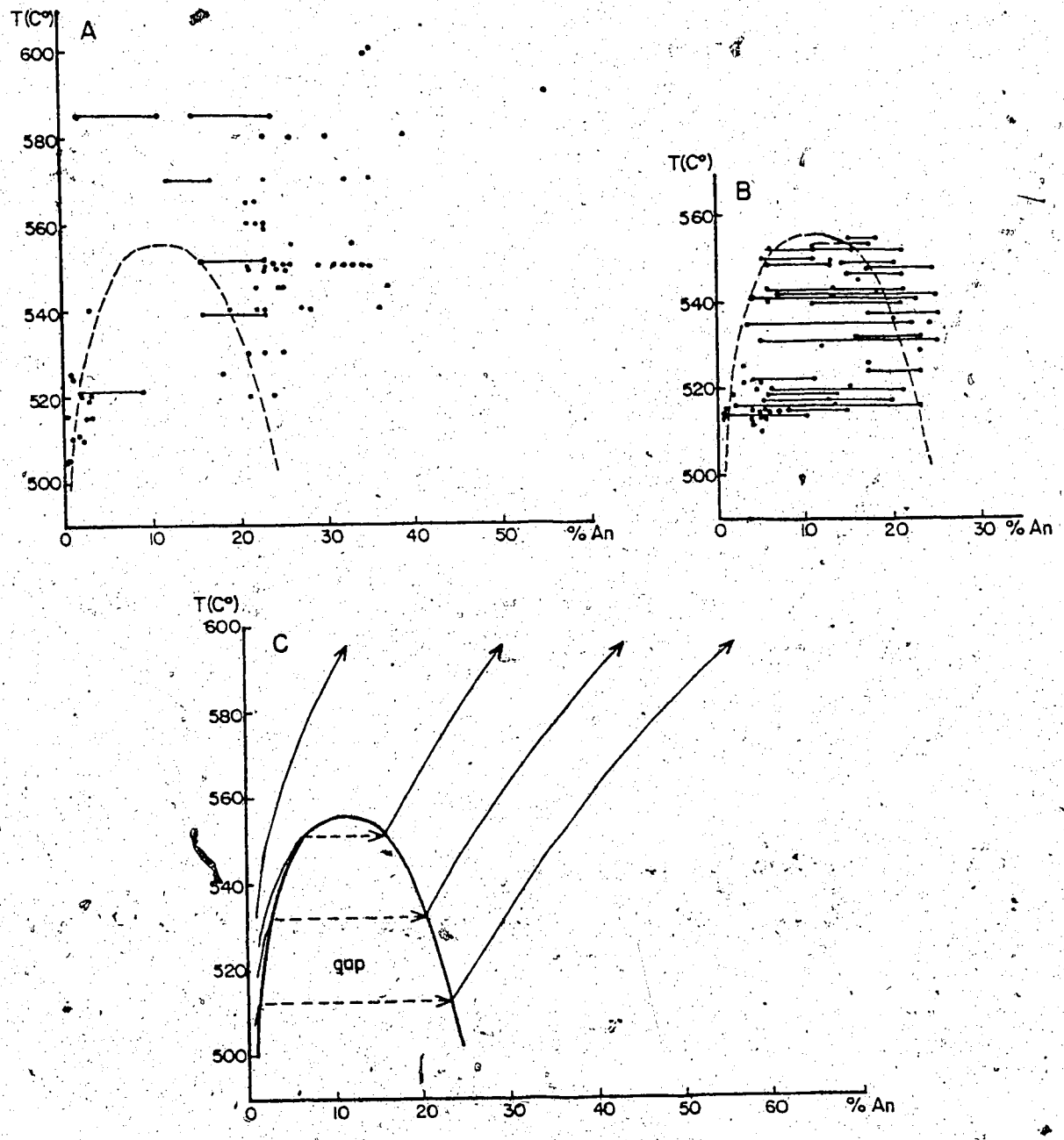

Figure 49. T-X diagrams of plagioclases from metabasites:
A analysed by electron microprobe
B analysed by optical methods
} lines join compositions from one sample
C proposed solvus; arrows indicate composition change with prograde crystallization in various chemical systems.

gher. This could be due to differing P/T regimes of metamorphism. But the garnet-biotite thermometer, applied to analyses reported in Crawford (1966) for the Vermont area, yields temperatures of 550-570°C for samples near the top of the solvus. Accepting Brown's model, one may conclude that the metamorphism in the Wakeham Bay area and in Vermont are of similar P/T regime.

The change in An content is the only chemical change in plagioclase that could be related to metamorphism. The K_2O content is low, shows little variation, and in no systematic manner.

B CALCIFEROUS AMPHIBOLES

Several authors have attempted to relate the chemistry of metamorphic calciferous amphiboles and the temperature-pressure conditions of metamorphism (Shido and Miyashiro, 1959; Engel and Engel, 1962; Fabriès, 1963; Kostyuk and Sobolev, 1969; Bard, 1969; Graham, 1974; Raase, 1974; see also Leake, 1968, and Saxena and Ekström, 1970).

It follows from their studies that systematic changes with increasing grade can be observed in calciferous amphiboles. They are:

1- actinolite -> blue-green hornblende -> green hornblende -> olive-green to brown hornblende;

2- acicular -> long prismatic -> short prismatic habit of

hornblende;

3- Na increases with T and P;

4- K and Ti increase with T;

5- Mn decreases with T;

6- Mg and Fe show little change with T and P; they are controled more by bulk rock composition;

7- $Al^{(4)}$ increases with T;

8- $Al^{(6)}$ increases mainly with P.

The most pronounced changes in hornblende composition occur in the upper amphibolite facies at the transition into the hornblende granulite facies.

In the chapter on mineralogy a compositional gap was demonstrated between actinolite and hornblende coexisting in the same rock.

Figure 50 shows the distribution of actinolite-alone, actinolite + hornblende, and hornblende-alone. Actinolite-alone occurs mainly at low grade; and the limit of its domain corresponds approximately to the 510-520°C isotherm. Hornblende-alone occurs at high grade; and the limit of its domain corresponds approximately to the 540° isotherm. Actinolite + hornblende occur in the intervening area, but also over the whole of the actinolite-alone domain. The small Aphebian basin northwest of Joy Bay contains no metabasites and the hornblendes occurring near it ($T < 540°C$) are in incompletely retrogressed Archean amphibolites.

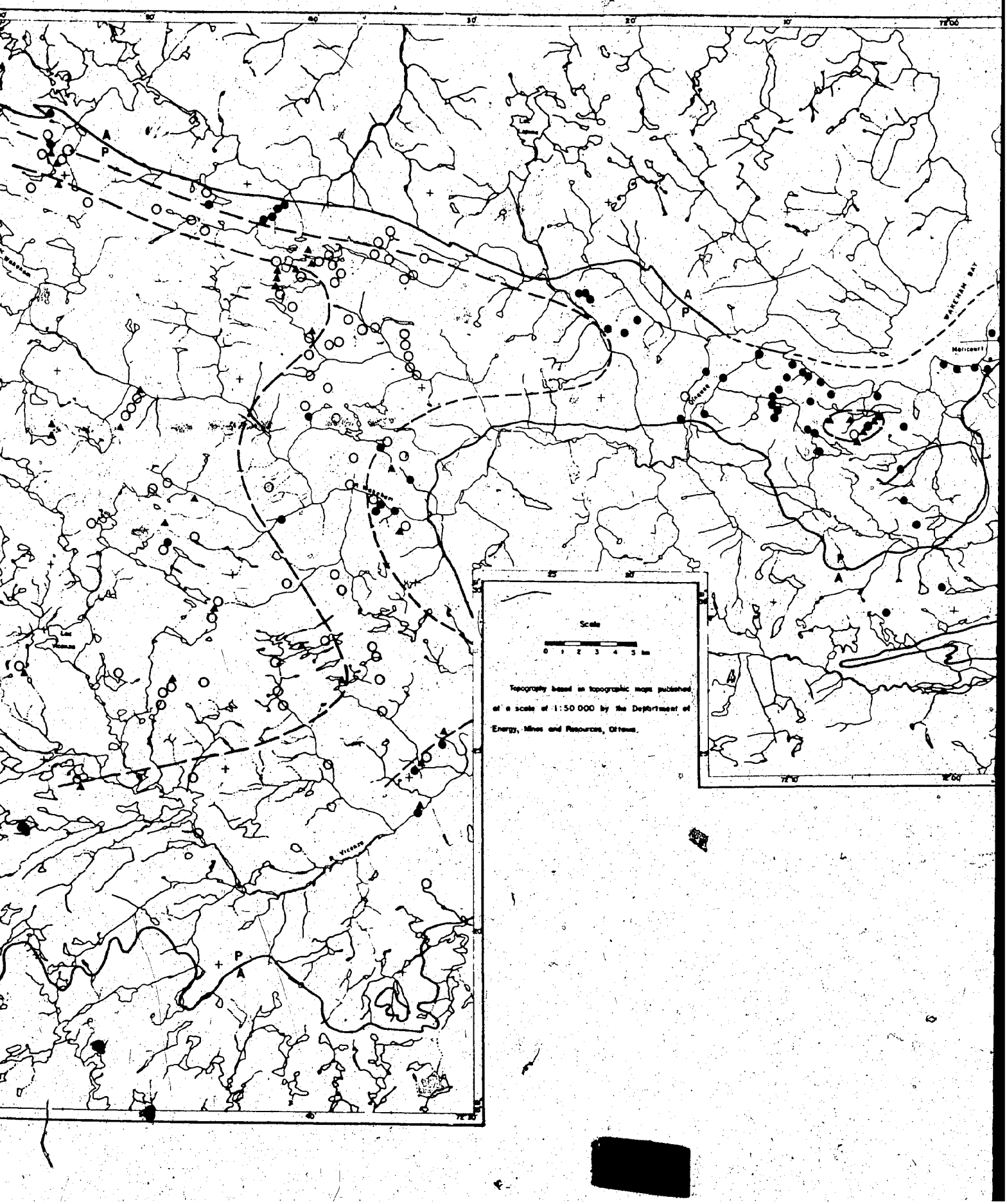
A
P
A
P
A
P
Scale
0 1 2 3 4 5 km
Topography based on topographic maps published at a scale of 1:50 000 by the Department of Energy, Mines and Resources, Ottawa.

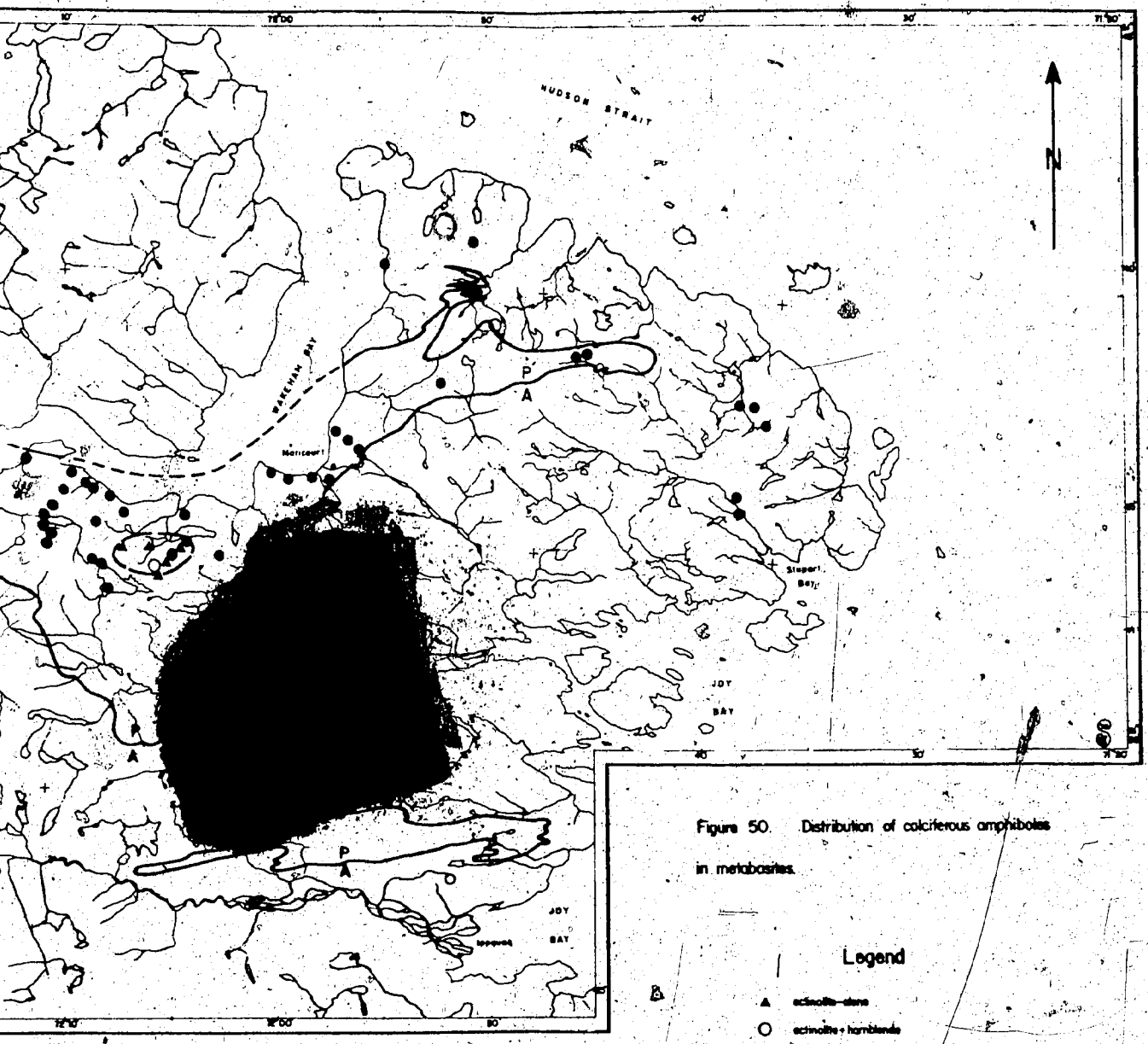

Figure 50. Distribution of calciferous amphiboles in metabasites.

Legend

- ▲ actinolite-alone
- ○ actinolite + hornblende
- ● hornblende-alone
- Limits of the actinolite-alone and of the hornblende-alone domains
- A / P contact between Archean and Aphebian rocks

An attempt has been made to relate the compositional gap to temperature in several T-X diagrams. Figure 51A is based on the Hallimond triangle (Fig. 35) and is a T-X plane through $Tremolite_{100}$ and $Pargasite_{60}$-$Tschermackite_{40}$. Figure 51B shows T versus the sum of the parameters that normally increase with temperature. Figure 51C uses the parameter (Al - (Na+K)) which in Kostyuk and Sobolev (1969) shows the most marked change with temperature. No very clear trend is brought out by this figure. However, taking the domain above 525°C, it is possible to draw a solvus closing somewhere above 580°C. The scatter of the data, especially below 525°C, illustrates well the sluggishness of reactions in amphiboles. The similarity in pattern in those three diagrams shows the interrelation between the various stoichiometric exchanges in the calciferous amphiboles. Figure 52 shows Ti versus T in hornblendes; little or no correlation is present. In the domain of temperature considered no T-X correlation appears within the hornblende group. The Fe-Mg distribution coefficient between actinolite and hornblende was calculated; it shows no relation to temperature.

It may be concluded that within the temperature domain considered (500-600°C) the main change in composition in calciferous amphiboles is from actinolite to hornblende i.e., disregarding the Fe/Mg ratio, from near Tr_{100} to about Pa_{50}-Ts_{30}-Tr_{20}. Although it is spread over a range in temperature, it is a discrete change that can be related to the

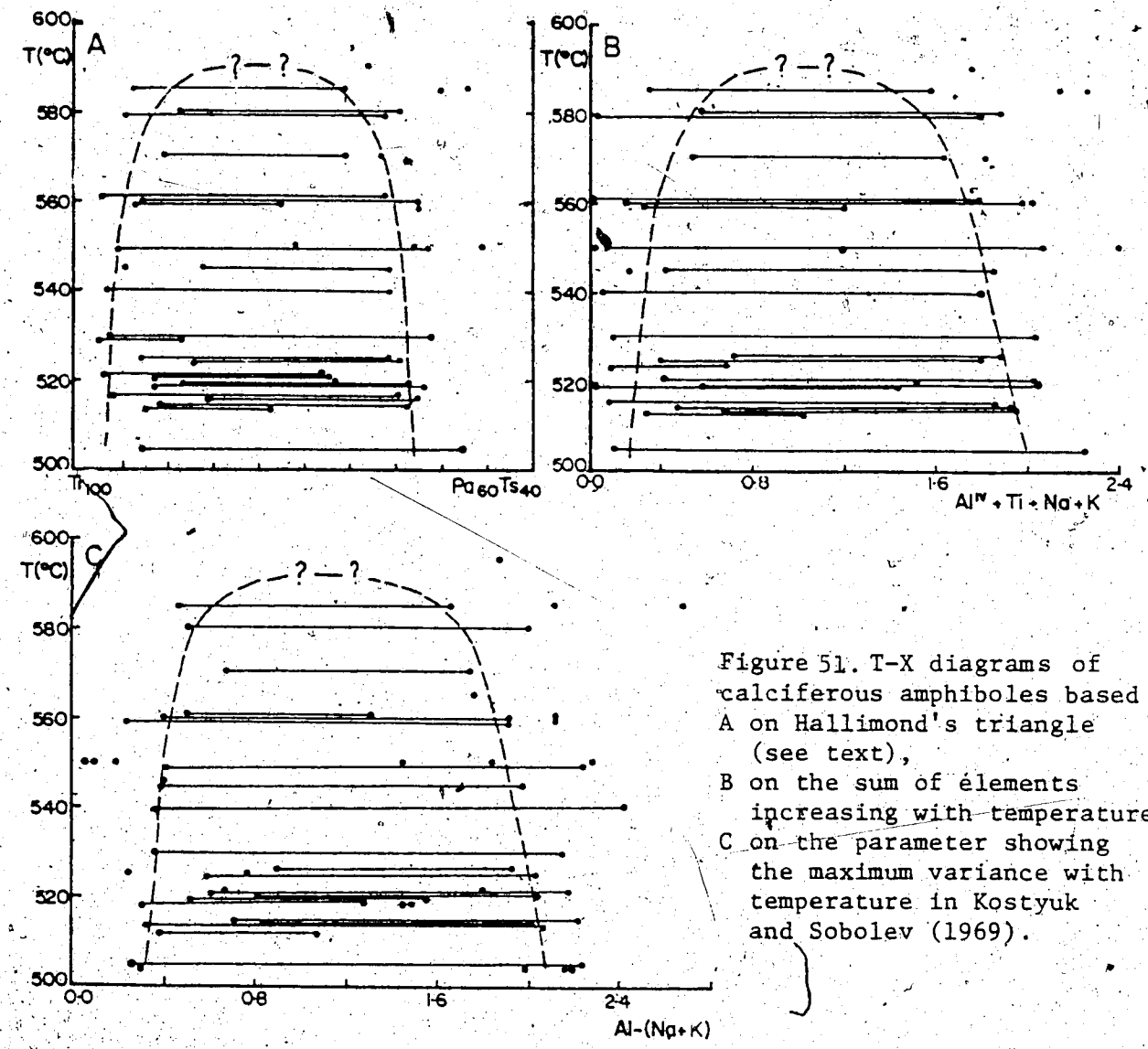

Figure 51. T-X diagrams of calciferous amphiboles based
A on Hallimond's triangle (see text),
B on the sum of elements increasing with temperature,
C on the parameter showing the maximum variance with temperature in Kostyuk and Sobolev (1969).

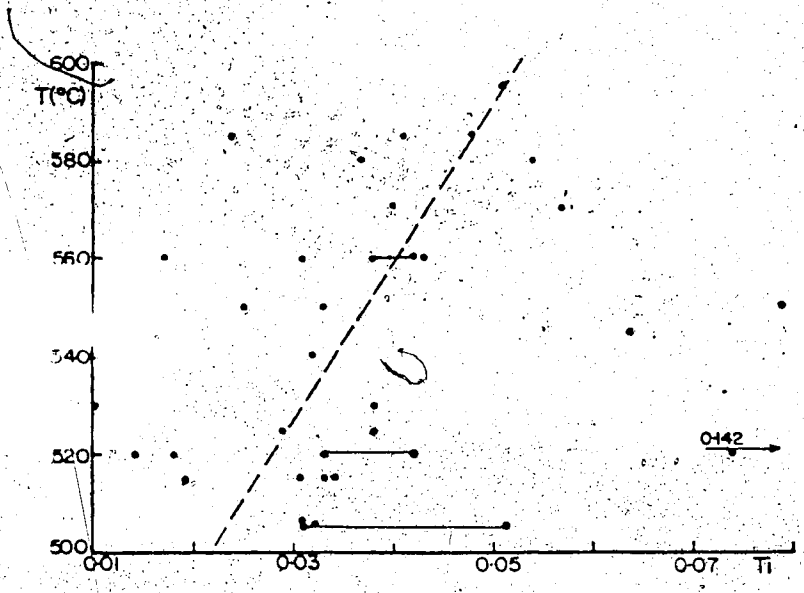

Figure 52. Relation between titanium in hornblendes and temperature.

albite-oligoclase transition in plagioclase, and both constitute the greenschist-amphibolite facies transition.

Once in the amphibolite facies the hornblende appears to vary little, although the paucicity of high grade hornblende analyses may fail to reveal the changes present. Indeed a colour change was observed in thin sections from blue-green to green to olive-green (from low to high grade). This colour change may result from subtle changes in the ratio of Fe^{3+}/Fe^{2+} and/or a slight increase in Ti which may also be partially reduced (to Ti^{3+}).

The change in composition of calciferous amphiboles with metamcrphic grade is hidden by the presence of a compositional gap; it could only become visible by reconstituting the bulk amphibole composition.

C OTHER MINERALS

Epidotes are abundant at low grade, decrease at medium grade, and are almost absent at high grade. This change is illustrated in Figure 53. An 'isograd' may be drawn to delimit the domain in which epidotes constitute normally more than 3% of the metabasite's mode. This 'isograd' corresponds approximately to the 540°C isotherm. Little change in composition was observed with increasing grade (see chapter on mineralogy, Figure 35): epidotes at medium to high grade trend towards clinozoisite. A composi-

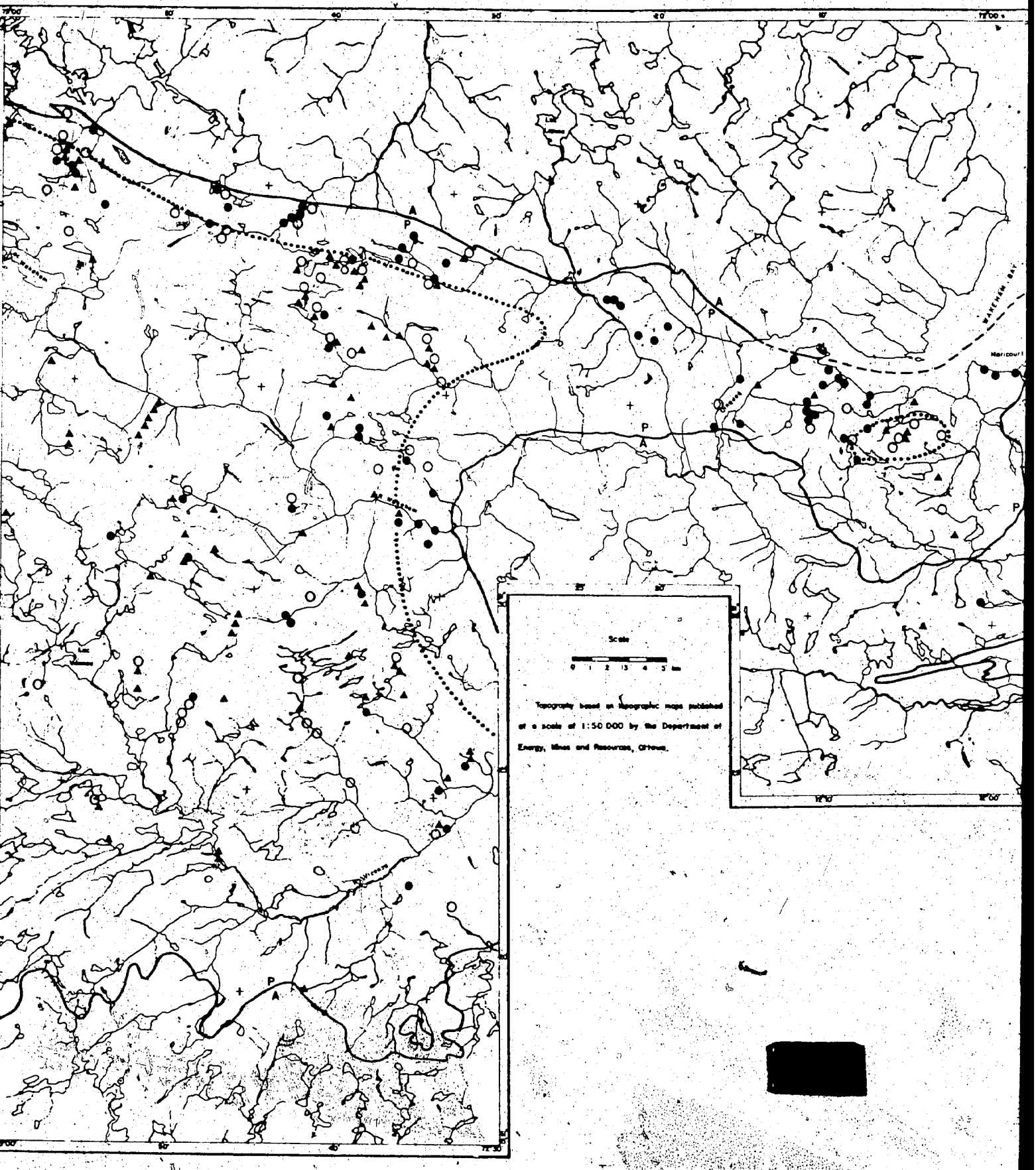
Scale
0 1 2 3 4 5 km
Topography based on topographic maps published at a scale of 1:50 000 by the Department of Energy, Mines and Resources, Ottawa.
WAKEHAM BAY
Maricourt

[redacted]

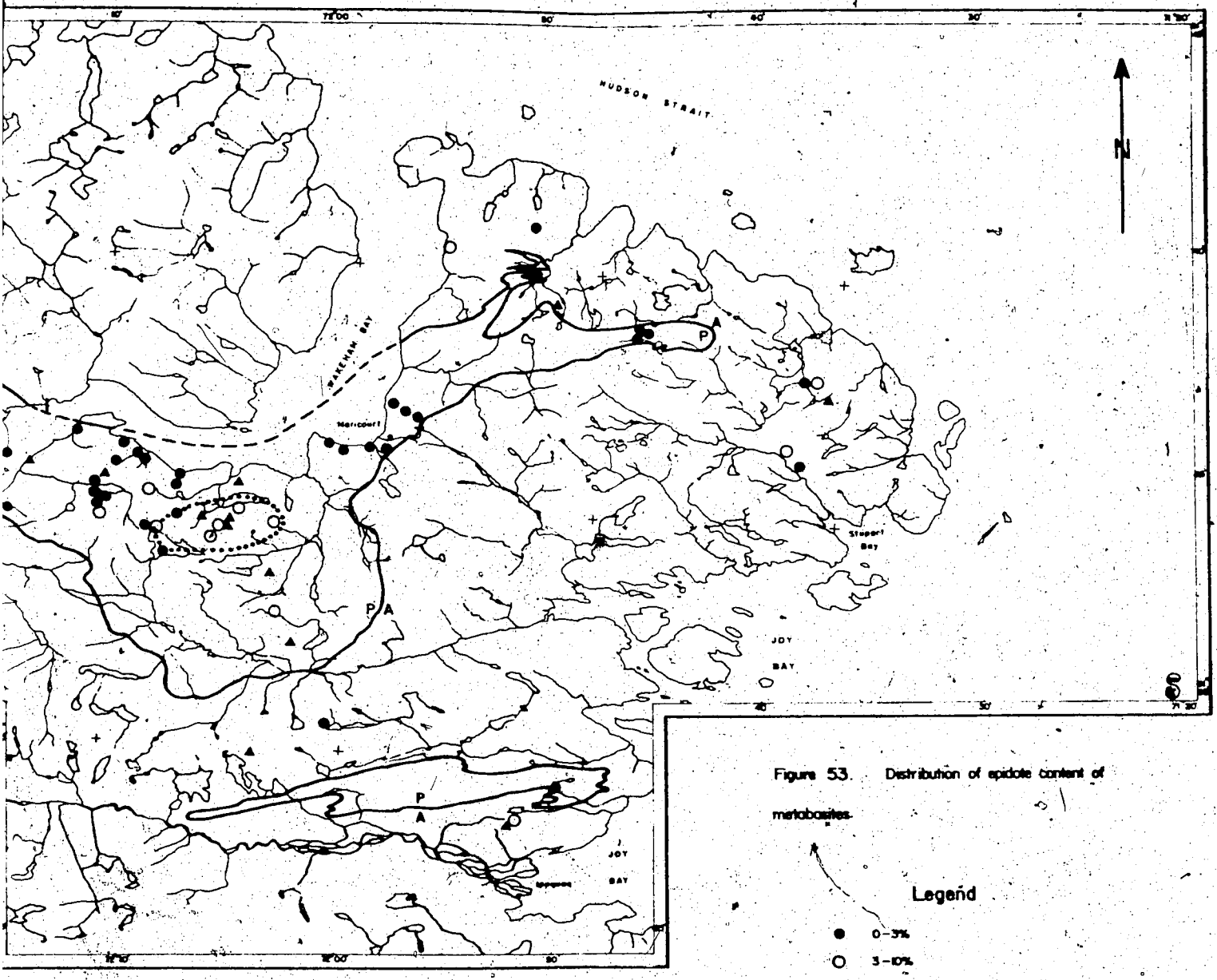

Figure 53. Distribution of epidote content of metabasites.

Legend

- 0-3%
- 3-10%
- >10%
- isograd of epidote >3% in metabasites
- A/P contact between Archean and Aphebian rocks

tional gap may be present but is not a prominent feature.

Chlorites are more abundant at low than at high grade. Figure 54 shows their distribution by modal abundance. Above the 540°C isotherm, they generally constitute less than 1% of the metabasites. The major variation in the composition of chlorite is the Fe/Mg ratio (Fig. 33). No correlation appears between this ratio or the distribution coefficient chlorite-hornblende and temperature. Neither is there any other significant chemical change with increasing grade.

Ilmenites were analysed; they are almost pure $FeTiO_3$ with no Fe_2O_3 in solid solution. Of the minor elements only Mn is present in significant amounts but shows no change with grade. Ilmenite is common only above the oligoclase isograd.

5. CONCLUSIONS

The presence of staurolite and kyanite as well as the sequence of index minerals observed in the Wakeham Bay area (biotite -> hornblende and almandine-garnet -> plagioclase) marks the Hudsonian metamorphism as one of intermediate P/T (Turner, 1968). The sequence is similar to the one produced by the Dalradian (Barrovian) metamorphism of Scotland. The metamorphism in East Otago (N.Z.) is of lower

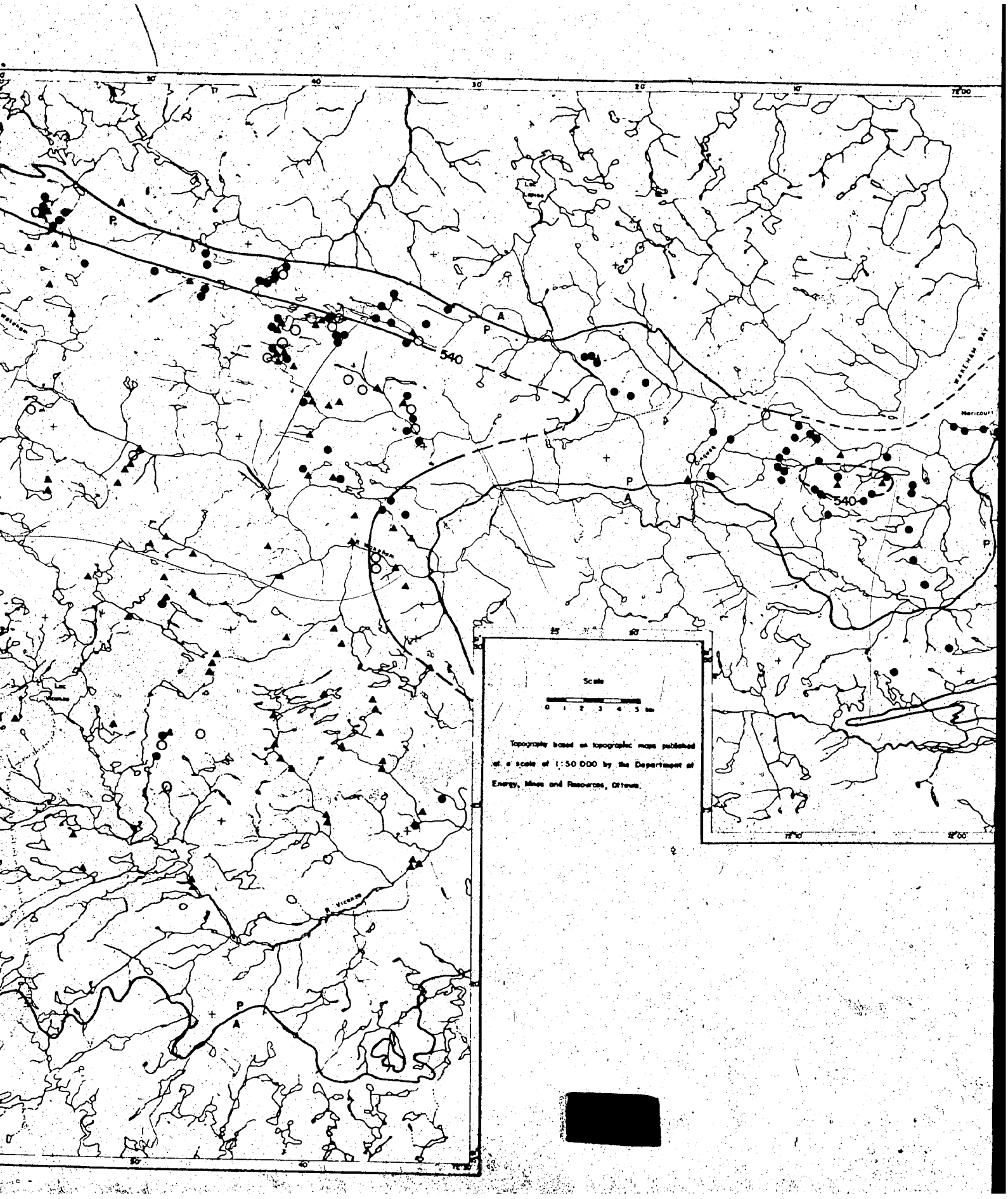
Scale
0 1 2 3 4 5 km
Topography based on topographic maps published at a scale of 1:50 000 by the Department of Energy, Mines and Resources, Ottawa.
540
540
P
A
Wakeham Bay
Maricourt

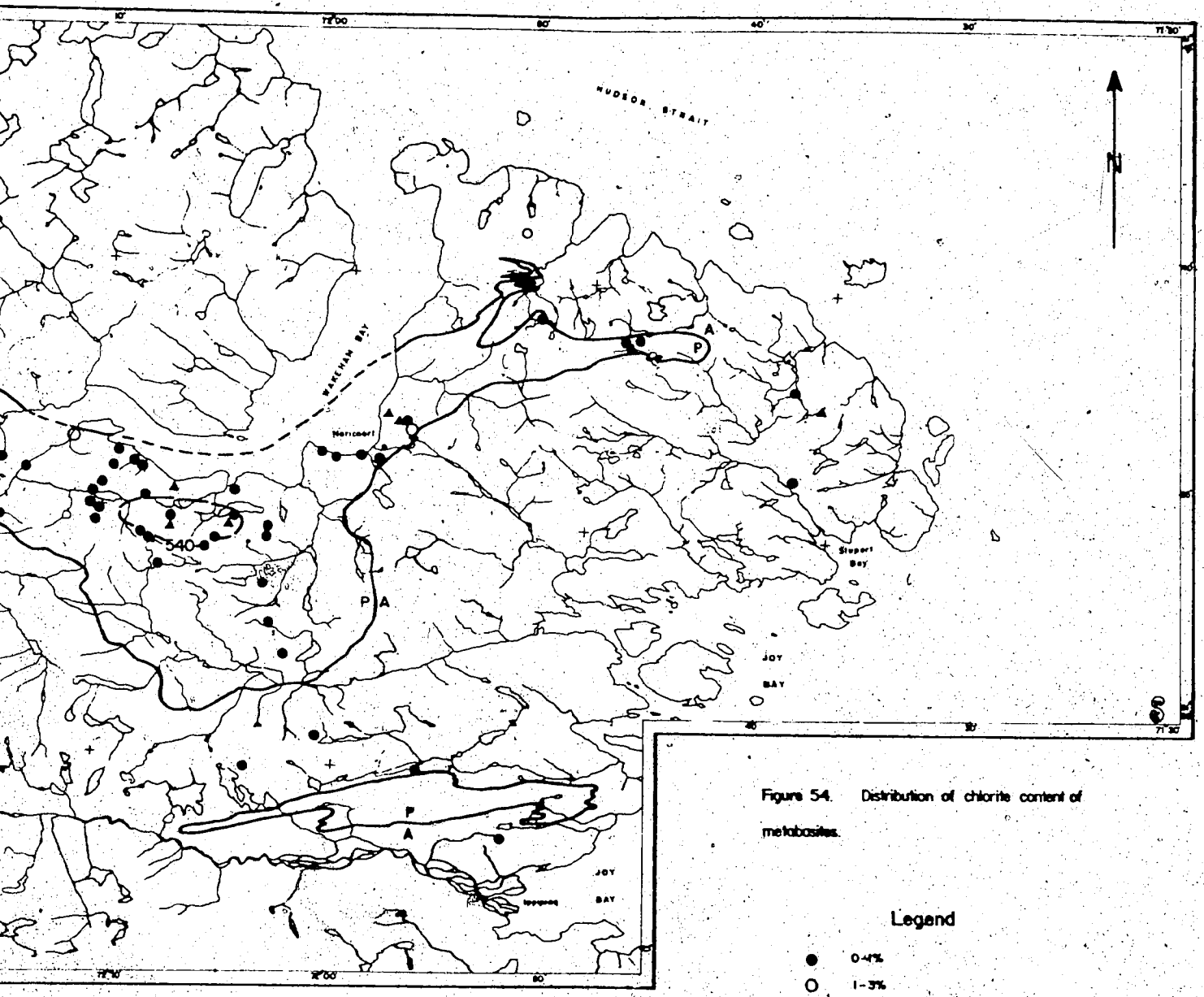

Figure 54. Distribution of chlorite content of metabasites.

Legend

- 0-1%
- 1-3%
- > 3%
- 540° 540° isotherm
- A P contact between Archean and Aphebian rocks

P/T, and the one in Vermont-New-Hampshire (U.S.A.) is a somewhat higher P/T type. This corresponds exactly to the baric type defined using the b_0 of potassic white micas and the scale of Sassi and Scolari (1974). The rarity of cummingtonite in the metabasites of the Wakeham Bay area also indicates an intermediate P/T metamorphism (Fabries, 1963; Bard, 1969). The garnet-biotite geothermometer combined with the plagioclase-garnet-Al_2SiO_5-quartz assemblage yields the following range of metamorphic conditions: 610°C (7.25 Kb) at highest grade, about 500° C (P unkwown) at lowest grade.

Some experimental data from the literature is shown in figure 55. The staurolite occurrences (580-585°C) are well within the staurolite stability domain. Liou et al. (1974) studied the evolution of natural metabasites near the greenschist-amphibolite facies transition. The sequence of events they have determined corresponds well with those described here:

- albite -> oligoclase coinciding with
- actinolite -> hornblende
- decrease, then disappearance of chlorite
- presence of epidote to higher temperature at relatively high pressure (epidote-amphibolite facies)
- incoming of ilmenite.

The temperature range of their transition zone corresponds reasonably well with that of the domain between actinolite-alone and hornblende-alone (Fig. 50).

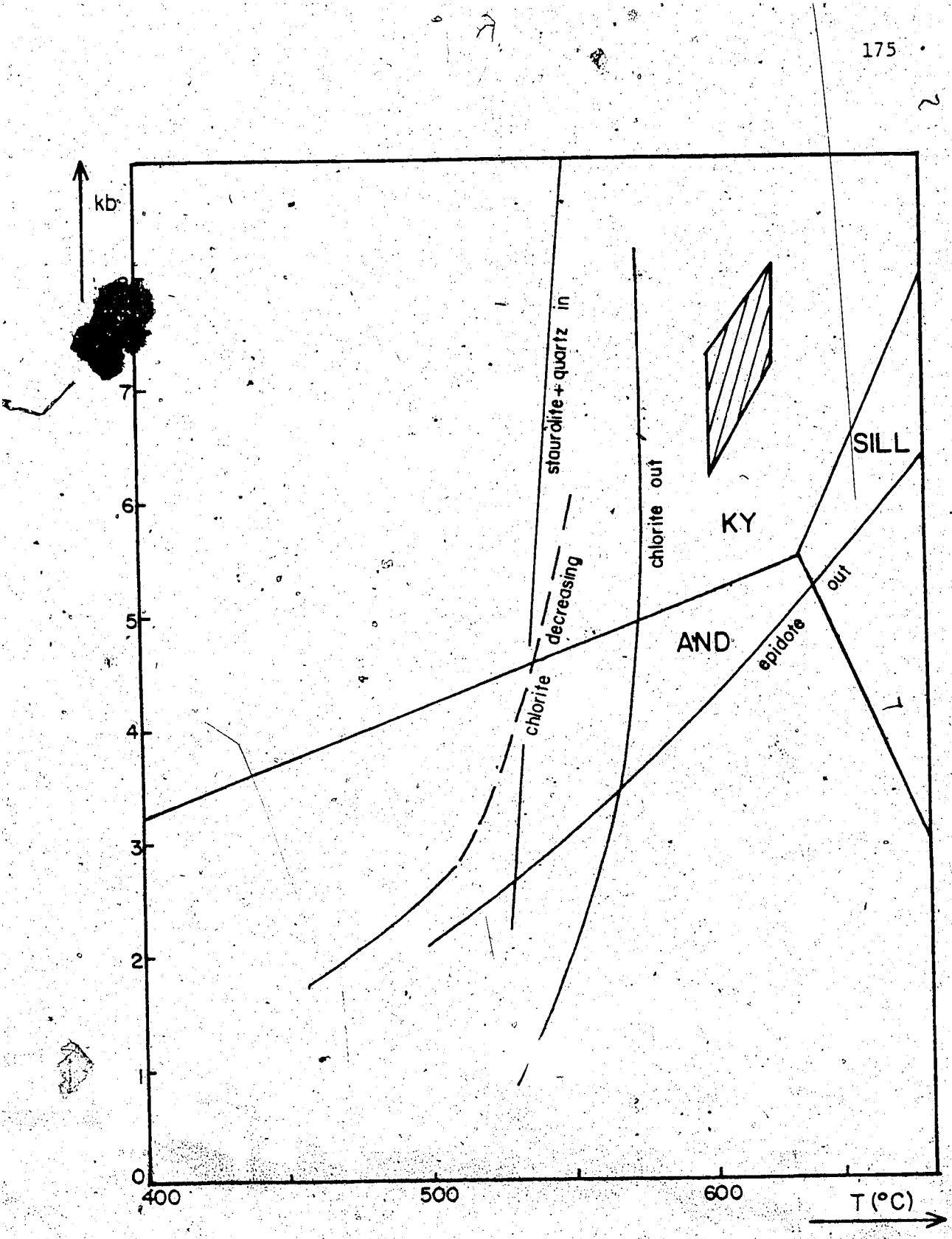

Fig. 55. Experimental data and T-P conditions during the Hudsonian metamorphism. Staurolite - quartz-in curve after Ganguly (1972); stability field of aluminium silicates after Richardson et al. (1969); other curves after Liou et al. (1974); hatched area: conditions of highest grade metamorphism in the Wakeham area.

The major feature in the distribution of isotherms (Fig. 47) is their parallelism with the Aphebian-Archean contact west of 72°W.[1] Away from the contact, although still parallel, the spacing between isotherms increases, i.e. the apparent gradient decreases. Interpolating between the highest grade conditions (7.25 Kb and 610°C) and 0 gives an average gradient of 25°C/km. Taking the spacing in the isotherms between the area just east of Maricourt and Joy Bay produces an angle of about 12° for the isothermal surface (dipping to the south). A similar calculation for the area north of the Monts Lune produces a dip of 60° near the Aphebian-Archean contact, shallowing to 30° away from it; this, assuming a 25°C/km gradient, a steeper gradient would result in shallower dips. In fact, a combination of both, i.e. steeper thermal gradient and steeper isothermal surface, can be postulated.

These phenomena are attributed to a basement effect ('effet de socle' of Fonteilles and Guitard, 1964 and 1968). According to them changes in temperature gradients in metamorphic terrains are due to:

- changes in conductivity (with temperature);
- changes in specific heat;
- changes in heats of reaction.

---

[1] This can also be observed on a broader regional scale (Westra, 1978)

The first two vary little between basement and cover. The last one, however, is quite different. The sum of heats of reaction for a given volume of rock is much larger in the cover where metamorphism is marked by a number of endothermic reactions, dehydration reaction and others. Whereas in the basement, the temperature can rise rapidly and reach a stage of equilibrium, in the cover the rise is slowed down through absorption of heat by metamorphic reactions.

In the eastern most part of the area, the isothermal surfaces between the end of the Aphebian belt (east of Maricourt) and the small basin near Joy Bay have a dip of about 12° (based on a gradient of 25°C/km). North of Monts Lune the isotherms are closely spaced, going from 580 to 520°C within 3-4 km with an increase in spacing towards lower temperature. The gradient is very steep in the zone corresponding to the transition greenschist-amphibolite facies which is a major dehydration step; but less steep at lower temperature, within the greenschist facies. Figure 56 is a model of isothermal surfaces for the Wakeham Bay area.

The deflection of the isotherms along the basement-cover contact illustrates a disequilibrium in the heat flow during metamorphism, disequilibrium which can also be observed in the high variance of amphibole and plagioclase analyses as related to temperature. This disequilibrium and deflection of the isotherms can be indirectly observed in the small difference in b_0 of the potassic white micas from the north and from the south of the western map area,

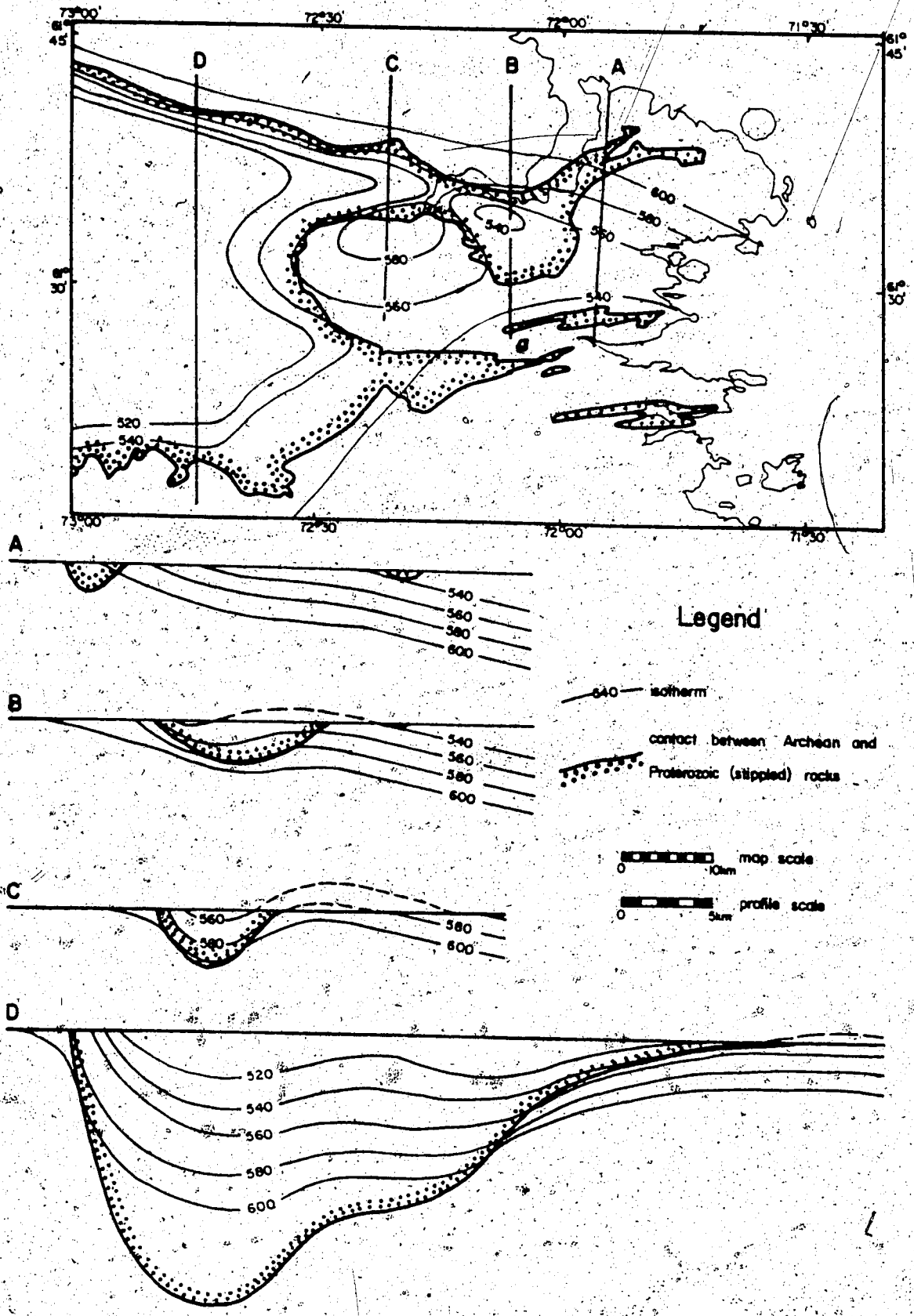

Fig. 56. Model of isothermal surfaces during the peak of Hudsonian metamorphism.

reflecting a slight difference in P/T regime: in the North the Aphebian cover was thick and as a result the temperature gradient was lower in its upper part than in the South where this cover was thinner.

This basement effect may be enhanced in the Monts Lune and in the small low-grade area just south of Wakeham Bay (see Figure 47) by the presence of thick competent sills which resisted penetrative deformation and constituted a barrier to the movement of fluids and, consequently, to the flow of heat.

CHAPTER VII

IGNEOUS PETROLOGY

1. INTRODUCTION

Igneous rocks form the bulk of the Aphebian sequence. They consist of mafic to ultramafic extrusives and high level intrusives (sills). Intermediate to acid rocks are rar Aphebian igneous rocks were subdivided as follows:

Upper Volcanic Group (UVG): tuffs, basalts, gabbroic sills, ultramafic sills, ultramafic lenses and pods.

Lower Volcanic Group (LVG): tuffs, basalts, gabbroic sills, ult amafic sills.

Volcano-Sedimentary Group (VSG): tuffs, basalts, gabbroic sills, ultramafic pods.

Diabase dykes.

All of these rocks have been metamorphosed and primary minerals are rare. Most of those occur in thick

sills where the lack of penetrative deformation has hindered the influx of water and the formation of hydrous (metamorphic) minerals. The observed primary minerals are:

- plagioclase and K-feldspar in some UVG and VSG felsic tuffs;
- olivine in UVG and LVG ultramafic sills;
- orthopyroxene in ultramafic rocks of the three groups;
- clinopyroxene, which is the most common, both in mafic and ultramafic sills (it appears often to have a composition of metamorphic pyroxene; the primary crystal has not been destroyed, it has merely changed its composition);
- kaersutite, in the ultramafic sills and the ultramafic base of gabbroic sills;
- zircon in gabbro sills and, in one case, in the basal part of an ultramafic sill;
- oxides (chromite, spinel, magnetite) and sulphides (pyrrhotite, pentlandite, chalcopyrite), in ultramafic and mafic sills and in basalts.

From these occurences, and from the presence of serpentine pseudomorphs, it it possible to conclude:

1- that in the ultramafic sills, olivine (and minor orthopyroxene) euhedral grains were included in large poekilitic crystals of clinopyroxene and sometimes kaersutite, accompanied by chromite (occasionally spinel), and a Ni-Fe sulphide, that exsolved into pyrrhotite, pentlandite, and chalcopyrite;

2- that in the mafic sills, orthopyroxene probably was absent, kaersutite occasionally present, and that clinopyroxene and plagioclase were the main minerals, with quartz as a phenocryst in some rocks;

3- that no information is available on the primary minerals of the extrusive rocks.

A study of the evolution of these rocks must thus be based on chemical analyses, of which 66 were made (Appendix IV). In addition, analyses are available from areas further west in the Cape Smith Belt: Shepherd (1957); Wilson et al. (1969); Moore (1977); Schwarcz and Fujiwara (1977). The first two are from stratigraphic equivalents of the Upper Volcanic Group, the latter two of both the Upper and the Lower Volcanic Groups. Rocks of the Wakeham Bay area are metamorphosed and there is no certitude that this metamorphism was isochemical. Chemical migrations must have been small for distinct igneous trends are recognizable in the variation diagrams below. However, some chemical exchanges did occur during metamorphism as revealed by the scatter in the trends. Analyses from other areas in the Cape Smith Belt are from less metamorphosed rocks.

2. MAJOR ELEMENT CHEMISTRY

Norm calculation and classification according to the scheme of Irvine and Baragar (1977) show these rocks to be mainly tholeiitic. This is clearly visible on an AFM diagram (Fig. 57); very few analyses plot in the calc-alkaline field; only the UVG tuffs with two analyses from Moore (1977) show a distinct calc-alkaline trend, similar to the trend of Cascades rocks (from Irvine and Baragar, 1971). The other rocks form a distinct tholeiitic trend.

The Cape Smith Belt is generally considered part of the Circum-Ungava Fold Belt with the Labrador Trough to the South-East and the Belcher Islands to the South-West; this fold belt can be extended to include the Thompson Belt in Manitoba. Both the Labrador Trough and the Thompson Belt contain abundant volcanic rocks. The Labrador Trough contains mostly mafic volcanics with some ultramafic sills; the Thompson Belt, mafic as well as abundant ultramafic rocks, and in that it resembles more the Cape Smith Belt. The Labrador Trough (Dimroth *et al.* 1970) and the Thompson Belt (Stephenson, 1974) volcanics both show a tholeiitic trend. However, unlike the Labrador Trough, both the Thompson Belt and the Cape Smith Belt trends extend into very magnesian compositions along the FM side and are on the whole less alkali-rich. In addition, they present a calc-alkaline trend that appears to be absent in the Labrador Trough.

In the Labrador Trough ultramafic rocks occur only

T UVG tuffs
X VSG tuffs
▲ UVG basalts
● UVG ultramafic sills } includes analyses from Shepherd (1959) and Wilson et al. (1969)
■ UVG gabbros
• Komatiites
□ LVG and VSG gabbros
△ LVG basalts
▼ Lower sequence } Schwarcz and Fujiwara (1977)
▽ Upper sequence
○ Moore (1977)

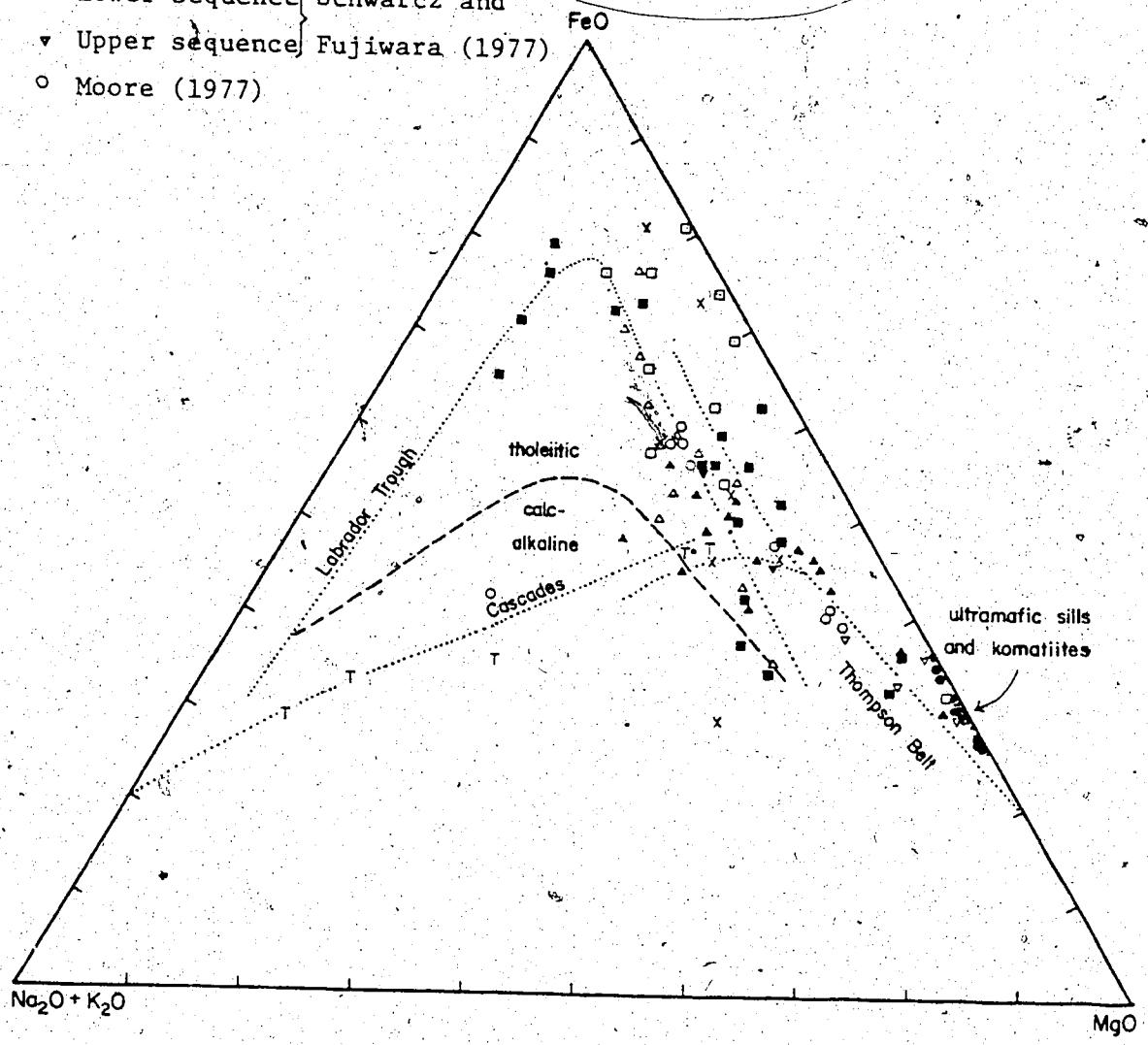

Figure 57. Analyses of Cape Smith Belt igneous rocks in the $Na_2O + K_2O$ -FeO* - MgO (weight percent triangle.

as thick differentiated sills along the eastern border in its south central part. In the Wakeham Bay area three types of ultramafic rocks have been observed:

1- a persistent string of pods no more than a few tens of metres thick, associated with basic volcanics (tuffs and some flows) in the Volcano-Sedimentary Group below the dolomite horizon; they have a composition of pyroxenite or olivine websterite (Fig. 58);

2- thick (up to 250 m) differentiated sills that occur mainly in the Upper Volcanic Group, but also in the Lower Volcanic Group; they are often above or below gabbro sills, but do not constitute their cumulate phase: they are distinctly different sills of lherzolitic bulk composition (Fig. 58); their central part may be occupied by an olivine-rich layer, mapped in the field as peridotite (the remainder as pyroxenite), of restricted lateral continuity; this layer appears to be the result of flowage differentiation (Bhattacharji, 1967);

3- lenses and layers in the Upper Volcanic Group, interlayered with basalts; they occasionally display polyhedral jointing; the presence of a 'bread-crust' structure on the upper surface of one layer, the top-to-bottom differentiation of this layer (unlike the sills), and the cylic alternation of some of these layers with basalts, suggest that these are extrusive.

This abundance of ultramafic rocks and the fact

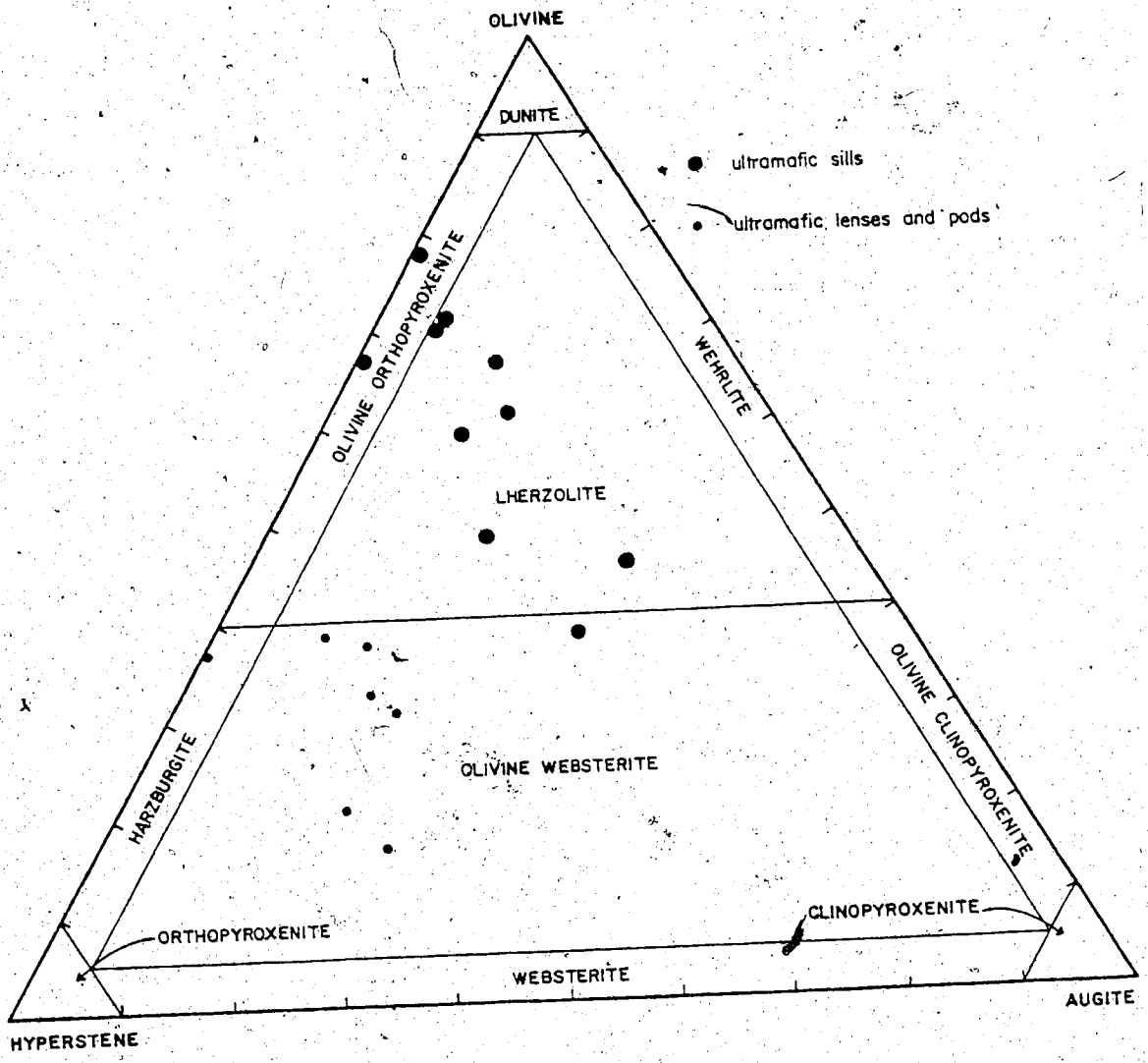

Figure 58. Analyses of Cape Smith Belt ultramafic rocks in the normative olivine-hypersthene-augite triangle.

that some are extrusive makes the Cape Smith Belt volcanics more akin to those of Archean greenstone belts than those of the Labrador Trough. Indeed ultramafic flows, called komatiites (Viljoen and Viljoen, 1969) are characteristic of Archean greenstone belts (for example the Abitibi Belt of Ontario and Quebec, the Barberton Mountain Land of South Africa, the Eastern Goldfields Province of Western Australia); they are often associated with Ni-Cu deposits similar to those of the Cape Smith or the Thompson Belt. Komatiites are characterized by unusual quench textures called spinifex texture (Nesbitt, 1971), by polyhedral jointing, and by their chemistry: high MgO, NiO, Cr_2O_3, low FeO*/(FeO*+MgO)[1] ratio, low TiO_2 and K_2O, and sometimes high CaO/Al_2O_3 ratio (Arndt et al., 1977).

In the Wakeham Bay area, no spinifex textures were observed in the third group of ultramafic rocks, owing to their original absence or to their destruction by metamorphic recrystallization; only chemistry can be used to compare them with komatiites. Schwarcz and Fujiwara (1977) describe quench textures in ultramafic rocks of the western end of the Cape Smith Belt. Figure 59 is a $CaO-MgO-Al_2O_3$ diagram for Cape Smith Belt analyses. They show a trend similar to those of the Abitibi and West Australia komatiites and to the Thompson Belt analyses; South African komatiites show a trend nearer the CaO-MgO side (higher CaO/Al_2O_3

---

[1] FeO* stands for total iron as FeO

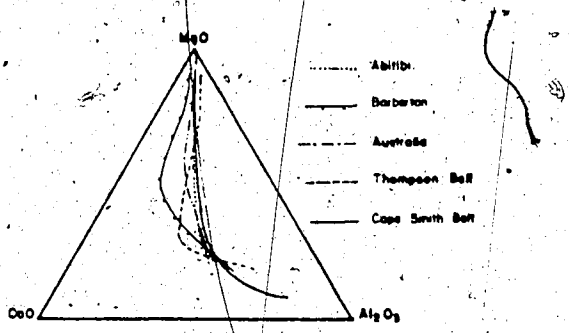

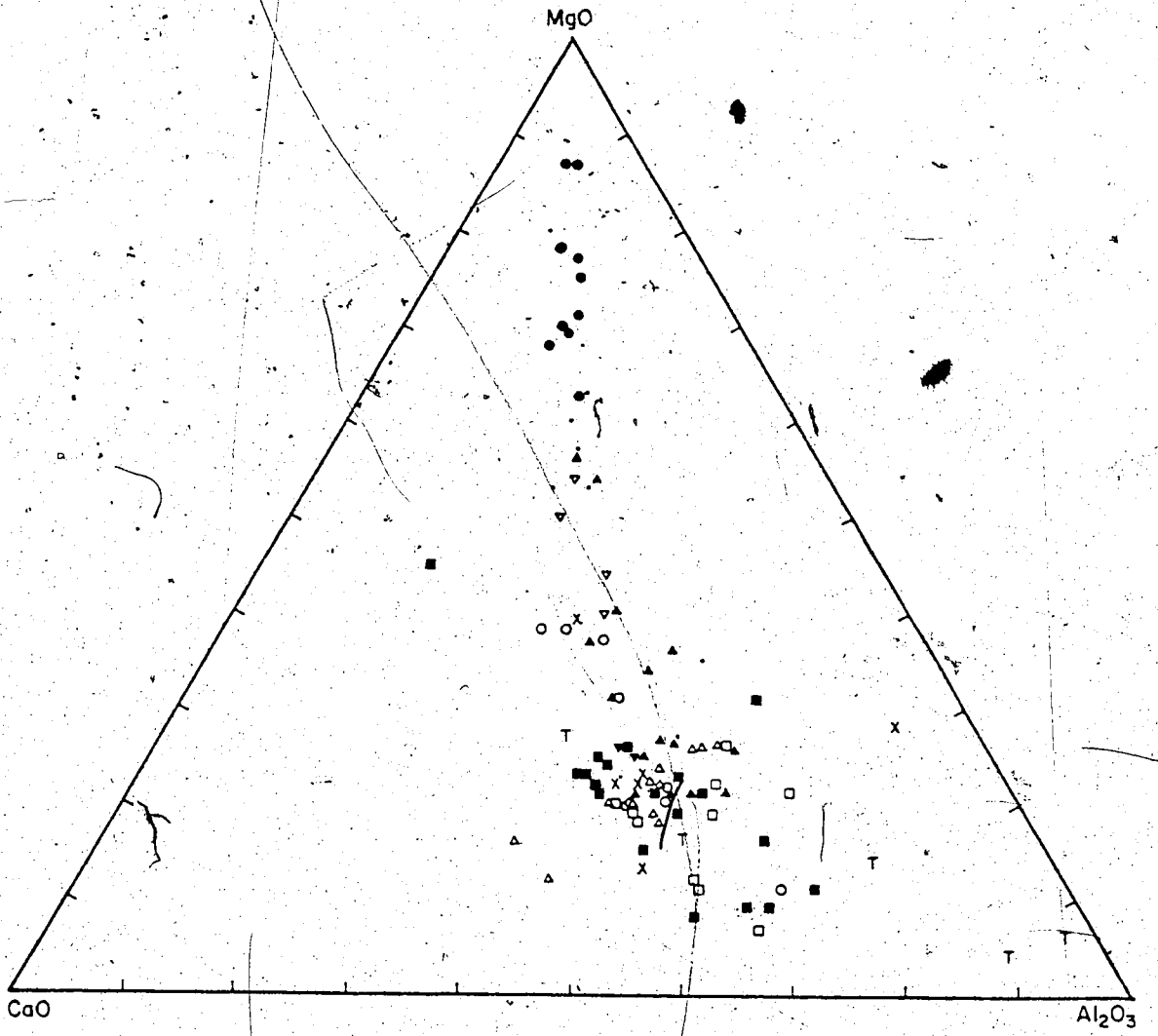

Figure 59. Analyses of Cape Smith Belt igneous rocks in the CaO - MgO - Al_2O_3 triangle. Same symbols as figure 57. Inset is a compilation of trends from various greenstone belts (Source of data: see text).

ratio). The vertical trend from the MgO corner to the centre of the triangle corresponds to olivine (+ orthopyroxene?) fractionation; it contains the ultramafic sills, the komatiites (UVG ultramafic lenses and some analyses from Schwarcz and Fujiwara, 1977), and, at its lower end, the komatiitic basalt (UVG basalts and some analyses from Moore, 1977, and from Schwarcz and Fujiwara, 1977). The inflection towards the Al_2O_3 corner corresponds to fractionation of olivine + clinopyroxene (+ orthopyroxene?); it contains the tholeiitic basalts and gabbro and the calc-alkaline rocks.

In Archean greenstone belts, komatiites are associated with tholeiitic, sometimes with calc-alkaline rocks. The three trends are best illustrated in a FeO versus MgO diagram (Jolly, 1975) Figure 60A shows the Cape Smith analyses in such a diagram; three trends are recognized that depart from a common point at about 8%[1] MgO, 11% FeO:

1- strong Mg enrichment at near constant Fe (magnesian series);

2- Fe enrichment with slight Mg decrease, followed by Fe and Mg decrease (tholeiitic series);

3- Fe and Mg depletion (calc-alkaline series).

The magnesian series comprises the ultramafic sills, the komatiites and komatiitic basalts. The tholeiitic series comprises the LVG and VSG basalts and gabbros, and

---

[1] weight percent, unless otherwise indicated

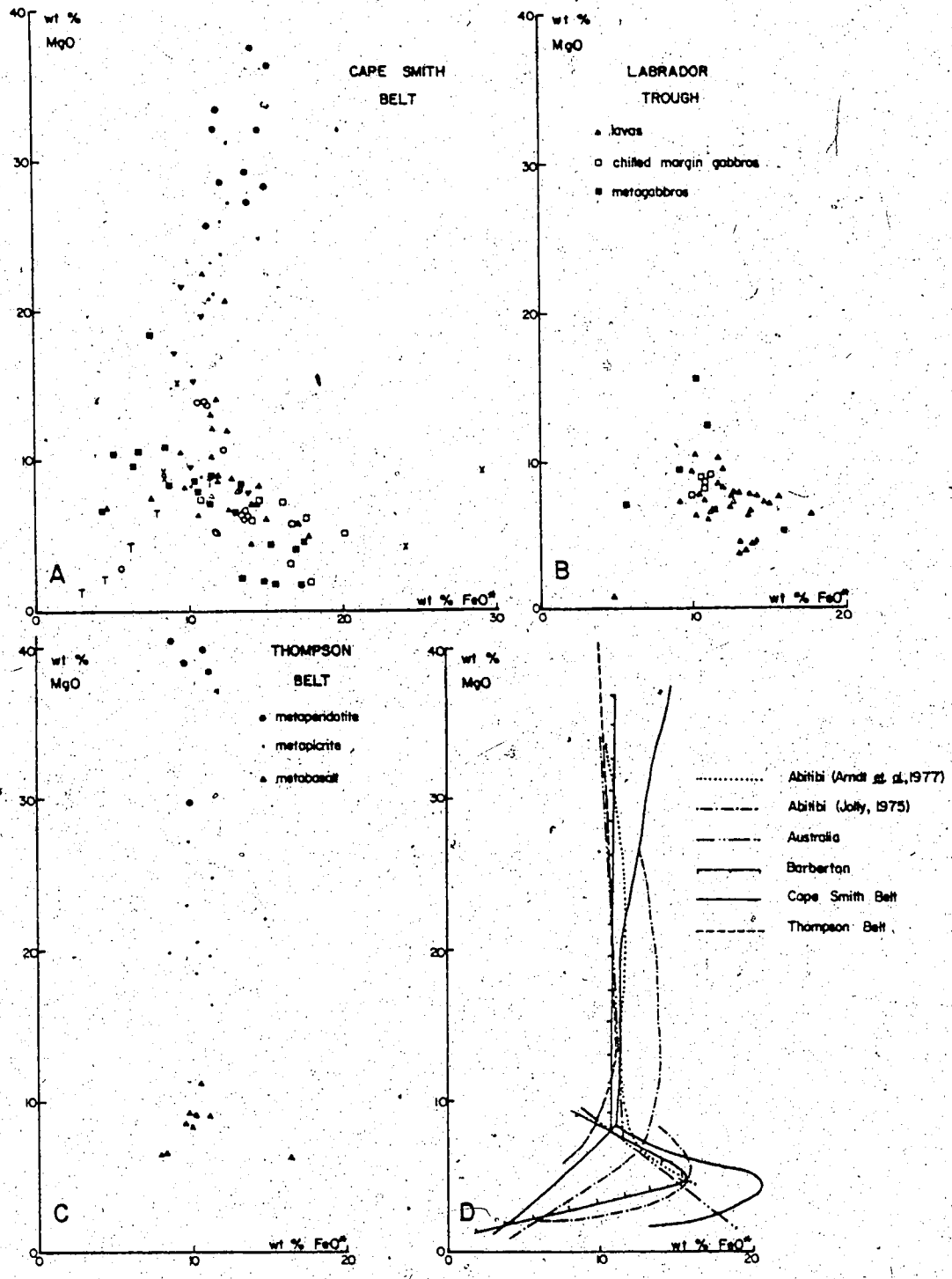

Figure 60. FeO*-MgO diagram for
A analyses from the Cape Smith Belt (symbols as in figure 57.),
B analyses from the Labrador Trough,
C analyses from the Thompson Belt,
D a compilation of trends in various greenstone belts (Source of data: see text).

the UVG gabbros, the calc-alkaline series, the UVG tuffs. The analyses of Moore (1977) correspond to rocks from the three series, those of Schwarcz and Fujiwara (1977) to the tholeiitic and the magnesian series. At the low FeO end of the tholeiitic trend, a few analyses show a wide MgO scatter; these may correspond to cumulates of gabbro. Figures 60B and C are FeO versus MgO plots of Labrador Trough and Thompson Belt analyses. In the Labrador Trough only a tholeiitic trend and, maybe, a calc-alkaline trend, are present; the scatter at the low-FeO end of the Labrador Trough tholeiitic trend is again attributed to cumulates in gabbro. In the Thompson Belt very distinct magnesian and tholeiitic trends are present; two analyses show a calc-alkaline tendency (compare the AFM diagram, Fig. 57). Figure 60D is a compilation of analyses from various areas with high-magnesium volcanism. It illustrates well the similarity of the Cape Smith Belt volcanism to that of Archean greenstone belts. The calc-alkaline series is abundant in the Abitibi only. In other areas it is subdued or absent. This may in part be due to lack of information; in Western Australia, for example, abundant felsic rocks accompany the mafic and ultramafic volcanism (Naldrett and Turner, 1977) and may represent a calc-alkaline trend.

Komatiites are distinguished from tholeiites not only on the basis of their Mg enrichment. The CaO/Al_2O_3 ratio was stressed by Viljoen and Viljoen (1969), but found less critical in the Abitibi greenstone belt (Arndt et al.,

1977). Indeed the inset of Figure 59 shows that this ratio is distinctly higher than 1 only for Barberton Mountain Land analyses. Figure 61 is a plot of Cape Smith Belt analyses; they have been subdivided into magnesian, tholeiitic, calc-alkaline and undefined on the basis of Figure 60. The magnesian series follows the $CaO/Al_2O_3 = 1$ line up to CaO = 10%; above that the scatter increases and the ratio decreases. The tholeiitic series shows a broad scatter, covering the field of the undefined analyses and together with the calc-alkaline series ($CaO/Al_2O_3 < 0.6$) delineates a broad cross-trend of constant ($CaO+Al_2O_3$). Indeed the sum $CaO+Al_2O_3 = 22.5$ appears as useful for distinguishing komatiites from tholeiites as a CaO/Al_2O_3 ratio.

Arndt et al. (1977) proposed an Al_2O_3 versus $FeO/(FeO+MgO)$ diagram to distinguish komatiites from tholeiites. Figure 62 is such a plot for the Cape Smith Belt analyses. The majority of the magnesian series falls in the komatiite field whereas the tholeiites and calc-alkaline series show a broad spread at right angle and overlap the aluminous end of the komatiite fields; this trend is similar to the Australian tholeiites. The group of undefined falls within or near the aluminous end of the komatiite field.

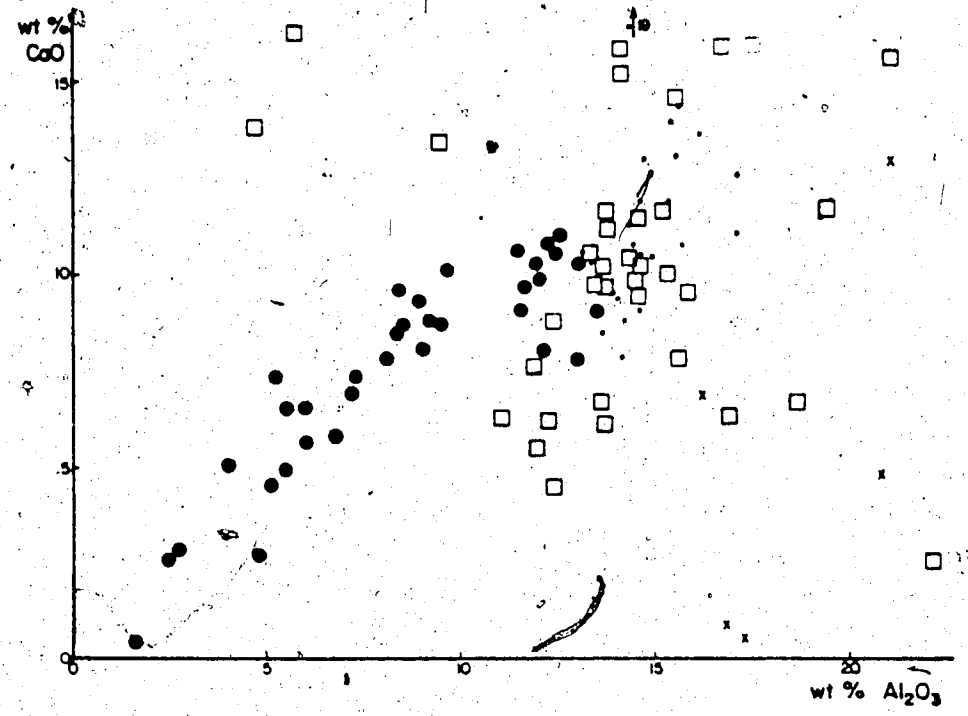

Figure 61. CaO-Al_2O_3 diagram for Cape Smith Belt analyses.

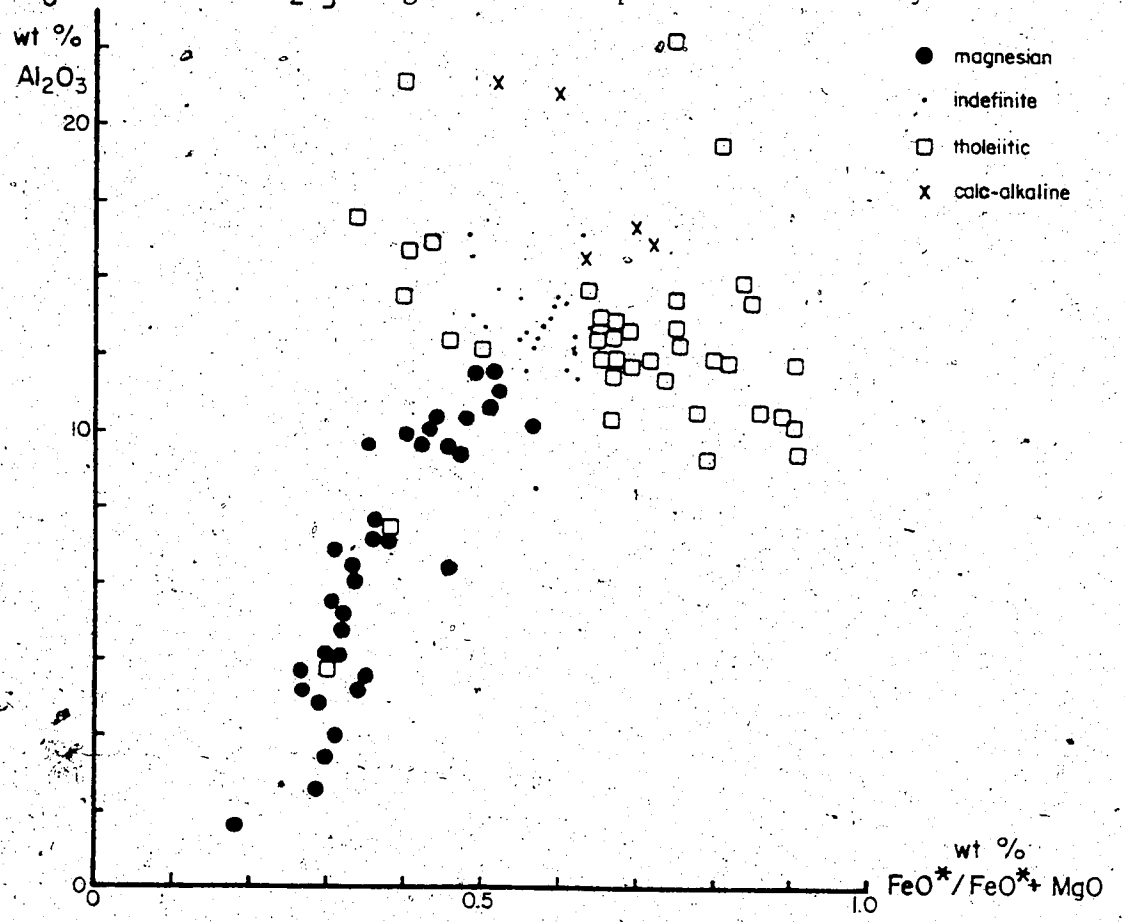

Figure 62. Al_2O_3-FeO*/(FeO*-MgO) diagram for Cape Smith Belt analyses.

3. MINOR ELEMENT CHEMISTRY

Discussion of the minor elements shown in the table of analyses in Appendix IV is hampered by the high detection limit (0.03 wt% element) and low accuracy when nearing this limit. The magnesian series is characterized by low TiO_2 (< 0.8%), K_2O (< 0.2 wt%)[1], and Na_2O, and high Cr_2O_3 and NiO. The Cr_2O_3 content varies from 1300 ppm in the basalts, to 3200 ppm in the ultramafic lenses (komatiites), and to 5800 ppm in the ultramafic sills whereas NiO is respectively < 300 ppm, 1200 ppm, and 1900 ppm.

The tholeiitic series is characterized by higher TiO_2 (about 2%), K_2O (about 0.4%), and Na_2O (1.0-2.5%); the other minor elements are mostly below detection limit. MnO shows little variation in the tholeiitic as well as in the magnesian series.

The analyses in Shepherd (1959), Wilson *et al.* (1969), Moore (1977), and Schwarcz and Fujiwara (1977) show a similar behaviour for the minor elements indicated. Wilson *et al.* (1969) show more accurate analyses for Ni, Cu, Co, and Zn. Ni and Cu reach very high levels in the ultramafic sill, which is mineralized; Co is about 150 ppm and Zn about 50 ppm. In the komatiitic basalts and komatiites, Ni is around 900 ppm, Cu around 100 ppm, Co around 80 ppm, and Zn

---

[1] sample 334 has an abnormaly high K_2O and is disregarded here

around 80 ppm.

The UVG gabbro sill is somewhat unusual for, despite a typical tholeiitic major element chemistry, it has low Ti and K.

4. PETROGENESIS

From the major element chemistry, three trends can be recognized in the Cape Smith Belt volcanics: a magnesian (komatiitic), a tholeiitic, and a calc-alkaline trend. The latter represents only a small part of the volcanic rocks now present and appears restricted to the upper part of the sequence. The magnesian trend although present in the lower part, becomes abundant only in the higher part of the sequence. The tholeiitic trend occurs throughout and represents the bulk of the volcanism. The magnesian series has a primitive composition, close to proposed mantle compositions, and has a low content in the incompatible elements (Ringwood, 1966) Ti and K. The tholeiitic series has a less primitive composition and higher content of incompatible elements; its composition is closer to oceanic tholeiites than continental tholeiites.

Komatiites are common only in Archean greenstone belts; they have been described in South Africa, Rhodesia, Canada, Australia, and India (Arndt et al., 1977); in South

Africa and Australia, they are associated with tholeiitic volcanism, in Canada (Abitibi) with tholeiitic and calc-alkaline volcanism. In these three regions significant amounts of felsic volcanics are present in the sequence. Some examples of high magnesian volcanics are known from younger terranes: in the South African Ventersdrop (2.3 b.y.) and Karoo (150-200 m.y.) volcanics (McIver, 1975), in the Aphebian Thompson Belt of Manitoba (Stephenson, 1974), in the lower Paleozoic Rambler Group of Newfoundland (Gale, 1973), in the Tertiary basalts of Baffin Bay (Clarke, 1970), in the Upper Cretaceous of Cyprus (Searle and Vokes, 1969). The Phanerozoic occurrences are either in a tensional continental environment (Baffin Bay and Karoo) and have higher Ti, some also higher K, than komatiites, or in a mid-oceanic ridge environment (Newfoundland and Cyprus) and have a primitive composition.

Tholeiitic and calc-alkaline extrusives constitute the major part of the Phanerozoic volcanism and their origin is relatively well understood, particularly in the light of present day global tectonic models. High magnesian, komatiitic, extrusives, because their major development took place at a time where these models may not apply, present a different problem.

Owing to the metamorphic (recrystallized) nature of the rocks in the Wakeham Bay area and the lack of detailed information on the other analyses of the Cape Smith Belt, it is not possible to define here, with certainty, the

compositional range of the extruding magmas, before their modification by igneous fractionation after extrusion or near surface intrusion. Indeed, because of the very low viscosity of these ultramafic liquids, significant differentiation can occur even in relatively thin flows. However, the similarity of their overall range of composition with that of volcanic rocks from less metamorphosed and/or better studied areas (Abitibi, South Africa, Western Australia, Baffin Bay) enables ones to use the compositions deduced there in petrogenic considerations.

A model for the genesis of komatiites must explain the extrusion of magmas with 33% or more MgO (about 50% normative olivine), i.e. magmas having an extrusion temperature of about 1650°C (Green, 1974). Factors to consider are:

1- composition of the komatiitic magma; in addition to high Mg, it has high Cr and Ni, but low Ti and K;
2- decrease in abundance with time; high magnesian magmas younger than the early Proterozoic are rare and tend to have somewhat lower Mg;
3- except for some of the Phanerozoic examples, they are ensialic, i.e. they are extruded onto a sialic crust;
4- the association with tholeiitic, and sometimes calc-alkaline volcanism and the common presence of significant amounts of felsic volcanics;
5- komatiites can be in various positions in the volcanic pile, but there may be a tendency for them to be near the base in older sequences.

Based on some of the above factors, various models have been proposed for the formation of komatiites:

1- Viljoen and Viljoen (1969): partial melting beneath a thin Archean eo-crust with a high geothermal gradient.

2- Clarke (1970): partial melting of garnet peridotite at 30 kb followed by olivine and eclogite fractionation.

3- McCall et al. (1971, p.284): "Remelting of deep-level cumulates" or "differentiates of the tholeiites by the agency of some as yet not understood mechanism, operative in depth...".

4- McIver and Lenthall (1974, p.327): "partial melting of a four phase eclogite mantle at depths of 90-100 km or more. Polybaric olivine and orthopyroxene fractionation were important in controlling the development of mafic and ultramafic komatiite-type extrusives and associated tholeiitic basalts..."

5- Green (1974, p.15): "...extrusion temperature (1650°±20°C) .... implies diapirism of upper mantle peridotite from a depth of at least 200 km."

6- Naldrett and Turner (1977): similar model but in two stages of partial melting, the first for the tholeiitic, the second for the komatiitic magma.

To produce a komatiitic magma by partial melting of the mantle, be it of pyrolite (Green and Ringwood, 1967) or garnet lherzolite (O'Hara, 1968) composition, a high degree of melting (about 75%) is required to match the com-

position of komatiite. An alternative would be to melt depleted mantle material, for example a mantle of more dunitic composition, the residue of partial melting which has produced a liquid of basaltic composition. Assuming a higher than present geothermal gradient for the Archean, such as proposed by Green (1974), Lambert (1976), Naldrett and Turner (1977) or Baer (1977) (Fig. 63), a depth of at least 200 km (about 70 kb and 1700-1750°C) is required to produce a melt that, rising adiabatically, would extrude at 1650°C. Under those T-P conditions a pyrolite upper mantle would produce only about 5% melt with a basaltic composition, enriched in incompatible elements; extrusion of this liquid could correspond to the tholeiites. To obtain a higher proportion of melt, and a liquid closer to a komatiite composition, it is necessary either to increase the temperature (at constant pressure) or decrease the pressure (at constant temperature). An increase in depth (and temperature) brings the geotherm outside the solidus of pyrolite. A decrease in pressure (at nearly constant temperature) is thus required. This could be the result of a diapiric up welling, induced maybe by the presence of a small portion of liquid, rising adiabatically. This adiabatic rise of mantle material will increase the percentage of melt, and in turn increase the buoancy and enhance the upward mouvement. To keep the liquid formed in equilibrium with the residual phases, i.e. to be able to proceed to a highly magnesian liquid composition, the upward flow must be rapid considering the low viscosity

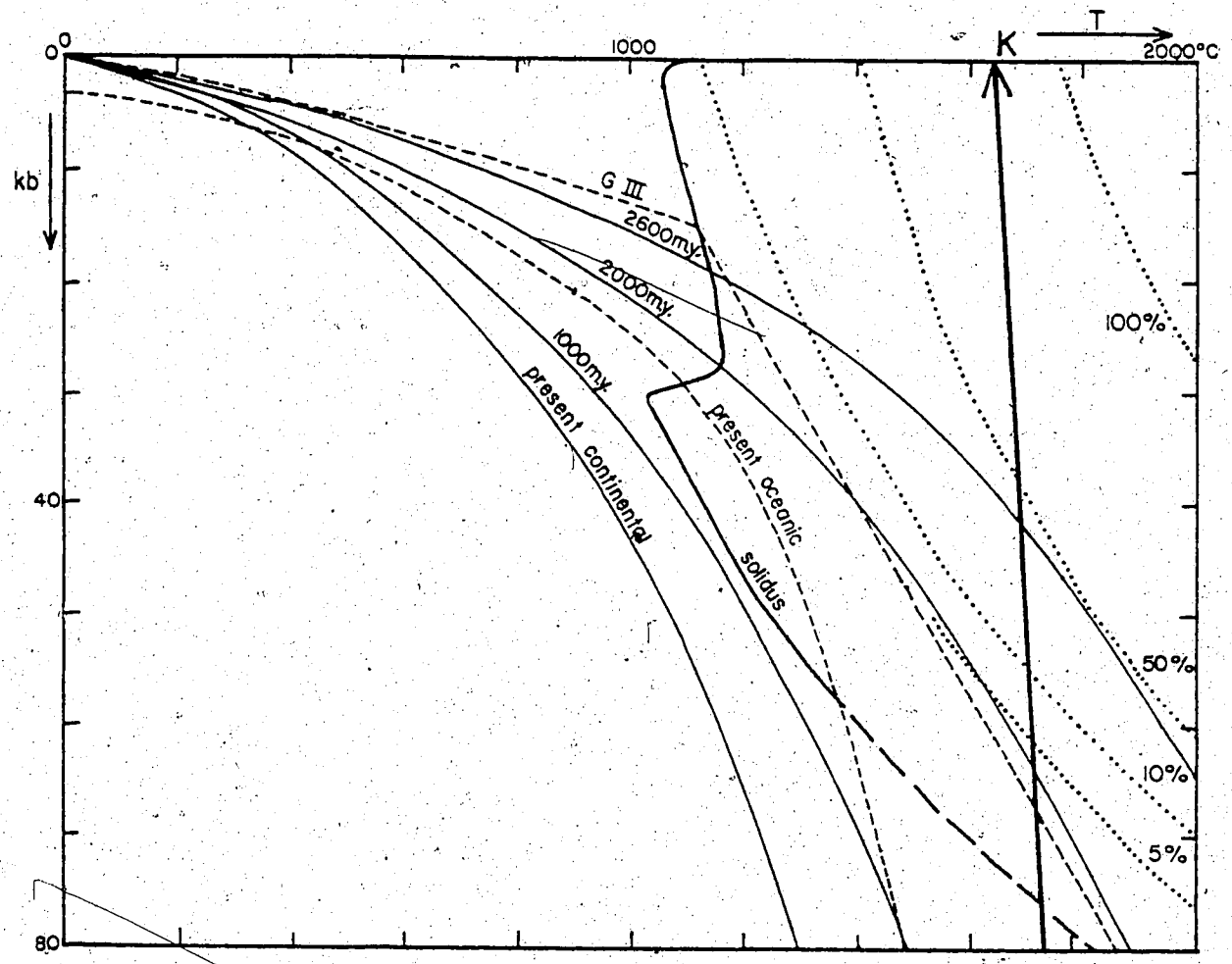

Fig. 63. A pressure-temperature diagram showing the path of a mantle diapir, rising adiabatically to extrude a komatiitic magma (K) at 1650°C, the pyrolite (+0.1% water) solidus and partial melting curves at 5, 10, 50, and 100%, and the model ILI geotherm (G III) after Green (1975). Present oceanic and continental geotherms after Clark and Ringwood (1964). Geotherm at 2600 m.y. after Lambert (1976) extrapolated beyond 1500°C. Geotherms at 1000 and 2000 m.y. interpolated between present continental and 2600 m.y. using data on change in heat generation with time in Lambert (1976).

of such a silica-poor liquid. Arndt et al. (1977) calculated a settling speed of 40 cm per hour for an olivine grain of 0.5 mm in a komatiitic lava with MgO=26% and SiO_2=46% compared with 0.04 cm per hour in a basaltic liquid. Upon reaching the base of the lithosphere, at a depth of about 50 km, the diapir would contain about 75% of liquid.

Extrusion of this magma would form komatiites; differentiation near the base of the lithosphere would account for the spread of composition of magnesian series (by olivine fractionation mainly) and for the tholeiitic series (by olivine and clinopyroxene fractionation). The felsic rocks that accompany the komatiites and tholeiites in the Archean greenstone belts are believed to be the result of partial melting of the sialic crust. The calc-alkaline series which are less common and tend to occur in the upper part of the sequences may be the result of one of the following: partial melting of the base of the volcanic sequence; hydration of the tholeiitic magma; partial melting of the lithosphere.

Other processes may be involved in the production of the komatiite-tholeiite sequence:

1- crystallization of orthopyroxene (without olivine) at an advanced stage of melting would increase the magnesian character of the magma;

2- liquid immiscibility, as described by Ferguson and Currie (1972) or by Gélinas et al. (1976), could enhance some of the differentiation processes;

3- frequent tapping of magma during the rise of the diapir could produce the various types of volcanics observed and would result in more dunitic melts near the end of the rise of the diapir.

CHAPTER VIII

GEOCHRONOLOGY AND STRATIGRAPHIC CORRELATION

1. GEOCHRONOLOGY

A PREVIOUS WORK

Beall et al. (1963) presented K-Ar and whole-rock Rb-Sr ages for rocks from the Cape Smith Belt, the gneisses immediately south of the belt, and the gneisses north of the belt. Their K-Ar ages show a broad range, from 1450 to 1650 m.y. in the rocks of the belt, and from 1550 to 1850 m.y. in the gneisses. The Rb-Sr ages of the gneisses vary from 2320 to 2700 m.y..

K-Ar dating by the Geological Survey of Canada shows an age of 1660±55 m.y. for the gneisses in the vicinity of the Belt, both south and north of it, and one age at 1639 m.y. for a hornblende schist within the belt. Gneisses and granites south of the belt, but away from it, in the

Superior Province yield ages in the range 2500-2600 m.y. (Wanless, 1969; Wanless et al., 1974).

Fryer (1972) presented whole-rock Rb-Sr ages of 3 groups of sediments and volcanics of the Circum-Ungava Geosyncline: Belcher Fold Belt, Flaherty Formation (1800 m.y.); Labrador Trough, Sokoman Iron Formation (1870 m.y.); Mistassini area, Temiscamie Formation (1790 m.y.).

Previous work, therefore, shows rocks of the Circum-Ungava Geosyncline to have been deposited at 1800-1900 m.y. and metamorphism in the Cape Smith Belt to have ended at about 1650 m.y., which is about 100 m.y. less than the peak of the Hudsonian Orogeny. The basement gneisses in the central part of the Ungava Peninsula were last affected by the Kenoran Orogeny, at about 2550 m.y. (Stockwell, 1973); and in the vicinity of the Cape Smith Belt this age was reset by the Hudsonian Orogeny, to about 1650 m.y..

B Rb-Sr AGE DETERMINATIONS

Four groups of samples of the Wakeham Bay area were chosen for isotopic analyses:

1- basement gneisses: from north of Maricourt;
2- volcanics from as low as possible in the volcanic sequence: from the Volcano-Sedimentary Group;
3- volcanics from as high as possible in the volcanic sequences: from the Upper Volcanic Group;

4- gabbro sills from the base of the Upper Volcanic Group.

Initially 10 samples were selected for each group. These were analysed rapidly by X-ray fluorescence spectrometry to obtain an indication of the amounts of Rb and Sr present in each. Using these data, 6 samples were chosen in each group to obtain the best possible spread in Rb/Sr ratios; except in the basement gneisses, the Rb content of the samples was low.

The samples from all four groups were analysed for their Rb content and isotopic composition; 4 samples of the first group and 6 each of the second and third group were analysed for their Sr content and isotopic composition. Details on the chemical preparation and the mass spectrometric analyses are given in Appendix II. The fully analysed samples are listed in Table 9, their isotopic composition given in Table 10, and their location plotted on Figure 64.

Isochron plots (Nicolaysen, 1961) were made for each of the 3 groups of data and the corresponding age calculated by means of the APL programme RBSRISOCHRON, written by H. Baadsgaard, using a decay constant of 1.42×10^{-11} y^{-1}.

The 4 samples of <u>basement gneisses</u> (Fig. 65) yield an age of 2893 ±53 m.y. with an initial $^{87}Sr/^{86}Sr$ ratio of 0.7040.

Table 9. List of samples analysed for Rb and Sr isotopes.

No	Field No	Description
Basement gneisses		
1	S50-1B	Grey medium-grained banded granodioritic hornblende biotite gneiss.
2	S50-1D	Pink medium-grained granitic biotite augen-gneiss.
3	S50-11B	Pinkish grey medium-grained massive tonalitic biotite hornblende gneiss.
4	S51-1A	Dark grey medium-grained banded granodioritic hornblende biotite gneiss.
Volcano-Sedimentary Group		
5	H7-6E	Tuff: quartz, plagioclase, biotite (35%), chlorite, epidote, sphene.
6	S7-4A	Tuff: quartz, plagioclase, b[illegible]ite (10%), chlorite, actinolite, epidote, calcite, sphene (tholeiitic basalt).
7	S7-4D	Tuff: quartz, plagioclase, chlorite, actinolite, hornblende, epidote, sphene (tholeiitic basalt).
8	S7-4G	Tuff: plagioclase, biotite (15%), chlorite, hornblende, epidote, calcite, ilmenite, zircon (calc-alkaline (high-alumina) basalt).
9	S7-4H	Tuff: quartz, biotite (1%), chlorite, hornblende, allanite, calcite, apatite, sphene, ilmenite (tholeiitic basalt).
10	S9-1H	Ultramafic: talc, chlorite, carbonate.
Upper Volcanic Group		
11	C28-2	Tuff: quartz, plagioclase, biotite (10%), chlorite, epidote, zircon, apatite, ilmenite (calc-alkaline rhyolite).
12	C32-2	Basalt: quartz, plagioclase, biotite (1%), chlorite, actinolite, hornblende, epidote, sphene, sulphide (tholeiitic basalt).
13	S15-4I	Basalt: plagioclase, biotite (3%), chlorite, actinolite, epidote, calcite, sphene (tholeiitic basalt).
14	S15-6D	Basalt: quartz, plagioclase, biotite (25%) chlorite, actinolite, hornblende, epidote, sphene (tholeiitic basalt).
15	S73-9A	Tuff: quartz, plagioclase, muscovite (13%), biotite (12%), chlorite, epidote, sphene, sulphide (tholeiitic andesite).
16	T5-6	Basalt: plagioclase, chlorite, actinolite, hornblende, epidote, sphene, calcite, sulphide (tholeiitic basalt).

Table 10. Rb-Sr analytical data.

No	Rb ppm	Sr ppm	$^{87}Rb/^{86}Sr$	$^{87}Sr/^{86}Sr$
Basement gneisses				
1	53.3	291	0.530	0.7239
2	226	336	1.945	0.7841
3	22.4	468	0.139	0.7103
4	39.9	381	0.303	0.7172
Volcano-Sedimentary Group				
6	34.7	183	0.548	0.7231
7	0.90	204	0.013	0.7058
8	0.68	215	0.009	0.7140
9	3.4	71.2	0.136	0.7122
10	0.16	14.7	0.032	0.7178
Upper Volcanic Group				
11	28.4	65.3	1.255	0.7447
12	0.44	173	0.007	0.7075
13	10.9	90.5	0.347	0.7145
14	76.7	79.5	2.792	0.7952
15	44.5	77.4	1.662	0.7503
16	0.57	101	0.017	0.7069

The common banding of the gneisses, at least on outcrop scale, if not on hand specimen scale, their heterogeneity in composition, as well as the presence of distinct metasediments (for example calcareous mica-schists) mixed with amphibolite, that appear concordantly interlayered, suggest that these gneisses are highly metamorphosed supracrustal rocks rather than orthogneisses. This age of 2900 m.y. is distinctly higher than the Kenoran age generally attributed to the rocks of the Superior Province of which the above gneisses are but an extension within the Churchill

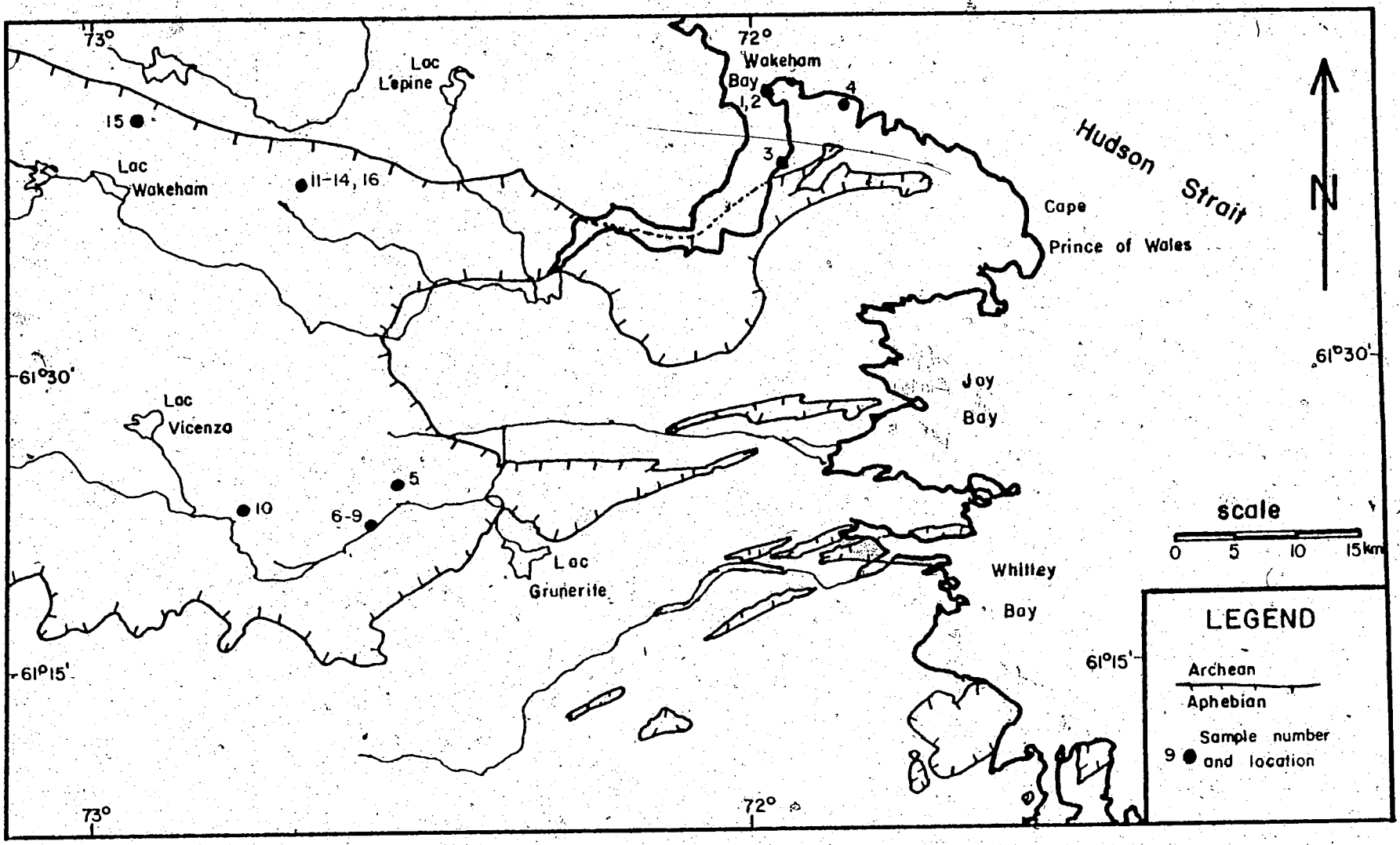

Fig. 64. Map of the Wakeham Bay area showing the location of samples analysed for Rb and Sr isotopes.

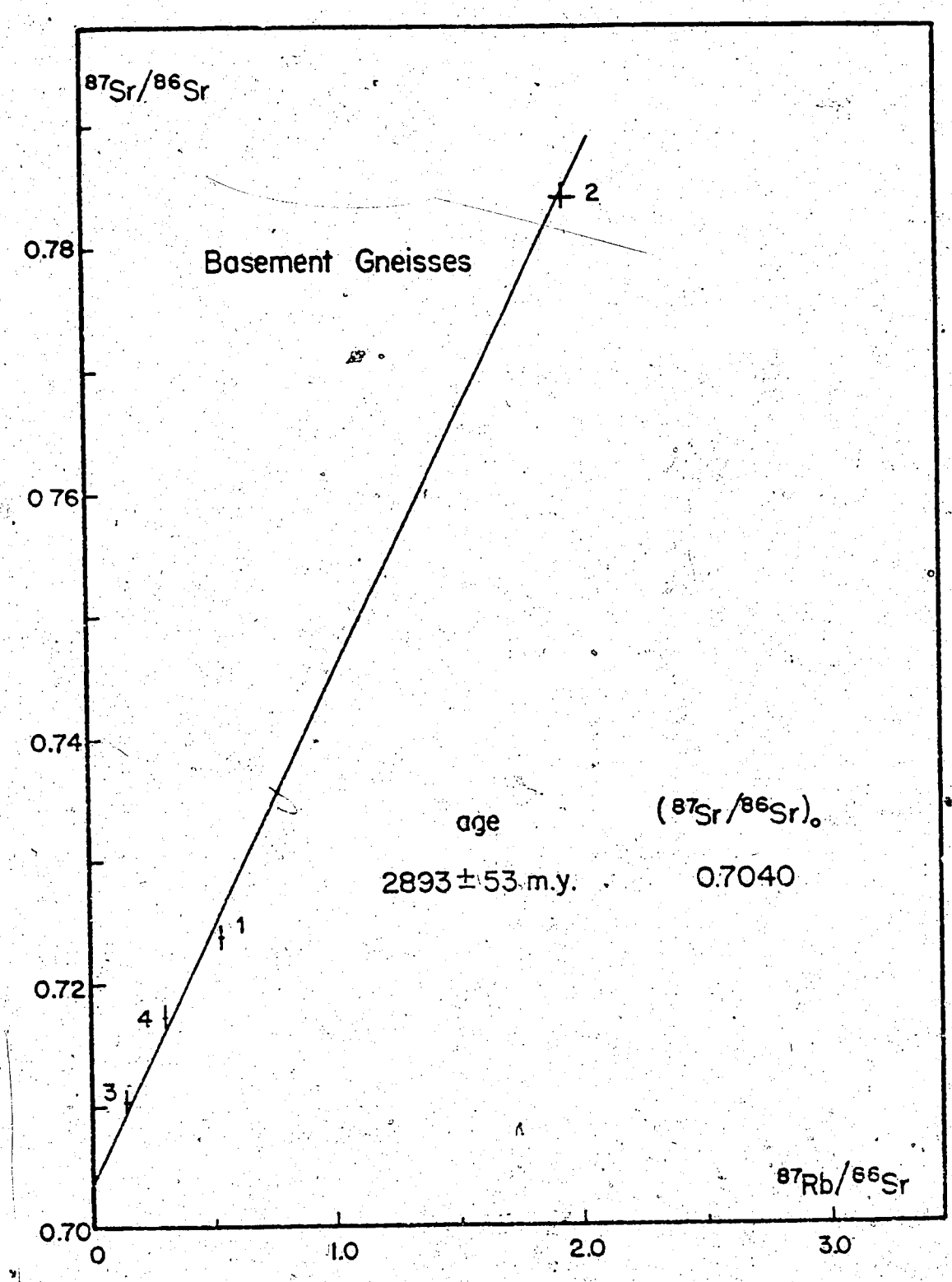

Fig. 65. Whole-rock Rb-Sr isochron plot of basement gneiss samples. All samples used for the isochron.

Province.

Early Archean rocks have been found in various localities of the Canadian Shield and Greenland. Figure 66 shows the Wakeham Bay area in relation to these other occurrences of early Archean rocks. Greenland is represented in its pre-drift location, using the continental fit of Bullard et al. (1965). The proximity to the Wakeham Bay area (600-700 Km) of both the Godthaabsfjord and the Saglek areas suggests that the North Atlantic Craton of Bridgewater et al. (1973) may have extended further west. The Wakeham Bay gneisses have a higher initial $^{87}Sr/^{86}Sr$ ratio (0.704) than the Amîtsoq gneiss (Bridgewater et al., 1973) or other Archean granitic rocks (Glickson, 1978). This tends to confirm their interpretation as supracrustal rocks. The age of 2900 m.y. could correspond to their age of deposition; it could also be correlated with the major metamorphic event observed in Greenland and Scotland at 2800-3000 m.y. (Bridgewater, et al., 1973). In both cases, the existence of a pre-2900 m.y. basement is implied.

This age of 2900 m.y. also raises the question of what was the effect of the Kenoran Orogeny in the northern part of the Ungava Peninsula: Was it more than a resetting of K-Ar ages? If the interlayered metasediments are indeed of the same age as the gneisses yielding the 2900 m.y. isochron, then no rocks, except maybe some basic dykes and some pegmatites, were observed in the Wakeham Bay area that could be related to the Kenoran Orogeny.

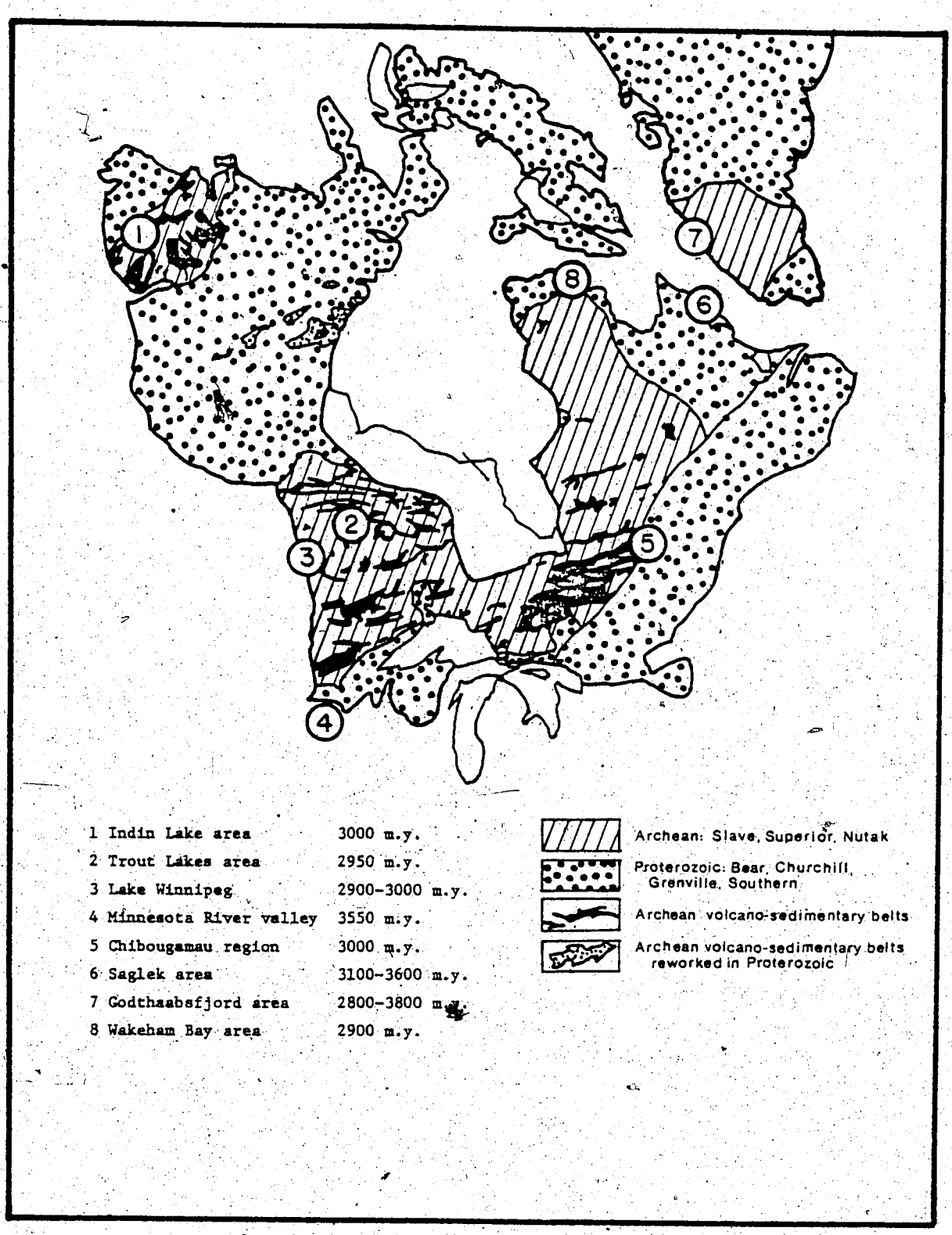

Fig. 66. The Wakeham Bay area compared to other occurences of early Archean rocks in the Canadian Shield and Greenland (after Baragar and Mc Glynn, 1976; Bridgewater et al., 1973; Hurst et al., 1975).

The isochron plot of the 6 Volcano-Sedimentary Group samples does not show a close fit to a line (Fig. 67). In particular samples 8 and 10, with almost no Rb, show a high $^{87}Sr/^{86}Sr$. Samples 5 to 9 are intermediate tuffs and 10 is a serpentinized ultramafic rock (peridotite ?). Any of these may have been subjected to a certain amount of metasomatism during metamorphism; and samples 8 and 10 have most probably gained some ^{87}Sr in this way. An isochron can be fitted to the other 4 samples; it yields an age of 2094±38 m.y. and an initial $^{87}Sr/^{86}Sr$ of 0.7068.

The isochron plot of the Upper Volcanic Group samples also show scatter (Fig. 68). Samples 11 and 15 are tuffs and are more liable to have undergone chemical exchanges during metamorphism than the others samples which are basalts. Sample 14, however, has a peculiar chemical compositon. The major element analysis shows a composition of basalt, but for a low Na_2O and a high K_2O content. Indeed, the thin section shows some 35% biotite which appears to replace the other minerals, mainly the actinolite and hornblende.

It is possible to trace three isochrons on Figure 68, giving a range in age from 1961 to 2335 m.y.. Isochrons I and II represent the maximum possible range. The 2191 and the 1961 m.y. isochrons are closest to the isochron obtained for the Volcano-Sedimentary Group samples both in age and in initial $^{87}Sr/^{86}Sr$.

An isochron combining all Aphebian samples (except

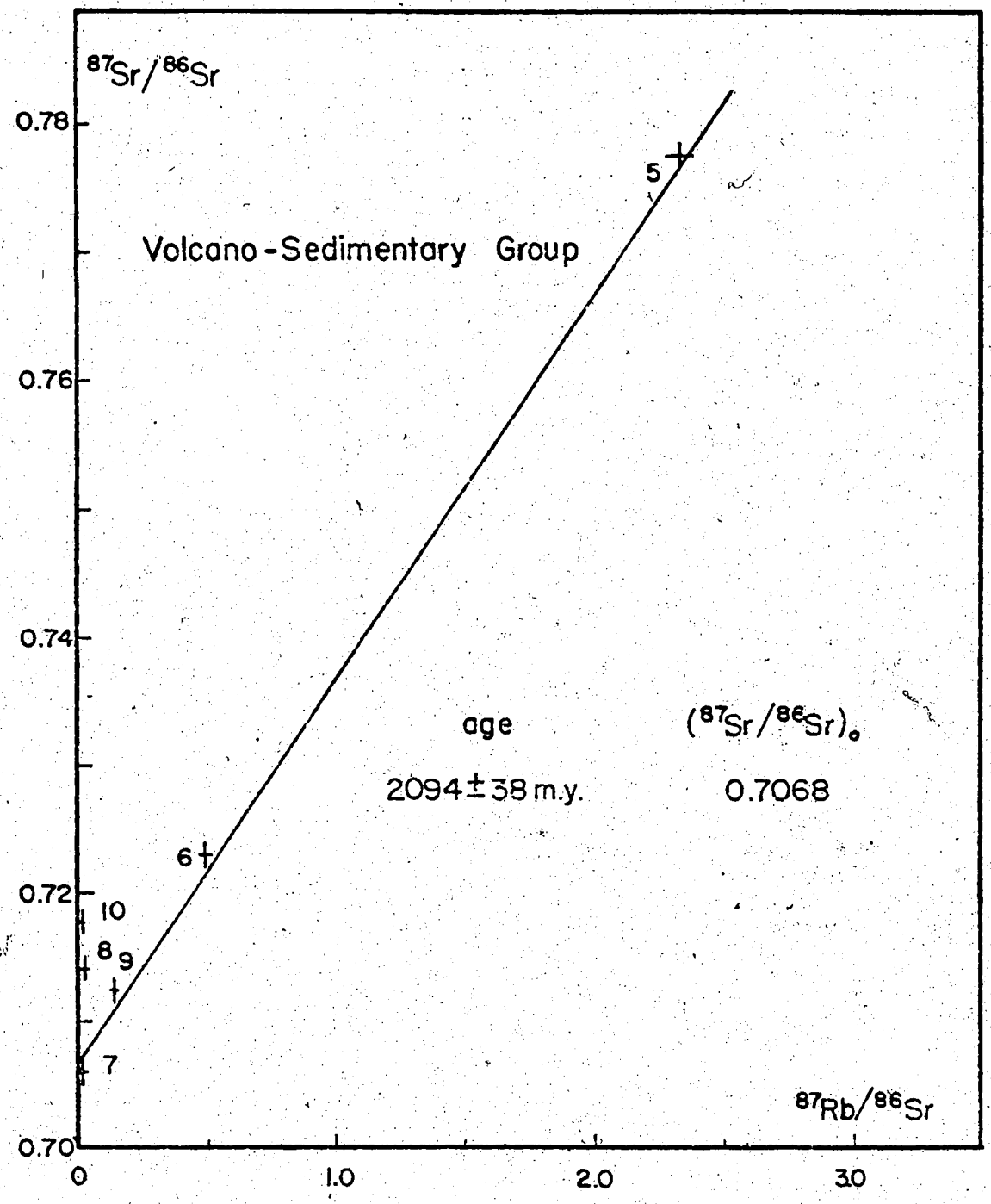

Fig. 67. Whole-rock Rb-Sr isochron plot of Volcano-Sedimentary Group samples. Samples 10 and 8 have been excluded from the isochron and age calculation.

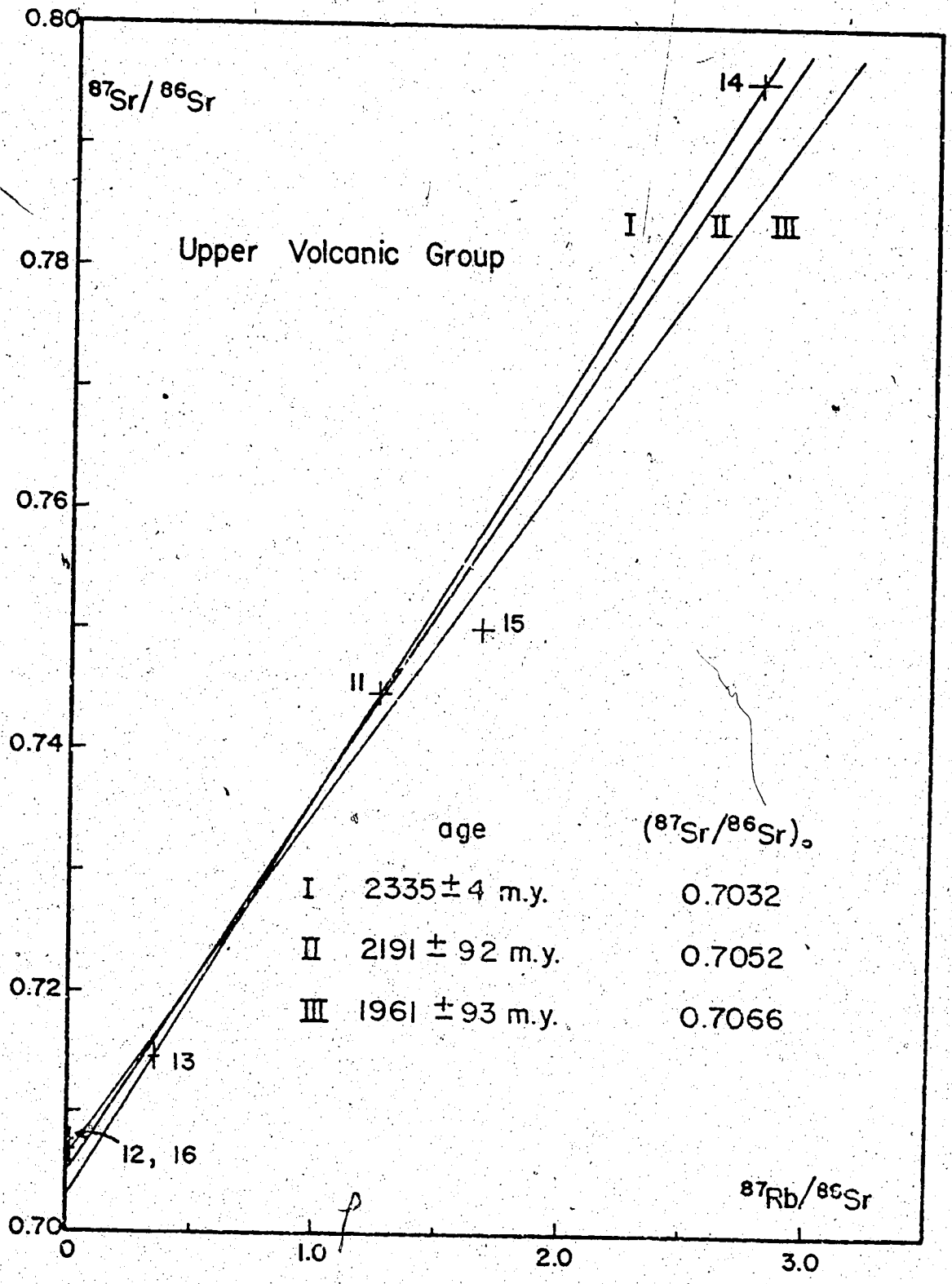

Ffg.68. Whole-rock Rb-Sr isochron plot of Upper Volcanic Croup samples.
Isochron I: samples 13,11,14.
Isochron II: all samples.
Isochron III: all samples except 14.

8 and 10) yields an age of 2154±60 m.y. with an initial $^{87}Sr/^{86}Sr$ of 0.7059 (Fig. 69). The close grouping of three Rb-poor samples near 0.706 adds to the credibility of the initial ratio of the isochron.

The volcanism of the Cape Smith Belt consists mainly of primitive tholeiites; but a calc-alkaline and a magnesian series were also recognized. In order to obtain a spread in the Rb/Sr ratio sufficient to plot isochrons, samples from all three series were analysed, thus adding somewhat to the scatter. The initial ratio (0.706) is higher than expected from primitive, mantle-derived volcanics.[1] However, such relatively high initial ratios are not rare amongst similar Proterozoic or Archean rocks:

- Green and Baadsgaard (1971), 0.702-0.706 on 2600 m.y. Yellowknife Group volcanics;
- Fryer (1972), 0.706 on 1800 m.y. Belcher Island Volcanics;
- Gates and Hurley (1973), 0.700-0.706 on 2000-2700 m.y. diabase dykes.

For the diabase dykes, contamination may be invoked. Green and Baadsgaard (1971) suggest, for the Yellowknife Group volcanics, a mantle source region with a higher Rb/Sr ratio than that of the source region of modern volcanics. This may also have been the case for the Wakeham

---

[1] The samples controlling this initial ratio (7, 12, 16) are from tholeiitic and the magnesian series.

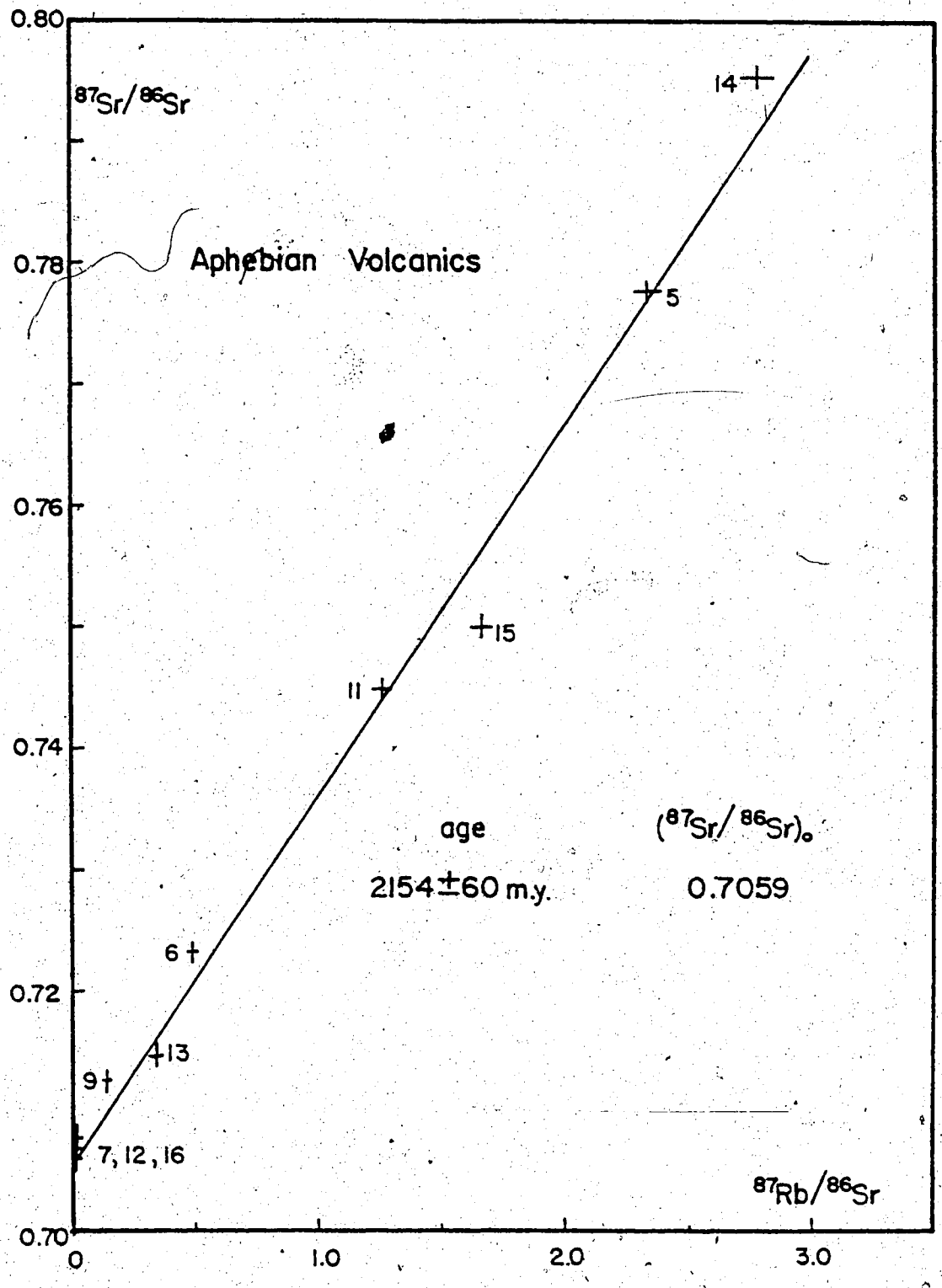

Fig. 69. Whole-rock Rb-Sr isochron plot of Aphebian volcanic rocks from the Upper Volcanic and Volcano-Sedimentary Groups.

Bay volcanics.

This age of 2100-2200 m.y. for the Aphebian volcanic rocks of the Wakeham Bay area is much older than those obtained by Fryer (1972) for other parts of the Circum-Ungava Geosyncline which could be considered equivalent on the basis of lithostratigraphic correlaton. (see discussion below on stratigraphic correlation).

An early Aphebian event (2000-2200 m.y.) has been recognized by Jackson and Taylor (1972) in the Aphebian fold belts on Baffin Island and Melville Peninsula. There, however, this event is represented by the resetting of the Rb-Sr whole-rock ages of some Archean rocks and by gneisses underlying later Aphebian supracrustals. An early Aphebian event has also been recorded in the Indin Lake area (see Fig. 66) by Frith et al. (1973), and in the Athabaska Lake region in northwestern, Saskatchewan (see for example Sassano et al., 1972).

2. STRATIGRAPHIC CORRELATION

Correlation of the stratigraphy determined in the Wakeham Bay area can be attempted with:

1- the rest of the Cape Smith Belt;

2- the rest of the Circum-Ungava Geosyncline.

Bergeron (1957) recognized, in the central part of the Cape Smith Belt, the Povungnituk or Lower Group and the Chukotat or Upper Group, separated by an angular unconformity with, in many places, a basal conglomerate. "The Povungnituk Group comprises mainly pelitic sediments, massive and pillowed basalts and intrusions of gabbroic and, in a few places, noritic sills. Minor dolomite, sandstone and iron formation are present. The Chukotat Group is composed in large part of pillowed basalts with ultrabasic and gabbroic sills and some slates and tuffs" (Bergeron in Dimroth et al. 1970). Subdivisions within those two groups do not appear to have been made by Bergeron (1957) nor others mapping the central part of the Cape Smith Belt (Beall, ms; Gold, 1962; De Montigny, 1962; Gélinas, 1962), and it is difficult to recognize any particular succession within these two groups from their reports or maps.

As stated previously, in the map area no angular unconformity nor basal conglomerate was found within the Aphebian succession. But by comparing with the maps of Beall (1959, 1960) and Gold (1962), it appears that the Povungnituk Group corresponds more or less to the Iron Group, Pelitic Group and Volcano-Sedimentary Group, and the Chukotat Group to the Lower and Upper Volcanic Group of the present study.

Baragar (1974) presents a geological column corresponding to a cross-section of the Cape Smith Belt at about 74°40'W. It shows from north to south:

1- metamorphic complex (north of the major EW fault);

2- Upper volcanic unit: mostly pillowed mafic lavas (≅ 17,000 feet);

3- upper sedimentary unit: mostly quartzites, quartzite conglomerates, and quartzite breccias; minor mafic volcanics (≅ 10,000 feet);

4- lower volcanic unit: massive mafic lavas and thin dolerite sills with interlayered quartzite, black shale, and minor pyroclastics (≅ 45,000 feet);

5- lower sedimentary unit: shale, thick-bedded quartzites, and dolomites (≅ 15,000 feet).

Ultramafic sills appear in the upper half of the lower volcanic unit and in the upper volcanic unit. It appears that his lower sedimentary unit corresponds to the Iron Group, Pelitic Group, and part of the Volcano-Sedimentary Group; his lower volcanic unit to the rest of the Volcano-Sedimentary Group and the Lower Volcanic Group; his upper sedimentary unit and upper volcanic unit to the Upper Volcanic Group of the Wakeham Bay area.

The Aphebian stratigraphic sequence of the Labrador Trough has been well described (Dimroth in Dimroth *et al.* 1970). It consists of three cycles of sandstone-precipitate-shale; volcanic rocks are associated with the shale part of each cycle. In the Wakeham Bay area such cycles are not obvious; this may be because the miogeoclinal domain, in which these cycles have been recognized in the

Labrador Trough, is restricted to a narrow band in the south of the Wakeham Bay area. The Wakeham Bay area Aphebian sequence, however, shows distinct similarities to that of the Lac des Chefs area in the northernmost Labrador Trough (Hardy, 1976) (see Table 11).

Table 11. Comparison of the Aphebian stratigraphic sequence of the Lac des Chefs area and Wakeham Bay area.

Lac des Chefs area	Wakeham Bay area
	Upper Volcanic Group
Volcanic rocks	Lower Volcanic Group
Pelitic sequence (upper half) Carbonated sequence	Volcano-Sedimentary Group
Pelitic sequence (lower half)	Pelitic Group
Iron formation Arenaceous sequence	Iron Group

This tentative correlation with the Lac des Chefs area can be extended to the stratigraphic sequence of the northern Labrador Trough (see Table 12). Additional similarities must be noted. In the Wakeham Bay area, a few thin horizons of iron-rich rock, interpreted as exhalites, occur above the dolomite horizon in the Volcano-Sedimentary Group (some also below), i.e. in a position similar to that of the upper iron formation of the Labrador Trough. The Larch River Slate, like the upper part of the Volcano-Sedimentary Group,

Table 12. Tentative correlation of Aphebian lithostratigraphic units of the Wakeham Bay area with the rest of the Circum-Ungava Geosyncline (After Dimroth et al., 1970, and Fryer, 1972).

Wakeham Bay	Labrador Trough (between 57 and 59°N.), after Dimroth (1970)	Labrador Trough (between 54 and 57°N.), after Dimroth (1970)	Belcher Island, after Jackson in Dimroth et. al. (1970)
Upper Volcanic Group Lower Volcanic Group	Thevenet Slate Hellancourt Basalt Larch River Slate	Willbob Basalt Thompson Lake Slate	Loaf Fm (Molasse-type) Omarolluk Fm (Flysch-type) Flaherty Fm (basalt)
Volcano-Sedimentary Group	upper iron-formation	Irene Lake Iron-Fm	Kipalu Iron-Fm
	Abner Dolomite	Murdoch Pyroclastics basalt	Mukpollo Fm (quartzite)
Pel ic Gro.	Chioak Fm (slate, conglomerate graywacke) Dragon Fm (slate, siltstone)	Menihek Slate	Rowatt Fm (quartzite, dolomite) Laddie Fm (argillite, quartzite, dolomite) Costello Fm (limestone, dolomite, argillite)
Iron Group.	Fenimore Iron-Fm	Sokoman Iron-Fm	Mavor Fm (dolomite)
	Allison Quartzite	Wishart Quartzite Denault Dolomite Attikamagen III Slate Swampy Bay Subgroup (slate, graywacke, conglomerate) Pistolet Subgroup (dolomite, sandstone, shale) Seward Subgroup (sandstone, dolomite, arkose)	Tukara Fm. (argillite, limestone, dolomite) McLeary Fm (dolomite, quartzite) Fairweather Fm (argillite, quartzite, dolomite, tuff, arkose, basalt) Eskimo Fm (basalt, argillite, tuff, agglomerate) Kasegalic Fm (dolomite, limestone, argillite)
ARCHEAN	ARCHEAN	ARCHEAN	ARCHEAN

consists of pelites interlayered with numerous gabbro sills. No equivalent, however, of the Thevenet Slate is observed in the Wakeham Bay area. Table 12 shows that, although similarities exist, lithostratigraphic correlation between the Wakeham Bay area and the Labrador Trough is at best tentative.

The Belcher Fold Belt, situated entirely within the miogeoclinal domain, shows quite a different stratigraphic succession (Jackson in Dimroth et al. 1970). Three cycles have been recognized there, but different from those of the Labrador Trough; they begin with basic volcanic rocks and end with interbedded massive dolomite and quartzite. In other words, whereas in the Labrador Trough each cycle is marked by a gradual increase in the instability of the depositional basin and in the amount of volcanism, in the Belcher Fold Belt each cycle begins with a pulse of volcanism accompanied by instability of the depositional basin, followed by a gradual increase in stability and decrease in volcanic activity. From this viewpoint, the Wakeham Bay area shows more affinity to the Labrador Trough than to the Belcher Fold Belt.

3. DISCUSSION and CONCLUSIONS

The Archean basement in the Wakeham Bay area consists of 2900 m.y. old gneisses. This is distinctly older than the Kenoran age previously accepted for the adjacent part of the Superior Province and the basement gneisses of the Churchill Province (see for example Dimroth, 1972). However, gneisses of this age, or older, have been found in various parts of the Canadian Shield and Greenland (Fig. 66). It should also be noted that the Ungava Peninsula is a particularly deeply eroded part of the Superior Province, as indicated by extensive occurrences in it of granulite facies rocks (Douglas, 1968). Granulite facies gneisses also occur near Douglas Harbour, northwest of Wakeham Bay. This extensive presence of granulite facies rocks also suggest that the Archean basement is here policyclic, i.e. that the Kenoran Orogeny reworked a basement.

The Aphebian sequence of the Wakeham Bay area yields an age of 2100-2200 m.y.; this is much older than that determined for the second cycle of the Labrador Trough and the Belcher Fold Belt by Fryer (1972). It indicates that the stratigraphic similarities between the Wakeham Bay area and the Labrador Trough are fortuitous, or rather, that they are the result of a similar sequence of tectonic events and source region-depositional basin relationships, which produced a stratigraphic sequence similar to one or two of the Labrador Trough cycles, but distinctly older.

Certain differences between the Cape Smith Belt and the Labrador Trough also point to an older age for the Cape Smith Belt Aphebian sequence.

1- The abundance of ultramafic sills and flows in the Cape Smith Belt compared with the Labrador Trough: ultramafic flows, komatiites, are more common in the Archean than in the Proterozoic or Phanerozoic.

2- The vertical nature of the deformation in the Cape Smith Belt, compared to the more tangential deformation in the Labrador Trough, suggests that it is more akin to an Archean tectonic style than to a Proterozoic tectonic style as discussed by Wynne-Edwards (1976).

Another difference between the two belts, although of unclear age significance, is the occurrence of extensive areas of rhyolite in the central part of the Cape Smith Belt (Taylor, 1974), whilst intermediate to acid volcanics are virtually absent in the Labrador Trough (Baragar in Dimroth et al., 1970).

CHAPTER IX

ECONOMIC GEOLOGY

1. INTRODUCTION

The Cape Smith Belt is well known for its Cu-Ni deposits associated with ultramafic rocks, none of which, however, have been brought to production, and the Asbestos Hill mine which has produced asbestos fibre concentrate since 1972. The formations in which these deposits occur extend into the Wakeham Bay area. Other potential resources are iron formation, stratiform sulphide deposits (Pb, Zn, and Cu?), and soapstone. Little exploration work has been done in the Wakeham Bay area, although an ultramafic sill near Lac Giraffe was drilled in the early 1960's and Cu-Ni indications were found (Dugas, 1971).

2. COPPER-NICKEL

The Donaldson and Katiniq deposits of New Quebec Raglan Mines Ltd occur in ultramafic rocks that are stratigraphic equivalents of the Upper Volcanic Group. The deposit of Expo-Ungava Mining Ltd., south of the Donaldson deposit, occurs in ultramafic rocks that are stratigraphic equivalents of the Lower Volcanic Group.

In the Wakeham Bay area, these ultramafic rocks are abundant only in the Upper Volcanic Group; some occur in the Lower Volcanic Group (see Fig. 70). Naldrett and Gasparrini (1971) discuss Archean Cu-Ni deposits of this type; the presence of abundant iron-sulphides in the country rocks is a favorable criterion. Numerous gossans occur in the Upper Volcanic Group, related to sediments, felsic to mafic tuffs, as well as to sulphurized (MacRae, 1974) basalts (see Fig. 70). Only one major ultramafic sill occurs in the Lower Volcanic Group. Cu-Ni sulphide concentrations may also occur in the basal (cumulate) part of gabbroic sills from the Upper and Lower Volcanic Group. The thick sills located in the hills just south of Wakeham Bay show abnormally high chalcopyrite/pyrrhotite and pentlandite/pyrrhotite ratios in the gabbros.

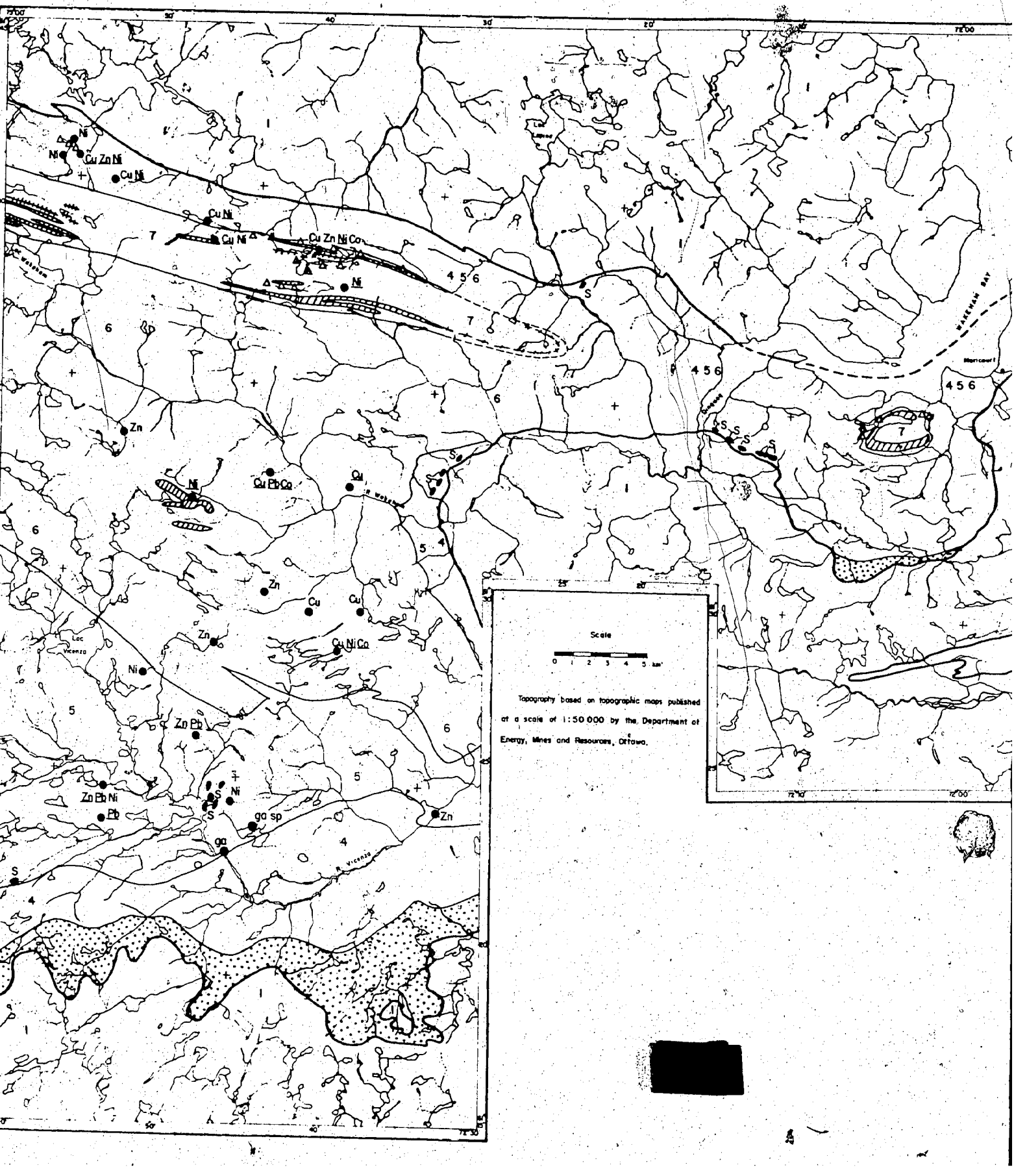
Ni
Cu Zn Ni
Cu Ni
Cu Ni
Cu Ni
Cu Zn Ni Co
Ni
Zn
Ni
Cu Pb Co
Cu
Zn
Cu
Cu
Zn
Cu Ni Co
Ni
Zn Pb
Zn Pb Ni
Pb
S
Ni
ga sp
ga
Zn
S
Loc Vicenza
R. Vicenza
Wakeham Bay
Scale
0 1 2 3 4 5 km
Topography based on topographic maps published at a scale of 1:50 000 by the Department of Energy, Mines and Resources, Ottawa.

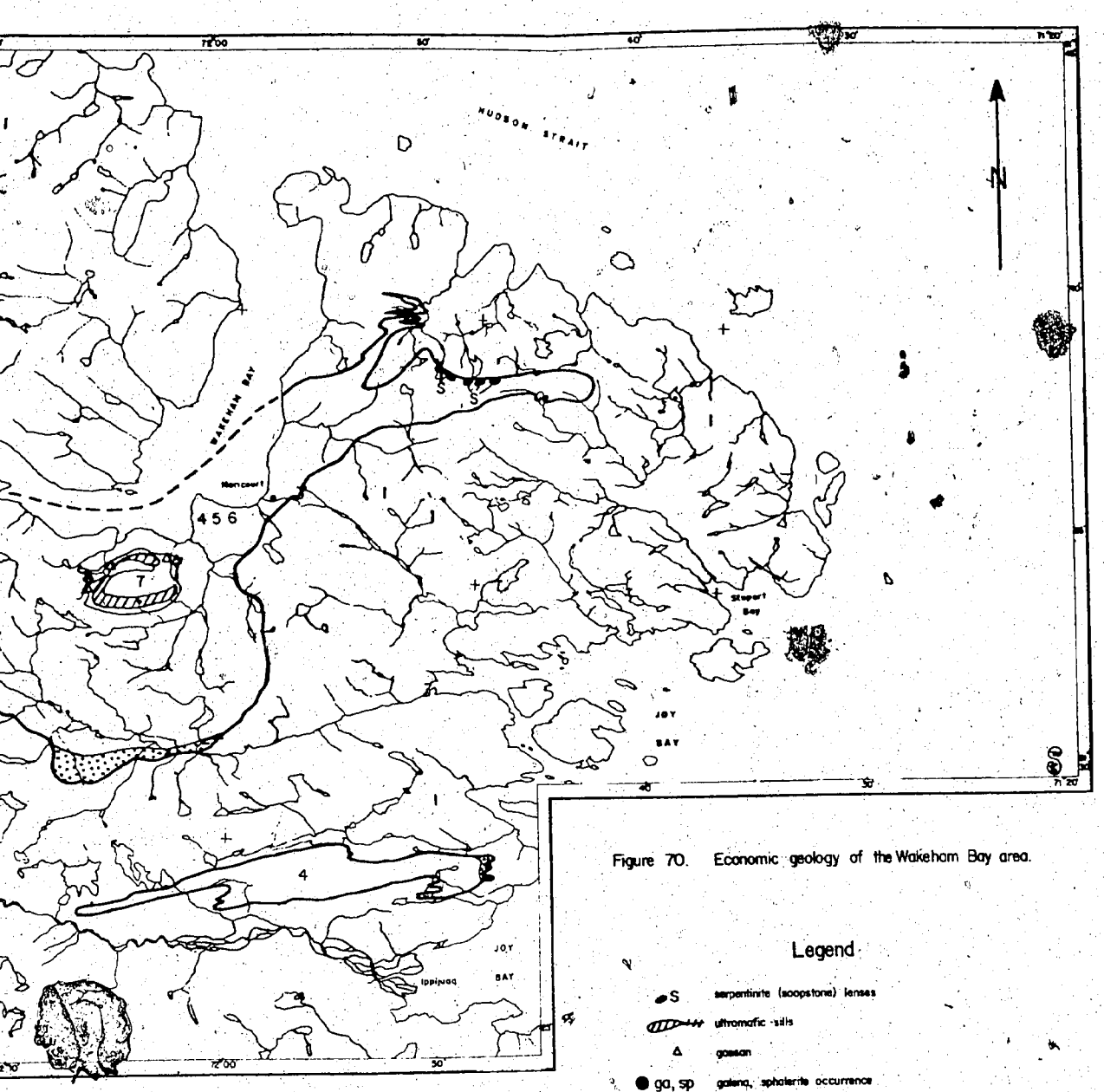

Figure 70. Economic geology of the Wakeham Bay area.

Legend

- S — serpentinite (soapstone) lenses
- ultramafic sills
- Δ — gossan
- ga, sp — galena, sphalerite occurrence
- Cu Pb Zn Ni Co — geochemical anomaly (stream sediment) $x > \bar{x} + 2s$ (where underlined: $x > \bar{x} + 3s$)
- 7 — Upper Volcanic Group
- 6 — Lower Volcanic Group
- 5 — Volcano-sedimentary Group
- 4 — Pelitic Group
- Ines Group
- I — Archean

3. ASBESTOS and SOAPSTONE

The ultramafic sill which contains the asbestos deposit of Asbestos Hill appears to occur at a stratigraphic level equivalent to the Volcano-Sedimentary Group (Collinas, 1961). No asbestos was observed in the ultramafic rocks of the Volcano-Sedimentary Group in the Wakeham Bay area. These rocks are generally talc-rich, sufficently so to be termed soapstone. They could provide a supply of raw material for Inuit handicraft. Their distribution is shown in Figure 70.

4. IRON FORMATION

Iron formation occurs in the Iron Group mostly in the southwest of the map area. Although it is mostly of the silicate- and carbonate-rich type, oxide-rich iron formation is also present. It may contain up to 70-80% iron oxide, although 40-50% is more common. Horizons of oxide iron formation are rarely more than a few meter thick. The distribution of iron formation is shown in Figure 70.

5. STRATIFORM SULPHIDE DEPOSITS

A potential for stratiform sulphide deposits exists in the Upper Volcanic Group and in the Volcano-Sedimentary Group. In the central parts of the Monts Lune, a horizon of what appears to be a sulphide-rich exhalite occurs within sediments and tuffs between the major sills on the north flank of these hills. Up to 1-2 m of massive to banded pyrite and pyrrhotite were observed. This horizon appears fairly continuous and the gossan it produces can be observed for over 10 km along strike. In the central part of the Monts Lune several gossans are found in felsic to intermediate tuffs. Gossans which are thought to be in the same or nearly the same stratigraphic horizon occur at the base of the thick sills just south of Wakeham Bay.

In the Volcano-Sedimentary Group a horizon about 1 m thick of felsic tuff, containing about 5% each of galena and sphalerite, was observed to the southeast of Lac Vicenza, somewhat below the dolomite horizon (Fig. 70). In the vicinity, a small (20 cm thick) galena-bearing quartz-carbonate vein cuts through mafic tuff.

Both types of stratiform sulphide showings can be correlated to rhyolites mapped by Taylor (1974) in the central Cape Smith Belt, near Nuvilik Lakes (equivalent to the Upper Volcanic Group) and near Lac Watts (equivalent to the Volcano-Sedimentary Group).

6. STREAM SEDIMENT GEOCHEMISTRY

Some 220 analyses of stream sediments collected during the mapping programme are available (Schimann, 1976). They are all from the western map area; all are analysed for Cu, Zn, Pb, Ni, Co, and Mn, a few for Ag and U (Table 13).

Table 13. Average and standard deviation of Cu, Zn, Pb, Ni, Co, and Mn in stream sediments from the western map area (all in ppm).

Element	n	$\bar{x}$	s
Cu	220	47	45
Zn	219	52	32
Pb	220	15	9
Ni	220	32	31
Co	220	18	22
Mn	220	442	559

In Figure 70, the anomalous values are plotted.[1] Several strong Cu, Ni, and Zn anomalies (up to Cu, Zn, Ni $\cong \bar{x} + 6s$) occur in the Upper Volcanic Group in the Monts Lune and further west towards the edge of the map area. Some of these appear to be related to gossans. A strong Ni anomaly occurs near Lac Giraffe, and a Cu, Ni, and Co (Co = $\bar{x} + 10s$) near Lac Dragon. Several scattered Cu and Zn anomalies occur in the Lower Volcanic Group. Several Zn, and Pb anomalies char-

[1] are considered anomalous: values larger than $\bar{x} + 2s$; those larger than $\bar{x} + 3s$ are underlined.

acterize the Volcano-Sedimentary Group.

7. CONCLUSIONS

Both field observations and geochemistry suggest that the area has a potential for Cu-Ni deposits in ultramafic rocks and for stratiform sulphide deposits (Cu, Zn, Pb) related to felsic to intermediate tuffs which may be distal equivalent of rhyolites found in the central part of the Cape Smith Belt. The iron formation which occurs in the area appears marginal under present economic conditions. No indication of asbestos was observed but several of the ultramafic lenses in the Volcano-Sedimentary Group are sufficently steatized to provide soapstone for local handicraft.

CHAPTER X

CONCLUSION

The Wakeham Bay area consists of an Archean basement of quartzo-feldspathic gneisses, amphibolites, and minor paragneisses, and of part of an Aphebian fold belt. The Aphebian sequence starts with sediments; these grade upward into the mafic volcanics and minor sediments which form about 80% of the sequence.

The fold belt forms an asymmetric synclinorium which in its eastern end splits in two and ends in isolated basins. The Aphebian rocks were deformed by differential vertical movements of rigid blocks of Archean basement along three systems of faults. Minor thrust faults resulted from the buckling of the thick and rigid volcanic pile. Little or no crustal shortening occurred.

The metamorphism reached mid-amphibolite facies (610°C, 7.25 kb) and was of intermediate P/T type. The P/T ratio is somewhat higher in the North, where the sequence is thicker, than in the South. A marked basement effect is recognized from the concentration of isothermal surfaces near

the basement-cover contact, and the parallelism of the isograds to this contact. It is concluded from this basement effect, that the metamorphism was a rapidly incoming single pulse, coeval with, and outliving somewhat the folding of the Aphebian cover.

The volcanism is essentially mafic and consists of massive and pillowed basalts intruded by numerous mafic to ultramafic sills. The majority of the volcanism is tholeiitic, akin to oceanic tholeiites; but in the upper part of the sequence a magnesian series is present, ultramafic lavas and high-level sills, similar to komatiites of Archean greenstone belts. Minor calc-alkaline extrusives are also present, mostly tuffs.

Two domains of sedimentation are recognized, a narrow miogeoclinal domain in the South and a eugeosynclinal domain in the North where sedimentation associated with the volcanism consists of shale and grauwacke.

Rb and Sr isotopic analyses indicated an age of 2900 m.y. for the quartzo-feldspathic gneisses of the Archean basement and an age of 2100-2200 m.y. for the volcanism. Closure of the K-Ar system of micas occurred at about 1650 m.y..

The stratigraphy defined for the Wakeham Bay area is at variance with the previously accepted one (Bergeron in Dimroth et al., 1970); but it can be followed westwards on geological maps, and correlates well with the stratigraphy described in the central part of the Cape Smith Belt by

Baragar (1974). Lithostratigraphic correlation can be made with the northern most part of the Labrador Trough (the Lac des Chefs area) and from there, with the rest of the Trough. This is based mainly on correlating the Iron Group with the Fenimore Iron Formation and the Sokoman Iron Formation further south. A similar correlation can be made with the Kipalu Iron Formation of the Belcher Islands. However, Rb/Sr dating (Fryer, 1971) shows these to be significantly younger (1760-1840 m.y.)[1] than the Iron Group of the Wakeham Bay area (>2150 m.y.). It appears thus that the lithostratigraphic similarity only reflects a similar sequence of events in different basins, at different times. In fact the similarity of the sedimentary part of the stratigraphic sequence of the Cape Smith Belt with a part of the sequence of the Labrador Trough is offset by the differences in the volcanism, namely the absence in the Labrador Trough of the komatiites which characterize the Upper Volcanic Group of the Cape Smith Belt.

Other differences are the structural trend and the tectonic style. In the Cape Smith Belt the trend is WSW-ENE, in line with the Thompson Belt, to which it is linked by gravity and magnetic anomalies in the Hudson Bay. In the Labrador Trough the trend is NNW-SSE and in the Belcher Islands it is NS, i.e. both of these are nearly at right angle to the Cape Smith-Thompson trend. In the Cape Smith

---

[1] normalized to a decay constant of 1.42×10^{-11} y^{-1}

Belt vertical tectonics predominate and little or no crustal shortening occurred; in the Labrador Trough the deformation is marked by decollement and large thrust faults; a 50% lateral shortening is estimated (Dimroth,1970).

Several authors (Gibb and Walcott, 1971; Thomas and Gibb, 1977; Demey and Burke, 1973) have considered the Cape Smith Belt (together with the Labrador Trough and the Thompson Belt) to be a suture between two colliding continents in a plate tectonics framework. This is based on the presence of a gravity anomaly, consistent with a model of continental collision and suture, on the interpretation of the basaltic rocks as allochtonous volcanic crust, of a major high-angle fault as a thrust, and of some felsic agglomerates as parts of an island-arc

Dimroth (1972) compared the Labrador Trough with Phanerozoic geosynclines and concluded that "the Labrador Trough is not a Precambrian suture, and evidence for active plate margins is absent in or around the Labrador Trough". Most of the arguments that he used are applicable to the Cape Smith Belt and additional ones can be invoked:

1- There is no discontinuity in the basement between South and North of the Belt in the Wakeham Bay area; the structural trends are the same and a late Archean diabase sill folded together with the Aphebian rocks can be followed in the basement around the end of the Belt.

2- The mafic and ultramafic volcanism of the Cape Smith Belt is different from the ophiolite complexes generated at

spreading centres. The mafic volcanics are more akin to oceanic tholeiites than continental tholeiites, but this only means that they are primitive.

3- Alpine-type serpentinites are absent; the only serpentinite bodies that could by likely candidates (VSG ultramafic lenses) are unrelated to faults or shear zones, follow the same stratigraphic horizon from the south side to the north side of the Belt, and are probably extrusive.

4- The minor calc-alkaline volcanics present are interstratified with the tholeiitic and the magnesian (ultramafic) volcanics and do not represent an island-arc.

5- Similarly, calc-alkaline intrusives, although they occur north of the Belt, are scarce.

6- The absence of mélange and of blue-schist facies metamorphism.

7- The absence of allochtonous masses and the continuity in stratigraphy from the south side to the north side around the end of the Belt, starting with the regolith on the basement and ending with the Upper Volcanic Group.

8- The predominance of vertical tectonics and absence of significant crustal shortening.

An alternative model can be presented. Mantle diapirism under a linear zone going from Wakeham Bay to the Thompson area or maybe further, caused faulting and subsidence acccompanied by volcanism during the period 2200-2150

m.y. ago. This resulted in the volcano-sedimentary sequence now visible. Sedimentation and volcanism may have carried on continuously or discontinuously until 1750-1650 m.y. ago, to form the additional 15-18 km of sediments and volcanics that were present at the time of metamorphism. In the Labrador Trough and the Belcher Islands a similar process took place but it started only 1900-1850 m.y. ago.

In the interval 1750-1650 m.y. ago, the major deformation and the metamorphism (Hudsonian Orogeny) took place and the locus of the mantle diapirism moved away from the Ungava Craton and waned.

The regional gravity low over the northern Ungava Peninsula is due to crustal thickening as a result of accumulation of sediments and volcanics. The density contrast between the Archean basement immediately north and south of the Belt can be attributed to the presence of granulite facies rocks in the North.

A scenario for the evolution of the Wakeham Bay area and its surroundings will now be presented.

At 2900 m.y. or earlier a gneissic basement was present; sedimentation and volcanism may have occurred subsequently, followed by deformation and high-grade metamorphism at 2600-2500 m.y. (Kenoran Orogeny). The pre-Kenoran basement is only inferred and the Archean paragneisses may be of the same age as the quartzo-feldspathic gneisses that yielded a 2900 m.y. minimum age.

At about 2300 m.y. a weak tensional regime over

large parts of the Ungava Craton is indicated by diabase dykes.

At about 2200 m.y. the beginning of subsidence resulted in a transgression over a peneplaned continent. The sedimentation begins with local coastal sandstones followed by a shallow marine environment in which iron formation is deposited. Subsidence increases and a sequence of shale is deposited. This shale sequence is interrupted near its top by a carbonate episode. Volcanism, which becomes a significant part of the series a little before deposition of the carbonate horizon, had already started during deposition of the Iron Group, at least in the central part of the geosyncline. The pelitic sedimentation ends abruptly and is followed by coarse detrital sedimentation, coastal to continental sandstone and arkose with minor conglomerate and local dolomitic breccia. This episode may be locally discordant. It is followed by immature marine sediments (shale and grauwacke) interstratified with and subordinate to mafic and ultramafic volcanics. Two horizons of sandstone and minor conglomerate occur after the first and after the second third of this sequence. These horizons may represent short lived regressions.

The 2200 m.y. transgressive sedimentary sequence can be observed essentially anywhere in the area, but the relative thicknesses vary. The sediments are thicker in the South, where a miogeoclinal domain may be distinguished which contains little volcanics, than in northern eugeosync-

linal domain which starts with a thin plateform sequence covered by thick volcanics and immature sediments. The thicknesses that can be estimated are 8-16 km in the eugebsynclinal domain and 2-3 km in the miogeoclinal domain. To this must be added a thickness of eroded rocks of 15-18 km to account for the now observed metamorphic grade.

The volcanism is essentially tholeiitic with komatiitic rocks in the upper part of the sequence and, once, in the lower part. Minor calc-alkaline extrusives are also present.

The Aphebian sequence was deformed, folded and faulted in response to differential vertical movements of rigid basement blocks. The deformation was accompanied and outlived by metamorphism. This metamorphism corresponded to a single relatively rapid pulse; hence the main deformation must have been short-lived. The age of deformation and metamorphism is not certain. It must have occurred between 2150 m.y. (age of the volcanism) and 1650 m.y. (closure of the K-Ar system in micas). Two possibilities exist:

1- deformation and metamorphism shortly after deposition of the rocks (>2100 m.y.) and uplift (following denudation) past the 350-400°C isotherm at about 1650 m.y.;

2- deposition at 2200-2150 m.y., minor faulting before, during, and after deposition along the EW to WSW-ENE direction; main deformation, metamorphism and uplift during the Hudsonian Orogeny at 1750-1650 m.y.; uplift (following denudation) past the 350-400°C isotherm at about 1650

m.y..

During the Hadrynian, a weak tensional regime included the Cape Smith Belt as indicated by 675 m.y. old diabase dykes. These dykes are parallel to the faults limiting the Hudson Strait Graben (Wade et al., 1977). This structure may have formed then or during the Mesozoic in response to the opening of the North-Atlantic and be related to the Baffin Basin System of graben.

No direct information is available on the Paleozoic in the area. Plateform-type sedimentation occurred in Ungava Bay and Hudson Bay where it extended into the Mesozoic. This plateform sedimentation may have covered most of the Ungava Craton (and the Wakeham Bay area) at some time during the Paleozoic (Ordovician?).

During the Quaternary, an ice cap covered the area until some 8000 y. ago, leaving it freshly eroded, covered with a thin and discontinuous layer of till, and underlining the preexisting structures. Subsequent isostatic readjustment lowered the relative sea-level by up to 400 feet and provided a high energy environment for the erosion of the till. This resulted in a belt of excellent outcrop conditions along the coast. This process of denudation of the high grounds and redeposition of the till in the major valleys and bays is still ongoing and is the only geological process visibly active at present.

BIBLIOGRAPHY

Abraham, K., Hörmann, P.K., and Raith, M. (1974): Progressive metamorphism of basic rocks from the southern Hohe Tauern area, Tyrol (Austria). N. Jb. Miner. Abh. 122, 1-35.

Airth, W.B. (1933): Cape Smith sulphide deposits. Can. Min. J. 54, 53-54.

Albee, A.L. (1965): Distribution of Fe, Mg and Mn between coexisting garnet and biotite in natural mineral assemblages. J. Geol. 73, 155-164.

Albee, A.L. (1965): Phase equilibria in three assemblages of kyanite-zone pelitic schists, Lincoln Mountain Quadrangle, Central Vermont. J. Petrol. 6, 246-301.

Arndt, N.T., Naldrett, A.J., and Pyke, D.R. (1977): Komatiitic and iron-rich tholeiitic lavas of Munro Township, Northeast Ontario. J.Petrol. 18, 319-369.

Atherton, M.P. (1965): The composition of garnet in regionally metamorphosed rocks. In: Pitcher, W.S. and Flinn, G.W. ed.: Controls of metamorphism. Oliver & Boyd, London, 281-290.

Atherton, M.P. (1968): The variation in garnet, biotite and chlorite composition in medium grade pelitic rocks from the Dalradian, Scotland, with particular reference to the zonation in garnet. Contr. Mineral. Petrol. 1, 347-371.

Baer, A.J. (1977): Speculations on the evolution of the lithosphere. Precambrian Res. 5, 249-260.

Banno, S. and Kanehira, K. (1961): Sulfide and oxide minerals in schists of the Sanbagawa and central Abukuma metamorphic terranes. Japan J. Geol. Geogr. 22, 331-348.

Baragar, W.R.A. (1974): Volcanic studies in the Cape Smith-Wakeham Bay belt, New Quebec. In Report of Activities, Part A. Geol Surv. Canada, Paper 74-1A, 155-157.

Baragar, W.R.A. and McGlynn, J.C. (1976): Early Archean basement in the Canadian Shield: a review of the evidence. Geol. Surv. Canada, Paper 76-14.

Bard, J.P. (1969): Le métamorphisme régional progressif des Sierras d'Aracena en Andalousie occidentale (Espagne). Thesis, Montpelier (France), 398 p.

Barron, B.J. (1974): The use of coexisting calcite-ankerite solid solutions as a geothermometer. Contr. Mineral. Petrol. 47, 77-80.

Barth, T.F.W. (1956): Studies in gneiss and granite. Skrifter Norske Vidensk. Akad., Mat.-Naturv. Klasse, 1, 1-35.

Beall, G.H. (1959): Preliminary report on the Cross Lake area, New Quebec. Quebec Dept. Mines, P.R. 396.

Beall, G.H. (1960): Preliminary report on the Laflamme Lake area, New Quebec. Quebec Dept. Mines, P.R. 435.

Beall, G.H.(ms): Final report on Cross Lake and Laflamme Lake areas. Quebec Dept. Nat. Res., unpublished.

Beall, G.H., Hurley, P.M. Fairbarn, H.W., and Pinson, W.H. jr. (1963): Comparison of K-Ar and whole-rock Rb-Sr dating in New-Quebec and Labrador. Am. J. Sci. 261, 571-580.

Bergeron, R. (1957): Preliminary report on Cape Smith-Wakeham Bay belt. Quebec Dept. Mines, P.R. 355.

Bergeron, R. (1959): Preliminary report on Povungnituk Range area, New Quebec. Quebec Dept. Mines, P.R. 392.

Best, M.G. and Weiss, L.E. (1964): Mineralogical relations in some pelitic hornfelses from the southern Sierra Nevada, California. Am. Mineral. 49, 1240-1266.

Bhattacharji, S. (1967): Scale model experiments on flowage differentiation in sills. In: Wyllie, P.J, ed., Ultramafic and related rocks, John Wiley and Sons, 69-70.

Bostock, H.S. (1970): Physiographic sub-divisions of Canada. In: Douglas, R.J.W. ed. (1970), 9-30.

Bridgewater, D., Watson, J., and Windley, B.F. (1973): The Archean Craton of the North Atlantic region. Roy. Soc. London, Phil. Trans., A 273, 493-512.

Brown, W.L. (1962). Peristerite unmixing in the plagioclases and metamorphic facies series. Norsk Geol. Tidsskr. 42, 354-382.

Bullard, E.C., Everett, J.E., and Smith, A.G. (1965): The fit of the continents around the Atlantic. Roy. Soc. London, Phil. Trans., A 258, 41-51.

Chinner, G.A. (1960): Pelitic gneisses with varying ferrous/ferric ratios from Glen Clova, Angus, Scotland. J. Petrol. 1, 178-217.

Cipriani, C., Sassi, F.P., and Scolari, A. (1974): Metamorphic white micas: definitions of paragenetic fields. Schweiz. Mineral. Petrogr. Mitt. 51, 259-302.

Cipriani, C., Sassi, F.P., and Viterbo-Bassani, C. (1968): La composizione delle miche chiare in rapporto con le costanti reticolari e col grado metamorfico. Rend. Soc. Ital. Mineral. Petrol. 24, 153-187.

Clark, S.P., and Ringwood, A.E. (1964): Density distribution and constitution of the mantle. Rev. Geophys. 2, 35-88.

Clarke, D.B. (1970): Tertiary basalts of Baffin Bay: possible primary magma from the mantle. Contr. Mineral. Petrol. 25, 203-225.

Cooper, A.F. (1972): Progressive metamorphism of metabasic rocks from the Haast Schist Group of Southern New Zealand. J. Petrol. 13, 457-492.

Cooper, A.F. and Lovering, J.F. (1970): Greenschist amphiboles from Haast River, New Zealand. Contr. Mineral. Petrol. 27, 11-24.

Crawford, M.L. (1966): Composition of plagioclase and associated minerals in some schists from Vermont, U.S.A. and South Westland, New Zealand, with interferences about the peristerite solvus. Contr. Mineral. Petrol. 13, 269-294.

Currie, K.L. (1966): Geology of the New Quebec Crater. Geol. Surv. Canada, Bull. 50, 36 p.

Dahl, O. (1969): Irregular distribution of iron and magnesium among coexisting biotite and garnet. Lithos 2, 311-322.

Dallmeyer, R.D. (1974a): The role of crystal structure in controlling the partitioning of Mg and Fe^{2+} between coexisting garnet and biotite. Am. Mineral. 59, 201-203.

Dallmeyer, R.D. (1974b): Metamorphic history of the northeastern Reading Prong, New York and northern New Jersey. J.Petrol. 15, 325-359.

Davis, J.C. (1973): Statistics and data analysis in geology. John Wiley & Sons, Inc., New York, 550 p.

De Montigny, P.A. (1959): [illegible]inary report on the Upper Deception River area, N[illegible]ec. Quebec Dept. Mines, P.R. 398.

Dewey, J.F. and Burke, K.C.A. (1973): Tibetan, Variscan, and Precambrian basement reactivation: Products of continental collision. J. Geol. 81, 683-692.

Dimroth, E. (1972): The Labrador Geosyncline revisited. Amer. J. Sci. 272, 487-506.

Dimroth, E., Baragar, W.R.A., Bergeron, R., and Jackson, G.D. (1970): The filling of the Circum-Ungava Geosyncline. In: Baer, A.J. ed. (1970): Basins and geosynclines of the Canadian Shield. Geol. Surv. Canada, Paper 70-40, 45-142.

Dobretsov, N.L. (1968): Paragenetic types and compositions of metamorphic pyroxenes. J. Petrol. 9, 358-377.

Douglas, R.J.W. (1968): Geological map of Canada. Geol. Surv. Canada, Map 1250A.

Douglas, R.J.W. ed. (1970): Geology and economic minerals of Canada. Geol. Surv. Canada, Econ. Geol. Rept. 1., 838p.

Dugas, J. (1971): Mineralization in the Cape Smith-Wakeham Bay area. Min. Rich. nat. Quebec, Sp. 9.

Engel, A.E.J. and Engel, C.G. (1958): Progressive metamorphism and granitization of the major paragneiss, northwest Adirondack Mountains, New York, Part I, Total rock. Geol. Soc. Am. Bull. 69, 1369-1414.

Engel, A.E.J. and Engel, C.G. (1960): Progressive metamorphism and granitization of the major paragneiss, northwest Adirondack Mountains, New York, Part. II, Mineralogy. Geol. Soc. Am. Bull. 76, 483-508.

Engel, A.E.J. and Engel, C.G. (1962): Hornblendes formed during progressive metamorphism of amphibolites, northwest Adirondack Mountains, New York. Bull. Geol. Soc. Am. 73, 1499-1514.

Ernst, W.G. (1963): Significance of phengitic micas from low-grade schists. Am. Mineral. 48, 1357-1373.

Evans, B.W. and Trommsdorff, V. (9174): Stability of enstatite + talc, and CO_2-metamorphism of metaperidotite, Val d'Efra, Lepontine Alps. Am. J. Sc. 274, 274-296.

Fabriès, J. (1963): Les formations cristallines et métamorphiques du Nord-Est de la province de Séville (Espagne). Thesis, Nancy (France), 267 p.

Fahrig, W.F., and Eade, K.E. (1968): Chemical evolution of the Canadian Shield. Can. J. Earth Sci. 5, 1242-1252.

Fahrig, W.F., Eade, K.E., and Adams, J.A.S. (1967): Abundance of radioactive elements in crystalline shield rocks. Nature 214, 1002-1003.

Fahrig, W.F., Irving, E., and Jackson, G.D. (1971): Paleomagnetism of the Franklin diabase. Can. J. Earth Sci. 8, 455-467.

Ferguson, J. and Currie, K.L. (1972): Silicate immiscibility in the ancient "basalts" of the Barberton Mountain Land, Transvaal. Nat. Phys. Sci. 235, 86-89.

Fettes, D.J., Graham, C.M., Sassi, F.P. and Scolari, A. (1976): The basal spacing of potassic white micas and facies series variation across the Caledonides. Scott. J. Geol. 12, 227-236.

Fleming, P.D. (1973): Mg-Fe distribution between coexisting garnet and biotite, and the status of fibrolite in the andalusite-staurolite zone of the Mt Lofty Ranges, South Australia. Geol. Mag. 109, 477-482.

Flint, R.F. (1971): Glacial and Quaternary geology. John Wiley and Sons, Inc., New York, 892 p.

Fonteilles, M. and Guitard, G. (1964): L'"effet de socle" dans le métamorphisme hercynien de l'enveloppe paléozoïque des gneiss des Pyrénées. Comptes Rendus de l'Académie des Sciences. 258 gr. 9, 4299-4302.

Fonteilles, M. and Guitard, G. (1968): L'effet de socle dans le métamorphisme. Bull. Soc. fr. Minéral Cristallogr. 91, 185-206.

Frith, R.A., Frith, R., Helmstaedt, H., Hill, J., and Leatherbarrow, R. (1974): Geology of the Indin Lake area, District of Mackenzie. In Report of Activities, Part 1A. Geol Surv. Canada, Paper 74-1A, 165-171.

Fritsch, W., Meixner, H. and Wieseneder, H. (1967): Zur quantitativen Klassification der Kristallinen Schiefer. 2. Mitt[illegible] N. Jb. Mineral. Mh., 364-376.

Frost, M.J. (1962): Metamorphic grade and iron-magnesium distribution between co-existing garnet-biotite and garnet-hornblende. Geol. Mag. 97, 427-438.

Fryer, B.J. (1972): Age determinations in the Circum-Ungava Geosyncline and the evolution of Precambrian banded iron-formation. Can. J. Earth Sci. 9, 652-663.

Gale, G.H. (1973): Paleozoic basaltic komatiite and ocean-floor basalts from northeastern Newfoundland. Earth Planet. Sci. Lett. 18, 66-74.

Ganguly, J. (1972): Staurolite stability and related parageneses: theory, experiments, and applications. J. Petro. 13, 335-365.

Ganguly, J. and Kennedy, G.C. (1974): The energetics of natural garnet solid solution 1. Mixing of the aluminosilicate end-members. Contr. Mineral. Petrol. 48, 137-148.

Gary, M., McAfee, R. jr., and Wolf, C.L. ed. (1972): Glossary of geology. Am. Geol. Institute, 805 p.

Gates, T.M. and Hurley, P.M. (1973): Evaluation of Rb-Sr dating methods applied to the Matachewan, Abitibi, Mackenzie, and Sudbury dyke swarms in Canada. Can. J. Earth Sci. 10, 900-919.

Gélinas, L. (1962): Preliminary report on Lake Watts area, New Quebec. Quebec Dept. Nat. Res., P.R. 471.

Gélinas, L., Brooks, C., and Trzcienski, W.E. jr. (1976): Archean varioli tes-quenched immiscible liquids. Can. J. Earth Sci. 13, 210-230.

Ghent, E.D. (1976): Plagioclase-garnet-Al_2SiO_5-quartz: a potential geobarometer-geothermometer. Am. Mineral. 61, 710-714.

Gibb, R.A. and Walcott, R.I. (1971): A Precambrian suture in the Canadian Shield. Earth and Plant. Sci. Letters, 10, 417-422.

Glickson, A.Y. (1978): On the basement of Canadian Greenstone Belts. Geoscience Can. 5, 3-12.

Gold, D.P. (1962): Preliminary report on Lake Brisebois area, New Quebec. Quebec Dept. Nat. Res. R.P. 470.

Goulet, N. (1971): Etude pétrologique, structurale, et géochronologique des formations cristallines du quart nord-est de la feuille SAINT-GABRIEL-de-BRANDON. Thesis, Grenoble (France), 203 p.

Graham, C.M. (1974): Metabasite amphiboles of the Scottish Dalradian. Contr. Mineral. Petrol. 47, 165-185.

Green, D.C. and Baadsgaard, H. (1971): Temporal evolution and petrogenesis of an Archean crustal segment at Yellowknife, N.W.T., Canada. J. Petro. 12, 177-217.

Green, D.H. (1974): Genesis of Archean peridotitic magmas and constraints on Archean geothermal gradients and tectonics. Geology 3, 15-18.

Green, J.C. (1963): High level metamorphism of pelitic rocks in northern New Hampshire. Am. Mineral. 48, 991-1023.

Green, O.H. and Ringwood, A.E. (1967): The genesis of basaltic magmas. Contr. Mineral. Petrol. 15, 103-190.

Gunning, H.C. (1933): Sulphide deposits at Cape Smith, east coast of Hudson Bay. Geol. Surv. Can., Sum. Rept 1933 pt. D, 139-154.

Hallimond, A.F. (1943): On the graphical representation of the calciferous amphiboles. Am. Mineral. 18, 65-89.

Hardy, R. (1976): Région des Lacs Robert et des Chefs. Min. Rich. nat. Quebec, R.G. 171, 99 p.

Harker, R.I. and Tuttle, O.F. (1955): Studies in the system $CaO-MgO-CO_2$. Part 1. Am. J. Sci. 253, 209-224.

Hess, H.H. (1949): Chemical composition and optical properties of common clinopyroxenes, Part 1., Am. Mineral. 34, 621-666.

Hietanen, A. (1969): Distribution of Fe and Mg between garnet, staurolite, and biotite in aluminum-rich schist in various metamorphic zones north of the Idaho batholith. Am. J. Sci. 267, 422-456.

Hörmann, P.K. and Raith, M. (1973): Bildungsbedingungen von Al-Fe(III)-Epidoten. Contr. Mineral. Petrol. 38, 307-320.

Holdaway, M.J. (1971): Stability of andalusite and the aluminum silicate phase diagram. Am. J. Sci. 271, 97-131.

Hounslow, A.W. and Moore, J.M. (1967): Chemical petrology of Grenville schists near Fernleigh, Ontario. J. Petrol. 8, , 1-28.

Hsu, L.C. (1968): Selected phase relationships in the system Fe-Al-Mn-Si-O-H. J. Petrol. 9, 40-83.

Hunt, J.A. and Kerrick, D.M. (1977): The stability of sphene: experimental redetermination and geologic implications. Geochim. Cosmochim. Acta 41, 279-288.

Hurst, R.W., Bridgewater, D., Collerson, K.D., and Wetherill, G.W. (1975): Rb/Sr systematics in very early Archean gneisses from Saglek Bay, Labrador. Earth Planet. Sci. Letters 27, 393-403.

Irvine, T.N. (1967): Chromian spinel as a petrogenetic indicator: part 2. Petrologic applications. Can. J. Earth Sci. 4, 71-103.

Irvine, T.N. and Baragar, W.R.A. (1971): A guide to the chemical classification of the common volcanic rocks. Can. J. Earth Sci. 8, 523-547.

Jackson, G.A. and Taylor, F.C. (1972): Correlation of major Aphebian rock units in the northeastern Canadian Shield. Can. J. Earth Sci. 9, 1650-1669.

James, H.L. (1955): Zones of regional metamorphism in the Precambrian of northern Michigan. Geol. Soc. Am. Bull. 66, 1455-1488.

Jolly, W.J. (1975): Subdivison of Archean lavas of the Abitibi area, Canada, from Fe-Mg-Ni-Cr relations. Earth Planet. Sci. Lett. 27, 200-210.

Klein, C. (1969): Two-amphibole assemblages in the system actinolite-hornblende-glaucophane. Am. Mineral. 54, 212-237.

Kostyuk, E.A. and Sobolev, V.S. (1969): Paragenetic types of calciferous amphiboles of metamorphic rocks. Lithos 2, 67-81.

Kretz, R. (1959): Chemical study of garnet, biotite, and hornblende from gneisses of southwestern Quebec, with emphasis on distribution of elements in coexisting minerals. J. Geol. 67, 371-402.

Kretz, R. (1960): Geological observations in northern New Quebec. Geol. Surv. Canada. Paper 60-12.

Lacroix, A. (1939): Observations sur quelques minéraux de Madagascar. Bull. Soc. fr. Mineral. Cristallogr. 62, 300-308.

Lambert, R.St.J. (1959): The mineralogy and metamorphism of the Moine schists of the Morar and Knoydart districts of Inverness-shire. Trans. Roy. Soc. Edinburgh 63, 553-588.

Lambert, R.St.J. (1976): Archean thermal regimes, crustal and upper mantle temperatures, and a progressive evolutionary model for the Earth. In: Windley, B.F. ed. The early history of the Earth; John Wiley and Sons, 363-374.

Leake, B.E. (1968): A catalog of analysed calciferous and subcalciferous amphiboles together with their nomenclature and associated minerals. Geol. Soc. Am. Spec. Paper 98, 210 p.

Lidiak, E.G. (1965): Petrology of andesitic, spilitic and keratophyric flow rocks, north-central Puerto-Rico. Geol. Soc. Am. Bull. 76, 57-88.

Liou, F.G., Kuniyoshi, S. and Ito, K. (1974): Experimental studies of the phase relations between greenschist and amphibolite in a basaltic system. Am. J. Sc. 274, 613-632.

Lowden, J.A. (1963): Age determination by the Geological Survey of Canada; Report 4, Isotopic ages. Geol. Surv. Canada, Paper 63-17.

Lyons, J.B. and Morse, S.A. (1970): Mg/Fe partitioning in garnet and biotite from some granitic, pelitic, and calcic rocks. Am. Mineral. 55, 232-245.

MacRae, N.D. (1974): Sulfurization of basalt under thermal metamorphic conditions to produce cordierite-bearing rocks. Can. J. Earth Sci. 11, 246-253.

McCall, G.J.H. and Leishman, J. (1971): Clues to the origin of Archean eugeosynclinal peridotites and the nature of serpentinisation. Spec. Publs. Geol. Soc. Aust. 3, 281-299.

McIver, J.R. (1975): Aspects of some high magnesia eruptives in Southern Africa. Contr. Mineral. Petrol. 51, 99-118.

McIver, J.R. and Lenthall, D.H. (1974): Mafic and ultramafic extrusives of the Barberton Mountain Land in terms of CMAS system. Precambrian Res. 1, 327-343.

Mielke, H. and Schreyer, W. (1972): Magnetite-rutile-assemblages in metapelites of the Fichtelgebirge, Germany. Earth Planet. Sci. Lett. 16, 423-428.

Miyashiro, A. (1958): Regional metamorphism of the Gossisyo-Takanuki district in the central Abukuma Plateau. J. Fac. Sci., Univ. Tokyo, Sec. II, 11, 219-272.

Moore, J. M. jr. (1977): Orogenic volcanism in the Proterozoic of Canada. In: Baragar, W.R.A., Coleman, L.C. and Hall, J.M., ed. Volcanic regimes in Canada. Geol. Assoc. Can. Spec. Paper 16, 127-148.

Naldrett, A. and Turner, A.R. (1977): The geology and petrogenesis of a greenstone belt and related nickel sulfide mineralization. Precambrian Res. 3, 43-103.

Naldrett, A.J. and Gasparrini, E.L. (1971): Archean Nickel Sulphide Deposits in Canada: their Classification Geological Setting and Genesis with Some Suggestions as to Exploration. Geol. Soc. Australia, Spec. Publ. 3, 201-226.

Nesbitt, R.W. (1971): Skeletal crystal forms in the ultramafic rocks of the Yilgarn block, Western Australia: Evidence for an Archean ultramafic liquid. Geol. Soc. Aust. Spec. Publs, 3, 331-348.

Nicolaysen, L.O. (1961): Graphic interpretation of discordant age measurement on metamorphic rocks. Ann. N.Y. Acad. Sci. 91, 198-206.

[redacted]tsch, K.H. (1970): Experimentelle Bestimmung der oberen Stabilitätsgrenze von Stilpnomelan. Fortschr. Mineral. (Suppl.) 47, 48-49.

[redacted], M.J. (1968): The bearing of phase equilibria studies in synthetic and natural systems of the origin and evolution of basic and ultrabasic rocks. Earth Sci. Rev. 4, 69-133.

Orville, P.M. (1972): Plagioclase cation exchange equilibria with aqueous chloride solution: results at 700°C and 2000 bars in the presence of quartz. Am. J. Sci. 272, 234-272.

Perchuk, L.L. (1967): The biotite-garnet geothermometer. Dokl. Akad. Nauk SSSR 177, 131-134 (transl.).

Phinney, W.C. (1963): Phase equilibria in the metamorphic rocks of St. Paul Island and Cape North, Nova Scotia. J. Petrol. 4, 90-130.

Prest, V.K. (1970): Quaternary geology. In Douglas, R.J.W. ed. (1970), 675-764.

Prest, V.K., Grant, D.R., and Rampton, V.N. (1967): Glacial map of Canada. Geol. Surv. Canada, map 1253A.

Raase, P. (1964): Al and Ti contents of hornblende, indicators of pressure and temperature of regional metamorphism. Contr. Mineral. Petrol. 45, 231-236.

Raith, M. (1976): The Al-Fe(III)epidote miscibility gap in metamorphic profile through the Penninic series of the Tauern Window, Austria. Contr. Mineral. Petrol. 57, 99-117.

Reinhardt, E.W. (1968): Phase relations in cordierite-bearing gneisses from the Gananoque area, Ontario. Can. J. Earth Sci. 5, 455-482.

Richardson, S.W., Bell, P.M., and Gilbert, M.C. (1969): Experimental determination of kyanite-andalusite and andalusite-sillimanite equilibria; aluminum silicate triple point. Am. J. Sci. 267, 259-272.

Ringwood, A.E. (1966): The chemical composition and origin of the Earth. In: Huxley, P.M.,ed. Advances in Earth Science, Cambridge, Mass. Inst. Tech. Press. 287-356.

Rosenberg, P.E. (1967): Subsolidus relations in the system $CaCO_3$-$MgCO_3$-$FeCo_3$ between 350°C and 550°C. Am. Mineral. 52, 787-796.

Sassano, G.P., Baadsgaard, H., and Morton, R.D. (1972): Rb-Sr isotopic systematics of the Foot Bay Gneiss, Donaldson Lake Gneiss, and pegmatite dykes from the Fay Mine, N.W. Saskatchewan. Can. J. Earth Sci. 9, 1368-1381.

Sassi, F.P. and Scolari, A. (1974): The b_0 value of the potassic white micas as a barometric indicator in low-grade metamorphism of pelitic schists. Contr. Mineral. Petrol. 45, 143-152.

Saxena, S.K. (1969): Silicate solid solutions and geothermometry: 3. Distribution of Fe and Mg between coexisting garnet and biotite. Contr. Mineral. Petrol. 22, 259-267.

Saxena, S.K. and Ekström, T.K. (1970): Statistical chemistry of calcic amphiboles. Contr. Mineral. Petrol. 26, 276-284.

Schimann, K. (1976): Géochimie des sédiments de ruisseau, Région de la Rivière Wakeham, Nouveau-Québec. Min. Rich. nat. Quebec, D.P. 421, 6 p.

Schwarcz, F.J. and Fujiwara, Y. (1977): Komatiitic basalts from the Proterozoic Cape Smith range in northern Quebec, Canada. In: Baragar, W.R.A., Coleman, L.C. and Hall, J.M. ed. Volcanic regimes in Canada. Geol. Assoc. Can. Spec. Paper 16, 193-202.

Searle, D.L. and Vokes, F.M. (1969): Layered ultrabasic lavas from Cyprus. Geol. Mag., 106, 515-530.

Sen, S.K. and Chakraborty, K.E. (1968): Magnesium-iron exchange equilibrium in garnet-biotite and metamorphic grade. N. Jb. Miner. Abh. 108, 181-207.

Sheperd, M. (1960): Petrography and mineralogy of the Cross Lake area, Ungava, New-Quebec. Ph.D thesis, Univ. Toronto.

Shido, F. (1958): Plutonic and metamorphic rocks of the Nakoso and Iritono districts in the central Abukuma Plateau. J. Fac. Sci., Univ. Tokyo, Sec. II, 11, 131-217.

Shido, F. and Miyashiro, A. (1959): Hornblendes of basic metamorphic rocks. J. Fac. Sci., Univ. Tokyo, Sec II, 12 85-102.

Smith, D. (1970): Mineralogy and petrology of the diabasic rocks in a differentiated olivine diabase sill complex, Sierra Ancha, Arizona. Contr. Mineral. Petrol. 2, 95-113.

Smith, D.G.W. (1976): Quantitative energy dispersive microanalysis. Microbeam techniques, Smith, D.G.W. ed., Miner. Ass. Canada, Short Course handbook, 1, 63-106.

Stephenson, J.F. (1974): Geology of the Ospwagan Lake (East Half) area. Manitoba Mines Branch, Publ. 74-1.

Stevenson, I.M. (1968): A geological reconnaissance of Leaf River map-area, New Quebec and Northwest Territories. Geol. Surv. Canada, Mem. 356.

Stockwell, C.H. (1964): Fourth report on structural provinces, orogenies and time-classification of rocks of the Canadian Precambrian Shield. Geol. Surv. Canada, Paper 64-17, Pt. II.

Stockwell, C.H. (1973): Revised Precambrian time-scale for the Canadian Shield. Geol. Surv. Canada, Paper 72-52.

Stormer, J.C. (1975): A practical two-feldspar geothermometer. Am. Mineral. 60, 667-674.

Strens, R.G.J. (1965) Stability and relations of the Al-Fe epidotes. Min. Mag. 35, 464-475.

Taylor, F.C. (1974): Reconnaissance geology of a part of the Precambrian Shield, Northern Quebec and Northwest Territories. Geol. Surv. Canada, Paper 74-21.

Thomas, M.D. and Gibb, R.A. (1977): Gravity anomalies and deep structure of the Cape Smith fold belt, northern Ungava, Quebec. Geology, 5, 169-172.

Thompson, A.B. (1976): Mineral reactions in pelitic rocks: II. Calculation of some P-T-X(Fe-Mg) phase relations. Am. J. Sci. 276, 425-454.

Thompson, P.H. (1973): Mineral zones and isograds in 'impure' calcareous rocks, an alternative means of evaluating metamorphic grade. Contr. Mineral. Petrol. 42, 63-80.

Tracy, R.J., Robinson, P., and Thompson, A.B. (1976): Garnet composition and zoning in the determination of temperature and pressure of metamorphism, central Massachusetts. Am. Mineral. 61, 762-775.

Tröger, W.E. (1959): Die optische Bestimmung der gesteinsbildende Minerale. Teil 1: Bestimmungstabellen, 3. Aufl. 147 S. E. Schweizerbart'sche Verlagsbuchhandlung, Stuttgart.

Tröger, W.E. (1967): Die optische Bestimmung der gesteinsbildende Mineral. Teil 2: Textband, 1. Aufl. 822 S. E. Schweizerbart'sche Verlagsbuchhandlung, Stuttgart.

Turner, F.J. (1968): Metamorphic petrology, mineralogical and field aspects. McGraw Hill Book Co., New York, 403 p.

Velde, B. (1965): Phengite micas: synthesis, stability, and natural occurrence. Am. J. Sci. 263, 886-913.

Velde, B. (1967): The Si^{+4} content in natural phengites. Contr. Mineral. Petrol. 14, 250-258.

Viljoen M.J. and Viljoen, R.P. (1969a): An introduction to the geology of the Barberton granite-greenstone terrain. In: Upper Mantle Project Spec. Publs. Geol. Soc. S. Afr. 2, 9-28.

Viljoen, M.J. and Viljoen, R.P. (1969b): The geology and geochemistry of the lower ultramafic unit of the Onverwacht Group and a proposed new class of igneous rock. In: Upper Mantle Project, Spec. Publs. Geol. Soc. S. Afr. 2, 55-85.

Viljoen, M.J. and Viljoen, R.P. (1969c): Evidence for the existence of a mobile extrusive peridotitic magma from the Komati Formation of the Onverwacht Group. In: Upper Mantle Project, Spec. Publs. Geol. Soc. S. Afr. 2, 87-112.

Viljoen, M.J. and Viljoen, R.P. (1969d): The geological and geochemical significance of the upper formations of the Onverwacht Group. In: Upper Mantle Project, Spec. Publs Geol. Soc. S. Afr. 2, 113-151.

Viljoen, M.J. and Viljoen, R.P. (1969e): Evidence for the composition of the primitive mantle and its products of partial melting from a study of the rocks of the Barberton Mountain Land. In: Upper Mantle Project, Spec. Publs. Geol. Soc. S. Afr. 2, 275-295.

Wade, J.A., Grant, A.C., Sanford, B.V., and Barss, M.S. (1977): Basement structure, eastern Canada and adjacent areas. Geol. Surv. Canada, map 1400A.

Wanless, R.K. (1969): Isotopic age map of Canada. Geol. Surv. Canada, Map 1256A.

Wanless, R.K., Stevens, R.D., Lachance, G.R., and Delabio, R.N.D. (1974): Age determinations and geological studies. K-Ar isotopic ages, Report 12, Geol. Surv. Canada, Paper 74-2.

Wenk, E., and Keller, F. (1969): Isograde in Amphibolitserien der Zentralalpen. Schweiz. Miner. Petr. Mitt. 49, 157-198.

Westra, L. (1978): Metamorphism in the Cape Smith-Wakeham Bay area north of 61 degrees. In: Metamorphism of the Canadian Shield. Geol. Surv. Canada, Paper 78-10, in print.

Wilson, H.D.B., Kilburn, L.C., Graham, A.R. and Ramlal, K. (1969): Geochemistry of some Canadian nickeliferous ultrabasic intrusions. Monogr. Econ. Geol. 4, 294-309.

Winkler, H.G.F. (1974): Petrogenesis of metamorphic rocks, 3rd. edition. Springer Verlag, Berlin, 320 p.

Wones, D.E. and Eugster, H.P. (1965): Stability of biotite: experiment, theory, and applications. Am. Mineral. 50, 1278-1272.

Wynne-Edwards, H.R. (1976): Proterozoic ensialic orogenesis: The millipede model of ductile plate tectonics Amer. J. Sci. 276, 927-953.

Wynne-Edwards, H.R. and Hay, P.W. (1963): Coexisting cordierite and garnet in regionally metamorphosed rocks from the Westport area, Ontario. Can. Mineral. 7, 453-478.

APPENDIX I

ELECTRON MICROPROBE WHOLE-ROCK ANALYSIS

1. PREVIOUS WORK

Several methods of sample preparation for whole-rock analysis with the electron microprobe have been tried since 1964. Three groups can be recognized: pressed powder, fusion with flux, and direct fusion.

Arrhenius *et al.* (1964) suggested a pressed powder technique for very fine material and a fusion technique involving the addition of equal amounts of flux to the samples and the production of a bead using a Pt loop dipped into the melt.

Gulson and Lovering (1968), Reed (1970), and Mori *et al.* (1971) adapted the flux fusion technique, suggested by Norrish and Chappell (1967), for X-ray fluorescence analysis, to microprobe analysis. Reed recommended the omission of the La_2O_3 from the flux. Wittkopp and O'Day (1973) recommended reducing the flux:sample ratio to 3:1 with fusion in

a graphite crucible for 10 minutes at 1100°C. Inman (1972) recommended using a flux made up of five parts $Li_2B_4O_7$ and one part Li_2CO_3 and mixing in 5:1 proportions with the sample. Fusion is then carried out in a gold crucible for 9 hours at 1025°C in air.

A direct fusion technique was proposed by Rucklidge et al. (1970) in which rock samples are melted in graphite crucibles in a Pt-wound quench furnace. Hydrogen is passed through the furnace to prevent excessive oxidation of the graphite. Temperatures used are approximately 100°C above the liquidus for the particular compositions involved.

Nicholls (1974), and also Brown (1977), likewise used direct fusion techniques, but employing iridium or molybdenum strip heaters. Nicholls carried out fusion in air, while Brown used a vessel pressurized with argon. In these methods, strip temperatures between 1600 and 2000°C and loads of 10-20 mg were used.

All of these techniques suffer from particular disadvantages. Pressed powders are suitable only when the grain size can be kept well below the size of the analysed volume and substantially less than the depth of electron penetration (1-5 microns). If this is not the case, the volume analysed may not be representative of the bulk composition, and also, normal ZAF corrections are not applicable. Furthermore, powders have to be carbon-coated to render them conductive; the film deposited to achieve this commonly breaks when the samples are transferred from air to vacuum

and vice versa.

In microprobe analysis, the introduction of large amounts of flux to assist in fusion gives rise to poor accuracy and sensitivity. The reduction of the amount of flux, to say 3 parts flux against 1 part sample, reduces these problems, but then loss of iron to the Pt-crucible increases as the viscosity goes up. All methods involving the addition of flux also have the disadvantage that both flux and sample have to be weighed accurately. Flux melting has the advantage of minimizing vaporization losses, and of being able to accommodate all rock compositions.

Direct melting of samples also suffers from disadvantages. Where a muffle-furnace or a quench-furnace is used, crucibles are necessary. Alumina crucibles are costly and cannot be reused. When a graphite crucible is used for such direct fusions, there is a loss of Fe and other transition metals into the crucible and also reduction of some of the oxides to the metal. Some of these problems are avoided with the use of the strip furnace, but others are introduced; the composition of 10-20 mg of powder is unlikely to be representative of a sample, even if the rock has been reduced to -325 mesh. Commonly, quench magnetite appears in the glass (especially at the upper surface where the temperature is not as high as that of the strip itself (1600-2000°C). Inert atmosphere must be used with some strip metals (only Ir and Re can be used in air), increasing the complexity of the apparatus and the time required for mel-

ting. Molybdenum has several advantages, but must be used in inert atmosphere, contaminates the glasses significantly (0.3-0.8 wt%), and absorbs Fe and Ti from the glass (Brown, 1977; Cameron-Schimann, 1978). Such effects are enhanced by the high surface to volume ratio of the glass in strip furnaces. This high ratio, combined with high strip temperatures will also increase alkali volatilization. These effects can be reduced by using a short run time, which in turn tends to produce inhomogeneous glasses (Brown, 1977).

2. DEFINITION of the PROBLEM

To be analysable on the electron microprobe a prepared rock sample must be:

1- Homogeneous at the scale of the volume excited by the electron beam; in the present case it was decided that a convenient method of analysing a volume as large as possible was to use a rastered beam to sweep over four areas of about 600 x 500 microns, thus analysing a volume of 4 x 10^{-6} cm^3 (average depth of penetration of the electron beam: 3 microns. This is possible with energy dispersive analysis. With wavelength dispersive analysis, the volume would be reduced by 2 orders of magnitude.) The rock sample must therefore be homogenised at the scale of 4 x $10^{-6}cm^3$ or $10^{-5}g$.

2- Non-porous: using a porous sample and a non-porous standard or sample and standard of different porosity means different conditions of X-ray production and normal ZAF corrections would not be applicable. Furthermore, samples have to be conductive, and the carbon film deposited to achieve this commonly breaks when porous samples are transferred from air to vacuum and vice versa. This problem could be overcome by mixing the sample with colloidal graphite (D.G.W. Smith, 1978, personal communication).

3- Polishable: this condition is related to the previous one.

4- Undiluted: the peak to background ratio of a dilute sample is decreased relative to an undilute sample and consequently the limit of detection is increased and the accuracy decreased.

In addition to this, the prepared sample should be representative of the original sample, at least within the limits of precision of the analytical method, i.e. it must have the same composition, with no contamination and no loss (or only known and non-essential losses). The preparation method should be rapid and inexpensive to take advantage of the possibilities of electron microprobes equipped for energy dispersive analysis.

3. PRELIMINARY WORK

To define a *modus operandi* for the solution of the above problem, it was necessary to determine certain physical dimensions and parameters, for example sample size, evaporation losses from melts, diffusion in melts, limits of glass forming compositions, etc... Various avenues were explored based on previous work. The first that was tried was the pressed powder method; it was found inadequate for reasons given above. Consequently glasses, and in particular glasses undiluted by fluxes, are considered to be suitable.

A HOMOGENEITY and REPRESENTATIVITY

To produce a glass from a powdered rock sample, the volume analysed by the electron microprobe ($4 \times 10^{-6} cm^3$ or $10^{-5} g$) must be representative of the sample, *i.e.* it must have a composition indistinguishable from that of the sample (within the limits of precision of the analytical method used). Firstly, the scale of homogeneity of the rock powder must be determined, *i.e.* the size of the smallest aliquot to be melted which will be representative of the sample. Secondly, it must be determined if melting to form a glass will reduce this size to that of the analysed volume.

The problem of sampling error is discussed by Wilson (1964) and Ingamells *et al.* (1972). Considering the

rock powder as a bimineralic mixture, the sampling error is obtained from:

$$R = [(pq)/n]^{0.5}.(B-H)/K$$

p,q = proportions of the two minerals

B,H = concentrations of the element considered in each mineral

K = overall concentration of this element

n = effective number of grains in sample

$n = w/d(D \times 10^{-4})^3$

w = sample weight in grammes

d = density of powder

D= effective diameter of grains in microns.

This simplification (only two phases present) enables one to calculate an approximate sampling error for an element by taking the mineral with the highest concentration of that element as phase 1 and the rest of the minerals as phase 2. For example, in a granite composed of quartz, K-feldspar, albite, and biotite, R(Fe) can be calculated by taking biotite as phase 1 and quartz + K-feldspar + albite as phase 2. But if this granite were to contain hematite, hematite would be taken as phase 1, for the higher the concentration of an element in a phase, compared to its average concentration in the rock, the larger R will be for a given sampling size.

As an example, a grain size analysis has been made

on a sample of granite run through a jaw-crusher, a rotary mill, and finally for about 4 min in a swing-mill (Table 14).

Table 14. Grain size distribution of 40 g of granite run through a jaw-crusher, a rotary mill, and in a swing-mill for 4 mn

nominal diameter D microns	fraction by weight
100	0.1
65	0.1
42	0.1
28	0.1
18	0.1
12	0.1
7.6	0.1
5.0	0.1
3.3	0.1
2.1	0.1

effective diameter = sum of D x g
= 28.3 microns

For a granite as above containing 1.5% FeO, all in biotite (6% of the rock and containing 25% FeO), the sampling error for various sampling sizes will be as follows:

relative error	sample size
0.1%	1 g
0.3%	100 mg
1%	10 mg

In fact rock powder for chemical analysis is often

coarser. A -70 mesh powder, (effective diameter 70 microns) will give the following errors:

relative error	sample size
0.4%	1g
1.4%	100mg
4.4%	10mg

For minor elements, especially when concentrated in a single phase, the sampling error will be much larger.

Considering the sensitivity and precision of the electron microprobe, a sample size of 0.1-0.5 g can be considered sufficient.

Fusion of this 0.1-0.5 g of rock powder must result in a reduction of the sampling size to 10^{-5} g. Two mechanisms will tend to homogenize the melt:

1- self-diffusion of the elements in the melt;

2- convection and/or mixing due to the movement of air bubbles in the melt.

Some information is available in the literature for the first mechanism, mainly from synthetic systems (Borom and Pask, 1968; Eitel, 1964; Sippel, 1963; Towers et al., 1953 and 1957; Winchell, 1971). From a compilation and comparison of the data found in these studies, the diffusion coefficients (D) at about 1400°C are:

5×10^{-5} cm^2/s for Na

1×10^{-6} cm^2/s for Ca (and Fe^{2+})

1×10^{-7} cm^2/s for Si

A convenient estimate of the magnitude of the diffusion is the mean-square displacement (Ramberg, 1952):

$$x^2 = 2Dt$$

where x is the average length of the path of the diffusing particles through time t. For example taking t = 300 s, the mean displacement is:

0.08 mm for Si

0.24 mm for Ca (and Fe^{2+})

1.73 mm for Na

A sample size of 0.1 g is equivalent to a sphere of 2 mm radius. Diffusion alone is thus sufficient only for Na.

Some information is available in the literature on the second mechanism. Shimada (1954) gives a diffusion coefficient of 10^{-3} cm^2/s for Ca at 1400°C, from an experiment which includes the effect of convection. This is three orders of magnitude greater than diffusion without convection. The mean displacement for Ca increases to 8 mm and that for Si, by comparison, to 2.4 mm. However, Shimada's work was performed on a low viscosity system ($CaO + Na_2O$ = 25%) and in a granite composition homogenization will be achieved only at temperatures above 1400°C.

B GLASS MAKING

The most common method of making a glass from rock powder is to put some rock powder in a crucible and insert this crucible into a furnace, which is subsequently set to a temperature above the liquidus of the rock. Common crucible materials are silica glass, porcelain, recrystallized alumina, alundum®, platinum-group metals, all of which can used in air, and graphite which must be used in vacuum, or in inert or reducing atmosphere.

The use of crucibles is restricted by their limit of resistance to heat and to the corrosive action of silicate melts, especially basic melts. Silica glass recrystallizes above 1100°C and porcelain crucibles soften above the same temperature. Alundum® is infiltrated and pierced by mafic melts. Recrystallized alumina and platinum-group metals can be used over the whole range of temperature required for the melting of most rocks. However, recrystallized alumina contaminates the melts and platinum-group metals absorb transition elements from the melt. These effects are not too serious on short runs (less than 15 min for batches of 3-5 g). Graphite can be used to temperatures sufficiently high to melt all types of rocks; it must be used in an oxygen-free enclosure which complicates its use. But even then it has a tendency to burn by reducing transition element oxides to the metal; the CO_2 produced results in frothing of the melt. Very rapid fusion may reduce this

problem at the expense of homogeneity. Compared to recrystallized alumina and platinum-group metals, graphite is inexpensive, and can often be reused which is not the case for the first two materials.

Various types of furnace were considered. At the time of these experiments, the muffle furnaces available at the Department of Geology could reach a temperature of only 1350°C, which is insufficient to melt most rocks. An induction furnace was tried at the Department of Physics, using graphite crucibles as susceptors. The temperatures that can be reached are sufficient to melt most rocks, the system is flexible, and melting could be done rapidly by employing a crucible-susceptor combination that can be used in air; but a vacuum or inert atmosphere system makes its use, slow and cumbersome.

Some experimentation was done with strip heating. A molybdenum strip was used, in vacuum. The method was found to be flexible and rapid. But small quantities of powder must be used, increasing the sampling error beyond acceptable limits. The melt is contaminated by the molybdenum strip; this seems to be in part due to a thin layer of molybdenum oxide present on the metal and the contamination would be lessened by preheating in a reducing atmosphere. The glasses produced were not homogeneous. However, experimentation with this method was not extensive and improvements could be made (Brown, 1977).

Homogeneous glasses can be produced rapidly and

with a minimum of equipment by using a flux. The method used for X-ray fluorescence analysis (Norrish and Chappell, 1967) can be adopted. La_2O_3 is not necessary as matrix corrections are routinely made. The main drawback is the low sensitivity resulting from the seven-fold dilution. This dilution ratio can be reduced. Experiments with $Li_2B_4O_7$ alone, showed that it is possible to produce a glass in a Pt-Au crucible over a Mecker burner with a flux:rock (granite or basalt) ratio as high as 1:2. But using such low proportions of flux increases the time required for the fusion, and the absorption of transition elements by the crucible, and decreases the life-time of the crucible.[1]

The conclusion drawn from this preliminary work is that a method should be used that does not require crucibles; a method that is also rapid and of low cost. The method that was developed for this purpose, and which is described in the following section, uses an image furnace.

---

[1] a significant factor considering their price

3. THE IMAGE FURNACE

An image furnace is a device for projecting the image of a high intensity radiation source onto the surface of the object to be heated. The source can be a carbon arc, a short-arc lamp, a filament lamp, or the sun. The optical device may consist of paraboloidal or ellipsoidal mirrors, or of lenses.

The efficiency of an image furnace is proportional to:

1- the fraction of the energy supplied by the source that can be focussed onto the object to be heated;

2- the albedo of the object within the spectral range of emission of the source, or to be more accurate, within the spectral range of the radiation that reaches the object.

Several studies have been made of the radiative properties of geological material; of those the studies of Adams and Felice (1967) and Hovis and Callahan (1966) are particularly useful. They show (see Fig. 71A) that in the spectral range 0.4-22 microns:

1- felsic igneous rocks have a higher albedo than mafic ones, as might be expected from their colour;

2- the albedo increases strongly as the particle size decreases; the albedo of an unsorted powder is similar to that of the finest fraction;

3- the albedo increases from 0.4 microns to the near-infrared and is low again above 5 microns;

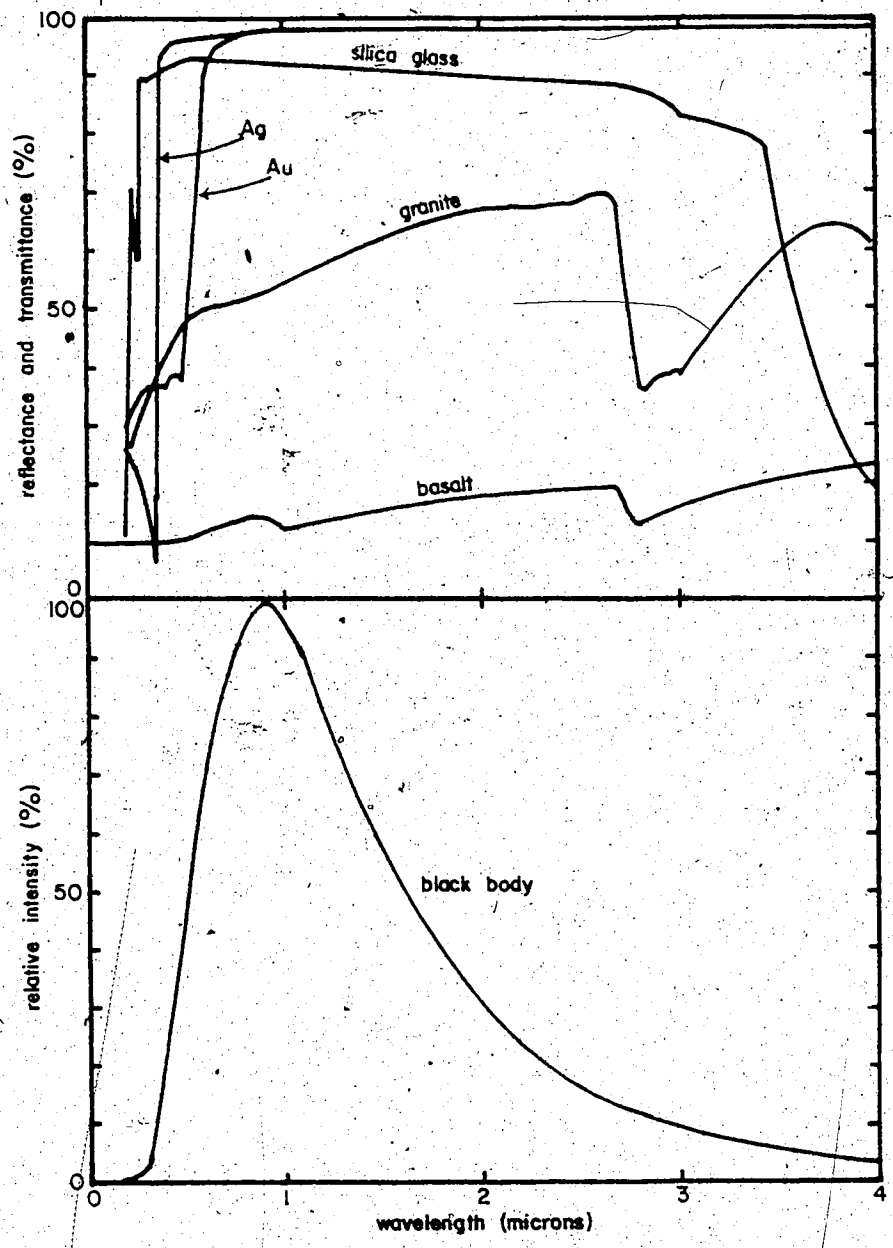

Fig. - Radiative properties of materials...
A- albedo of granite and basalt powders...
reflectance of gold and silver,
transmittance of silica glass (less than 1 cm thick).
B- spectral distribution of energy emitted by a black body at 3200° K.
After Adams and Felice (1967), Hovis and Callahan (1966) Harrison (1960), and Beder et al. (1971).

4- most rock types show strong absorption bands between 2 and 3 microns.

From these considerations, one should choose a source emitting in the ultraviolet or in the infrared, either above 5 microns or in the 2-3 micron range. In addition, the source should be as small as possible. However, ultraviolet and far-infrared radiations require special optical material.

Three compact light sources could be used: short-arc lamps, carbon arc, and incandescent lamps. Short-arc lamps emit most of their energy between 0.25 and 1.1 micron. Carbon arcs are of various types; but in general a large proportion of the emitted energy is in the ultraviolet and visible. Both of these sources require rather complex and expensive power supplies. They have, however, the advantage of being of very high radiance (power per unit surface area) as they are nearly point sources. The incandescent lamp has an emission similar to that of a black-body with a maximum (at 3000°K) at 0.9 micron, i.e. a large proportion of the energy is in the infrared. Its spectral efficiency for the present purpose is about equivalent to that of a carbon arc or a short-arc lamp. It has the disadvantage of a lower radiance (larger source at equal power), but the advantage of low cost, simplicity, and flexibility: its power output can easily be varied with an ordinary variac unit from 0 to 100% (according to the type of material to be melted). In the prototype, a 120 V - 2000 W tungsten-halogen lamp with a

silica glass envelope is used (type BWA of G.T.E. Sylvania). At 120 V, it approximates a black-body radiation source at 3200°K (see Fig. 71B). Such high temperature can be reached, while retaining a high average rated life (350 hr), by the use of the tungsten-halogen cycle. The presence of a silica glass envelope rather than ordinary glass, in addition to making possible the use of the tungsten-halogen cycle, extends the spectral range of the emitted radiation.

The fraction of the energy emitted by the source that reaches the object to be heated depends on the geometrical and optical characteristics of the furnace and on the materials used for the mirrors and windows.

In the prototype, the mirrors are first surface gold-coated mirrors. Gold and silver have the highest reflectance within the spectral range considered (Harrison, 1960). The reflectance of gold decreases sharply below 0.6 micron, but a lamp, such as the one used, emits little energy below that (see Fig. 71C); gold also has the advantage of being chemically inert. Such mirrors should not be used above a few 100°C and cooling must be used where necessary. Most of the optical components of the image furnace are located outside a vacuum chamber that contains the sample. The window of this chamber is of silica glass (General Electric type 105) and has a near 100% transmittance from 0.3 to 2.7 microns and more than 70% between 0.25 and 3.5 microns (Beder et al., 1971) (see Fig. 71A). This interval contains over 95% of the energy radiated by the

lamp. Other materials suitable for that wavelength range are much more expensive, such as synthetic sapphire, and/or less heat resistant, such as LiF.

The optics of the image furnace (Fig. 72 and Plate 1) consist of:

1- a main mirror: ellipsoidal, diameter 16", clearance (from apex to near focal point) 5", working distance (from apex to far focal point) 20", and a collecting efficiency of 50%;[1]

2- a backup mirror; hemispherical, diameter 3";

3- a collector mirror: conical, height 5", diameters 7" and 1.8".

The source (lamp) is located at the near focal point of the main mirror which collects 50% of the energy emitted and focusses it to the far focal point (sample position). The backup mirror collects the other 50% of the emitted energy and sends it back through the source onto the main mirror. Because of the finite size of the source (0.35" x 1.38") the image formed by the main mirror is large, about 3.5" in diameter. The irradiance of this image is not homogeneous; the inner 1" diameter circle, which is the surface to be heated, receives about 30% of the energy. The collector mirror (conical) concentrates on this surface a major

---

[1] catalogue number 3E-16-5-20, Special Optics, Cedar Grove, New Jersey

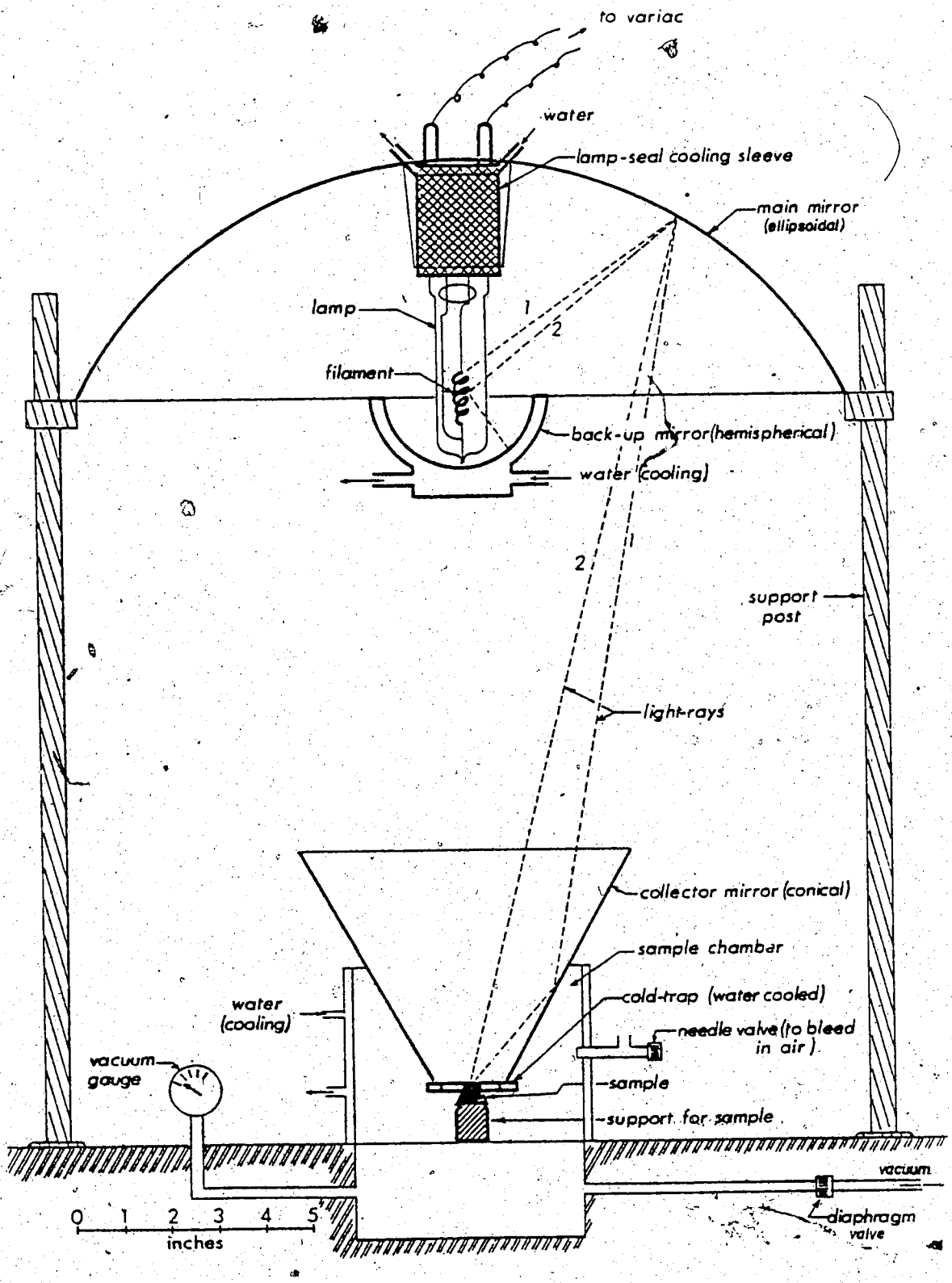

Figure 72. Sketch of the image furnace.

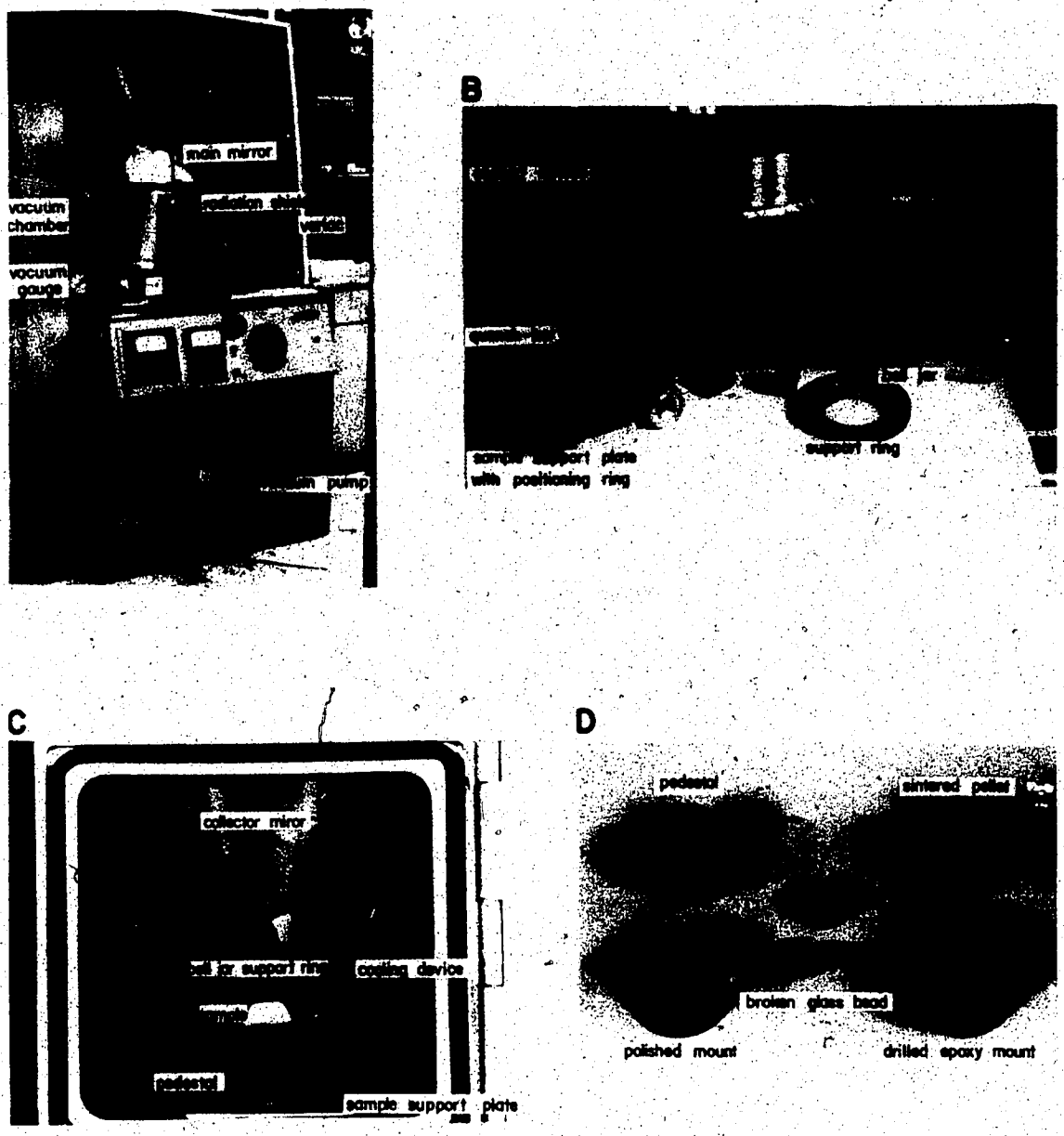

Plate I. The image furnace

A. General view

B. The vacuum chamber

C. Inside of the vacuum chamber with sample ready to fuse

D. Steps in sample preparation

portion of the outer 70% of the beamed energy. It is estimated that in this manner the irradiance in the inner 1" circle is increased by 100-150%.

The main mirror and the lamp are air-cooled. The backup mirror and the lamp-seal area are water-cooled. The sample sits in a vacuum chamber which is water cooled, as is the ring that supports the small bell-jar. This bell-jar is made from a silica-glass crucible (15 ml wide form) whose rim is ground flat to hold vacuum.

The image furnace was built on a disused vacuum coating unit. The sample chamber is connected to a mechanical vacuum pump. A diffusion pump can also be connected if a hard vacuum is ever required. A needle valve is provided on the chamber to bleed in air or an inert gas, while a diaphragm valve between the chamber and the pump permits rapid and flexible control of the vacuum. In normal operation a pressure of between 1/4 - 3/4 atm. is maintained and controlled with a Bourdon gauge; other gauges are available for hard vacuum. The upper part of the apparatus is enclosed in a thin aluminium casing to shield the operator from the ultraviolet radiation of the lamp and others from its glare.

4. FUSION PROCEDURE

A PREPARATION

The rock sample is ground to 100% -100 microns (see Table 14). A useful and simple test of grain size can be carried out; no grains should be detectable between the fingers if the powder is fine enough. The sample must be ground fine not only to decrease the sampling error, but also to aid in the melting which will be more rapid with fine powder.

During direct fusion some of the volatile elements are lost: H_2O, CO_2, S, Cl, P (in part). If this loss occurs during fusion in the image furnace, some of the evaporate is deposited onto the bell-jar reducing its transmittance. To avoid this, the sample is preheated. About 0.5-2.0 g of powder in a 4 ml porcelain crucible is heated for 12 hours at 1000°C in a muffle furnace. This eliminates most of the volatiles that are lost during direct fusion, and produces a sintered pellet which can easily be tipped out of the crucible in one piece (see Plate 1). If a loss-on-ignition determination is required, it can be done at this stage. The preheating is done in large batches by using a tray made from refractory bricks holding about 40 porcelain crucibles.

B FUSION

The sintered pellet is tipped from the crucible to sit inverted on the top of an inconel[1] pedestal and then introduced into the chamber of the image furnace. The chamber is evacuated to 3/4 or 1/4 atm. depending upon whether the composition of the sample is basic or acid. The purpose of having this partial vacuum is to extract air bubbles that are trapped in the melt. The voltage is then increased until fusion begins to occur, then further increased by 10 to 20 volts (maximum of 120 volts), and held there for about 5 minutes for samples that melt readily, or 10 minutes for more refractory material. The reason for not using a harder vacuum is that components of the melt can be lost by vapour transport during melting, the lower the pressure, the greater the loss. Loss by this mechanism increases as the viscosity of the melt drops, hence higher pressures are used with the less viscous melts. After melting is complete, the sample is removed from the furnace and quenched with an aluminium bar.

The upper half or two-thirds of the pellet are melted, the lower part acting as the hearth, and thereby eliminating the problem of contamination by crucible walls. The elimination of the bubbles not only makes a glass that

---

[1] 72% Ni, 6-10% Fe, 14-17% Cr; this alloy has a good resistance to oxidation at high temperature. Ordinary steel would produce scales during the fusion.

is easily polished, but also aids in the homogenization process. This mixing can be enhanced in viscous melts by varying the pressure during the melting.

C PROCESSING

Glass chips of sufficient size to produce a polished surface of 3-4 mm^2 are mounted in epoxy resin, 12 or more per 1" diameter petrographic mount. A convenient way is to prepare epoxy resin blanks, drill 12 holes a few millimetres deep, embed the glass chips in fresh epoxy resin, and set the mount upside down on a glass plate, for example a petrographic slide, for curing. In this manner all chips will be at the same level, near the surface of the mount, making for easier grinding. The glass plate should be coated beforehand with a silicone-based liquid[1] for easier removal of the mounts after curing of the epoxy resin.

Grinding and polishing is done as for other polished mounts used in electron microprobe work. But it is preferable to let the mounts harden for several days before grinding. Also the grinding, prior to polishing, must be done on silicon carbide paper and not on a cast-iron wheel and glass plates with silicon carbide powder, as is done with rock samples. Care must be taken in the identification

---

[1] for example Buehler Release Agent

of the samples, at the pre-fusion stage and at the polishing stage. A convenient system for sample identification is to cut a groove along the side of the mount before embedding the glass chips and counting the sample positions always in the same pattern. After polishing, the samples are carbon-coated.

D ANALYSIS

The procedure used for analysis is very similar to that outlined by Smith and Gold (1976). An energy dispersive technique is used which gives fully quantitative analyses for major and minor elements from Na to Zn, plus Zr and Ba. Thus 22 elements are determined simultaneously and automatically. Analyses are collected for a period of 400 s using a rastered beam sweeping over an area of 300 x 250 or 600 x 500 microns. If the rock is acid and the melt, from which the glass was formed, was very viscous, minor residual inhomogeneities can be averaged out by selecting 4 such areas and sweeping each for 100 s. The data produced is processed through the FORTRAN IV programme 'EDATA' which applies all necessary corrections for background, overlap, escape peaks, drift, as well as ZAF effects.

E VAPORIZATION LOSSES

As mentioned above, some of the components of the rock powder are lost in the glass making; H_2O, CO_2, S, Cl, and P (partly). Such losses will occur in all direct melting methods. Phosphorus losses can be minimized by using a melting time which is as short as possible. These losses do not detract much from the usefulness of the method, but other losses may be more significant, and alkalies are of particular concern.

At temperatures above 1000°C, the partial pressure of vapour of some of the constituents of rocks is sufficiently high that losses may occur, and be a potential source of error in the analysed composition. To a first approximation, a melt may be considered as a mixture of oxides. At the surface of the melt, an oxide MO(l) is in equilibrium with its vapour constituted by MO(g), M(g), O(g) etc... The surface of the enclosing chamber is at a much lower temperature and the vapour pressure of MO is lower there than near the surface of the melt; a gradient of concentration is established and mass transfer occurs. In soft vacuum and at atmospheric pressure, the mass loss rate is pressure dependent and is a diffusion-controlled process. Calculations have been made to establish the mass loss rate on simple systems. With a system as complex as a natural rock such calculations are of little use and direct experimentation is more useful.

Information is available in the literature on ex-

periments done in four fields: pure oxides, synthetic glasses, tektites, and lunar materials.

Tables of vapour pressure of oxides (Brewer, 1953) are useful only in that they give a relative order of vaporization of oxides. A glass is not only a mixture of oxides, it is a framework of silica groups to which are bonded the other oxides. The vapour pressure of an oxide will be a function of the dissociation energy of the framework, the dissociation energy of the oxide, the vaporization energy of the oxide and of the element. In addition, the rate of vaporization will also be controlled by diffusion in the glass.

Experiments on synthetic glass are done at atmospheric pressure. The rates of losses measured vary, from 3 to 150 x 10^{-4} mg/cm^2 at 1400-1500°C (Dietzel and Merker, 1957; Oldfield and Wright, 1962). The losses are mainly sodium.

Experiments on tektites and those on lunar rocks are more akin to the present problem as they deal with natural (complex) systems, one of granitic, the other of basaltic composition. The results on tektites are contradictory. Walter and Carron (1964) found weight losses at 10^{-6} atm. of 3-7 x 10^{-2} mg/cm^2.mn at 2000-2100°C and 1.4 x 10^{-3} mg/cm^2.mn at 1780°C. The vapour pressure at 1600°C is measured as 0.3 atm.. Centolanzi and Chapman (1966) measured a vapour pressure of $.10^{-5}$ atm. at 1600°C and mass loss rates that vary (at 1825°C) from 1 mg/cm^2.mn at 0.1 atm to 0.1 mg/cm^2.mn at

1 atm. These results are quite contradictory; the method used by Centolanzi and Chapman (1966), direct measurement of weight loss by evaporation, is more similar to the present situation.

Biggar and O'Hara (1972) measured mass loss rates for Na_2O and K_2O of 0.1 mg/cm^2.mn at 1175°C and pressure on the order of 10^{-7} to 10^{-8} atm. for a tholeiite. De Maria et al. (1971) measured the vapour pressure of lunar basalts. Their findings are shown in Figure 73. The differences between the two samples may be related to differences in viscosity: sample 12022, 7 poises and sample 12065, 11 poises at 1400°C (Weill et al., 1971). Vaporization losses may be significant for alkalis and iron if hard vacuum is used during melting.

In conclusion, it appears that vaporization losses will be negligeable if the pressure during melting is kept above 0.1 atmosphere for low viscosity melts (basalts, ultramafic rocks, peralkaline rocks) and 0.01 atmosphere for high viscosity melts (granites, granodiorites).

F UNITS of GLASS-FORMING COMPOSITIONS

Limits of glass-forming compositions are set in two ways:

1- the ability of the furnace to melt a given composition;

2- the ability of a melt to form a glass upon cooling.

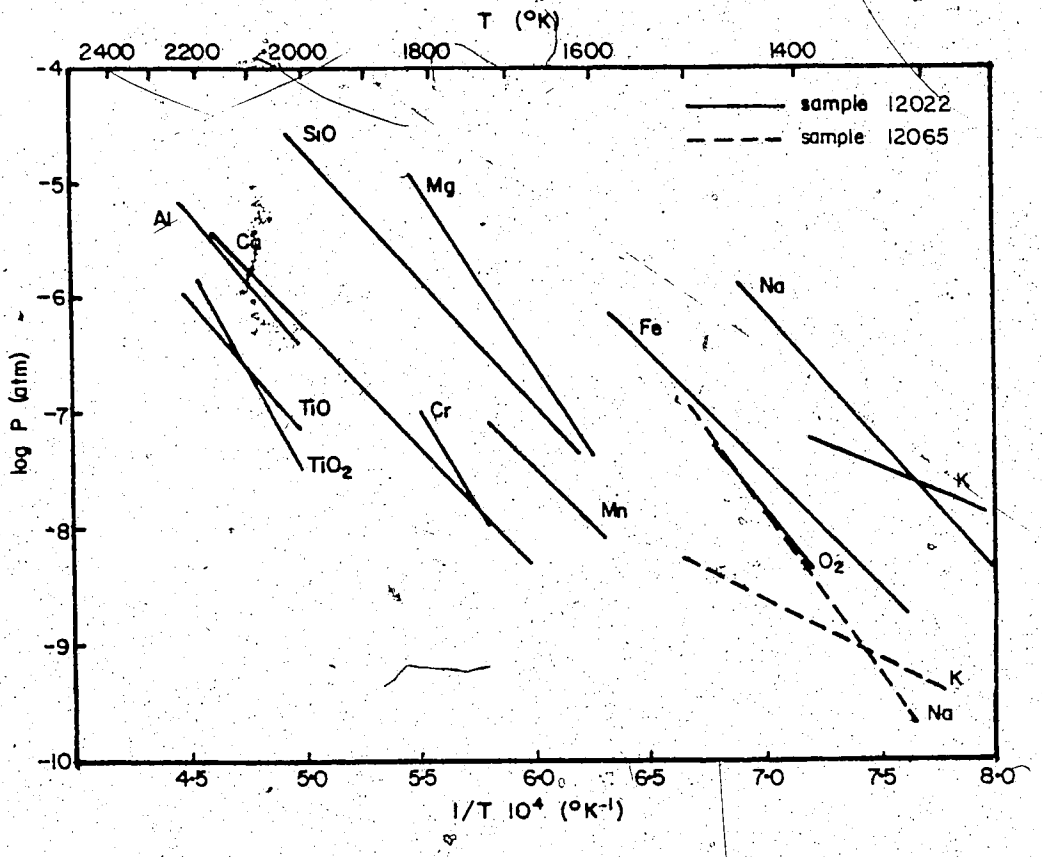

Figure 73. Vaporization behaviour of lunar basalts in vacuum. After De Maria et al. (1971).

Certain rock compositions cannot be melted in the image furnace, because of their high liquidus temperature (ultramafic compositions with MgO > 45%), and/or their high albedo (SiO_2 + Al_2O_3 > 85-90%).

Certain rock compositions do not form homogeneous glasses because:

1- the melt does not solidify as a glass (it recrystallizes, even upon rapid quenching), or

2- liquid immiscibility produces an inhomogeneous glass.

The formation of glass is discussed by Rawson (1967). Most materials melt to a liquid with a viscosity comparable to that of water (0.02 poise), and when this liquid is cooled it crystallizes rapidly. Certain materials melt to liquids with very high viscosity (10^5 to 10^7 poises). These liquids may be supercooled sufficiently to form a glass instead of crystallizing. Of interest to the present study is, of course, that SiO_2 is a glass-forming oxide. But whether a liquid cools to form a glass depends not only on its composition, but also on the rate of cooling which in turn is dependent on the volume considered. Some compositions may form a glass at the scale of a few milligrammes, but not at the scale considere,d here 0.1-1 g.

Most rocks can be considered as a mixture of silica, alumina, alkali and alkaline-earth oxides, and iron oxide. The case of rocks containing significant amounts of sulphate, sulphide, phosphate, and carbonaceous matter will

be discussed later. Table 15 shows lower limits of silica content for glass-formation in some synthetic systems.

Table 15. Limits of glass forming compositions in silicate systems after Imaoka (1962).

System	Glass-formation range (mol. % SiO_2)
SiO_2 - K_2O	100.0 - 45.5
SiO_2 - Na_2O	100.0 - 42.0
SiO_2 - BaO	100-0 - 60.0
SiO_2 - CaO	100.0 - 43.3
SiO_2 - MgO	100.0 - 57.5

Ternary systems of the same oxides show silica limits intermediate between the two binary systems, sometimes somewhat lower (Imaoka and Yamazaki, 1968). Most natural systems contain also alumina; it may act as a network former like silica ($Al_2O_3 < R_2O$) or as both a network former and a network modifier ($Al_2O_3 > R_2O$). Igneous rock compositions beyond the glass-forming domain are reached only in ultramafic rocks (high MgO) and in carbonatites (high CaO, and CO_2).

Fields of liquid immiscibility can be observed in a number of phase diagrams shown in Levin et al. (1964 and 1969). Such fields, however, are temperature dependent and in most cases are outside natural compositions.

Some experiments were carried out with iron-rich compositions. Compositions with more than 20-25% Fe_2O_3 show

immiscibility with formation of a silica-rich and an oxide-rich liquid, each quenching as a glass.

Volatile-rich compositions also present a problem. During the preheating stage (12 hours at 1000°C) carbonates and sulphides are transformed into oxides[1], carbonaceous matter burns, and CO_2 and SO_2 are eliminated with H_2O. Phosphates and sulphates are not dissociated at this temperature but are in the image furnace, especially under vacuum as the fusion is normally done; P and S evaporate and coat the bell-jar (which is near the sample) decreasing drastically the irradiance of the sample. Samples containing more than 1-2% of phosphate or sulphate should be melted at atmospheric pressure. If more than 4-5% phosphorus is present another melting technique should be used.

---

[1] this may produce non-glass forming compositions

5. DISCUSSION

A ADVANTAGES and DISADVANTAGES

There are a number of significant advantages to the technique outlined:

1- Because the sample forms its own hearth, there are no problems of contamination on the one hand, or loss of material to the crucible on the other. There does not appear to be any vertical compositional gradient, paralleling the temperature gradient; the reason is probably the speed of the melting coupled with the mixing effect of bubbles streaming out of the melt. At the same time, diffusion in the glass is sufficiently rapid to homogenize it.

2- Sample preparation is rapid, at least as rapid as the preparation of glass discs for XRF analysis.

3- Because dilution of the sample with flux is unnecessary in most cases, sensitivity and accuracy are high; peak:background ratios are maintained at a maximum.

4- Cost of preparation of samples is low. This can become an important factor when large numbers of analyses have to be performed.

5- The volume of glass formed from a 0.5-2.0 g sample is statistically representative of the original rock sample if it has been powdered to the suggested grain size.

6- Operation of the equipment is very simple and flexible. Temperature, vacuum and atmosphere (if required) can all be easily controlled. The glasses can be produced by any careful person of normal intelligence after a very short period of training.

7- The energy dispersive technique advocated for the microprobe is extremely rapid compared to conventional wavelength dispersive techniques or to standard XRF techniques. It permits the simultaneous analysis of 22 elements with an accuracy that is as good as the wavelength and XRF techniques in the major and minor element ranges. Because of the lack of focussing requirements with EDA, it is unnecessary to obtain the perfection of polish on the mounts that would be required with the fully focussing crystal spectrometers employed in WDA, and a broadly rastered beam can be used to analyse a much larger volume.

The technique also has some disadvantages, most of which are related to the direct melting method rather than to the technique used. Volatile elements are lost from the samples. These include H_2O, CO_2, Cl, F, S, P (in part), probably Pb and possibly other elements in the Pb and S groups. The method has certain limits in terms of the compositions which can be handled. The furnace is capable of heating dark-coloured powders to 1600-1700°C but light-coloured samples can only be raised to 1400-1500°C. The temperatures

could undoubtedly be increasedwith further modifications to the optical design. Outside a certain composition range, it is difficult or impossible to form a glass. Thus if Al_2O_3 + SiO_2 < 45%, although a melt can be formed, it cannot be quenched before it recrystallizes. Hence, glasses cannot be prepared by the technique outlined, from ultramafics or from carbonate-rich sediments. If SiO_2 + Al_2O_3 > 85-90%, the melt is very viscous and has a high temperature liquidus. Silicates with Fe_2O_3 > 20-25% often show immiscibility phenomena with the formation of a silica-rich and an oxide-rich liquid. If large amounts of phosphorus are present in a sample (more than 4-5%), it evaporates in the image furnace and coats the silica-glass isolation window, thereby causing a reduction in the efficiency of the furnace. A similar effect may be expected with sulphate-rich rocks. Most of these problems can be avoided by the introduction of flux ($Li_2B_4O_7$) in 1:1 to 2:1 ratio with sample, with subsequent melting being carried out in air. For the most accurate analysis the sample and flux should be weighed. However, in most cases, satisfactory accuracy is achieved by assuming that the difference between the oxide totals of the elements analysed and 100% has the composition of the flux. Where the Fe content is high, it must be calculated partly as Fe_2O_3 and partly as FeO; wet chemical analysis of glasses, with and without flux, have shown that the iron is only partly oxydized; about 65% of the total iron is present as Fe_2O_3

B TIME of SAMPLE PREPARATION.

Time is required to fill the porcelain crucibles with samples, to note down their numbers and the number of the crucible used and to place them in the muffle furnace for sintering. A batch of 30 to 40 can be done in about 2.5 hours or less, i.e. about 4 minutes per sample. Melting can be carried out at the rate of about 4-8 samples/hour, i.e. about 10 minutes/sample including all manipulations. Further time is expended in making epoxy mounts, drilling holes in them to take the glass fragments, choosing suitable glass grains and mounting them. Overall it takes about 2-3 hours for a batch of 30-40 samples, i.e., about 4.5 minutes/sample. Polishing times clearly vary according to the facilities that are available. However, we have found that 6 mounts (each containing twelve glasses) can be polished with the expenditure of about 4 h real time during a two-day period. Thus, about 3.5 minutes/sample is expended in polishing. This gives a total time expended per sample in preparation of about 20 minutes. The time taken for analysis is about 8 minutes/sample, another 4 minutes are required for data manipulation and perhaps 3 minutes for computer reduction.

C COST

The cost of building the equipment we have illustrated here was about $3,000, (1974 dollars), i.e. the same as half a dozen platinum crucible for flux melting. However, a significant portion of this figure was taken up by experimental versions and the cost of rebuilding on the final pattern would be closer to $2,000. The cost of production would, of course, be considerably reduced if the equipment was built in quantity rather than a one-off basis.

The porcelain crucibles cost around 30¢ each and can be used 5-10 times. The lamp costs about $50 with an average rated life of 350 h (with a longer life if used at less than 120 volts). An average of 6 samples/hour gives a cost/sample of about 2.5¢. The cost of materials for mounting and polishing is difficult to estimate. However, it is probably of the order of 50¢/sample, giving a total cost in materials of about 60¢/sample. Thus the total costs of preparation including labour and materials is probably less than $3/sample.

The computing costs per sample are about $1.50 (for an average silicate rock). Using round figures of $100/hour for microprobe costs, each sample costs about $16.50 to analyse. Thus the total cost of obtaining a fully quantitative analysis for 22 elements is close to $20/sample, provided always that the samples are run in batches of sufficient quantity.

D ANALYTICAL RESULTS

Table 16 lists energy dispersive electron microprobe analyses of glasses made in the image furnace, using the procedure outlined above, and the corresponding known compositions.

Mg, and to a lesser extent Na, are low on most microprobe analyses due to build-up of an oil film on the detector window during the period in which these glasses were analysed (this problem was corrected subsequently).

The analyses of standard samples (T-1, BCR-1, AVG-1) show good agreement with the "best" or "usable values", and there is no significant variation from glass to glass and from one spot to another on the same glass. There is no detectable loss of Na or K, as expected from the discussion above.

In the case of sample R145, it is difficult to decide which of the three analyses is best (wet chemical, X-ray fluorescence, or microprobe). Samples H42 and R182 are examples of extreme compositions (aluminous and ultramafic respectively). Again there is no significant difference between the two glasses of each sample. Sample R184 shows that rocks containing refractory minerals, such as spinel or garnet, can be melted completely without forming inhomogeneities.

6. CONCLUSIONS

Direct melting of powdered rock samples with an image furnace, using the procedure outlined above, is a rapid and low-cost method of preparing samples for microprobe analysis. The method is applicable to a broad spectrum of compositions. In fact, aside from some extreme compositions, the limit of the method is only the glass-forming ability of the rocks themselves. Where this limit is reached, mixing at 1:1 by volume of $Li_2B_4O_7$ and powdered sample enables direct melting (at atmospheric pressure). The analytical results agree well with known compositions and demonstrate the inter- and intra-glass homogeneity of a variety of compositions, including refractory mineral-bearing rocks.

Combining direct melting of rock samples with the energy dispersive capability of an electron microprobe and a suitable data processing programme, results in a method of whole-rock analysis that compares favourably, in speed and quality of analysis of major elements, with other modern methods, such as X-ray fluorescence analysis.

Table 16. Comparison between "known composition" and electron microprobe analyses of glasses produced from a variety of rock types with the image furnace. All analyses are recalculated to 100%, volatile-free. Microprobe analyses were made using one 400 s count with scanning set at 300 x 250 microns.

		T-1 tonalite				
	"Best	Glass A[2]			Glass B	
	values"[1]	1[3]	2	3	1	2
Si	29.71	30.30	30.00	29.76	29.94	29.57
Ti	0.36	0.38	0.35	0.42	0.44	0.39
Al	8.80	9.17	9.08	8.91	8.94	9.25
Fe	4.21	4.57	4.46	4.38	4.32	4.54
Mn	0.09	0.08	0.06	0.07	0.06	0.07
Mg	1.14	0.93	0.92	0.88	0.86	0.93
Ca	3.70	3.86	3.82	3.78	3.72	3.91
Na	3.31	3.25	3.38	3.27	3.51	3.34
K	1.04	1.01	1.01	0.99	0.95	0.94

		AVG-1 andesite				BCR-1 basalt	
	"Usable	Glass	Glass	Glass	"Usable	Glass	Glass	Glass
	values"[4]	A	B	C	values"	A	B	C
Si	28.29	28.58	28.72	28.63	25.90	26.20	26.10	26.11
Ti	0.64	0.59	0.61	0.66	1.34	1.37	1.31	1.36
Al	9.24	9.34	9.33	9.31	7.32	7.38	7.34	7.30
Fe	5.39	5.51	5.30	5.36	10.62	10.62	10.69	10.61
Mn	0.08	0.04	-	-	0.15	0.05	0.09	0.09
Mg	0.95	0.59	0.59	0.59	2.13	1.62	1.72	1.63
Ca	3.62	3.56	3.52	3.53	5.04	4.96	5.06	4.98
Na	3.24	3.13	3.02	3.03	2.46	2.28	2.30	2.46
K	2.47	2.49	2.49	2.52	1.41	1.44	1.38	1.40

			R145 rhyolite			
	Wet	XRF[6]	Glass A		Glass B	
	chem.[5]		1	2	1	2
Si	32.09	33.88	32.73	32.58	32.52	32.47
Ti	0.24	0.20	0.21	0.23	0.23	0.25
Al	8.69	7.18	8.66	8.67	8.64	8.62
Fe	2.00	1.81	2.12	2.11	2.23	2.19
Mn	0.03	0.03	-	-	-	-
Mg	1.00	0.72	0.91	0.88	0.86	0.87
Ca	3.07	2.70	3.21	3.20	3.20	3.19
K	1.31	1.53	1.45	1.44	1.42	1.44

Table 16. Cont'd...

	DS/An39 Antrim basalt[7]					R182 ultramafic		
	Wet chem.[8]	Glass A 1	Glass A 2	Glass B 1	Glass B 2	Wet chem.[8]	Glass A	Glass B
Si	24.94	24.23	24.31	24.29	24.71	20.35	20.34	20.39
Ti	0.63	0.60	0.58	0.71	0.64	0.36	0.47	0.43
Al	7.91	7.74	7.78	7.72	7.89	2.99	2.79	2.64
Fe	7.78	9.06	8.89	8.66	8.77	11.09	12.93	12.14
Mn	0.13	0.14	0.15	0.16	0.13	0.14	0.17	0.12
Mg	3.85	3.63	3.62	3.42	3.47	18.74	17.57	17.63
Ca	7.65	7.58	7.50	7.44	7.57	1.85	2.42	2.28
Na	1.78	1.79	1.86	1.99	1.90	0.44	0.23	0.10
K	0.61	0.61	0.61	0.59	0.60	0.43	0.40	0.39
Cr	-	-	-	-	-	-	0.29	0.28
Ni	-	-	-	-	-	-	0.22	0.20

	H42 metabentonite[9]				R184 gneiss[10]		
	Wet chem.[11]	Glass A 1	Glass A 2	Glass B 1	Wet chem.	Glass A	Glass B
Si	28.34	29.16	28.97	28.91	29.81	30.48	30.10
Ti	0.19	0.14	0.21	0.23	0.45	0.35	0.43
Al	12.96	12.22	12.25	12.07	10.74	10.99	11.09
Fe	0.83	1.47	1.50	1.52	4.60	4.85	4.92
Mn	-	-	-	-	0.02	-	-
Mg	2.85	2.20	2.21	2.21	1.39	1.12	1.16
Ca	0.43	1.25	1.21	1.24	0.54	0.55	0.55
Na	0.09	-	-	-	1.39	1.24	1.23
K	6.59	6.76	6.75	6.59	3.38	3.55	3.50

1: "Best values" as per Abbey (1972).
2: Glasses A and B are made with the image furnace, glass C is made by Roedder.
3: 1, 2, and 3 are analyses of the same glass on different spots.
4: "Usable values" as per Abbey (1972).
5: Wet chemical analysis: A. Stelmach, analyst.
6: X-ray fluorescence analysis at University of Durham.
7: Wet chemical analysis and glass analyses on different samples.
8: Wet chemical analysis: A. Stelmach, analyst; not of same sample as glasses.
9: A.P.I. reference clay.
10: Garnet-cordierite-spinel gneiss.
11: Analysis from A.P.I..

7. REFERENCES

Adams, J.B. and Felice, A.L. (1967): Spectral reflectance 0.4 to 2.0 microns of silicate rock powders. J. Geophys. Res., 72, 5705-5716.

Arrhenius, G., Fitzgerald, R., Frederiksen, K., Holm, B., Sinkankas, J., Bonnatti, E., Boström, K., Lynn, D., Matthias, B., Geballe, T. and Korkisch, J. (1964): Valence band structure and other La Jolla problems in microprobe analysis. Electrochem. Soc. Meeting, Electrotherm. and Metall. Div. Extended Abstracts, No 214, 100-103.

Beder, E.C., Bass, C.D. and Shackleford W.L. (1971): Transmissivity and absorption of fused quartz between 0.22 micron and 3.5 microns from room temperature to 1500°C. App. Optics 10, 2263-2268.

Biggar, G.M. and O'Hara, M.J. (1972): Volatilisation from lavas and small planets. In: Progress in exp. petrology, Nat. Env. Res. Council, Publ. Series D, No 2, p 107.

Borom, M.P. and Pask, J.A. (1968): Kinetics of dissolution and diffusion of the oxides of iron in sodium disilicate glass. J. Amer. Ceram. Soc., 51, 490-498.

Brewer, L. (1953): The thermodynamic properties of the oxides and their vaporization processes. Chem. Rev., 52, 1-70.

Brown, R.W. (1977): A sample technique for whole rock analysis with the electron microprobe. Geochim. Cosmochim. Acta, 41, 435-438.

Cameron-Schimann, M. (1978): Electron microprobe study of uranium minerals and its application to some Canadian deposits. Univ. Alberta, PhD Thesis, 343 p.

Centolanzi, F.J. and Chapman, D.R. (1966): Vapor pressure and tektite glass and its bearing on tektite trajectories determined from aerodynamic analysis. J. Geophys. Res., 71, 1735-1749.

De Maria G., Balducci, G., Guido, M. and Piacente V. (1971): Mass spectrometric investigation of the vaporization process of Apollo 12 lunar samples. Proc. 2nd. Lun. Sc. Conf., 2, 1367-1380.

Dietzel, A. and Merker, L. (1957). Enstehung von Inhomogenitäten in der Glasschmelze durch Verdampfung einzelner Glasbestandteile. I. Glastech. Ber., 30, 134-138.

Eitel, W. (1964): Silicate Science. Academic Press, 5 vol.

Gulson, B.L. and Lovering, J.F. (1968): Rock analysis using the electron probe. Geochim. Cosmochim. Acta, 32, 119-122.

Harrison, T.R. (1960): Radiation pyrometry and its underlying principles of radiant heat transfer. J.Wiley and Sons, N.Y., 234 p.

Hovis, W.A. and Callahan, W.R. (1966): Infrared reflectance spectra of igneous rocks, tuffs, and red sandstone from 0.5 to 22 microns. J. Opt. Soc. America, 56, 639-643.

Imaoka, M. (1962): Glass-formation range and glass structure. In: Adv. Glass Technology, Tech. Paper, VI, Intern. Congr. Glass. Tech., Wash., D.C., 149-164.

Imaoka, M. and Yamazaki I.T, (1968): Glass-formation ranges of ternary systems. I. Silicates of A group elements. Rep. Inst. Ind. Sci. Univ. Tokyo, 18, 241-273 (in Japanese).

Ingamells, C.O., Engels, J.C. and Switzer, P. (1972): 24th Intern. Geol. Congress, sect. 10, 405-415.

Inman, C. (1972): A technique for preparation of small heterogeneous samples for bulk chemical analysis by electron-microprobe. Anal. Chim. Acta, 60, 468-471.

Levin, E.M., Robbins, C.R. and McMurdie, H.F. (1964): Phase diagrams for ceramists. Amer. Ceram. Soc. Inc. 601 p.

Levin, E.M., Robbins, C.R. and McMurdie, H.F. (1969): Phase diagrams for ceramists: 1969 supplement. Amer. Ceram. Soc. Inc. 626 p.

Mori, T., Jakkes, P., and Nagaoka, M. (1971): Major element analysis of silicate rocks using #lectron microanalyser. Sci. Rep. Kanazawa Univ., 16, 113-120.

Nicholls, I.A. (1974): A direct fusion method of preparing silicate rock glasses for energy-dispersive electron microprobe analysis. Chem. Geol., 14, 151-157.

Norrish, K.N. and Chapell, B.W. (1967): X-ray fluorescence spectrography. In: Zussman J. ed. Physical Methods in the Determination of Minerals Academic Press, 514 p., p 161-214.

Oldfield, L.T. and Wright, R.D. (1962): The volatilization of constituents from borosilicate glass at elevated temperatures. In: Adv. Glass Technology, Tech. Paper, VI, Intern. Congr. Glass. Tech., Wash., D.C., 35-51.

Ramberg, H. (1952): The origin of metamorphic and metasomatic rocks. Univ. Chicago Press, 317 p.

Rawson, H. (1967): Non-metallic solids, vol. 2: Inorganic glass-forming systems. Academic; N.Y., 317 p.

Reed, S.J.B. (1970): The analysis of rocks in the electron probe. Geochim. Cosmochim. Acta, 34, 416-421.

Rucklidge, J.C., Gibb, G.F., Fawcett, J.J. and Gasparrini, E.L. (1970): Rapid rock analysis by electron probe. Geochim. Cosmochim. Acta, 34, 416-421.

Shimada, H. (1954): Glasströmungen in elektrisch beheitzten Modellwannen. Glastechn. Ber., 27, 151-159.

Sippel, R.F. (1963): Sodium self diffusion in natural minerals. Geochim. Cosmochim. Acta, 27, 107-120.

Smith, D.G.W. and Gold, C.M. (1976): A scheme for fully quantitative energy dispersive analysis. Adv. X-ray Anal. 18, 191-201.

Towers, H. and Chipman, J. (1957): Diffusion of calcium and silicon in a lime-alumina-silica slag. Trans. AIME, 209, 769-773.

Towers, H., Paris, M., and Chipman, J. (1953): Diffusion of calcium ion in liquid slag. Trans. AIME, 197, 1455-1458.

Walter, L.S. and Carron, M.K. (1964): Vapor pressure and vapor fractionation of silicate melts of tektite composition. Geochim. Cosmochim. Acta, 28, 937-951.

Weill, D.F., McCallum, I.S., Bottinga, Y., Drake, M.J., and McKay, G.A. (1971): Mineralogy and petrology of some Apollo 11 igneous rocks. Proc. Apollo 11 Lunar Sci. Conf. (1970) 1, 937-955.

Wilson, A. D. (1964): The sampling of silicate rock powders for chemical analysis. The Analyst, 89, 18-30.

Winchell, P. (1971): Diffusion of ^{24}Na, ^{124}Sb, and ^{13}C in melts from the albite-sodium disilicate systems. J. Amer. Ceram. Soc., 54, 63-64.

Wittkopp, R. and O'Day, M. (1973): Whole rock chemical analysis using the electron microprobe. Anal. Letters, 6, 1021-1028.

APPENDIX II

ANALYTICAL TECHNIQUES

1. ELECTRON MICROPROBE

The electron microprobe was used intensively to analyse minerals and whole-rocks. A fully quantitative energy dispersive method was used in most cases. Some of the plagioclases were analysed by a rapid method described in the next section. The fully quantitative method, very similar to that outlined by Smith and Gold (1976) analyses for major and minor elements from Na to Zn, plus Zr and Ba. Thus 22 elements are determined simultaneously and automatically. The analytical conditions were:

- excitation voltage: 15 kV;
- beam current (aperture current): 0.33×10^{-6} ampere;
- a correction is applied for drift in beam current/probe current ratio by taking calibration measurements with a Faraday cage every 1 to 2 hours;
- counting time: 400 s;

- the counting time is electronically ajusted for dead time and counting losses associated with the pile-up rejection system (Smith, 1976, p.78-80);
- the beam was focussed or scanning, (from 16 x 16 to 600 x 400 microns) depending on the object analysed.

The data (cumulated counts, "true counting time etc...) were accumulated on cassette tapes for the standards and the samples, and processed with a FORTRAN IV programme (EDATA), which applies all necessary corrections for background, overlap, escape peak, drift, as well as ZAF effects.

With a system analysing simultaneously for 22 elements a problem of standards arises. Although EDATA has a default standard option it would be desirable to accumulate counts on standards for every element at each run. In order to avoid counting on many standards at each run, and lose, thus, some of the advantage of this method of analysis, rapidity, an attempt has been made to produce two glasses containing together the 22 elements; the amount of each element in the glasses is sufficient to decrease the statistical error, on counts cumulated for 400 s, to a negligeable level. Because of the lack of adequate equipment at the time this was done, the two glasses produced were found to be somewhat inhomogeneous and contaminated. A specific area of each glass was carefully and repeatedly analysed and the glass subsequently used as secondary standard. Table 17 lists their composition. Mineral standards were used on some

occasions to increase the reliability of the results (garnet and biotite analyses).

Table 17. Composition of glass standards in weight percent oxide and element; in each standard, the elements which were used are underlined.

	Standard 108				Standard 109		
	oxide	S.D.*	element		oxide	S.D.	element
Na	9.598	0.070	7.12	Na	0.198	/	0.15
Al	25.044	0.068	13.26	Mg	23.333	0.061	14.07
Si	42.604	0.098	19.92	Al	1.498	0.042	0.79
K	0.048	/	0.04	Si	49.157	0.152	22.98
Ca	12.941	0.052	9.25	K	5.377	0.061	4.46
Y	0.809	0.026	0.55	Ca	0.088	/	0.06
Mn	2.801	0.028	2.17	Ti	3.555	0.044	2.13
Co	1.665	0.016	1.31	Cr	1.278	0.030	0.87
Cu	1.715	0.051	1.37	Fe**	/	/	8.34
Zr	0.878	0.045	0.65	Co	0.041	/	0.03
Ba	1.897	0.063	1.70	Ni	1.233	0.042	0.97
O	/	/	42.66	Zn	2.618	0.074	2.10
				O	/	/	43.05

* standard deviation: n = 14
** Fe_2O_3 = 9.084; FeO = 2.540; S.D. = 0.050 on total oxide percent.

Several methods of locating analytical points were tried. The most efficient method is to examine the polished thin section with a microscope equipped for transmitted as well as reflected light, choose an area of interest, draw a line with india Ink from the edge of the section to this area and take a photomicrograph (x 50, for example) in reflected light including the end of this line. This can be done before or after carbon-coating. It is advantageous to

use a Polaroid® camera and be able to mark immediatly on the photo the points to analyse.

The quality of the analyses is difficult to judge accurately. It depends upon many parameters: data processing, choice of standards, stability of operating conditions and operator's care in monitoring these conditions, in particular the beam current/probe current ratio, quality of carbon coating, absence of contamination of the excited volume.

The quality of the results obtainable with the EDATA programme is demonstrated in Smith and Gold (1976) and need not be discussed here.

The standards used were the glass standards (see table above) or minerals chosen, from those available in the electron microprobe laboratory, on the basis of their adequacy for the analyses done and the reliability of their composition.

Stability of operating conditions (excitation voltage) was monitored continously during analyses or at intervals of 1 to 2 hours (beam current/probe current ratio) by making calibrations with a Faraday cage.

The quality of carbon coating and its reproducibility were assured by thorough cleaning of the polished thin sections before coating, the use of a hard vacuum, coating to a constant conductivity on a test glass plate, and by verifying the conductivity of the sections after coating.

Contamination of the excited volume is of little

concern in whole-rock analysis because of the size of the glass chips; in mineral analysis such a contamination can be detected by comparing the structural formulae calculated with the theoretical one. Some analyses were discarded on that basis.

Mg, and to a lesser extent Na, were found to be systematically low; the reason was a build-up of oil on the detector window.[1] In most cases this error could be considered negligeable. Garnet analyses done before correction of the above problem were corrected empirically by adding 0.3% MgO to the analysis because the error on MgO significantly affected the temperature calculated by the biotite-garnet thermometer. The figure of 0.3% was obtained from comparison of a series of rocks, analysed during that period with their X-ray fluorescence analyses.

2. RAPID ANALYSIS of PLAGIOCLASE

The composition of plagioclase in fine-grained metabasites of the greenschist and lower amphibolite facies is often difficult to determine by optical methods because of the small size of the grains and the common absence of twinning and cleavage. An alternative rapid method is desir-

---

[1] this problem was corrected subsequently

able.

Because plagioclase can be considered as a simple solid solution series between albite and anorthite (the K content is generally small in low grade metamorphic plagioclase), ZAF corrections can be avoided. It is also unnecessary to subtract the background because it varies continuously as the average atomic number increases.

An electron microprobe equipped for energy dispersive analysis is used to record and output the total number of counts for the energy ranges corresponding to the Kα lines of Na, Al, Si, and Ca. In the present case an ARL EMX electron microprobe, equipped with an ORTEC energy dispersive analyser recording X-ray pulses on 1024 channels (0 to 10,240 eV) was used. The analytical conditions were:

- excitation voltage: 15kV;
- beam current[1] : 0.33×10^{-6} ampere;
- counting 'time' based on fixed integrated beam current: 1×10^5 ($\cong$300 s) for standards and 3×10^4 ($\cong$100 s) for samples;
- the counting period has been electronically adjusted for dead-time and counting losses associated with the pile-up rejection system (Smith, 1976 p 78-83).

Total counts (peak + continuum) were integrated over the following regions of interest: channels 94 to 112 eV for Na,

---

[1] terminology as in Rucklidge (1976)

140 to 157 eV for Al, 162 to 186 eV for Si, and 357 to 381 eV for Ca. The ratio of beam current to probe current is measured before and after recording the counts for the standards and at intervals of 1 to 2 hours thereafter. The recorded counts are then recalculated to a constant beam current/probe current ratio. The recorded X-ray spectrum should be monitored for any peak shift (Smith, 1976, p 90-91) through the analytical run as correction could not easily be made for this.

A set of calibration curves, one each for Na, Al, Si, and Ca, are made, using plagioclases of known composition or, as here, a set of synthetic glasses of composition An_0, An_{20}, An_{40}, An_{60}, An_{80}, and An_{100} (Fig. 74). The counts obtained on each sample point for Na, Al, Si, and Ca are compared with the calibration curves to yield four An-values which are then averaged. Because of low count rate, the Ca and the Na an value are of little significance near the sodic and calcic end-member composition respectively. These calibration curves are valid only if no elements other than Na, Al, Si, and Ca are present in significant amount. Working with fine-grained rocks increases the probability of contamination of the excited volume by minerals other than plagioclase, below the polished surface. This can be verified by monitoring each recorded spectrum on the CRT display. Contamination of the excited volume by ferro-magnesian minerals and iron-rich epidote are thus easily detected. A small Fe-Kα peak will generally be present when working with

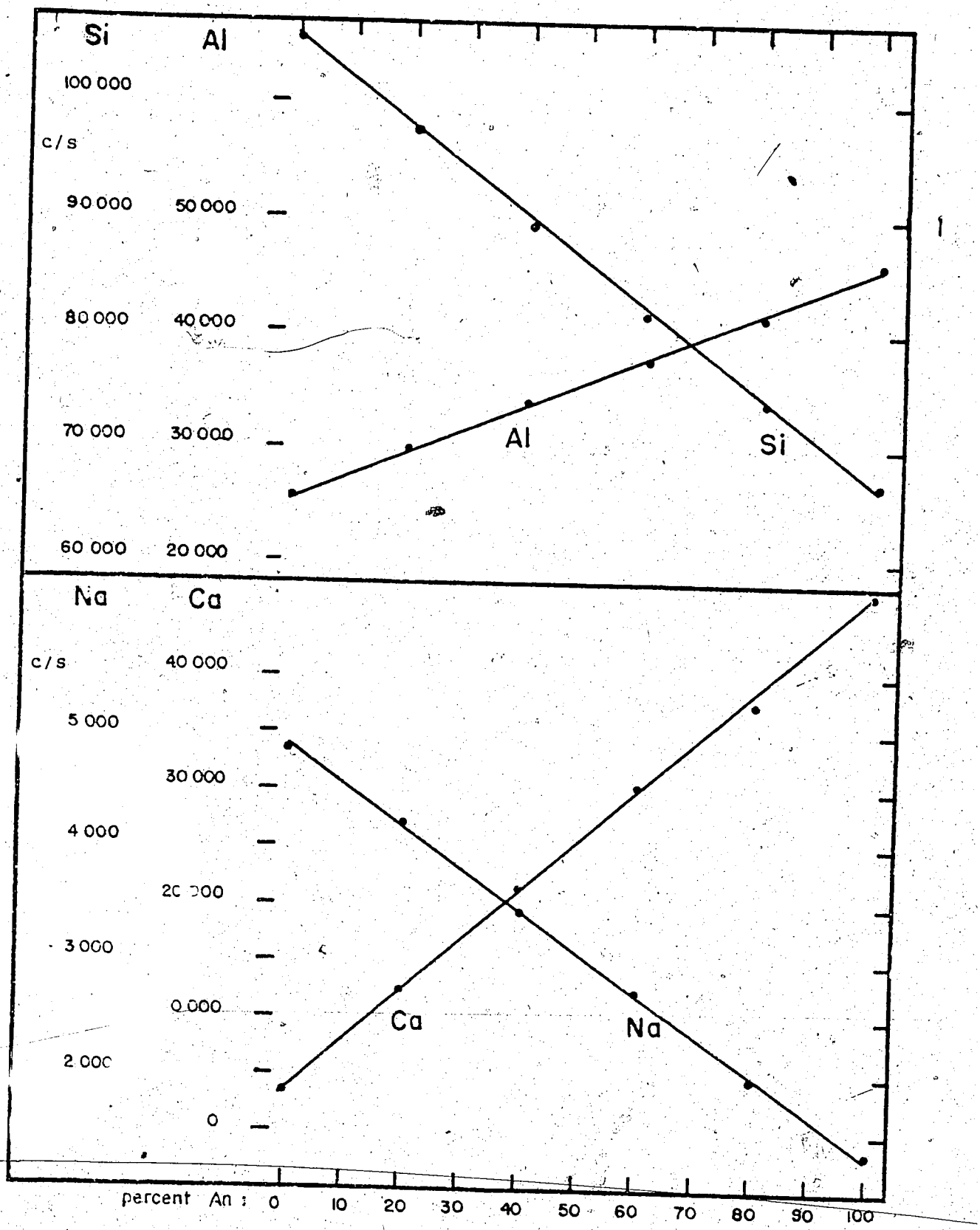

Fig. 74. Example of calibration curves for rapid analysis of plagioclase: total counts per region of interest for 3x10⁴ integrated beam current, 0,107 probe current/beam current ratio, 0.33x10⁻⁶A beam current, and 15 KeV excitation voltage.

metabasites due to the addition of counts from the iron normally present in the feldspars to those from the 'corona' (Sm 1976; p.102) of the electron beam.

In cases where the four An-values do not fall within a narrow range (±2% An), it is generally easy to recognize the cause of the discrepancy using the four variables.

If a focussed beam is used, sodium will tend to be mobilized resulting in lower Na counts; similar Al, Si, and Ca An-values and a high Na An-value may be diagnosed as sodium mobilization and averaging the Al, Si, and Ca An-value will minimize the error. Use of beam scanning over an area of 20 x 20 to 40 x 40 microns is recommended for sodic plagioclases.

Contamination of the excited volume by quartz results in higher Si counts; similar Na, Al, and Ca An-values and a lower Si An-value. The average of the Na, Al, and Ca An-value will be close to the actual value if the contamination is not too large.

If contamination by epidote occurs, little can be done but reanalyze, except in the simplest case of compositions near the albite and clinozoisite end-member where the Si An-value will be closest to the actual An content. This last case may be diagnosed by the An-values having the following order:

$$Ca > Na > Al > Si.$$

Contamination by calcite or apatite are recogni-

zable by high Ca An-value and similar Na, Al, Si An-value.

A precision of ±2% An or better should be obtained using this method. A counting time of 100 s gives a number of counts sufficient for the precision to be expected from this method. One can therefore carry out 50 to 100 analyses per day, depending on the time required to locate a new analysis point, change sample etc... An equivalent time is usually required to process the recorded data. This could easily be reduced by computer processing: standardize the data to a constant beam current/probe current ratio, calculate best fit curves for the Na, Al, Si, and Ca An-values of the standards, from this, calculate the Na, Al, Si, and Ca An-value for each analysis.

This method can also be used for alkali feldspar by making a calibration curve for $KAlSi_3O_8$-$NaAlSi_3O_8$. Here, however, only the K and Na curve can be used to determine the Ab/Or ratio; the Si and Al will show little variation, but can serve as a check for contamination. Extension of the method to ternary feldspars is possible but would require computer data handling for the method to remain convenient and rapid.

Table 18 compares known An contents of plagioclase with rapid analysis results. Only sample 23 shows a significant difference (21 to 25). The points analysed in WDA were different and this may explain the difference in result.

Table 18. Comparison of rapid analysis with fully quantitative analysis.

	fully-quantitative	rapid analysis				
	An	Na An	Al An	Si An	Ca An	Average An
23 point 1	21[1]	26	26	24	26	25.5
23 point 2		23	28	24	26	25.0
EP/S11-2	75.6[2]	77	74	75	76	75.5
639-17	0[3]	-2	1	0	0	0

1 energy dispersive analysis
2 wet chemical analysis, Carmichael, Univ. of California
3 wavelength dispersive analysis, electron microprobe laboratory, Univ. of Alberta

3. ISOTOPIC ANALYSIS

A CHEMISTRY

1/ Rubidium

An amount of sample estimated to contain 20 micrograms of Rb, but not exceeding 1.5 g, is accurately weighed into a 50 ml platinum dish. Vapour distilled HF (5 ml), demineralized distilled water (5 ml), and concentrated H_2SO_4 (5 drops) are added and the whole left on a hot plate for several hours to decompose the sample. About 20 micrograms of almost pure ^{87}Rb spike is added and equilibrated for 2 or more hours with the sample, which is then evaporated to dryness and ignited at 900°C for 30 mn to eliminate the excess H_2SO_4 and produce oxides and insoluble sul-

phates of all constituents, except Mg and the alkalis. The residue is leached with water; the leachate is transferred to a 2 ml centrifuge tube with a capillary tube and 1-4 drops of 'suprapure' concentrated $HClO_4$ added to precipitate the potassium and rubidium as perchlorates. After centrifugation, the supernatant liquid is poured off as completely as possible, the precipitate washed quickly once with water and then dissolved in 1-3 drops of water in preparation for mass spectrometric analysis.

2/ Strontium

An amount of sample estimated to contain about 20 micrógrammes of normal Sr, but not exceeding 1 g, is accurately weighed into a 100 ml teflon beaker, 10 ml each of vapour distilled concentrated HNO_3 and HF added. The covered teflon beaker is set on a hot plate for about 2 hours, or until the sample is decomposed, then evaporated to dryness at 120°C. The residue is moistened with 1/2 ml water (distilled, demineralized); a spike consisting of almost pure ^{84}Sr is added, followed by 10 ml of 1:1 HNO_3 and a few ml of water. The beaker is set on a hot plate for one hour, then the solution evaporated to dryness at 140°C. The residue is moistened with 1 ml of water, 10 ml of 1:1 HNO_3 added, and the solution stirred and heated quickly to begin dissolution; 40 ml of water are added and the beaker covered and heated for several hours to insure equilibration and dissolution. The cover is then removed and the solution eva-

porated down to about 5 ml.

This solution is transferred to a 1.5 ml centrifuge tube and centrifuged. The supernatant liquid is transferred to a 20 ml beaker, the centrifuge tube cleaned of the solids by rinsing with water, and the solution poured back into the centrifuge tube. One to three drops of strontium-free $BaCl_2$ solution (about 10 mg total Ba) are added. $Ba(NO_3)_2$ is precipitated by adding 95+% HNO_3, and strontium coprecipitates with the $Ba(NO_3)_2$. The solution is heated and cooled to dissolve and reprecipitate. The precipitate is left to sit overnight, then centrifuged. The supernatant liquid is poured off, the precipitate transferred to a 3 ml centrifuge tube using concentrated HNO_3 to rinse it. It is centrifuged again and the supernatant liquid poured off. The precipitate is washed with concentrated HNO_3 and the supernatant liquid poured off as completely as possible. A drop of water and 1 ml 2.5 N HCL are added and the precipitate is dissolved by heating.

The sample solution is transferred to a precalibrated 1x18 cm cation exchange column containing Dowex® 50W-X8 (200-400 mesh) resin. Elution is done with 2.5 N HCl and a 20 ml fraction (situated between about 5 and 75 ml) containing the strontium is collected. The solution is evaporated and the residue stored in a covered 20 ml beaker in preparation for mass spectrometric analysis.

B MASS SPECTROMETRY

Both the rubidium solution and the strontium solution were loaded on tantalum filaments. These filaments are degassed before loading by heating them in vacuum for about 2 hours with a current of 4-4.5 A (resulting in a filament temperature of about 1500°C). To load the filament, it is first oxidized by briefly bringing it to red heat in air, then the solution (of Rb or Sr) is loaded drop by drop onto the filament and evaporated under a heat lamp. Rb is treated with H_2SO_4 to convert it to sulphate and Sr with $HClO_4$ to convert it ultimately to oxide. Both the Rb and Sr were analysed using single filaments.

A 6" radius of curvature, 60° sector, single focussing solid source mass spectrometer, equipped with a CARY 31 vibrating reed amplifier with a 10^{11} ohm resistor, designed and built by Dr. G.L. Cumming of the Department of Physics, University of Alberta, was used. This spectrometer is equipped with peak-switching facility and chart and digital output. The rubidium was analyzed by surface ionization of the Ta filament using a 1.3 A filament current and a 3.5 kV accelerating voltage. The 87/85 ratio was measured by peak-switching. Ranges of closely linear peaks were chosen on the chart output and running means of the isotopic ratio calculated from the digital output. Where a progressive increase in the mean 87/85 ratio of each range with time could be observed in a run, the first mean 87/85 ratio was used,

assuming it had the least mass discrimination. If not, an average was taken of the various ratios.

The strontium analyses were done by H. Baadsgaard on a Vacuum Generators Micromass 30 spectrometer. It is a 12" radius of curvature, 90° sector, single collecting solid source instrument, with an on-line Hewlett-Packard computer. The Sr 86/88, 87/86, and 84/86 ratios were measured by peak-switching. A 2.6-3.4 A filament current and a 8.0 kV accelerating voltage were used. The mean ratios in this case were not calculated by the on-line computer but by hand.

The mass spectrometric data (i.e. Rb 87/85; Sr 86/88, 87/86, 84/86) and the chemical data (i.e. sample weight used for Rb and for Sr, amount of ^{87}Rb and ^{85}Rb in the Rb spike and of ^{84}Sr, ^{86}Sr, ^{87}Sr, ^{88}Sr in the Sr spike) were processed using the APL programme RBSRCOM written by H. Baadsgard. The programme calculates ppm Rb, ppm Sr, ppm $^{87}Sr^{*}$, $^{87}Rb/^{86}Sr$, $^{87}Sr/^{86}Sr$, and a factor of mass discrimination of the Sr analysis. A ratio of 2.541 for $^{85}Rb/^{87}Rb$ is used to calculate ppm Rb and $^{86}Sr/^{88}Sr$ is normalized to 0.1194.

The errors on the results are estimated to be 2% for $^{87}Rb/^{86}Sr$ and 0.1% for $^{87}Sr/^{86}Sr$.

4. REFERENCES

Rucklidge, J.C. (1976): Electron microprobe instrumentation. In: Microbeam techniques, Smith, D.G.W. ed., Miner. Ass. Canada, Short course handbook, 1, 1-44.

Smith, D.G.W. (1976): Quantitative energy dispersive microanalysis. Microbeam techniques, Smith, D.G.W. ed., Miner. Ass. Canada, Short course handbook, 1, 63-106.

Smith, D.G.W., and Gold, C.M. (1976): A scheme for fully quantitative energy dispersive analysis. Adv. X-ray Anal. 18, 191-201.

APPENDIX III

DATA HANDLING AND COMPUTER USE

Extensive use of computer facilities was made in the following fields: structural study, biotite-garnet thermometer, isochron and age calculation in geochronology, thin section description, processing of the electron microprobe analyses not only for the processing of the raw data, but also to store the analyses and effect various calculations on them.

The use of the computer for the structural study and for the development of the biotite-garnet thermometer has been described in chapters III and IV respectively, the use in geochronology is mentioned in appendix II, and no more will be said here about these applications.

Thin section descriptions were stored in short form in a file, together with information on the geographical and stratigraghic location of the sample (see Appendix IV). Four programmes were written by C. Gold to use this file:

- TEST searches the file and extracts sets of numbers of

samples with a given characteristic: presence of a mineral in a given percentage range, rock type, formation etc...

- COMPAR uses the above sets to produce sub-sets with certain characteristics; coexistence or non-coexistence of two or more minerals for example.
- PRINT lists the heading line or the total entry for the samples of a set.
- PLOT produces maps of sample points corresponding to a set.

The programme EDATA (electron microprobe data processing) prints the weight percent of elements for each analysis, in addition to information on corrections etc... It can also list the weight percent element in a line file, one line per analysis with the format 30F8.3 (The 8 first spaces are empty and can be used to add H_2O, CO_2 etc...). Programmes were written which use such line files as input.

CONVOX calculates weight percent oxides and is used mainly with whole-rock analyses. Fe is calculated as FeO, but provision is made for calculating part or all Fe as Fe_2O_3 and for adding H_2O^+ and CO_2.

FORMU calculates structural formulae and weight percent oxides for minerals on the basis of specified number of anions. The oxides can be calculated to a total of 100% or to any other total. Both of these programmes produce an output in tabular form (10 analyses per page) and in line

form for storing or futher manipulation. For example the line file output of CONVOX was used in a norm calculation programme (an input modified version of IRVINE, written by C. Gold).

Finally, the system's programme *FMT was used to produce the thesis. This was done partly using terminals at the University of Alberta, partly using terminals in Montreal, at Centennial College and at Ecole Polytechnique, connected to the University of Alberta computer through DATAPAC, a national shared data packet switching network managed by the Computer Communications Group of Trans Canada Telephone System.

APPENDIX IV

DATA TABLES

1. NOTES to the TABLE of THIN SECTION DESCRIPTIONS

This table is a computer file containing short thin section descriptions. It was produced as a computer file in order to retrieve rapidly certain portions of the information: list samples with a given assemblage, those with a given amount of a certain mineral, list samples from a given part of the map area or from a given formation, plot samples on a map etc... This is done by means of four programmes TEST, COMPAR, PRINT, and PLOT, which are described in the previous section.

Each entry consists of a heading line followed by 1-2 lines listing the minerals and their percentage. Each line of an entry starts with the sample number. The heading line follows with the field sample number (initial, traverse number, outcrop number), coordinates, formation, rock type.

The coordinates are Transverse Universal Mercator

coordinates of zone 18, given in hundreds of metres and with 10 km added to the northing.

Example: 207 178 correspond to 6220700m 6807800m.

This change in scale simplified the use of the plotting programme.

The formations are coded as follows:

1- East of 72°25':

E 1 Archean

A gneiss

B amphibolite

C miscellaneous

E 2 Early Aphebian

A diabase

B regolith

Aphebian

E 3 iron formation

E 4 pelites and psammites

E 5 basic rocks and serpentinites

E 6 dolomites and calc-schists

E 7 pelites and para-amphibolites

E 8 quartzite and quartz-schists

E 9 orthoamphibolites

E10 quartz-schists, quartzites, pelites (includes felsic tuffs)

E11 sills (gabbro, pyroxenite, peridotite).

2- West of 72°25'

W 1 Archean

A gneiss

B amphibolite

W 2 Early Aphebian

A diabase

B regolith

Aphebian

W 3 Iron Group

W 4 Pelitic Group

W 5 Volcano-Sedimentary Group

W 6 Lower Volcanic Group

W 7 Upper Volcanic Group

W 8 north flank of geosyncline (North of Monts Lune).

The rock types are coded as follows:

AMP	amphibolite	TFB	basic tuff
SCT	schist (pelitic)	TFI	intermediate tuff
GNS	gneiss	FLS	felsic tuff (felsite)
ACT	actinolitite	AGL	agglomerate
CIP	marble	UM	ultramafic rocks
CST	calc-schist	IF	iron formation
COR	hornfels	CGL	conglomerate
DIA	diabase	SS	sandstone
MBT	basalt	GWK	grauwacke
MBG	gabbro	RGL	regolith
MBX	basite (undefined)	XX	undefined rock

MBY pyroclastic rock

The second and third line of each entry list the mineral present (FORMAT A4) and its percentage (FORMAT F3.1). The decimal value is used as follows:

.1 trace

.5 less than 1% but more than trace

.9 percentage not determined or included with another mineral; this was often used for quartz and plagioclase in metabasites where the grains were small and difficult to distinguish

.8 maybe present

.7 in special position (vein etc...).

The minerals are coded as follows:

QZ	quartz	CORD	cordierite
FP	feldspar	STAU	staurolite
MICR	microline	AND	andalusite
AB	albite	TURM	tourmaline
OLIG	oligoclase	ZIRC	zircon
AN	plagioclase (An>40)	SPH	sphene
SCAP	scapolite	RUTI	rutile
BIOT	biotite	SPIN	spinel
MUSC	muscovite	AP	apatite
PHLO	phlogopite	ACCS	accessory minerals
PARG	paragonite	ALTR	alteration mineral
MICA	mica	MRAD	radioactive ACCS

STIL	stilpnomelane	ALL	allanite
TALC	talc	CARB	carbonate
SERP	serpentine	CC	calcite
CHEQ	chlorite (Fe=Mg)	CARX	second carbonate?
CHFE	chlorite (Fe>Mg)	DOL	dolomite
CHMG	chlorite (Fe<Mg)	SID	siderite
CHLR	chlorite	INCO	unknown mineral
OPX	orthopyroxene	OP	opaque mineral
CPX	clinopyroxene	SULF	sulphide
AMPH	amphibole	GRPH	graphite
ANTH	anthophyllite-gedrite	MT	magnetite
CUMM	cummingtonite-grunerite	ILM	ilmenite
TREM	tremolite	PO	pyrrhotite
ACT	actinolite	PY	pyrite
HORN	hornblende	PN	pentlandite
OL	olivine	CPY	chalcopyrite
EP	epidote	GA	galena
ZOIS	zoisite	SP	sphalerite
GRNA	garnet	HEM	hematite

Table 19. Thin section descriptions.

```
 1.C 6. 1A    671 270 E 1C SCT
 1.QZ  45  PLAG10  BIOT30  MUSC 2  EP  10  ZIRC  1 SPH  2
 1.AP   1  OP    1 MICR  7
 2.C 6. 1C    671 272 E 1B AMP
 2.QZ   8 PLAG15  BIOT10  HORN60  EP  15  TURM  1 OP   1
 3.C 6. 7C    669 287 E 4  SCT
 3.QZ  30  PLAG20  MICR  8 BIOT40  MUSC10  AP    1 OP   1
 3.CC   1 MRAD  1
 4.C 6. 9A    670 291 E 4  SCT
 4.QZ  30  PLAG10  MICR  8 BIOT25  MUSC30  CC    1 OP   3
 4.ZIRC 1 AP    1
 5.C 6. 9B    670 291 E 4  SCT
 5.QZ  50  FP  35  BIOT15  ZI[illegible]  1 GRNA  1 OP   1
 6.C 7. 1A    644 298 E 5  AMP
 6.QZ   8 PLAG20  BIOT15  HORN6[illegible]  1 ILM  2
 7.C 7. 3A    635 298 E 1B AMP
 7.QZ  15  PLAG  1 BIOT 5  HOR[illegible]NA15  ILM  3  AP    1
 7.ALL  5
 8.C 8. 2     615 424 E 7  AMP
 8.QZ  20  FP  10  BIOT 5  HORN60  GRNA 2  ILM  2  ALL   8
 9.C 9. 1A    627 436 E 7  AMP
 9.QZ  25  PLAG10  BIOT 5  HORN50  GRNA10  ILM  2  SULF  1
 9.ALL  5
10.C 9. 1B    627 436 E 4  SCT
10.QZ  40  OLIG40  BIOT20  MUSC 2  GRNA 1  ZIRC  1 AP    1
10.OP
11.C 9. 2C    626 437 E 9  AMP
11.QZ   8 PLAG30  CHMG 3  HORN60  CARX10  ILM  1  MRAD  1
11.SULF 1
12.C 9. 3     625 439 E 9  AMP
12.QZ  40  PLAG  9 HORN60  SPH  3  PO    1 CPY   1 ALL   1
13.C 9. 4B    621 440 E 9  AMP
13.PLAG20  CHMG 5  HORN65  CARB 5  ILM  5  ALL   1
14.C 9. 5D    616 443 E 9  AMP
14.QZ  15  PLAG 5  BIOT  1 CHEQ10  HORN60  GRNA10  CARB 5
14.ILM 10  MRAD  1 ALL   1  SPH  1
15.C 9. 9A    607 425 E 9  AMP
15.QZ   8 PLAG 1  HORN80  GRNA10  AP    5 CC    1 CARB  8
15.ILM 10  ALL   1
16.C 9.12     597 424 E 9  AMP
16.QZ   7 PLAG 5  EP   1  SPH  4  CC    7 HORN50  ALL   1
17.C 9.13     590 426 E 9  AMP
17.QZ   9 PLAG40  HORN50  CC  10  CARB  9 ILM  4  SPH   5
17.AP   5 SULF  1  MRAD  1
18.C10. 9     497 379 E 4  SCT
18.QZ  45  PLAG15  BIOT15  MUSC20  CHFE  1 TURM 1  AP    1
18.ZIRC 1 OP   2
19.C10.13     497 394 E 9  AMP
19.PLAG15  CHEQ  1 HORN70  EP  10  CARB 5  SPH  2  SULF  1
20.C10.14     497 396 E 9  AMP
```

Table 19. Cont'd...

20.QZ	9	PLAG15	HORN80	EP	1	ZIRC	1	SPH	5	AP	1
20.ILM	3	MRAD	1								
21.C10.15A		498 398 E 9	AMP								
21.QZ	9	PLAG40	HORN55	SPH	5	OP	1	ALL	1		
22.C10.16A		495 401 E 9	AMP								
22.QZ	1	PLAG35	HORN65	CARB	1	AP	1	SPH	2	ILM	1
22.ALL	1										
23.C10.16B		495 401 E 9	AMP								
23.QZ	8	PLAG35	HORN60	CARB	3	SPH	3	ILM	1	ALL	1
24.C10.17		495 405 E 9	AMP								
24.QZ	9	HORN	9	GRNA	9	CC	9	CARB	9	ILM	9
25.C10.19		499 409 E 9	AMP								
25.PLAG15		HORN70	EP	15	SPH	2	SULF	5			
26.C10.21A		503 415 E 9	AMP								
26.QZ	9	PLAG50	HORN20	CUMM30		ILM	3	AP	1	SULF	1
26.ALL	1										
27.C10.21B		503 415 E 9	FLS								
27.QZ	80	MICR	9	PLAG15		MUSC	3	OP	1	ZIRC	1
28.C11. 5B		535 321 E 3	IF								
28.QZ	40	CHMG	1	CUMM30		SID	30	CARB	9	OP	1
29.C11.13		533 330 E 3	IF								
29.CUMM99		OP	1								
30.C11.14		533 331 E 4	SCT								
30.QZ	45	PLAG10	BIOT20	MUSC20		ZIRC	1	AP	1	TURM	1
30.ALL	1	OP	2								
31.C11.28		523 378 E 9	AMP								
31.QZ	9	PLAG27	CHMG	1	BIOT	1	HORN70	SPH	1	ILM	2
31.ALL	1										
32.C11.36		517 404 E 9	AMP								
32.QZ	8	PLAG20	HORN70	EP	5	CARB	2	SPH	2	SULF	1
33.C12. 9		662 486 E 1C	CIP								
33.QZ		FP	PHLO	CHMG		TREM		CC	80	OP	2
34.C13. 1B		634 509 E 1C	SCT								
34.QZ	25	PLAG50	MICR	1	BIOT15		HORN	5	EP	5	CARB 1
34.ZIRC	1	AP	1	OP	1						
35.C13. 6		659 510 E 4	SCT								
35.QZ	35	PLAG30	BIOT20	MUSC15		GRNA	1	ZIRC	1		
36.C15. 1A		716 475 E 5	AMP								
36.QZ	9	PLAG30	BIOT	1	CHEQ	4	CUMM	1	HORN60	GRNA	1
36.ALL	1	AP	1	ILM	5	SULF	1				
37.C15. 1B		716 476 E 9	AMP								
37.QZ	9	FP	35	BIOT	1	CHEQ	1	HORN55	CUMM	8	GRNA 7
37.AP	1	ALL	1	ILM	5						
38.C15. 1C		716 477 E 4	SCT								
38.QZ	65	BIOT10	MUSC25	CHEQ	1	TURM	1	OP	1		
39.C15. 1D		716 478 E 9	AMP								
39.QZ	8	SCAP	8	PLAG10		BIOT	1	HORN85	CARB	5	SPH 1
39.ILM	1	AP	1	MRAD	1						
40.C15. 3A		708 478 E 5	UM								
40.TREM49		ANTH49	OP	1	CARB	1					

Table 19. Cont'd...

```
41.C15. 3B   708 478 E 5  UM
41.TREM90  ANTH  9 OPX  5  MICA  9 CARB 2  OP   1
42.C15. 4B   705 478 E 5  UM
42.TREM98  ANTH  9 MICA  9 OP   1  CARB 1
43.C15. 5A   700 477 E 5  UM
43.QZ    1 PLAG 2  MICR 2  PHLO 2  TREM 7  CPX   8 CARB 2
43.OP    2 EP   1  INCO 1
44.C15. 6A   695 477 E 5  UM
44.ANTH40  TREM 1  OPX 40  CHMG10  CARB10  OP   1
45.C15. 9A   680 487 E 5  MBX
45.FP    1 BIOT  1 EP  45  ACT 50  SPH  2  OP   3  HORN  1
46.C15. 9B   679 487 E 7  AMP
46.QZ   10  PLAG15  BIOT  1 CHEQ  1 INCO 3  HORN70  CC    1
46.SPH   3  ILM  1  AP    1 ALL   1
47.C15.10A   670 480 E 5  UM
47.CHMG20  ANTH45  CC  30  SID   9 OP   3
48.C16. 3B   445 390 E 7  AMP
48.QZ    9 PLAG20  BIOT 3  CHMG10  HORN60  DOL  3  CC    8
48.SPH   2 ALL   1 PO   1  MT    5 ILM  5 CPY  1 RUTI  5
49.C16. 4A   445 392 E 7  SCT
49.QZ   55  FP    9 BIOT25  MUSC10  TURM 2  GRNA 5  AP    1
49.ZIRC  1 MRAD  1 OP   7
50.C16. 4B   445 392 E 7  SCT
50.QZ   70  FP    9 BIOT10  MUSC10  CHMG 5  GRNA 3  TURM 2
50.ZIRC 1  AP   2  OP   1
51.C16. 9    448 402 E 9  AMP
51.QZ    1 PLAG30  CHLR 2  ACT 65  EP   7  SPH  2  CARB 3
51.INCO 3  HORN  9
52.C16.13    458 416 E 9  AMP
52.QZ   55  PLAG  9 BIOT 3  HORN35  AP   1  ILM  7  ALL   1
53.C20. 1     66 331 W 6  MBT
53.QZ    8 PLAG10  BIOT 1  CHEQ 3  ACT 50  EP  30  SPH  6
53.SULF  1
54.C20. 2     66 332 W 6  MBT
54.QZ    8 FP    8 CHPE10  ACT 35  EP  35  SPH 10  CARB10
54.SULF 1
55.C20.13A    98 367 W 6  MBT
55.QZ    5 FP    8 BIOT  1 CHLR 5  ACT 40  EP  35  CARB 3
55.SPH  10  SULF 2
56.C20.13B    98 372 W 6  MBG
56.QZ    5 PLAG10  CHMG10  ACT 50  EP  30  SPH  7
57.C21. 6    94   8 W 2A DIA
57.PLAG  9 CPX   9 OL.  9 SERP  9 OP   9
58.C28. 2    205 470 W 7  TFI
58.QZ 25  PLAG55  BIOT10  CHLR 2  EP   8 ZIRC  1 AP    1
58.ILM 11
59.C29. 6B   242 464 W 7  MBG
59.PLAG20  ACT 60  EP  10  CC   4  SPH  2  SULF 1  HORN  9
60.C31. 1.1  237 470 W 7  UM
60.SERP45  CPX 40  CHEQ10  MT    9 ILM  9 CPY  9
```

Table 19. Cont'd...

```
61.C31. 1.2  237 470 W 7  UM
61.SERP70  CPX   9 CHEQ  9 OPX   8 MT    9 ILM   9 CPY   9
62.C31. 1.3  237 470 W 7  UM
62.SERP70  CPX   9 CHEQ  9 MT    9 ILM   9 CPY   9
63.C31. 2    234 467 W 7  UM
63.PHLO  1 CHMG10  ACT 10  CPX 60  EP  25  CARB  5 SPH  2
64.C31. 3    230 465 W 7  SCT
64.QZ  65  FP    9 BIOT15  CHLR15  EP    8 GRNA 3  ZIRC 2
64.AP    5 OP   2
65.C31. 7    218 463 W 7  MBT
65.ANTH86  CHLR  8 EP    8 SPH  4  PO   9  PN    1 CPY   5
66.C31. 8    217 461 W 7  MBT
66.PLAG  1 CHMG30  ACT 65  EP   5  SPH  3  HORN  9
67.C32. 2    230 455 W 7  MBT
67.QZ    1 PLAG10  BIOT  1 CHEQ10  ACT 70  EP  10  SPH  4
67.SULF 2  HORN  9
70.D 2.14    681 488 E 5  UM
70.CHMG20  ANTH50  EP   7  SPIN10  CARB10  OP   3
71.D 6. 4A   688 280 E 4  SCT
71.QZ   9 PLAG40  BIOT35  MUSC15  SPH  5  OP   5  TURM 3
71.ZIRC 2
72.D 9. 5A   581 342 E 4  SCT
72.QZ  65  BIOT10  MUSC20  TURM 1  ZIRC  1 OP   4
73.D 9. 7    578 343 E 9  AMP
73.PLAG15  HORN65  EP  15  SPH  3  CARB 3  ILM   5 MRAD  1
74.D 9.13    571 355 E 9  AMP
74.QZ   1  PLAG15  HORN60  CPX 10  SPH  8  EP  10  MRAD  1
75.D13. 1A   568 371 E 9  AMP
75.QZ   9 PLAG30  HORN65  EP   3  SPH  1  ILM  3  AP   8
75.SULF  1   MRAD  1
76.D13. 1C   568 371 E 9  AMP
76.QZ   9 PLAG20  HORN70  EP  15  CC   4  SPH  3  SULF  1
77.D13.13    519 388 E 9  AMP
77.QZ   9 PLAG20  HORN60  EP  10  CC  10  SPH  3  ILM   1
78.D13.16A   516 389 E 9  AMP
78.QZ   9 PLAG25  HORN70  ALL  1  AP   1  ILM  5
79.D13.16B   516 389 E 9  AMP      P
79.QZ   9 PLAG30  HORN65  ALL  1  SPH  1  ILM  4  CPY  1
80.H 1. 6A   306  81 W 3  IF
80.QZ   9 CUMM  9 DOL   9 SID   8 MT    9
81.H 1. 6F   307  79 W 3  IF
81.QZ  50  BIOT 3  CHMG 6  GRNA15  SID  4  SPH   1 MRAD  1
81.OP  20
82.H 1. 7A   309  79 W 3  IF
82.QZ  55  AB   6  BIOT 7  CHFE 4  GRNA 3  SID  8  OP  20
83.H 1. 7E   310  79 W 3  IF
83.QZ  55  BIOT  1 CHFE15  CUMM  1 GRNA10  SID  3  OP  15
84.H 1. 8A   313  77 W 3  IF
84.QZ  60  BIOT 2  CHFE15  GRNA10  OP  15
85.H 1. 8B   314  77 W 3  IF
```

Table 19. Cont'd...

```
85.QZ  55  BIOT  1 CHFE20  AP    1 OP  25
86.H 1. 9E   318  73 W 3  IF
86.STIL 5  CHFE  1 CUMM65  CARB30  OP    1
87.H 2. 1A   319  75 W 3  SCT
87.QZ  55  BIOT 3  CHFE40  ZIRC  1 GRPH  1
88.H 2. 1B   319  75 W 3  IF
88.QZ  45  STIL20  CHFE  1 GRNA 5  SID 20  OP  10
89.H 2. 1D   319  75 W 3  SS
89.QZ  85  MUSC10  CHFE 5  OP   1
90.H 2. 1E   319  75 W 3  SS
90.QZ  85  CHFE15  ZIRC  1
91.H 2. 2    321  79 W 3  SS
91.QZ  40  AB    9 MUSC20  BIOT 5  CHLR  1 EP   1  CARB 3
91.ZIRC  1 OP    1
92.H 2. 5    316  94 W 3  SS
92.QZ  80  PLAG 1  BIOT 3  CHFE10  GRNA 1  CARB 2  ZIRC  1
92.OP   2
93.H 5. 1    225 256 W 6  MBT
93.PLAG15  BIOT 5  [illegible]  EP   8  CARB 1  SPH  7  SULF 3
93.ACT 55  HORN [illegible]  1
94.H 5. 6C   227 [illegible] W 6  AGL
94.
95.H 5.10    227 241 W 6  MBG
95.QZ    9 PLAG20  CHFE 7  ACT 55  EP  13  SPH  3  SULF 2
95.HORN  9
96.H 5.16B   230 234 W 6  MBX
96.AB  30  BIOT  1 CHEQ 7  ACT 50  EP  10  SPH  4  HORN  9
96.MRAD  1
97.H 5.20B   236 229 W 6  MBY
97.QZ    9 AB  40  BIOT12  CHEQ20  EP   4  SPH  4  CC  20
97.CARB  8 MRAD  1
98.H 5.28A   254 206 W 5  SCT
98.QZ  35  AB  15  BIOT25  MUSC20  CHEQ  1 EP   5  TURM  1
98.SPH   1 OP   1
99.H 5.29    256 205 W 5  MBY
99.QZ    9 PLAG45  BIOT  1 CHMG15  EP  10  SPH  3  ACT 20
99.CC  10  CARB  8 MRAD  1  HORN  1
100.H 5.30A  257 204 W 5  SS
100.QZ  70 MICR15  PLAG15  MUSC  5 OP   1
101.H 5.30C  257 203 W 5  MBY
101.QZ  15  PHLO  1 CHMG45  TREM  1 DOL 40  SPH  1 ILM  3
101.SULF  1  ZIRC  1
102.H 5.33   259 196 W 5 SCT
102.QZ  25  PLAG20  BIOT15  MUSC25  CHEQ 5  CC  10  CARB  8
102.OP   1
103.H11. 5   277 340 W 6  AMP
103.QZ    8 PLAG30  CHMG 3  ACT 45  EP  20  CARB  1 SPH  2
103.HORN  9
104.H11. 7F  291 325 W 5  SCT
104.QZ  40  PLAG35  BIOT20          4  TURM 1  OP   2
```

Table 19. Cont'd...

```
105.H11. 7J    291 325 W 5  SCT
105.QZ  30  PLAG  9 BIOT18  CHMG20  EP   1  CARB20  OP   4
106.H11. 7L    291 325 W 5  SCT
106.QZ   9 PLAG  9 BIOT  9 CHMG  9 EP    9 CARB  9
106.SPH  9 OP    9 INCO  9
107.H11. 7P    291 325 W 5  SCT
107.QZ  50  PLAG30  BIOT10  MUSC 5  CHEQ  1 GRNA 1  OP   3
108.H11. 7S    291 325 W 5  SCT
108.QZ   9 PLAG  9 CHMG  9 ACT   9 EP    9 SPH   9 AP    9
109.H11. 9E    291 326 W 5  SCT
109.QZ  47  PLAG40  BIOT 5  MUSC 5  CHEQ  1 EP    8 AP    1
109.SPH  1 ZIRC  8 OP   2
110.H11.10B    293 327 W 5  SCT
110.QZ  35  PLAG15  BIOT15  CHMG15  CC  15  CARB  9 EP    5
110.SPH  1  OP   3
111.H11.10C    293 327 W 5  SCT
111.QZ   9 PLAG  9 MUSC  9 CHMG  9 SPH   9 OP    9
112.H11.10D    293 327 W 5  SS
112.QZ  40  PLAG45  MUSC 4  BIOT 4  CHEQ  1 CARB 5  SPH   5
112.OP   5
113.H11.10H    293 327 W 5  TFI
113.QZ  20  PLAG20  BIOT10  CHLR15  HORN15  CC  15  CARB15
113.SPH  1 ILM  5  SULF 1
114.H11.10J    293 327 W 5  AMP
114.PLAG13  BIOT 1  ACT 50  CARB 4  SPH  2  OP    1 HORN  9
114.MRAD  1
115.H11.10K    293 327 W 5  AMP
115.PLAG25  BIOT 2  CHMG 4  ACT 61  EP   1  CARB 3  SPH  3
115.ILM  1  HORN  9   MRAD  1
116.H12. 5C    287 336 W 5  AMP
116.QZ   9 PLAG25  BIOT  1 CHLR 7  HORN41  ALL  1  CARB 2
116.SPH  1 ILM  4  HEM   1
117.H12. 5E    287 336 W 5  AMP
117.QZ   9 PLAG20  CHEQ 7  HORN68  CARB  1 SPH  1  ILM  4
117.HEM  1 ALL   1  MRAD  1
118.H12. 6B    296 334 W 4  SCT
118.QZ  70  PLAG  8 BIOT15  MUSC10  CHEQ 2  EP    1 TURM  1
118.AP   1 SPH   1 OP   1
119.H12. 6C    297 334 W 4  SCT
119.QZ  80  PLAG  9 BIOT15  CHEQ 2  GRNA  1 TURM  1 AP    1
119.OP   1
120.H12. 7G    301 335 W 4  SCT
120.QZ   9 PLAG  1 BIOT  9 CHMG  9 CC    9 TURM  9 OP    9
121.H12.10B    303 332 W 4  SCT
121.QZ  52  PLAG  8 BIOT30  MUSC 3  GRNA10  TURM  1 AP    1
121.ILM  5
122.H12.10G    303 332 W 4  SCT
122.QZ   9 BIOT  9 CHFE  9 CARB  9 ILM   9 GRNA  9
123.H13.36     279 340 W 6  AMP
123.QZ   9 PLAG15  HORN70  CARB 5  SPH  3  ILM  7  ALL   5
```

Table 19. Cont'd...

```
124.H13.53     278 338 W 6  MBX
124.QZ     9 CHEQ  9 HORN  9 EP     9 SPH    9 MRAD  9 SULF10
125.H13.110    277 336 W 6  AMP
125.QZ     9 PLAG15  CHEQ 2  HORN77  ALL  1  SPH   1 ILM  5
125.SULF  1
126.H13.112    277 336 W 6  AMP
126.PLAG30  [illegible]N66  EP   1  SPH  3  ILM  6  SULF  1 MRAD  1
127.H13.1[illegible]  277 335 W 6  AMP
127.PLAG25  [illegible]N64  ALL  2  CARB 1  SPH  2  ILM  5  SULF 1
128.H13.114    277 335 W 6  AMP
128.QZ     9 PLAG30  HORN58  EP   3  SPH  3  CARB 1  ILM  5
128.MRAD  1
129.H13.116    277 335 W 6  AMP
129.PLAG30  CHEQ 3  HORN54  ALL  2  CARB 4  [illegible]  1  ILM  6
129.SULF 1
130.H13.118    277 335 W 6  AMP
130.QZ     9 PLAG10  CHEQ 2  HORN80  ALL  2  [illegible]H  1  ILM  5
131.L 1. 2     127 171 W 5  MBT
131.PLAG10  BIOT  1 CHEQ 5  ACT 50  EP  30  SPH  7  SULF 2
131.HORN  9
132.L 1. 9     121 188 W 5  MBT
132.QZ     9 PLAG20  BIOT 4  CHEQ 6  ACT 40  EP  20  CC  10
132.SULF 3  SPH  4  HORN  9
133.L 1.10A    120 190 W 5  TFB
133.QZ  15  PLAG  9 BIOT25  CHLR20  ACT  5  CC  25  EP  10
133.SPH  4  SULF 2
134.L 1.10C    120 189 W 5  CST
134.QZ  20  PLAG  9 BIOT  1 CHMG20  CC  70  TURM  1 ZIRC  1
135.L 4. 2A    238 382 W 6  SCT
135.QZ  40  PLAG  9 BIOT 5  CHEQ30  EP  20  GRNA 4  SPH  4
135.[illegible]O  3  CPY  1
136.L 4. 2B    238 382 W 6  MBG
136.QZ     9 PLAG20  BIOT 4  CHEQ15  HORN40  EP  10  CC  15
136.SPH  3  SULF 1  ILM  4
137.L 4. 3A    236 387 W 6  MBG
137.QZ     9 PLAG  9 BIOT  9 CHEQ  9 ACT   9 EP    9 SPH   9
137.ILM  9 HORN  9
138.L 4.13     248 419 W 6  MBT
138.QZ  15  PLAG  9 BIOT 1  CHLR10  ACT 30  EP  10  CC  30
138.SPH  7  HORN  9
139.L 4.15A    253 421 W 6  MBG
139.PLAG20  CHEQ10  ACT 50  EP  15  CC    1 SPH  5  HORN  9
140.L 5. 6     263 349 W 6  MBT
140.PLAG20  CHMG 5  ACT 60  EP  15  SPH  7  SULF  1 HORN  9
141.L 5.11     264 362 W 6  MBG
141.PLAG15  CHMG 5  ACT 70  EP   5  SPH  7  HORN  9
142.L 7. 1     147 391 W 6  MBT
142.QZ     9 PLAG10  BIOT 7  CHLR 7  ACT 50  EP  25  SPH  3
142.SULF  5 HORN  9
143.L 7. 2     147 391 W 6  MBT
```

Table 19. Cont'd...

```
143.QZ    7 AB  15  CHLR 8  EP  10  ACT 60  CC    7 SPH  8
143.SULF 1
144.L 7. 6    145 389 W 6  MBT
144.QZ    9 PLAG 8  BIOT  5 CHLR 7  ACT 60  EP  15  CC   7
144.SPH 10  SULF 2  HORN  9
145.L 7. 7B   144 387 W 6  MBG
145.QZ    9 PLAG15  BIOT 5  CHLR 3  ACT 50  EP  20  CARB 1
145.SPH  5  SULF 2  HORN  1
146.L 7. 8    143 385 W 6  MBT
146.PLAG10  BIOT 3  CHEQ 5  ACT 42  EP  35  CARB  5 SPH 5
146.HORN  9
147.L 7.11    142 383 W 6  MBG
147.PLAG17  BIOT 3  CHLR10  ACT 33  EP  30  CARB  1 SPH  5
147.SULF 2  HORN  9
148.L 7.15    140 381 W 6  MBG
148.QZ    2  PLAG18  BIOT 2  CHEQ 7  STIL 1  ACT 33  EP  30
148.SPH   6  SULF 1  HORN  9   MRAD  1
149.L 7.17B   139 379 W 6  MBT
149.PLAG15  BIOT  1 CHEQ 9  ACT 41  EP  30  SPH  5  SULF  1
149.HORN  9
150.L 7.23    136 373 W 6  MBG
150.QZ    1  PLAG10  BIOT 8  CHEQ 7  ACT 38  EP  30  SPH  6
150.SULF  1
151.M 2. 9    290 156 W 4  SCT
151.QZ   30  PLAG20  MUSC15  BIOT15  CHEQ15  EP   1  SPH  3
151.OP    2  AP    1
152.M 2.10A   278 161 W 4  SCT
152.QZ    9 MUSC  9 BIOT  9 CHLR  9 GRNA  9 OP    9
153.M 2.13    294 161 W 4  SCT
153.QZ   25  PLAG28  MUSC10  BIOT15  CHEQ15  TURM 2  SPH  2
153.OP    3  AP    1
154.M 2.16    312 146 W 4  SCT
154.QZ   15  CHEQ 2  ACT 60  EP  10  CARB10  SPH  3  OP    1
154.HORN  9
155.M 8. 8    203 234 W 6  AGL
155.QZ    9 BIOT  9 CHFE  9 EP    9 PO    9 CPY   9
156.M 9. 1B   308 184 W 4  SCT
156.QZ    9 BIOT  9 CHLR  9 ACT   9 EP    9 CARB  9 SPH   9
156.OP    9
157.M 9. 1K   306 182 W 4  CIP
157.QZ    9 BIOT  9 CC    9 OP    9
158.M 9. 3    303 181 W 4  SCT
158.QZ    9 PLAG  8 BIOT  9 EP    9 OP    9 TURM  9
159.P 3. 9    122 323 W 6  MBG
159.QZ   10  PLAG 8  BIOT 5  CHEQ10  ACT 53  EP   1  CARB 6
159.SPH   6  SULF 2  HORN  9   MRAD  1
160.P 3.10    123 325 W 6  UM
160.SERP35  CHEQ  8 TREM55  CC  10  SPH   1
161.P 4. 1A   140 247 W 5  MBG
161.QZ    8 PLAG15  BIOT 4  CHEQ 7  ACT 50  EP  20  SPH  4
```

Table 19. Cont'd...

```
161.SULF  1 HORN  9
162.P 4. 8     140 256 W 6  SCT
162.QZ  34  PLAG  8 MUSC10  BIOT10  CHEQ20  EP  15  GRNA 3
162.TURM  1 ZIRC  1 OP   7
163.P 4. 9     140 260 W 6  SCT
163.QZ  60  BIOT10  EP   5  TURM 5  PO  18  CPY  2
164.P 4.23     145 303 W 6  TPB
164.QZ  17  PLAG  8 BIOT20  CHEQ 5  EP  20  CARB30  SPH  4
164.OP   4
165.P 5. 2     239 265 W 6  AGL
165.QZ    9 PLAG  9 BIOT  9 CHLR  9 ACT   9 EP    9 SPH   9
166.P 5.17A    220 284 W 6  SCT
166.QZ  21  PLAG  9 BIOT 6  CHLR25  EP    1 CARB40  SPH  8
167.P 5.22B    218 287 W 6  SS
167.QZ  70  PLAG17  MUSC  1 BIOT 3  EP    1 CARB 3  SPH   8
167.ZIRC  1 OP   7
168.P 7. 9      87 246 W 6  MBG
168.QZ   3  PLAG17  BIOT 1  CHEQ10  ACT 49  EP   7  CARB 8
168.SPH  5  SULF  1
169.P 7.10      86 247 W 6  MBG
169.QZ    9 PLAG20  BIOT  1 CHEQ10  ACT 50  EP   4  CARB10
169.SPH  6  OP    1 MRAD  1   HORN  9
170.P 7.27C     74 271 W 5  CGL
170.QZ    9 MICR  9 PLAG  9 MUSC  9 CARB  9
171.P 9. 6      87 106 W 3  SCT
171.QZ  58  PLAG  9 MUSC 5  BIOT12  GRNA 7  CARB 5  MT  13
172.P 9.18      69 111 W 4  SCT
172.QZ  80  PLAG  9 MUSC 5  BIOT 7  CHLR 5  TURM  1 SPH  3
172.ZIRC  1 OP   1
173.P 9.27A     79 140 W 5  UM
173.TREM97  CHMG 3  SPH   1 OP    1
174.P 9.27C     79 140 W 5  UM
174.TALC  9 SERP  9 CHLR  9 CARB  9 TREM  9 OP    9
175.P 9.27D     79 140 W 5  UM
175.TREM90  CARB10  OP    1
176.R 1.11     619 294 E 4  SCT
176.QZ  25  PLAG25  BIOT46  MRAD  1 AP    1 ZIRC  1 OP   6
177.R 1.16     593 311 E 1B AMP
177.PLAG25  HORN65  BIOT10  EP    1 SPH   1 MRAD  1
178.R 2. 7     563 297 E 1B AMP
178.QZ    9 PLAG20  BIOT  1 HORN56  EP  20  CC   4  CARB  8
178.SPH   1 SULF  1 ZIRC  1
179.R 5.13B    163 325 W 6  MBG
179.QZ   5  PLAG10  BIOT 1  CHEQ16  ACT 45  EP  20  CARB  1
179.SPH  3  MRAD  1
180.R 6. 3     105 525 W 8  SCT
180.QZ  33  PLAG30  MUSC30  BIOT15  CHFE  1 ZIRC  1 SPH   1
180.OP   2
181.R 6.14      95 506 W 7  MBT
181.QZ    9 PLAG45  BIOT  1 CHMG  1 ACT 45  EP   3  SPH  3
```

Table 19. Cont'd...

181.CARB	3	PO	5	CPY	5										
182.R 6.17		96	502	W	7	FLS									
182.QZ	90	PLAG	9	MICR	9	BIOT	3	CHEQ	5	EP	1	SPH	2		
182.AP	1														
183.R 6.21		96	495	W	7	MBX									
183.QZ	9	PLAG10		CHEQ	8	ACT	30	EP	50	SPH	2	RUTI	8		
183.SULF	1	INCO	1												
184.R 9. 9		59	526	W	7	TPB									
184.QZ	8	PLAG15		BIOT	1	MUSC	1	CHMG35		EP	20	CARB30			
184.SPH	1	OP	1												
185.R10. 2		174	498	W	8	SCT									
185.QZ	25	OLIG23		BIOT	1	CHMG	1	AMPH50		DOL	2	EP	1		
185.OP	2	AP	1	ZIRC	1	MRAD	1	RUTI	8						
186.R12. 1B		164	231	W	5	MBG									
186.QZ	9	PLAG30		BIOT20		ACT	30	EP	10	SPH	7	AP	1		
186.OP	1	MRAD	1	HORN	9										
187.R12. 1C		164	232	W	5	MBG									
187.PLAG30		BIOT	2	ACT	55	EP	10	SPH	1	HORN	9	[illegible]	1		
188.R12. 5A		167	238	W	5	SS									
188.QZ	76	PLAG	9	BIOT	4	MUSC15		CHEQ	2	ZIRC	1	[illegible]	1		
188.SPH	2														
189.R12. 7A		167	239	W	5	MBG									
189.QZ	8	PLAG10		CHLR	3	ACT	75	EP	10	CC	1	SPH	3		
189.SULF	5	HORN	9	MRAD	1										
190.R12. 9		168	241	W	5	TPB									
190.QZ	35	PLAG	9	CHMG50		ACT	5	EP	5	SPH	5	SULF	1		
190.HORN	9														
191.R12.10		169	242	W	6	MBT									
191.QZ	9	PLAG15		BIOT20		ACT	50	EP	10	SPH	3	HORN	9		
191.MRAD	1														
192.R12.12B		170	244	W	6	MBG									
192.QZ	30	PLAG30		STIL	1	CHFE10		ACT	20	SPH	5	ILM	5		
192.PO	1	CPY	1	MRAD	1										
193.R12.13		170	245	W	6	UMX									
193.ACT	69	CHMG30		SPH	1	AP	1	OP	1	SULF	1				
194.R12.32		190	277	W	6	MBT									
194.PLAG15		CHLR	5	ACT	40	EP	35	SPH	4	SULF	1	HORN	1		
195.R12.36		191	282	W	6	MBT									
195.QZ	9	PLAG35		BIOT	1	CHLR	5	ACT	20	EP	35	SPH	3		
195.SULF	1														
196.R12.42		193	286	W	6	MBT									
196.QZ	9	PLAG15		BIOT10		CHLR	5	ACT	45	EP	20	SPH	5		
196.SULF	5	CC	7	INCO	7	HORN	9								
197.R13.22		187	244	W	6	MBX									
197.QZ	9	PLAG15		CHLR	3	ACT	60	EP	15	SPH	4	CC	5		
197.SULF	5	HORN	9												
198.R14. 4D		263	242	W	6	MBY									
198.QZ	9	PLAG35		BIOT10		CHMG35		EP	1	CC	15	SPH	2		
198.SULF	1	MT	1	ZIRC	1										
199.R14. 8C		262	248	W	6	MBG									

Table 19. Cont'd...

```
199.QZ  10  PLAG  1 BIOT 1  CHLR15  ACT 55  EP  15  SPH  4
199.SULF 1  MRAD  1
200.R14.12     252 268 W 6  MBT
200.QZ  15  PLAG  1 CHLR10  ACT 55  EP  15  SPH  4  OP    5
200.HORN  9
201.R14.26     230 297 W 6  MBT
201.QZ    9 PLAG10  STIL 5  CHFE10  ACT 60  EP  10  SPH  5
201.ILM  2  SULF  1   HORN  9
202.R15. 3     285 232 W 5  MBX C
202.QZ  35  PLAG  9 CHMG10  ACT 40  EP  10  CC   5  SPH  4
202.SULF  5 MRAD  1   HORN  9
203.R15. 4B    285 233 W 5  MBY
203.QZ    9 PLAG15  BIOT10  CHMG50  EP  10  CC  10  SPH  4
203.SULF  5 ZIRC  8 MRAD  1
204.R15. 5     285 235 W 6  MBX
204.QZ    9 PLAG15  CHLR 5  ACT 70  EP  10  CC   9 SPH  5
204.SULF  5 HORN  9   MRAD  1
205.R15.11     283 250 W 6  MBG
205.QZ    9 PLAG15  BIOT 3  CHEQ10  ACT 60  EP  15  SPH  3
205.SULF 1  MRAD  1   HORN  9
206.R15.15     280 262 W 6  MBT
206.QZ    9 PLAG 5  BIOT 1  CHLR10  ACT 65  EP  20  CARB  9
206.SPH  5  SULF  5 HORN  1
207.R15.17     279 266 W 6  MBG
207.QZ    9 PLAG20  CHLR 5  ACT 55  EP  20  SPH  3  MRAD  1
207.HORN  9
208.R15.18     278 267 W 6  MBG
208.QZ    9 PLAG15  CHLR10  ACT 60  EP  10  CARB  1 SPH  4
208.HORN  9
209.R15.27B    260 295 W 6  MBG
209.QZ    9 PLAG 5  CHLR 5  ACT 70  EP  20  SPH  2  HORN  9
210.R15.29     258 300 W 6  UM
210.QZ    8 PLAG 4  CHMG 5  TREM80  EP   2  CARB10  SPH  3
210.
211.R15.30     256 302 W 6  MBT
211.QZ    9 PLAG15  CHLR 5  ACT 70  EP  10  SPH  5  HORN  9
212.R15.31     256 303 W 6  MBG
212.QZ    9 PLAG10  BIOT  1 CHLR 5  ACT 40  EP  35  CARB 3
212.SPH  3  SULF  1 HORN  9
213.R17.16A    170 217 W 5  MBY
213.QZ  50  PLAG  9 BIOT40  CHLR 3  EP    8 CARB10  SPH  1
213.ILM  1  MRAD  1
214.R20. 2A    285 357 W 5  MBY
214.QZ    9 PLAG20  BIOT 3  CHMG30  ACT 30  CC  15  CARB  8
214.ILM  2  MRAD  1
215.R20. 2C    290 355 W 5  SCT
215.QZ  79  PLAG  9 BIOT15  CHEQ 3  AP    1 ZIRC  1 OP   2
215.TURM 1
216.R20. 2E    295 352 W 5  MBX
216.QZ    9 PLAG25  BIOT  1 CHLR 4  HORN65  ALL   1 CARB 3
```

Table 19. Cont'd...

```
216.AP    1  SPH    1 ILM  5
217.R20.  4     291 364 W 6  AMP
217.QZ    8 PLAG20  ACT 70  EP  10  MRAD  1 SPH  2  SULF 2
217.HORN  9
218.R20.  7     282 371 W 6  AMP
218.QZ    8 PLAG20  ACT 70  EP   5  SPH  3  ILM  2  HORN  9
219.R20.  8     279 368 W 6  AMP
219.QZ   10  PLAG  9 CHEQ 1  HORN83  ALL   1 SPH   1 ILM  6
220.R22. 1B    218 344 W 6  MBT
220.QZ    9 PLAG25  BIOT  5 CHEQ 5  STIL 3  ACT 60  EP   5
220.CARB 3  SPH 10  SULF  5 HORN  9
221.R22. 2D    218 342 W 6  SS
221.QZ   83  PLAG  9 BIOT 3  MUSC10  CHFE 2  EP    1 ZIRC  1
221.CARB  1 SPH  1  OP   1
222.R22. 7B    225 328 W 6  MBG
222.QZ   20  PLAG  8 BIOT  1 CHEQ30  EP  40  GRNA  1 AP   1
222.SPH   7  PO   3  CPY   1 ZIRC  1
223.R22. 7C    225 328 W 6  MBG
223.QZ   10  BIOT25  CHFE 5  HORN10  GRNA  5 EP  40  SPH  5
223.PO    4  CPY   5 ZIRC  1
225.S 1. 6     278  70 W 3  IF
225.QZ   64  CUMM15  GRNA10  CARB 1  AP    1 OP  10
226.S 2.1.1    291  98 W 3  SS
226.QZ   89  MICR 5  PLAG 5  BIOT  1 MUSC 1  ZIRC  1 OP    1
227.S 2.1.2    291  98 W 3  SS
227.QZ   89  MUSC10  ZIRC  1 OP   1
228.S 2.1.3    291  98 W 3  IF
228.QZ   81  BIOT  1 STIL 1  CUMM 3  CARB  1 ZIRC  1 OP  15
229.S 2.1.4    291  98 W 3  IF
229.QZ   64  STIL 1  CUMM10  CARB15  ZIRC  1 OP  10
230.S 2.1.5    291  98 W 3  IF
230.QZ   71  STIL 1  CUMM 3  CARB  1 OP  25
231.S 2.1.6    291  98 W 3  IF
231.QZ   34  STIL  1 CHFE  1 CUMM 1  DOL 35  OP  10
232.S 2.1.7    291  98 W 3  IF
232.QZ   74  STIL 1  CHFE  1 CUMM 3  CARB 2  OP  20
233.S 2.1.9    291  98 W 3  IF
233.QZ   45  STIL44  CARB10  OP   1
234.S 2.1.10   291  98 W 3  SS
234.QZ   97  BIOT 1  CHEQ 2  ZIRC  1
235.S 2.1.11   291  98 W 3  IF  SC
235.QZ   15  DOL 15  STIL70
236.S 2.1.12   291  98 W 3  IF
236.QZ   53  CC  45  CARB  9 STIL  1 CUMM 2
237.S 2.1.14   291  98 W 3  SCT
237.QZ   48  BIOT10  MUSC25  TURM 2  OP  15
238.S 2.1.15   291  98 W 3  IF
238.QZ   89  STIL10  BIOT 1  CHFE  1 OP    1
239.S 3.1.2    316  87 W 3  IF
239.QZ   20  BIOT  1 STIL10  CHFE20  CARB30  OP  20
```

Table 19. Cont'd...

```
240.S 3.1.3    315  87 W 3  IF
240.QZ  50  BIOT  1 CUMM 2  CC  45  CARB  8
241.S 4.13A    258 117 W 3  SCT
241.QZ  76  BIOT 5  MUSC 8  CHEQ10  AP    1 OP   1
242.S 4.14A    263 123 W 3  SCT
242.QZ  37  AB  37  BIOT 2  MUSC 3  CHEQ 1  AP   1  OP   1
243.S 4.14C    264 124 W 3  IF
243.QZ  29  STIL70  OP   1
244.S 4.14D    264 124 W 3  IF
244.QZ  10  STIL50  CUMM28  ALL   1 CARB 2  AP    1
245.S 4.17A    263 142 W 4  IF
245.QZ  40  STIL40  SND 15  OP   5
246.S 4.22A    238 137 W 4  SCT
246.QZ  68  FP    9 BIOT 5  MUSC10  CHEQ10  GRNA 5  CC    1
246.CARB  1 ZIRC  1 GRPH 2
247.S 4.25B    234 128 W 4  SCT
247.QZ  58  MUSC15  CHEQ 2  AB  15  CARB10  OP    1
248.S 4.32A    240 113 W 3  IF
248.QZ  90  OP  10  ZIRC  1
249.S 4.32B    241 111 W 3  IF
249.QZ  85  OP  15  ZIRC  1
250.S 6. 7F    319 224 W 6  SCT
250.QZ    9 FP    9 BIOT  9 CHEQ  9 EP    9 ZOIS  9 GRNA  9
250.TURM  9 ZIRC  9 OP    9
251.S 6. 8A    319 224 W 6  SCT
251.QZ  50  FP    8 BIOT15  CHEQ 3  ACT  1  EP  29  TURM  1
251.OP   2                                    9
252.S 6. 8E    319 223 W 6  SCT
252.QZ  48  AB    8 BIOT10  CHEQ 5  EP  35  TURM 1  OP   1
253.S 6.12A    319 220 W 6  TFI
253.QZ  30  AB    8 CHEQ40  EP  20  AP    1 SPH 10
254.S 6.13A    318 218 W 6  MBG
254.QZ  35  CHTE 5  HORN51  EP   3  AP   1  ILM  4  SPH  1
254.ZIRC  1
255.S 6.14     315 216 W 5  CGL
255.QZ  40  MICR20  PLAG20  MUSC16  BIOT 4  ZIRC  1 SPH   1
256.S 6.14A    315 216 W 5  SS
256.QZ  54  MICR20  PLAG20  BIOT 1  CHEQ 2  ZIRC  1 SPH  2
256.OP   1
257.S 6.15     309 215 W 5  SCT
257.QZ  78  MUSC15  BIOT 3  CHMG  1 CARB 2  TURM 1  ZIRC  1
257.SPH   1 OP   1
258.S 6.16     308 211 W 5  CGL
258.QZ  55  PLAG40  MUSC 5  BIOT  1 ZIRC  1 OP    1
259.S 6.16E    308 210 W 5  MBG
259.QZ  25  BIOT 4  CHEQ 5  ACT 42  EP  20  SPH  3  SULF 1
259.MRAD  1   HORN  9
260.S 6.17E    307 208 W 5  AGL
260.QZ    9 BIOT  9 CHLR  9 ACT   9 EP    9 SPH   9 SULF  9
260.
```

Table 19. Cont'd...

261.S 6.18 304 204 W 5 MBG
261.QZ 10 AB 42 STIL 3 CHLR 8 HORN40 EP 1 AP 1
261.SPH 1 ILM 4 MRAD 1
262.S 7. 2A 293 191 W 5 SCT
262.QZ 9 BIOT 9 CHFE 9 GRNA 9 CC 9 AP 9 ZIRC 9
262.OP 9
263.S 7. 2B 293 191 W 5 SCT
263.QZ 15 BIOT10 CHLR 5 GRNA69 ZIRC 1 OP 2
264.S 7. 4A 304 184 W 5 TFB
264.QZ 8 PLAG44 BIOT10 CHMG10 TREM10 EP 10 CARB15
264.SPH 1
265.S 7. 4B 305 185 W 5 TFB
265.QZ 8 PLAG20 BIOT 1 CHMG 8 TREM40 EP 30 SPH 2
266.S 7. 4D 305 184 W 5 TFB
266.QZ 9 PLAG13 CHMG 5 ACT 65 EP 15 SPH 2 HORN 9
266.MRAD 1
267.S 7. 4E 308 183 W 5 TFB
267.PLAG 9 CHMG 5 TREM70 EP 10 CARB 5 SPH 1
268.S 7. 4G 304 183 W 5 TFB
268.PLAG15 BIOT15 CHEQ50 HORN10 EP 5 CC 1 ILM 5
268.ZIRC 1
269.S 7. 4H 304 183 W 5 TFB
269.QZ 10 BIOT 1 CHFE20 HORN58 ALL 1 CC 8 AP 1
269.SPH 1 ILM 3
270.S 7. 5 307 184 W 5 MBX
270.QZ 9 PLAG10 CHEQ 5 HORN80 EP 1 CC 1 AP 1
270.SPH 2 ILM 1 SULF 1 MRAD 1
271.S 7. 5A 307 184 W 5 SCT
271.QZ 56 PLAG20 BIOT10 MUSC10 CHEQ 1 EP 2 CC 1
271.AP 1 OP 1
272.S 9. 1C 188 189 W 5 IF
272.QZ 28 STIL20 CUMM30 CARB20 AP 1 OP 2
273.S 9. 1F 188 189 W 5 UM
273.TALC69 CHMG10 CC 20 DOL 9 OP 1
274.S 9. 2D 213 244 W 5 SS
274.QZ 55 PLAG38 MICR 9 MUSC 5 BIOT 2 CHLR 1 ZIRC 1
274.SPH 1 OP 1
275.S 9. 2L 210 246 W 5 SCT
275.QZ 78 PLAG 9 BIOT 1 MUSC 3 CHMG15 TURM 1 ZIRC 1
275.SPH 2 OP 1
276.S13. 2C 296 221 W 5 SCT
276.QZ 73 PLAG 9 MUSC20 BIOT 5 CHEQ 1 TURM 1 ZIRC 1
276.SPH 2
277.S13. 5C 286 235 W 6 COR
277.QZ 76 PLAG 9 BIOT12 CHLR 3 CC 8 ZIRC 1 SPH 1
278.S14. 4A 253 381 W 6 SCT
278.QZ 61 MUSC20 BIOT15 CHLR 1 EP 1 AP 1 ZIRC 1
278.GRNA 2 TURM 1 OP 1
279.S14. 4B 253 381 W 6 MBG
279.QZ 8 OLIG35 CHEQ10 CHFE 1 ACT 45 EP 1 CC 5

Table 19. Cont'd...

279.AP 1 ILM 2 HORN 9 SULF 1
280.S14. 4C 253 382 W 6 MBG
280.QZ 17 BIOT 1 CHMG 7 HORN70 SPH 1 ILM 5 MRAD 1
281.S14. 4D 253 382 W 6 MBG
281.QZ 9 PLAG20 CHEQ 1 ACT 72 EP 2 ILM 3 SPH 2
281.HORN 9 SULF 1 ALL 1 MRAD 1
282.S14.10A 248 397 W 6 MBT
282.QZ 10 PLAG 9 CHEQ 1 ACT 70 EP 16 CC 1 SPH 3
282.HORN 9
283.S14.13A 238 403 W 6 MBT
283.QZ 9 PLAG10 CHEQ 4 ACT 64 EP 17 SPH 4 SULF 1
283.HORN 9
284.S14.15A 237 414 W 6 SCT
284.QZ 89 PLAG 9 CHEQ 4 HORN 4 ZIRC 1 SPH 1 OP 3
285.S14.15C 237 414 W 6 AGL
[illegible] 9 PLAG 9 BIOT 9 CHLR 9 ACT 9 EP 9 SPH 9
[illegible] 9 HORN 9
[illegible]A 238 422 W 6 MBT
[illegible]9 PLAG10 BIOT 1 CHEQ10 ACT 53 EP 20 SPH 5
[illegible] HORN 9
[illegible] 236 424 W 6 SCT
[illegible] PLAG 9 BIOT30 CHLR25 EP 1 ACT 1 CC 1
[illegible] 236 424 W 6 SS
[illegible] PLAG 9 BIOT 4 CHEQ 1 MUSC 4 ZIRC 1 AP 1
[illegible] 1 OP 1
[illegible]S14.17C 236 424 W 6 SS
289.QZ 84 PLAG 1 MUSC 2 BIOT10 CHLR 1 EP 1 ZIRC 1
288.SPH 1 OP 2
290.S14.17D 236 424 W 6 MBG
290.QZ 8 PLAG17 BIOT 7 CHLR 6 EP 7 ACT 49 SPH 5
290.SULF 1 HORN 9 ALL 1
291.S14.17E 236 424 W 6 SS
291.QZ 69 PLAG13 BIOT 4 MUSC 4 AP 1 ZIRC 1 SPH 1
292.S14.17F 236 424 W 6 SS
292.QZ 72 PLAG15 MICR 8 MUSC 5 BIOT 4 CC 1 AP 1
292.ZIRC 1 SPH 1 OP 7
293.S14.17G 236 424 W 6 MBT
293.QZ 9 PLAG17 BIOT10 CHEQ 1 ACT 61 EP 5 SPH 5
293.SULF 2 HORN 9
294.S14.21A 227 438 W 6 MBT
294.QZ 8 PLAG15 CHEQ 5 ACT 50 EP 25 SPH 4 SULF 1
294.HORN 9
295.S14.21B 227 438 W 6 TFB
295.QZ 32 PLAG 8 BIOT 1 CHEQ30 EP 5 CC 20 SPH 3
295.OP 2 MRAD 1
296.S14.22A 231 439 W 6 SCT
296.QZ 28 PLAG28 BIOT10 CHEQ 3 MUSC30 EP 1 OP 1
297.S15. 1A 220 441 W 7 UM
297.SERP 9 CHEQ 9 TREM 9 CPX 9 CARB 9 OP 9

Table 19. Cont'd...

```
298.S15. 1B   220 441 W 7  UM
298.SERP  9 CHEQ  9 CPX   9 OP    9 ALTR  9 OL    9 OPX   8
299.S15. 1C   220 442 W 7  UM
299.SERP  9 CHEQ  9 CPX   9 OP    9 OL    9 OPX   8
300.S15. 1D   220 443 W 7  UM
300.OL    9 CPX   9 SERP  9 CHMG  9 AMPH  9 TREM  9 QZ    9
300.OP    9 SPIN  8
301.S15. 1E   220 444 W 7  UM
301.SERP  9 CHLR  9 AMPH  9 TREM  9 OP    9 SPIN  8 OL    9
301.CPX   9
302.S15. 2A   220 444 W 7  UM
302.CUMM  9 TREM  9 AMPH  9 CPX   9
303.S15. 2B   220 444 W 7  MBG
303.OLIG  9 CUMM  9 TREM  9 AMPH  9 EP    9 SPH   9
304.S15. 2C   220 444 W 7  MBG
304.OLIG 8 BIOT 3  ACT 45  EP  25  ZOIS16  SPH  3
305.S15. 2D   220 445 W 7  MBG
305.QZ    9 PLAG 5  BIOT 5  ACT 50  EP  20  ZOIS18  SPH  2
305.SULF  1 HORN  9   MRAD  1
306.S15. 2E   220 445 W 7  MBG
306.QZ    9 OLIG 5  BIOT 2  ACT 60  EP  21  ZOIS10  SPH  2
306.SULF  1 HORN  9   MRAD  1
307.S15. 2F   220 445 W 7  MBG
307.QZ    9 OLIG10  BIOT 2  CHMG16  ACT 40  EP  30  SPH  2
307.OP    1 HORN  9   MRAD  1
308.S15. 2G   220 445 W 7  MBG
308.QZ    8 OLIG 7  INCO  9 CHEQ  1 ACT 61  EP  30  SPH  2
308.SULF  1 HORN  9   ZIRC  1
309.S15. 2H   220 446 W 7  MBG
309.OLIG 7  CHEQ 3  ACT 58  EP  30  SPH  2  OP    1 MRAD  1
310.S15. 2I   220 446 W 7  MBG
310.PLAG 7  ACT 60  EP  30  AP    1 SPH  3  OP    1 MRAD  1
311.S15. 2K   220 446 W 7  MBG
311.QZ    9 AB  40  BIOT  1 ACT 56  EP  10  SPH  4  MRAD  1
311.HORN  9
312.S15. 2L   220 447 W 7  MBG
312.AB  20  BIOT 1  ACT 58  CHEQ 3  EP  15  SPH  3  HORN  9
312.MRAD  1
313.S15. 2M   220 447 W 7  MBG
313.QZ  10  AB    8 BIOT10  CHEQ 8  ACT 49  EP  20  SPH  3
313.MRAD  1
314.S15. 2N   220 448 W 7  MBG
314.QZ    9 AB  15  CHMG  1 ACT 62  EP  20  SPH  3  MRAD  1
315.S15. 2P   220 448 W 7  COR
315.QZ  97  PLAG  9 PHLO  1 CHMG  1 TREM 1  SPH  2
316.S15. 2R   220 449 W 7  COR
316.QZ  80  PLAG  9 BIOT 5  CHMG 1  ACT  4  EP   4  GRNA 2
316.TURM 1  SPH  3  RUTI  1
317.S15. 2S   220 449 W 7  COR
317.QZ  70  PLAG  7 BIOT  9 CHMG  9 EP    9 GRNA  9 TURM  9
```

Table 19. Cont'd...

```
317.ZIRC  9 SPH   9
318.S15. 4A   218 452 W 7  GWK
318.QZ  20  PLAG  9 BIOT 3  CHEQ 1  ACT 30  EP  38  SPH  4
318.OP   4
319.S15. 4D   218 442 W 7  MBX
319.QZ  18  OLIG  9 BIOT  1 CHEQ 7  ACT 40  EP  30  SPH  4
319.OP    1 SULF  8
320.S15. 4E   218 443 W 7  SCT
320.QZ  48  PLAG  8 BIOT 7  MUSC20  TURM  1 OP  25  MRAD  1
321.S15. 4F   218 443 W 7  MBT
321.PLAG  1 BIOT  1 CHMG15  TREM79  EP   3  SPH  3  SULF  1
322.S15. 4G   218 443 W 7  MBT
322.CHMG10  ACT 81  EP   4  SPH  5  HORN  9
323.S15. 4H   218 444 W 7  MBT
323.AB    1 CHMG15  ACT 73  EP   8  SPH  4  HORN  9
324.S15. 4I   218 444 W 7  MBT
324.PLAG 4  BIOT 3  CHMG 5  ACT 61  EP  20  CARB  5 SPH  5
324.SULF 1  MRAD  1
325.S15. 4K   218 445 W 7  MBT
325.PLAG 4  BIOT  1 CHMG 8  ACT 72  AMPH  8 EP  10  SPH  5
325.SULF 1  HORN  9
326.S15. 4M   218 445 W 7  UM
326.CHMG20  ACT 76  SPH  3  OP   1  HORN  9
327.S15. 4N   218 445 W 7  UM
327.CHMG25  ACT 63  CARB10  SPH   8 OP   2
328.S15. 4P   218 446 W 7  UM
328.TALC  1 CHEQ20  TREM72  OP   8
329.S15. 4Q   218 446 W 7  UM
329.TALC  1 CHLR20  TREM74  CARB 1  OP   6
330.S15. 4R   218 446 W 7  UM
330.CHMG32  ACT 60  CARB 4  OP   4
331.S15. 4T   218 446 W 7  MBT
331.PLAG20  CHLR  8 HORN60  EP  15  SPH  5  MRAD  1
332.S15. 4V   218 457 W 7  MBT
332.PLAG 5  CHMG10  ACT 70  EP  10  CARB  1 SPH  4  SULF 1
333.S15. 6C   217 461 W 7  SCT
333.QZ  55  BIOT10  MUSC20  EP   5  OP  10
334.S15. 6D   217 461 W 7  MBT
334.QZ    9 PLAG10  BIOT25  CHMG 1  ACT 40  EP  20  SPH  3
334.SULF 1  HORN  9
335.S1 . 7    217 461 W 7  TFI
335  _  5  CHMG15  TREM15  EP   5  SPH   9 OP  15
336.S16. 1A   221 492 W 1A  GNS
336.QZ  30  MICR 5  OLIG50  BIOT  1 MUSC 7  CHFE 7  CC   1
336.AP    1 ZIRC  1 OP   1
337.S16. 1C   221 492 W 8  SCT
337.QZ  78  PLAG  9 BIOT10  CC  10  AP    1 MRAD  1 OP    1
338.S16. 1D   221 492 W 8  SCT
338.QZ  40  BIOT10  GRNA25  CARB  1 OP  25  ACCS  1
339.S16. 1E   221 492 W 8  CIP
```

Table 19. Cont'd...

```
339.QZ    9 PLAG15  BIOT 5  CHMG  1 AMPH60  DOL 13  EP    1
339.MRAD  1 RUTI 1  OP   1
340.S16. 1F   221 492 W 8  SCT
340.QZ    9 PLAG  9 BIOT  9 CHLR  9 GRNA  9 CC    9  OP    9
341.S16. 1G   221 492 W 8  CIP
341.QZ   30  PLAG  9 BIOT 2  CHMG 5  AMPH50  EP   2  CC   10
341.AP    1 RUTI  1 PO   1
342.S16. 1H   221 492 W 8  SCT
342.QZ   70  PLAG  9 MUSC10  BIOT15  GRNA 2  TURM  1 AP    1
342.RUTI  1 OP   2
343.S16. 1K   221 491 W 8  AMP
343.QZ    9 PLAG15  BIOT  1 CHMG 1  HORN77  EP    1 CARX 6
343.RUTI 1  SULF  1 MRAD  1
344.S16. 1M   221 491 W 8  SCT
344.QZ   58  PLAG  9 BIOT 5  CHMG 5  EP   5  CARX20  AP   1
344.RUTI 1  PO  15
345.S16. 1P   221 491 W 8  AMP
345.QZ    9 PLAG15  CHMG  1 HORN72  ALL  3  CARX 7  SPH   1
345.ILM  3
346.S16. 1Q   221 491 W 8  CST
346.QZ   35  PLAG  9 BIOT15  CHMG 3  CC  20  DOL   9 INCO 7
346.AP    1 MRAD  1 RUTI  1 PO  20  GRPH  9
347.S16. 1R   221 491 W 8  AMP
347.QZ   10  CHMG  1 HORN85  ALL  2  SPH  2  ILM  1
348.S16. 2B   220 491 W 8  SCT
348.QZ   66  PLAG  9 MUSC20  CHMG 2  BIOT10  TURM 1  ZIRC 1
348.OP    1 INCO  1
349.S16. 2E   220 491 W 8  SCT
349.QZ   32  BIOT32  CHMG 3  DOL 33  CC    8 AP    1 OP    1
350.S16. 3C   217 489 W 8  AMP
350.QZ   15  CHEQ  1 HORN72  GRNA10  AP   1  ILM  2  ALL   1
350.ZIRC  1
351.S16. 3D   217 489 W 8  SCT
351.QZ   73  PLAG  9 BIOT20  CHMG  1 EP   3  GRNA 2  TURM 1
351.AP    1 OP    1 INCO 1
352.S16. 3E   216 487 W 8  AMP
352.PLAG 1  CHMG10  ACT 87  CARB 1  ACCS  1 MT   1
352.BIOT  1  RUTI  1  MRAD  1
353.S16. 3G   216 487 W 8  AMP
353.QZ    9 PLAG20  CHMG 2  CUMM25  HORN50  ILM  3  SULF  1
353.MRAD  1
354.S16. 4A   215 485 W 8  AMP
354.PLAG25  CHMG 1  HORN68  ALL   1 SPH  3  ILM  3  SULF  1
355.S16. 4B   215 485 W 8  AMP
355.QZ    9 PLAG20  HORN73  EP   4  SPH  2  SULF 1
356.S16. 4C   215 485 W 8  AMP
356.QZ    9 PLAG 5  CHMG 1  HORN88  ALL  1  SPH   1 ILM  5
357.S16. 4D   214 484 W 8  AMP
357.QZ    9 PLAG15  CHMG  1 HORN77  ALL  2  CARX 2  SPH  1
357.ILM  3
```

Table 19. Cont'd...

358.S16. 4F 213 484 W 8 SCT
358.QZ 82 BIOT10 CHEQ 1 GRNA 1 CARB 2 ZIRC 1 SPH 1
358.SULF 5
359.S16. 4I 212 483 W 8 AMP
359.QZ 1 PLAG15 BIOT 1 CHMG 1 HORN78 AP 1 ALL 1
359.SPH 1 ILM 5
360.S16. 4L 211 483 W 8 CST
360.QZ 17 PLAG 3 CHMG 5 HORN10 CC 64 CARB 9 OP 1
360.MRAD 1
361.S16. 4N 210 482 W 8 MBY
361.QZ 20 PLAG 9 BIOT 1 CHMG34 HORN35 CARB 7 ALL, 1
361.ILM 4 SULF 1
362.S16. 4P 209 482 W 8 AMP
362.QZ 9 PLAG15 HORN75 CARB 5 ALL 1 SPH 1 ILM 5
362.EP 7 INCO 7 SULF 1
363.S16. 5A 208 481 W 8 AMP
363.QZ 9 PLAG15 HORN73 CARX 6 ALL 5 SPH 4 ILM 2
364.S50. 1E 614 544 E 2A DIA
364.PLAG30 HORN30 CPX 18 GRNA20 SPH 1 OP 2
365.S50. 7B 634 508 E 1C CIP
365.PLAG 1 SCAP20 PHLO20 CPX 20 CC 20 AP 1 SPH 1
365.OP 1
366.S50.13C 619 468 E 6 CST
366.QZ 25 CUMM47 HORN 5 CPX 20 OP 3
367.S51. 1B 677 541 E 2A DIA
367.PLAG30 HORN35 CPX 15 GRNA15 SPH 2 OP 3
368.S51. 7A 670 519 E 1B AMP
368.QZ 9 PLAG17 HORN65 EP 3 CARX 8 SPH 3 ILM 4
368.SULF 1 MRAD 1
369.S51.12B 670 501 E 6 CIP
369.QZ 1 SCAP 8 PHLO10 CHMG 1 TALC 1 TREM10 DOL 77
369.OP 1
370.S51.12C 671 500 E 4 SCT
370.QZ 1 MICR20 PLAG15 SCAP10 BIOT20 EP 1 CORD 8
370.ALL 1 AP 1 SPH 1 OP 2 ALTR 1
371.S53. 2A 498 427 E 4 SCT
371.QZ 51 MICR 9 PLAG 9 BIOT30 GRNA15 CARB 1 MRAD 1
371.OP 1 TURM 1
372.S53. 2C 498 426 E 4 SCT
372.QZ 38 PLAG32 BIOT 8 CHLR 5 CARX10 TURM 1 AP 1
372.ZIRC 1 OP 2
373.S53. 2D 498 425 E 6 CIP
373.QZ 2 MICR 1 PHLO 5 CHMG 1 TREM 3 CC 88 DOL 9
373.OP 1
374.S53. 2E 500 424 E 4 SCT
374.QZ 67 PLAG10 MUSC 5 BIOT 5 CHEQ10 GRNA 2 TURM 1
374.MRAD 1 AP 1 OP 1
375.S53. 2F 500 424 E 8 SCT
375.QZ 72 AB 15 BIOT 4 MUSC 4 CHEQ 4 ZIRC 1 AP 1
375.OP 1

Table 19. Cont'd...

376.S53. 3B 506 422 E 7 AMP
376.PLAG37 HORN60 SPH 3 AP 8 ALL 1 ILM 1
377.S53. 4A 512 418 E 7 AMP
377.QZ 9 PLAG15 BIOT 1 HORN55 GRNA20 CARB 3 ALL 1
377.ILM 6
378.S53. 4B 514 417 E 7 AMP
378.QZ 44 PLAG10 BIOT 1 CHEQ 1 HORN25 GRNA 4 CARX 5
378.SULF 5 MT 5 MRAD 1
379.S53. 5A 522 414 E 7 SCT
379.QZ 86 HORN10 CHEQ 2 OP 2
380.S53. 6A 528 408 E 9 AMP
380.AB 25 CHMG10 HORN50 ANTH10 ALL 1 MRAD 1 AP 1
380.ILM 5 CPY 1 PY 1
381.S53. 6B 528 407 E 9 AMP
381.QZ 25 PLAG 9 HORN65 ALL 3 CARB 3 MRAD 1 SPH 2
381.ILM 2
382.S53.11E 547 400 E10 FLS
382.QZ 1 PLAG70 MUSC15 BIOT12 CHMG 1 SPH 3 ZIRC 1
383.S54. 2A 786 419 E 2A DIA
383.QZ 1 PLAG35 SCAP 3 HORN32 CPX 10 GRNA15 SPH 3
383.RUTI 1 CARB 1 ILM 5 PO 5 CPY 1
384.S54. 2B 785 425 E 1B AMP
384.QZ 9 PLAG25 SCAP15 CHMG 1 HORN58 ALL 1 SPH 2
384.SULF 1 RUTI 1 ILM 1 MRAD 1
385.S54. 3 780 431 E 1A GNS
385.QZ 70 PLAG 9 SCAP10 BIOT10 EP 10 AP 1
386.S55. 7A 796 453 E 1B AMP
386.CHMG20 HORN57 EP 20 OP 3
387.S55. 7D 791 460 E 1A GNS
387.QZ 25 PLAG20 HORN30 ALL 4 GRNA15 SPH 3 OP 3
387.ZIRC 1
388.S55. 7G 788 459 E 1A GNS
388.PLAG48 BIOT48 CUMM 2 AP 1 OP 2 ZIRC 1
389.S55. 7H 785 460 E 1B AMP
389.QZ 1 PLAG30 HORN40 CPX 30
390.S56. 1A 749 463 E 1A GNS
390.PLAG40 BIOT 6 CHMG11 ANTH40 ALL 2 ILM 1 PY 1
390.CPY 1
391.S56. 1B 749 460 E 1A GNS
391.QZ 45 PLAG 9 BIOT20 MUSC10 KY 15 GRNA10 ZIRC 1
391.OP 1
392.S57. 1B 686 286 E 5 ACT
392.BIOT15 CHMG 5 ACT 80 MRAD 1
393.S57. 2A 689 285 E 1 XX
393.QZ 2 PLAG23 BIOT20 CARX40 INCO10 ALL 2 MT 2
393.PY 1 CPY 1
394.S58. 3B 539 269 E 3 IF
394.QZ 40 BIOT15 CUMM20 GRNA20 CARB 2 MRAD 1 OP 3
395.S59. 3A 474 382 E 5 UM
395.CHMG17 TREM80 CARB 3

Table 19. Cont'd...

```
396.S59. 3B    474 382 E 5  UM
396.TALC108 CHMG15  ANTH25  CARB50  OP    1
397.S59. 4A    458 386 E 5  UM
397.BIOT29  TREM70  OP   1
398.S59. 4B    458 386 E 5  UM
398.TALC15  CHMG10  TREM70  OP    1 ANTH 5
399.S59. 4D    458 387 E 5  UM
399.CHMG24  TREM75  CARB 1  OP   1
400.S59. 4E    458 387 E 5  UM
400.TALC33  ANTH33  CARB33  OP   1
401.S59. 4F    458 388 E 5  UM
401.TALC25  CHMG22  ANTH25  DOL 25  SID   9 OP   3
402.S59. 4G    458 390 E 4  SCT
402.QZ  56  MUSC25  BIOT10  GRNA 7  TURM  1 ZIRC  1 MRAD  1
402.OP   2
403.S59. 4J    458 391 E 7  PLS
403.QZ    9 PLAG  9 MUSC  9 BIOT  9 CHMG  9 EP    9 SPH   9
403.OP  50
404.S59. 4M    458 392 E 7  SCT
404.QZ  69  MICR  8 PLAG  9 MUSC  1 BIOT20  CC  10  CARB  9
404.TURM 1  AP    1 OP    1
405.S59. 5A    458 394 E 7  AMP
405.QZ  10  CHMG  1 HORN76  ALL   1 GRNA 3  CARX 5  SPH  2
405.ILM  4  SULF 2
406.S59. 5B    458 395 E 7  SCT
406.QZ  48  MUSC30  BIOT10  CHMG 5  STAU 5  TURM  1 ALL   1
406.OP   2
407.S59. 7     468 413 E 9  AMP
407.PLAG40  HORN45  EP  12  SPH  3  PO    1 PY    1 CPY   1
408.S60. 1B    528 394 E 9  TFB
408.PLAG65  BIOT  1 CHMG15  ACT 15  AP    1 ZIRC  1 SULF 2
408.ILM  2     OP   1
409.S60.10     541 398 E 9  TFI
409.QZ  20  PLAG60  BIOT15  EP   7  ZOIS 3  OP    1
410.S61. 2A    539 394 E 9  TFI
410.QZ  35  BIOT 8  ACT 10  EP   5  ZOIS32  SPH   1 OP  10
411.S61. 2B    539 394 E 9  TFI
411.QZ  30  BIOT20  AMPH  1 EP  20  ZOIS30  CHMG  1 SPH   1
411.MRAD  1
412.S61. 4     543 385 E11  AMP
412.QZ  10  PLAG10  MICR  8 BIOT20  ACT 20  CPX 30  ALL  6
412.OP   4
413.S61. 5A    542 387 E11  UM
413.CHMG45  ACT 50  OP   5  HORN  9
414.S61. 5B    542 387 E11  UM
414.SERP15  CHMG30  TREM50  OP   5
415.S61. 5C    542 387 E11  UM
415.SERP20  CHMG25  TREM52  OP   3
416.S61. 5F    543 388 E11  UM
416.SERP55  CHMG10  CHEQ10  TREM20  OP    5
```

Table 19. Cont'd...

```
417.S61. 5L    545 389 E11  UM
417.CHMG20  TREM75  OP   5
418.S61. 5M    545 389 E11  UM
418.BIOT 3  CHMG15  TREM75  OP   7
419.S61. 5P    547 390 E11  MBG
419.QZ    8 PLAG25  BIOT 1  ACT 50  EP  20  SPH  3  SULF 1
419.MRAD  1
420.S61. 5R    547 390 E11  MBG
420.QZ    8 PLAG15  BIOT  1 ACT 73  EP  10  SPH  2  SULF  1
420.MRAD  1
421.S61. 6C    549 392 E11  UM
421.CHMG30  TREM58  OL   2  CPX  5  OP   5
422.S61. 6D    550 393 E11  MBG
422.QZ    9 PLAG13  HORN72  EP  13  SPH  1  SULF 1  MRAD  1
423.S61. 6F    551 394 E11  MBG
423.QZ    9 PLAG10  CHMG10  ACT 37  EP  40  SPH  2  SULF 1
424.S61. 7A    554 398 E11  MBG       P
424.PLAG15  ACT 68  ZOIS15  SPH  8 PO   1  CPY  1
425.S61. 7B    555 398 E11  MBG       P
425.PLAG10  HORN75 EP   5  CARX 5  AP    5 SPH  2  PO   3
425.CPY   5
426.S61. 7D    556 399 E11  MBG
426.OLIG15  HORN72  EP   4  CARB 3  SPH  5  PO   1  CPY   5
426.PN    1
427.S61. 7E    557 399 E11  UM
427.CHMG30  TREM68  OP   2  INCO  1
428.S62. 2A    569 393 E11  MBG
428.CHMG 1  HORN97  EP    1 SPH  2
429.S62. 2B    569 393 E11  MBG
429.QZ   90  MICR  9 PLAG  9 CHMG 1  MUSC  1 HORN 2  EP   5
429.SPH   1  ILM  1  ZIRC  1
430.S62. 4A    571 400 E11  UM
430.CHMG35  TREM60  ALTR  5 MT   15 ILM  1  PO   1
430.PN    1  CPY  1
431.S63. 1B    634 508 E 1A GNS
431.QZ    9  MICR35  PLAG15  BIOT 8  TREM10  CPX 15  EP   1
431.CC    6  SPH  1  OP    1 MRAD  1
432.S64. 6A1   554 408 E 9  MBT
432.PLAG25  HORN20  EP  35  SPH  5  CPX 15
433.S64. 6A2   554 408 E 9  MBT
433.PLAG55  HORN18  CPX 10  EP  10  SPH  7
434.S64. 6A3   554 408 E 9  MBT
434.PLAG35  HORN 5  CPX 20  EP  29  SPH  6
435.S64. 6B    554 408 E 9  MBT
435.PLAG45  CPX 35  EP  13  CARB  1 SPH  7
436.S65. 1     667 504 E 1A GNS
436.QZ   15  MICR 5  PLAG40  BIOT 3  CHFE15  MUSC  1 HORN15
436.CPX   3  EP     9 SPH  2  SULF 2  MRAD  1
437.S65. 2     721 478 E 9  AMP
437.PLAG30  HORN40  CPX 27  EP    1 SPH  1  SULF 2
```

Table 19. Cont'd...

```
438.S66. 1A   469 388 E 5  UM
438.CHMG 3  TREM95  CARB  1 OP   2
439.S67. 4A   486 426 E 4  SCT
439.QZ  54  MICR10  PLAG10  MUSC 5  BIOT10  CHEQ10  ZIRC  1
439.SPH  1  OP    1
440.S67. 4B   486 426 E 6  CST
440.QZ  10  PLAG10  PHLO15  CHMG 1  TREM15  AMPH 1  CARB48
440.SPH  1
441.S67. 4C   486 426 E 6  CST
441.QZ   9 PLAG30  BIOT10  CHEQ 1  HORN20  CARB33  SPH  3
441.OP   3
442.S67. 4D   486 426 E 5  UM
442.CHMG10  TREM83  CARX 5  OP   2  QZ   1
443.S67. 4L   487 427 E 4  AMP
443.QZ   9 PLAG15  BIOT 1  CHLR 3  HORN67  ALL  1  SPH  1
443.ILM  15 CARB10  SULF  5
444.S67. 5A   465 435 E 4  SCT
444.QZ  77  PLAG  9 MUSC10  BIOT10  CHEQ 1  TURM  1 AP   1
444.OP   1
445.S67. 5B   462 435 E 4  SCT
445.QZ  80  MICR  9 PLAG  9 MUSC 1  BIOT15  AP   1  ZIRC  1
445.OP   3
446.S68. 1B   232 100 W 2A DIA
446.QZ  10  PLAG40  MUSC 1  BIOT10  CHEQ10  OL   1  EP  20
446.CARB 1  AP   1  SPH  4  OP   2
447.S68. 4A   229 104 W 3  IF
447.QZ  59  BIOT 5  CHEQ10  GRNA 4  CARX10  OP  12
448.S68. 4C   229 104 W 3  IF
448.QZ   5  STIL  5 CUMM65  CARX15  MT  15
449.S68. 7C   209 111 W 3  SCT
449.QZ  52  PLAG  9 MUSC30  BIOT 5  CHLR 5  SID  5  CP   3
450.S68.14C   196 160 W 4  SCT
450.QZ  76  PLAG  9 MUSC10  BIOT 5  CHEQ 5  CC   3  OP   1
451.S68.18A   187 165 W 5  MBG
451.QZ   9 PLAG10  CHLR 5  ACT 65  EP  15  SPH  5  SULF  1
451.HORN  9
452.S68.19A   186 166 W 5  IF
452.STIL90  AMPH 8  ILM  1  SPH  1  PO   1
453.S68.20A   186 168 W 5  MBG
453.QZ   9 PLAG 7  BIOT 6  CHMG 5  ACT 58  EP  20  TURM  1
453.SPH  4  PO    5 CPY   5 HORN  9
454.S70. 5    207 178 W 5  FLS
454.QZ  70  PLAG10  MUSC10  BIOT 1  ZIRC   GA   5  SP   5
455.S70. 7    183 195 W 6  MBG
455.QZ   8 PLAG30  CHEQ 3  ACT 47  EP  15  SPH  5  SULF  1
455.HORN  9
456.S72. 1A   163 346 W 6  MBT
456.QZ   9 PLAG15  BIOT 5  CHEQ10  ACT 48  EP   8  CC   5
456.SPH  8  SULF 1  HORN  9  MRAD  1
457.S72. 1B   163 347 W 6  SCT
```

Table 19. Cont'd...

457.QZ 66 PLAG 9 BIOT 8 CHEQ10 EP 10 TURM 1 SPH 3
457.OP 2
458.S72. 2A 163 346 W 6 SS
458.QZ 75 PLAG15 MUSC10 SPH 1 OP 1
459.S72. 5A 161 343 W 6 UM
459.PLAG 5 CHMG30 TREM59 EP 3 SPH 3 ZIRC 1
460.S72. 5B 161 342 W 6 UM
460.SERP30 CHEQ25 TREM30 AMPH10 OP 5
461.S72. 5C 160 342 W 6 UM
461.SERP45 CHEQ20 OL 5 CPX 5 OPX 5 OP 10 TREM10
462.S72. 5D 160 341 W 6 UM
462.SERP62 CHMG15 CPX 15 OPX 8 OP 8
463.S72. 5E 159 340 W 6 UM
463.SERP15 CHMG10 OL 40 CPX 26 OPX 2 OP 7
464.S72. 6A 155 342 W 6 MBT
464.QZ 9 PLAG 7 BIOT 2 CHEQ 5 ACT 32 EP 40 SPH 10
464.PO 3 PN 5 CPY 5 HORN 9
465.S72. 8A 156 334 W 6 UM
465.TREM83 AMPH 9 CHEQ15 SPH 1 OP 2
466.S72. 8B 156 334 W 6 UM
466.SERP30 CHEQ30 TREM34 CARB 1 OP 5
467.S73. 1A 92 535 W 8 SCT
467.QZ 35 PLAG 9 MUSC10 BIOT 4 CHEQ25 CC 10 TURM 1
467.SPH 4 OP 2
468.S73. 2B 90 533 W 8 SCT
468.QZ 46 PLAG 9 BIOT10 CHMG 3 HORN20 EP 4 CC 10
468.CARB 9 TURM 1 RUTI 1 OP 7
469.S73. 2C 90 532 W 8 SCT
469.QZ 30 PLAG 9 BIOT15 CHMG20 HORN 7 GRNA 7 EP 1
469.SPH 3 OP 3 RUTI 1 CC 15 CARB 9
470.S73. 3B 90 530 W 8 SCT
470.QZ 70 PLAG 9 MUSC 2 BIOT20 EP 6 TURM 1 OP 1
471.S73. 6A 89 520 W 8 MBG
471.PLAG15 ACT 78 EP 5 SPH 2 ILM 1 HORN 9
472.S73. 9A 90 514 W 7 FLS
472.QZ 48 PLAG 9 MUSC13 BIOT12 CHMG 6 EP 12 SPH 5
472.SULF 4
473.S73. 9B 90 514 W 7 TRI
473.QZ 54 PLAG 9 CHEQ17 HORN 7 EP 12 SPH 5 ILM 2
473.SULF 1
474.S73.11C 89 512 W 7 MBG
474.PLAG10 CHMG10 ACT 45 AMPH 5 EP 25 SPH 3
475.S73.11E 89 511 W 7 MBG
475.QZ 25 PLAG 9 CHMG40 EP 10 CARB25 SPH 1
476.S73.11G 88 511 W 7 MBG
476.QZ 9 PLAG 7 CHMG10 ACT 40 EP 40 SPH 2 HORN 9
477.S73.11H 88 511 W 7 MBG
477.QZ 9 PLAG10 CHEQ 1 ACT 80 EP 5 SPH 4 ILM 9
477.HORN 9 MRAD 1 SULF 9
478.S73.11I 88 510 W 7 MBG

Table 19. Cont'd...

478.QZ 9 AB 20 CHEQ 5 ACT 45 EP 25 SPH 5 AP 1
478.CC 1 HORN 9 MRAD 1
479.S73.13 86 511 W 7 TFB C
479.QZ [redacted] PLAG20 MUSC30 PARG 8 CHFE 3 CARB40 SULF 5
480.S74 94 474 W 7 MBT
480.PL TREM42 CHMG10 MUSC30 SPH 3 PO 8 PN 1
480.CPY
481.S75. 5A 178 338 W 6 MBG
481.PLAG20 BIOT10 CHEQ 7 ACT 44 EP 15 SPH 4 MRAD 1
482.S75. 7A 179 318 W 6 MBT
482.PLAG15 CHEQ 5 ACT 51 EP 25 SPH 4 SULF 1 HORN 1
483.S75. 7B 179 319 W 6 MBG
483.PLAG20 BIOT 1 ACT 50 EP 25 SPH 5 SULF 1 HORN 9
484.S75. 8A 163 312 W 6 MBX
484.QZ 4 PLAG10 BIOT 5 CHEQ 1 ACT 34 EP 40 SPH 6
484.CC 1 SULF 1 HORN 9
485.S75. 9A 164 314 W 6 MBG
485.AB 20 CHFE10 STIL10 HORN51 EP 1 SPH 8 OP 1
485.MRAD 1
486.S79. 1 250 463 W 7 MBT
486.AB 5 BIOT 2 CHMG 3 ACT 79 EP 10 SPH 1 CC 1
486.MRAD 1
487.S79. 2 246 465 W 7 MBG
487.QZ 9 AB 40 CHMG 1 ACT 52 EP 3 SPH 4 ILM 1
487.HORN 9 MRAD 1
488.S79. 3A 254 456 W 7 MBG
488.QZ 9 PLAG26 ACT 50 EP 20 SPH 4 HORN 9
489.S79. 3B 254 456 W 7 MBG
489.QZ 9 PLAG20 ACT 55 EP 20 SPH 4 SULF 1 HORN 9
490.S79. 4 251 453 W 7 MBT
490.QZ 9 PLAG15 ACT 61 EP 20 SPH 4 SULF 1 HORN 9
491.S80. 1 225 454 W 7 UM
491.TREM68 CHMG25 SPH 7
492.S80. 2A 229 456 W 7 MBT
492.QZ 9 PLAG10 BIOT 1 CHLR 3 ACT 75 EP 7 SPH 5
492.CPY 1 PO 1
493.S80. 2B 229 456 W 7 UM
493.CHMG10 TREM78 SPH 1 RUTI 1 OP 2
494.S81. 7A 279 482 W 8 SCT
494.QZ 30 PLAG 9 BIOT20 MUSC25 CHEQ 2 GRNA20 TURM 1
494.OP 2
495.S81. 7B 279 481 W 8 SCT
495.QZ 10 PLAG 9 BIOT20 MUSC33 CHMG 1 STAU 5 GRNA30
495.GRAP 1
496.S81. 9A 273 429 W 6 AMP
496.QZ 9 PLAG20 CHEQ 5 ACT 48 EP 20 SPH 3 CARB 3
496.ILM 1 HORN 9 SULF 1
497.S81.10A 266 428 W 6 AMP
497.QZ 9 PLAG15 CHLR 3 ACT 57 EP 20 SPH 3 SULF 2
497.HORN 9

Table 19. Cont'd...

498.S81.12A	258	433	W	6	AMP								
498.QZ	9	PLAG20	BIOT	1	CHEQ	2	ACT	44	EP	30	SPH	3	
498.SULF	1	HORN	9										
499.S82. 2B	297	406	W	6	AMP								
499.QZ	9	PLAG30	HORN56		EP	10	SPH	2	CARB	1	ILM	2	
499.ACT	9	SULF	1										
500.S82. 3A	294	409	W	6	AMP								
500.QZ	9	PLAG15	CHEQ	2	ACT	72	EP	7	SPH	4	SULF	1	
500.HORN	9												
501.S82. 4A	292	411	W	6	AMP								
501.QZ	9	PLAG 7	CHEQ	1	ACT	72	EP	15	SPH	3	CARB	2	
501.SULF	1	HORN	9										
502.S82. 4B	292	411	W	6	AMP								
502.QZ	9	PLAG 7	CHEQ	2	ACT	67	EP	20	SPH	4	SULF	1	
502.HORN	9												
503.S82. 5	292	415	W	6	AMP								
503.QZ	9	PLAG10	BIOT	1	CHEQ	1	ACT	70	EP	16	SPH	4	
503.SULF	1	HORN	9										
504.S82. 6A	291	418	W	6	AMP								
504.QZ	9	PLAG23	BIOT	1	CHEQ	2	ACT	61	EP	6	SPH	2	
504.AP	1	ILM	5	HORN	9	SULF	5	ALL	1				
505.S82. 6B	291	418	W	6	AMP								
505.QZ	9	PLAG35	CHEQ	2	ACT	53	ALL	3	SPH	4	ILM	3	
505.HORN	9												
506.S82. 7A	290	423	W	6	AMP								
506.QZ	9	PLAG35	CHEQ	5	ACT	43	EP	5	SPH	5	CARB	5	
506.ILM	2	HORN	9										
507.S82. 7B	290	423	W	6	AMP								
507.QZ	9	PLAG10	CHEQ	1	ACT	70	EP	15	SPH	5	HORN	9	
508.S82. 8A	289	427	W	6	AMP								
508.QZ	9	MRAD	1	PLAG10	ACT	84	EP	4	SPH	4	HORN	9	
509.S82. 8B	289	427	W	6	AMP								
509.QZ	9	PLAG35	CHEQ	1	ACT	52	EP	4	SPH	2	ILM	7	
509.HORN	9	SULF	1	ALL	1								
510.S82. 9A	289	420	W	6	AMP								
510.QZ	9	PLAG 5	CHEQ	3	ACT	46	EP	40	SPH	4	CARB	1	
510.SULF	2	HORN	9										
511.S82. 9B	289	420	W	6	AMP								
511.QZ	9	PLAG15	CHEQ	5	ACT	59	EP	15	SPH	4	CARB	1	
511.SULF	2	HORN	9										
512.S83. 1A	306	476	W	8	IF								
512.QZ	50	CUMM25	CARB	9	CC	24	OP	1					
513.S83. 1B	306	476	W	8	CST								
513.QZ	10	CHMG45	TREM45		RUTI	1	SULF	2					
514.S83. 2	311	476	W	8	SS								
514.QZ	58	PLAG 1	CC	40	SID	1	MT	1	PO	1			
515.S83. 6A	298	466	W	8	AMP								
515.QZ	9	PLAG20	ACT	76	ALL	1	SPH	1	ILM	3	HORN	9	
516.S83. 6B	298	466	W	8	AMP								
516.QZ	9	PLAG25	CHEQ	1	ACT	72	ALL	1	SPH	1	SULF	1	

Table 19. Cont'd...

```
516.ILM  2  HORN  9
517.S83. 7A    292 458 W 8  AMP
517.QZ    9 PLAG30  BIOT 1  CHEQ 3  ACT 54  ALL  2  SPH  3
517.CC    7 ILM  4  HORN  9
518.S83. 7B    292 458 W 8  AMP
518.QZ    9 PLAG25  BIOT  1 CHEQ 8  HORN54  ALL  3  SPH  1
518.CARB 6  ILM  3
519.S83. 8A    293 456 W 7  UM
519.TALC43  CHEQ35  TREM 4  SPH   1 CARB  9 CC  15  SPH  1
519.OP   3
520.S83. 8B    293 456 W 7  AMP
520.QZ    9 PLAG15  BIOT 3  CHMG 2  ACT 57  EP  20  SPH  3
520.HORN  9
521.S83. 8C    293 456 W 7  AMP
521.QZ    9 PLAG15  ACT 70  EP  10  SPH  4  CARB 1  SULF  1
521.HORN  9   MRAD  1
522.S83.10     288 455 W 7  MBT
522.QZ    1 PLAG10  CHEQ  1 ACT 81  EP   5  SPH  4  SULF  1
522.HORN  9   MRAD  1
523.T 3. 5     252 456 W 7  MBX
523.QZ    9 PLAG10  BIOT 3  ACT 68  EP  15  SPH  4  HORN  9
524.T 3. 8     251 464 W 7  MBT
524.PLAG 5  CHMG 3  ACT 72  EP  15  SULF  1 INCO 5  HORN  9
524.MRAD  1
525.T 3.15     248 460 W 7  MBT
525.PLAG 8  CHMG 3  ACT 71  EP  15  SPH  3  SULF  1 HORN  9
526.T 5. 5     238 462 W 7  MBT
526.PLAG25  CHMG15  ACT 55  EP   3  SPH  2  SULF  1
527.T 5. 6     238 462 W 7  MBT
527.PLAG15  CHEQ 2  ACT 61  EP  15  SPH  4  CARB 3  SULF  1
527.HORN  9
528.S16. 1B    221 492 W 2B RGL
528.QZ  50  BIOT20  MUSC25  GRNA 5  ZIRC  1 SPH   1 MRAD  1
528.OP    1
529.S73. 3A     90 530 W 8  CIP
529.QZ  45  PLAG  9 BIOT 4  HORN 5  CC  45  DOL   9 TURM 1
529.RUTI  1 SPH   1 OP    1
530.C23. 4     178 495 W 8  MBX
530.QZ    1 PLAG  1 ACT 75  HORN  9 BIOT  1 EP  10  ZOIS10
530.SPH  5  PO    1 MT    1 RUTI  1 MRAD  1
531.C23. 7A    179 489 W 8  AMP
531.QZ  15  PLAG  9 HORN74  SPH   1 AP    1 ILM  5  MRAD  1
531.CPY   1
532.C23. 8C    178 476 W 7  MBX
532.QZ  20  PLAG  9 ACT 72  HORN  9 EP   5  SPH  3  MRAD  1
532.AP    1
533.C23. 9     177 474 W 7  MBT.
533.PLAG 3  ACT 80  HORN  9 EP   5  SPH 10  CHLR  1 CPY   5
533.PY    1
534.C26.10     279 465 W 8  MBT
```

Table 19. Cont'd...

```
534.QZ   6  PLAG  9 ACT 81  HORN  9 EP   4  CHLR  5 SPH  4
534.ILM  3  PO    5 CPY   5
535.R 6. 4    105 524 W 8  AMP
535.QZ  20  PLAG10  HORN51  ACT   1 CHLR 5  ALL   1 INCO 5
535.CC   5  AP    1 ILM  4
536.R 6. 9A   101 512 W 8  MBG
536.QZ  20  PLAG  9 ACT 67  HORN  9 EP  10  SPH  2  OP   1
537.R 6.12     97 508 W 7  MBG
537.QZ   8 PLAG 2  ACT 57  HORN  9 EP  30  SPH  2  PY   5
537.CPY  1 CHMG 7
538.R 8. 2    113 487 W 7  MBT
538.PLAG  1 ACT 80  HORN  9 EP   3  ZOIS  9 CHLR  9 SPH 10
538.CC   7  CARB  9
539.R 8. 8    107 459 W 6  MBT
539.PLAG10  ACT 51  HORN  9 EP  30  CHLR 5  SPH  3  PO   1
539.CPY  1
540.R 9. 7B    60 526 W 7  MBG
540.QZ   8 PLAG15  ACT 53  HORN  9 CHLR 3  EP  25  SPH  3
540.PO   5 CPY   5
541.R10.13    170 480 W 7  MBX
541.QZ   1  PLAG  1 ACT 87  HORN  9 CHMG 5  EP   3  SPH  4
541.PO   1
542.S74. 1A   151 485 W 7  MBT
542.QZ  20  PLAG  9 ACT 66  HORN  9 EP   7  SPH  7  PY   1
542.CPY  1 MRAD  1
543.S74. 3A    81 493 W 7  MBT
543.QZ   8 PLAG  1 ACT 68  HORN  9 CHLR15  EP   6  SPH 10
543.PO   5 CPY   5
544.S81. 4B   271 467 W 8  AMP
544.QZ  25  PLAG  9 ACT 67  HORN  9 CHMG  1 EP   3  SPH  1
544.ILM  4  RUTI  8
545.S81. 5B   273 473 W 8  AMP
545.QZ  25  PLAG  9 ACT 70  HORN  9 CHMG  5 SPH  1  ALL  5
545.ILM  3  CPY   5
546.S81. 6    279 479 W 8  AMP
546.QZ  25  PLAG  9 HORN68  ACT   9 ALL   5 AP   5 SPH  1
546.RUTI  8 ILM  5
547.S82. 2A   297 406 W 6  AMP
547.QZ  15  PLAG  9 ACT 74  HORN  9 CHEQ 1  EP   3  SPH  2
547.ALL  1  ILM  5
548.S83. 3    310 473 W 8  MBT
548.PLAG 1  ACT 91  HORN  9 EP   7  RUTI 1  MRAD  1
549.C29. 4    242 462 W 7  MBX
549.QZ   9 PLAG40  ACT 47  HORN  9 CHLR 5  EP   1 SPH  2
549.OP   5
550 D 6. 7    687 288 E 4  SCT
550.QZ  64  MUSC 1  BIOT15  GRNA15  ILM  1  CHLR 3  EP   1
550.ALL  9
551.D12.22    737 473 E 4  SCT
551.QZ  40  PLAG30  MUSC  1 BIOT20  GRNA 5  KY   5  ZIRC  5
```

Table 19. Cont'd...

```
551.HEM   1 PO    1
552.R 9. 6     60 527 W 7  SCT
552.QZ  69  MUSC20  TURM  1 GRNA 1  ILM 10
553.C 6. 7B    660 286 E 4  SCT
553.QZ  80  PLAG  9   BIOT10  GRNA10  ILM   1 ZIRC  1
554.C17. 9  385 452 E 9  AMP
554.QZ    9 PLAG15  HORN79  ILM  5  ALL  1
555.C17.10    388 452 E 9  AMP
555.QZ    9 PLAG25  HORN67  ILM  7  ALL  1  SPH   1
556.C17.11A   390 451 E 9  TFI
556.QZ    9 PLAG70  BIOT15  ILM  5  PO  10  ZIRC  1
557.C17.11B   391 450 E 9  AMP
557.QZ    9 PLAG50  HORN44  BIOT 1  ILM  5  ALL   1 AP    1
558.C17.12    392 449 E 9  AMP
558.QZ    9   PLAG25  HORN70  ILM  5  ALL   1 AP    1
559.C17.15A   402 435 E 9  AMP
559.QZ    9 PLAG10  HORN85  ILM  5  ALL   1
560.C17.15B   411 433 E 9  AMP
560.QZ    9 PLAG10  HORN84  ILM  5  CC   1  ALL   1 AP    1
561.C17.15C   418 440 E 9  AMP
561.QZ    9 PLAG15  HORN84  SPH  1  AP   1  ALL   1
562.D 5.14    728 473 E 1A GNS
562.QZ  45  PLAG10  BIOT20  HORN15  GRNA10  ALL   1 ILM   1
564.H 1. 8C   318 074 W 3  SCT
564.QZ  42  PLAG  8 CHFE20  BIOT 4  GRNA 4  MUSC20  ILM 10
565.H 1.14A   292 072 W 3  SCT
565.QZ  90  PLAG  8 CHFE 5  BIOT 1  GRNA 3  MT   1
567.H11. 9A   291 326 W 5  SCT
567.QZ  58  PLAG  9 MUSC10  BIOT 1  CHLR20  EP   5  GRNA 1
567.ILM  3  TURM 2
568.L 3.10D   244 377 W 6  SCT
568.QZ  65  PLAG  9 BIOT15  MUSC10  CHEQ 1  GRNA 3  EP   5
568.MT   1  ILM   1
569.P 1. 3    233 373 W 6  SCT
569.QZ  73  PLAG  9 BIOT 4  EP  15  GRNA 3  CHMG 4  SPH  1
569.TURM 1
570.S 4.12    254 116 W 4  SCT
570.QZ  5   BIOT45  GRNA50  ILM   1
571.S 5. 4A   252 234 W 6  SCT
571.QZ  47  PLAG  9 MUSC20  CHEQ10  BIOT 5  EP   5  GRNA 3
571.OP  10
572.S50.13B   610 469 E 4  GNS
572.QZ  40  PLAG20  BIOT10  GRNA30  ZIRC  1
573.S51.22A   659 464 E 9  GNS
573.QZ   1  HORN10  BIOT45  GRNA20  SPIN20  ILM  3  ALL   8
573.ZIRC 1
```

2. NOTES to the TABLE of WHOLE-ROCK ANALYSES

All whole-rock analyses were done by energy dispersive electron microprobe analysis on glasses made in the image furnace. All glasses were produced by direct melting except for number 43 and 45 which were made with flux as can be seen from the low analytical total. The analyses were recalculated to oxide percentages using the programme CONVOX.

Table 20. Analyses of igneous rocks

Number	1	2	3	4	5	6
Sample	095	192	199	205	207	208
SiO_2	48.69	50.57	51.40	54.59	51.48	48.88
TiO_2	2.09	3.76	1.70	1.77	1.43	1.86
Al_2O_3	14.57	13.81	13.67	12.16	14.48	13.34
V_2O_3	/	/	/	/	/	/
Cr_2O_3	/	/	/	/	/	/
FeO	17.72	20.16	16.13	14.50	12.12	16.63
MnO	0.19	0.18	0.14	0.16	0.10	0.18
CoO	/	/	/	/	/	/
NiO	/	0.06	/	/	/	/
ZnO	/	/	/	/	/	/
BaO	/	/	/	/	/	/
MgO	6.01	4.93	6.92	7.20	5.97	5.77
CaO	10.59	4.67	9.66	7.87	11.40	10.66
Na_2O	/	1.44	0.15	1.37	2.89	2.45
K_2O	0.14	0.14	0.24	0.39	0.14	0.23
P_2O_5	/	0.29	/	/	/	/
Total 1	100.00	100.00	100.00	100.00	100.00	100.00
Total 2	97.45	98.66	97.73	97.86	98.08	98.19

Number	7	8	9	10	11	12
Sample	209	222	223[1]	264	265	266
SiO_2	50.08	43.58	50.12	48.75	50.50	49.87
TiO_2	0.96	2.85	2.53	0.68	0.61	1.13
Al_2O_3	15.53	19.38	15.84	17.06	16.60	15.29
V_2O_3	/	/	/	/	/	/
Cr_2O_3	0.06	/	/	/	/	/
FeO	10.87	17.88	16.53	8.64	8.39	11.51
MnO	0.09	0.32	0.12	/	0.05	0.10
CoO	/	/	/	/	/	/
NiO	0.07	0.06	/	/	/	/
ZnO	/	/	0.05	/	/	/
BaO	/	/	0.11	/	/	/
MgO	7.20	4.10	3.12	9.12	8.57	7.95
CaO	13.09	11.68	9.55	12.62	13.68	11.87
Na_2O	1.98	/	/	1.71	1.55	2.09
K_2O	0.08	/	2.00	1.43	0.17	0.19
P_2O_5	/	0.15	/	/	/	/
Total 1	100.00	100.00	100.00	100.00	100.00	100.00
Total 2	98.00	98.11	97.84	99.30	99.27	99.27

Note: FeO is total iron; / signifies 'not detected'; total 2 is the analytical total, total 1 the recalculated total.
[1] contains 0.06 ZrO_2.

Table 20. Cont'd...

Number	13	14	15	16	17	18
Sample	267	268	269	261	093	191
SiO_2	59.93	31.62	40.00	54.01	46.23	52.79
TiO_2	0.69	4.13	2.90	2.22	2.70	1.66
Al_2O_3	9.44	22.08	15.23	13.60	15.31	13.57
V_2O_3	/	/	/	/	0.07	0.07
Cr_2O_3	0.47	/	/	/	/	/
FeO	9.06	28.40	24.12	17.98	16.92	11.55
MnO	0.13	0.27	0.21	0.24	0.18	0.10
CoO	/	/	0.04	/	0.04	/
NiO	/	0.07	0.05	/	/	0.04
ZnO	/	0.17	/	/	/	/
BaO	/	/	/	/	/	/
MgO	15.1	9.45	4.24	1.84	5.55	7.46
CaO	13.46	2.56	11.77	6.68	10.14	8.46
Na_2O	0.64	0.59	0.75	3.04	2.57	2.50
K_2O	0.06	0.51	0.46	0.39	0.31	1.82
P_2O_5	/	0.17	0.23	/	/	/
Total 1	100.00	100.00	100.00	100.00	100.00	100.00
Total 2	99.08	101.78	98.68	98.28	97.54	99.15

Number	19	20	21	22	23	24
Sample	195	196	197	200	201	204
SiO_2	49.47	49.32	47.93	49.10	49.89	50.62
TiO_2	1.70	2.55	1.92	1.65	3.36	1.76
Al_2O_3	15.56	13.64	14.07	14.63	12.37	13.42
V_2O_3	/	/	0.10	/	0.08	/
Cr_2O_3	/	/	/	/	/	/
FeO	14.38	14.90	13.88	14.35	17.68	14.01
MnO	0.11	0.15	0.14	0.12	0.20	0.15
CoO	0.07	/	/	/	/	/
NiO	/	0.05	/	/	/	/
ZnO	0.04	/	/	0.07	/	/
BaO	/	/	/	/	/	/
MgO	8.13	5.95	4.34	7.08	4.91	6.89
CaO	7.80	10.31	15.90	10.16	8.80	9.79
Na_2O	2.55	2.42	1.46	2.65	2.42	3.11
K_2O	0.19	0.74	0.25	0.20	0.29	0.25
P_2O_5	/	/	/	/	/	/
Total 1	100.00	100.00	100.00	100.00	100.00	100.00
Total 2	99.53	97.98	97.54	97.75	98.00	98.07

Table 20. Cont'd...

Number	25	26	27	28	29	30
Sample	206	211	432	433	446	058
SiO_2	48.88	52.20	51.22	51.36	53.68	68.19
TiO_2	1.27	1.47	1.89	1.72	1.79	0.52
Al_2O_3	15.72	14.08	14.04	14.34	18.56	17.27
V_2O_3	/	/	0.08	0.09	/	/
Cr_2O_3	/	/	0.07	0.15	/	/
FeO	12.48	12.92	7.53	4.64	9.02	2.98
MnO	0.08	0.08	0.06	0.09	/	/
CoO	/	/	/	/	/	/
NiO	/	/	0.04	/	/	/
ZnO	/	/	/	/	/	/
BaO	/	/	/	/	/	0.06
MgO	8.60	7.49	7.41	6.60	3.48	1.26
CaO	10.75	7.89	15.23	19.01	6.70	0.60
Na_2O	2.03	3.35	2.19	1.93	4.21	7.89
K_2O	0.19	0.14	0.24	0.08	1.82	1.24
P_2O_5	/	/	/	/	0.44	/
Total 1	100.00	100.00	100.00	100.00	100.00	100.00
Total 2	98.47	98.39	98.38	99.62	98.53	101.24

Number	31	32	33	34	35	36
Sample	182	184	412	472	067	324
SiO_2	67.73	47.99	53.80	54.63	51.23	51.10
TiO_2	0.73	0.77	0.29	1.93	0.79	0.72
Al_2O_3	16.75	20.96	10.55	20.84	12.51	11.36
V_2O_3	/	0.07	/	0.06	/	/
Cr_2O_3	/	0.08	/	/	0.18	0.18
FeO	4.59	7.95	11.36	6.30	11.44	11.49
MnO	/	0.08	0.06	/	0.11	0.14
CoO	/	/	/	/	/	/
NiO	/	/	/	/	0.08	/
ZnO	/	/	/	/	/	/
BaO	/	/	/	0.09	/	/
MgO	1.80	6.44	8.40	4.11	11.05	12.93
CaO	0.85	12.99	11.48	4.84	11.00	10.50
Na_2O	7.23	2.49	3.23	4.82	1.50	1.35
K_2O	0.32	0.17	3.85	2.40	0.11	0.24
P_2O_5	/	/	/	/	/	/
Total 1	100.00	100.00	100.00	100.00	100.00	100.00
Total 2	100.73	99.52	98.35	99.40	98.78	98.96

Table 20. Cont'd...

Number	37	38	39	40	41	42
Sample	325	334	490	527	297	298
SiO_2	50.64	48.95	50.86	52.56	45.61	43.88
TiO_2	0.77	0.82	1.02	0.83	0.21	0.12
Al_2O_3	11.55	13.54	14.90	13.50	5.19	5.50
V_2O_3	/	/	/	/	/	/
Cr_2O_3	0.21	0.12	0.05	0.06	0.46	0.41
FeO	11.79	12.51	11.88	11.53	13.95	15.18
MnO	0.11	0.08	0.12	0.05	0.16	0.16
CoO	/	0.05	/	/	/	/
NiO	0.08	/	/	/	0.14	0.22
ZnO	/	/	0.06	/	/	/
BaO	/	/	/	/	/	/
MgO	14.11	11.79	8.42	12.09	26.99	28.00
CaO	9.10	9.21	10.50	7.80	7.30	6.54
Na_2O	1.51	0.19	2.05	1.46	/	/
K_2O	0.14	2.75	0.15	0.13	/	/
P_2O_5	/	/	/	/	/	/
Total 1	100.00	100.00	100.00	100.00	100.00	100.00
Total 2	99.42	98.96	99.40	98.06	99.86	100.45

Number	43	44	45	46	47	48
Sample	299	300	301	273	326	328
SiO_2	41.68	43.49	41.91	48.52	48.58	46.84
TiO_2	/	0.19	/	0.17	0.55	0.37
Al_2O_3	2.49	3.97	2.72	4.78	8.40	6.79
V_2O_3	/	/	/	/	/	/
Cr_2O_3	0.82	0.44	0.76	0.18	0.36	0.48
FeO	15.26	14.73	14.29	12.52	11.51	12.71
MnO	0.17	0.15	/	0.05	0.10	0.09
CoO	/	/	/	/	/	/
NiO	0.17	0.16	0.27	0.16	0.09	0.19
ZnO	/	/	/	/	0.11	/
BaO	/	/	/	/	/	/
MgO	36.77	31.77	37.24	30.92	20.72	26.70
CaO	2.64	5.05	2.81	2.70	9.60	5.83
Na_2O	/	/	/	/	/	/
K_2O	/	/	/	/	/	/
P_2O_5	/	/	/	/	/	/
Total 1	100.00	100.00	100.00	100.00	100.00	100.00
Total 2	27.76	99.61	26.04	99.18	98.74	99.88

Table 20. Cont'd...

Number	49	50	51	52	53	54
Sample	329	330	331	491	492	493
SiO_2	46.78	46.95	51.94	48.00	51.73	47.23
TiO_2	0.46	0.49	0.89	0.54	0.85	0.48
Al_2O_3	7.19	8.07	13.13	9.17	14.62	8.40
V_2O_3	/	/	/	/	/	/
Cr_2O_3	0.40	0.44	0.07	0.39	/	0.41
FeO	12.19	12.20	10.86	11.81	10.24	11.59
MnO	0.08	0.15	0.06	0.07	0.08	0.11
CoO	/	/	/	/	/	/
NiO	0.17	0.20	0.05	0.14	/	0.15
ZnO	0.08	0.07	/	/	/	/
BaO	/	/	/	/	/	/
MgO	25.74	23.66	8.72	21.07	8.13	23.11
CaO	6.92	7.77	10.60	8.82	11.80	8.52
Na_2O	/	/	3.43	/	2.43	/
K_2O	/	/	0.26	/	0.14	/
P_2O_5	/	/	/	/	/	/
Total 1	100.00	100.00	100.00	100.00	100.00	100.00
Total 2	100.37	99.74	98.32	99.77	98.08	98.25

Number	55	56	57	58	59	60
Sample	302	303	304	305	306	307
SiO_2	51.12	49.44	49.88	50.03	50.77	49.90
TiO_2	0.36	0.26	0.31	0.43	0.43	0.47
Al_2O_3	5.73	17.53	20.96	16.72	15.54	15.44
V_2O_3	0.08	0.07	0.08	0.06	0.07	/
Cr_2O_3	0.52	0.17	0.08	/	0.08	/
FeO	7.62	5.21	4.38	6.46	6.86	10.46
MnO	0.09	0.07	0.06	/	0.06	0.13
CoO	/	/	/	/	/	/
NiO	0.09	0.05	/	/	/	/
ZnO	/	/	/	/	/	/
BaO	/	/	/	/	/	/
MgO	18.12	10.22	6.53	9.43	10.88	8.44
CaO	16.29	16.04	15.72	16.04	14.60	14.01
Na_2O	/	0.85	1.83	0.70	1.08	1.05
K_2O	/	0.10	0.20	0.14	0.14	0.11
P_2O_5	/	/	/	/	/	/
Total 1	100.00	100.00	100.00	100.00	100.00	100.00
Total 2	98.55	99.50	100.02	98.99	99.59	99.10

Table 20. Cont'd...

Number	61	62	63	64	65	66
Sample	309	311	312	313	314	487
SiO_2	50.86	49.85	51.03	50.71	52.48	52.18
TiO_2	0.64	1.46	0.95	0.99	0.96	1.00
Al_2O_3	15.64	17.05	14.69	14.45	16.90	14.60
V_2O_3	0.07	0.07	/	/	/	/
Cr_2O_3	/	/	/	0.06	0.11	/
FeO	8.75	11.44	10.49	11.54	8.52	12.29
MnO	0.08	0.07	/	0.13	/	0.19
CoO	/	/	/	/	/	/
NiO	/	0.05	0.04	0.05	0.08	/
ZnO	/	/	/	/	/	0.05
BaO	/	/	/	/	/	/
MgO	8.19	6.78	7.72	8.73	10.74	7.08
CaO	14.36	11.12	13.10	10.81	6.26	9.11
Na_2O	1.34	1.99	1.78	1.59	3.82	2.90
K_2O	0.06	0.13	0.29	0.96	0.13	0.60
P_2O_5	/	/	/	/	/	/
Total 1	100.00	100.00	100.00	100.00	100.00	100.00
Total 2	99.73	98.02	99.15	99.63	100.02	99.39

3. NOTES to TABLES of MINERAL ANALYSES

All minerals analysed are by energy dispersive electron microprobeanalysis and they are recalculated to oxide percentages and structural formulae using the programme FORMU. The output of this programme was used directly to produce the tables; consequently all numbers are to three decimal places. This does not represent the precision of the analyses. In a general way, the quality of the analyses was verified by comparing calculated structural formulae with the theoretical one.

In the oxide percentages, all the iron is given as FeO, except for epidote where it is given as Fe_2O_3; the first total is 100% for anhydrous minerals or a theoretical anhydrous total for hydrous minerals; the second total is the analytical total calculated by stoichiometry from element percentages.

The plagioclases were recalculated on the basis of 32 oxygens for:

$Z = (12-x)Si + xAl^{(4)}$

$Y = Al^{(6)} + Fe^{3+} + Ti + V + Cr$

$X = Na + Ca + Fe^{2+} + Ni + Zn + K$

Iron was included as Fe^{2+} in X up to X=4, the remainder, if any, as Fe^{3+} in Y.

The quality of the analyses was checked as such:

$Al^{(4)} = Ca\ (+ Fe^{2+} + Ni + Zn)$

Sum of Y = 4

Sum of X = 4

An is the percentage of anorthite, Ca/Sum of X.

The <u>biotites</u> were recalculated on the basis of 22 bivalent anions:

$Z = (8-x)Si + xAl^{(4)}$

$Y = Al^{(6)} + Ti + V + Cr + Fe$ (all as Fe^{2+}) $+ Mn + Co + Ni + Cu + Zn + Mg$

$X = K + Ca + Ba + Na$

The charge balance was calculated as:

$K + Na + 2Ca + 2Ba + Al^{(6)} + Ti + V + Cr - (6 - \text{sum of } Y) - Al^{(4)}$

It is a measure of the amount of Fe^{3+} present and/or the analytical error.

The <u>chlorites</u> were recalculated on the basis of 28 bivalent anions:

$Z = (8-x)Si + xAl^{(4)}$

$Y = Al^{(6)} + Ti + Cr$

$X = Fe^{2+} + Mg$ ($+ Mn + Co + Ni + Zn + Ca + Na$)

The charge balance was calculated as:

$Y - Al^{(4)} - (12 - \text{sum of } X+Y)$

It is a measure of the amount of Fe^{3+} present in Y and/or

the analytical error.

The amphiboles were recalculated on the basis of 23 bivalent anions:

$$Z = (8 - x)Si + xAl^{(4)}$$

$$Y = Al^{(6)} + Ti + V + Cr + Fe^{2+} + Mn + Ni + Zn + Mg \equiv 5$$

$$X+A = Ba + Ca + Na + K \equiv 2\text{-}3$$

No attempt has been made to estimate Fe^{3+}.

The epidotes were recalculated on the basis of 25 bivalent anions:

$$Z = (10-x)Si + xAl^{(4)} \quad (x \geq 4)$$

$$Y = Al^{(6)} + Ti + Fe^{3+} + V + Cr \equiv 2$$

$$X = Ca + Fe^{2} + (+ Mn + Co + Zn + Ba + Na) \equiv 4$$

All iron was included in Y as Fe^{3+}; where Y was larger than 2, part of the iron was added to X as Fe^{2+} up to X = 4.

Ps is the percentage of $Ca_2Al_2FeSi_3O_{12}(OH)$, Fe^{3+}/Sum of Y.

The garnets were recalculated on the basis of 24 oxygens:

$$Z = (6-x)Si + xAl^{(4)}$$

$$Y = Al^{(6)} + Ti + Fe^{3+} + V + Cr \equiv 4$$

$$X = Fe^{2+} + Mn + Mg + Ca (+ Ni + Zn + Ba + Co + Cu) \equiv 6$$

All iron was included in X as Fe^{2+}; where X was larger than 6, part of the iron was added to Y as Fe^{2+} up to Y = 4.

The ilmenites were recalculated on the basis of 6 oxygens. Ti being very near to 2 in all analysis, all Fe was

taken as Fe^{2+}. Silicon was excluded from the structural formula calculation. A small amount of SiO_2 is present in almost all analyses; some Si may be present in the lattice, but the SiO_2 present in the analyses could also be due to X-rays from the corona[1]

The carbonates were recalculated on the basis of 6 bivalent anions (CO_3^{2-}). CO_2 is calculated by stoichiometry. Here again some SiO_2 is present in most analyses, and was excluded from the structural formulae. In some cases (448), it is clearly due to contamination of the excited volume. Because of the small beam diameter that had to be used in most cases, the carbonates destabilized during the analysis; consequently the analytical total is meaningless (C not analysed) and total 2 is not given.

Table 30 contains miscellaneous minerals, The number of bivalent anions forming the basis of the structural formula calculation is shown at the bottom of each structural formula. $Al^{(4)}$ was calculated by difference as usual with the remaining Al as AL6. In the spinels, the iron was divided into Fe^{3+} and Fe^{2+} so as to complete the site A preferentially, assuming vacancies in the site B. For the prehnites, the iron was divided into Fe^{3+} and Fe^{2+} so as to balance out X and Y.

---

[1] The zone of diffuse electron flux surrounding the electron beam, at least 900 micron in diameter, from which X-rays are detected in energy dispersive, but not in wavelength dispersive analysis because of the focussing of the crystals

TABLE 21. PLAGIOCLASES.

MINERAL NO	012. PLAG	023. PLAG	043. PLAG	051. PLAG	181. PLAG	181. PLAG	181. PLAG	308. AB	376. PLAG	380. PLAG
STRUCTURAL FORMULAE										
SI 4+	9.784	11.070	10.573	11.657	11.355	11.036	11.036	11.857	10.541	11.114
AL IV	2.216	0.930	1.437	0.343	0.645	0.964	0.964	0.143	1.459	0.396
SUM OF Z	12.000	12.000	12.000	12.000	12.000	12.000	12.000	12.000	12.000	12.000
AL VI	4.008	4.020	4.040	3.983	4.010	4.001	4.001	4.010	4.014	3.995
TI 4+	0.016	0.0	0.0	0.0	0.0	0.0	0.0	0.0	0.0	0.0
FE 3+	0.0	0.007	0.0	0.059	0.0	0.022	0.022	0.0	0.0	0.022
CR 3+	0.012	0.0	0.0	0.0	0.007	0.0	0.0	0.0	0.008	0.007
SUM OF Y	4.036	4.027	4.025	4.042	4.017	4.023	4.023	4.010	4.022	4.024
FE 2+	0.018	0.013	0.021	0.005	0.011	0.0	0.0	0.042	0.015	0.0
NI	0.0	0.0	0.0	0.0	0.0	0.0	0.0	0.0	0.006	0.0
ZN	0.007	0.0	0.0	0.0	0.015	0.006	0.006	0.0	0.0	0.0
CA	2.130	0.842	1.377	0.271	0.620	0.905	0.906	0.127	1.393	0.822
NA	1.764	3.114	2.504	3.661	3.282	3.068	3.070	3.740	2.550	3.169
K	0.017	0.031	0.021	0.063	0.018	0.026	0.026	0.035	0.018	0.021
SUM OF X	3.936	4.000	3.923	4.000	3.946	4.005	4.008	3.944	3.982	4.012
NO OF ANIONS	32	32	32	32	32	32	32	32	32	32
AN	55	21	35	7	16	23	23	3	35	21
WEIGHT PERCENT OXIDES										
SIO2	54.227	62.508	59.316	66.215	64.394	62.245	62.238	67.728	59.059	62.757
TIO2	0.114	0.0	0.0	0.0	0.0	0.0	0.0	0.0	0.0	0.0
AL2O3	29.268	23.713	25.997	20.846	22.397	23.756	23.758	20.128	26.015	23.385
CR2O3	0.086	0.0	0.0	0.0	0.053	0.0	0.0	0.0	0.054	0.050
FEO	0.122	0.133	0.141	0.431	0.075	0.145	0.146	0.287	0.098	0.152
NIO	0.0	0.0	0.0	0.0	0.0	0.0	0.0	0.0	0.040	0.0
ZNO	0.050	0.0	0.0	0.0	0.115	0.044	0.044	0.0	0.0	0.0
CAO	11.016	4.440	7.208	1.438	3.283	4.766	4.767	0.679	7.283	4.334
NA2O	5.045	9.070	7.246	10.728	9.601	8.927	8.932	11.020	7.371	9.231
K2O	0.072	0.137	0.092	0.290	0.082	0.116	0.115	0.157	0.080	0.092
CL	0.0	0.0	0.0	0.062[1]	0.0	0.0	0.0	0.0	0.0	0.0
TOTAL 1	100.000	100.000	100.000	100.000	100.000	100.000	100.000	100.000	100.000	100.000
TOTAL 2	102.182	101.243	101.116	100.782	101.413	101.759	101.598	102.004	101.059	102.582

[1] DISREGARDED IN STRUCTURAL FORMULA CALCULATION

TABLE 21. CONT'D...

MINERAL NO	496. AB	498. AB	499. PLAG	503. PLAG	504. PLAG	509. PLAG	509. AB	516. PLAG	517. PLAG	522. PLAG
STRUCTURAL FORMULAE										
SI 4+	11.959	11.964	11.243	11.077	11.872	11.872	12.030	11.203	11.156	11.114
AL IV	0.041	0.036	0.757	0.923	0.128	0.128	0.0	0.797	0.844	0.886
SUM OF Z	12.000	12.000	12.000	12.000	12.000	12.000	12.030	12.000	12.000	12.000
AL VI	4.004	4.017	3.982	4.016	3.980	4.010	3.985	4.002	4.037	4.001
FE 3+	0.0	0.0	0.011	0.0	0.020	0.0	0.015	0.0	0.0	0.0
CR 3+	0.0	0.0	0.007	0.0	0.0	0.0	0.0	0.0	0.0	0.0
SUM OF Y	4.004	4.017	4.000	4.016	4.000	4.010	4.000	4.002	4.037	4.001
FE 2+	0.044	0.027	0.055	0.023	0.031	0.018	0.013	0.028	0.017	0.038
CO	0.0	0.0	0.0	0.0	0.0	0.007	0.0	0.0	0.0	0.0
ZN	0.0	0.012	0.005	0.008	0.020	0.015	0.0	0.008	0.009	0.011
CA	0.058	0.039	0.723	0.920	0.125	0.103	0.063	0.813	0.827	0.908
NA	3.789	3.796	3.173	2.932	3.759	3.773	3.715	3.058	2.984	2.932
K	0.035	0.034	0.028	0.038	0.038	0.036	0.031	0.036	0.039	0.036
SUM OF X	3.926	3.908	3.984	3.921	3.973	3.952	3.822	3.943	3.876	3.925
NO OF ANIONS	32	32	32	32	32	32	32	32	32	32
AN	2	1	18	24	3	3	2	21	22	23
WEIGHT PERCENT OXIDES										
SIO2	68.416	68.475	63.546	62.559	67.722	67.824	68.964	63.355	63.127	62.760
AL2O3	19.635	19.683	22.726	23.666	19.879	20.057	19.381	23.023	23.433	23.414
CR2O3	0.0	0.0	0.052	0.0	0.0	0.0	0.0	0.0	0.0	0.0
FEO	0.300	0.183	0.449	0.155	0.346	0.123	0.193	0.188	0.115	0.258
COO	0.0	0.0	0.0	0.0	0.0	0.049	0.0	0.0	0.0	0.0
ZNO	0.0	0.091	0.038	0.059	0.154	0.115	0.0	0.062	0.072	0.085
CAO	0.310	0.210	3.816	4.852	0.665	0.551	0.336	4.291	4.368	4.783
NA2O	11.181	11.208	9.250	8.541	11.062	11.120	10.987	8.921	8.711	8.541
K2O	0.159	0.151	0.123	0.168	0.172	0.161	0.140	0.160	0.174	0.159
TOTAL 1	100.000	100.000	100.000	100.000	100.000	100.000	100.000	100.000	100.000	100.000
TOTAL 2	101.697	101.413	101.979	101.099	101.583	100.494	100.812	100.706	100.507	100.849

TABLE 21. CONT'D...

MINERAL NO	531. PLAG	532. PLAG	534. PLAG	536. PLAG	537. PLAG	541. PLAG	544. PLAG	545. PLAG	546. PLAG	547. PLAG
STRUCTURAL FORMULAE										
SI 4+	11.006	10.974	10.998	11.035	11.025	11.033	11.019	11.062	10.971	11.923
AL IV	0.994	1.026	1.002	0.965	0.975	0.967	0.981	0.938	1.029	0.077
SUM OF Z	12.000	12.000	12.000	12.000	12.000	12.000	12.000	12.000	12.000	12.000
AL VI	4.008	3.996	4.012	3.998	3.985	3.998	4.012	4.011	4.021	4.024
FE 3+	0.022	0.0	0.0	0.0	0.062	0.002	0.0	0.0	0.0	0.0
CR 3+	0.0	0.007	0.0	0.008	0.0	0.0	0.007	0.007	0.009	0.0
SUM OF Y	4.030	4.003	4.012	4.006	4.047	4.000	4.019	4.018	4.030	4.024
FE 2+	0.010	0.036	0.048	0.032	0.003	0.053	0.022	0.029	0.028	0.052
MN	0.0	0.0	0.0	0.0	0.0	0.010	0.0	0.0	0.0	0.0
NI	0.0	0.0	0.009	0.0	0.0	0.0	0.006	0.0	0.0	0.0
ZN	0.0	0.0	0.0	0.0	0.0	0.0	0.006	0.011	0.011	0.005
BA	0.0	0.003	0.0	0.0	0.0	0.0	0.0	0.003	0.0	0.0
CA	0.915	0.995	0.922	0.912	0.893	0.900	0.951	0.898	1.006	0.046
NA	3.049	2.912	2.983	3.016	3.069	3.003	2.928	2.965	2.820	3.759
K	0.026	0.037	0.023	0.041	0.035	0.038	0.027	0.036	0.030	0.038
SUM OF X	4.000	3.983	3.985	4.001	3.997	3.949	3.940	3.940	3.895	3.900
NO OF ANIONS	32	32	32	32	32	32	32	32	32	32
AN	23	25	23	23	22	23	24	23	26	1
WEIGHT PERCENT OXIDES										
SIO2	62.053	61.806	61.999	62.225	62.097	62.188	62.163	62.412	61.873	68.195
AL2O3	23.929	23.996	23.979	23.745	23.701	23.742	23.898	23.691	24.162	19.899
CR2O3	0.0	0.052	0.0	0.058	0.0	0.0	0.049	0.052	0.066	0.0
FEO	0.217	0.244	0.325	0.218	0.438	0.371	0.146	0.198	0.186	0.355
MNO	0.0	0.0	0.0	0.0	0.0	0.067	0.0	0.0	0.0	0.0
NIO	0.0	0.0	0.066	0.0	0.0	0.0	0.045	0.0	0.0	0.0
ZNO	0.0	0.0	0.0	0.0	0.0	0.0	0.049	0.085	0.085	0.040
BAO	0.0	0.046	0.0	0.0	0.0	0.0	0.0	0.042	0.0	0.0
CAO	4.815	5.231	4.853	4.799	4.693	4.734	5.009	4.731	5.295	0.247
NA2O	8.869	8.462	8.675	8.774	8.918	8.732	8.521	8.629	8.204	11.091
K2O	0.116	0.163	0.103	0.181	0.153	0.166	0.119	0.160	0.131	0.172
TOTAL 1	100.000	100.000	100.000	100.000	100.000	100.000	100.000	100.000	100.000	100.000
TOTAL 2	101.450	101.157	100.182	100.434	100.159	100.208	102.020	101.192	101.566	102.456

TABLE 22 . BIOTITES.

MINERAL NO	035. BIOT	043. BIOT	049. BIOT	064. BIOT	106. BIOT	121. BIOT	122. BIOT	135. BIOT	152. BIOT	152. BIOT
STRUCTURAL FORMULAE										
SI 4+	5.424	5.551	5.485	5.532	5.540	5.525	5.482	5.575	5.542	6.181
AL IV	2.576	2.449	2.515	2.468	2.460	2.475	2.518	2.425	2.458	1.819
SUM OF Z	8.000	8.000	8.000	8.000	8.000	8.000	8.000	8.000	8.000	8.000
AL VI	0.948	0.778	0.573	0.679	0.765	0.709	0.581	0.701	0.552	2.584
TI 4+	0.231	0.143	0.304	0.229	0.199	0.258	0.119	0.202	0.266	0.088
V 3+	0.0	0.011	0.013	0.008	0.007	0.0	0.006	0.012	0.0	0.011
FE 2+	2.485	1.803	2.664	3.051	2.612	2.982	3.964	2.663	3.555	1.307
MN	0.009	0.016	0.039	0.013	0.021	0.022	0.021	0.016	0.062	0.028
NI	0.007	0.0	0.006	0.005	0.0	0.008	0.014	0.007	0.0	0.0
ZN	0.005	0.004	0.0	0.015	0.008	0.006	0.016	0.0	0.0	0.0
MG	1.995	2.039	2.105	1.740	2.079	1.690	1.291	2.162	1.366	0.597
SUM OF Y	5.693	5.794	5.704	5.740	5.691	5.675	6.012	5.763	5.801	4.615
BA	0.013	0.0	0.0	0.0	0.0	0.0	0.0	0.0	0.0	0.0
CA	0.0	0.009	0.0	0.0	0.009	0.0	0.0	0.0	0.008	0.0
K	1.780	1.767	1.914	1.843	1.894	1.898	1.666	1.780	1.755	1.814
SUM OF X	1.793	1.776	1.914	1.843	1.894	1.898	1.666	1.780	1.755	1.814
CL	0.0	0.016	0.0	0.0	0.0	0.0	0.0	0.0	0.0	0.0
NO OF ANIONS	22	22	22	22	22	22	22	22	22	22
CH'GE BALANCE	+.194	+.042	+.027	+.023	+.089	+.065	-.140	+.021	-.068	+1.194
WEIGHT PERCENT OXIDES										
SIO2	36.016	37.832	35.954	35.910	36.515	35.909	34.574	36.812	35.372	44.151
TIO2	2.044	1.297	2.646	1.980	1.743	2.233	1.000	1.777	2.257	0.841
AL2O3	19.851	18.661	17.173	17.333	18.032	17.555	16.582	17.515	16.298	26.681
V2O3	0.0	0.095	0.108	0.066	0.055	0.0	0.050	0.103	0.0	0.102
FEO	19.729	14.689	20.871	23.678	20.579	23.168	29.888	21.019	27.122	11.162
MNO	0.070	0.126	0.299	0.099	0.163	0.171	0.153	0.125	0.467	0.237
NIO	0.057	0.0	0.049	0.043	0.0	0.062	0.108	0.056	0.0	0.0
ZNO	0.041	0.039	0.0	0.128	0.075	0.055	0.140	0.0	0.0	0.0
BAO	0.229	0.0	0.0	0.0	0.0	0.0	0.0	0.0	0.0	0.0
MGO	8.891	13.897	9.259	7.581	9.193	7.370	5.464	9.577	5.851	2.863
CAO	0.0	0.055	0.0	0.0	0.055	0.0	0.0	0.0	0.049	0.0
K2O	9.272	9.445	9.841	9.383	9.790	9.677	8.240	9.216	8.785	10.164
CL	0.0	0.063	0.0	0.0	0.0	0.0	0.0	0.0	0.0	0.0
TOTAL 1	96.200	96.200	96.200	96.200	96.200	96.200	96.200	96.200	96.200	96.200
TOTAL 2	96.264	95.499	94.708	94.428	92.976	93.194	95.606	96.334	89.937	96.005

TABLE 22. CONT'D...

MINERAL NO	162. BIOT	171. BIOT	246. BIOT	250. BIOT	263. BIOT	278. BIOT	351. BIOT	371. BIOT	391. BIOT	391. BIOT
STRUCTURAL FORMULAE										
SI 4+	5.644	5.657	5.568	5.587	5.550	5.545	5.510	5.411	5.458	5.431
AL IV	2.356	2.343	2.432	2.413	2.450	2.455	2.490	2.589	2.542	2.569
SUM OF Z	8.000	8.000	8.000	8.000	8.000	8.000	8.000	8.000	8.000	8.000
AL VI	0.814	0.475	0.763	0.751	0.789	0.727	0.841	1.004	0.824	0.873
TI 4+	0.145	0.130	0.210	0.167	0.214	0.212	0.180	0.059	0.272	0.21
V 3+	0.012	0.0	0.012	0.0	0.013	0.0	0.006	0.0	0.007	0.014
FE 2+	2.653	2.660	2.938	2.762	3.304	2.674	2.452	3.497	1.733	2.193
MN	0.041	0.203	0.065	0.023	0.045	0.028	0.0	0.0	0.0	0.010
NI	0.006	0.010	0.0	0.013	0.006	0.009	0.006	0.0	0.0	0.010
ZN	0.0	0.012	0.0	0.008	0.005	0.015	0.008	0.0	0.0	0.0
MG	2.078	2.403	1.767	2.050	1.348	2.071	2.288	1.237	2.784	2.410
SUM OF Y	5.749	5.893	5.755	5.798	5.736	5.850	5.781	5.797	5.680	5.727
BA	0.0	0.0	0.0	0.024	0.0	0.0	0.0	0.0	0.0	0.0
CA	0.040	0.0	0.010	0.0	0.0	0.011	0.0	0.0	0.0	0.0
NA	0.0	0.0	0.0	0.0	0.0	0.0	0.0	0.0	0.0	0.029
K	1.659	1.818	1.711	1.734	1.776	1.811	1.719	1.873	1.811	1.778
SUM OF X	1.699	1.818	1.721	1.754	1.776	1.821	1.719	1.873	1.811	1.807
NO OF ANIONS	22	22	22	22	22	22	22	22	22	22
CH'GE BALANCE	+.091	-.027	+.007	+.085	+.065	+.246	+.031	+.144	+.042	+.049
WEIGHT PERCENT OXIDES										
SIO2	37.438	37.001	36.444	36.695	35.801	36.514	36.767	34.661	37.197	36.473
TIO2	1.283	1.133	1.829	1.458	1.832	1.854	1.601	0.505	2.464	1.882
AL2O3	17.842	15.638	17.742	17.631	17.725	17.781	18.860	19.526	19.463	19.611
V2O3	0.101	0.0	0.096	0.0	0.104	0.0	0.049	0.0	0.056	0.113
FEO	21.042	20.795	22.987	21.686	25.481	21.051	19.558	26.779	14.609	17.608
MNO	0.318	1.570	0.502	0.176	0.344	0.220	0.0	0.0	0.0	0.076
NIO	0.048	0.085	0.0	0.108	0.052	0.073	0.051	0.0	0.0	0.085
ZNO	0.0	0.107	0.0	0.067	0.040	0.130	0.072	0.0	0.0	0.0
BAO	0.0	0.0	0.0	0.409	0.0	0.0	0.0	0.0	0.0	0.0
MGO	9.248	10.546	7.758	9.036	5.836	9.152	10.246	5.318	12.733	10.296
CAO	0.250	0.0	0.060	0.0	0.0	0.070	0.0	0.0	0.0	0.0
NA2O	0.0	0.0	0.0	0.0	0.0	0.0	0.0	0.0	0.0	0.101
K2O	8.631	9.326	8.782	8.935	8.986	9.354	8.996	9.411	9.679	9.365
TOTAL 1	96.200	96.200	96.200	96.200	96.200	96.200	96.200	96.200	96.200	96.200
TOTAL 2	92.663	95.476	94.485	95.111	96.533	94.229	95.304	96.584	91.696	95.074

TABLE 22 . CONT'D...

MINERAL NO	402. BIOT	494. BIOT	495. BIOT	495. BIOT	498. BIOT	503. BIOT	520. BIOT	528. BIOT	550. BIOT	551. BIOT
STRUCTURAL FORMULAE										
SI 4+	5.414	5.520	5.477	5.716	5.602	5.638	5.789	5.497	5.435	5.461
AL IV	2.586	2.480	2.523	2.284	2.398	2.362	2.211	2.503	2.565	2.539
SUM OF Z	8.000	8.000	8.000	8.000	8.000	8.000	8.000	8.000	8.000	8.000
AL VI	0.826	0.954	0.899	0.684	0.754	0.534	0.791	0.791	0.791	0.942
TI 4+	0.233	0.166	0.174	0.046	0.172	0.179	0.183	0.099	0.203	0.233
V 3+	0.0	0.0	0.0	0.0	0.0	0.0	0.0	0.0	0.0	0.010
CR 3+	0.006	0.0	0.0	0.0	0.0	0.0	0.0	0.0	0.0	0.0
FE 2+	2.967	2.150	2.228	1.262	2.564	2.408	1.976	3.424	3.613	2.188
MN	0.0	0.0	0.0	0.0	0.018	0.015	0.012	0.055	0.018	0.0
NI	0.009	0.011	0.006	0.0	0.006	0.011	0.009	0.008	0.014	0.0
CU	0.0	0.0	0.0	0.0	0.0	0.0	0.054	0.0	0.0	0.0
ZN	0.015	0.006	0.012	0.0	0.009	0.0	0.0	0.005	0.013	0.0
MG	1.731	2.471	2.515	1.476	2.284	2.405	2.906	1.468	1.093	2.395
SUM OF Y	5.787	5.758	5.834	5.086	5.766	5.790	5.674	5.850	5.745	5.765
BA	0.0	0.0	0.0	0.008	0.029	0.018	0.0	0.0	0.0	0.004
CA	0.0	0.0	0.0	0.0	0.0	0.020	0.140	0.0	0.0	0.0
NA	0.0	0.0	0.0	0.144	0.0	0.0	0.063	0.0	0.0	0.0
K	1.712	1.676	1.604	1.582	1.837	1.632	1.618	1.811	1.881	1.587
SUM OF X	1.712	1.676	1.604	1.734	1.866	1.670	1.813	1.811	1.881	1.589
NO OF ANIONS	22	22	22	22	22	22	22	22	22	22
CH'GE BALANCE	-.028	+.074	-.012	+.884	+.119	-.201	+.141	+.048	+.055	-.006
WEIGHT PERCENT OXIDES										
SIO2	35.410	37.345	36.988	40.742	36.909	37.697	39.206	35.246	34.542	36.968
TIO2	2.029	1.496	1.567	0.438	1.509	1.588	1.653	0.842	1.712	2.094
AL2O3	18.934	19.713	19.603	27.685	17.230	17.678	15.773	17.917	18.095	19.981
V2O3	0.0	0.0	0.0	0.0	0.0	0.0	0.0	0.0	0.0	0.083
CR2O3	0.047	0.0	0.0	0.0	0.0	0.0	0.0	0.0	0.0	0.0
FEO	23.200	17.387	17.985	10.750	20.138	19.251	16.000	26.246	27.454	17.709
MNO	0.0	0.0	0.0	0.0	0.141	0.120	0.099	0.417	0.136	0.0
NIO	0.070	0.091	0.054	0.0	0.048	0.090	0.079	0.067	0.113	0.0
CUO	0.0	0.0	0.0	0.0	0.0	0.0	0.489	0.0	0.0	0.0
ZNO	0.131	0.059	0.113	0.0	0.084	0.0	0.0	0.041	0.111	0.0
BAO	0.0	0.0	0.0	0.153	0.488	0.307	0.0	0.0	0.0	0.061
MGO	7.596	11.218	11.396	7.057	10.098	10.789	13.204	6.317	4.661	10.379
CAO	0.0	0.0	0.0	0.0	0.0	0.123	0.883	0.0	0.0	0.0
NA2O	0.0	0.0	0.0	0.531	0.0	0.0	0.221	0.0	0.0	0.0
K2O	8.783	8.892	8.493	8.845	9.495	8.557	8.594	9.106	9.374	8.425
TOTAL 1	96.200	96.200	96.200	96.200	96.200	96.200	96.200	96.200	96.200	96.200
TOTAL 2	96.167	95.274	95.647	95.714	95.166	94.160	91.465	96.382	96.701	91.592

TABLE 22. CONT'D...

MINERAL NO	551. BIOT	552. BIOT	553. BIOT	562. BIOT	564. BIOT	564. BIOT	565. BIOT	567. BIOT	568. BIOT	569. BIOT
STRUCTURAL FORMULAE										
SI 4+	5.485	5.455	5.397	5.541	5.282	5.496	5.576	5.531	5.579	5.627
AL IV	2.515	2.545	2.603	2.459	2.718	2.504	2.424	2.469	2.421	2.373
SUM OF Z	8.000	8.000	8.000	8.000	8.000	8.000	8.000	8.000	8.000	8.000
AL VI	0.942	0.717	0.839	0.548	0.508	0.859	0.540	0.749	0.926	0.641
TI 4+	0.204	0.236	0.205	0.274	0.605	0.344	0.237	0.218	0.204	0.198
V 3+	0.007	0.009	0.006	0.008	0.017	0.010	0.0	0.018	0.0	0.011
CR 3+	0.0	0.0	0.0	0.0	0.0	0.0	0.0	0.018	0.0	0.006
FE 2+	2.273	2.564	3.949	2.086	4.124	3.810	3.554	2.612	2.401	2.556
MN	0.0	0.012	0.015	0.0	0.033	0.027	0.077	0.016	0.020	0.029
CO	0.0	0.0	0.0	0.0	0.008	0.0	0.0	0.0	0.0	0.0
NI	0.0	0.0	0.008	0.0	0.0	0.0	0.0	0.0	0.0	0.0
ZN	0.0	0.0	0.027	0.005	0.006	0.006	0.011	0.0	0.0	0.0
MG	2.376	2.186	0.747	2.899	0.374	0.484	1.277	2.044	2.070	2.272
SUM OF Y	5.802	5.724	5.799	5.820	5.675	5.540	5.696	5.675	5.621	5.713
BA	0.021	0.0	0.003	0.0	0.007	0.0	0.0	0.005	0.0	0.0
CA	0.0	0.009	0.043	0.019	0.014	0.0	0.0	0.016	0.011	0.0
K	1.512	1.883	1.666	1.677	1.595	1.867	2.018	1.858	1.824	1.896
SUM OF X	1.533	1.892	1.672	1.696	1.616	1.867	2.018	1.879	1.835	1.896
NO OF ANIONS	22	22	22	22	22	22	22	22	22	22
CH'GE BALANCE	-.013	+.033	-.002	-.012	-.293	+.016	+.067	+.073	+.176	+.075
WEIGHT PERCENT OXIDES										
SIO2	37.030	35.993	34.074	37.419	33.072	34.778	35.293	36.461	37.237	37.157
TIO2	1.835	2.073	1.721	2.459	5.034	2.893	1.996	1.907	1.811	1.739
AL2O3	19.799	18.263	18.438	17.226	17.139	18.054	15.917	17.999	18.950	16.882
V2O3	0.058	0.070	0.047	0.068	0.130	0.081	0.0	0.145	0.0	0.089
CR2O3	0.0	0.0	0.0	0.0	0.0	0.0	0.0	0.152	0.0	0.049
FEO	18.345	20.225	29.804	16.837	30.870	28.820	26.890	20.582	19.161	20.176
MNO	0.0	0.091	0.111	0.0	0.243	0.199	0.573	0.126	0.157	0.223
COO	0.0	0.0	0.0	0.0	0.065	0.0	0.0	0.0	0.0	0.0
NIO	0.0	0.0	0.062	0.0	0.0	0.0	0.0	0.0	0.0	0.0
ZNO	0.0	0.0	0.229	0.050	0.055	0.052	0.090	0.0	0.0	0.0
BAO	0.363	0.0	0.043	0.0	0.106	0.0	0.0	0.082	0.0	0.0
MGO	10.765	9.678	3.164	13.137	1.572	2.055	5.423	9.043	9.268	10.066
CAO	0.0	0.058	0.256	0.119	0.080	0.0	0.0	0.096	0.067	0.0
K2O	8.004	9.748	8.251	8.885	7.834	9.267	10.017	9.607	9.550	9.820
TOTAL 1	96.200	96.200	96.200	96.200	96.200	96.200	96.200	96.200	96.200	96.200
TOTAL 2	92.616	92.506	90.881	91.566	86.952	89.401	90.114	92.634	90.832	92.002

TABLE 22. CONT'D...

MINERAL NO	570. BIOT	571. BIOT	572. BIOT	573. BIOT	573. BIOT	573. BIOT	444. BIOT	469. BIOT	469. BIOT	552. BIOT
STRUCTURAL FORMULAE										
SI 4+	5.521	5.608	5.533	5.390	5.361	5.327	5.457	5.561	5.564	5.521
AL IV	2.479	2.392	2.467	2.610	2.639	2.673	2.543	2.439	2.436	2.479
SUM OF Z	8.000	8.000	8.000	8.000	8.000	8.000	8.000	8.000	8.000	8.000
AL VI	0.665	0.769	0.470	0.637	0.657	0.650	0.858	0.777	0.829	0.782
TI 4+	0.229	0.142	0.142	0.113	0.118	0.132	0.178	0.151	0.147	0.201
V 3+	0.006	0.006	0.006	0.006	0.0	0.009	0.0	0.0	0.0	0.0
FE 2+	3.959	2.809	3.779	1.449	1.450	1.496	2.583	2.043	1.965	2.937
MN	0.088	0.032	0.033	0.0	0.0	0.0	0.012	0.014	0.009	0.022
CO	0.0	0.0	0.0	0.0	0.005	0.011	0.0	0.0	0.0	0.0
ZN	0.013	0.0	0.020	0.0	0.005	0.006	0.007	0.0	0.0	0.0
MG	0.771	1.999	1.491	3.819	3.808	3.731	2.136	2.809	2.781	1.810
SUM OF Y	5.731	5.757	5.941	6.024	6.043	6.035	5.774	5.794	5.730	5.754
BA	0.0	0.0	0.0	0.004	0.0	0.0	0.003	0.007	0.031	0.0
CA	0.0	0.0	0.0	0.009	0.022	0.0	0.0	0.0	0.011	0.0
K	1.883	1.818	1.823	1.667	1.616	1.682	1.778	1.738	1.769	1.785
SUM OF X	1.883	1.818	1.823	1.680	1.638	1.682	1.081	1.767	1.811	1.785
NO OF ANIONS	22	22	22	22	22	22	22	22	22	22
CHARGE BALANCE	+.029	+.094	-.091	-.143	-.161	-.174	+.051	+.057	+.122	+.045
WEIGHT PERCENT OXIDES										
SIO2	34.601	36.828	34.932	37.242	37.094	36.695	36.141	37.795	37.612	36.106
TIO2	1.910	1.238	1.192	1.035	1.083	1.212	1.569	1.354	1.317	1.769
AL2O3	16.715	17.610	15.735	19.036	19.351	19.420	19.112	18.445	18.727	18.095
V2O3	0.050	0.049	0.048	0.050	0.0	0.075	0.0	0.0	0.0	0.0
FEO	29.659	22.052	28.526	11.969	11.993	12.320	20.449	16.508	15.879	22.962
MNO	0.654	0.252	0.245	0.0	0.0	0.0	0.092	0.110	0.063	0.170
COO	0.0	0.0	0.0	0.0	0.043	0.091	0.0	0.0	0.0	0.0
ZNO	0.114	0.0	0.174	0.0	0.050	0.053	0.064	0.0	0.0	0.0
BAO	0.0	0.0	0.0	0.071	0.0	0.0	0.044	0.119	0.537	0.0
MGO	3.243	8.806	6.317	17.707	17.679	17.246	9.492	12.740	12.615	7.942
CAO	0.0	0.0	0.0	0.055	0.142	0.0	0.0	0.0	0.071	0.0
K2O	9.253	9.364	9.030	9.034	8.767	9.068	9.236	9.215	9.379	9.158
TOTAL 1	96.200	96.200	96.200	96.200	96.200	96.200	96.200	96.200	96.200	96.200
TOTAL 2	93.409	91.756	93.395	92.520	91.881	91.854	95.787	94.801	94.542	96.462

TABLE 22. CONT'D...

MINERAL NO	010. BIOT	050. BIOT	087. BIOT	106. BIOT	119. BIOT	262. BIOT	338. BIOT	342. BIOT	348. BIOT	358. BIOT
STRUCTURAL FORMULAE										
SI 4+	5.440	5.453	5.456	5.511	5.503	5.505	5.491	5.516	5.577	5.552
AL IV	2.560	2.547	2.544	2.489	2.497	2.495	2.509	2.484	2.423	2.448
SUM OF T	8.000	8.000	8.000	8.000	8.000	8.000	8.000	8.000	8.000	8.000
AL VI	0.860	0.789	0.577	0.720	0.764	0.739	0.697	0.848	0.874	0.819
TI 4+	0.243	0.257	0.275	0.177	0.201	0.210	0.171	0.207	0.167	0.164
V 3+	0.012	0.0	0.0	0.0	0.009	0.0	0.010	0.0	0.0	0.0
FE 2+	2.434	2.552	4.055	2.515	2.606	3.078	2.631	2.399	2.137	2.872
MN	0.012	0.015	0.056	0.019	0.017	0.034	0.016	0.0	0.015	0.021
ZN	0.0	0.009	0.0	0.0	0.0	0.0	0.0	0.0	0.100	0.0
MG	2.106	2.085	0.803	2.362	1.152	1.694	2.281	2.256	2.532	1.892
SUM OF Y	5.667	5.707	5.766	5.799	5.749	5.735	5.806	5.710	5.735	5.768
BA	0.0	0.003	0.006	0.0	0.0	0.0	0.020	0.006	0.004	0.0
CA	0.0	0.008	0.0	0.0	0.0	0.0	0.0	0.0	0.011	0.0
NA	0.046	0.0	0.0	0.0	0.0	0.0	0.0	0.014	0.015	0.0
K	1.818	1.811	1.870	1.827	1.827	1.827	1.810	1.755	1.704	1.765
SUM OF X	1.864	1.822	1.876	1.827	1.827	1.827	1.830	1.795	1.734	1.765
CL	0.0	0.0	0.028	0.0	0.0	0.010	0.019	0.0	0.011	0.0
NO OF ANIONS	22	22	22	22	22	22	22	22	22	22
	+.074	+.039	-.044	+.034	+.044	+.036	+.015	+.068	+.102	+.068
WEIGHT PERCENT OXIDES										
SIO2	36.171	36.078	34.030	36.519	36.359	35.724	36.110	36.814	38.203	36.444
TIO2	2.152	2.258	2.283	1.560	1.766	1.814	1.497	1.841	1.499	1.434
AL2O3	19.293	18.729	16.515	18.043	18.279	17.807	17.886	18.867	18.881	18.194
V2O3	0.103	0.0	0.0	0.0	0.076	0.0	0.082	0.0	0.0	0.0
FEO	19.351	20.190	30.239	19.928	20.587	24.622	20.689	19.139	17.244	22.542
MNO	0.093	0.166	0.416	0.152	0.131	0.261	0.127	0.0	0.116	0.167
ZNO	0.0	0.081	0.0	0.0	0.0	0.0	0.0	0.0	0.091	0.0
BAO	0.0	0.048	0.101	0.0	0.0	0.0	0.335	0.099	0.066	0.0
MGO	9.396	9.257	3.363	10.501	9.538	7.374	10.064	10.101	11.468	8.333
CAO	0.0	0.048	0.0	0.0	0.0	0.0	0.0	0.0	0.070	0.0
NA2O	0.158	0.0	0.0	0.0	0.0	0.0	0.0	0.049	0.052	0.0
K2O	9.483	9.396	9.148	9.496	9.467	9.301	9.336	9.292	9.023	9.086
CL	0.0	0.0	0.103	0.0	0.0	0.040	0.074	0.0	0.044	0.0
TOTAL 1	96.200	96.200	96.200	96.200	96.200	96.200	96.200	96.200	96.200	96.200
TOTAL 2	95.776	95.356	97.046	95.547	95.598	96.117	95.381	96.213	95.598	95.455

TABLE 23 - CHLORITES.

MINERAL NO	496. CHEQ	498. CHEQ	501. CHEQ	504. CHEQ	522. CHEQ	547. CHEQ	048. CHMG	181. CHMG	181. CHMG	181. CHMG
STRUCTURAL FORMULAE										
SI 4+	5.409	5.393	5.333	5.286	5.310	5.299	5.316	5.413	5.398	5.391
AL IV	2.591	2.607	2.667	2.714	2.690	2.701	2.684	2.587	2.602	2.609
SUM OF Z	8.000	8.000	8.000	8.000	8.000	8.000	8.000	8.000	8.000	8.000
AL VI	2.762	2.768	2.739	2.824	2.807	2.752	2.762	2.726	2.775	2.781
TI 4+	0.011	0.011	0.0	0.0	0.0	0.015	0.010	0.0	0.0	0.0
CR 3+	0.0	0.0	0.0	0.0	0.016	0.0	0.011	0.015	0.014	0.012
SUM OF Y	2.773	2.779	2.739	2.824	2.807	2.767	2.772	2.741	2.789	2.793
FE 2+	4.522	4.392	4.245	4.955	3.469	4.879	3.122	3.279	3.222	3.207
MN	0.049	0.051	0.054	0.041	0.032	0.041	0.036	0.036	0.035	0.038
CO	0.010	0.0	0.0	0.0	0.011	0.0	0.0	0.0	0.0	0.0
NI	0.017	0.012	0.021	0.010	0.024	0.017	0.0	0.0	0.011	0.0
ZN	0.027	0.0	0.024	0.022	0.021	0.027	0.018	0.039	0.016	0.020
MG	4.490	4.660	4.846	4.071	5.528	4.218	5.985	5.783	5.770	5.798
CA	0.017	0.015	0.033	0.020	0.027	0.012	0.0	0.023	0.030	0.028
NA	0.0	0.0	0.0	0.0	0.0	0.0	0.0	0.047	0.065	0.046
SUM OF X+Y	11.905	11.909	11.962	11.943	11.919	11.961	11.933	11.948	11.938	11.936
NO OF ANIONS	28	28	28	28	28	28	28	28	28	28
CHARGE BALANCE	-.028	+.080	+.038	+.047	+.081	+.024	+.057	+.037	+.048	+.052
WEIGHT PERCENT OXIDES										
SIO2	25.822	25.876	25.637	24.934	26.116	25.030	26.446	26.779	26.763	26.751
TIO2	0.068	0.069	0.0	0.0	0.0	0.093	0.066	0.0	0.0	0.0
AL2O3	21.683	21.862	22.049	22.164	22.938	21.853	22.986	22.298	22.619	22.692
CR2O3	0.0	0.0	0.0	0.0	0.099	0.0	0.070	0.093	0.089	0.076
FEO	25.807	25.192	24.397	27.944	20.397	27.555	18.569	19.392	19.098	19.022
MNO	0.273	0.287	0.304	0.230	0.185	0.226	0.214	0.208	0.204	0.221
COO	0.059	0.0	0.0	0.0	0.068	0.0	0.0	0.0	0.0	0.0
NIO	0.103	0.073	0.124	0.061	0.145	0.099	0.0	0.0	0.070	0.0
ZNO	0.177	0.0	0.158	0.143	0.138	0.175	0.122	0.259	0.107	0.138
MGO	14.383	15.004	15.631	12.885	18.242	13.368	19.977	19.197	19.194	19.302
CAO	0.075	0.066	0.149	0.089	0.123	0.052	0.0	0.105	0.141	0.129
NA2O	0.0	0.0	0.0	0.0	0.0	0.0	0.0	0.119	0.165	0.119
TOTAL 1	88.450	88.450	88.450	88.450	88.450	88.450	88.450	88.450	88.450	88.450
TOTAL 2	87.291	85.816	86.312	87.191	87.731	88.806	87.394	87.323	87.178	87.266

TABLE 23 - CONT'D...

MINERAL NO	300. CHMG	380. CHMG	520. CHMG	534. CHMG	543. CHMG	544. CHMG	545. CHMG	051. CHLR	517. CHLR	535. CHLR
STRUCTURAL FORMULAE										
SI 4+	5.739	5.286	5.599	5.310	5.607	5.346	5.362	5.570	5.385	5.554
AL IV	2.261	2.714	2.401	2.690	2.393	2.564	2.638	2.430	2.615	2.446
SUM OF Z	8.000	8.000	8.000	8.000	8.000	8.000	8.000	8.000	8.000	8.000
AL VI	2.329	2.730	2.368	2.705	2.305	2.795	2.681	2.606	2.726	2.513
TI 4+	0.0	0.011	0.0	0.0	0.0	0.0	0.010	0.0	0.0	0.0
CR 3+	0.030	0.013	0.0	0.0	0.060	0.0	0.0	0.0	0.0	0.0
SUM OF Y	2.359	2.744	2.368	2.705	2.365	2.795	2.691	2.606	2.726	2.611
FE 2+	0.904	2.839	3.467	3.989	3.351	3.856	3.918	4.397	3.550	5.088
MN	0.0	0.0	0.029	0.035	0.035	0.031	0.023	0.063	0.023	0.036
CO	0.0	0.0	0.0	0.0	0.010	0.007	0.007	0.0	0.0	0.0
NI	0.011	0.0	0.018	0.0	0.025	0.027	0.024	0.030	0.011	0.0
ZN	0.0	0.0	0.018	0.0	0.0	0.016	0.011	0.023	0.006	0.0
MG	8.676	6.366	6.101	5.218	6.207	5.316	5.286	4.731	5.630	4.295
CA	0.0	0.014	0.017	0.047	0.020	0.014	0.010	0.061	0.0	0.033
SUM OF X+Y	11.950	11.963	12.018	11.994	11.953	12.062	11.970	11.911	11.946	11.965
NO OF ANIONS	28	28	28	28	28	28	28	28	28	28
CH'GE BALANCE	-.048	+.023	-.018	+.006	-.013	-.062	+.040	+.089	+.054	-.130
WEIGHT PERCENT OXIDES										
SIO2	30.605	26.544	27.543	25.746	27.640	26.005	26.048	26.668	26.483	26.132
TIO2	0.0	0.077	0.0	0.0	0.0	0.0	0.062	0.0	0.0	0.0
AL2O3	20.766	23.193	19.905	22.192	19.647	22.115	21.924	20.454	22.284	19.795
CR2O3	0.201	0.083	0.0	0.0	0.377	0.0	0.0	0.0	0.0	0.0
FEO	5.765	17.041	20.388	23.125	19.744	22.424	22.755	25.166	20.870	28.619
MNO	0.0	0.0	0.170	0.201	0.205	0.176	0.129	0.359	0.132	0.202
COO	0.0	0.0	0.0	0.0	0.063	0.043	0.041	0.0	0.0	0.0
NIO	0.071	0.0	0.112	0.0	0.155	0.166	0.145	0.180	0.064	0.0
ZNO	0.0	0.0	0.119	0.0	0.0	0.106	0.069	0.151	0.040	0.0
MGO	31.041	21.449	20.137	16.975	20.529	17.350	17.231	15.199	18.577	13.558
CAO	0.0	0.064	0.076	0.211	0.091	0.065	0.045	0.273	0.0	0.144
TOTAL 1	88.450	88.450	88.450	88.450	88.450	88.450	88.450	88.450	88.450	88.450
TOTAL 2	85.624	88.690	84.812	87.403	84.473	88.192	87.510	86.907	85.678	87.539

TABLE 23 CONT'D...

MINERAL NO	538. CHLR	540. CHLR	541. CHLR
STRUCTURAL FORMULAE			
SI 4+	5.384	5.261	5.584
AL IV	2.616	2.739	2.416
SUM OF Z	8.000	8.000	8.000
AL VI	2.583	2.738	2.579
CR 3+	0.028	0.0	0.078
SUM OF Y	2.611	2.738	2.657
FE 2+	3.251	4.118	2.923
MN	0.038	0.036	0.028
NI	0.024	0.0	0.029
MG	6.057	5.097	6.074
CA	0.020	0.013	0.170
SUM OF X+Y	12.001	12.002	11.881
NO OF ANIONS	28	28	28
CH'GE BALANCE	+.004	-.001	+.041
WEIGHT PERCENT OXIDES			
SIO2	26.643	25.422	27.875
AL2O3	21.826	22.453	21.157
CR2O3	0.173	0.0	0.492
FEO	19.231	23.787	17.444
MNO	0.224	0.207	0.167
NIO	0.148	0.0	0.179
MGO	20.111	16.524	20.345
CAO	0.093	0.057	0.791
TOTAL 1	88.450	88.450	88.450
TOTAL 2	86.556	83.999	86.822

TABLE 24 . ACTINOLITES.

MINERAL NO	051. ACT	181. ACT	181. ACT	186. ACT	186. ACT	300. ACT	308. ACT
STRUCTURAL FORMULAE							
SI 4+	7.554	7.913	7.991	8.043	7.778	7.403	7.584
AL IV	0.446	0.87	0.009	0.0	0.222	0.597	0.416
SUM OF Z	8.000	8.000	8.000	8.043	8.000	8.000	8.000
AL VI	0.305	0.130	0.130	0.391	0.105	0.260	0.347
TI 4+	0.010	0.0	0.0	0.0	0.0	0.0	0.009
V 3+	0.0	0.006	0.0	0.0	0.0	0.007	0.007
CR 3+	0.032	0.0	0.008	0.005	0.0	0.034	0.010
FE 2+	1.557	1.189	1.250	2.414	2.669	0.629	1.934
MN	0.022	0.019	0.019	0.033	0.025	0.009	0.033
NI	0.007	0.0	0.0	0.0	0.0	0.0	0.009
ZN	0.0	0.009	0.011	0.0	0.0	0.009	0.0
MG	3.177	3.656	3.588	2.008	2.210	4.175	2.703
SUM OF Y	5.100	5.009	4.956	4.851	5.009	5.142	5.052
BA	0.002	0.0	0.0	0.0	0.0	0.004	0.0
CA	1.896	1.949	1.951	1.818	2.010	1.824	1.933
NA	0.065	0.034	0.027	0.056	0.059	0.318	0.044
K	0.010	0.0	0.0	0.037	0.019	0.015	0.021
SUM OF X+A	1.973	1.983	1.978	1.911	2.088	2.161	1.998
NO OF ANIONS	23	23	23	23	23	23	23
WEIGHT PERCENT OXIDES							
SIO2	52.489	55.927	56.336	54.648	51.874	53.044	51.977
TIO2	0.089	0.0	0.0	0.0	0.0	0.0	0.082
AL2O3	4.427	1.300	0.691	2.255	1.848	5.334	4.438
V2O3	0.0	0.056	0.0	0.0	0.0	0.061	0.058
CR2O3	0.280	0.0	0.072	0.045	0.0	0.311	0.090
FEO	12.933	10.050	10.539	19.610	21.279	5.387	15.846
MNO	0.184	0.161	0.160	0.263	0.196	0.073	0.265
NIO	0.062	0.0	0.0	0.0	0.0	0.0	0.077
ZNO	0.0	0.085	0.106	0.0	0.0	0.088	0.0
BAO	0.041	0.0	0.0	0.0	0.0	0.066	0.0
MGO	14.810	17.339	16.971	9.157	9.891	20.075	12.432
CAO	12.298	12.856	12.842	11.530	12.508	12.201	12.366
NA2O	0.231	0.125	0.100	0.195	0.203	1.174	0.157
K2O	0.056	0.0	0.0	0.197	0.102	0.086	0.114
S	0.0	0.0	0.084	0.0	0.0	0.0	0.0
TOTAL 1	97.900	97.900	97.900	97.900	97.900	97.900	97.900
TOTAL 2	96.994	97.161	97.931	98.331	97.563	97.085	97.470

TABLE 24. CONT'D...

MINERAL NO	496. ACT	498. ACT	499. ACT	501. ACT	503. ACT	504. ACT	509. ACT	509. ACT	516. ACT	517. ACT
STRUCTURAL FORMULAE										
SI 4+	7.442	7.824	7.640	7.033	7.519	7.703	7.701	7.587	7.798	7.701
AL IV	0.558	0.176	0.360	0.967	0.481	0.297	0.299	0.413	0.202	0.299
SUM OF Z	8.000	8.000	8.000	8.000	8.000	8.000	8.000	8.000	8.000	8.000
AL VI	0.509	0.153	0.268	0.503	0.415	0.280	0.208	0.336	0.248	0.678
TI 4+	0.0	0.0	0.009	0.030	0.009	0.013	0.0	0.010	0.0	0.0
V 3+	0.011	0.010	0.0	0.010	0.0	0.0	0.010	0.007	0.006	0.000
CR 3+	0.0	0.029	0.008	0.013	0.008	0.0	0.0	0.007	0.006	0.0
FE 2+	2.077	1.757	1.966	2.034	1.705	2.092	2.174	2.183	1.577	1.421
MN	0.031	0.034	0.025	0.035	0.028	0.025	0.031	0.033	0.025	0.023
CO	0.0	0.0	0.0	0.0	0.0	0.0	0.0	0.007	0.0	0.0
NI	0.005	0.009	0.010	0.011	0.0	0.0	0.0	0.009	0.0	0.000
ZN	0.008	0.007	0.011	0.012	0.0	0.009	0.0	0.028	0.008	0.0
MG	2.566	3.059	2.799	2.804	2.893	2.638	2.689	2.503	3.214	2.901
SUM OF Y	5.207	5.058	5.096	5.420	5.058	5.057	5.112	5.123	5.061	4.960
BA	0.008	0.0	0.0	0.0	0.0	0.0	0.0	0.0	0.0	0.0
CA	1.888	1.926	1.916	1.682	1.915	1.902	1.894	1.864	1.855	1.773
NA	0.104	0.0	0.037	0.094	0.062	0.049	0.052	0.051	0.040	0.093
K	0.025	0.015	0.0	0.019	0.032	0.025	0.018	0.021	0.022	0.018
SUM OF X+A	2.025	1.941	1.953	1.795	2.009	1.976	1.964	1.936	1.917	1.884
NO OF ANIONS	23	23	23	23	23	23	23	23	23	23
WEIGHT PERCENT OXIDES										
SIO2	50.625	54.035	52.344	47.925	51.994	52.576	52.385	51.504	54.350	54.238
TIO2	0.0	0.0	0.084	0.270	0.086	0.116	0.0	0.087	0.0	0.165
AL2O3	5.582	1.931	3.651	8.499	5.259	3.341	2.924	4.312	2.662	5.840
V2O3	0.097	0.083	0.0	0.084	0.0	0.0	0.087	0.062	0.056	0.090
CR2O3	0.0	0.254	0.066	0.110	0.068	0.0	0.0	0.064	0.057	0.0
FEO	16.888	14.508	16.106	16.572	14.095	17.074	17.681	17.721	13.140	11.968
MNO	0.251	0.275	0.202	0.279	0.228	0.204	0.249	0.262	0.204	0.195
COO	0.0	0.0	0.0	0.0	0.0	0.0	0.0	0.057	0.0	0.0
NIO	0.045	0.080	0.087	0.097	0.0	0.0	0.0	0.075	0.0	0.079
ZNO	0.073	0.067	0.106	0.111	0.0	0.088	0.0	0.254	0.072	0.0
BAO	0.139	0.0	0.0	0.0	0.0	0.0	0.0	0.0	0.0	0.0
MGO	11.711	14.175	12.867	12.821	13.421	12.080	12.275	11.402	15.028	13.235
CAO	11.988	12.414	12.254	10.700	12.357	12.115	12.023	11.811	12.069	11.554
NA2O	0.367	0.0	0.132	0.330	0.220	0.173	0.182	0.177	0.144	0.336
K2O	0.135	0.079	0.0	0.102	0.173	0.134	0.095	0.113	0.119	0.101
TOTAL 1	97.900	97.900	97.900	97.900	97.900	97.900	97.900	97.900	97.900	97.900
TOTAL 2	96.846	97.609	97.038	94.810	97.092	97.148	96.467	95.992	95.458	96.114

TABLE 24. CONT'D...

MINERAL NO	520. ACT	522. ACT	532. ACT	537. ACT	538. ACT	540. ACT	541. ACT	543. ACT	544. ACT	545. ACT
STRUCTURAL FORMULAE										
SI 4+	7.772	7.839	7.810	7.703	7.874	7.700	7.842	7.790	7.817	7.905
AL IV	0.228	0.161	0.190	0.297	0.126	0.300	0.158	0.210	0.183	0.095
SUM OF Z	8.000	8.000	8.000	8.000	8.000	8.000	8.000	8.000	8.000	8.000
AL VI	0.205	0.185	0.175	0.243	0.158	0.217	0.084	0.253	0.227	0.137
TI 4+	0.0	0.0	0.0	0.0	0.0	0.0	0.0	0.035	0.0	0.0
V 3+	0.009	0.006	0.0	0.0	0.0	0.0	0.0	0.009	0.010	0.006
CR 3+	0.041	0.034	0.006	0.012	0.009	0.008	0.028	0.018	0.012	0.015
FE 2+	1.165	1.297	1.619	1.408	1.128	1.585	1.101	1.168	1.502	1.510
MN	0.028	0.025	0.029	0.017	0.020	0.037	0.021	0.011	0.031	0.023
CO	0.0	0.011	0.0	0.0	0.0	0.0	0.0	0.0	0.0	0.005
NI	0.009	0.013	0.0	0.0	0.006	0.0	0.005	0.010	0.012	0.011
ZN	0.010	0.013	0.0	0.0	0.0	0.0	0.0	0.0	0.0	0.010
MG	3.566	3.463	3.257	3.379	3.721	3.259	3.807	3.514	3.297	3.379
SUM OF Y	5.053	5.047	5.086	5.059	5.042	5.106	5.046	5.018	5.091	5.096
CA	1.934	1.921	1.915	1.940	1.936	1.902	1.965	1.864	1.869	1.866
NA	0.024	0.0	0.0	0.027	0.0	0.042	0.013	0.073	0.0	0.0
K	0.018	0.0	0.008	0.017	0.0	0.016	0.011	0.020	0.010	0.009
SUM OF X+A	1.976	1.921	1.923	1.984	1.936	1.960	1.989	1.957	1.879	1.875
NO OF ANIONS	23	23	23	23	23	23	23	23	23	23
WEIGHT PERCENT OXIDES										
SIO2	54.834	55.108	54.320	53.926	55.819	53.525	55.497	55.114	54.644	55.238
TIO2	0.0	0.0	0.0	0.0	0.0	0.0	0.0	0.329	0.0	0.0
AL2O3	2.590	2.061	2.154	3.209	1.710	3.050	1.454	2.781	2.432	1.376
V2O3	0.080	0.057	0.0	0.0	0.0	0.0	0.0	0.079	0.090	0.055
CR2O3	0.365	0.307	0.050	0.103	0.085	0.074	0.247	0.164	0.106	0.137
FEO	9.829	10.900	13.462	11.783	9.556	13.169	9.319	9.882	12.548	12.614
MNO	0.230	0.204	0.234	0.141	0.170	0.308	0.176	0.091	0.258	0.190
COO	0.0	0.093	0.0	0.0	0.0	0.0	0.0	0.0	0.0	0.047
NIO	0.076	0.111	0.0	0.0	0.055	0.0	0.044	0.092	0.106	0.092
ZNO	0.093	0.119	0.0	0.0	0.0	0.0	0.0	0.0	0.0	0.092
MGO	16.862	16.333	15.202	15.870	17.696	15.199	18.075	16.680	15.464	15.843
CAO	12.736	12.607	12.434	12.670	12.809	12.338	12.977	12.309	12.197	12.168
NA2O	0.087	0.0	0.0	0.099	0.0	0.152	0.048	0.267	0.0	0.0
K2O	0.099	0.0	0.043	0.091	0.0	0.087	0.063	0.113	0.055	0.049
TOTAL 1	97.900	97.900	97.900	97.900	97.900	97.900	97.900	97.900	97.900	97.900
TOTAL 2	96.901	96.180	96.654	96.067	95.953	89.561	96.167	96.292	97.177	97.175

TABLE 24. CONT'D...

MINERAL NO	546. ACT	547. ACT	548. ACT
STRUCTURAL FORMULAE			
SI 4+	7.527	7.405	7.770
AL IV	0.473	0.595	0.230
SUM OF Z	8.000	8.000	8.000
AL VI	0.375	0.417	0.254
TI 4+	0.015	0.016	0.0
V 3+	0.0	0.011	0.0
CR 3+	0.020	0.008	0.033
FE 2+	1.739	2.138	1.007
MN	0.024	0.029	0.019
NI	0.010	0.009	0.006
CU	0.0	0.0	0.0
ZN	0.005	0.007	0.0
MG	2.953	2.466	3.730
SUM OF Y	5.141	5.101	5.049
CA	1.832	1.908	1.920
NA	0.077	0.087	0.0
K	0.020	0.025	0.007
SUM OF X+A	1.921	2.020	1.927
NO OF ANIONS	23	23	23
WEIGHT PERCENT OXIDES			
SIO2	52.020	50.285	55.299
TIO2	0.141	0.140	0.0
AL2O3	4.972	5.828	2.923
V2O3	0.0	0.094	0.0
CR2O3	0.179	0.069	0.294
FEO	14.370	17.352	8.572
MNO	0.200	0.231	0.162
NIO	0.082	0.075	0.051
ZNO	0.045	0.062	0.0
MGO	13.694	11.235	17.810
CAO	11.814	12.090	12.751
NA2O	0.276	0.306	0.0
K2O	0.107	0.134	0.038
TOTAL 1	97.900	97.900	97.900
TOTAL 2	97.442	97.981	95.970

TABLE 25. HORNBLENDES.

MINERAL NO	012. HORN	023. HORN	048. HORN	051. HORN	181. HORN	186. HORN	186. HORN	186. HORN	186. HORN	308. HORN
STRUCTURAL FORMULAE										
SI 4+	6.638	6.574	6.235	6.730	7.956	6.286	6.384	6.302	6.348	6.501
AL IV	1.362	1.426	1.765	1.270	0.044	1.714	1.616	1.698	1.652	1.499
SUM OF Z	8.000	8.000	8.000	8.000	8.000	8.000	8.000	8.000	8.000	8.000
AL VI	0.821	0.832	1.360	0.802	0.231	1.051	0.962	1.063	1.069	1.122
TI 4+	0.052	0.070	0.048	0.040	0.0	0.051	0.032	0.035	0.031	0.031
V 3+	0.007	0.0	0.008	0.0	0.0	0.008	0.021	0.011	0.013	0.005
CR 3+	0.011	0.0	0.008	0.0	0.006	0.0	0.0	0.0	0.0	0.0
FE 2+	2.065	2.319	4.697	1.865	1.204	2.894	2.893	2.910	2.903	2.251
MN	0.031	0.030	0.034	0.025	0.019	0.046	0.046	0.042	0.046	0.037
NI	0.0	0.0	0.0	0.007	0.0	0.0	0.0	0.0	0.007	0.016
ZN	0.0	0.0	0.0	0.0	0.0	0.008	0.0	0.0	0.015	0.0
MG	2.163	1.907	1.996	2.387	3.499	1.085	1.153	1.078	1.054	1.641
SUM OF Y	5.150	5.158	5.151	5.126	4.959	5.143	5.026	5.139	5.138	5.103
CA	1.888	1.811	1.773	1.907	1.882	1.861	1.882	1.867	1.866	1.850
NA	0.300	0.452	0.373	0.286	0.123	0.411	0.466	0.411	0.378	0.354
K	0.045	0.066	0.069	0.032	0.0	0.130	0.135	0.133	0.125	0.050
SUM OF X+A	2.233	2.329	2.215	2.225	2.005	2.402	2.473	2.411	2.369	2.254
NO OF ANIONS	23	23	23	23	23	23	23	23	23	23
WEIGHT PERCENT OXIDES										
SIO2	44.845	43.946	42.740	45.871	56.333	40.987	41.600	41.089	41.406	43.664
TIO2	0.467	0.620	0.442	0.367	0.0	0.445	0.280	0.304	0.265	0.275
AL2O3	12.511	12.804	18.175	11.980	1.650	15.295	14.250	15.273	15.058	14.933
V2O3	0.062	0.0	0.070	0.0	0.0	0.063	0.169	0.088	0.107	0.046
CR2O3	0.092	0.0	0.070	0.0	0.054	0.0	0.0	0.0	0.0	0.0
FEO	16.681	18.534	13.909	15.199	10.190	22.561	22.539	22.684	22.637	18.075
MNO	0.246	0.239	0.279	0.202	0.158	0.358	0.351	0.322	0.351	0.292
NIO	0.0	0.0	0.0	0.058	0.0	0.0	0.0	0.0	0.060	0.136
ZNO	0.0	0.0	0.0	0.0	0.0	0.067	0.0	0.0	0.134	0.0
MGO	9.804	8.553	9.180	10.918	16.624	4.749	5.039	4.717	4.614	7.394
CAO	11.908	11.301	11.347	12.130	12.440	11.328	11.447	11.361	11.357	11.594
NA2O	1.047	1.559	1.319	1.004	0.450	1.384	1.533	1.384	1.272	1.228
K2O	0.238	0.344	0.369	0.172	0.0	0.663	0.691	0.678	0.638	0.263
TOTAL 1	97.900	97.900	97.900	97.900	97.900	97.900	97.900	97.900	97.900	97.900
TOTAL 2	98.165	98.709	98.363	97.115	97.237	98.237	98.563	98.238	98.053	97.822

TABLE 25. CONT'D...

MINERAL NO	376. HORN	380. HORN	496. HORN	498. HORN	499. HORN	501. HORN	503. HORN	504. HORN	509. HORN	509. HORN
STRUCTURAL FORMULAE										
SI 4+	6.645	6.282	6.494	6.538	6.603	6.777	6.505	6.900	6.519	6.386
AL IV	1.355	1.718	1.506	1.462	1.397	1.223	1.495	1.100	1.481	1.614
SUM OF Z	8.000	8.000	8.000	8.000	8.000	8.000	8.000	8.000	8.000	8.000
AL VI	0.830	1.208	0.935	0.972	1.008	0.849	0.953	0.769	0.947	1.039
TI 4+	0.057	0.033	0.033	0.034	0.038	0.014	0.142	0.074	0.033	0.042
V 3+	0.0	0.0	0.011	0.006	0.007	0.0	0.0	0.008	0.018	0.011
CR 3+	0.0	0.0	0.008	0.014	0.0	0.010	0.007	0.0	0.006	0.0
FE 2+	1.981	1.685	2.648	2.354	2.645	2.212	2.050	2.288	2.700	2.741
MN	0.035	0.009	0.029	0.034	0.028	0.031	0.029	0.030	0.033	0.033
CO	0.0	0.0	0.0	0.0	0.0	0.0	0.006	0.0	0.0	0.0
NI	0.0	0.0	0.013	0.009	0.0	0.012	0.010	0.008	0.008	0.0
ZN	0.007	0.0	0.011	0.020	0.0	0.016	0.009	0.012	0.023	0.005
MG	2.248	2.318	1.506	1.712	1.492	2.090	1.777	1.863	1.399	1.290
SUM OF Y	5.158	5.253	5.194	5.155	5.218	5.234	4.983	5.152	5.167	5.161
BA	0.0	0.0	0.0	0.0	0.0	0.011	0.0	0.0	0.0	0.0
CA	1.840	1.644	1.836	1.863	1.751	1.790	1.938	1.870	1.837	1.843
NA	0.389	0.632	0.358	0.293	0.310	0.243	0.335	0.256	0.338	0.389
K	0.023	0.021	0.064	0.073	0.058	0.031	0.073	0.073	0.095	0.081
SUM OF X+A	2.252	2.297	2.258	2.229	2.119	2.064	2.346	2.199	2.270	2.338
NO OF ANIONS	23	23	23	23	23	23	23	23	23	23
WEIGHT PERCENT OXIDES										
SIO2	45.058	43.117	42.890	43.659	43.857	45.655	43.832	46.344	42.933	42.021
TIO2	0.511	0.297	0.291	0.298	0.337	0.122	1.276	0.657	0.293	0.368
AL203	12.571	17.035	13.677	13.790	13.553	11.840	13.995	10.647	13.568	14.811
V203	0.0	0.0	0.095	0.051	0.061	0.0	0.0	0.068	0.148	0.090
CR203	0.0	0.0	0.070	0.122	0.0	0.081	0.059	0.0	0.052	0.0
FEO	16.061	13.822	20.906	18.790	21.001	17.814	16.515	18.374	21.261	21.559
MNO	0.279	0.069	0.223	0.268	0.221	0.247	0.229	0.238	0.257	0.260
COO	0.0	0.0	0.0	0.0	0.0	0.0	0.054	0.0	0.0	0.0
NIO	0.0	0.0	0.105	0.071	0.0	0.097	0.083	0.069	0.067	0.0
ZNO	0.064	0.0	0.100	0.177	0.0	0.142	0.079	0.114	0.206	0.041
BAO	0.0	0.0	0.0	0.0	0.0	0.194	0.0	0.0	0.0	0.0
MGO	10.229	10.675	6.675	7.670	6.649	9.446	8.035	8.397	6.180	5.695
CAO	11.646	10.533	11.318	11.612	10.857	11.253	12.390	11.722	11.294	11.316
NA2O	1.360	2.237	1.218	1.008	1.062	0.846	1.166	0.887	1.149	1.321
K2O	0.122	0.115	0.330	0.384	0.303	0.165	0.388	0.384	0.492	0.416
TOTAL 1	97.900	97.900	97.900	97.900	97.900	97.900	97.900	97.900	97.900	97.900
TOTAL 2	97.799	98.865	97.487	98.581	95.042	95.389	97.031	97.637	97.019	97.191

TABLE 25. CONT'D...

MINERAL NO	516. HORN	517. HORN	522. HORN	531. HORN	531. HORN	532. HORN	534. HORN	535. HORN	537. HORN	538. HORN
STRUCTURAL FORMULAE										
SI 4+	6.563	6.594	6.533	6.488	6.588	6.462	7.110	6.368	7.082	6.975
AL IV	1.437	1.406	1.467	1.512	1.412	1.538	0.890	1.632	0.918	1.025
SUM OF Z	8.000	8.000	8.000	8.000	8.000	8.000	8.000	8.000	8.000	8.000
AL VI	0.980	0.957	1.053	1.059	1.101	1.063	0.816	0.948	0.652	0.629
TI 4+	0.043	0.064	0.032	0.045	0.042	0.038	0.025	0.041	0.017	0.018
V 3+	0.007	0.012	0.009	0.012	0.0	0.008	0.0	0.010	0.006	0.0
CR 3+	0.006	0.010	0.012	0.0	0.0	0.0	0.007	0.0	0.012	0.041
FE 2+	2.071	2.006	1.646	2.082	1.867	2.126	1.897	2.435	1.713	1.525
MN	0.023	0.029	0.024	0.032	0.021	0.028	0.029	0.023	0.023	0.019
CO	0.0	0.012	0.009	0.0	0.0	0.0	0.0	0.0	0.0	0.0
NI	0.0	0.014	0.007	0.0	0.0	0.010	0.0	0.0	0.0	0.010
ZN	0.005	0.023	0.009	0.0	0.0	0.0	0.005	0.0	0.0	0.0
MG	1.967	1.983	1.828	1.929	2.053	1.833	2.303	2.001	2.667	2.831
SUM OF Y	5.102	5.110	4.829	5.159	5.084	5.106	5.082	5.458	5.090	5.073
BA	0.0	0.0	0.0	0.0	0.0	0.0	0.0	0.0	0.0	0.002
CA	1.824	1.843	2.084	1.793	1.773	1.860	1.791	1.604	1.887	1.892
NA	0.435	0.314	0.277	0.407	0.464	0.405	0.251	0.412	0.220	0.340
K	0.070	0.078	0.023	0.045	0.049	0.054	0.020	0.058	0.040	0.046
SUM OF X+A	2.329	2.235	2.300	2.245	2.286	2.319	2.062	2.074	2.147	2.270
NO OF ANIONS	23	23	23	23	23	23	23	23	23	23
WEIGHT PERCENT OXIDES										
SIO2	44.312	44.579	44.818	43.858	44.973	43.533	48.777	42.531	48.722	48.106
TIO2	0.387	0.579	0.296	0.402	0.384	0.341	0.225	0.362	0.151	0.161
AL2O3	13.847	13.552	15.828	14.744	14.552	14.863	9.927	14.616	9.166	9.680
V2O3	0.063	0.100	0.080	0.099	0.0	0.065	0.0	0.087	0.054	0.0
CR2O3	0.051	0.086	0.105	0.0	0.0	0.0	0.061	0.0	0.107	0.359
FEO	16.721	16.212	13.501	16.827	15.232	17.120	15.560	19.438	14.090	12.576
MNO	0.182	0.232	0.193	0.254	0.166	0.224	0.237	0.182	0.188	0.156
COO	0.0	0.103	0.080	0.0	0.0	0.0	0.0	0.0	0.0	0.0
NIO	0.0	0.114	0.057	0.0	0.0	0.083	0.0	0.0	0.0	0.0
ZNO	0.042	0.211	0.085	0.0	0.0	0.0	0.050	0.0	0.0	0.089
BAO	0.0	0.0	0.0	0.0	0.0	0.0	0.0	0.0	0.0	0.0
MGO	8.913	8.994	8.414	8.748	9.404	8.287	10.598	8.965	12.311	0.036
CAO	11.498	11.629	13.341	11.311	11.293	11.691	11.469	9.997	12.114	13.101
NA2O	1.517	1.096	0.981	1.420	1.635	1.408	0.889	1.418	0.779	12.180
K2O	0.369	0.413	0.122	0.237	0.261	0.284	0.106	0.304	0.217	1.210
TOTAL 1	97.900	97.900	97.900	97.900	97.900	97.900	97.900	97.900	97.900	97.900
TOTAL 2	95.881	96.250	97.013	97.937	98.225	97.549	96.609	95.957	96.180	96.555

TABLE 25. CONT'D...

MINERAL NO	540. HORN	541. HORN	543. HORN	544. HORN	545. HORN	546. HORN	547. HORN	548. HORN
STRUCTURAL FORMULAE								
SI 4+	6.799	7.441	7.191	6.422	6.643	6.604	6.579	6.614
AL IV	1.201	0.559	0.809	1.578	1.357	1.396	1.421	1.386
SUM OF Z	8.000	8.000	8.000	8.000	8.000	8.000	8.000	8.000
AL VI	0.783	0.325	0.544	1.075	0.958	0.968	0.940	0.979
TI 4+	0.024	0.010	0.019	0.079	0.031	0.054	0.029	0.037
V 3+	0.011	0.005	0.009	0.007	0.008	0.009	0.011	0.006
CR 3+	0.005	0.044	0.017	0.007	0.007	0.009	0.012	0.036
FE 2+	2.042	1.300	1.529	2.156	2.016	2.068	2.503	1.407
MN	0.027	0.024	0.022	0.027	0.024	0.021	0.026	0.018
CO	0.0	0.0	0.0	0.0	0.008	0.0	0.0	0.0
NI	0.0	0.009	0.012	0.011	0.0	0.007	0.005	0.008
ZN	0.0	0.0	0.0	0.006	0.0	0.0	0.0	0.0
MG	2.255	3.382	2.997	1.760	2.081	1.966	1.609	2.585
SUM OF Y	5.147	5.099	5.149	5.128	5.133	5.122	5.135	5.076
CA	1.856	1.924	1.804	1.830	1.827	1.811	1.848	1.883
NA	0.321	0.103	0.257	0.387	0.342	0.381	0.355	0.301
K	0.029	0.015	0.039	0.028	0.060	0.054	0.081	0.072
SUM OF X+A	2.206	2.042	2.100	2.245	2.229	2.246	2.284	2.256
NO OF ANIONS	23	23	23	23	23	23	23	23
WEIGHT PERCENT OXIDES								
SIO2	46.097	52.069	49.842	43.245	45.037	44.680	43.729	45.792
TIO2	0.214	0.097	0.176	0.710	0.277	0.487	0.254	0.340
AL2O3	11.409	5.249	7.954	15.158	13.314	13.568	13.314	13.895
V2O3	0.089	0.048	0.078	0.059	0.067	0.080	0.095	0.048
CR2O3	0.047	0.385	0.148	0.057	0.060	0.075	0.098	0.317
FEO	16.551	10.879	12.674	17.360	16.341	16.725	19.885	11.646
MNO	0.216	0.196	0.176	0.215	0.191	0.165	0.203	0.151
COO	0.0	0.0	0.0	0.0	0.070	0.0	0.0	0.0
NIO	0.0	0.078	0.106	0.096	0.0	0.056	0.043	0.072
ZNO	0.0	0.0	0.0	0.055	0.0	0.0	0.0	0.0
MGO	10.256	15.878	13.939	7.953	9.464	9.016	7.176	12.009
CAO	11.742	12.566	11.674	11.500	11.564	11.433	11.463	12.167
NA2O	1.122	0.370	0.919	1.345	1.194	1.329	1.218	1.075
K2O	0.156	0.085	0.214	0.148	0.319	0.286	0.421	0.389
TOTAL 1	97.900	97.900	97.900	97.900	97.900	97.900	97.900	97.900
TOTAL 2	91.728	96.184	95.512	97.520	97.122	97.289	98.261	96.531

TABLE 26. EPIDOTES.

MINERAL NO	051. EP	181. EP	308. EP	496. EP	498. EP	499. EP	501. EP	503. EP	504. EP	509. EP
STRUCTURAL FORMULAE										
SI 4+	5.950	5.985	6.139	6.099	5.967	5.954	6.027	5.998	6.028	6.031
AL IV	4.050	4.015	4.000	4.000	4.033	4.046	4.000	4.002	4.004	4.000
SUM OF Z	10.000	10.000	10.139	10.099	10.000	10.000	10.027	10.000	10.028	10.031
TI 4+	0.0	0.008	0.008	0.0	0.0	0.014	0.0	0.0	0.011	0.009
FE 3+	0.628	0.649	0.784	1.299	0.932	1.134	1.025	0.755	1.082	1.178
V 3+	0.011	0.025	0.013	0.046	0.029	0.052	0.026	0.026	0.033	0.009
SUM OF Y	2.011	2.017	1.966	1.934	2.000	2.008	2.000	2.000	1.995	2.000
FE 2+	0.018	0.012	0.0	0.0	0.049	0.0	0.014	0.041	0.0	0.021
MN	0.006	0.0	0.0	0.0	0.008	0.005	0.012	0.017	0.005	0.0
CO	0.0	0.0	0.0	0.0	0.0	0.0	0.0	0.0	0.012	0.0
ZN	0.006	0.008	0.006	0.0	0.0	0.0	0.012	0.0	0.012	0.022
BA	0.0	0.0	0.0	0.0	0.0	0.0	0.006	0.0	0.0	0.0
CA	3.970	3.980	3.752	3.900	3.937	3.999	3.896	3.923	3.898	3.879
SUM OF X	4.000	4.000	3.758	3.900	3.994	4.004	3.940	3.981	3.927	3.922
NO OF ANIONS	25	25	25	25	25	25	25	25	25	25
PS	31	32	40	67	47	56	51	38	54	59
WEIGHT PERCENT OXIDES										
SIO2	38.532	38.730	39.862	38.795	38.259	37.905	38.560	38.691	38.536	38.467
TIO2	0.0	0.073	0.071	0.0	0.0	0.120	0.0	0.0	0.097	0.077
AL2O3	29.718	29.202	28.417	24.689	27.508	26.130	26.714	28.477	26.372	25.911
FE2O3	5.564	5.689	6.764	10.984	8.360	9.596	8.836	6.824	9.198	10.169
V2O3	0.092	0.205	0.106	0.369	0.232	0.415	0.208	0.206	0.266	0.074
CR2O3	0.107	0.092	0.090	0.111	0.120	0.128	0.224	0.150	0.140	0.119
MNO	0.042	0.0	0.0	0.0	0.058	0.041	0.093	0.131	0.040	0.0
ZNO	0.051	0.073	0.051	0.0	0.0	0.0	0.101	0.0	0.103	0.191
BAO	0.0	0.0	0.0	0.0	0.0	0.0	0.098	0.0	0.0	0.0
CAO	23.994	24.037	22.740	23.152	23.564	23.765	23.266	23.622	23.255	23.093
TOTAL 1	98.100	98.100	98.100	98.100	98.100	98.100	98.100	98.100	98.100	98.100
TOTAL 2	98.954	99.256	98.997	99.436	98.367	99.711	97.942	98.776	98.291	97.645

TABLE 26.. CONT'D...

MINERAL NO	517. EP	522. EP	532. EP	534. EP	536. EP	537. EP	538. EP	540. EP	541. EP	544. EP
STRUCTURAL FORMULAE										
SI 4+	6.183	6.067	5.990	5.957	6.176	5.960	5.941	5.971	5.967	5.989
AL IV	4.000	4.000	4.010	4.043	4.000	4.040	4.059	4.029	4.033	4.011
SUM OF Z	10.183	10.067	10.000	10.000	10.041	10.000	10.000	10.000	10.000	10.000
AL VI	0.655	1.041	1.165	0.718	1.041	1.204	1.078	1.182	1.165	0.943
TI 4+	0.0	0.0	0.0	0.009	0.0	0.0	0.0	0.0	0.008	0.009
FE 3+	1.119	0.811	0.880	1.229	0.931	0.773	0.877	0.797	0.715	1.002
V 3+	0.068	0.041	0.029	0.031	0.019	0.012	0.026	0.012	0.025	0.030
CR 3+	0.013	0.045	0.010	0.013	0.008	0.011	0.038	0.009	0.087	0.016
SUM OF Y	1.855	1.938	2.000	2.000	2.000	2.000	2.019	2.000	2.000	2.000
FE 2+	0.0	0.0	0.0	0.088	0.005	0.053	0.0	0.086	0.035	0.055
MN	0.011	0.0	0.0	0.0	0.0	0.0	0.0	0.0	0.0	0.016
NI	0.0	0.012	0.0	0.0	0.0	0.0	0.005	0.008	0.0	0.008
ZN	0.005	0.011	0.0	0.0	0.0	0.0	0.0	0.0	0.0	0.0
BA	0.0	0.013	0.0	0.0	0.006	0.0	0.007	0.004	0.0	0.0
CA	3.834	3.923	3.880	3.886	3.738	3.941	3.989	3.871	3.960	3.894
NA	0.0	0.0	0.0	0.0	0.123	0.0	0.0	0.0	0.0	0.0
SUM OF X	3.850	3.959	3.964	3.974	3.909	3.994	4.001	3.969	3.995	3.973
NO OF ANIONS	25	25	25	25	25	25	25	25	25	25
PS	60	41	44	61	47	39	43	40	36	50
WEIGHT PERCENT OXIDES										
SIO2	39.594	39.021	38.605	37.848	39.907	38.431	38.108	38.468	38.454	38.322
TIO2	0.0	0.0	0.0	0.073	0.0	0.0	0.0	0.0	0.068	0.076
AL2O3	25.291	27.504	28.300	25.664	27.307	28.686	27.957	28.484	28.423	26.891
FE2O3	9.527	6.934	7.537	11.127	7.615	7.084	7.476	7.566	6.422	8.993
V2O3	0.545	0.326	0.232	0.243	0.157	0.094	0.209	0.099	0.200	0.240
CR2O3	0.109	0.368	0.083	0.105	0.064	0.087	0.307	0.072	0.711	0.133
MNO	0.082	0.0	0.0	0.0	0.0	0.0	0.0	0.0	0.0	0.124
NIO	0.0	0.099	0.0	0.0	0.0	0.0	0.041	0.066	0.0	0.067
ZNO	0.041	0.098	0.0	0.0	0.0	0.0	0.0	0.0	0.0	0.0
BAO	0.0	0.205	0.0	0.0	0.097	0.0	0.116	0.065	0.0	0.0
CAO	22.913	23.546	23.343	23.041	22.542	23.719	23.835	23.279	23.822	23.255
NA2O	0.0	0.0	0.0	0.0	0.410	0.0	0.0	0.0	0.0	0.0
TOTAL 1	98.100	98.100	98.100	98.100	98.100	98.100	98.100	98.100	98.100	98.100
TOTAL 2	97.775	98.687	98.837	98.780	98.312	98.664	97.963	87.112	98.169	99.349

TABLE 26. CONT'D...

MINERAL NO	547. EP	548. EP	308. ZOIS	499. ZOIS	538. ZOIS
STRUCTURAL FORMULAE					
SI 4+	5.976	6.142	5.995	5.968	5.949
AL IV	4.024	4.000	4.005	4.032	4.051
SUM OF Z	10.000	10.142	10.000	10.000	10.000
AL VI	0.631	1.643	1.245	0.523	1.006
TI 4+	0.0	0.008	0.0	0.010	0.0
FE 3+	1.292	0.235	0.719	1.445	0.951
V 3+	0.061	0.023	0.024	0.022	0.035
CR 3+	0.016	0.013	0.012	0.0	0.008
SUM OF Y	2.000	1.914	2.000	2.000	2.000
FE 2+	0.034	0.0	0.052	0.021	0.054
MN	0.007	0.0	0.006	0.005	0.0
CO	0.006	0.0	0.0	0.0	0.0
NI	0.008	0.0	0.006	0.0	0.0
ZN	0.0	0.0	0.0	0.005	0.0
BA	0.006	0.0	0.008	0.0	0.0
CA	3.934	3.828	3.904	3.968	3.946
SUM OF X	3.995	3.828	3.924	3.978	4.000
NO OF ANIONS	25	25	25	25	25
PS	65	12	36	72	48
WEIGHT PERCENT OXIDES					
SIO2	37.831	40.519	38.697	37.676	38.113
TIO2	0.0	0.068	0.0	0.085	0.0
AL2O3	24.998	31.581	28.749	24.394	27.486
FE2O3	11.157	2.065	6.617	12.304	8.563
V2O3	0.480	0.186	0.191	0.177	0.281
CR2O3	0.132	0.111	0.101	0.0	0.061
MNO	0.056	0.0	0.047	0.039	0.0
COO	0.048	0.0	0.0	0.0	0.0
NIO	0.066	0.0	0.046	0.0	0.0
ZNO	0.0	0.0	0.0	0.045	0.0
BAO	0.089	0.0	0.133	0.0	0.0
CAO	23.242	23.571	23.519	23.378	23.596
TOTAL 1	98.100	98.100	98.100	98.100	98.100
TOTAL 2	100.312	98.639	99.563	99.704	98.150

TABLE 17. GARNETS.

MINERAL NO	035. GRNA CORE	035. GRNA EDGE	049. GRNA EDGE	064. GRNA CORE	106. GRNA EDGE	121. GRNA EDGE	122. GRNA EDGE	122. GRNA CORE	135. GRNA EDGE	135. GRNA CORE
STRUCTURAL FORMULAE										
SI 4+	5.964	5.970	6.017	6.032	6.054	6.014	5.998	6.002	6.012	6.052
AL IV	0.036	0.030	0.0	0.0	0.0	0.0	0.022	0.0	0.0	0.0
SUM OF Z	6.000	6.000	6.017	6.032	6.054	6.014	6.000	6.002	6.012	6.052
AL VI	4.035	4.058	3.930	3.917	3.978	3.911	4.022	4.017	4.023	3.978
TI 4+	0.0	0.0	0.0	0.0	0.008	0.0	0.0	0.0	0.0	0.0
FE 3+	0.0	0.0	0.070	0.061	0.0	0.089	0.0	0.0	0.0	0.0
CR 3+	0.0	0.0	0.0	0.0	0.007	0.0	0.0	0.0	0.0	0.0
SUM OF Y	4.035	4.058	4.000	4.000	3.993	4.000	4.020	4.017	4.023	3.978
FE 2+	4.520	4.532	3.939	3.507	3.762	3.615	4.156	3.766	3.129	2.635
MN	0.375	0.436	0.967	0.957	0.714	1.109	0.543	1.124	1.045	1.457
NI	0.021	0.012	0.011	0.013	0.013	0.016	0.006	0.014	0.0	0.005
ZN	0.0	0.0	0.005	0.020	0.023	0.0	0.0	0.0	0.0	0.0
BA	0.0	0.0	0.0	0.0	0.0	0.0	0.0	0.0	0.0	0.004
MG	0.735	0.660	0.283	0.122	0.044	0.197	0.070	0.056	0.153	0.061
CA	0.315	0.287	0.796	1.381	1.342	1.078	1.196	1.009	1.615	1.765
SUM OF X	5.966	5.927	6.001	6.000	5.892	6.015	5.971	5.969	5.942	5.941
NO OF ANIONS		24	24	24	24	24	24	24	24	24
WEIGHT PERCENT OXIDES										
SIO2	37.095	37.089	37.055	37.313	37.563	37.061	37.045	36.965	37.553	37.819
TIO2	0.0	0.0	0.0	0.0	0.066	0.0	0.0	0.0	0.0	0.0
AL2O3	21.482	21.543	20.532	20.560	20.939	20.447	21.074	20.989	21.315	21.089
CR2O3	0.0	0.0	0.0	0.0	0.054	0.0	0.0	0.0	0.0	0.0
FEO	33.608	33.657	29.512	26.389	27.905	27.283	30.690	27.729	23.365	19.684
MNO	2.756	3.200	7.027	6.988	5.229	8.068	3.960	8.173	7.707	10.751
NIO	0.161	0.095	0.085	0.103	0.098	0.125	0.046	0.110	0.0	0.039
ZNO	0.0	0.0	0.045	0.160	0.194	0.0	0.0	0.0	0.0	0.0
BAO	0.0	0.0	0.0	0.0	0.0	0.0	0.0	0.0	0.0	0.069
MGO	3.069	2.751	1.171	0.505	0.183	0.814	0.290	0.231	0.640	0.258
CAO	1.830	1.664	4.572	7.975	7.769	6.201	6.896	5.803	9.416	10.293
TOTAL 1	100.000	100.000	100.000	100.000	100.000	100.000	100.000	100.000	100.000	100.000
TOTAL 2	102.629	102.995	99.408	100.199	100.371	99.987	102.437	102.827	102.401	102.265

TABLE 27. CONT'D...

MINERAL NO	495. GRNA EDGE	495. GRNA CORE	528. GRNA EDGE	528. GRNA CORE	550. GRNA CORE	550. GRNA EDGE	551. GRNA EDGE	551. GRNA EDGE	552. GRNA EDGE	553. GRNA EDGE
STRUCTURAL FORMULAE										
SI 4+	5.966	5.964	5.997	5.997	5.981	5.981	6.020	6.029	6.035	6.024
AL IV	0.034	0.036	0.003	0.003	0.019	0.019	0.0	0.0	0.0	0.0
SUM OF Z	6.000	6.000	6.000	6.000	6.000	6.000	6.020	6.029	6.035	6.024
AL VI	4.072	4.008	4.005	4.030	4.026	4.042	4.028	3.914	3.985	3.965
FE 3+	0.0	0.0	0.0	0.0	0.0	0.0	0.0	0.070	0.0	0.0
CR 3+	0.0	0.0	0.0	0.0	0.007	0.0	0.0	0.0	0.013	0.006
SUM OF Y	4.072	4.008	4.005	4.030	4.033	4.042	4.028	3.984	3.998	6.001
FE 2+	4.523	4.559	3.944	3.848	3.724	4.389	4.640	4.661	4.330	4.500
MN	0.014	0.041	1.108	1.044	0.703	0.081	0.113	0.115	0.202	0.282
NI	0.0	0.006	0.018	0.014	0.011	0.0	0.006	0.015	0.015	0.010
ZN	0.0	0.0	0.025	0.0	0.010	0.0	0.010	0.016	0.019	0.015
BA	0.0	0.0	0.0	0.0	0.0	0.0	0.0	0.0	0.006	0.003
MG	0.712	0.551	0.188	0.160	0.0	0.103	0.870	0.917	0.344	0.0
CA	0.660	0.849	0.710	0.890	1.513	1.374	0.278	0.276	1.016	1.185
SUM OF X	5.909	6.006	5.993	5.956	5.961	5.947	5.917	6.000	5.932	5.995
NO OF ANIONS	24	24	24	24	24	24	24	24	24	24
WEIGHT PERCENT OXIDES										
SIO2	37.367	37.126	36.870	36.999	37.051	37.100	37.668	37.553	37.517	37.064
AL2O3	21.817	21.360	20.904	21.113	21.258	21.373	21.382	20.685	21.019	20.696
CR2O3	0.0	0.0	0.0	0.0	0.053	0.0	0.0	0.0	0.101	0.050
FEO	33.862	33.931	28.988	28.381	27.576	32.550	34.707	35.227	32.175	33.100
MNO	0.103	0.301	8.039	7.608	5.143	0.595	0.837	0.847	1.485	2.046
NIO	0.0	0.048	0.134	0.107	0.085	0.0	0.044	0.115	0.117	0.074
ZNO	0.0	0.0	0.212	0.0	0.085	0.0	0.083	0.134	0.160	0.122
BAO	0.0	0.0	0.0	0.0	0.0	0.0	0.0	0.0	0.101	0.040
MGO	2.994	2.301	0.777	0.664	0.0	0.428	3.653	3.833	1.434	0.0
CAO	3.857	4.933	4.076	5.127	8.749	7.953	1.626	1.606	5.892	6.807
TOTAL 1	100.000	100.000	100.000	100.000	100.000	100.000	100.000	100.000	100.000	100.000
TOTAL 2	102.506	102.950	103.441	103.107	102.022	102.187	100.262	102.072	99.894	99.697

TABLE 27. CONT'D...

MINERAL NO	152. GRNA EDGE	162. GRNA EDGE	171. GRNA EDGE	246. GRNA CORE	250. GRNA CORE	250. GRNA EDGE	263. GRNA EDGE	263. GRNA CORE	278. GRNA EDGE	351. GRNA EDGE
STRUCTURAL FORMULAE										
SI 4+	5.993	6.029	6.020	6.020	6.000	6.008	5.987	6.006	6.018	5.976
AL IV	0.007	0.0	0.0	0.0	0.0	0.0	0.013	0.0	0.0	0.024
SUM OF Z	6.000	6.029	6.020	6.020	6.000	6.008	6.000	6.006	6.018	6.000
AL VI	4.029	3.905	3.940	3.995	4.001	4.028	4.008	3.981	3.930	4.032
TI 4+	0.0	0.0	0.0	0.012	0.013	0.0	0.0	0.016	0.0	0.0
FE 3+	0.0	0.083	0.050	0.0	0.0	0.0	0.0	0.0	0.069	0.0
V 3+	0.0	0.0	0.0	0.0	0.0	0.0	0.0	0.007	0.0	0.0
CR 3+	0.0	0.0	0.0	0.0	0.0	0.006	0.0	0.0	0.0	0.0
SUM OF Y	4.029	3.988	3.990	4.007	4.014	4.034	4.008	4.004	3.999	4.032
FE 2+	3.131	2.653	1.597	2.137	2.166	2.919	3.758	2.946	3.511	4.158
MN	2.027	1.443	3.748	2.719	1.800	1.139	0.994	1.450	1.129	0.286
CO	0.0	0.0	0.008	0.012	0.014	0.0	0.0	0.0	0.0	0.0
NI	0.019	0.013	0.011	0.031	0.021	0.015	0.016	0.018	0.016	0.012
ZN	0.006	0.006	0.0	0.0	0.006	0.0	0.013	0.007	0.009	0.008
BA	0.004	0.0	0.0	0.0	0.0	0.0	0.0	0.0	0.0	0.0
MG	0.091	0.083	0.055	0.0	0.0	0.088	0.082	0.0	0.218	0.450
CA	0.681	1.802	0.581	1.044	1.963	1.772	1.152	1.554	1.117	1.051
SUM OF X	5.959	6.000	6.000	5.943	5.970	5.933	6.010	5.975	6.000	5.965
NO OF ANIONS	24	24	24	24	24	24	24	24	24	24
WEIGHT PERCENT OXIDES										
SIO2	36.782	37.495	36.796	37.120	37.473	37.555	36.912	37.234	37.182	37.270
TIO2	0.0	0.0	0.0	0.100	0.112	0.0	0.0	0.130	0.0	0.0
AL2O3	21.016	20.605	20.431	20.898	21.198	21.358	20.966	20.939	20.600	21.462
V2O3	0.0	0.0	0.0	0.0	0.0	0.0	0.0	0.055	0.0	0.0
CR2O3	0.0	0.0	0.0	0.0	0.0	0.045	0.0	0.0	0.0	0.0
FEO	22.973	20.342	12.039	15.753	16.174	21.814	27.698	21.839	26.443	30.999
MNO	14.688	10.597	27.045	19.790	13.271	8.406	7.233	10.616	8.234	2.109
COO	0.0	0.0	0.061	0.091	0.110	0.0	0.0	0.0	0.0	0.0
NIO	0.147	0.102	0.087	0.240	0.166	0.117	0.120	0.137	0.121	0.090
ZNO	0.053	0.054	0.0	0.0	0.053	0.0	0.106	0.058	0.078	0.065
BAO	0.064	0.0	0.0	0.0	0.0	0.0	0.0	0.0	0.0	0.0
MGO	0.374	0.347	0.227	0.0	0.0	0.369	0.338	0.0	0.903	1.885
CAO	3.903	10.458	3.314	6.007	11.443	10.336	6.626	8.992	6.439	6.119
TOTAL 1	100.000	100.000	100.000	100.000	100.000	100.000	100.000	100.000	100.000	100.000
TOTAL 2	102.845	99.873	101.352	101.700	101.240	101.410	102.522	102.321	100.115	103.197

TABLE 27. CONT'D...

MINERAL NO	351. GRNA CORE	371. GRNA EDGE	371. GRNA CORE	391. GRNA EDGE	391. GRNA EDGE	402. GRNA EDGE	402. GRNA CORE	494. GRNA CORE	494. GRNA EDGE	495. GRNA EDGE
STRUCTURAL FORMULAE										
SI 4+	5.950	5.977	5.947	6.036	5.998	5.986	5.970	5.976	5.972	5.926
AL IV	0.050	0.023	0.054	0.0	0.002	0.014	0.030	0.024	0.028	0.074
SUM OF Z	6.000	6.000	6.000	6.036	6.000	6.000	6.000	6.000	6.000	6.000
AL VI	3.990	3.989	4.000	3.991	3.929	4.022	4.017	4.027	4.021	3.98
FE 3+	0.010	0.011	0.0	0.0	0.071	0.0	0.0	0.0	0.0	0.011
CR 3+	0.0	0.0	0.0	0.0	0.0	0.0	0.0	0.0	0.006	0.0
SUM OF Y	4.000	4.000	4.000	3.991	4.000	4.022	4.017	4.027	4.027	4.000
FE 2+	4.011	4.001	4.067	4.281	4.270	4.369	4.347	4.534	4.528	4.532
MN	0.426	0.067	0.217	0.356	0.560	0.014	0.085	0.013	0.0	0.015
CO	0.0	0.0	0.0	0.0	0.0	0.0	0.0	0.010	0.0	0.006
NI	0.013	0.0	0.0	0.009	0.017	0.008	0.008	0.014	0.019	0.019
CU	0.0	0.0	0.0	0.0	0.0	0.0	0.0	0.0	0.0	0.046
ZN	0.007	0.0	0.0	0.005	0.0	0.0	0.0	0.005	0.017	0.007
BA	0.0	0.0	0.0	0.0	0.0	0.003	0.0	0.0	0.0	0.0
MG	0.372	0.153	0.133	0.950	0.853	0.371	0.220	0.628	0.735	0.727
CA	1.199	1.795	1.487	0.341	0.337	1.209	1.331	0.767	0.675	0.684
SUM OF X	6.028	6.016	6.029	5.942	6.037	5.924	5.991	5.971	5.974	6.038
NO OF ANIONS	24	24	24	24	24	24	24	24	24	24
WEIGHT PERCENT OXIDES										
SIO2	36.996	37.278	36.791	37.881	37.271	37.304	37.078	37.299	37.328	36.900
ZRO2	0.0	0.0	1.569[1]	0.0	0.0	0.0	0.0	0.0	0.0	0.0
AL2O3	21.312	21.230	20.840	21.250	20.726	21.339	21.324	21.448	21.474	21.466
CR2O3	0.0	0.0	0.0	0.0	0.0	0.0	0.0	0.0	0.049	0.0
FEO	29.891	29.911	30.078	32.122	32.251	32.549	32.280	33.831	33.840	33.821
MNO	3.129	0.491	1.583	2.636	4.109	0.107	0.620	0.093	0.0	0.112
COO	0.0	0.0	0.0	0.0	0.0	0.0	0.0	0.080	0.0	0.059
NIO	0.102	0.0	0.0	0.069	0.131	0.066	0.065	0.109	0.144	0.145
CUO	0.0	0.0	0.0	0.0	0.0	0.0	0.0	0.0	0.0	0.379
ZNO	0.060	0.0	0.0	0.046	0.0	0.0	0.0	0.046	0.146	0.058
BAO	0.0	0.0	0.0	0.0	0.0	0.048	0.0	0.0	0.0	0.0
MGO	1.553	0.642	0.551	3.999	3.557	1.553	0.916	2.629	3.083	3.038
CAO	6.956	10.448	8.588	1.997	1.954	7.036	7.716	4.465	3.936	3.973
TOTAL 1	100.000	100.000	100.000	100.000	100.000	100.000	100.000	100.000	100.000	100.000
TOTAL 2	103.110	102.056	102.545	98.380	100.875	102.943	103.016	103.230	103.466	103.488

[1] STRUCTURAL FORMULA CORRECTED FOR ZIRCON CONTAMINATION

TABLE 27. CONT'D...

MINERAL NO	562. GRNA EDGE	564. GRNA EDGE	565. GRNA EDGE	567. GRNA EDGE	568. GRNA EDGE	569. GRNA EDGE	570. GRNA EDGE	571. GRNA EDGE	572. GRNA EDGE	573. GRNA EDGE	573. GRNA EDGE
STRUCTURAL FORMULAE											
SI 4+	6.034	6.061	6.075	6.052	6.030	6.072	6.031	6.046	6.102	5.990	5.968
AL IV	0.0	0.0	0.0	0.0	0.0	0.0	0.0	0.0	0.0	0.0	0.032
SUM OF Z	6.034	6.061	6.075	6.052	6.030	6.072	6.031	6.046	6.102	5.990	6.000
AL VI	3.983	3.937	3.934	3.983	3.948	3.935	3.956	3.944	3.900	3.936	3.967
TI 4+	0.0	0.0	0.014	0.007	0.008	0.0	0.0	0.008	0.0	0.0	0.0
FE 3+	0.0	0.0	0.0	0.0	0.0	0.0	0.005	0.0	0.0	0.057	0.026
V 3+	0.0	0.0	0.0	0.0	0.0	0.006	0.0	0.0	0.0	0.0	0.0
CR 3+	0.0	0.0	0.0	0.0	0.006	0.008	0.0	0.012	0.008	0.007	0.007
SUM OF Y	3.983	3.937	3.948	3.990	3.960	3.949	3.961	3.964	3.908	4.000	4.000
FE 2+	3.847	3.693	2.819	3.655	3.019	3.019	4.398	2.912	4.003	3.331	3.312
MN	0.115	1.592	2.207	0.983	1.271	1.225	0.885	1.405	0.245	0.054	0.116
CO	0.0	0.0	0.0	0.0	0.006	0.0	0.0	0.0	0.0	0.0	0.012
NI	0.0	0.008	0.007	0.010	0.015	0.011	0.008	0.013	0.014	0.007	0.0
ZN	0.013	0.011	0.006	0.007	0.014	0.016	0.0	0.014	0.019	0.0	0.007
BA	0.0	0.006	0.0	0.0	0.0	0.005	0.003	0.004	0.0	0.0	0.0
MG	0.963	0.0	0.0	0.048	0.0	0.0	0.0	0.0	0.050	1.842	1.738
CA	1.020	0.664	0.882	1.204	1.666	1.656	0.706	1.610	1.602	0.798	0.845
SUM OF X	5.958	5.974	5.921	5.907	5.991	5.932	6.000	5.958	5.933	6.032	6.030
NO OF ANIONS	24	24	24	24	24	24	24	24	24	24	24
WEIGHT PERCENT OXIDES											
SIO2	38.277	37.059	37.388	37.477	37.433	37.768	36.833	37.533	37.974	38.767	38.565
TIO2	0.0	0.0	0.117	0.057	0.066	0.0	0.0	0.067	0.0	0.0	0.0
AL2O3	21.439	20.422	20.541	20.925	20.794	20.765	20.498	20.772	20.593	21.667	21.922
V2O3	0.0	0.0	0.0	0.0	0.0	0.046	0.0	0.0	0.0	0.0	0.0
CR2O3	0.0	0.0	0.0	0.0	0.047	0.065	0.0	0.094	0.063	0.060	0.058
FEO	29.171	26.995	20.744	27.060	22.406	22.451	32.148	21.612	29.782	26.213	25.789
MNO	0.863	11.490	16.040	7.189	9.313	8.998	6.383	10.300	1.803	0.415	0.982
COO	0.0	0.0	0.0	0.0	0.050	0.0	0.0	0.0	0.0	0.0	0.096
NIO	0.0	0.062	0.057	0.079	0.119	0.088	0.058	0.104	0.111	0.059	0.0
ZNO	0.113	0.094	0.046	0.056	0.119	0.132	0.0	0.120	0.162	0.0	0.058
BAO	0.0	0.089	0.0	0.0	0.0	0.075	0.054	0.068	0.0	0.0	0.0
MGO	4.097	0.0	0.0	0.198	0.0	0.0	0.0	0.0	0.209	7.997	7.537
CAO	6.039	3.789	5.086	6.960	9.653	9.612	4.027	9.330	9.303	4.821	5.094
TOTAL 1	100.000	100.000	100.000	00.000	100.000	100.000	100.000	100.000	100.000	100.000	100.000
TOTAL 2	97.968	99.277	100.376	99.762	98.537	99.640	100.931	99.544	99.910	99.476	100.990

TABLE 27. CONT'D...

MINERAL NO	152. GRNA CORE	005. GRNA EDGE	010. GRNA EDGE	050. GRNA EDGE	087. GRNA EDGE	106. GRNA EDGE	119. GRNA EDGE	262. GRNA EGDE	338. GRNA EDGE	342. GRNA EDGE
STRUCTURAL FORMULAE										
SI 4+	6.015	6.028	6.008	5.995	6.002	5.997	6.032	5.988	5.993	6.017
AL IV	0.0	0.0	0.0	0.009	0.0	0.003	0.0	0.012	0.007	0.0
SUM OF Z	6.015	6.028	6.008	6.000	6.002	6.000	6.032	6.000	6.000	6.017
AL VI	4.019	4.009	4.031	4.039	4.013	4.028	4.016	4.019	4.018	4.023
TI 4+	0.0	0.006	0.0	0.0	0.0	0.0	0.0	0.0	0.0	0.0
SUM OF Y	4.019	4.015	4.031	4.039	4.013	4.028	4.016	4.019	4.018	4.023
FE 2+	3.292	4.247	4.303	4.225	3.994	3.567	3.948	3.797	3.984	4.449
MN	1.830	0.251	0.733	0.482	1.375	0.747	0.682	1.119	0.488	0.169
NI	0.015	0.0	0.0	0.0	0.0	0.0	0.0	0.0	0.0	0.0
ZN	0.005	0.0	0.0	0.0	0.0	0.0	0.0	0.0	0.0	0.0
BA	0.0	0.0	0.0	0.0	0.003	0.0	0.0	0.0	0.0	0.0
MG	0.084	0.231	0.523	0.502	0.055	0.323	0.375	0.190	0.514	0.568
CA	0.715	1.190	0.379	0.736	0.551	1.322	0.908	0.873	0.990	0.747
SUM OF X	5.941	5.919	5.938	5.945	5.978	5.959	5.913	5.978	5.976	5.933
NO OF ANIONS	24	24	24	24	24	24	24	24	24	24
WEIGHT PERCENT OXIDES										
SIO2	36.970	37.494	37.221	37.283	36.681	37.449	37.552	36.939	37.420	37.548
TIO2	0.0	0.049	0.0	0.0	0.0	0.0	0.0	0.0	0.0	0.0
AL2O3	20.954	21.156	21.187	21.373	20.808	21.354	21.212	21.096	21.324	21.298
FEO	24.185	31.585	31.865	31.432	29.179	26.631	29.385	28.002	29.736	33.186
MNO	13.280	1.843	5.361	3.540	9.919	5.508	5.011	8.148	3.596	1.243
NIO	0.116	0.0	0.0	0.0	0.0	0.0	0.0	0.0	0.0	0.0
ZNO	0.042	0.0	0.0	0.0	0.0	0.0	0.0	0.0	0.0	0.0
BAO	0.0	0.0	0.0	0.0	0.046	0.0	0.0	0.0	0.0	0.0
MGO	0.348	0.963	2.172	2.097	0.224	1.355	1.564	0.788	2.155	2.376
CAO	4.104	6.910	2.194	4.275	3.143	7.703	5.276	5.026	5.769	4.348
TOTAL 1	100.000	100.000	100.000	100.000	100.000	100.000	100.000	100.000	100.000	100.000
TOTAL 2	102.986	101.729	101.821	101.536	101.560	101.419	101.318	101.433	100.086	101.794

TABLE 27. CONT'D...

MINERAL NO	348. GRNA EDGE	358. GRNA EDGE	374. GRNA EDGE	444. GRNA EDGE	469. GRNA EDGE	469. GRNA EDGE	552. GRNA EDGE	092. GRNA EDGE
STRUCTURAL FORMULAE								
SI 4+	6.042	6.045	6.002	5.988	6.007	5.986	6.054	6.071
AL IV	0.0	0.0	0.0	0.012	0.0	0.014	0.0	0.0
SUM OF Z	6.042	6.045	6.002	6.000	6.007	6.000	6.054	6.071
AL VI	4.016	3.992	4.038	4.034	4.015	4.012	4.011	3.959
SUM OF Y	4.016	3.992	4.038	4.034	4.015	4.012	4.011	3.959
FE 2+	4.198	3.454	4.049	536	3.759	3.925	3.449	3.110
MN	0.743	0.708	0.505	0.429	0.454	0.345	1.454	1.780
BA	0.0	0.0	0.0	0.0	0.0	0.010	0.0	0.0
MG	0.629	0.234	0.595	0.537	0.753	0.682	0.168	0.082
CA	0.322	1.526	0.430	0.453	0.998	1.027	0.804	0.948
SUM OF X	5.892	5.922	5.939	5.955	5.964	5.989	5.975	5.920
NO OF ANIONS	24	24	24	24	24	24	24	24
WEIGHT PERCENT OXIDES								
SIO2	37.605	37.837	37.286	37.117	37.826	37.547	37.462	37.501
AL203	21.207	21.196	21.283	21.279	21.450	21.426	21.060	20.744
FEO	31.238	25.842	32.749	33.614	28.297	29.431	25.513	29.971
MNO	5.456	5.229	3.705	3.138	3.379	2.555	10.625	12.984
BAO	0.0	0.0	0.0	0.0	0.0	0.157	0.0	0.0
MGO	2.625	0.983	2.482	2.232	3.181	2.870	0.696	0.339
CAO	1.869	8.914	2.495	2.619	5.866	6.013	4.645	5.463
TOTAL 1	100.000	100.000	100.000	100.000	100.000	100.000	100.000	100.000
TOTAL 2	101.812	101.046	102.675	101.857	101.590	102.075	101.206	101.379

TABLE 28. ILMENITES.

MINERAL NO	023. ILM	043. ILM	376. ILM	380. ILM	499. ILM	504. ILM	509. ILM	517. ILM	531. ILM	534. ILM
STRUCTURAL FORMULAE										
TI 4+	2.004	1.997	1.999	1.995	1.969	2.012	2.008	1.995	2.036	2.065
V 3+	0.0	0.0	0.002	0.0	0.0	0.0	0.0	0.0	0.0	0.0
FE 2+	1.827	1.887	1.905	1.935	1.931	1.881	1.870	1.902	1.833	1.758
MN	0.123	0.064	0.075	0.020	0.079	0.076	0.073	0.065	0.057	0.082
CO	0.0	0.0	0.0	0.0	0.0	0.0	0.002	0.0	0.0	0.0
NI	0.0	0.0	0.0	0.0	0.004	0.003	0.004	0.006	0.0	0.0
ZN	0.0	0.009	0.003	0.003	0.014	0.016	0.016	0.017	0.0	0.003
MG	0.0	0.039	0.0	0.041	0.0	0.0	0.0	0.0	0.019	0.008
CA	0.015	0.008	0.008	0.004	0.007	0.0	0.004	0.003	0.005	0.007
SUM OF A	1.965	2.007	1.991	2.003	2.035	1.976	1.969	1.993	1.914	1.858
NO OF CATIONS	3.983	4.004	3.994	4.001	4.017	3.988	3.985	3.996	3.956	3.929
NO OF ANIONS	6	6	6	6	6	6	6	6	6	6
WEIGHT PERCENT OXIDES										
SIO2*	0.278	0.0	0.072	0.067	0.250	0.0	0.151	0.161	0.128	0.114
TIO2	53.064	52.768	52.731	52.766	51.707	53.109	53.059	52.593	54.261	55.301
V2O3	0.0	0.0	0.052	0.0	0.0	0.0	0.0	0.0	0.0	0.0
FEO	43.495	44.830	45.169	45.991	45.583	44.625	44.410	45.073	43.909	42.310
MNO	2.889	1.501	1.748	0.473	1.849	1.774	1.723	1.511	1.353	1.950
COO	0.0	0.0	0.0	0.0	0.0	0.0	0.059	0.0	0.0	0.0
NIO	0.0	0.0	0.0	0.0	0.103	0.070	0.097	0.153	0.0	0.0
ZNO	0.0	0.232	0.079	0.093	0.372	0.422	0.422	0.449	0.0	0.072
MGO	0.0	0.524	0.0	0.542	0.0	0.0	0.0	0.0	0.258	0.114
CAO	0.274	0.145	0.149	0.069	0.137	0.0	0.079	0.060	0.091	0.138
TOTAL 1	100.000	100.000	100.000	100.000	100.000	100.000	100.000	100.000	100.000	100.000
TOTAL 2	100.150	100.301	101.182	101.628	100.137	100.119	99.306	98.111	103.269	101.423

* EXCLUDED FROM STRUCTURAL FORMULAE CALCULATIONS

TABLE 28. CONT'D...

MINERAL NO	535. ILM	547. ILM
STRUCTURAL FORMULAE		
TI 4+	2.022	1.989
V 3+	0.004	0.0
FE 2+	1.854	1.936
MN	0.064	0.075
ZN	0.002	0.010
CA	0.003	0.002
SUM OF A	1.923	2.023
NO OF CATIONS	3.958	4.012
NO OF ANIONS	6	6
WEIGHT PERCENT OXIDES		
SIO2[1]	0.262	0.0
TIO2	53.714	52.238
V2O3	0.110	0.0
FEO	44.288	45.714
MNO	1.518	1.741
ZNO	0.060	0.263
CAO	0.048	0.043
TOTAL 1	100.000	100.000
TOTAL 2	101.892	100.696

[1] EXCLUDED FROM STRUCTURAL FORMULAE CALCULATIONS

TABLE 29. CARBONATES.

MINERAL NO	171. CARB	371. CARB	448. CARB	479. CARB	514. CARB	538. CARB	171. CC	181. CC	371. CC	448. CC
STRUCTURAL FORMULAE										
FE 2+	0.106	0.082	0.714	0.433	0.402	0.018	0.022	0.020	0.017	0.123
MN	0.349	0.013	0.048	0.011	0.082	0.010	0.159	0.015	0.013	0.111
CO	0.0	0.0	0.0	0.0	0.0	0.0	0.002	0.0	0.0	0.0
NI	0.002	0.004	0.0	0.002	0.0	0.002	0.005	0.004	0.005	0.002
ZN	0.0	0.0	0.0	0.003	0.0	0.0	0.002	0.003	0.0	0.0
MG	0.098	0.020	0.187	0.559	0.463	0.020	0.004	0.021	0.008	0.003
CA	1.423	1.871	1.039	0.977	1.021	1.944	1.791	1.892	1.956	1.566
SUM OF A	1.978	1.990	1.988	1.985	1.988	1.994	1.985	1.955	1.999	1.805
C	2.000	2.000	2.000	2.000	2.000	2.000	2.000	2.004	2.000	2.000
NO OF ANIONS	6	6	6	6	6	6	6	6	6	6
WEIGHT PERCENT OXIDES										
SIO2	0.314	0.156	0.161	0.234	0.475	0.105	0.230	0.503	0.0	2.966
FEO	3.713	2.916	24.558	15.718	14.479	0.630	0.766	0.727	0.619	4.437
MNO	12.078	0.475	1.635	0.387	2.918	0.366	5.570	0.549	0.460	3.949
COO	0.0	0.0	0.0	0.0	0.0	0.0	0.076	0.0	0.0	0.0
NIO	0.082	0.160	0.0	0.058	0.0	0.060	0.185	0.146	0.202	0.089
ZNO	0.0	0.0	0.0	0.105	0.0	0.0	0.065	0.109	0.0	0.0
MGO	1.932	0.397	3.614	11.382	9.341	0.394	0.082	0.431	0.168	0.052
CAO	38.944	52.145	27.895	27.670	28.695	54.472	49.579	53.233	54.680	44.202
CO2	42.938	43.751	42.137	44.446	44.091	43.974	43.445	44.249	43.872	44.305
TOTAL T	100.000	100.000	100.000	100.000	100.000	100.000	100.000	100.000	100.000	100.000

TABLE 29. CONT'D...

MINERAL NO	479.	514.	538.
	CC	CC	CC
STRUCTURAL FORMULAE			
FE 2+	0.085	0.105	0.004
MN	0.008	0.049	0.013
NI	0.003	0.003	0.003
MG	0.050	0.075	0.005
CA	1.834	1.741	1.972
SUM OF A	1.980	1.973	1.997
C	2.000	2.000	2.000
NO OF ANIONS	6	6	6
WEIGHT PERCENT OXIDES			
SIO2	0.304	0.403	0.0
FEO	3.043	3.772	0.159
MNO	0.297	1.745	0.447
NIO	0.128	0.101	0.119
MGO	0.997	1.502	0.101
CAO	51.310	48.632	55.189
CO2	43.920	43.846	43.916
TOTAL 1	100.000	100.000	100.000

TABLE 30 . MISCELLANEOUS MINERALS.

MINERAL NO	479. MUSC	479. PARG	300. SERP	300. KAER	300. CPI	300. OL	300. SPIN	300. SPIN	573. SPIN	380. ANTH
STRUCTURAL FORMULAE										
SI 4+	6.405	6.054	1.809	6.376	1.920	1.012	-----	-----	-----	6.008
AL IV	1.595	1.946	-----	1.624	0.080	-----	4.073	15.377	15.659	1.992
SUM OF Z	8.000	8.000	-----	8.000	2.000	-----	-----	-----	-----	8.000
AL VI	4.027	3.944	-----	0.070	0.048	-----	-----	-----	-----	1.307
TI 4+	0.033	0.010	0.0	0.513	0.007	0.0	0.650	0.0	0.0	0.016
FE 3+	0.0	0.0	0.0	0.0	0.0	0.0	3.688	0.0	0.348	0.0
V 3+	0.045	0.008	0.0	0.019	0.0	0.0	0.094	0.0	0.025	0.0
CR 3+	0.013	0.0	0.0	0.143	0.042	0.0	7.443	0.685	0.010	0.0
SUM OF B	-----	-----	-----	-----	-----	-----	15.948	16.062	16.042	
FE 2+	0.104	0.056	0.530	0.807	0.156	0.323	6.245	2.835	5.306	2.534
MN	0.0	0.0	0.007	0.005	0.004	0.004	0.113	0.020	0.032	0.044
CO	0.0	0.0	0.002	0.0	0.0	0.0	0.0	0.009	0.025	0.0
NI	0.0	0.0	0.010	0.0	0.001	0.006	0.071	0.033	0.019	0.0
ZN	0.0	0.0	0.0	0.0	0.0	0.0	0.066	0.062	0.077	0.0
BA	0.0	0.0	0.0	0.0	0.0	0.0	0.0	0.0	0.004	0.0
MG	0.060	0.0	2.833	3.428	0.932	1.639	1.161	4.887	2.476	2.969
SUM OF Y	4.282	4.018	3.382	4.987	-----	-----	-----	-----	6.898	
CA	0.016	0.041	0.0	1.762	0.799	0.003	0.022	0.0	0.0	0.078
SUM OF A	-----	-----	-----	-----	1.989	1.975	7.678	7.846	7.939	-----
NA	0.129	1.681	0.0	0.765	0.0	0.0	0.0	0.0	0.0	0.697
K	0.719	0.180	0.0	0.102	0.0	0.0	0.0	0.0	0.0	0.0
SUM OF X	0.864	1.902	-----	-----	-----	-----	-----	-----	-----	-----
SUM OF X+A	-----	-----	-----	2.629	-----	-----	-----	-----	-----	0.775
NO. OF ANIONS	22	22	7	23	6	4	32	32	32	23
WEIGHT PERCENT OXIDES										
SIO2	52.927	49.661	41.422	44.299	52.538	40.255	0.137	0.144	0.0	40.986
TIO2	0.365	0.106	0.0	4.741	0.247	0.0	3.159	0.0	0.0	0.148
AL2O3	39.418	40.990	0.0	9.999	2.981	0.0	12.623	62.809	60.383	19.208
FE2O3	0.0	0.0	0.0	0.0	0.0	0.0	17.912	0.0	2.104	0.0
V2O3	0.467	0.078	0.0	0.162	0.0	0.0	0.427	0.0	0.141	0.0
CR2O3	0.135	0.0	0.0	1.255	1.441	0.0	34.407	4.175	0.056	0.0
FEO	1.023	0.546	14.504	6.701	5.098	15.382	27.277	16.315	28.829	20.667
MNO	0.0	0.0	0.193	0.043	0.129	0.192	0.488	0.114	0.170	0.151
COO	0.0	0.0	0.061	0.0	0.0	0.0	0.0	0.056	0.143	0.0
NIO	0.0	0.0	0.286	0.0	0.046	0.301	0.324	0.195	0.108	0.0
ZNO	0.0	0.0	0.0	0.0	0.0	0.0	0.325	0.404	0.472	0.0
BAO	0.0	0.0	0.0	0.0	0.0	0.0	0.0	0.0	0.045	0.0
MGO	0.331	0.0	43.535	15.978	17.120	43.750	2.845	15.788	7.550	13.589
CAO	0.120	0.313	0.0	11.427	20.399	0.121	0.076	0.0	0.0	0.498
NA2O	0.551	7.114	0.0	2.741	0.0	0.0	0.0	0.0	0.0	2.452
K2O	4.662	1.158	0.0	0.554	0.0	0.0	0.0	0.0	0.0	0.0
TOTAL 1	100.000	100.000	100.000	97.900	100.000	100.000	100.000	100.000	100.000	97.900
TOTAL 2	91.756	91.068	81.760	96.690	99.304	100.996	101.388	102.665	101.284	100.370

TABLE 30 .CONT'D...

MINERAL NO	535. PREH	501. PREH	491. PREH	494. STAU	495. STAU	495. STAU
STRUCTURAL FORMULAE						
SI 4+	2.966	2.997	2.981	7.903	7.883	7.879
AL IV	0.034	0.003	0.019	0.097	0.117	0.121
SUM OF Z	3.000	3.000	3.000	8.000	8.000	8.000
AL VI	1.960	1.955	1.980	17.915	17.906	17.973
TI 4+	0.006	0.0	0.004	0.104	0.123	0.118
FE 3+	0.030	0.034	0.015	0.0	0.0	0.0
V 3+	0.003	0.004	0.004	0.0	0.0	0.0
CR 3+	0.007	0.007	0.007	0.0	0.021	0.0
SUM OF Y	2.006	2.000	2.010	18.019	18.050	18.091
FE 2+	0.017	0.015	0.026	3.023	3.088	3.029
CO	0.0	0.0	0.0	0.0	0.008	0.0
NI	0.0	0.0	0.0	0.0	0.0	0.015
ZN	0.0	0.002	0.0	0.333	0.215	0.248
BA	0.004	0.006	0.0	0.0	0.0	0.0
MG	0.0	0.0	0.0	0.602	0.604	0.573
CA	1.975	1.969	1.974	0.0	0.0	0.0
K	0.004	0.0	0.0	0.019	0.014	0.0
SUM OF X	2.000	1.992	2.000	3.958	3.915	3.865
NO OF ANIONS	11	11	11	47	47	47
WEIGHT PERCENT OXIDES						
SIO2	42.989	43.454	43.266	27.854	27.816	27.828
TIO2	0.106	0.0	0.084	0.489	0.578	0.553
AL2O3	24.514	24.088	24.612	53.858	53.954	54.217
FE2O3	0.901	0.943	0.0	0.0	0.0	0.0
V2O3	0.054	0.073	0.065	0.0	0.0	0.0
CR2O3	0.137	0.137	0.120	0.0	0.094	0.0
FEO	0.0	0.0	0.710	12.737	13.026	12.791
COO	0.0	0.0	0.0	0.0	0.037	0.0
NIO	0.0	0.0	0.0	0.0	0.0	0.067
ZNO	0.0	0.041	0.0	1.589	1.025	1.188
BAO	0.131	0.222	0.0	0.0	0.0	0.0
MGO	0.0	0.0	0.0	1.423	1.430	1.358
CAO	26.724	26.642	26.743	0.0	0.0	0.0
K2O	0.043	0.0	0.0	0.354	0.040	0.0
TOTAL 1	95.600	95.600	95.600	98.000	98.000	98.000
TOTAL 2	95.864	94.794	95.211	100.385	100.892	100.887

4. NOTES to the TABLE of PLAGIOCLASE An CONTENT

Table 31 lists the An content of plagioclases, mostly from metabasites. Column 1 contains the sample number; column 2 and 3 the An content by microprobe analysis, column 2 by fully quantitative energy dispersive analysis, and column 3 by rapid analysis (see Appendix II); column 4 lists An content by universal stage, measuring the optic axial angle where the plagioclase could be assumed to be in the range of An_{0-25} and no ambiguity arises in 2V versus An. Column 5 lists what are considered to be the best values from columns 2, 3 and 4. Column 6 lists the corresponding temperature obtained from the garnet-biotite thermometer and interpolated on the map of isotherm distribution (fig. 47).

Table 31. An content of plagioclases (all in metabasites, except where marked by '*'); temperatures from the garnet-biotite thermometer.

No	microprobe quant.	microprobe semi-quant.	U-stage	best values	T°C
12	55			55	590
19		33,36,18,35		18,35	550
20		27,30		29	550
21		24,26		25	550
22		25,26		25	550
23		24,24		24	550
25		25,30,36		32	550
26		24,26		25	545
31		20,23		22	550
32		33,39,39		37	545
43*		35		35	620
51	7 (retrogressed)			7	585
58			11,11,13	12	530
59			0,4,6	3	535
74		31,31,33		32	550
75		24,24,29		26	550
76		33,34		34	550
77		35,37		36	500
79		27,28,30		28	500
96			5	5	515
97			5	5	515
98*			5	5	520
103			11,12,20,20,22	11,21	540
105*			13,13,13,15	13	550
113			2,6,6,11	5,11	550
114			14,14,20,20	14,20	550
115			16,18,22,25	17,24	550
			6,14,14,16,18 20,20,22	6,15,21	550
117			6,6,11,11,16,20	6,11 16,20	550
123			13,15,16,18,18		545
125			9,9,14,20,25	9,14,23	540
126			6,6,11,13,16		540
127			0,1,6,13,13,16	2,14	540
128			0,0,3,9,13	1,11	540
129			1,1,6,9,9,13 15,18,20	4,10,18	540
136			2,9,9,14,16	8,15	515
137			2,2,6,6	4	515
138			6,6,6	6	515
139			0,1,1	1	515
140			2,6,6,6,25	5,25	530
141			16,20,25,25	16,23	530

Table 31. Cont'd...

No	microprobe		U-stage	best values	C
	quant.	semi-quant.			
143			5	5	510
177		18,20,20		19	540
181	16,23,23			16,23	530
183			2,2,6	3	520
184		23,24		23	580
186		0,0		0	505
192		0,0		0	505
204			0,0,9,11	0,10	515
205			0,6,6	4	515
206			6	6	515
207			0,4,4	3	515
208			2,2,2,13,20,25	2,13,23	515
209			6,13	6,13	520
210			6,11,13	6,12	520
211			0,2,4	3	520
214			15,20,20,22	15,21	550
216			15,16,18,18	17	550
217			11,16,16,18	11,17	550
218			7,18,25,25	7,18,25	540
219			4,8,13,20,22	6,13,21	540
220			0,6,9	5	515
242*			5	5	540
247*			5	5	530
254			0,0,6	2	520
261			0,2,6	3	525
266		2,6,10		6	540
279			0,4,6,9	5	520
280				6	520
281			4,4,6,9	6	520
283			6,9	7	515
290			0,1,1	1	515
293			1,6,6,9	5	515
294			0,6,6	4	515
303			0	0	515
304			2,6,6	5	515
307			25,25,25	25	515
308			0,4,6,11	3,11	515
311			0,0,6,13	2,13	515
312			0,0,1,1	1	515
314			6,6,6,14	6,14	515
323			12,18,20,22	17,21,19	520
324			16,18,18,20,20	18	520
325			16,16,16,18,20	17	520
331			7,7,7	7	525
332			11,13,13,13	13	520
334			16,18,22,22,25	17,23	525

Table 31. Cont'd...

No	microprobe quant.	microprobe semi-quant.	U-stage	best values	T°C
376	35			35	570
380	21			21	550
383			45	45	620
384			35	35	620
389		33,35,35		35	620
390*			20	20	625
391*		26		26	625
393*		2		2	540
407		30,34		32	570
419		40,53,54,55 (relics)	45,60	54	540
420			19,22	20	540
422		37,38 (relic)		38	540
424		30,40 (relic)		35	540
425		2,5		3	540
426		25,29		27	540
431*			40	40	625
432		31,32,33		32	555
440*			40	40	580
453			0,0	0	515
464		0,3		2	510
474			6,6,11,22	6,11,22	540
478			6,11,13	6,12	550
479			5	5	540
485			5	5	510
496			22,25,25	24	535
482			0,6,18,25	3,18,25	535
488			20,22,25,25	23	530
490			16,16,20	16,20	525
492		21,22		21	525
496	2			2	515
499	18			18	525
501		2,5		3	520
503	24			24	520
504				3	520
505			4,11,11	4,11	520
506			4,6,6	5	520
508			14,16	15	520
509	3,2		0,4,9,9	2,9	520
511			0,9,18,22,22	5,21	520
516	21			21	560
517	22			22	545
520		25,25		25	545
522	23			23	540
526		21,22		21	530
530		39,39		39	580

Table 31. Cont'd...

No	microprobe quant.	microprobe semi-quant.	U-stage	best values	T°C
531	23			23	560
532	25			25	530
533		1,1,2		1	525
534	23			23	550
535	(retrogressed)		0,0	0	580
536	23			23	570
537	22			22	560
538		2		2	520
539		0,0,2		1	510
540		2,11		2,11	585
541	2,3			23	530
542		21,23			540
543		3,3		3	515
544	24			24	550
545	23			23	560
546	26			26	580
547	1			1	525
548		30		30	580
551*		25		25	600
554		15,23,25		15,24	570
555		12,17		12,17	570
557		20,20,26		22	565
558		20,21		21	565
559		23,24		23	550
56[illegible]		22,33,33		33	550
[illegible]61		25,27		26	555

5. NOTES to the TABLE of BIOTITE-GARNET TEMPERATURES

Table 32 lists the temperatures obtained from analyses of coexisting garnets and biotites using the geothermometer outlined in Chapter VI. All garnet and biotite analyses were made by energy dispersive microprobe techniques. Column 1 lists the sample number, column 2 the coordinates,

column 3 the temperature.

The temperature is obtained from the following ...ation:

$$f(T) = 399.647 + 72.7KD - 8.23bAl^{(6)} + 54.82bTi + 12.94bFe + 4.49bMg + 24.01bK + 22.38gFe - 26.23gMg + 4.38gCa + 12.42gMn - 80.76bXFe - 264.9gXFe$$

$$f(T) = 1000\exp[-100/(T^{\circ}C + 273)]$$

Al, Ti, etc... are from biotite (prefix b) and garnet (prefix g) structural formulae calculated on the basis of 22 and 24 bivalent anions respectively, and multiplied by 100.

$KD = b(Fe/Mg)/g(Fe/Mg) \times 1000$

$XFe = Fe/(Fe+Mg) \times 1000$

Table 32. Temperatures obtained from coexisting biotites and using equation 12 of Chapter VI.

No	location	T(°C)
10	627 593	590
35	659 510	605
49	445 392	596
50	445 392	588
64	230 465	547
87	319 75	546
106	291 325	535
106	291 325	555
119	297 334	569
121	303 332	566
122	303 332	537
135	238 382	538
152	278 161	554
162	140 256	504
171	87 106	542
246	238 137	501
250	319 224	514
262	293 191	551
263	293 191	535
278	253 381	559
338	221 492	581
342	221 492	583
348	220 491	586
351	217 489	572
358	213 484	528
371	498 427	523
391	749 460	623[1]
402	458 390	572
444	465 435	586
469	90 532	586
494	279 482	586
495	279 481	586[2]
528	221 492	553
550	687 288	547
551	737 473	601[1]
552	60 527	584
553	660 286	523
562	728 473	622
564	318 074	541
565	292 072	534
567	291 326	537
568	244 377	506
569	233 373	520
570	254 116	549
571	252 284	503
572	610 469	536
573	659 464	628

1: contains kyanite 2: contains staurolite

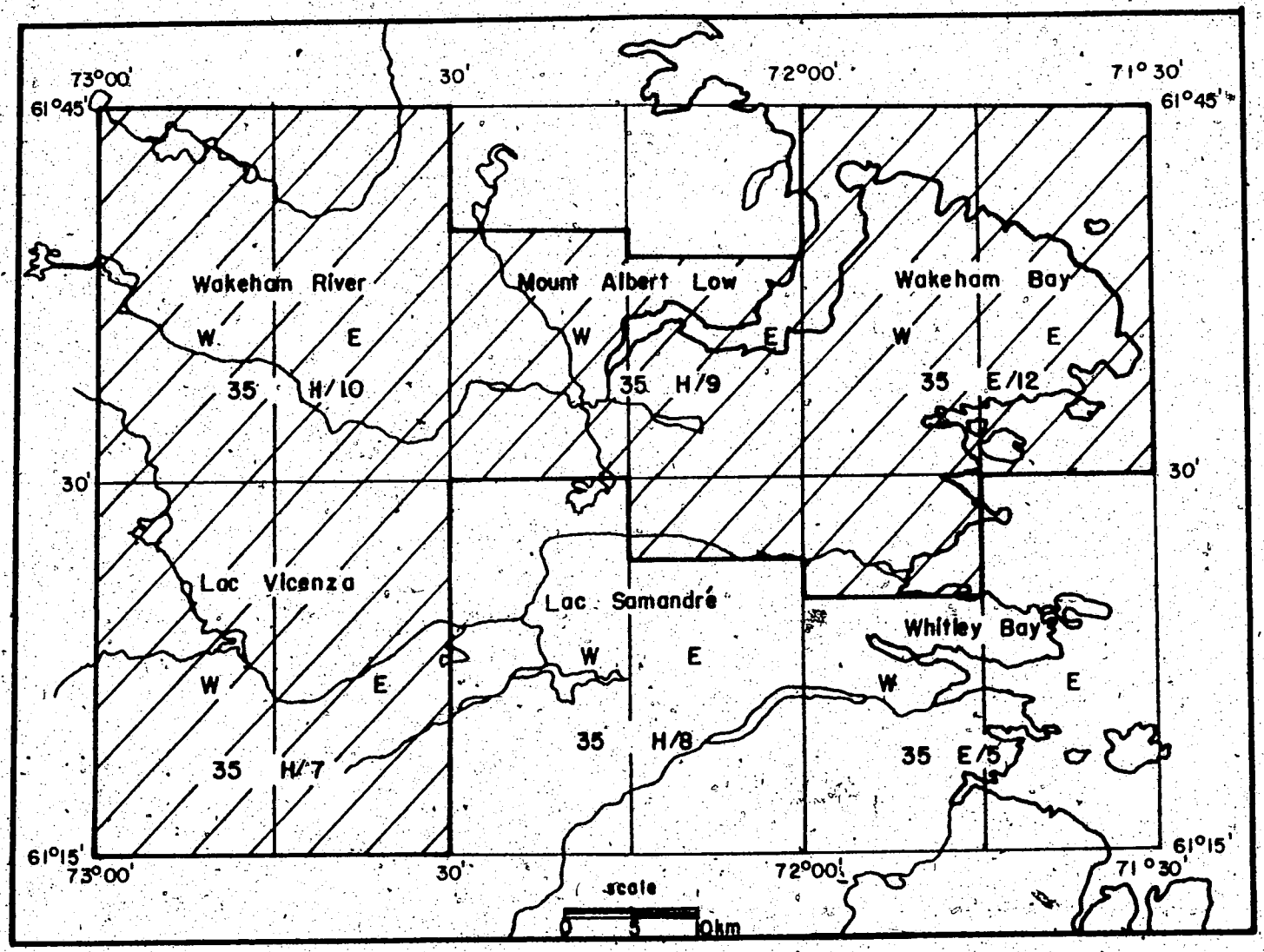

Fig. 14. Index to geological maps.

Table 1. Legend to geological maps and tectonic profiles.

Lithologies and stratigraphic units.

8	Hadrynian	τ	diabase dyke
	Aphebian		
7	Upper Volcanic Group	se	sediments (undifferentiated)
6	Lower Volcanic Group	s	sandstone, arkose, grit
5	Volcano-Sedimentary Group	q	quartzite (metamorphic equivalent of s)
4	Pelitic Group	a	argillite, shale
3	Iron Group	m	micaschist (metamorphic equivalent of a)
		d	dolomite and calschists
		if	iron formation (undifferentiated)
		lif	lean iron formation (iron rich sand-or siltstone)
		cif	silicate-carbonate iron formation
		gif	quartz-oxide iron formation
		ge	dark-green chlorite schist
		t	volcano-sediments (undifferentiated)
		tb	basic tuff
		ti	intermediate tuff
		tf	felsic tuff
		pα	para-amphibolite (metamorphic equivalent of t)
		b	volcanic rocks (undifferentiated)
		α	amphibolite (metamorphic equivalent of t and/ or b)
		oα	ortho-amphibolite (metamorphic equivalent of b)
		be	basic to intermediate extrusive rocks (undifferentiated)
		bf	flows
		bp	pillows
		bs	gabbroic (to dioritic) sills
		y	pyroxenitic sills
		p	peridotitic sills
		u	ultramafic rocks (undifferentiated)
2	Early Aphebian	τ	diabase dyke
1	Archean	n	quartzo-feldspathic gneiss
		α	amphibolite
		m	paragneisses (pelitic to calcareous schists)

Symbols.

Contact (defined, approximate)

Foliation (bedding): horizontal, vertical, inclined, top known (pillows)

Fault (defined,approximate)

Anticline (trace of axial surface)

Syncline (trace of axial surface)


71°45'
73
75
40'
45'
50
5
HUDSO

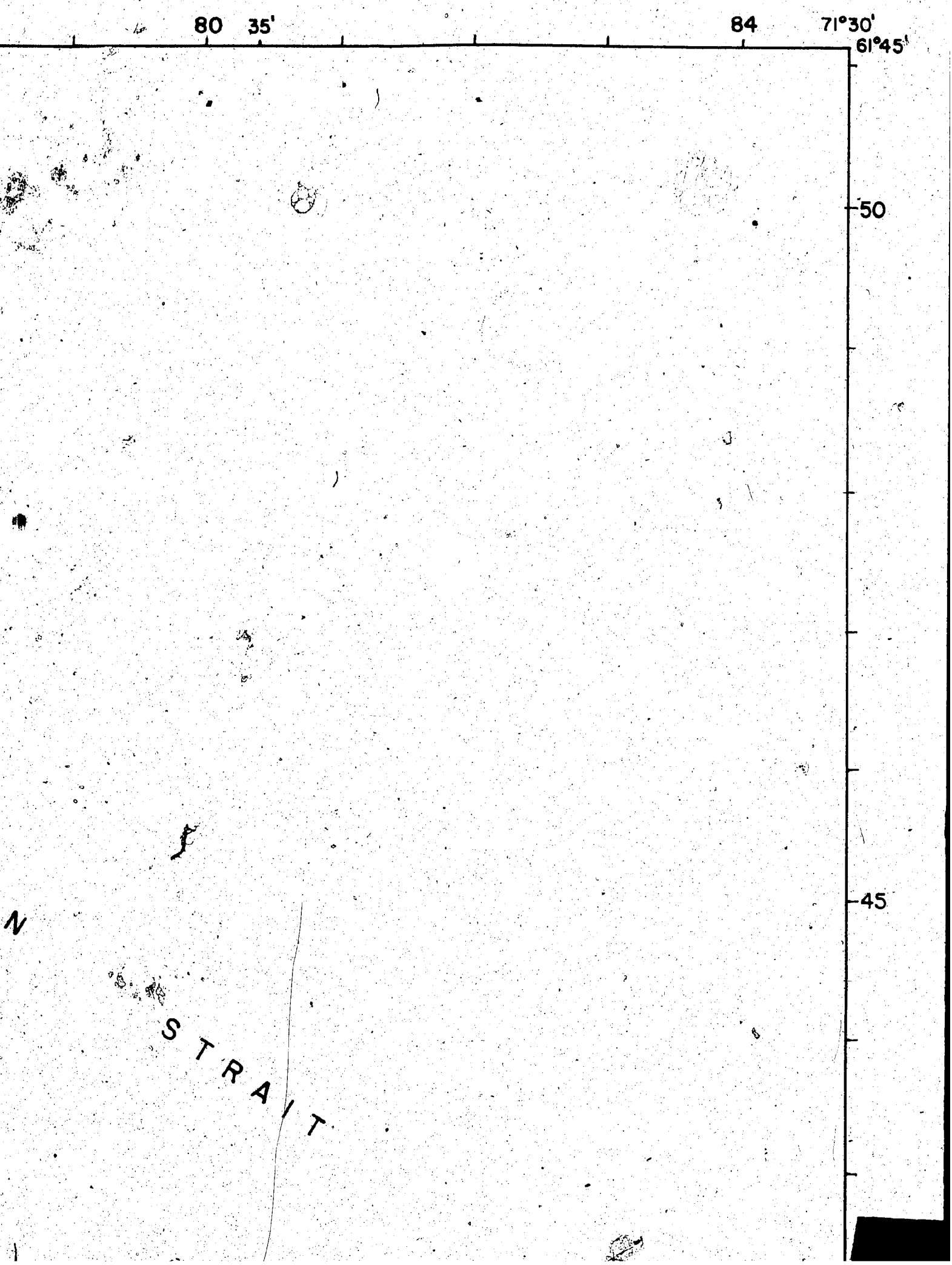
80 35'
84
71°30'
61°45'
50
45
N
STRAIT

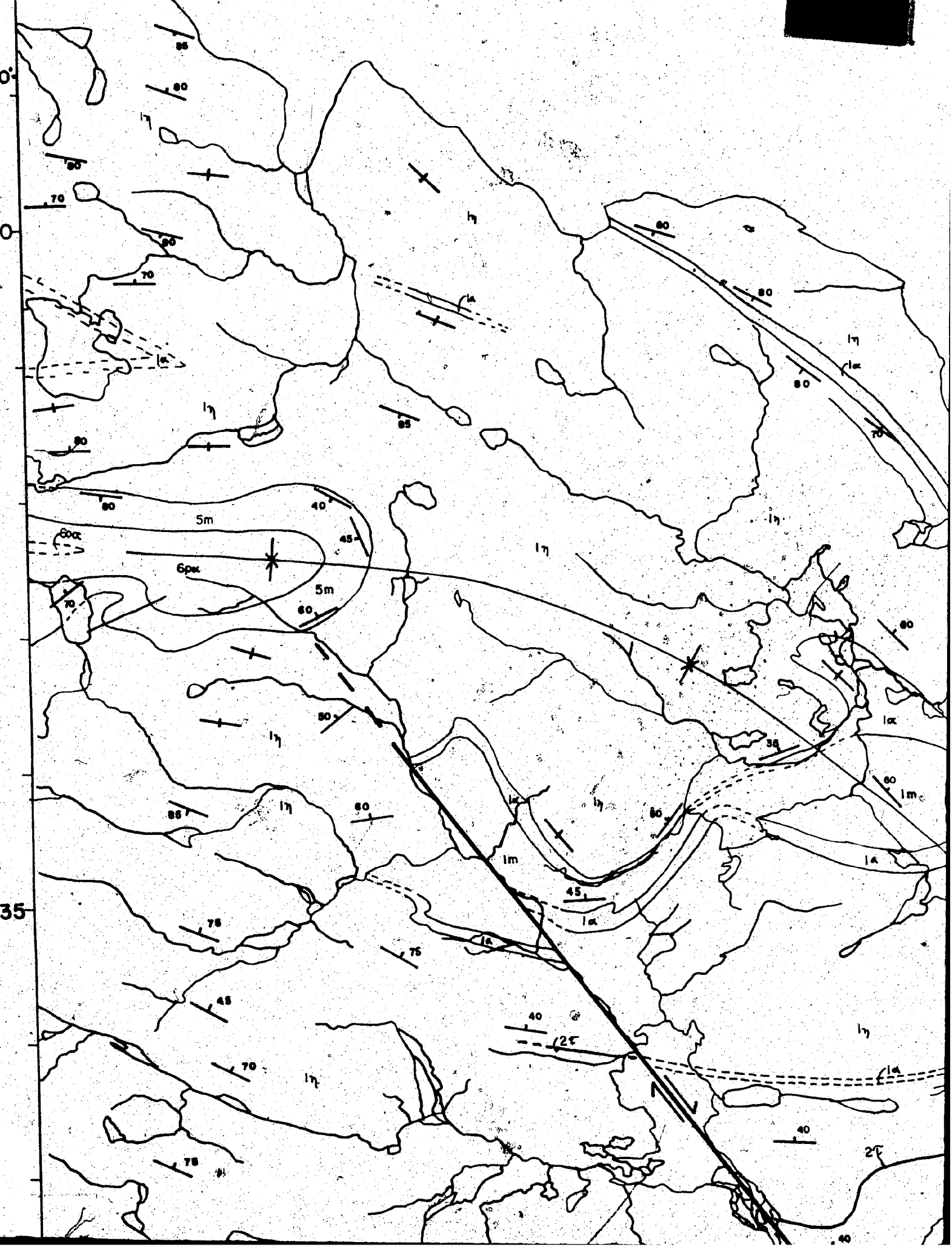
1η
1α
1m
5m
6pα
2τ
85
80
70
75
60
50
45
40
35

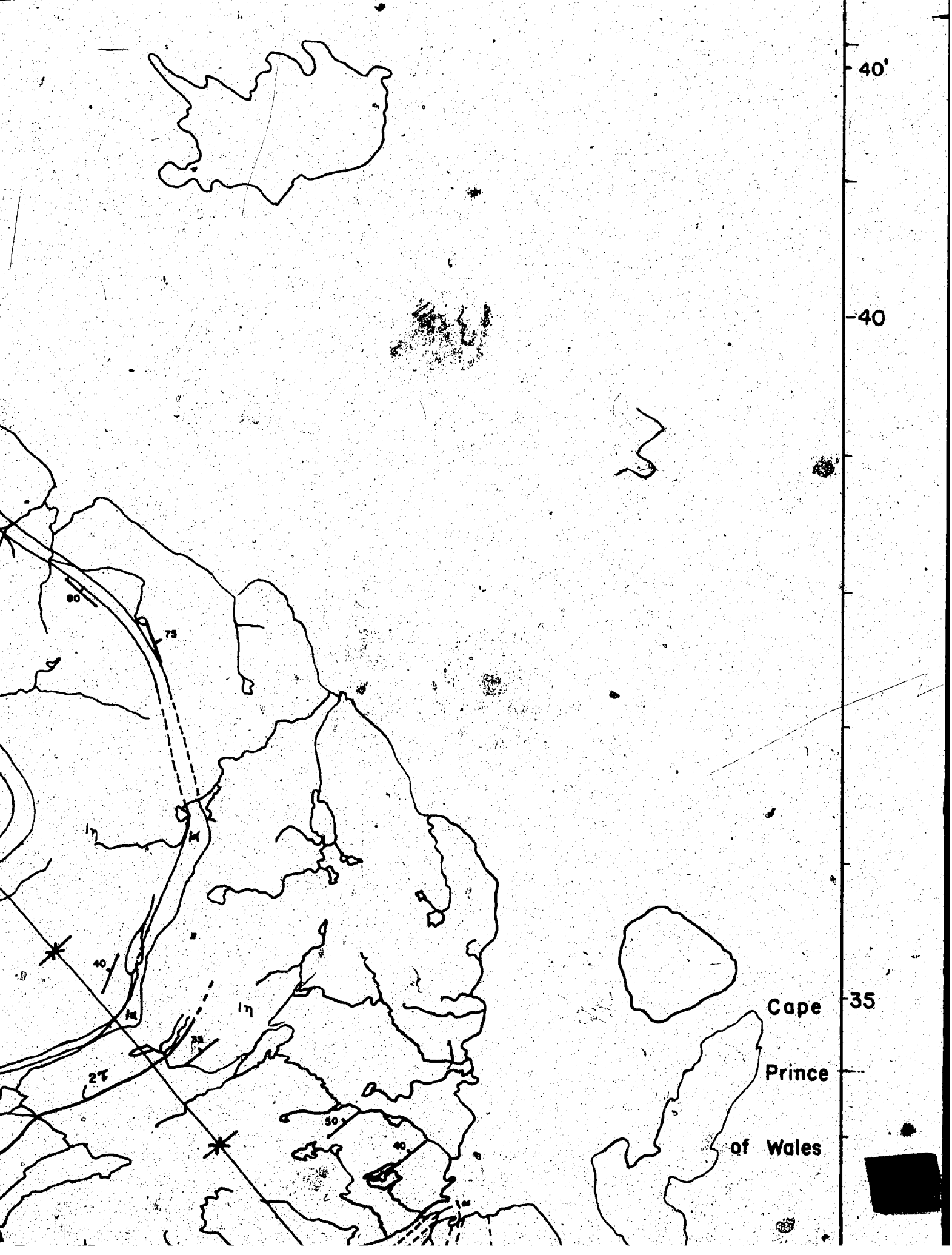
40'
40
35
Cape
Prince
of Wales

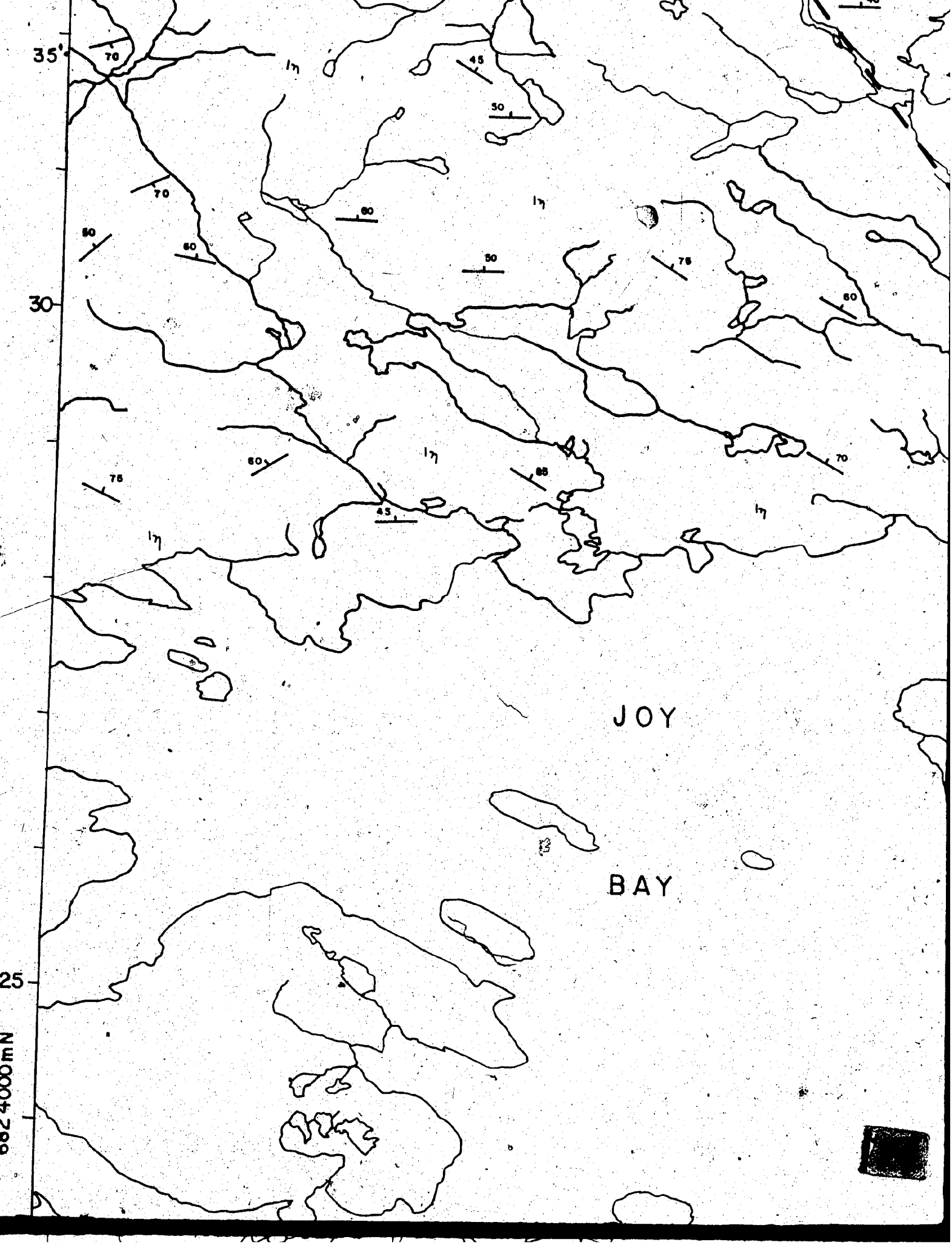
35'
30
25
JOY
BAY
70
45
50
70
60
50
60
50
75
60
75
60
70
65
45
lη
lη
lη
lη
6824000mN

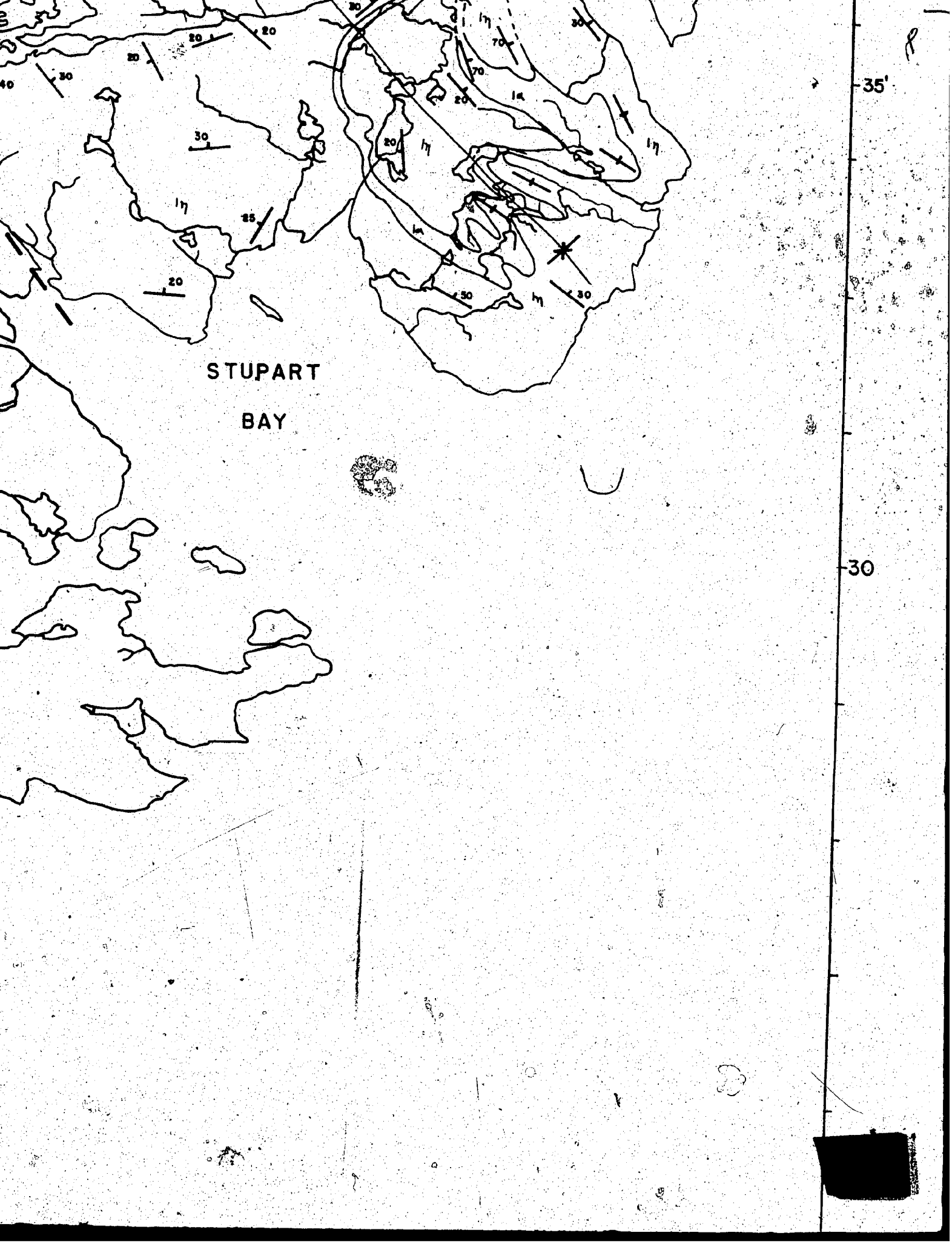
STUPART
BAY
35'
30

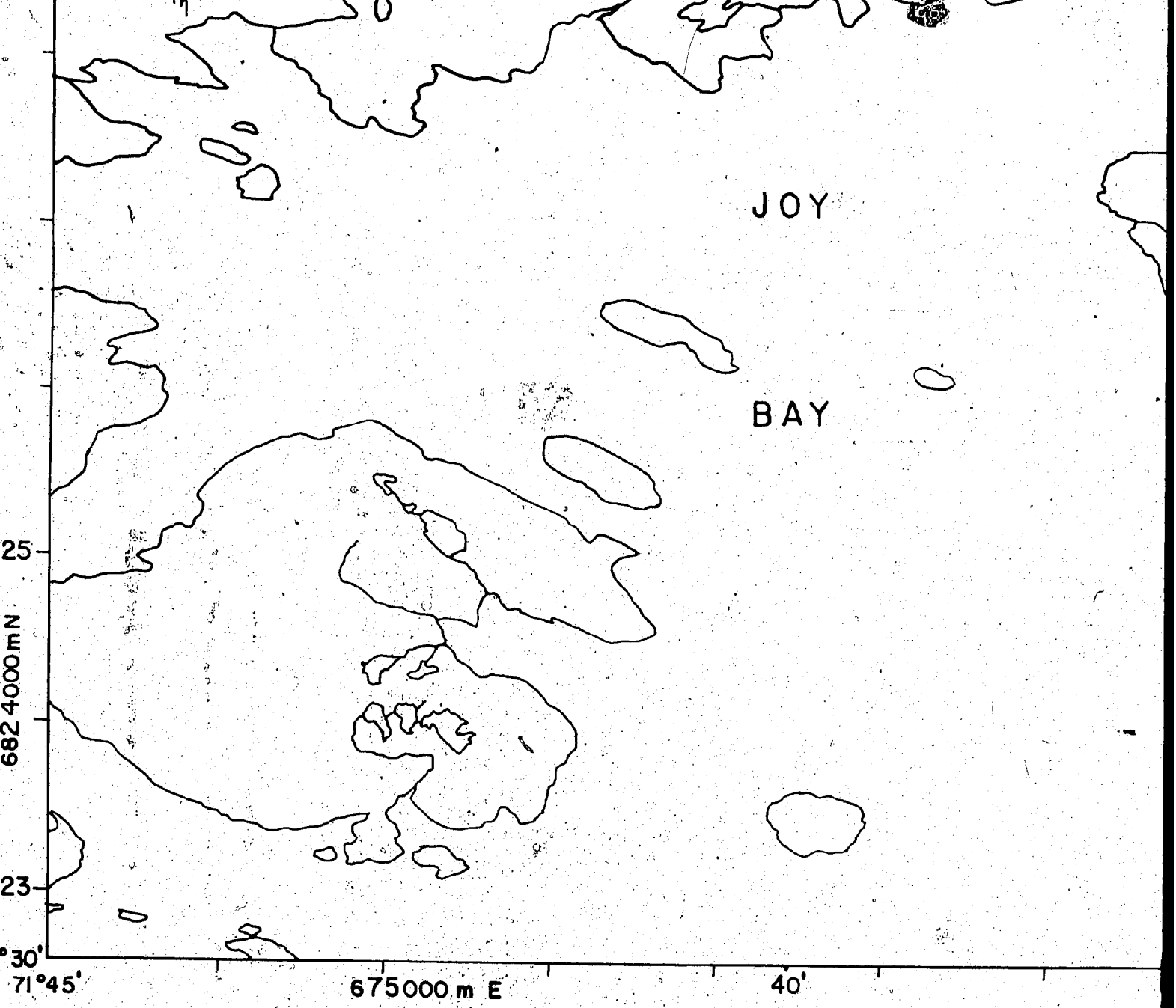

ogy by K. Schimann, L. Charlebois
P. Denis, 1972.

GEOL
WAKEHAM
QUE

gure 9.

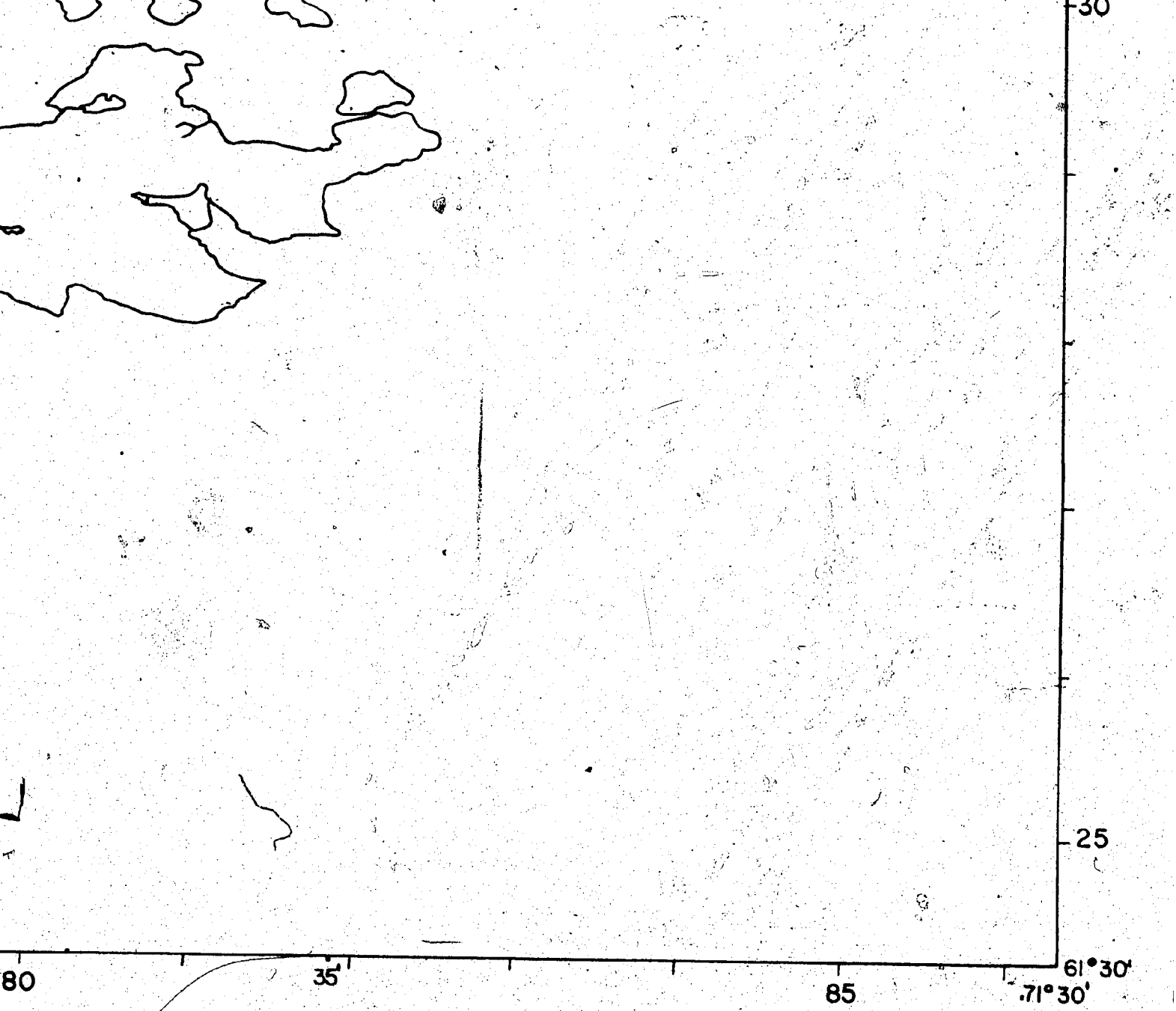

OGY

BAY E

EC

Topography based on topographic maps published at a scale of 1:50 000 by the Department of Energy, Mines and Resources, Ottawa.

UTM Grid 18V NTS 25 E/12E

scale

0 1 2km

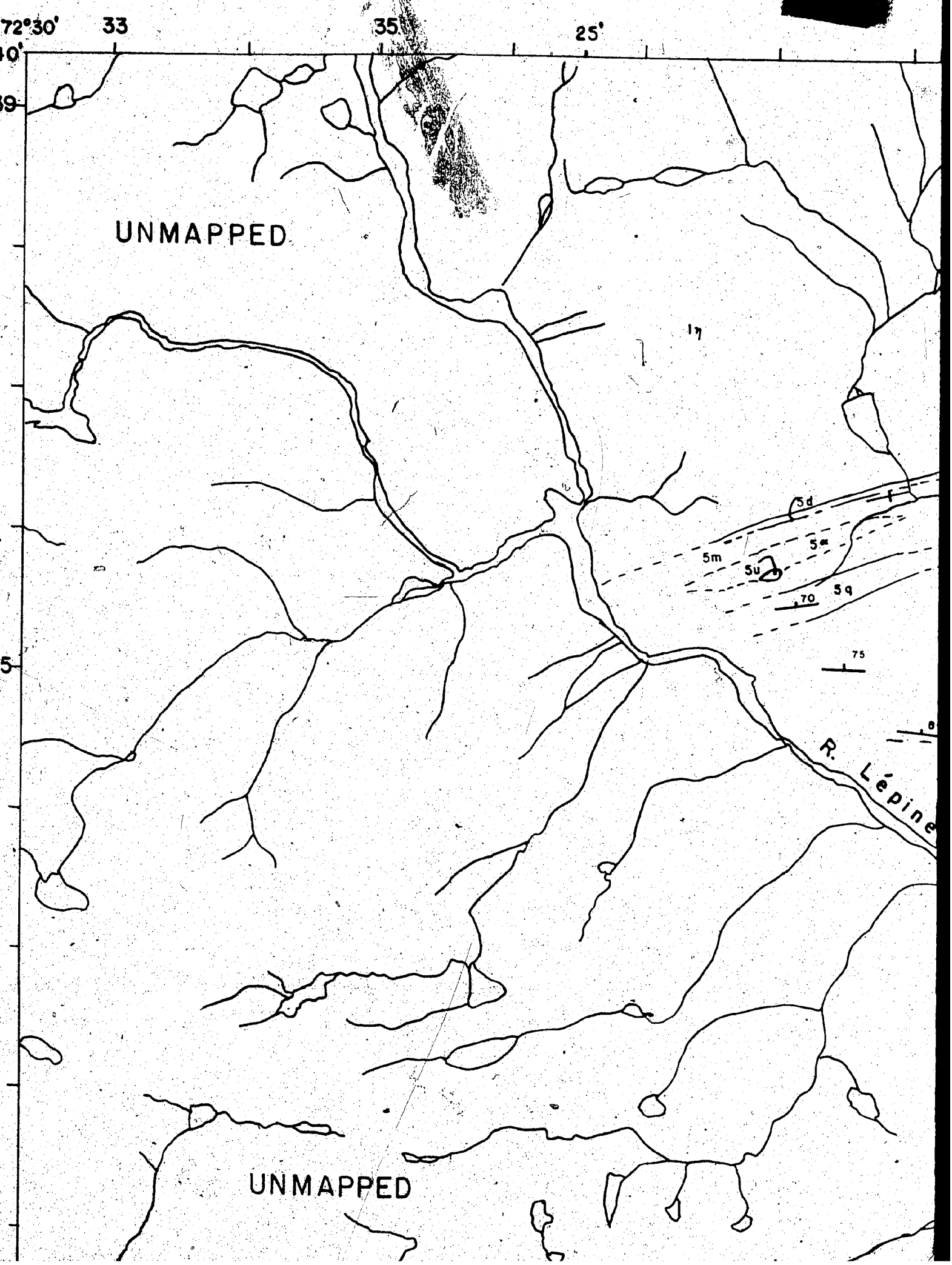
72°30'
33
35'
25'
UNMAPPED
1η
5d
5m
5u
5q
70
75
R. Lépine
UNMAPPED

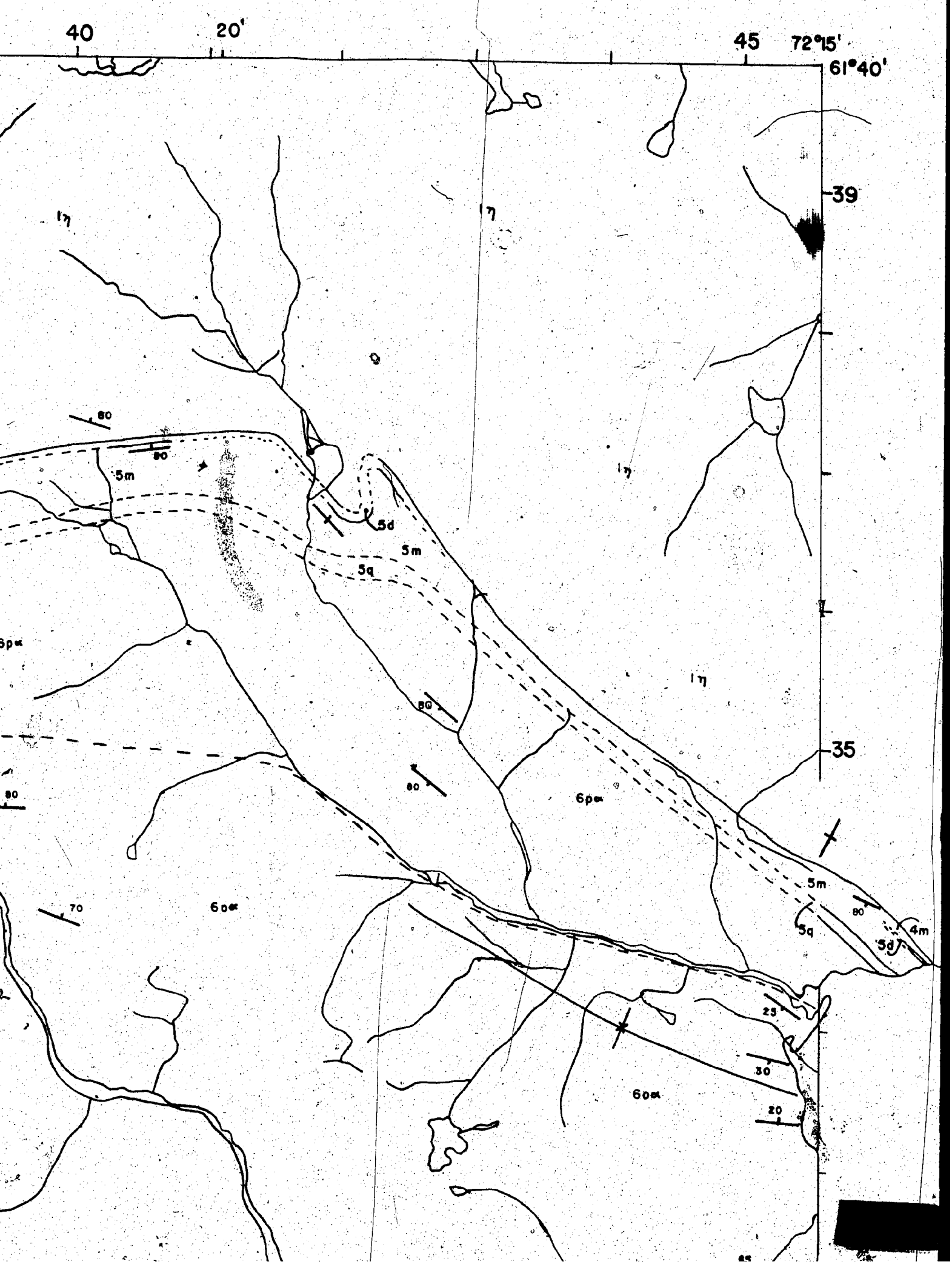
40
20'
45
72°15'
61°40'
39
35
1η
80
5m
5d
5q
6pα
70
6oα
4m
25
30
20

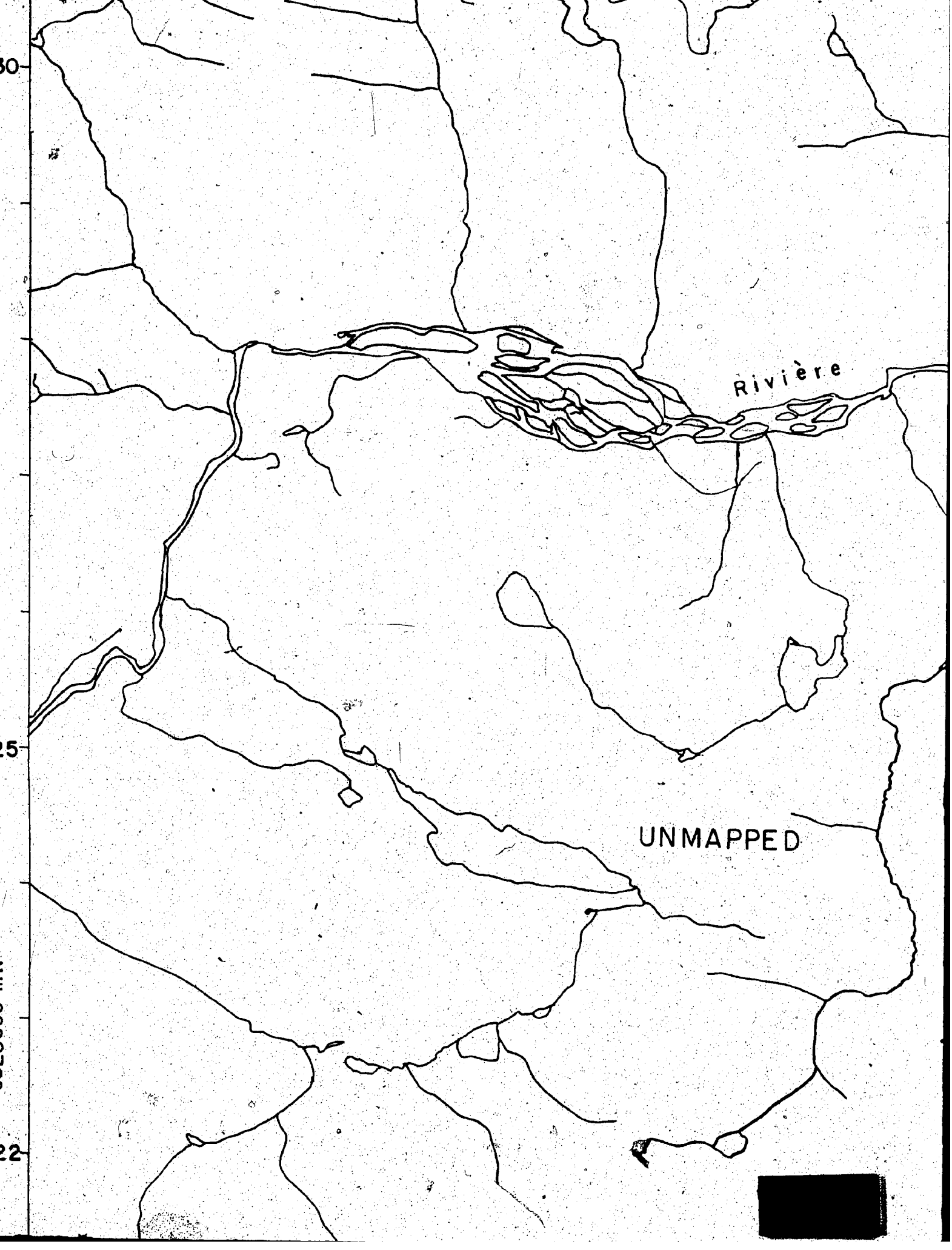
Rivière
UNMAPPED

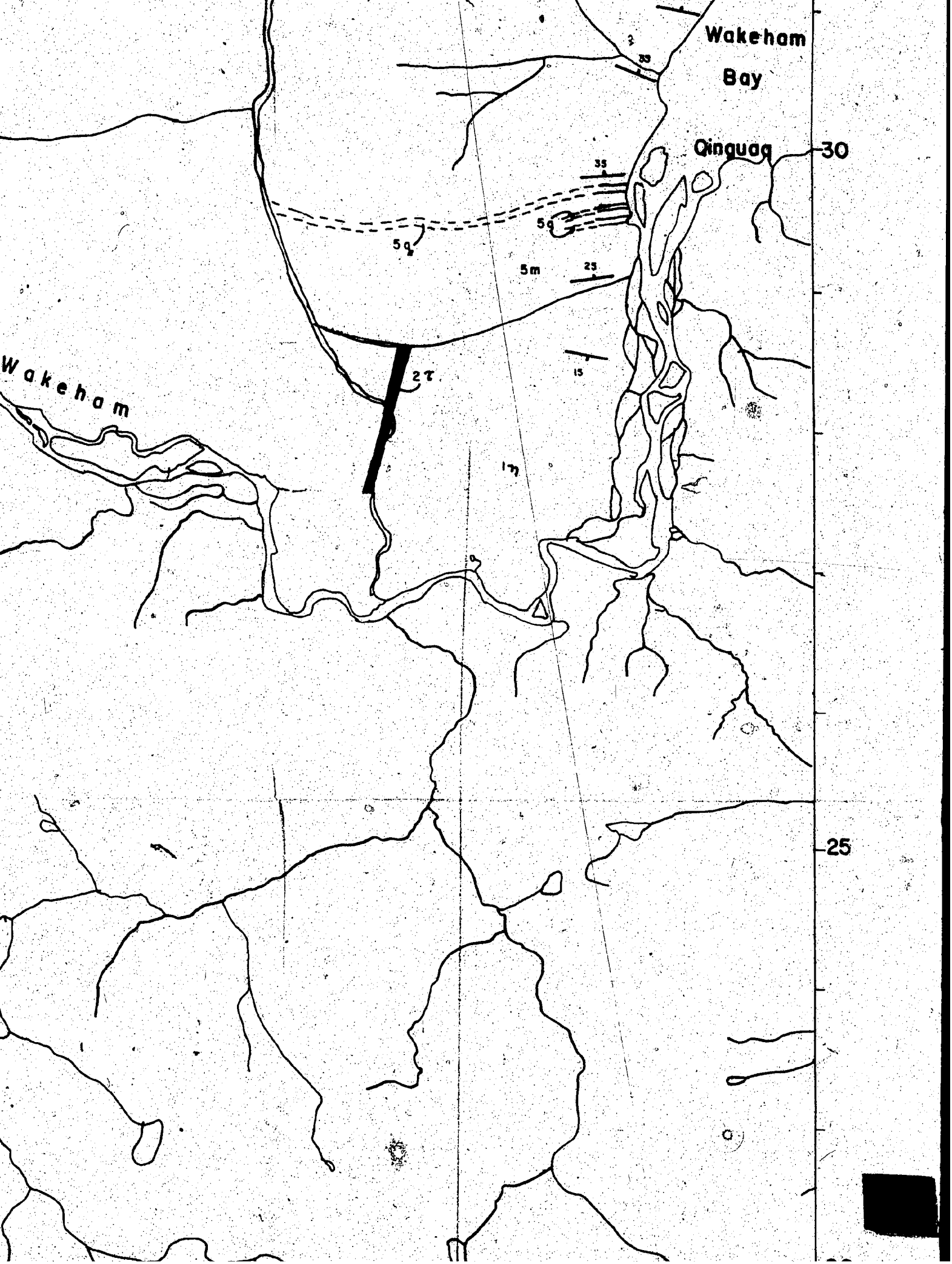
Wakeham
Bay
Qinguaq
30
25
Wakeham
35
5q
5m
23
15
2τ
1m

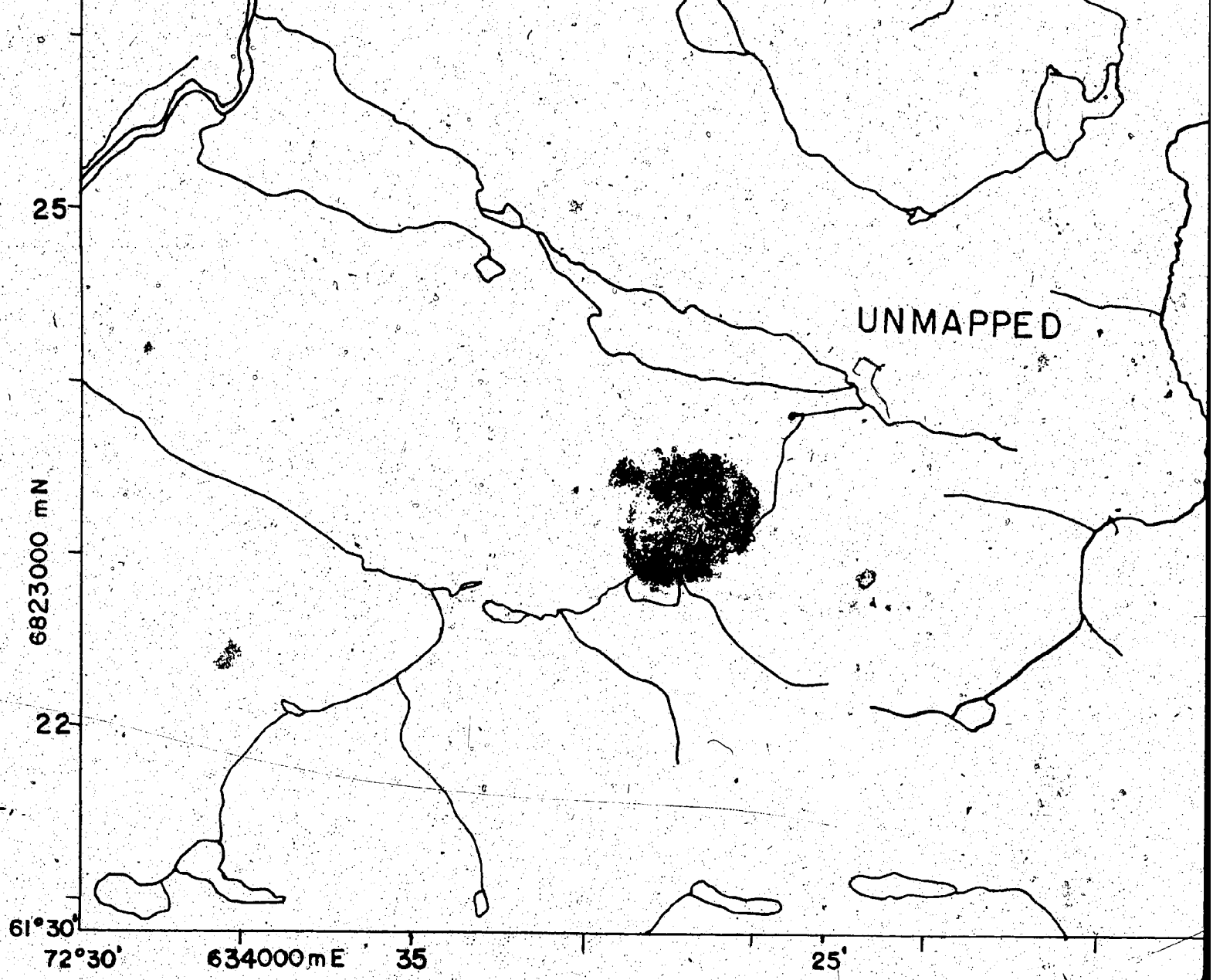

ology by K. Schimann and L. Charlebois, 1972.

GEOL

part of MOUNT ALB

QUE

igure 8.

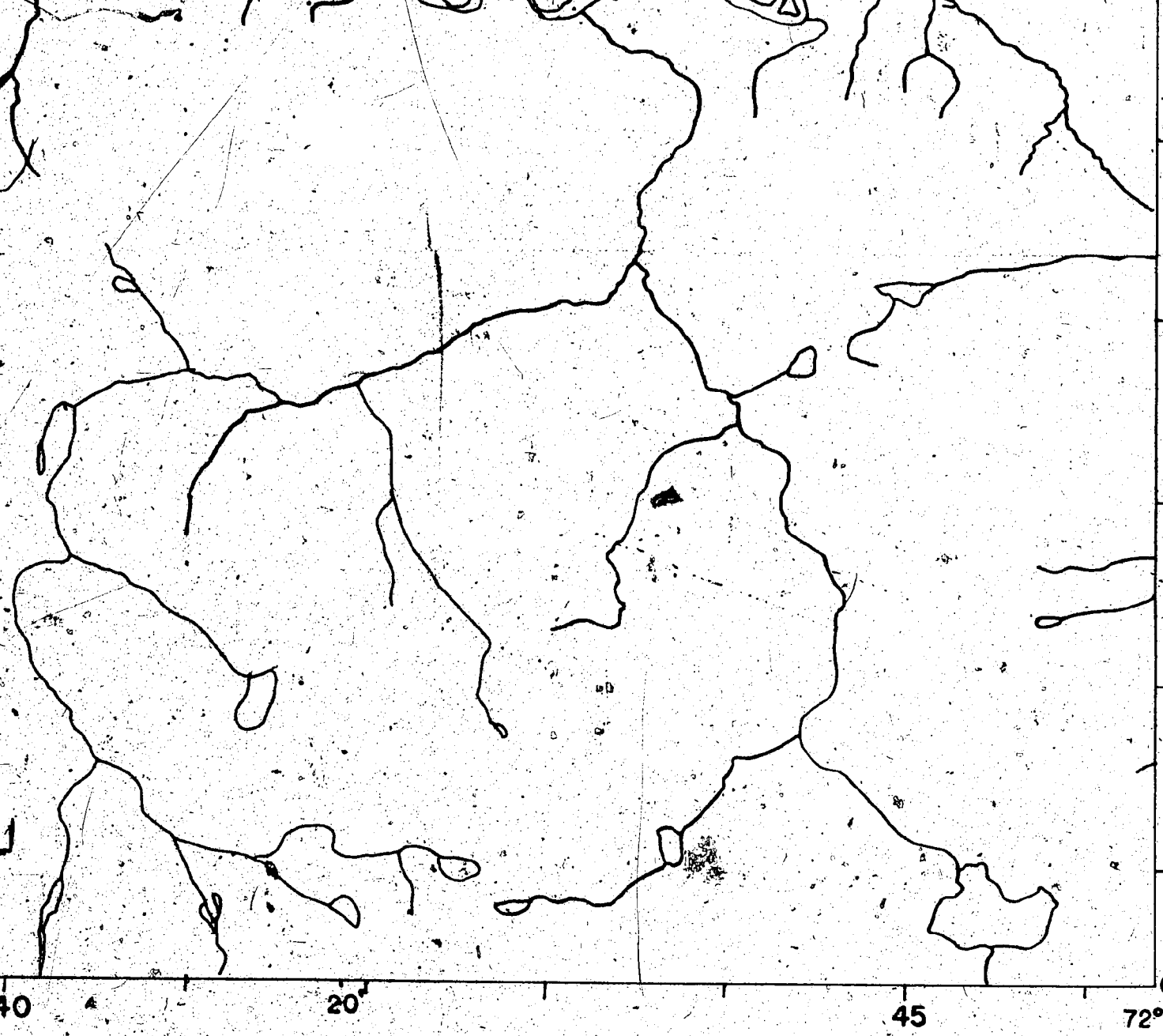

GY

RT LOW W

EC

Topography based on topographic maps published at a scale of 1:50 000 by the Department of Energy, Mines and Resources, Ottawa.

UTM Grid 18V NTS 35 H/9W

scale

0 1 2km

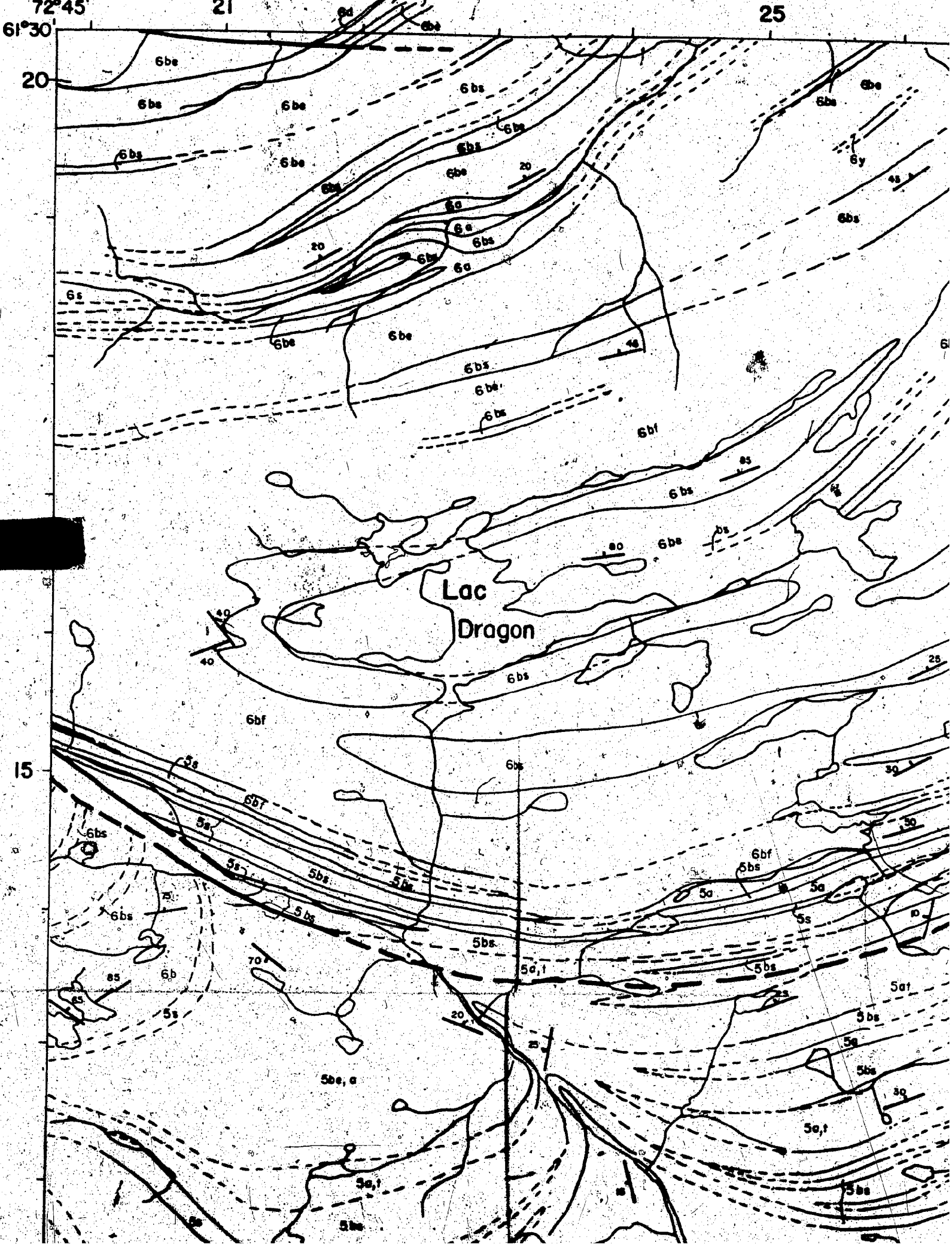
72°45
21
25
61°30
20
15
Lac
Dragon
6be
6bs
6a
6s
6bf
6y
5s
5bs
5a,t
5be, a
6b

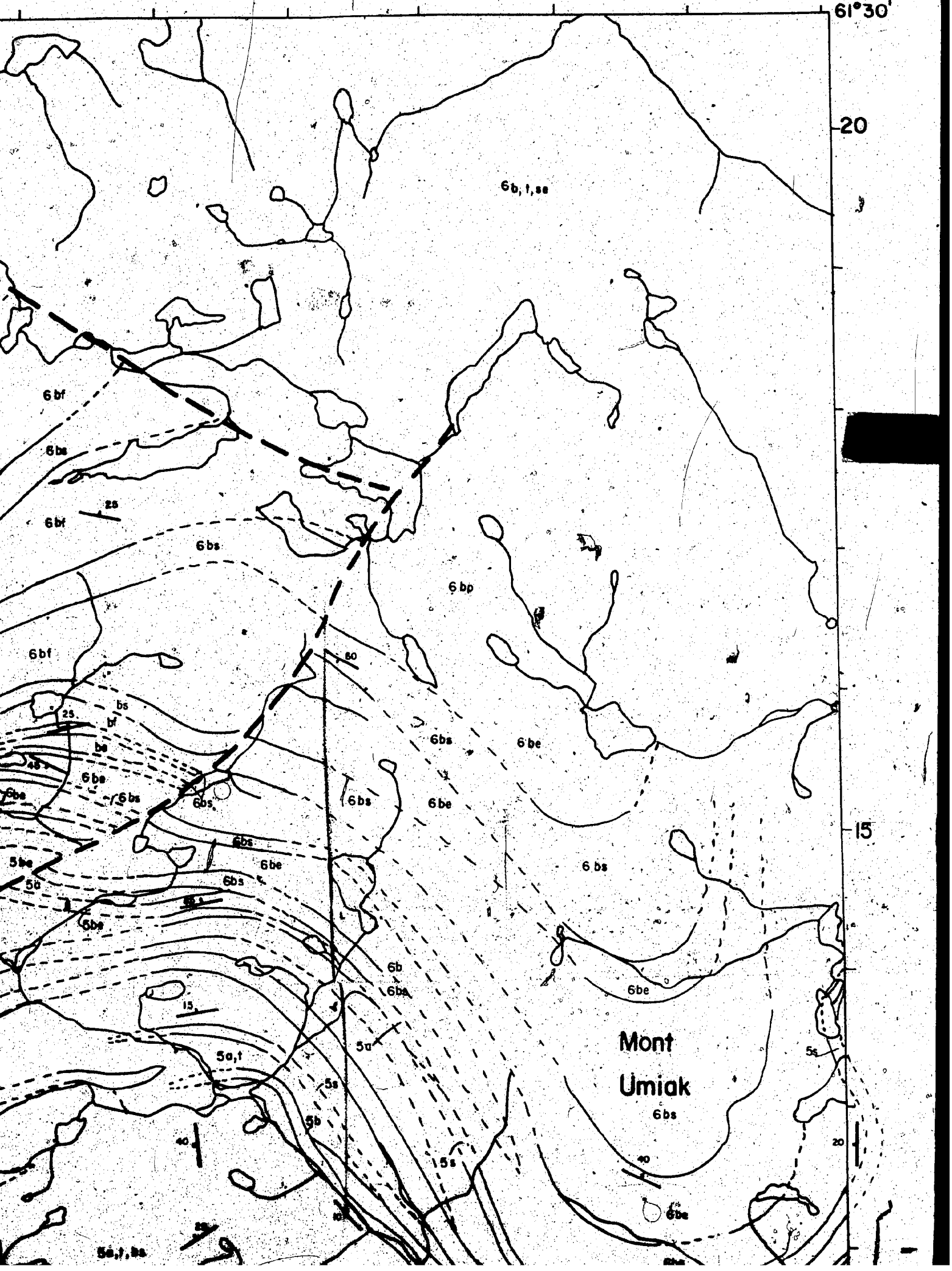
61°30'
20
15
6b, f, se
6bf
6bs
6bp
6be
6b
6ba
5a
5s
5b
5a,f
5a,f,ba
Mont
Umiak

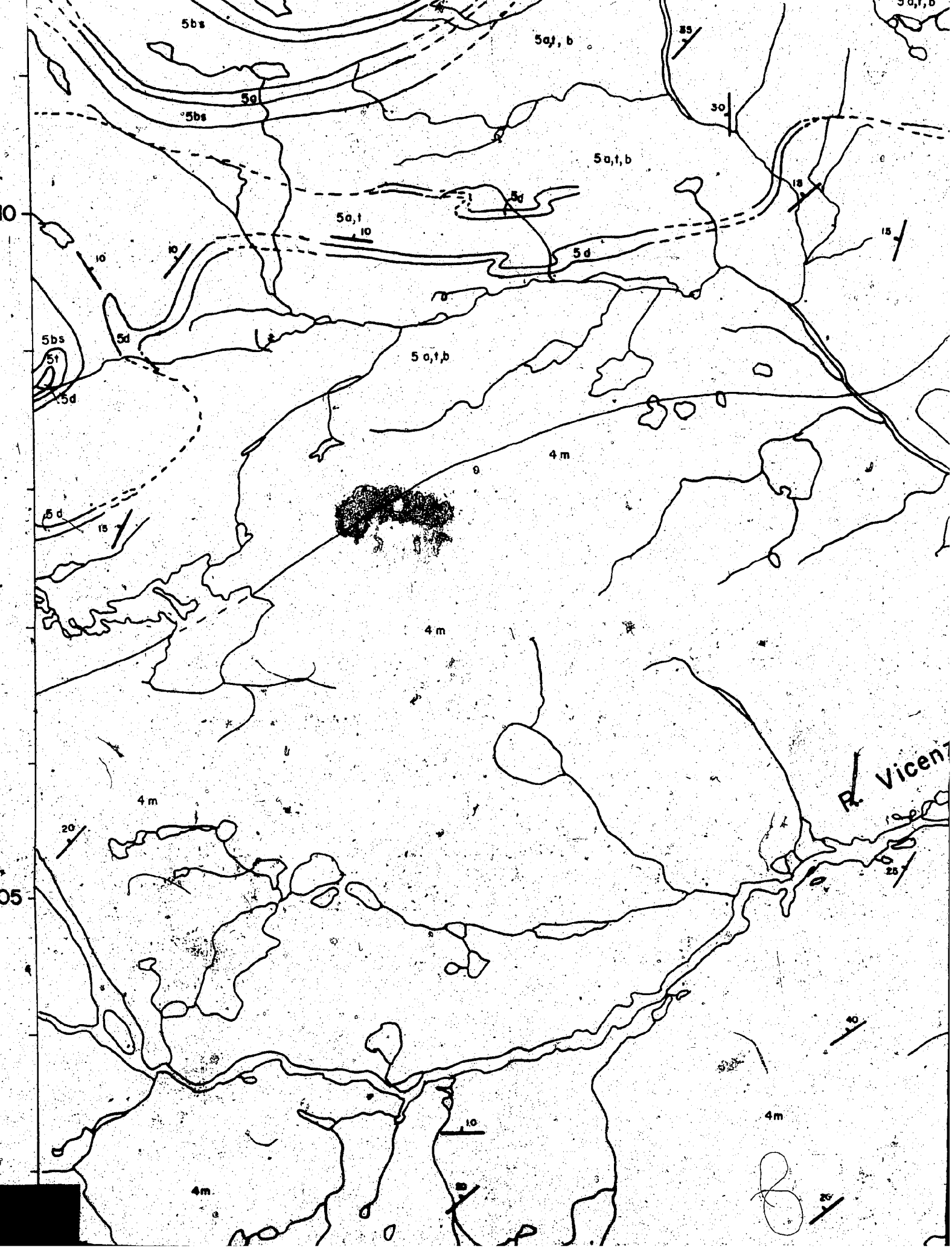
5bs
5g
5bs
5a,t, b
85
30
5a,t,b
18
5d
5a,t
10
15
10
10
5d
5bs
5t
5d
5 a,t,b
5d
15
4 m
4 m
4 m
20
R. Vicen
25
40
10
4m
4m
20

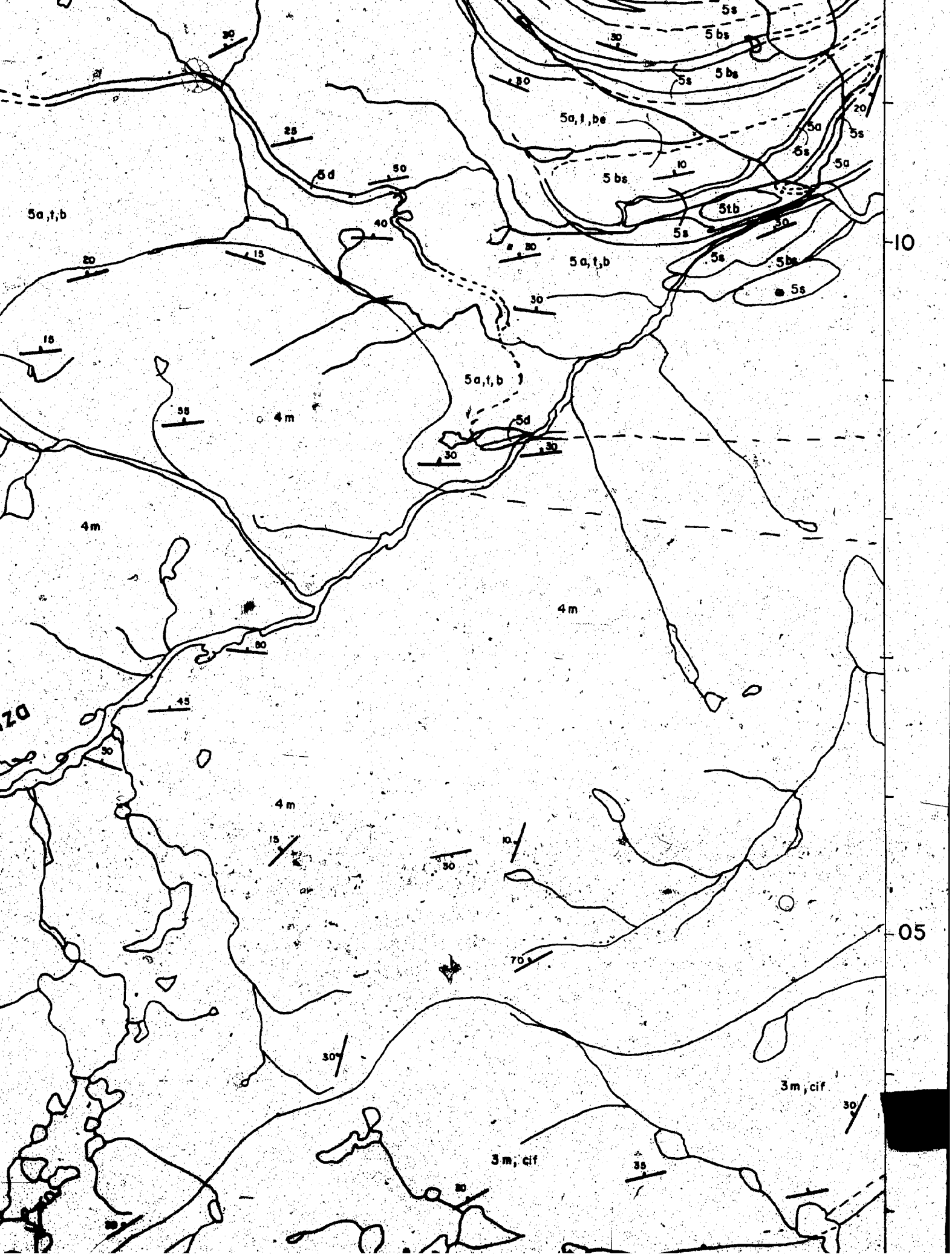
5s
5bs
5s
5bs
5a,t,be
5a
5s
5s
5a
5d
5 bs
5tb
5s
5a,t,b
5s
5bs
5s
5a,t,b
5a,t,b
4m
5d
4m
4m
4m
3m,cif
3m,cif
10
05

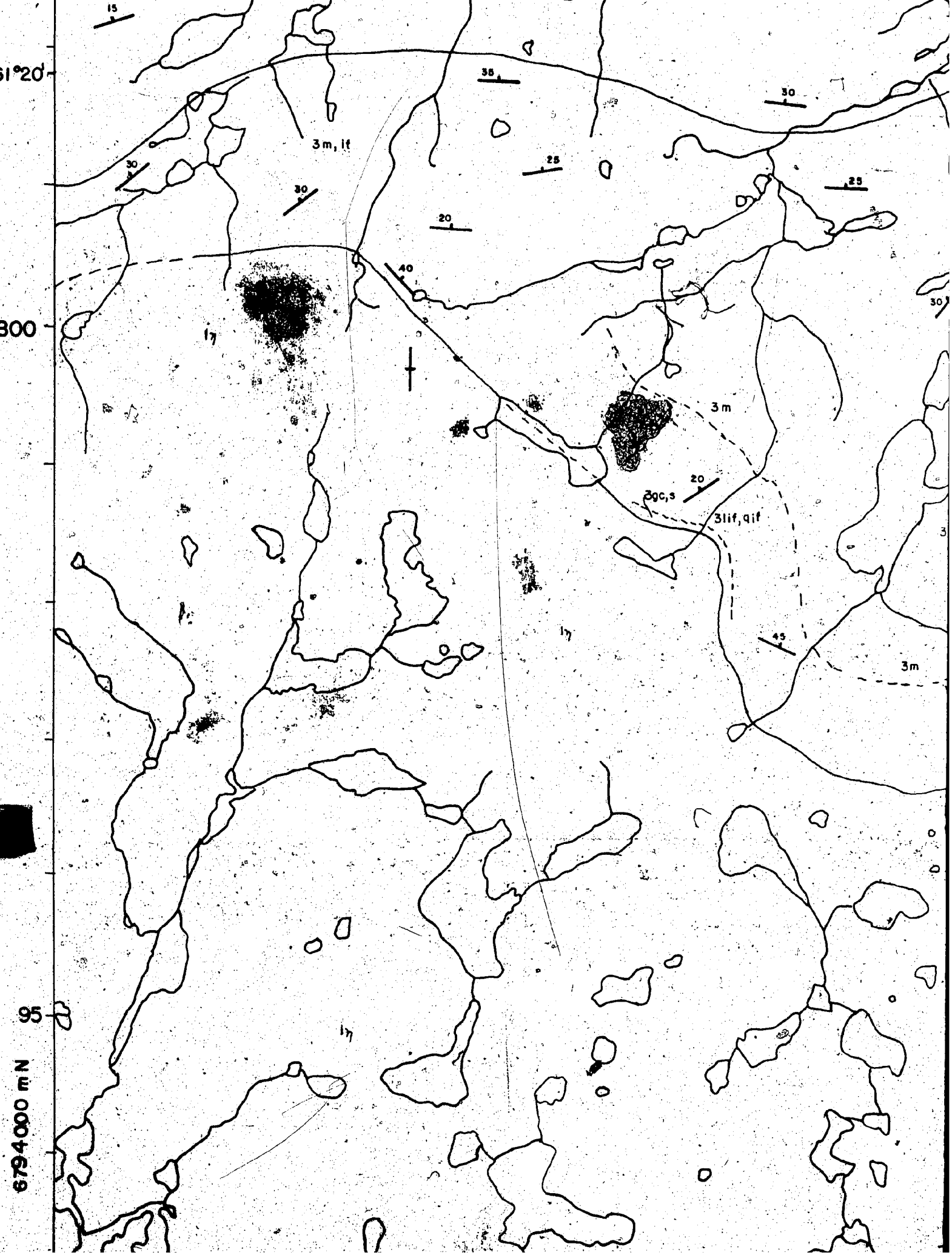
61°20'
300
95
6794000 mN
15
35
30
3m, lf
30
30
25
25
20
40
30
lη
3m
3gc,s
20
3lif, qif
45
3m
lη
lη

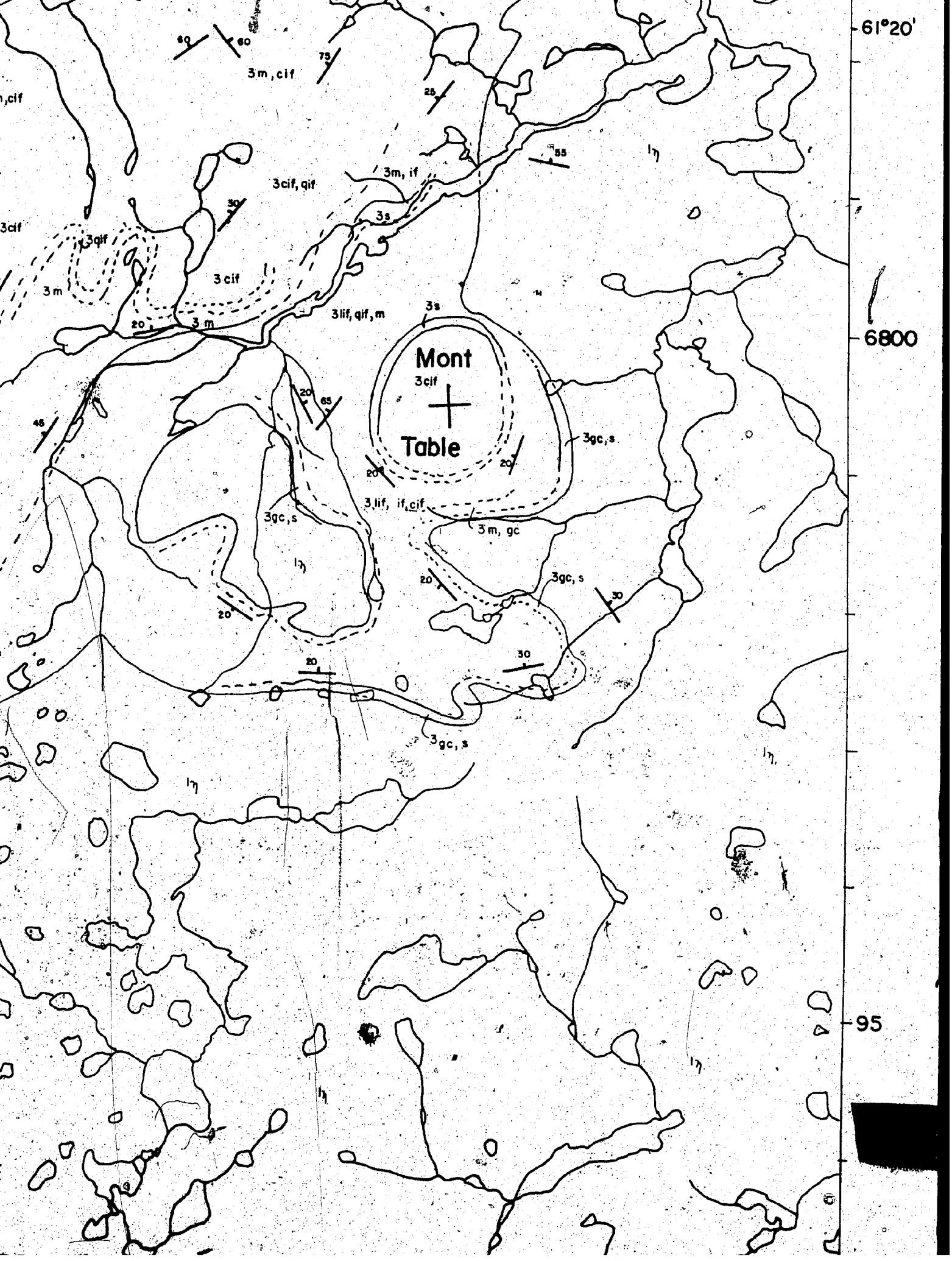
61°20'
6800
95
Mont
3cif
Table
3m, cif
3cif, qif
3m, if
3s
3qif
3cif
3m
3lif, qif, m
3gc, s
3lif, if, cif
3m, gc
lη

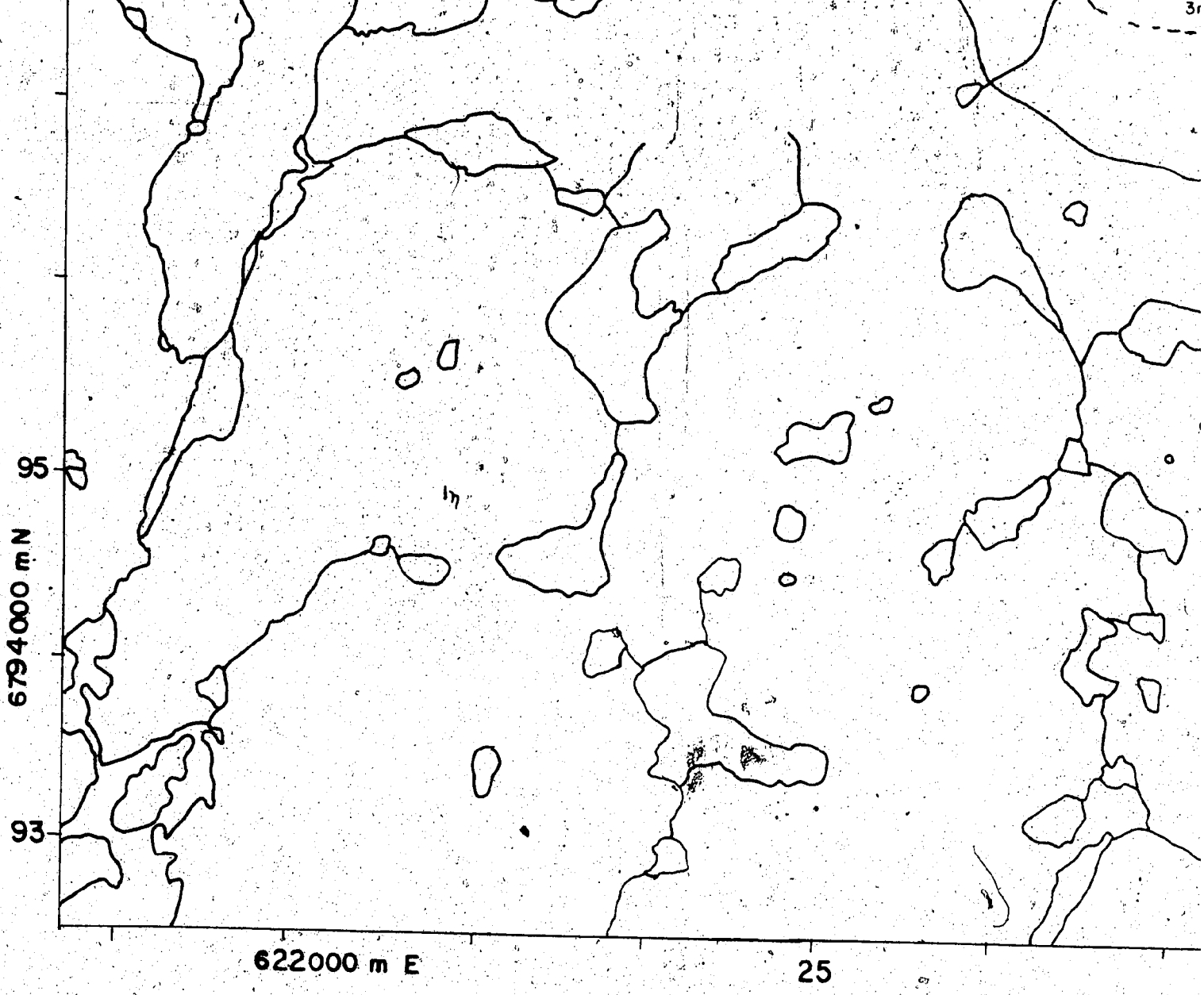

Geology by K. Schimann: 1971, 1972;
M. Hocq, W. Müller: 1971;
R. Côté and P. Sylvestre: 1972.

GEO
LAC VI
QUE

Figure 5.

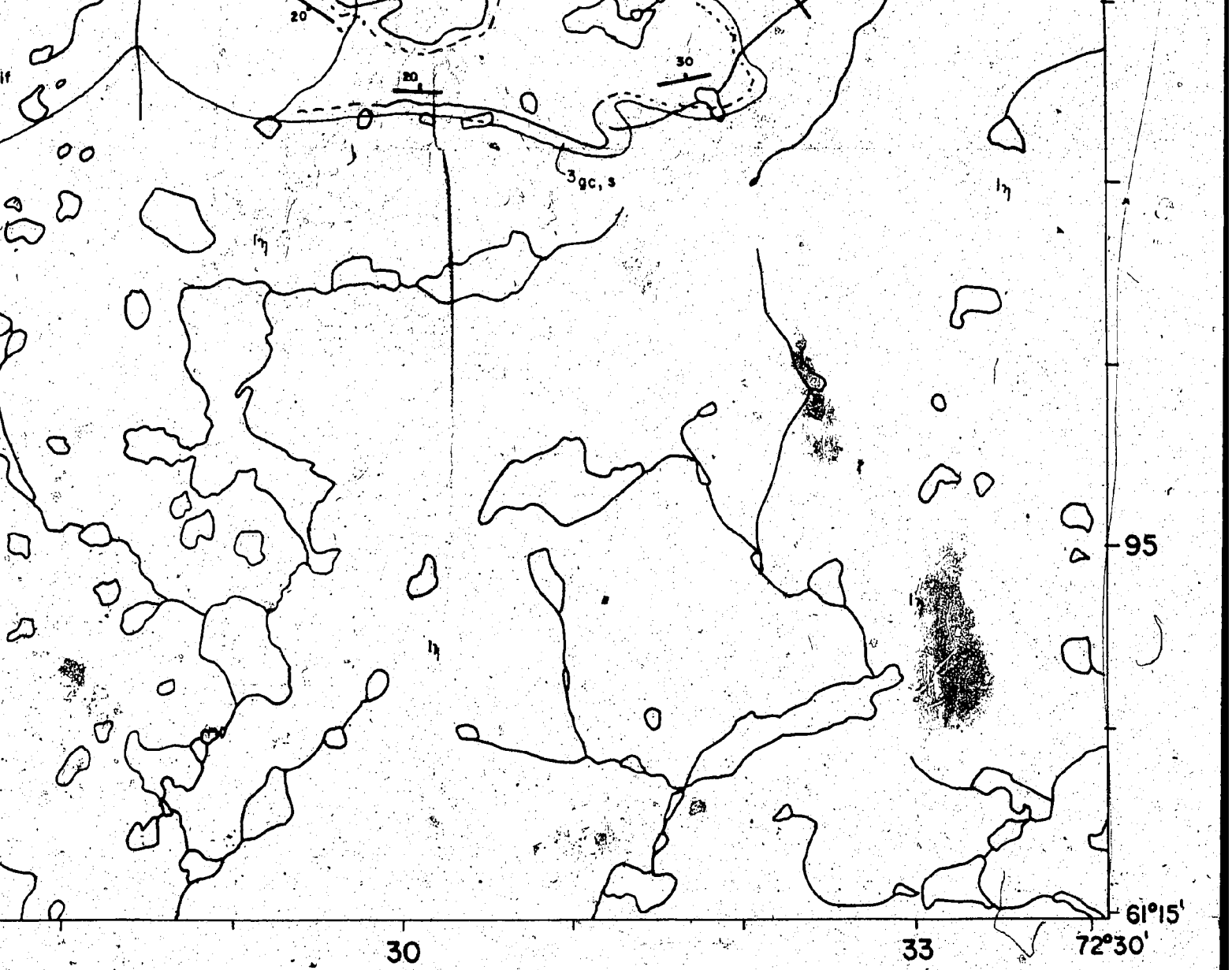

Topography based on topographic maps published at a scale of 1:50 000 by the Deparment of Energy, Mines and Resources, Ottawa.

UTM Grid 18V NTS 35 H/7E

scale

0 1 2km

OGY

NZA E

EC

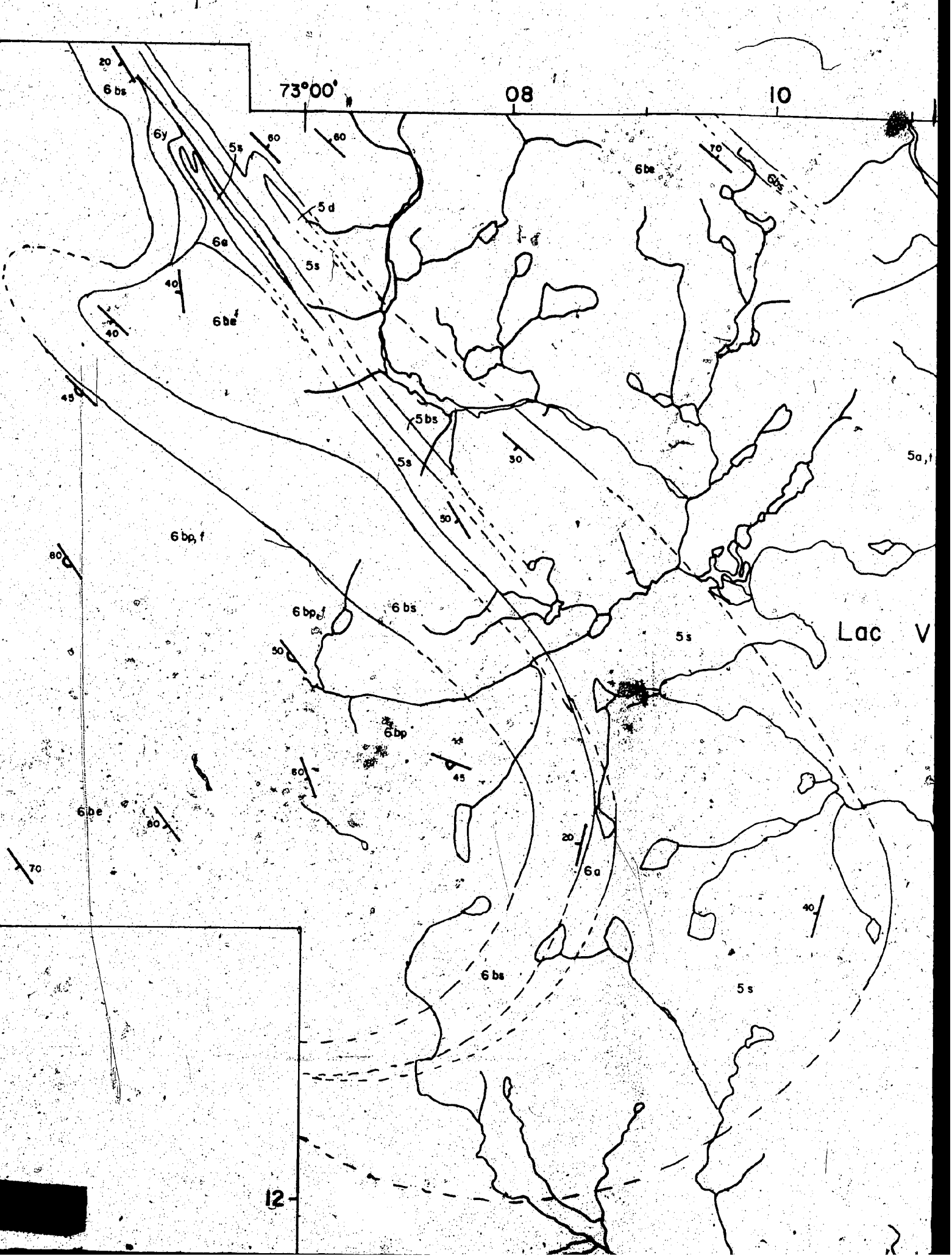
73°00'
08
10
12
Lac V
6 bs
6y
5s
5d
6e
6be
5bs
6 bp, f
6bp
6a
5a, t

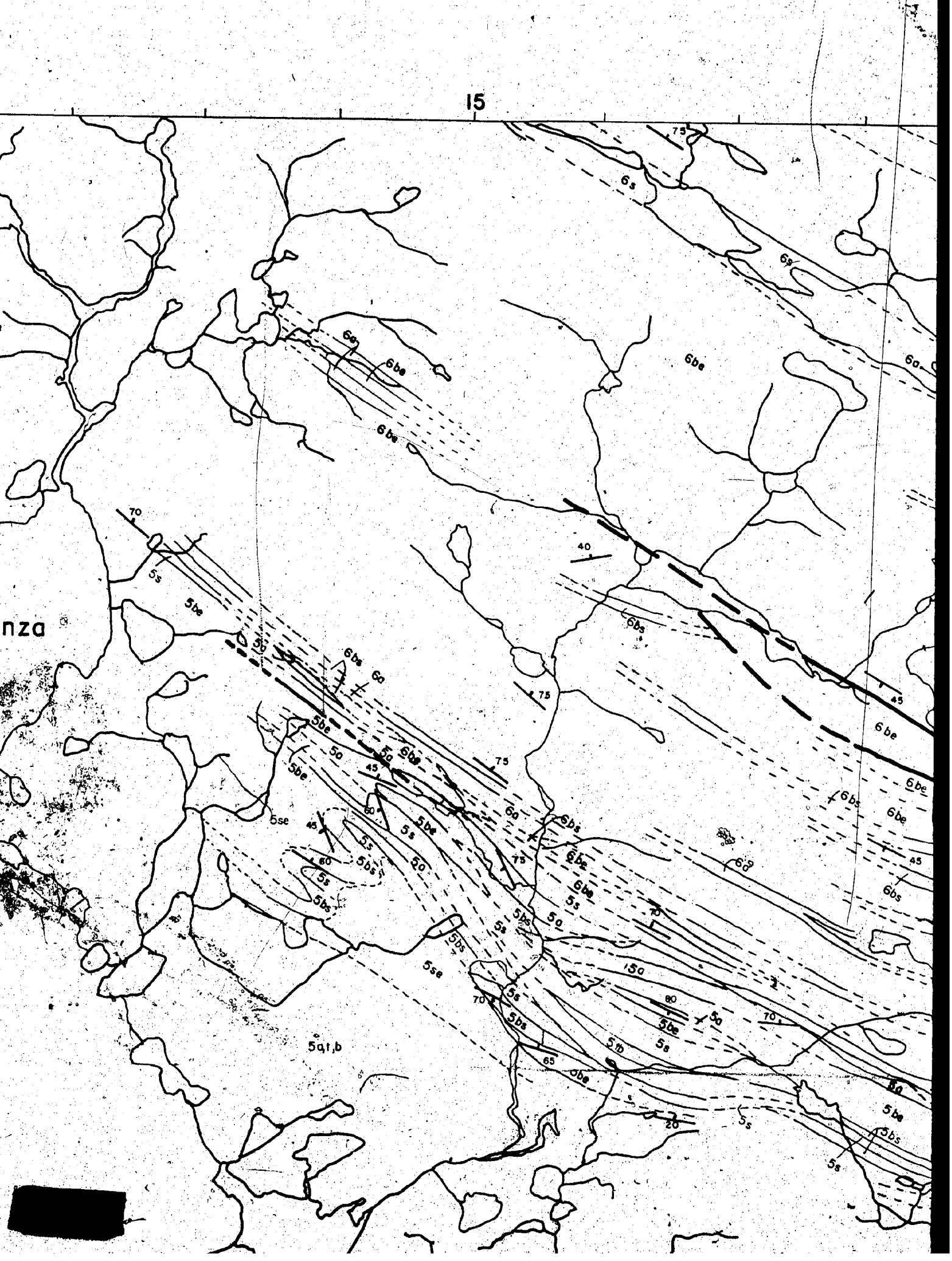
15
nza
6s
6a
6be
6bs
5s
5be
5a
5bs
5se
5a,b
5b
70
75
40
45
50
60
65

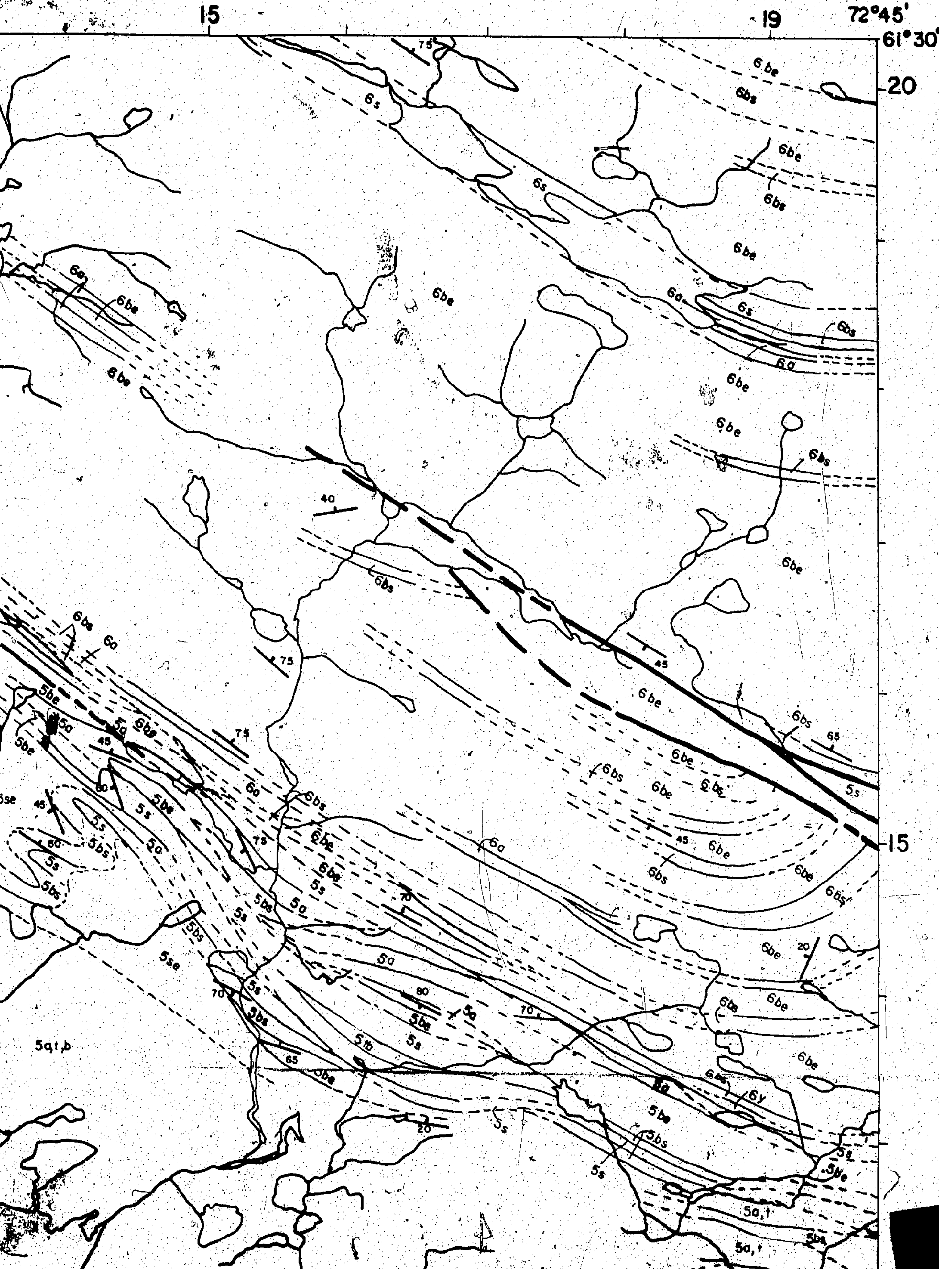
15
19
72°45'
61°30'
20
15
6be
6bs
6s
6a
5be
5bs
5a
5s
5se
5a,t,b
5a,t
6y

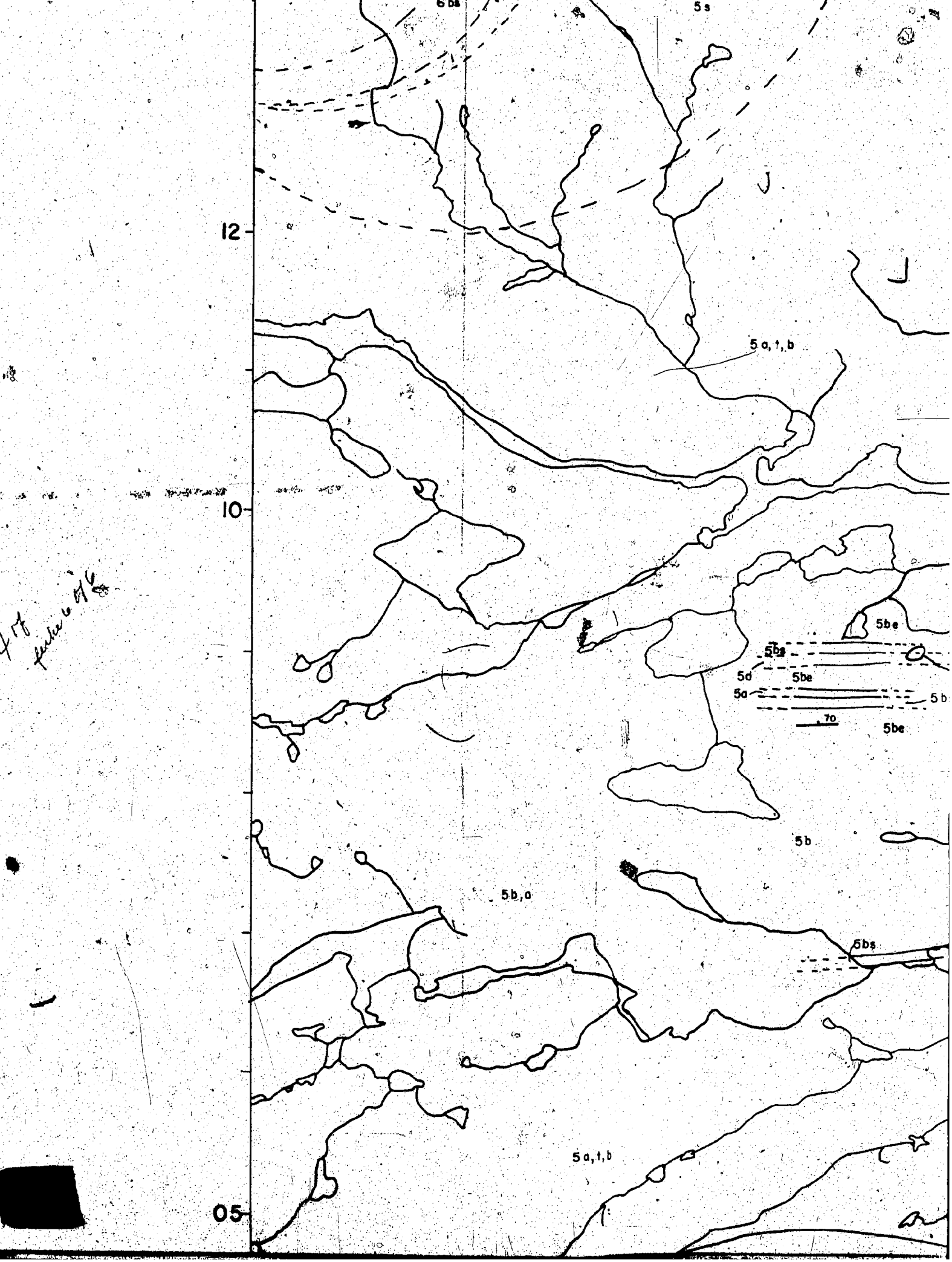
6 bs
5 s
12
5 a, t, b
10
5be
5bs
5d
5be
5a
5 b
70
5be
5b
5b, a
5bs
5 a, t, b
05

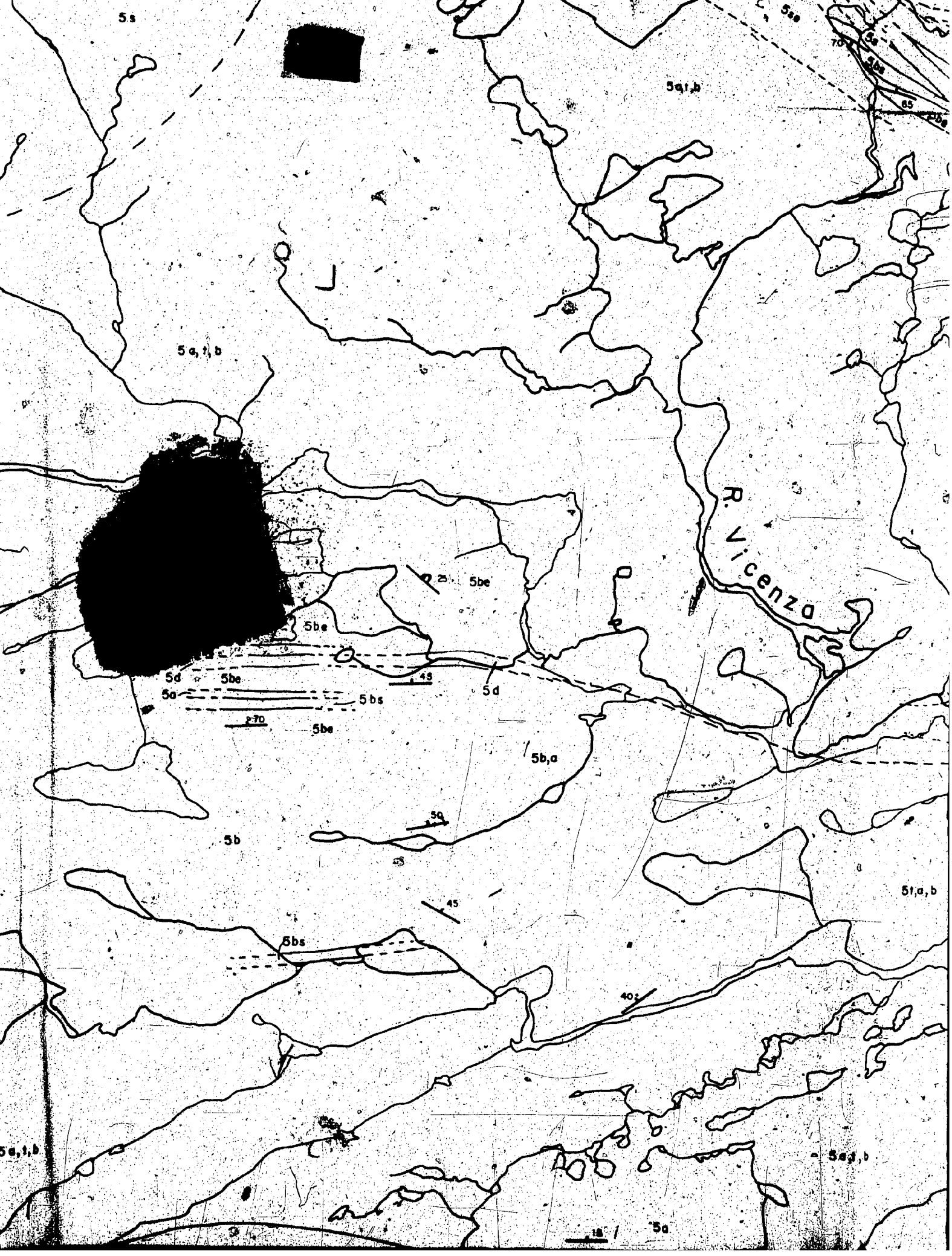
5s
5a,1,b
5a,1,b
5be
5be
5d
5be
5a
5bs
5d
5be
5b,a
5b
5bs
5a,1,b
5a,1,b
5a
R. Vicenza

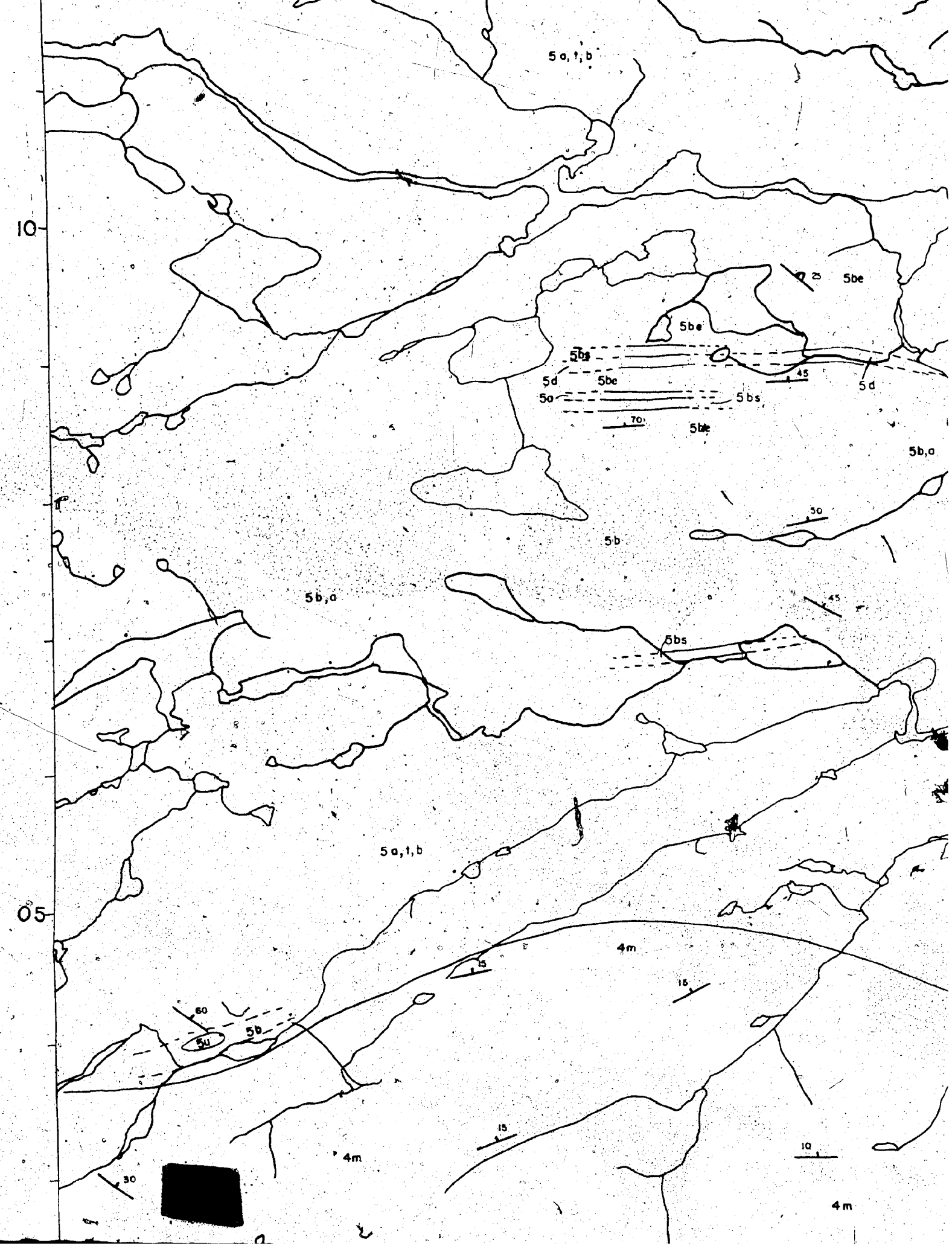
5a,1,b
10
5be
5be
5bs
5d
5be
5d
45
5a
5bs
70
5b
5b,a
30
5b
5b,a
45
5bs
5a,1,b
05
4m
15
15
60
5b
5u
15
4m
10
30
4m

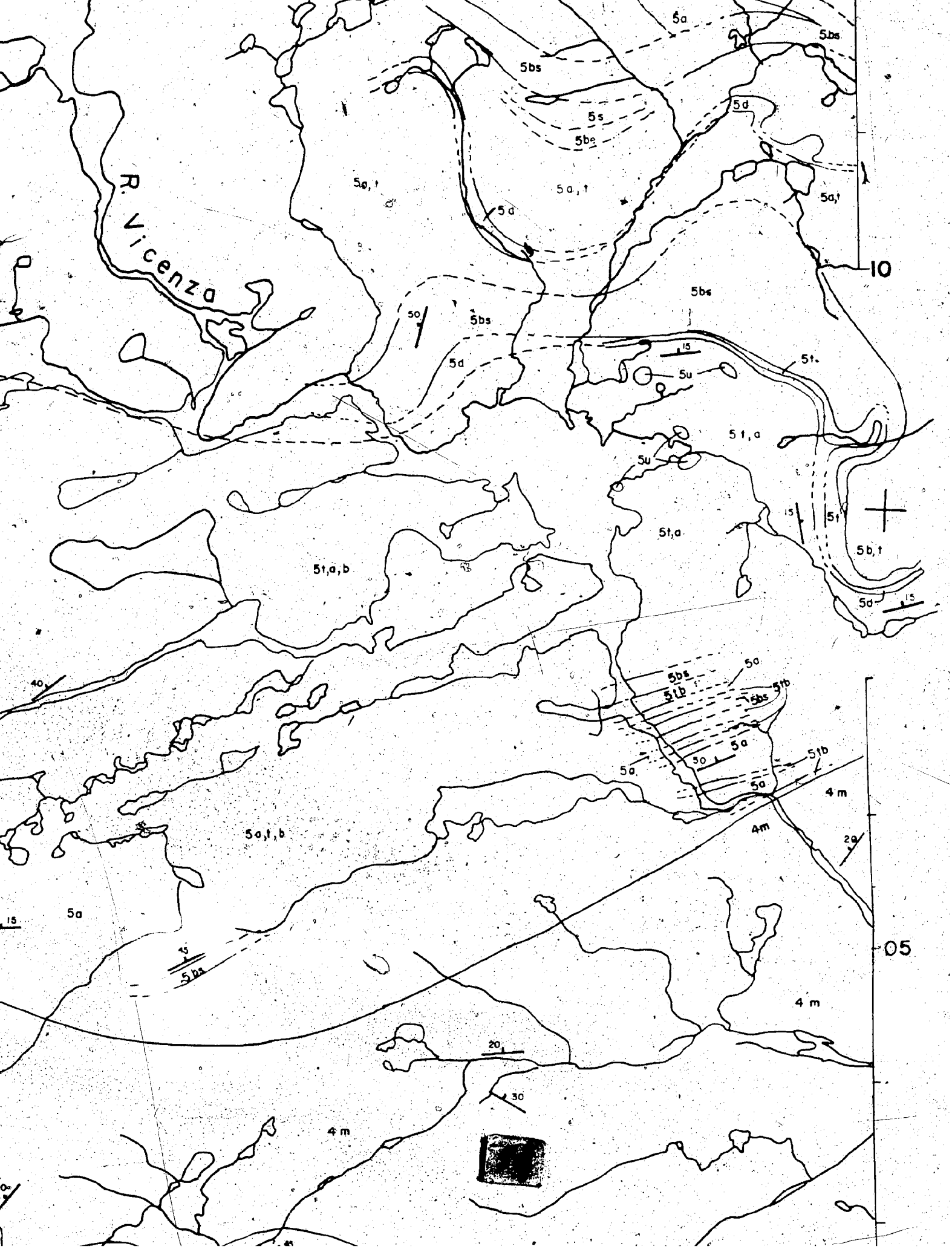
R. Vicenza
5a
5bs
5d
5s
5be
5a,f
10
5bs
5t.
5u
5t,a
5t,a,b
5b,f
5d
5bs
5a
5t,b
4m
5a,f,b
05
4m
20
30
4m

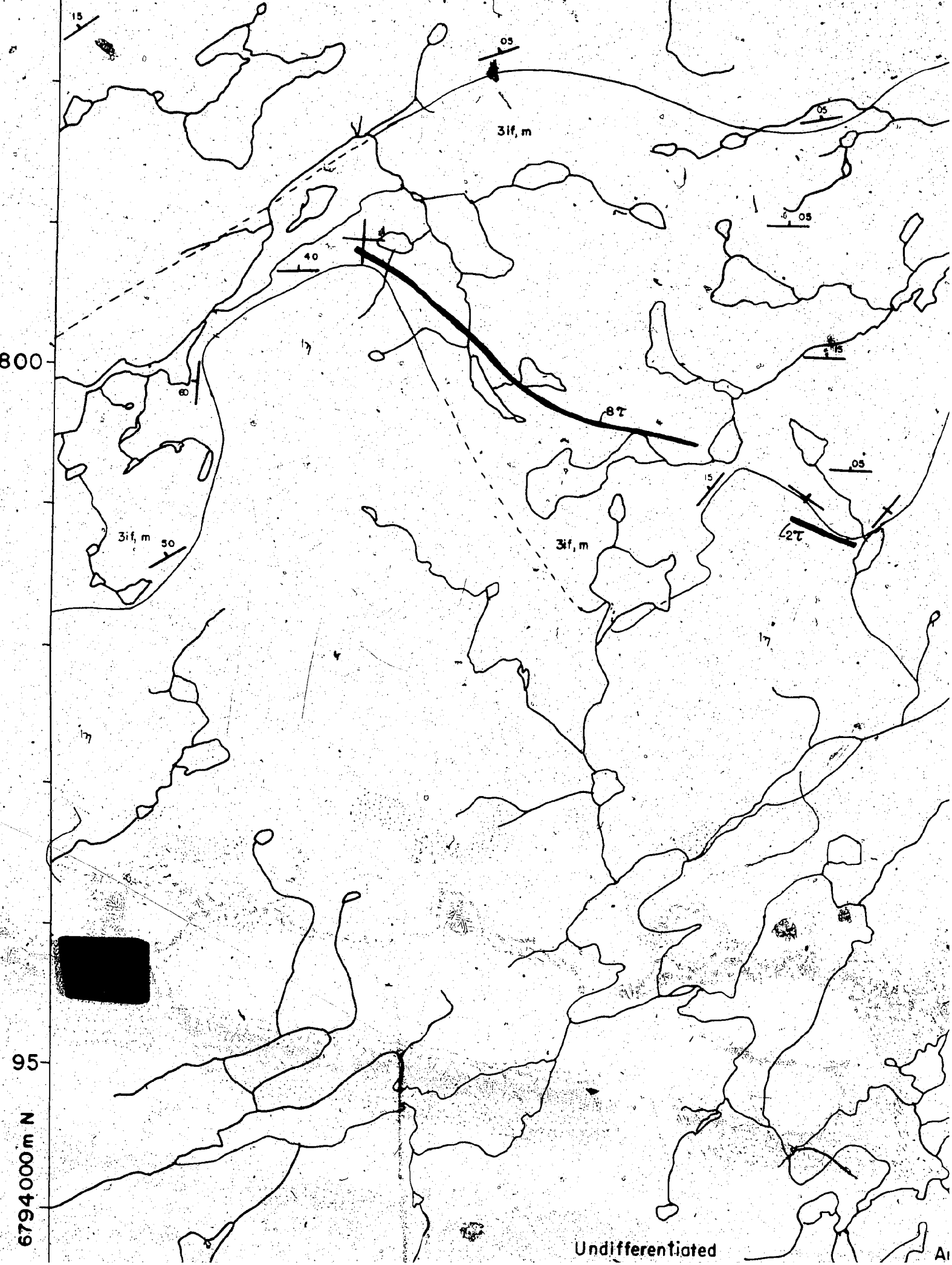
800
95
6794000 m N
15
05
05
05
40
15
80
3if, m
50
3if, m
3if, m
8τ
2τ
Undifferentiated

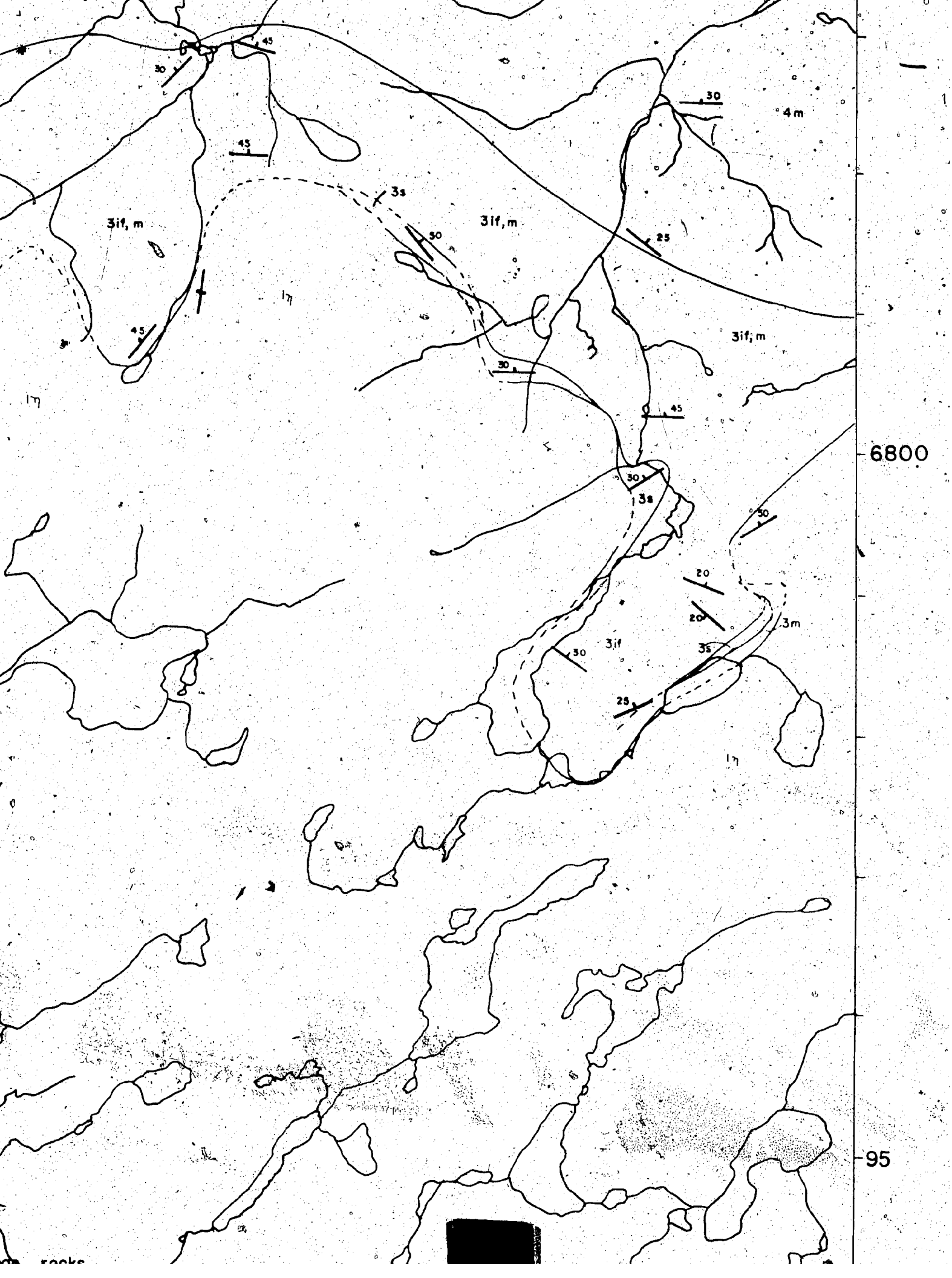
3if, m
3s
3if, m
4m
3if; m
6800
3s
3m
3if
95

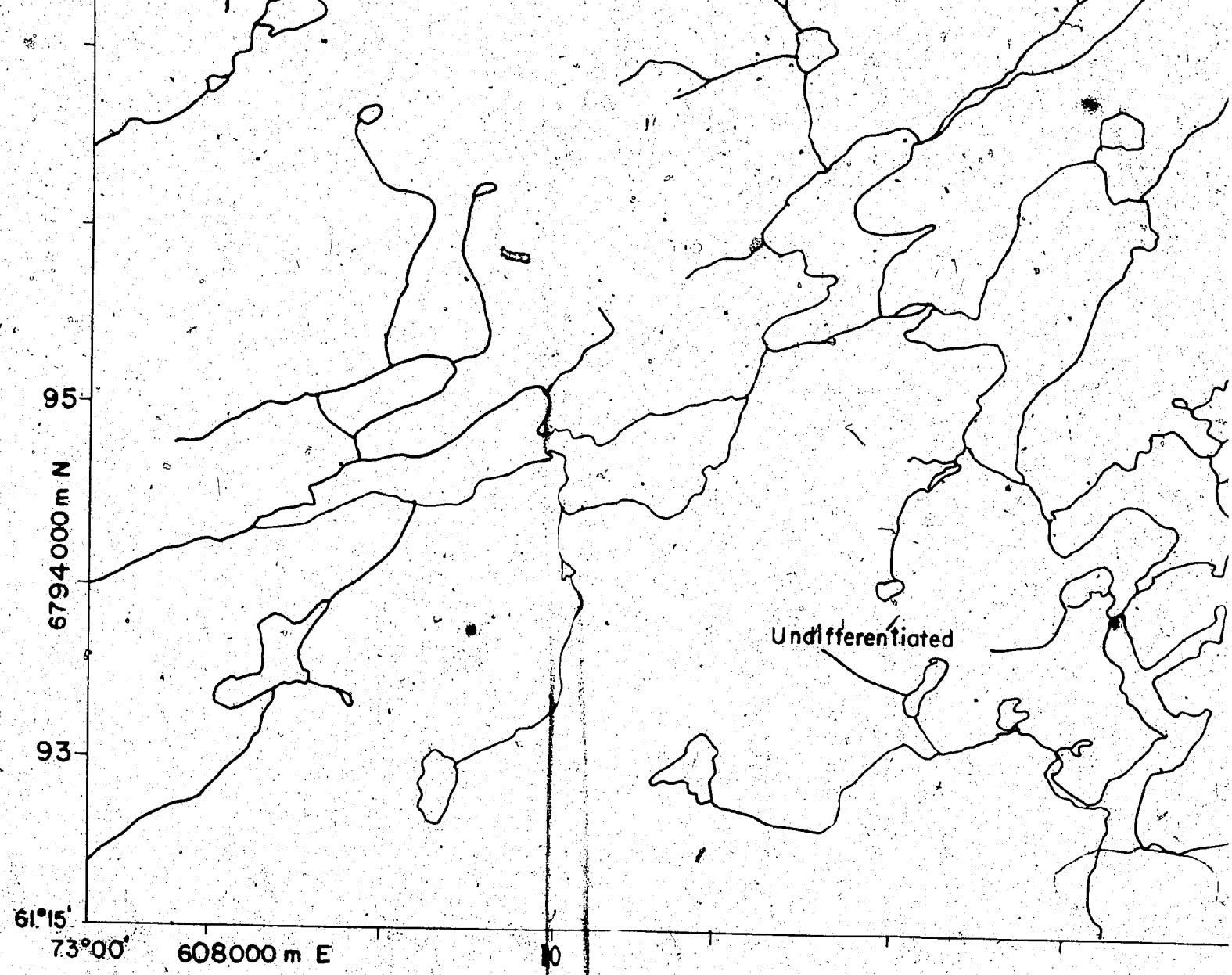

ology by K. Schimann; 1971, 1972;
Charlebois, R. Côté, M. Trudeau
d P. Sylvestre, 1972.

GEOL
LAC VIC
QUE

igure 6.

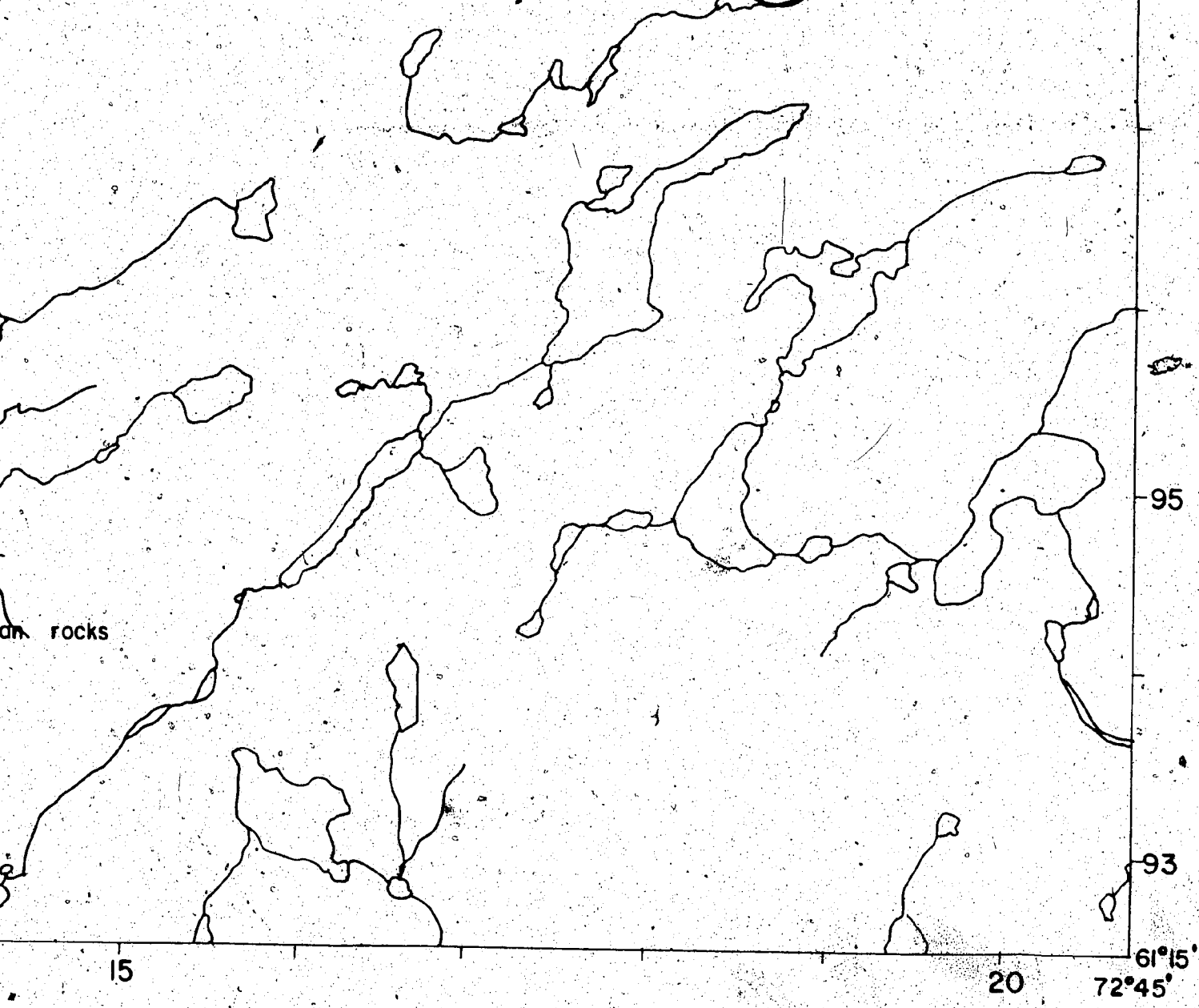

GY

NZA W

EC

Topography based on topographic maps published at a scale of 1:50 000 by the Department of Energy, Mines and Resources, Ottawa.

UTM Grid 18V NTS 35 H/7W

scale

0 1 2 km

[redacted]

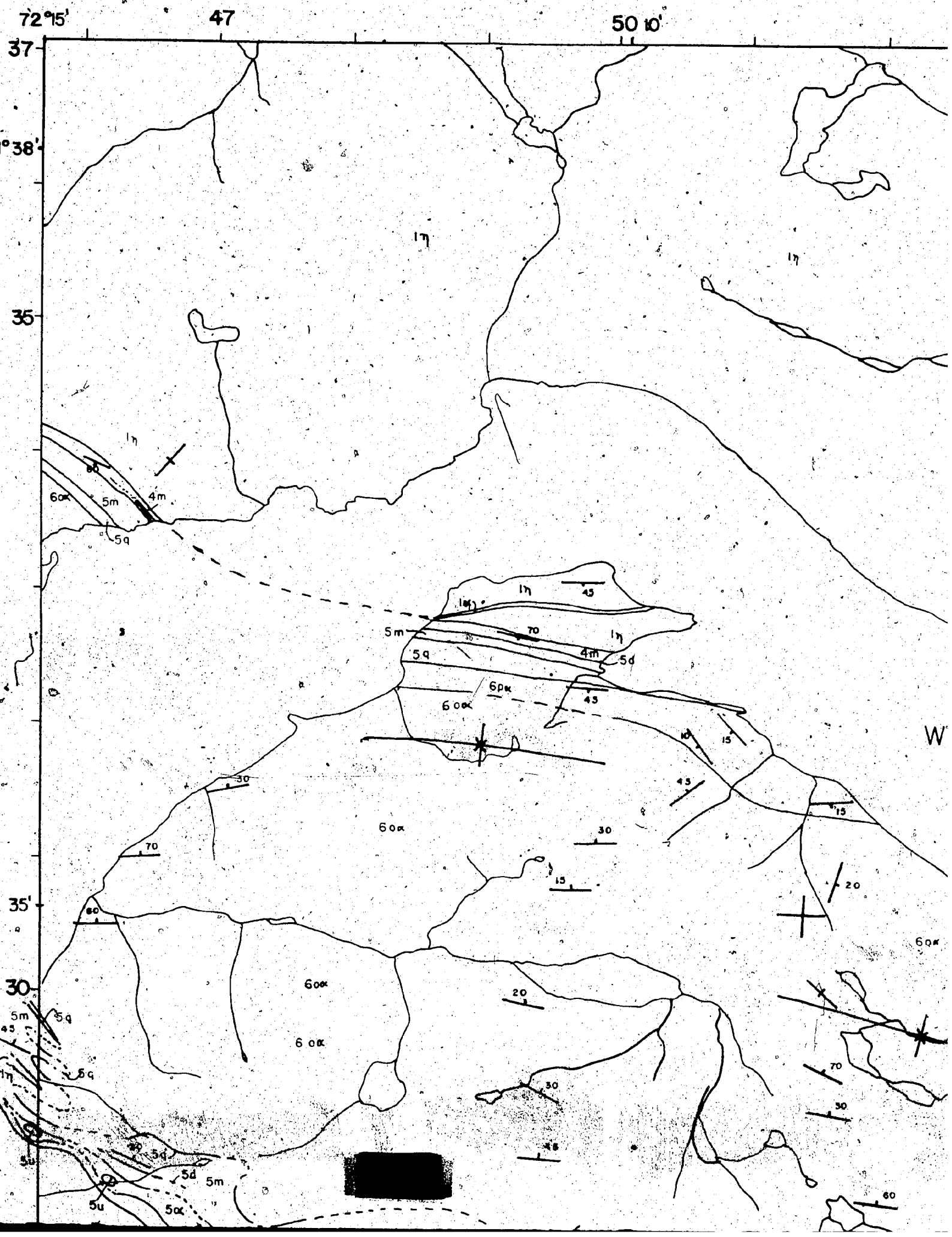
72°15'
47
50 10'
37
°38'
35
35'
30
1η
5m
5q
4m
5d
6pα
6 0α
5u
5α
W

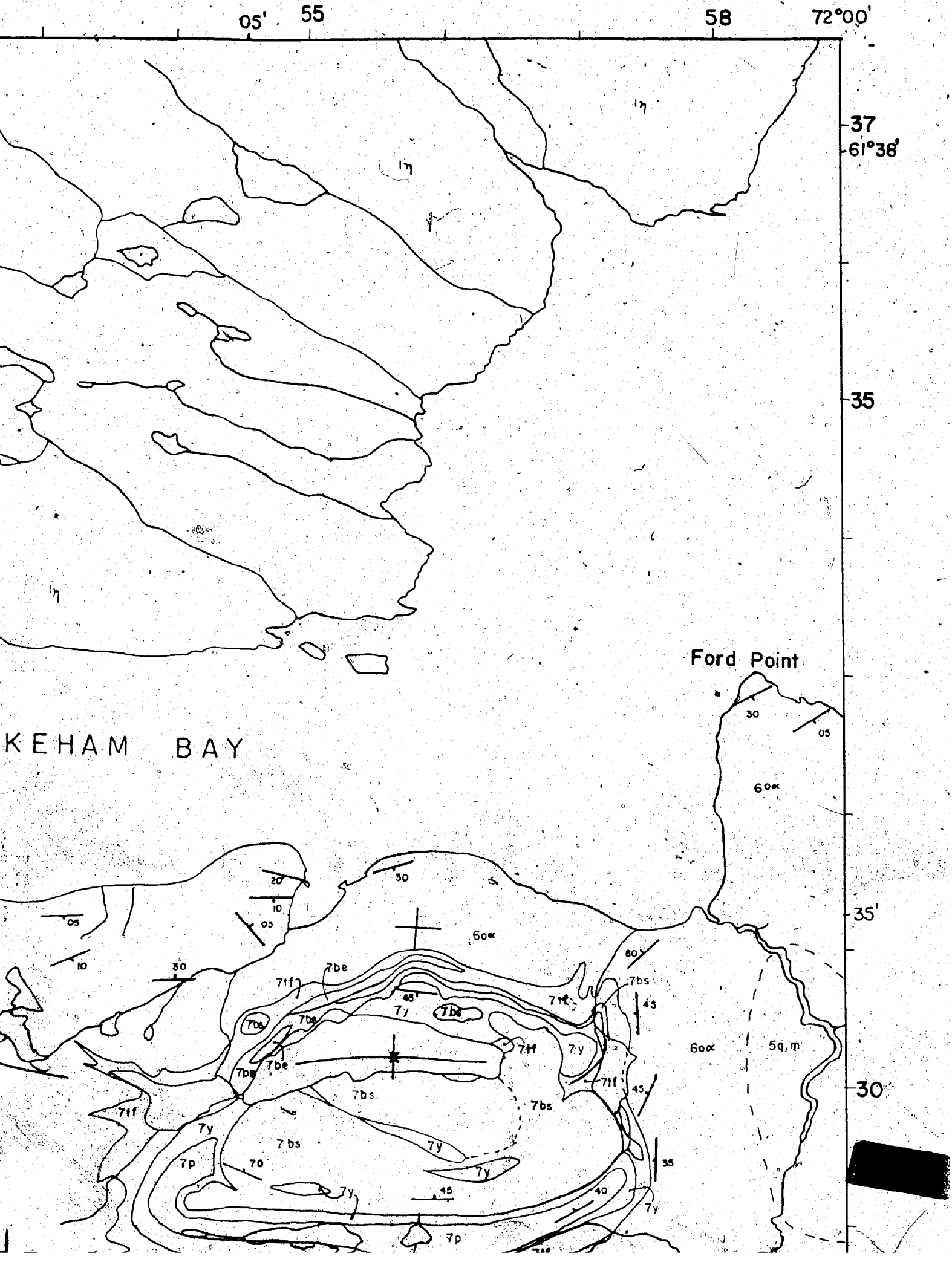
05'
55
58
72°00'
37
61°38'
35
Ford Point
KEHAM BAY
35'
30
60∝
5q, m
7bs
7y
7f
7be
7p

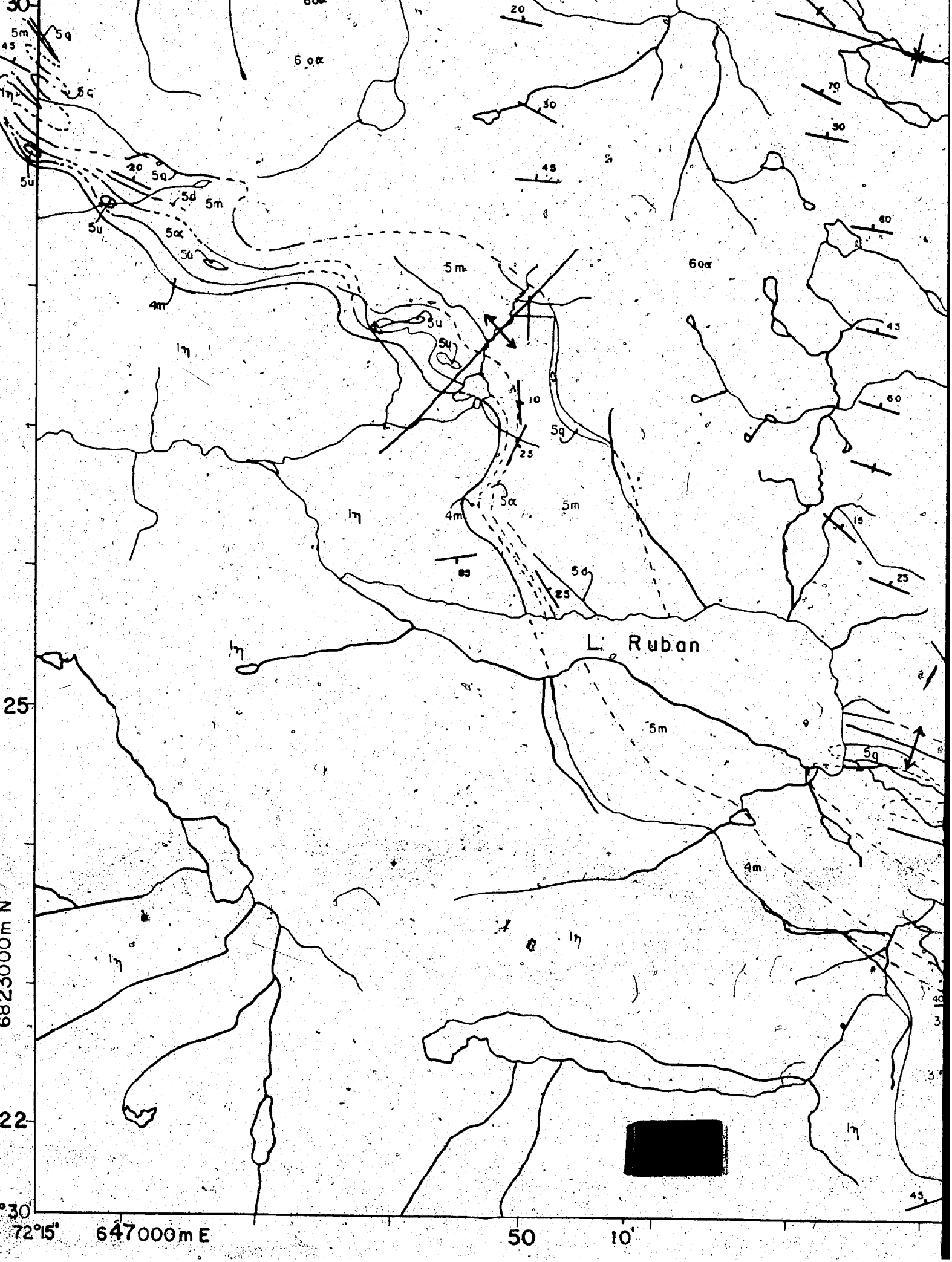
L. Ruban
[redacted]
30
25
22
72°15'
647000m E
50
10'
6823000m N

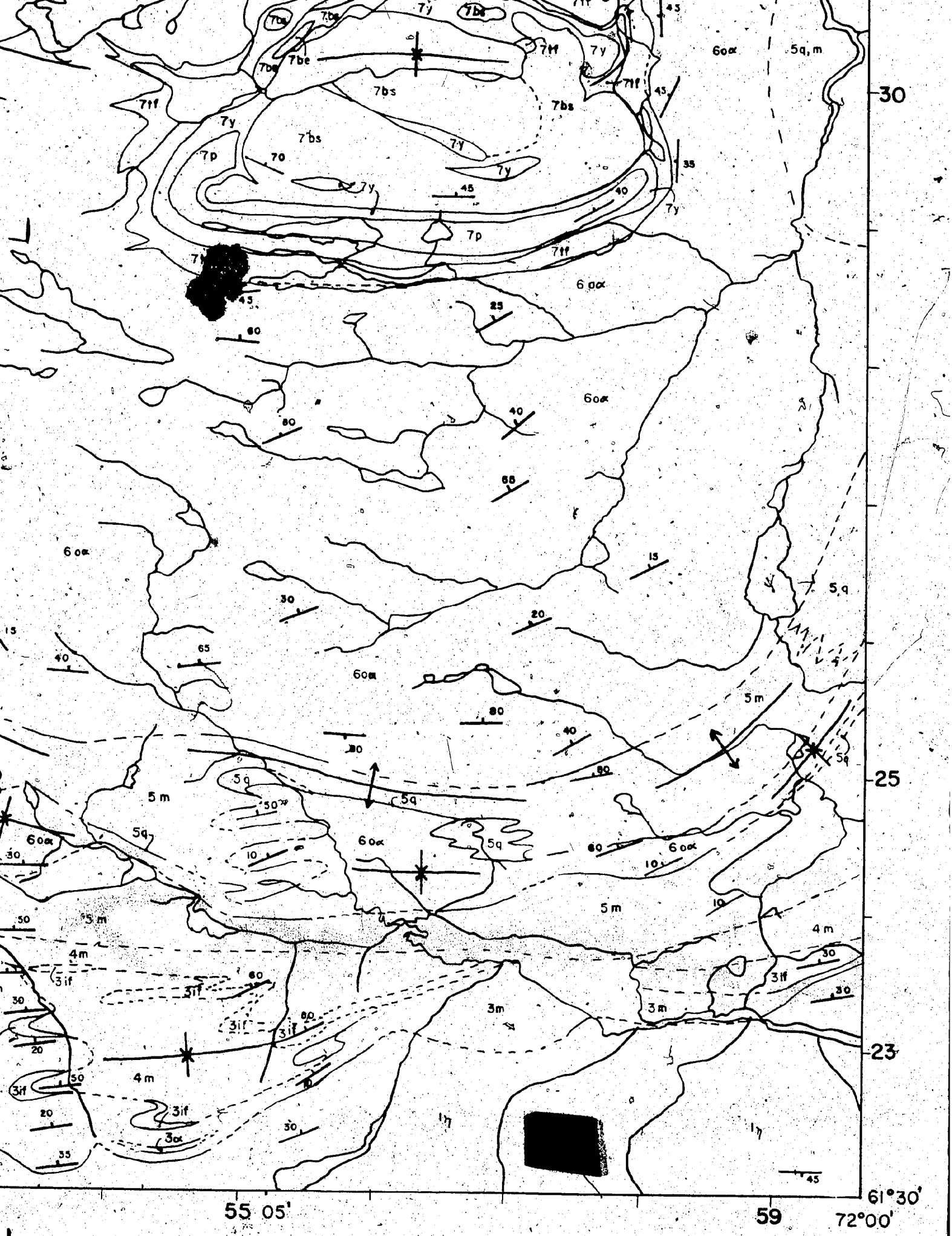
7be
7bs
7y
7p
7ff
6oα
5q, m
5q
5m
4m
3if
3m
3α
30
25
23
55 05'
59
72°00'
61°30'

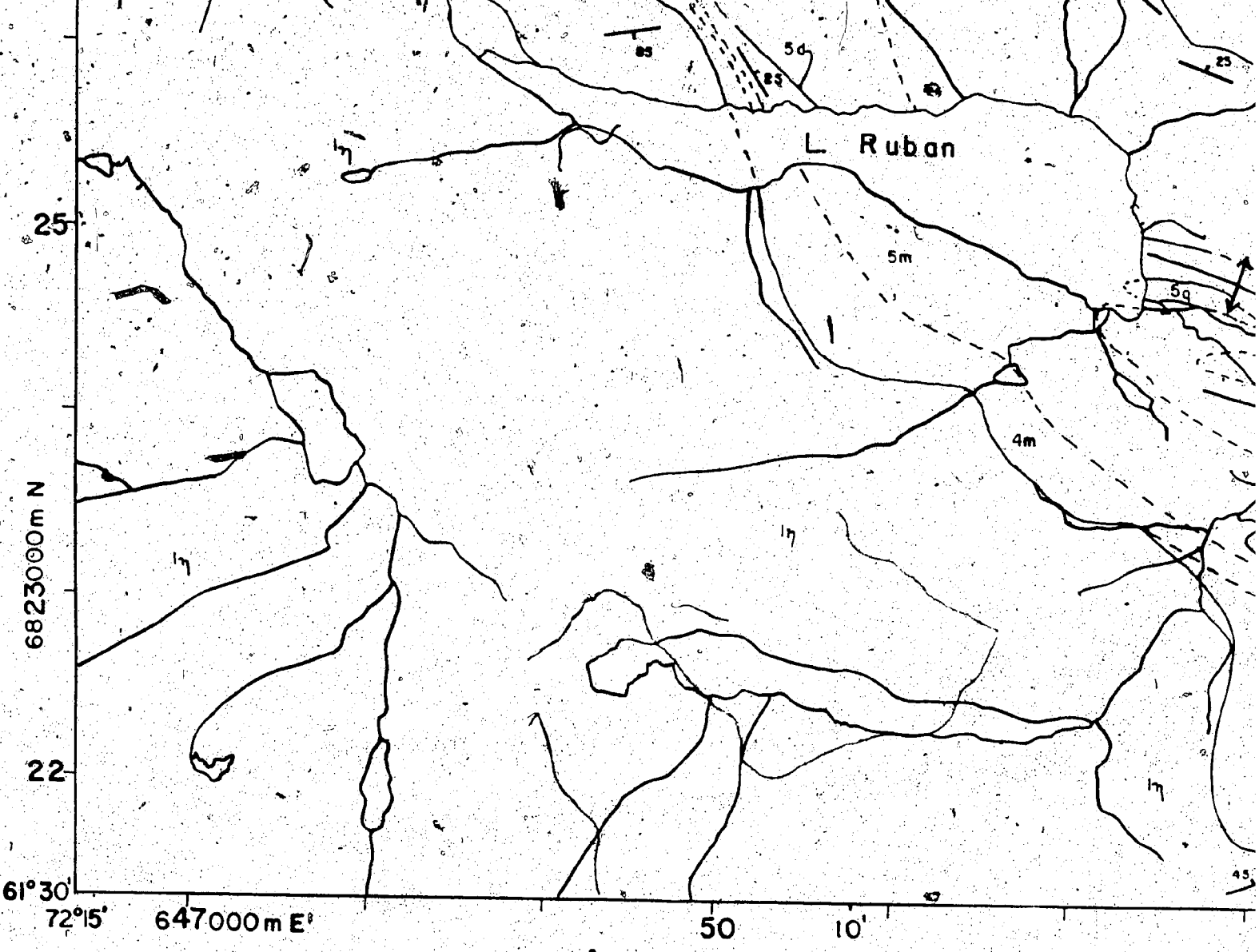

ology by K. Schlmann, L. Charlebois,
Côté and P. Denis, 1972.

GEOL

part of MOUNT ALBE

QUE

igure 7.

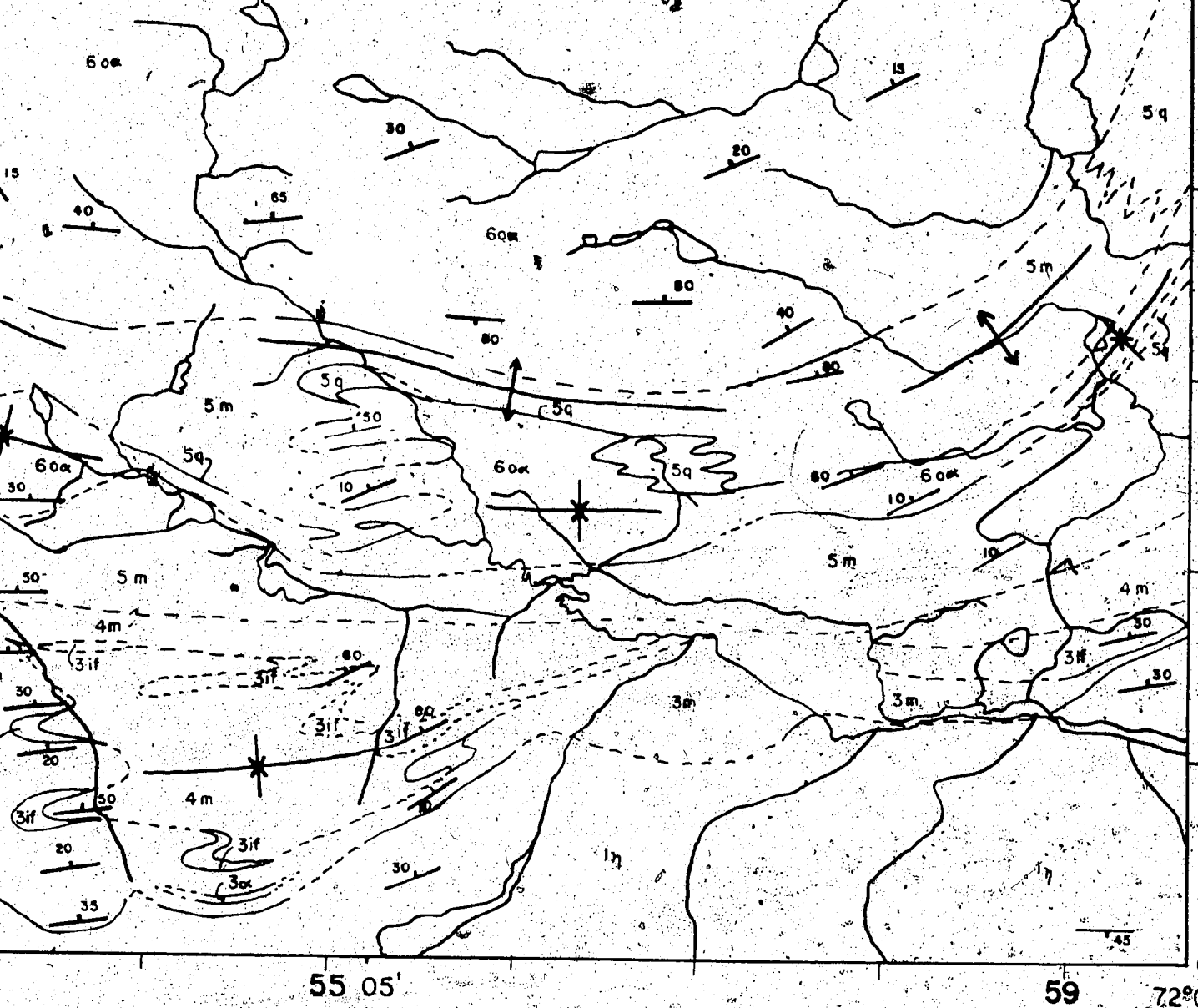

OGY

RT LOW E

EC

Topography based on topographic maps published at a scale of 1:50 000 by the Department of Energy, Mines and Resources, Ottawa.

UTM Grid 18V NTS 35 H/9E

scale

0 1 2km

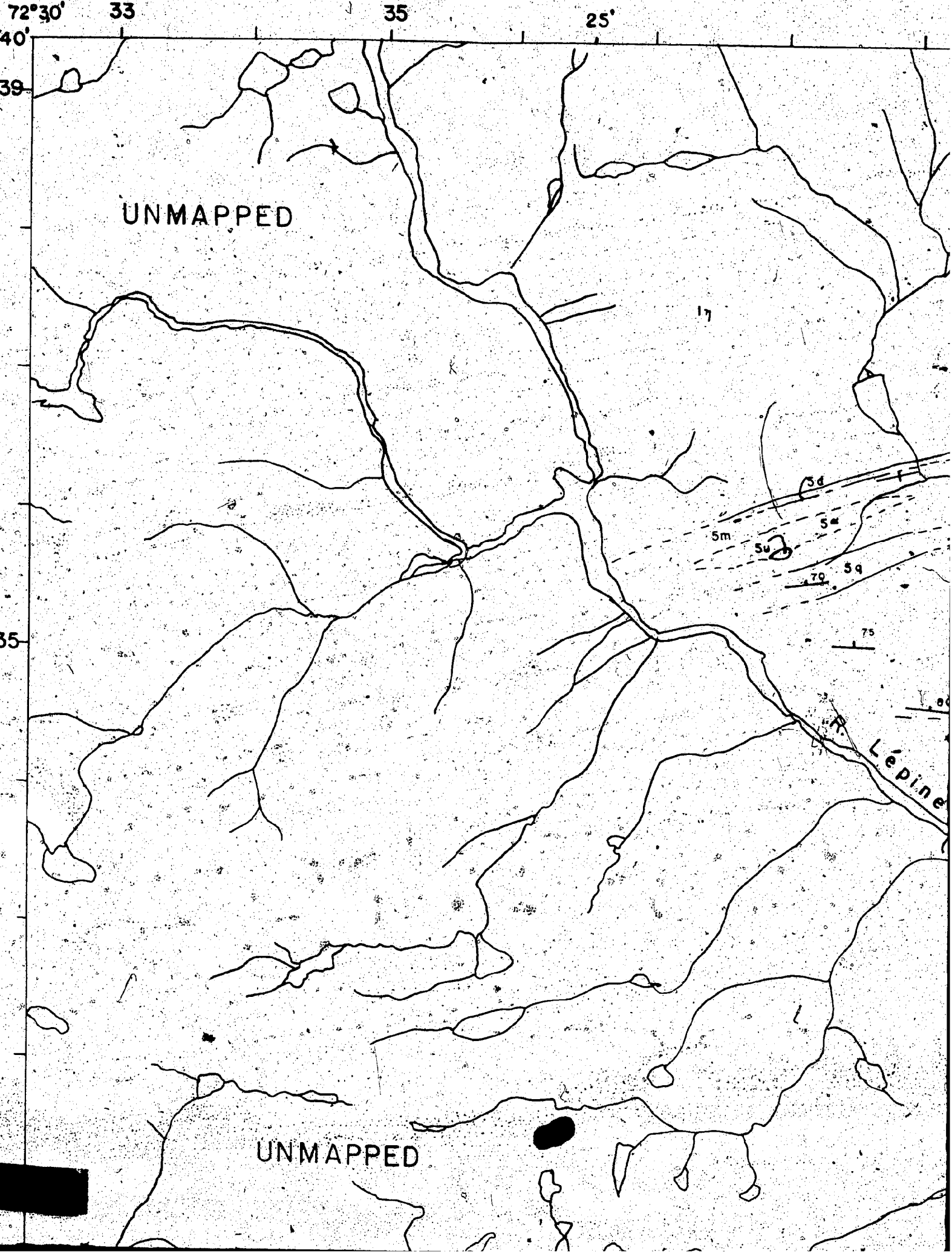
72°30'
33
35
25'
40'
39
35
UNMAPPED
17
5d
5m
5u
5q
70
75
R. Lépine
UNMAPPED

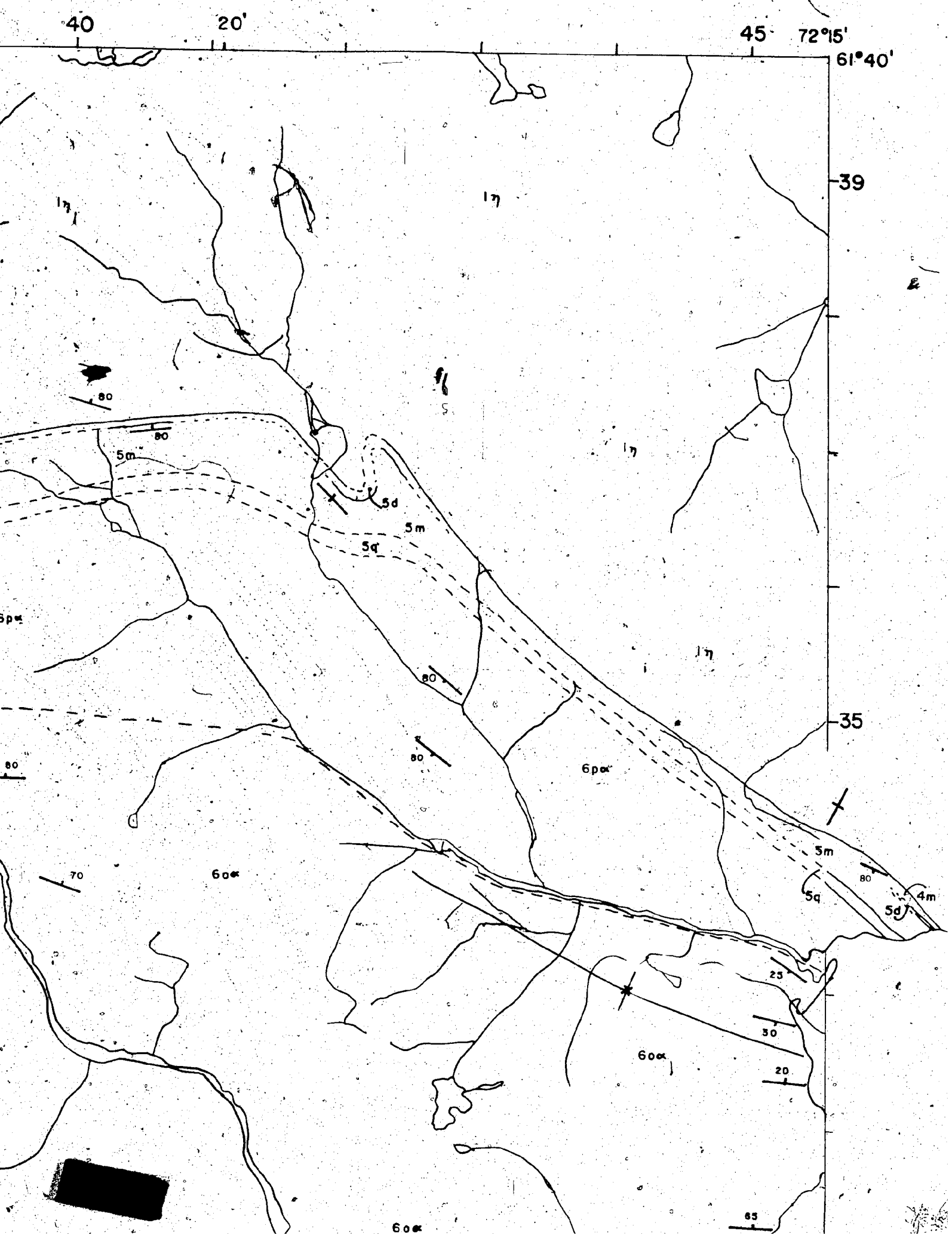
40
20'
45
72°15'
61°40'
39
35
1η
80
5m
5d
5q
6pα
6oα
70
4m
23
30
20
65

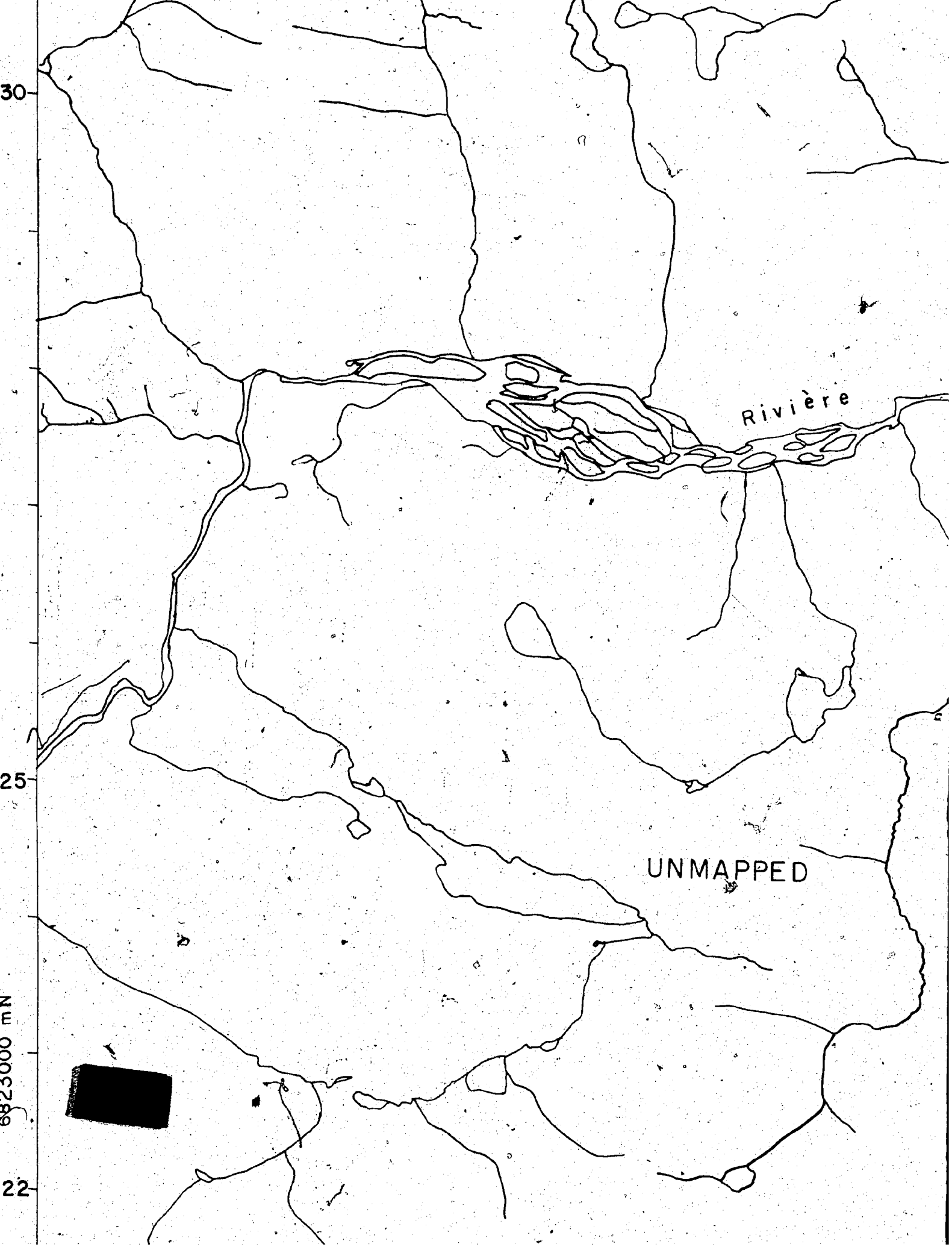
30
Rivière
25
UNMAPPED
6823000 mN
22

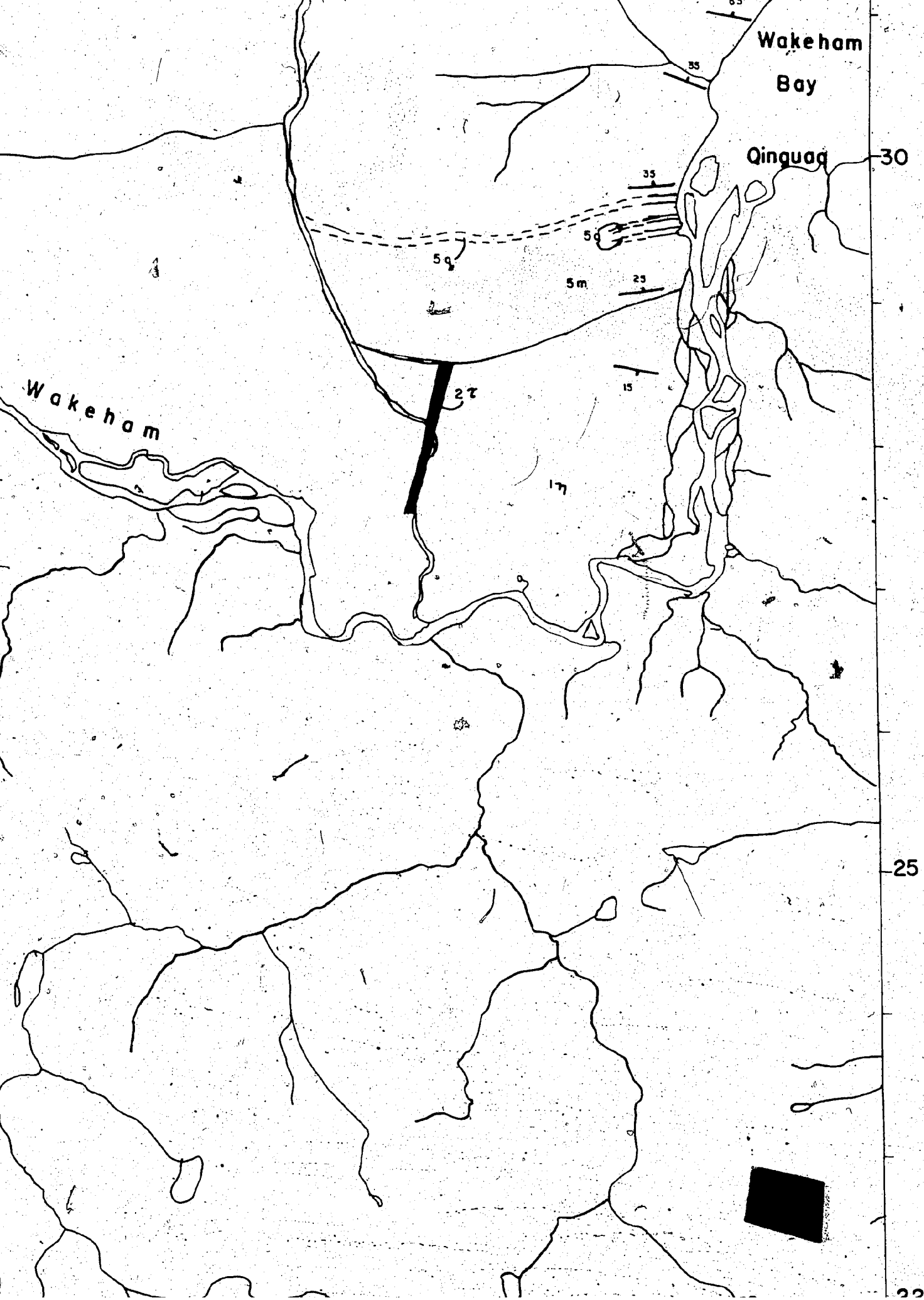
Wakeham
Bay
Qinquaq
30
25
Wakeham
35
50
5m
25
15
27
17

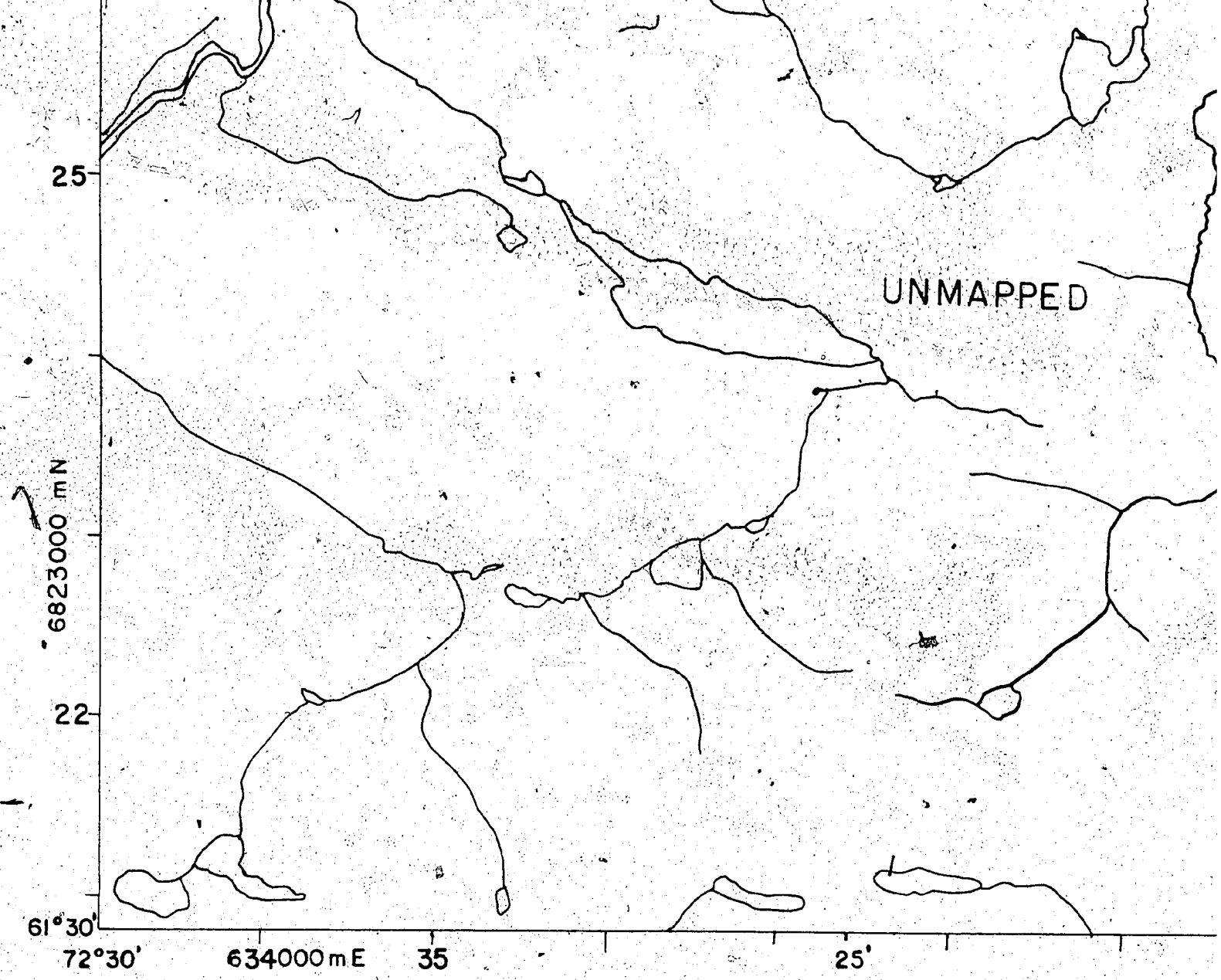

Geology by K. Schimann and L. Charlebois, 1972.

GEO

part of MOUNT ALB

QUE

Figure 8.

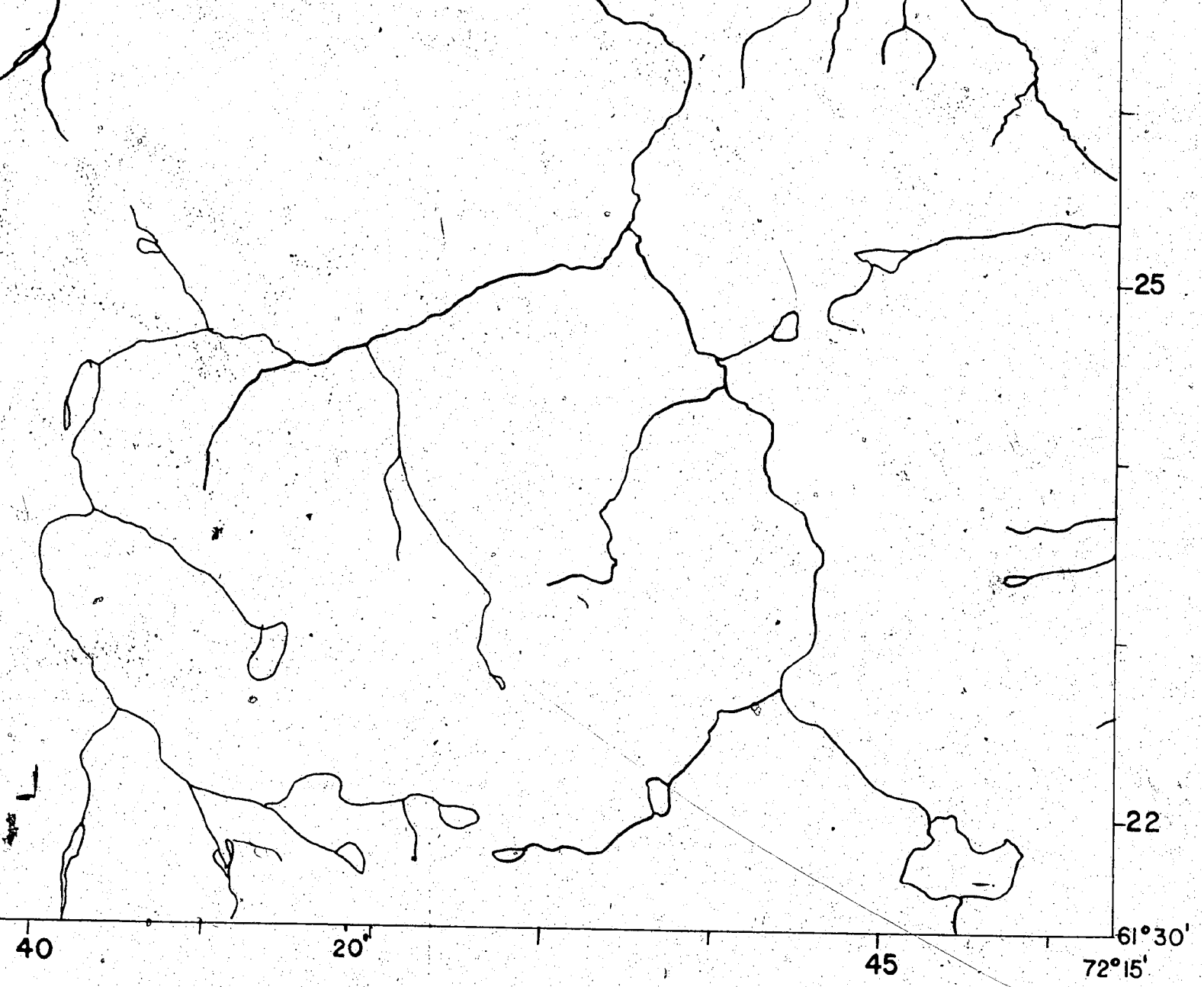

OGY
RT LOW W
EC

Topography based on topographic maps publishe
at a scale of 1:50 000 by the Department
Energy, Mines and Resources, Ottawa.

UTM Grid 18V NTS 35 H/9W

scale

0 1 2km


71°45'
°45'
73
75
40'
50
45
HUDSO

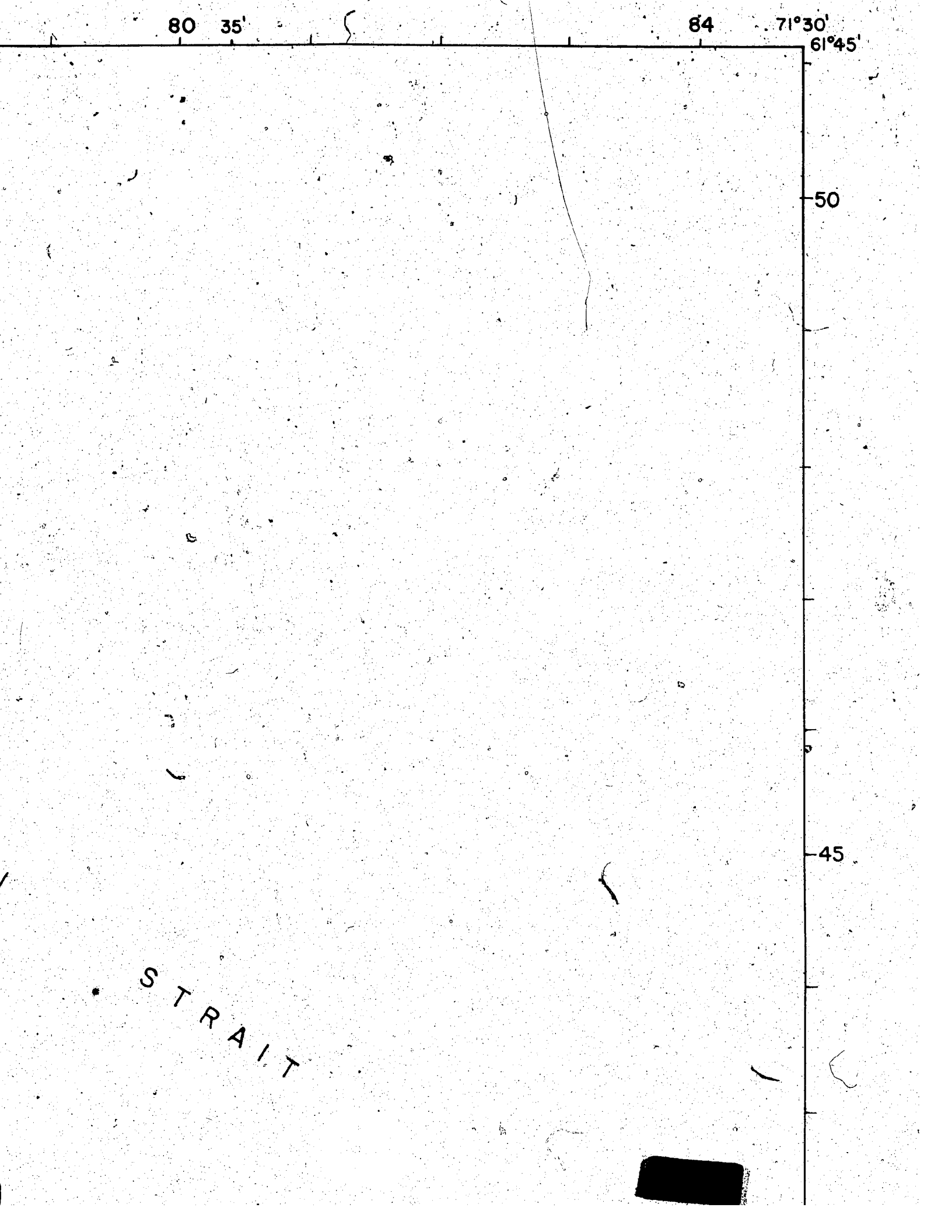
80 35'
84
71°30'
61°45'
50
45
STRAIT

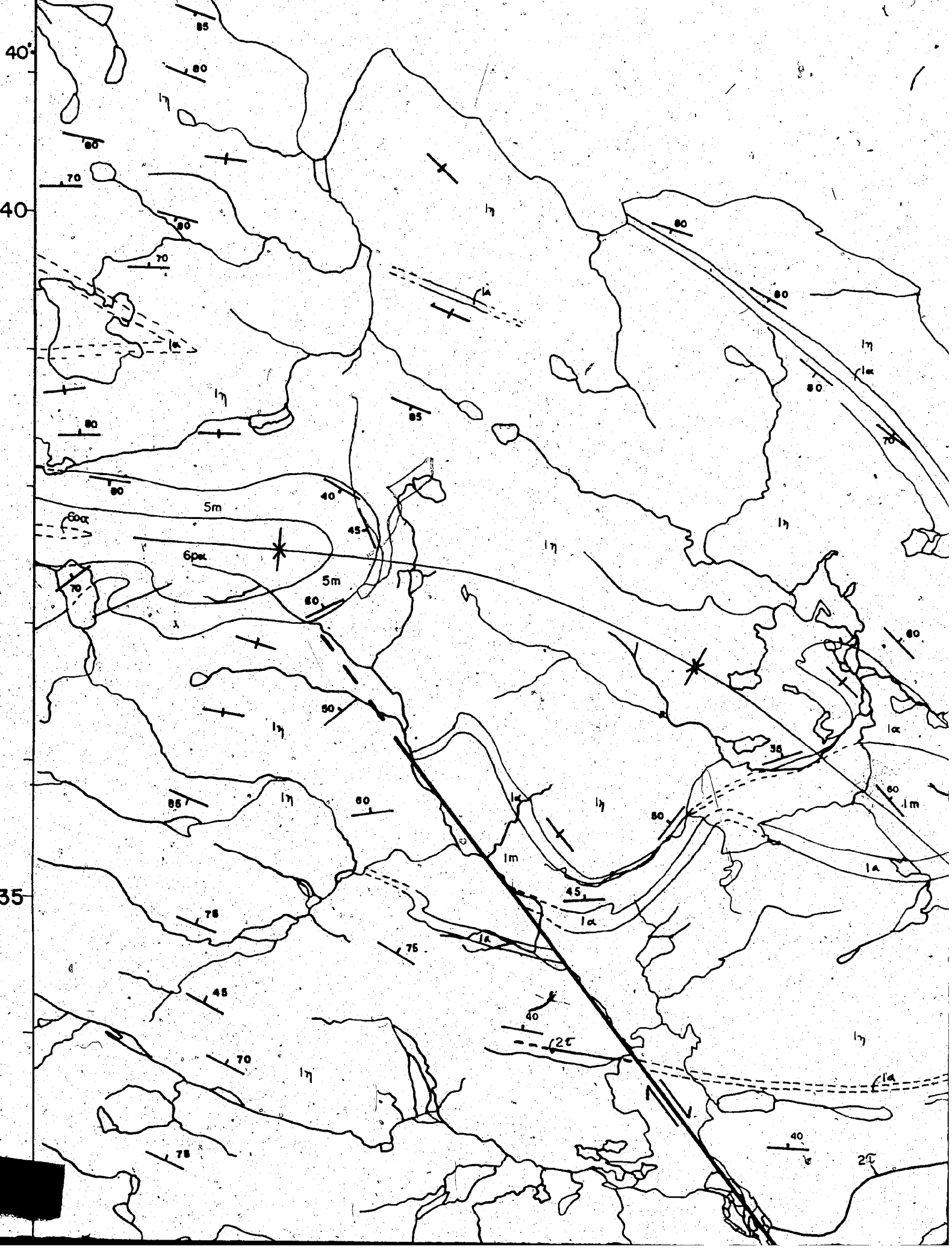
40°
40
35
85
80
70
60
50
45
40
75
35
5m
6pα
60α
1η
1α
1m
2τ

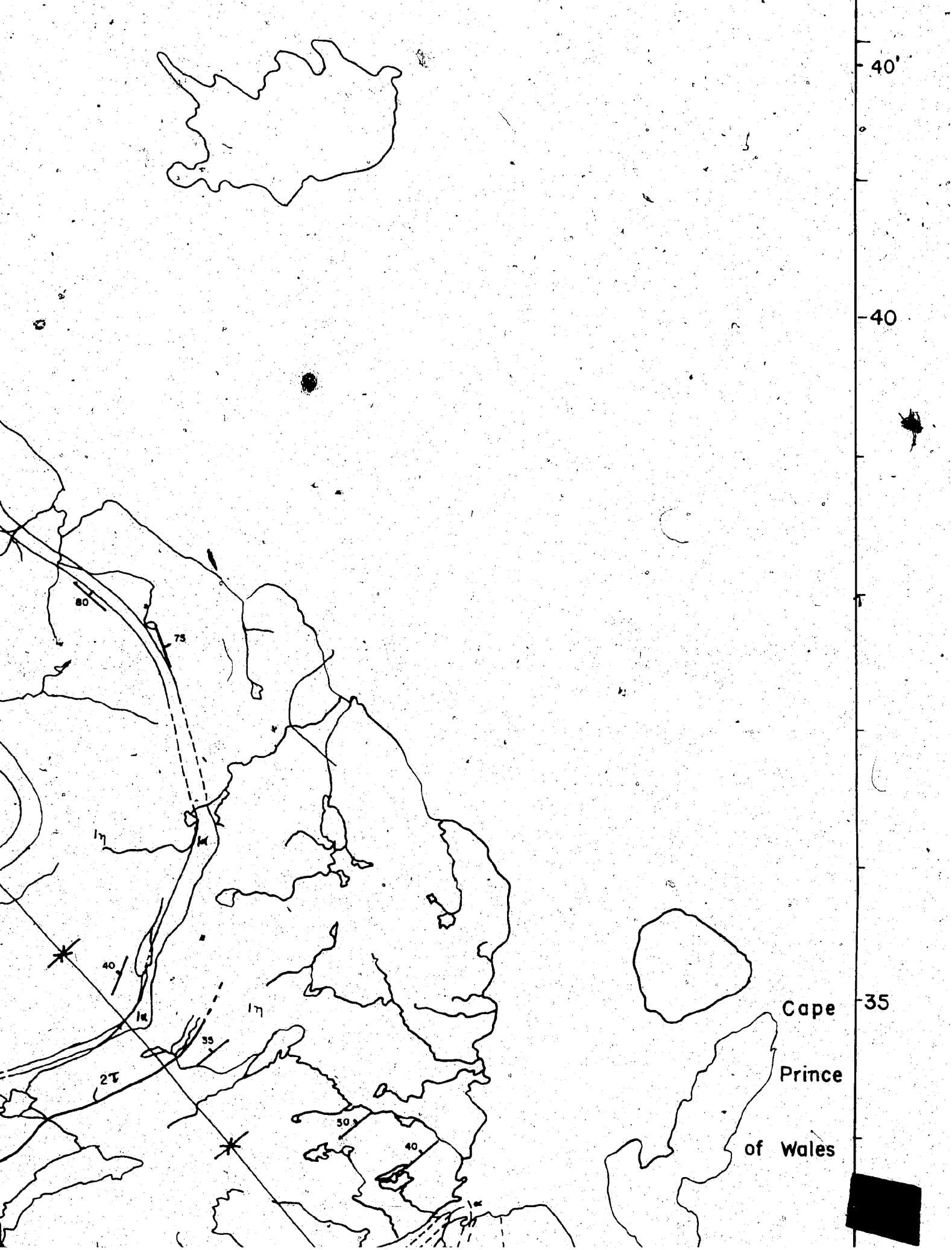
40'
40
35
80
75
1η
1κ
40
1κ
1η
35
2τ
50
40
1κ
Cape
Prince
of Wales

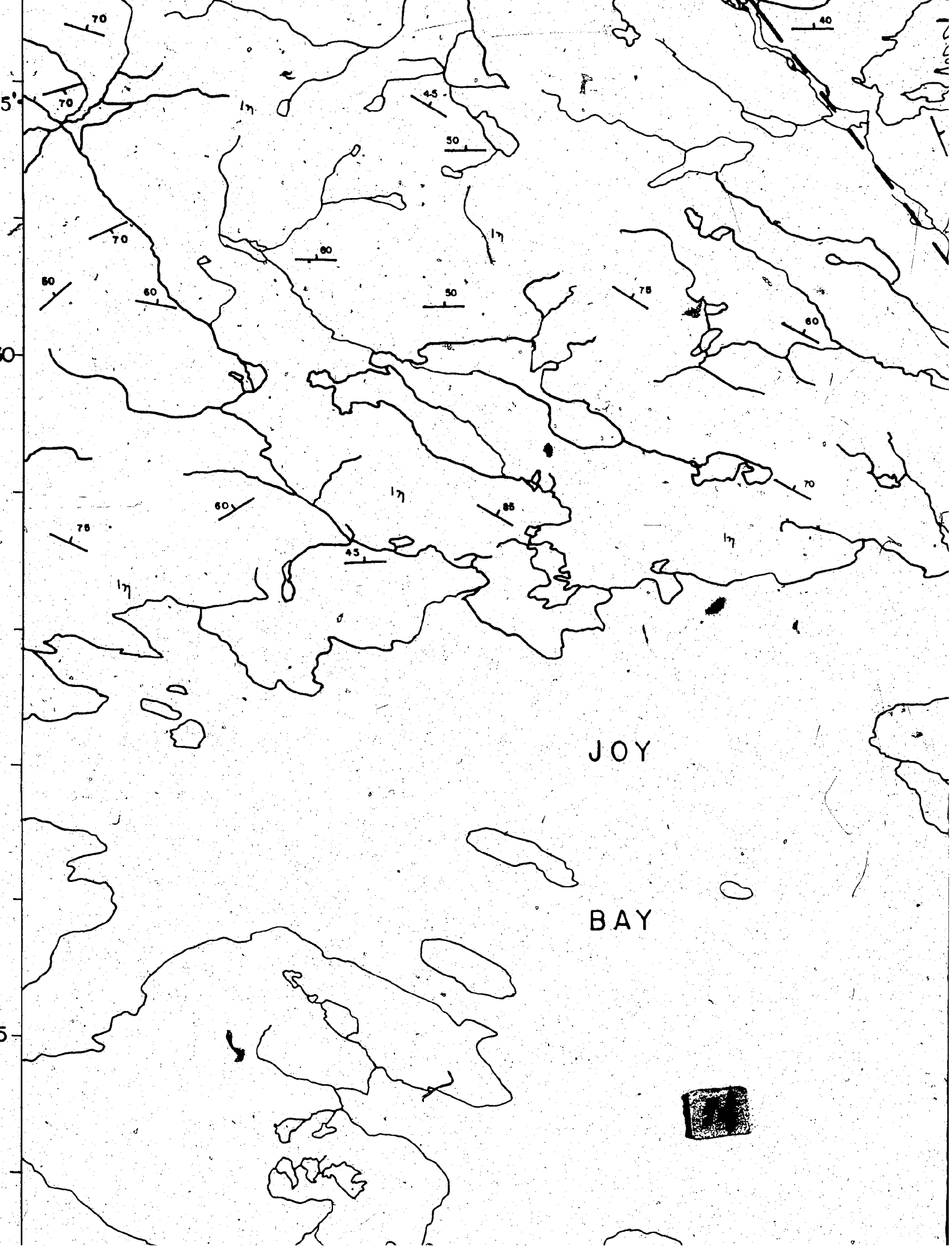
JOY
BAY

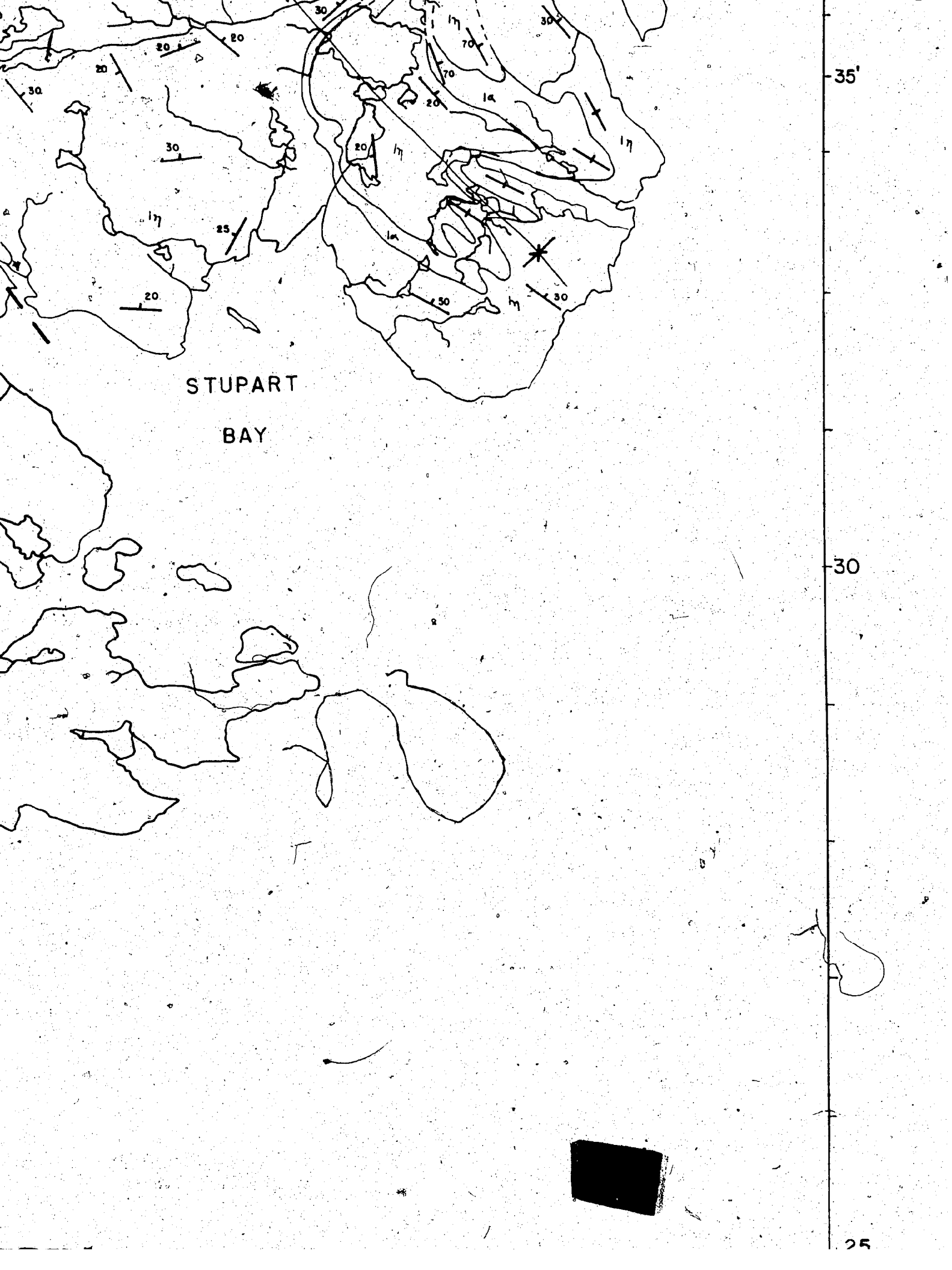
STUPART
BAY
35'
30
25

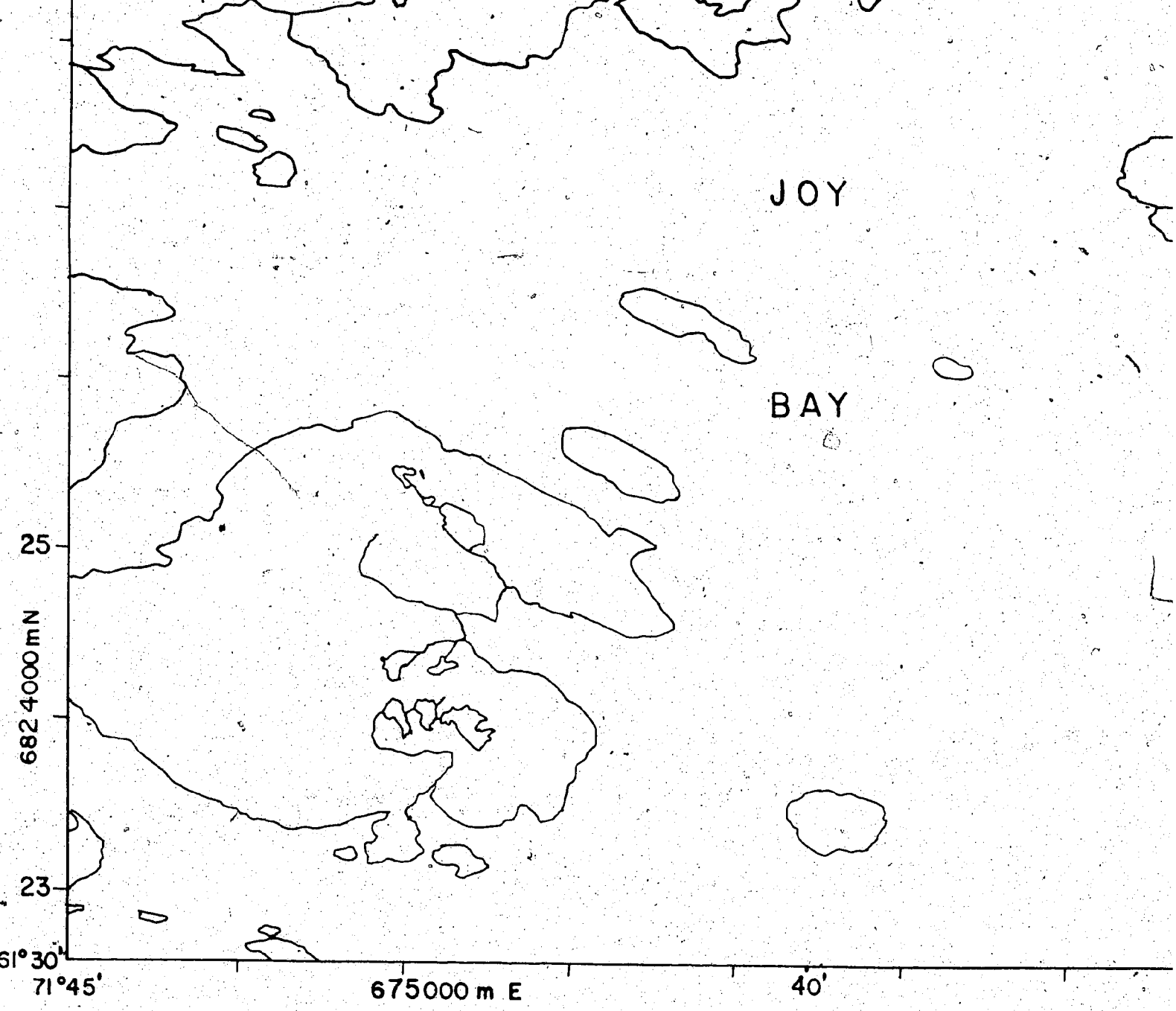

ology by K. Schimann, L. Charlebois
d P. Denis, 1972.

GEOL
WAKEHAN
QUE

igure 9.

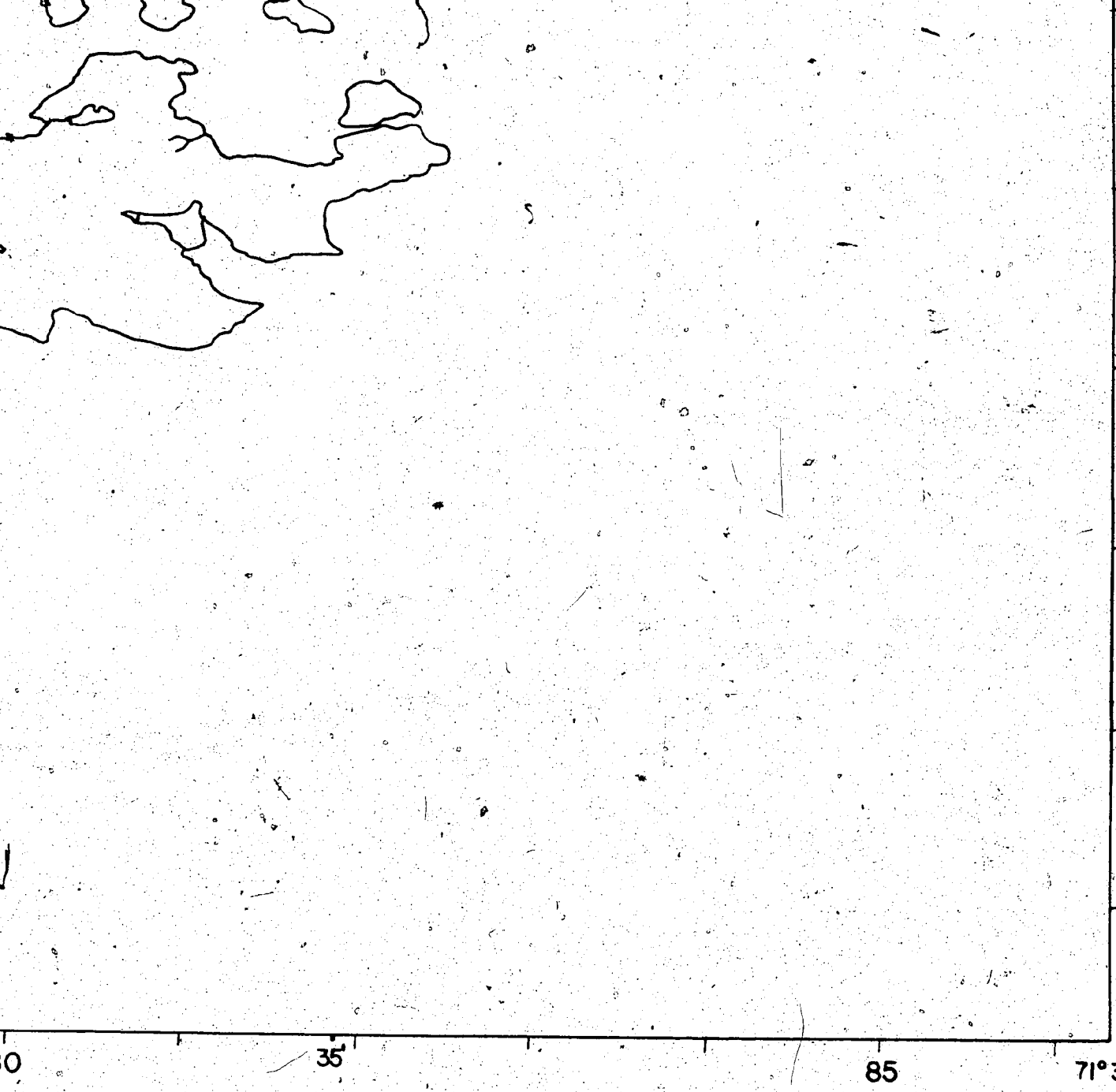

GY

BAY E

EC

Topography based on topographic maps published at a scale of 1:50 000 by the Department of Energy, Mines and Resources, Ottawa.

UTM Grid 18V NTS 25 E/12E

scale

0 1 2km

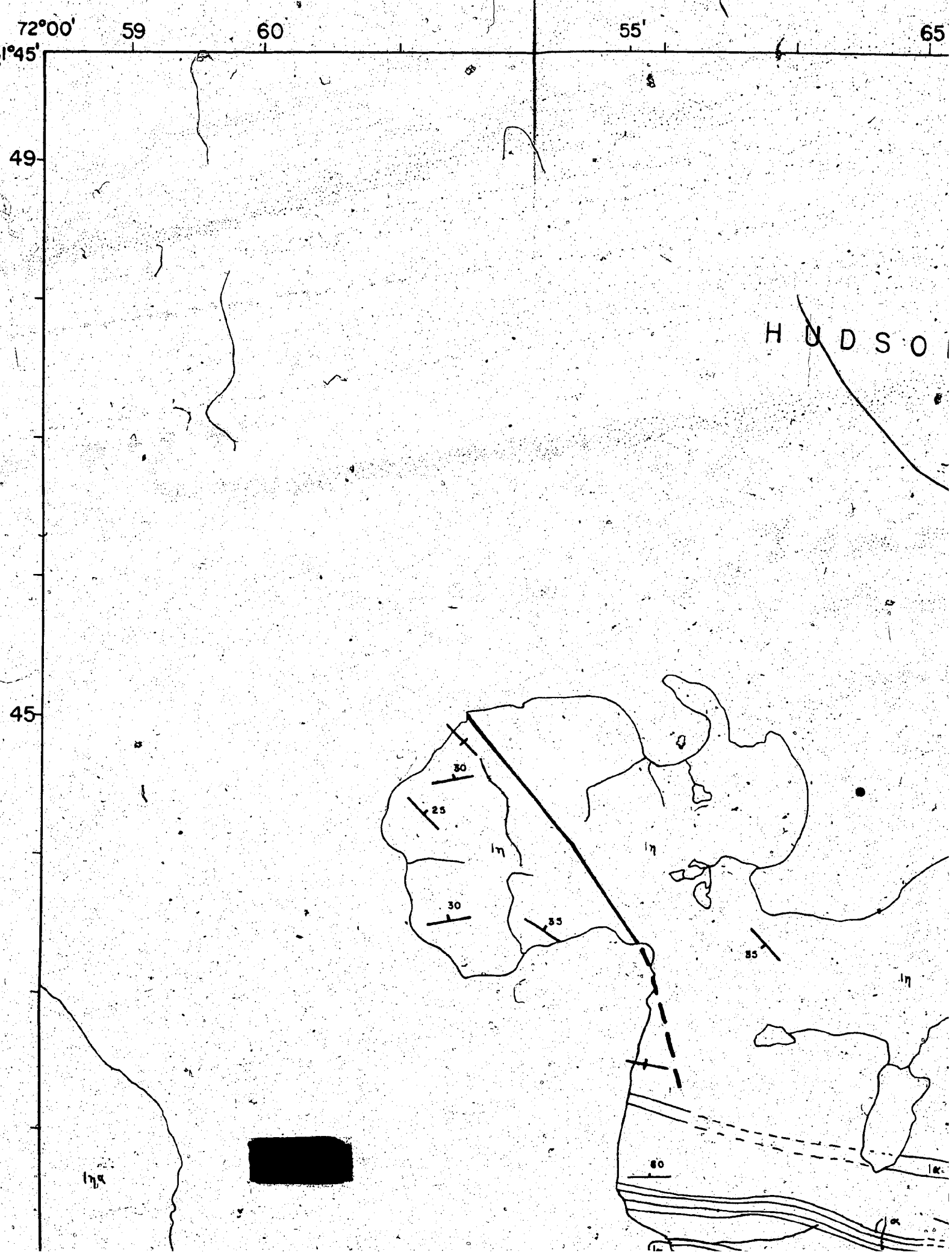
72°00'
59
60
55'
65
49
45
H U D S O
30
25
30
35
35
60

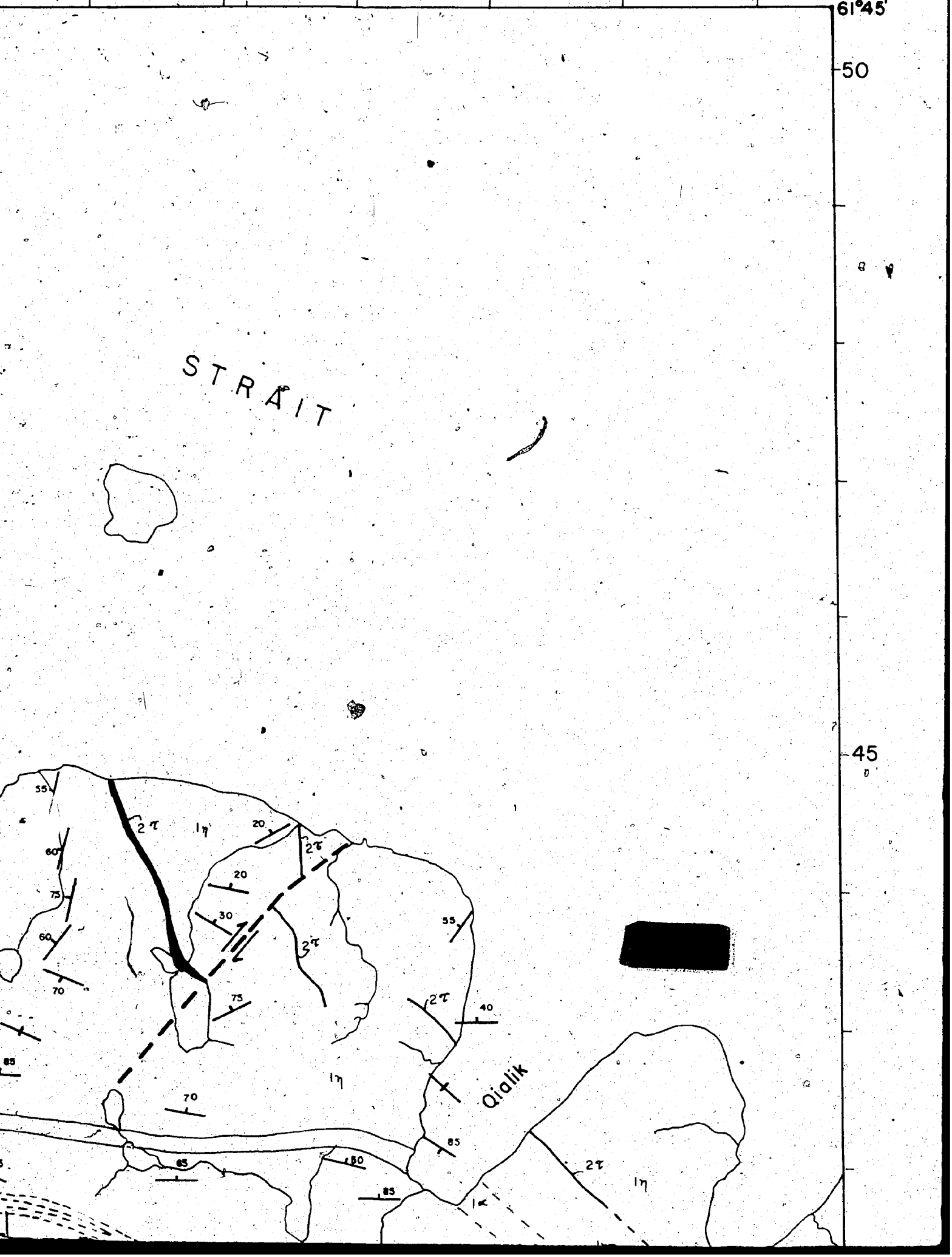
61°45'
50
45
STRAIT
Qialik
55
2τ
1η
20
60
75
30
70
85
40
80
1α

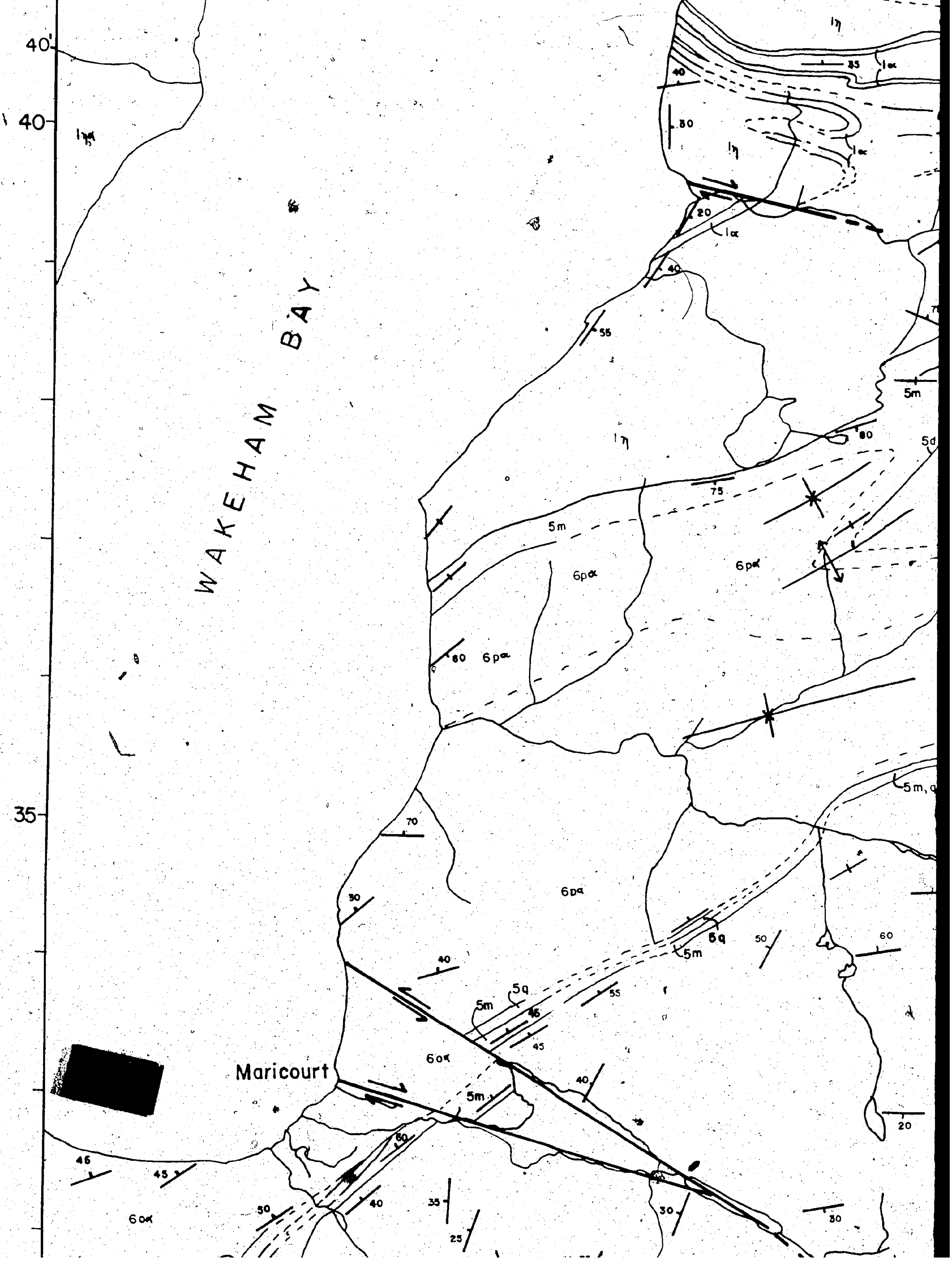
40'
40
35
WAKEHAM BAY
Maricourt
1η
1α
5m
5d
5q
6pα
6oα
5m, α

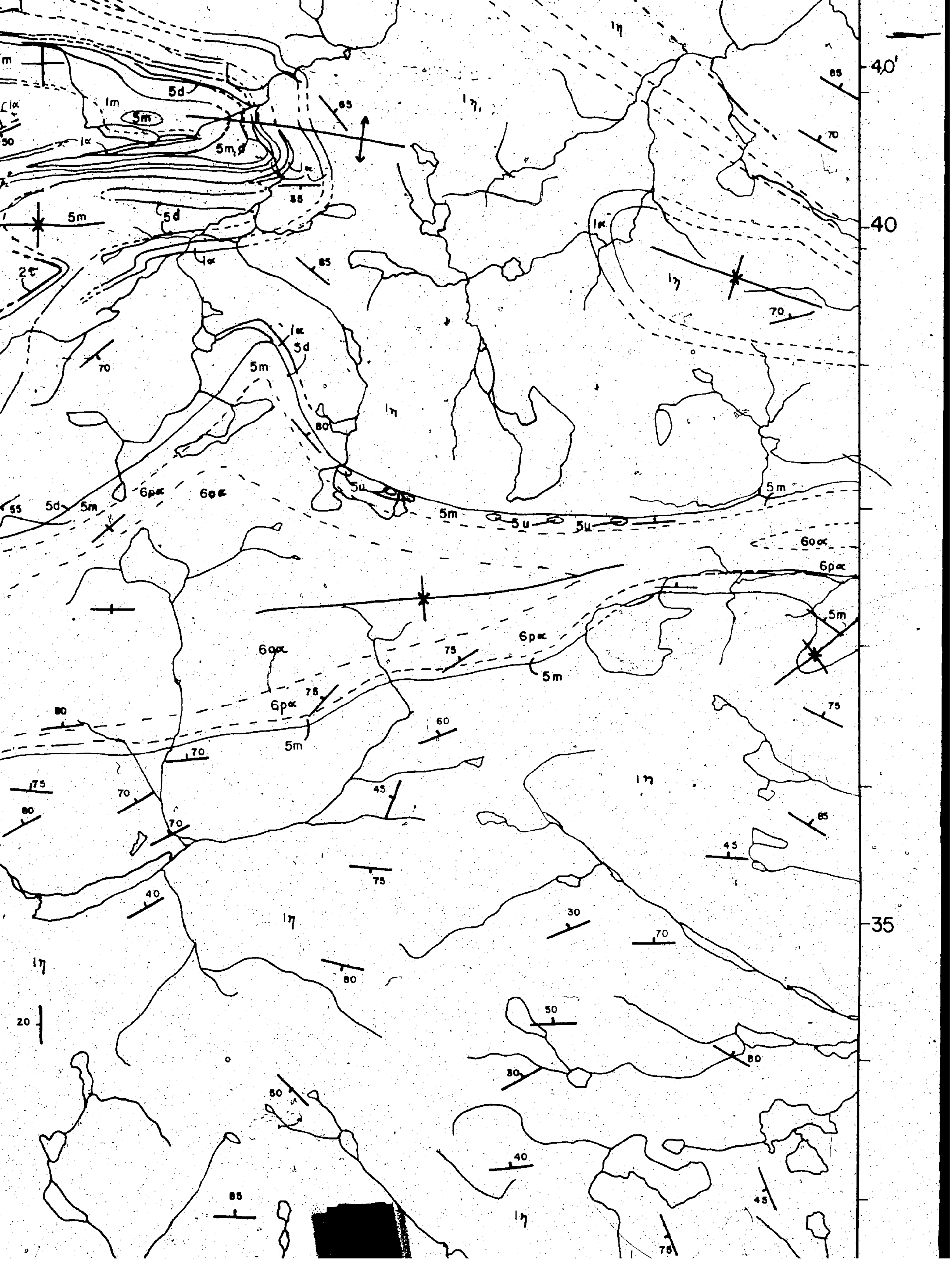

40'
40
35
1η
1m
5d
5m
5m,d
1α
2τ
5u
6pα
6oα
85
65
70
35
80
55
75
60
45
40
30
50
20

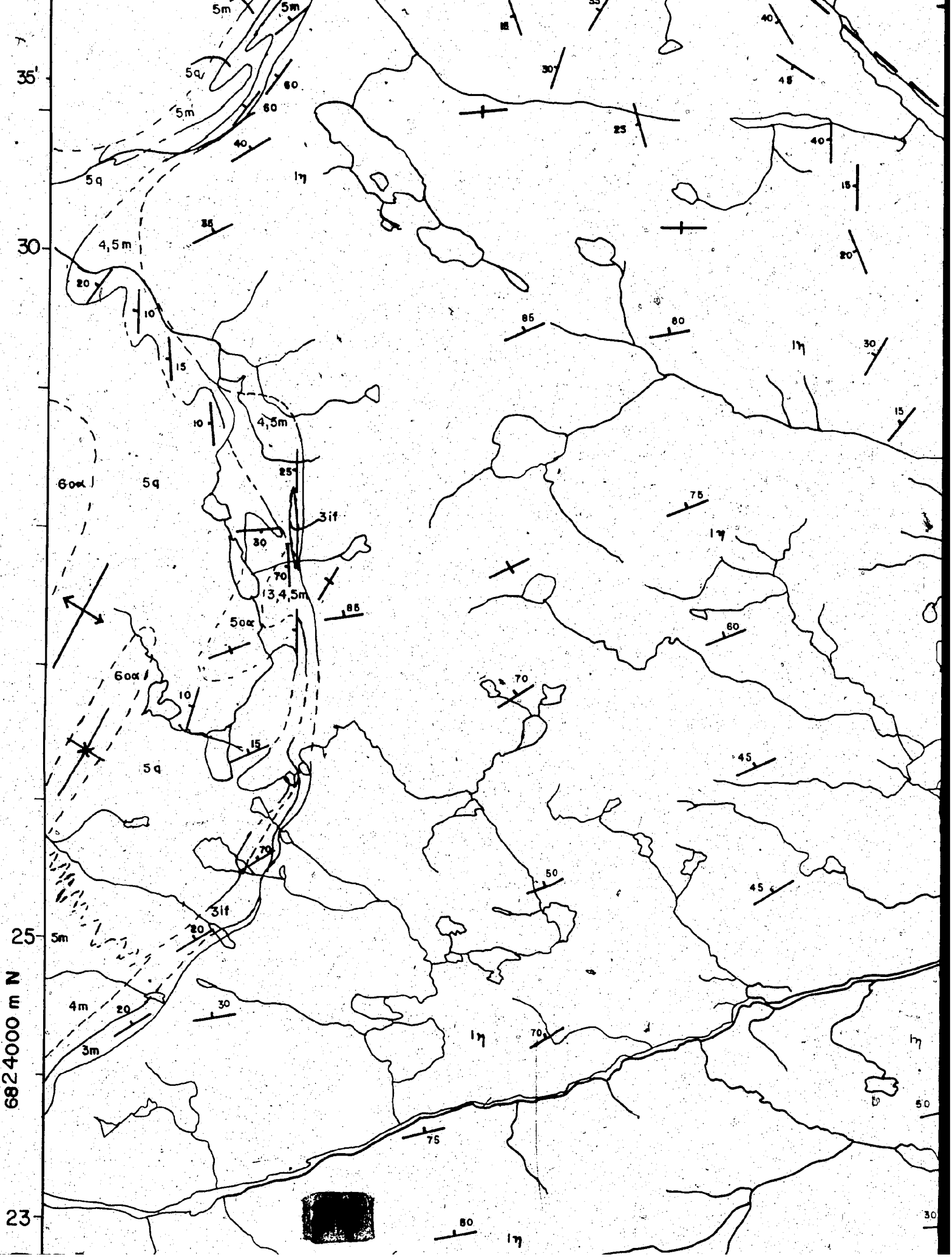
35'
30
25
23
6824000 m N
5m
5q
4,5m
6oα
3if
3,4,5m
5oα
4m
3m
1η

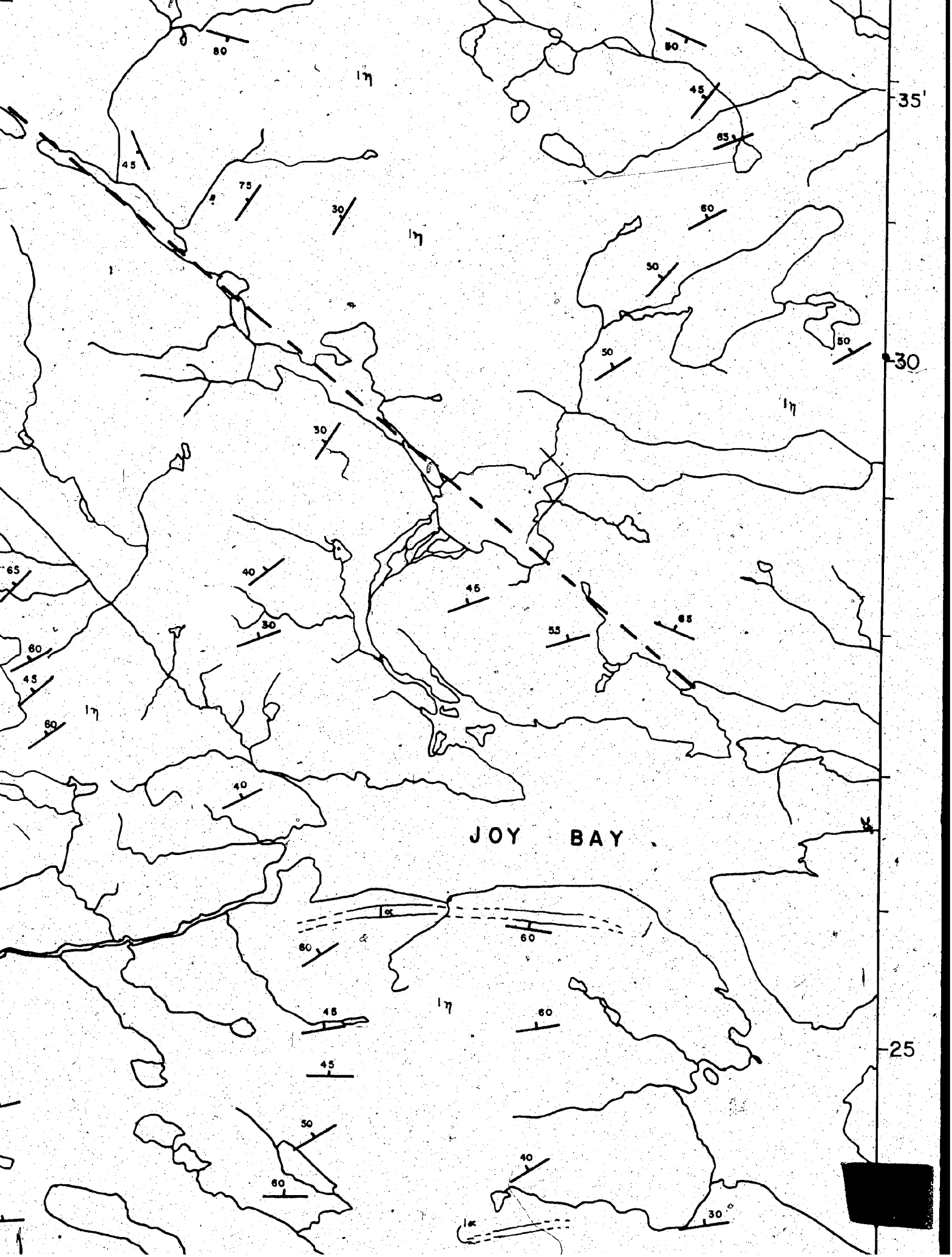
JOY BAY
35'
30
25

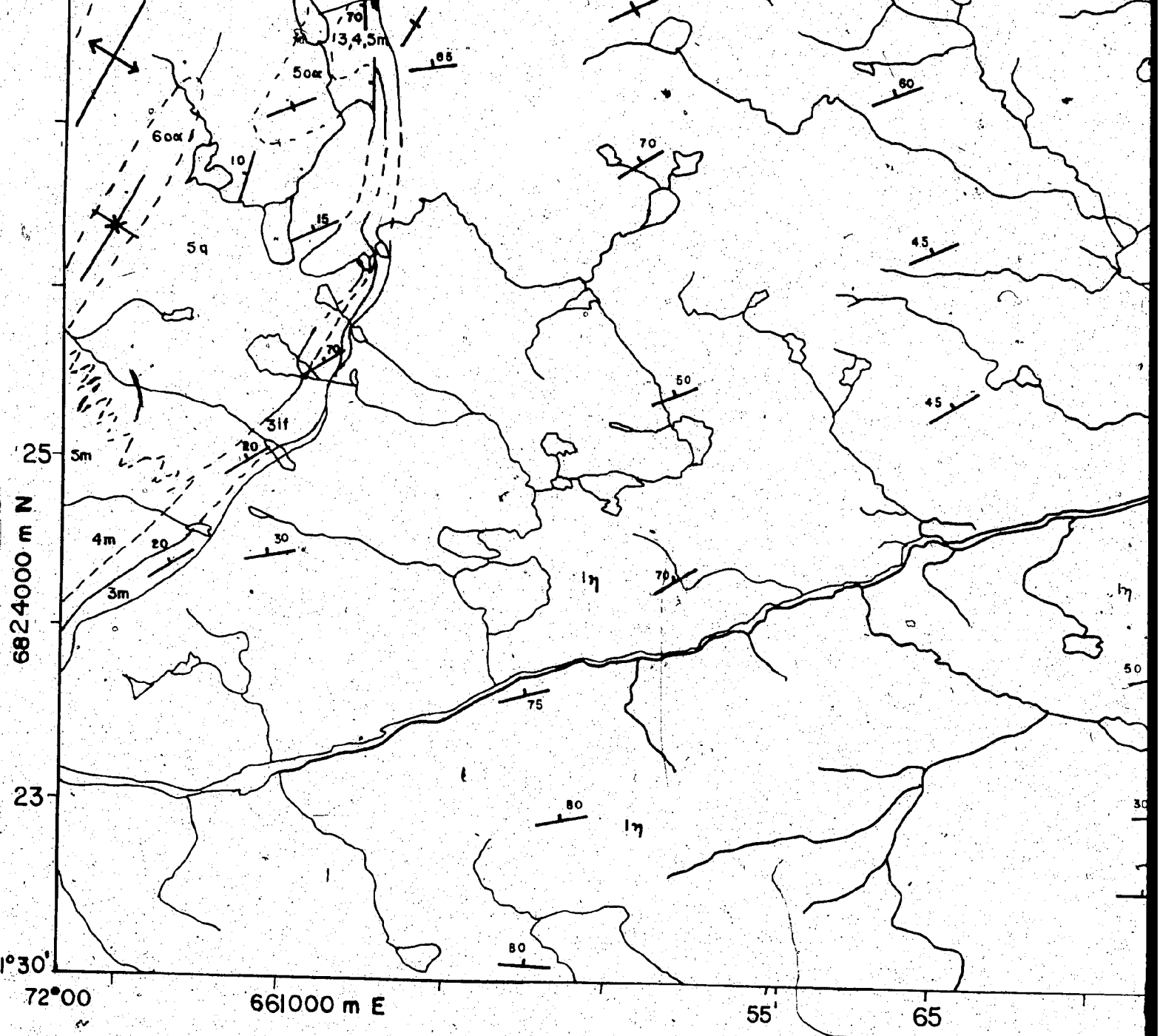

logy by K. Schlmann, L. Charlebois,
Côté and P. Denis, 1972.

GEOL
WAKEHAM
QUEE

gure 10.

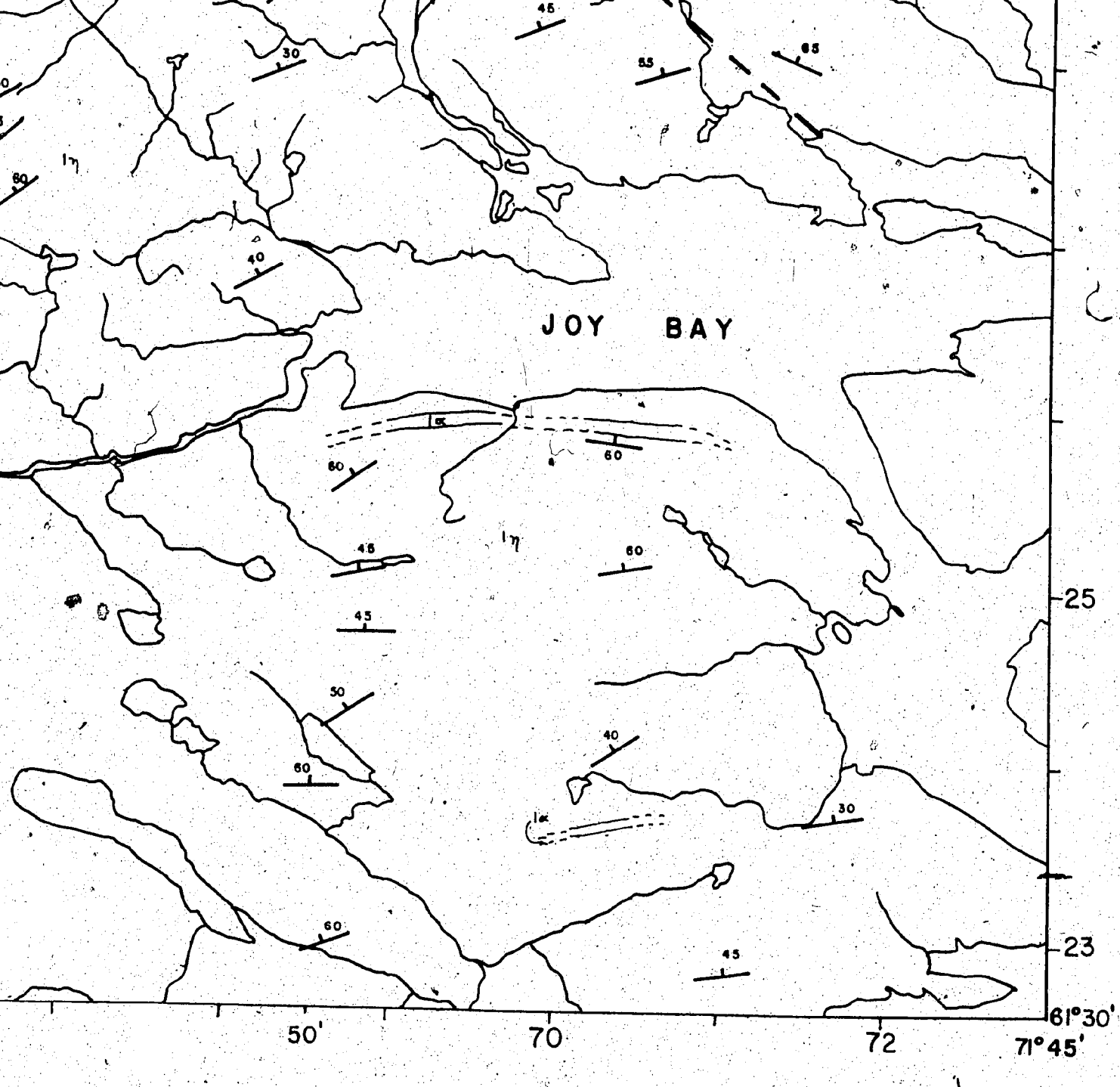

GY

BAY W

C

Topography based on topographic maps published at a scale of 1:50 000 by the Department of Energy, Mines and Resources, Ottawa.

UTM Grid 18V NTS 25 E/12W

scale

0 1 2km

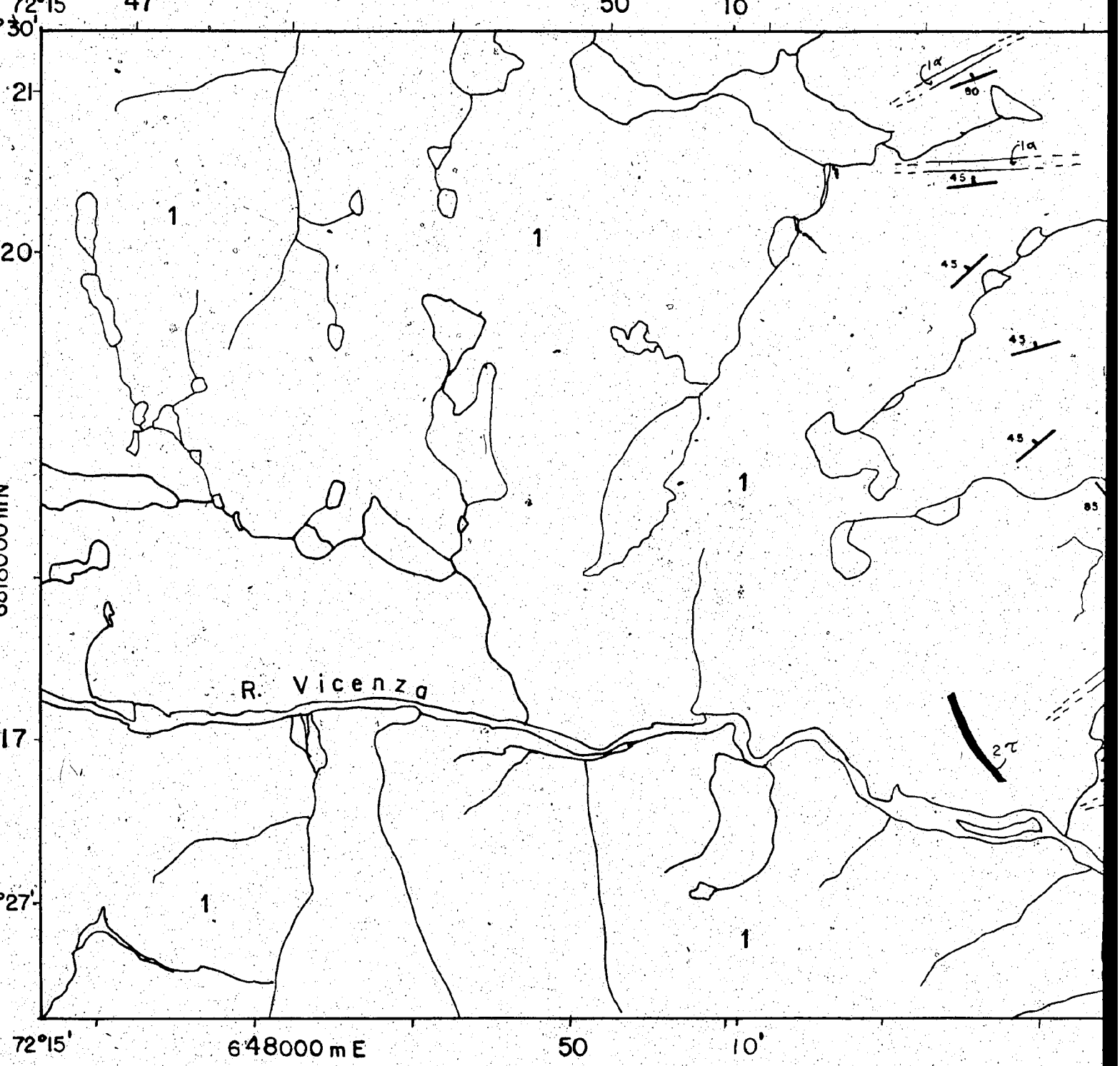

gy by K. Schimann, L. Charlebois,
é and P. Denis, 1972.

GEOL

part of LAC SAM

QUE

gure 11.

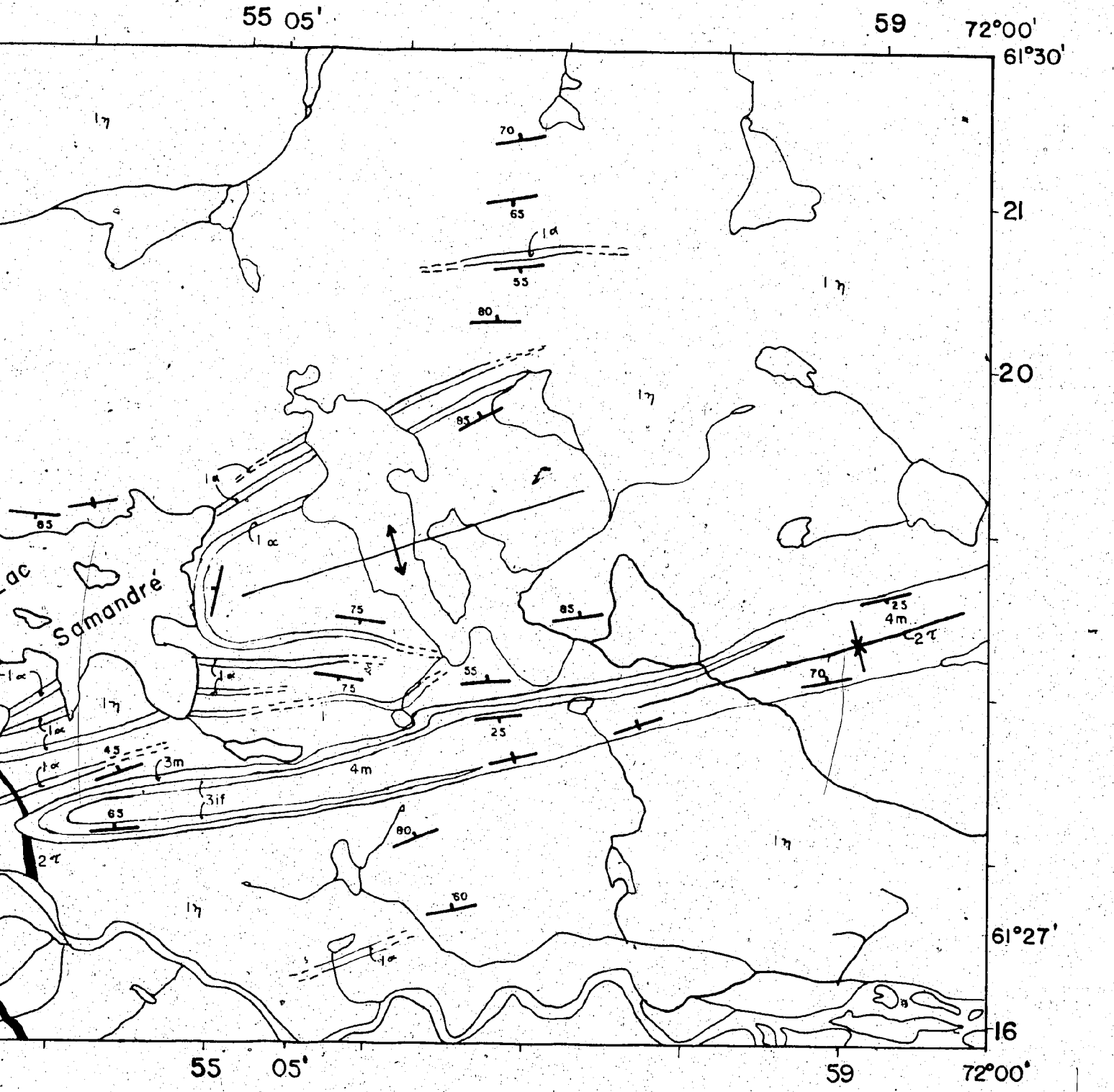

GY

NDRÉ E

C

Topography based on topographic maps published at a scale of 1:50 000 by the Department of Energy, Mines and Resources, Ottawa.

UTM Grid 18V NTS 35 H/8E

scale

0 1 2 km

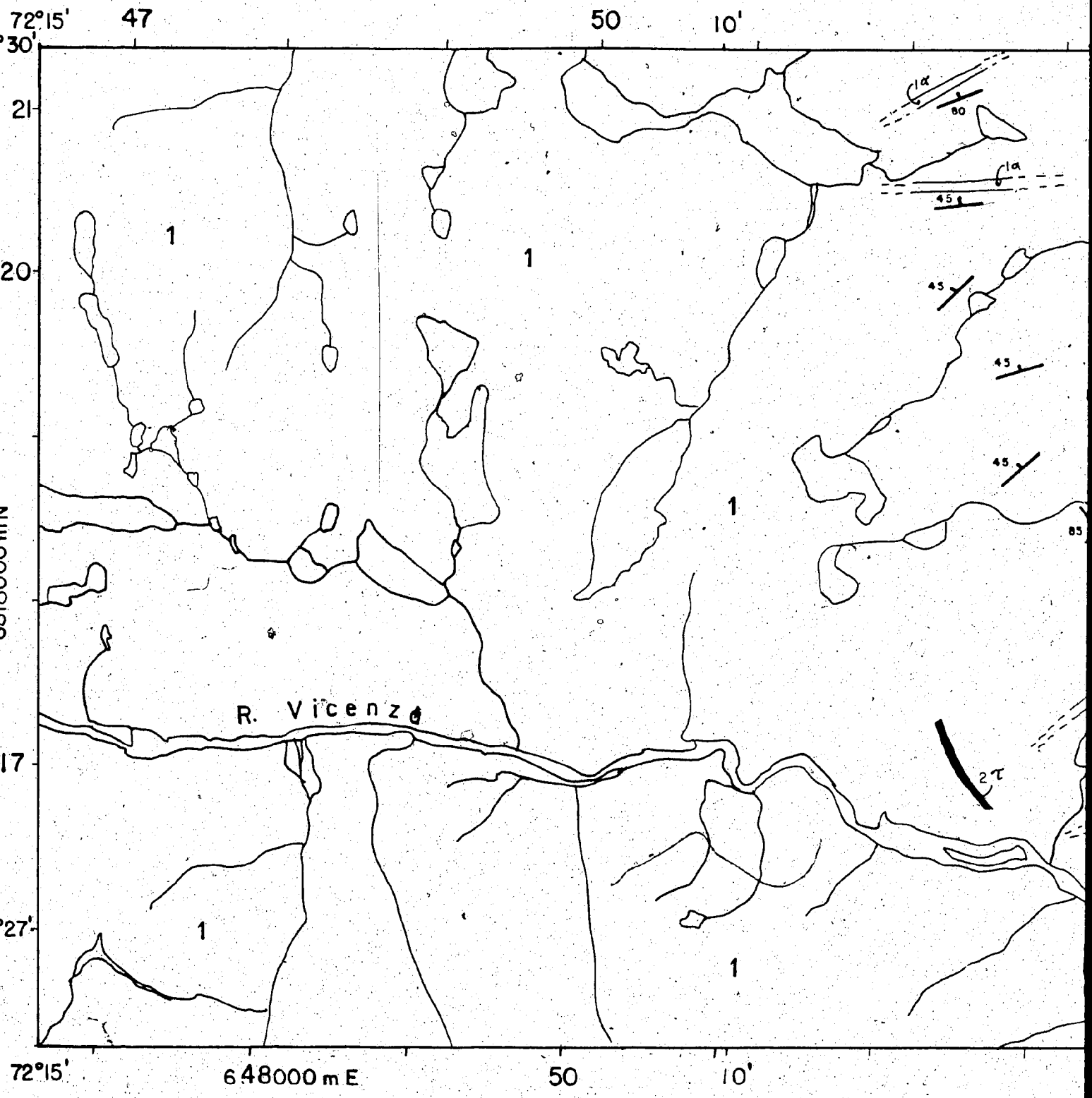

gy by K. Schimann, L. Charlebois,
é and P. Denis, 1972.

GEOL

part of LAC SAM

QUE

gure 11.

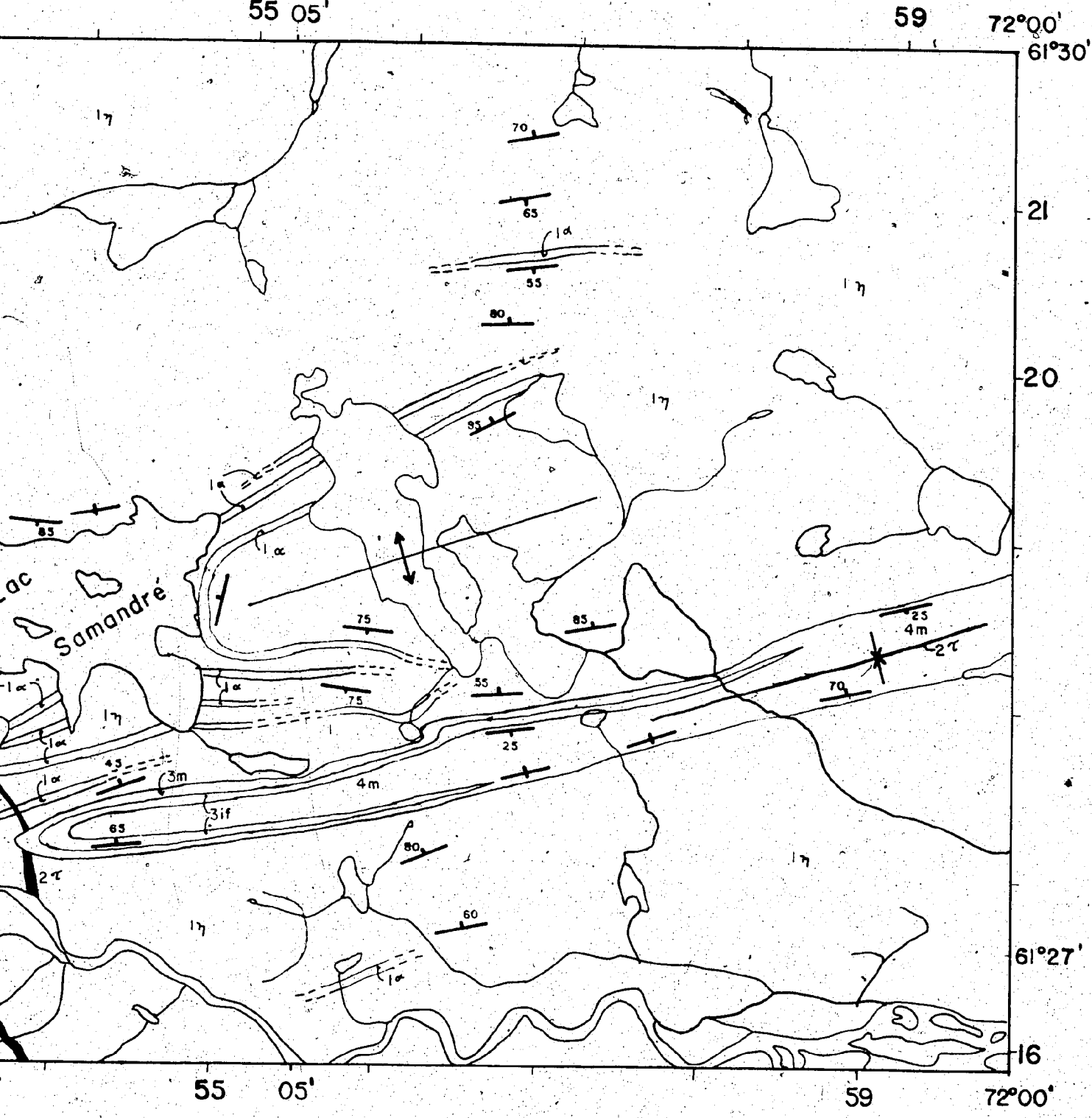

Topography based on topographic maps published at a scale of 1:50 000 by the Department of Energy, Mines and Resources, Ottawa.

UTM Grid 18V NTS 35 H/8E

scale

0 1 2 km

GY

NDRÉ E

C

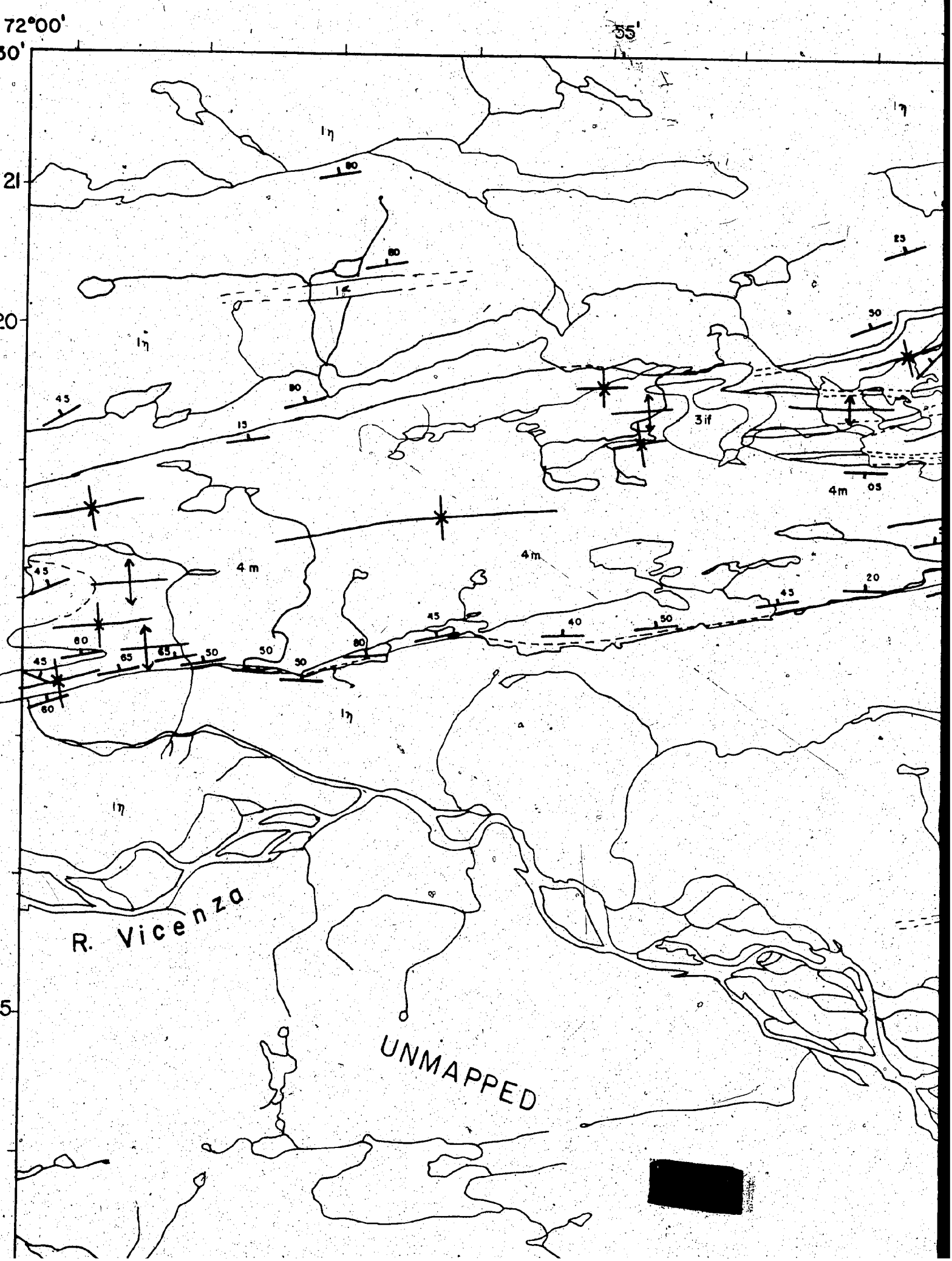
72°00'
55'
30'
21
20
5
1η
80
45
15
3if
4m
05
30
25
20
60
65
50
40
R. Vicenza
UNMAPPED

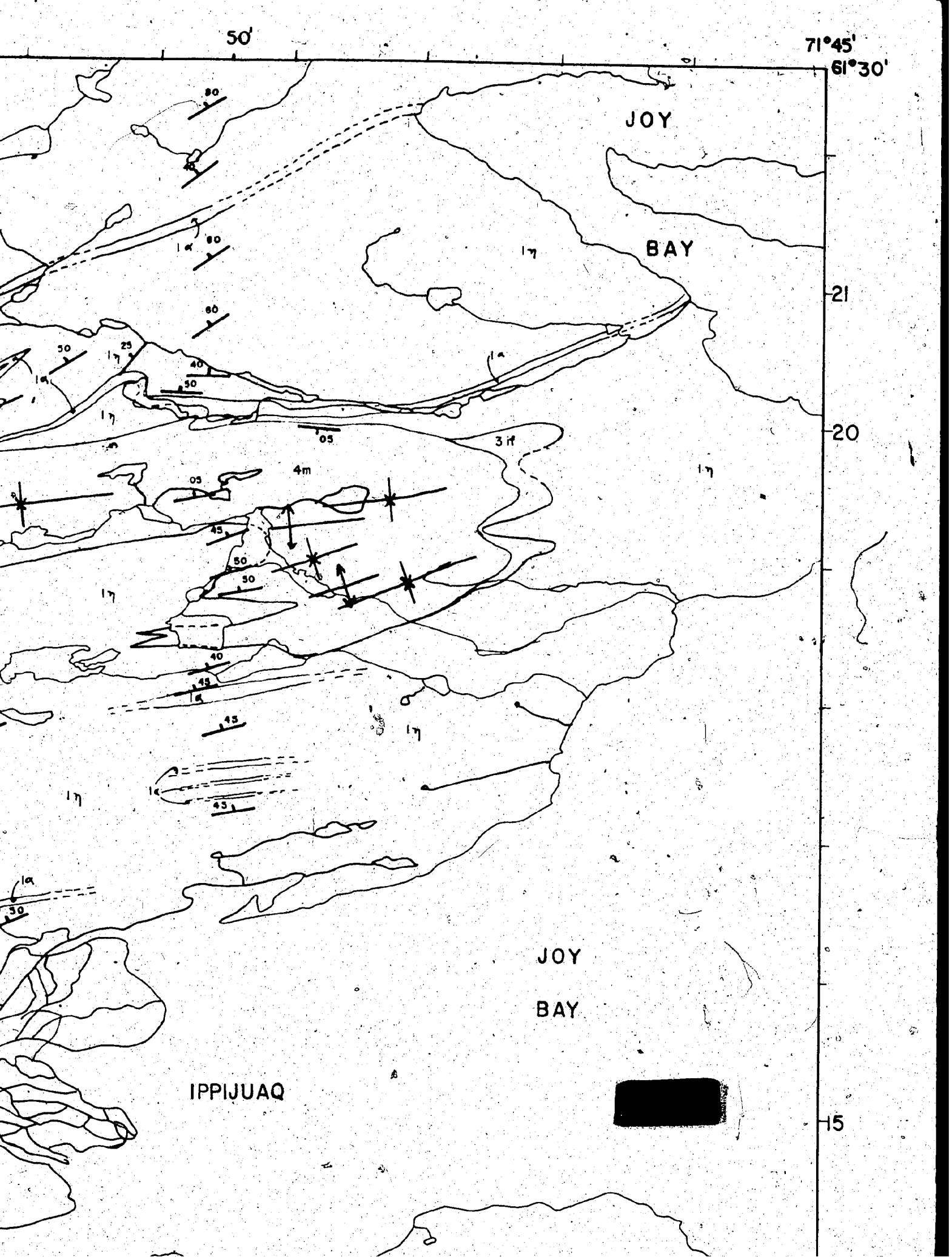
50'
71°45'
61°30'
JOY
BAY
21
20
15
JOY
BAY
IPPIJUAQ
80
60
30
25
40
05
3 if
4m
45
50
1η
1α

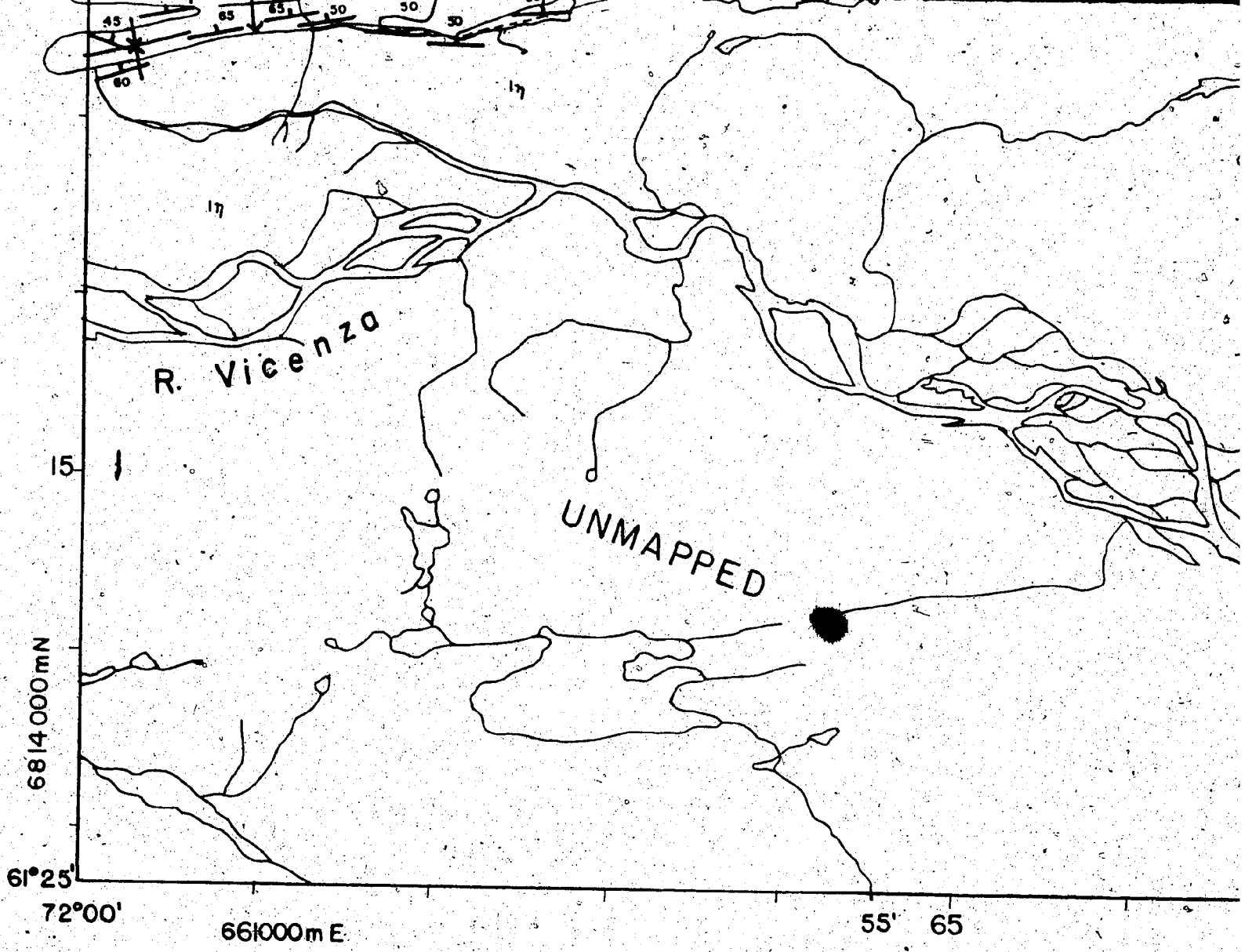

blogy by K. Schimann, L. Charlebois, Côté and P. Denis, 1972.

GEOI

part of WHITLEY

QUE

gure 12.

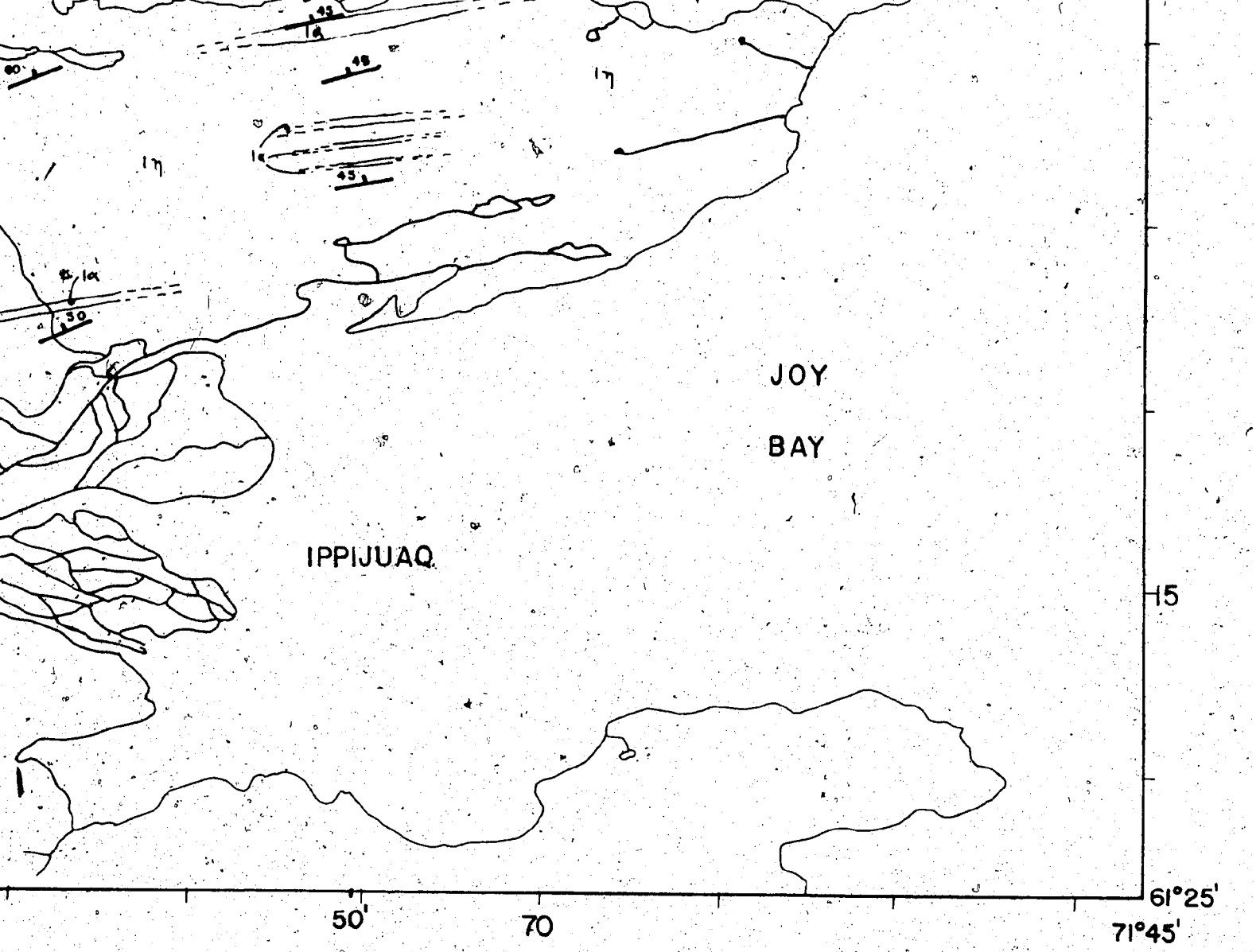

OGY

BAY W

EC

Topography based on topographic maps published at a scale of 1:50 000 by the Department of Energy, Mines and Resources, Ottawa.

UTM Grid 18V NTS 25 E/5W

scale

0 1 2km


s
g
y
b
u
pc
bp
bp, bf
60
70
80
30
45

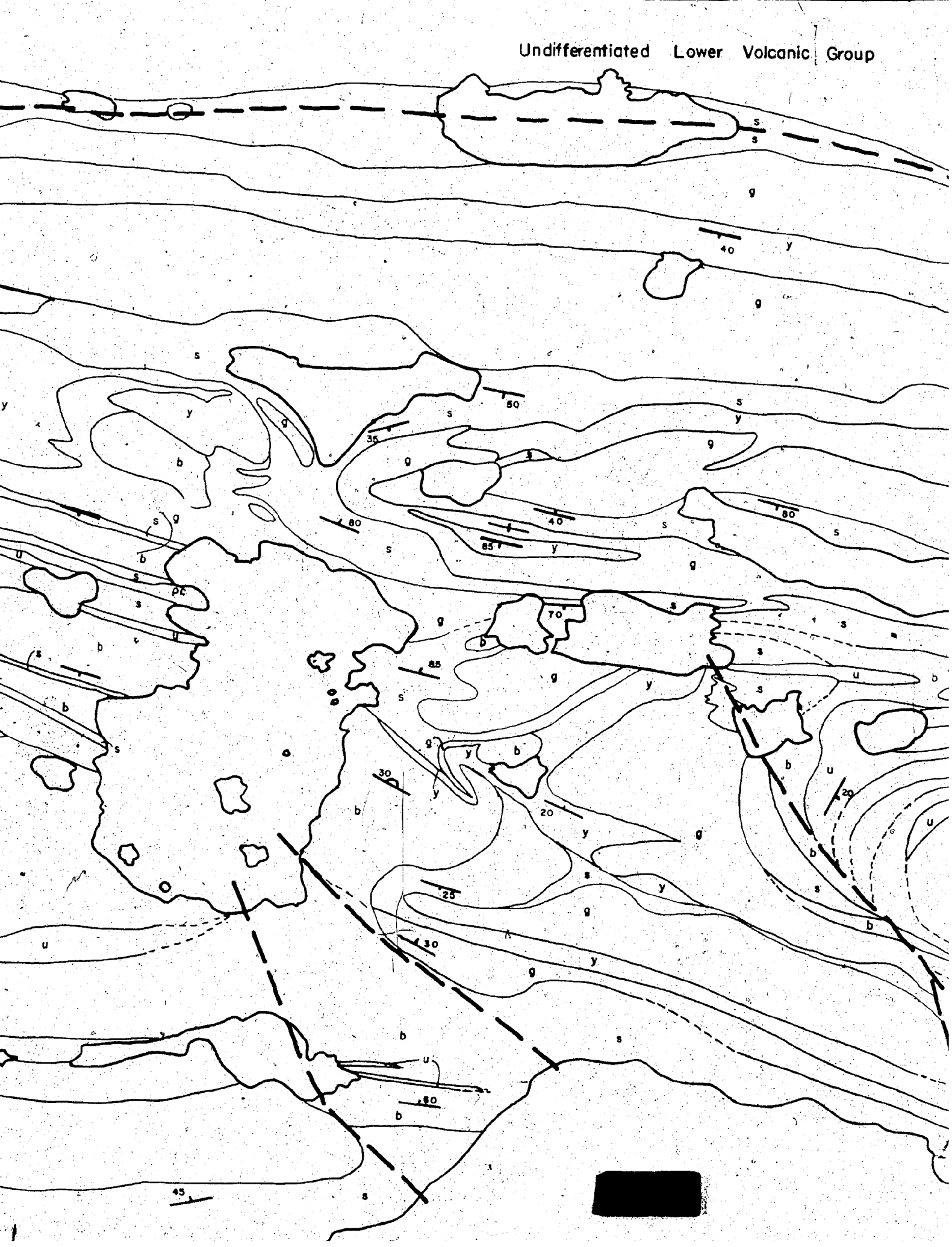
Undifferentiated Lower Volcanic Group

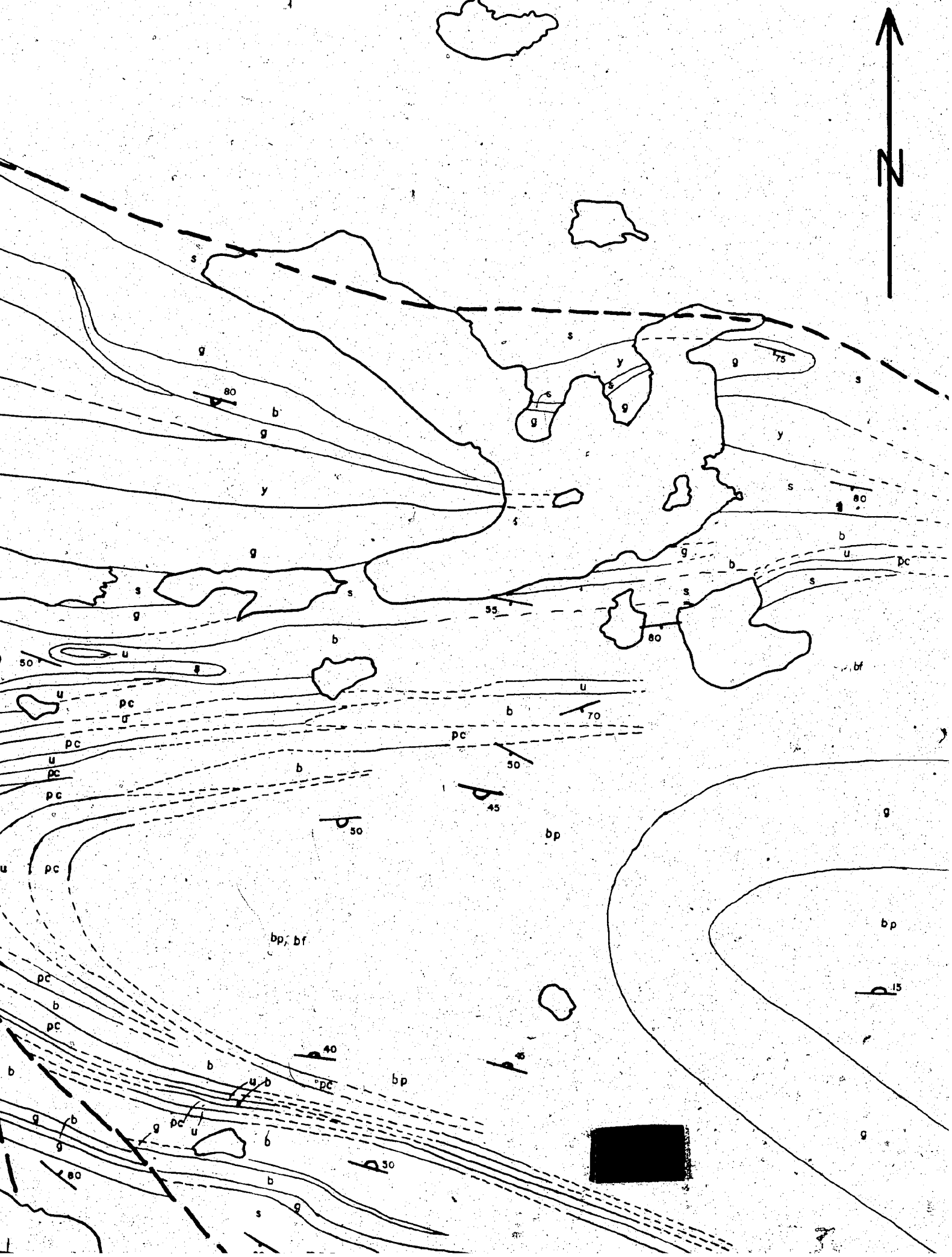
N
s
g
y
b
u
pc
bf
bp
bp, bf
80
75
55
50
70
45
40
30
15

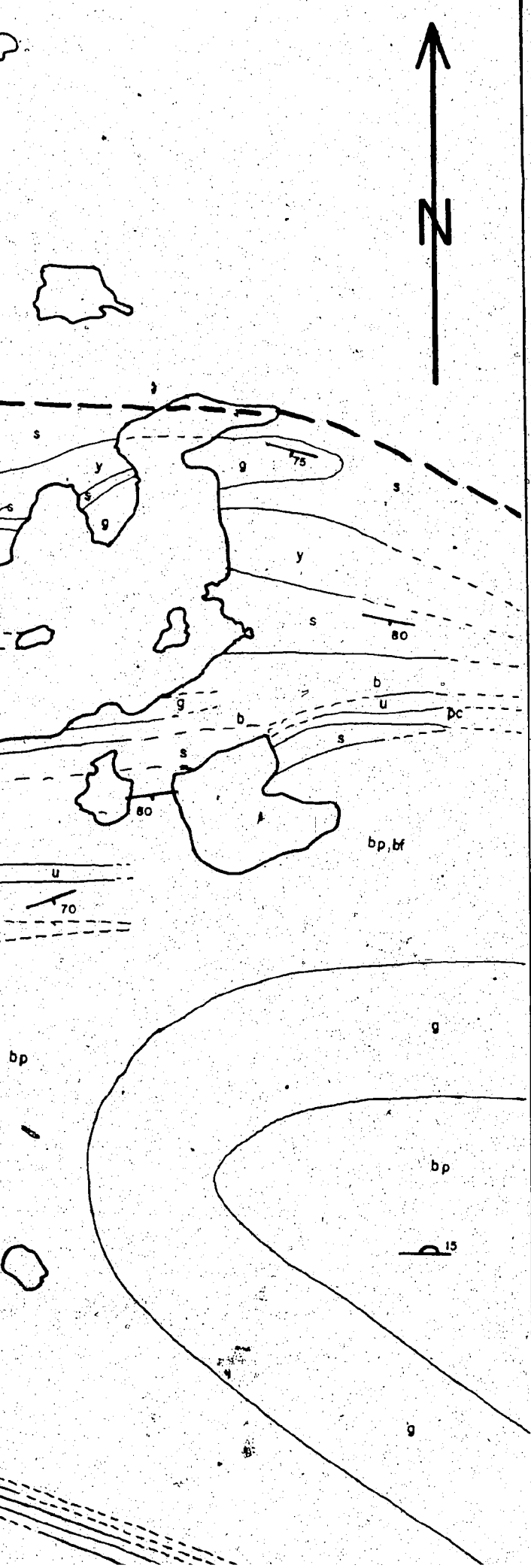

LEGEND

UPPER VOLCANIC GROUP

g	gabbro	sills
y	pyroxenite	sills
p	peridotite	sills
u	ultramafic flow (?)	
pc	picrite	
b	undifferentiated	basalt
bf	flow	basalt
bp	pillows	basalt
s	sediments, mostly detrital (and tuffs)	

SYMBOLS

- contact
- foliation (≃bedding), top known (pillows)
- fault

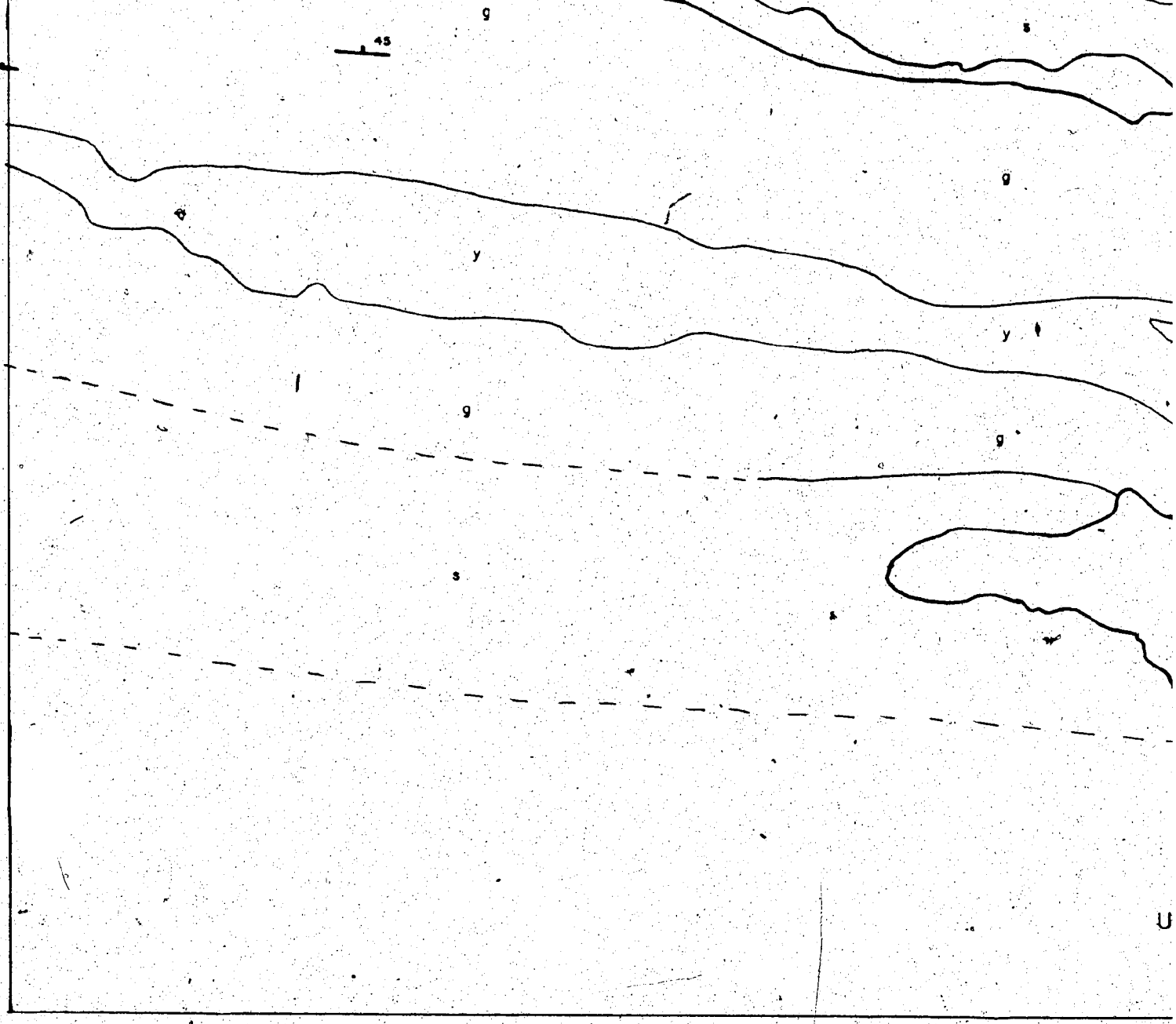

ology by K. Schimann, 1971, 1972;
Chorlebois and P. Trudel, 1972.

igure 13.

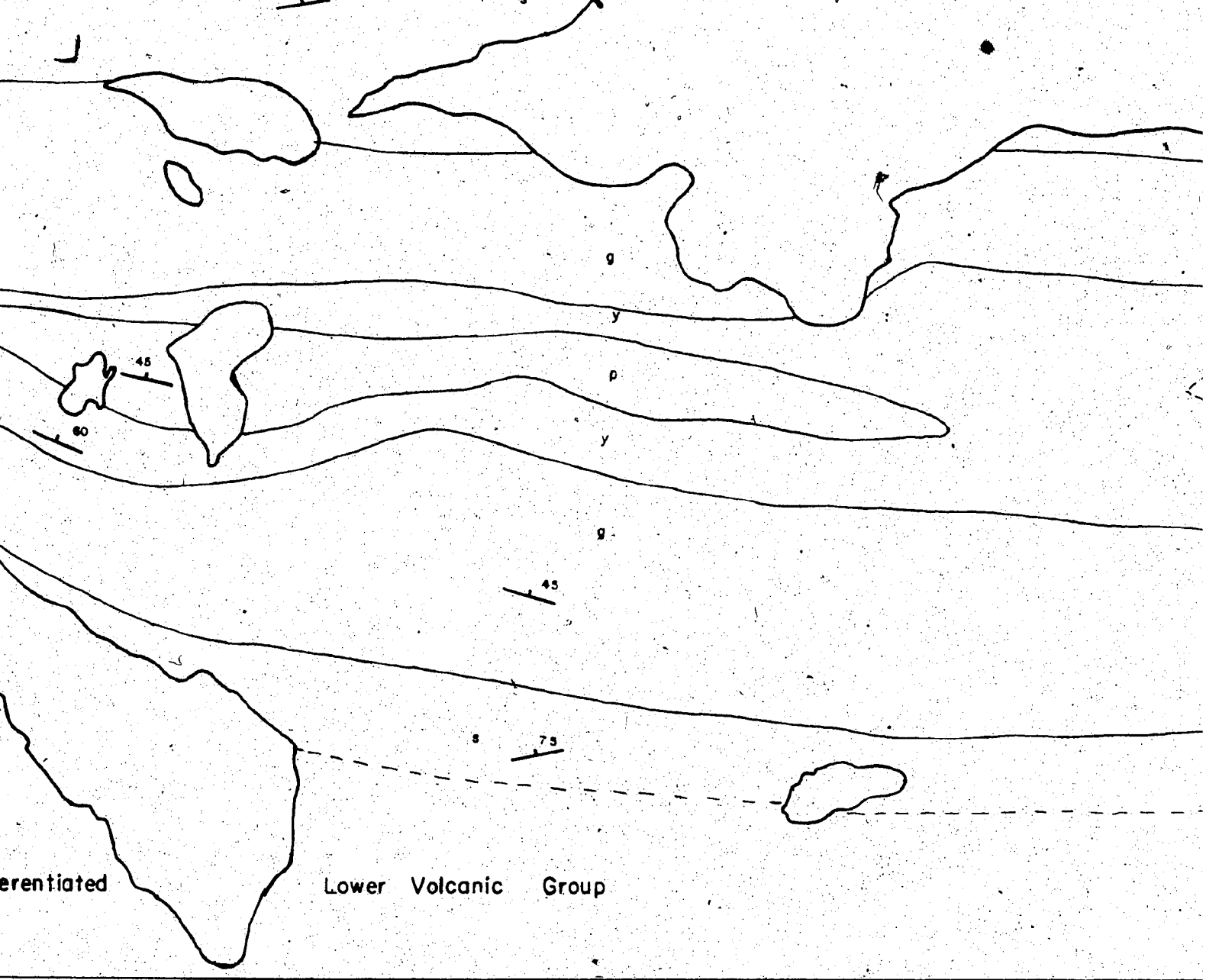

GEOLOGY
CENTRAL MONTS LUNE
QUEBEC

[redacted]

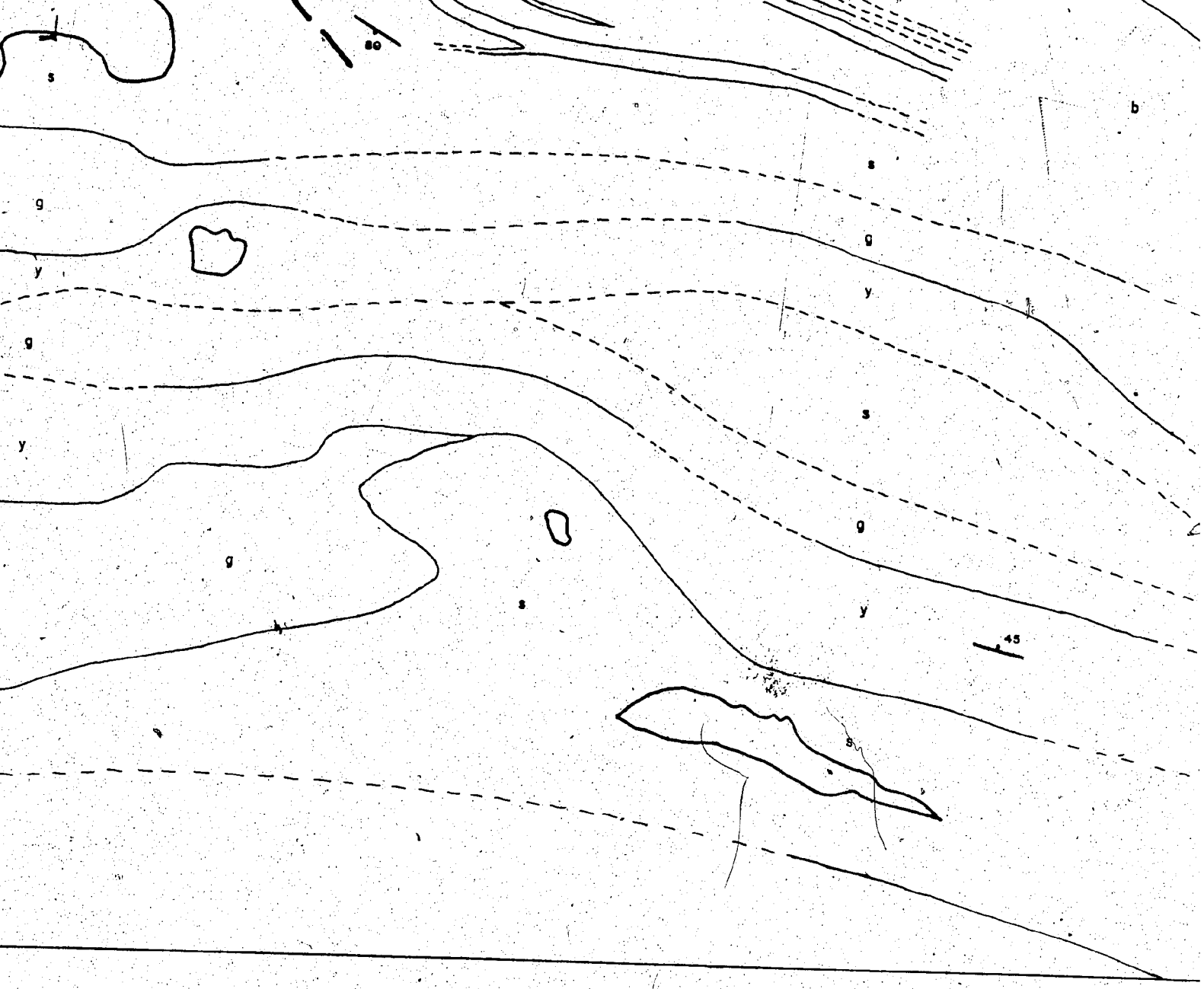

Topography based on enlargment of air photogr
A-16208-182 of the Department of Energy,
Mines and Resources, Ottawa, (uncorrected)

NTS 35 H/1(

Location shown on geological map Wakeham R

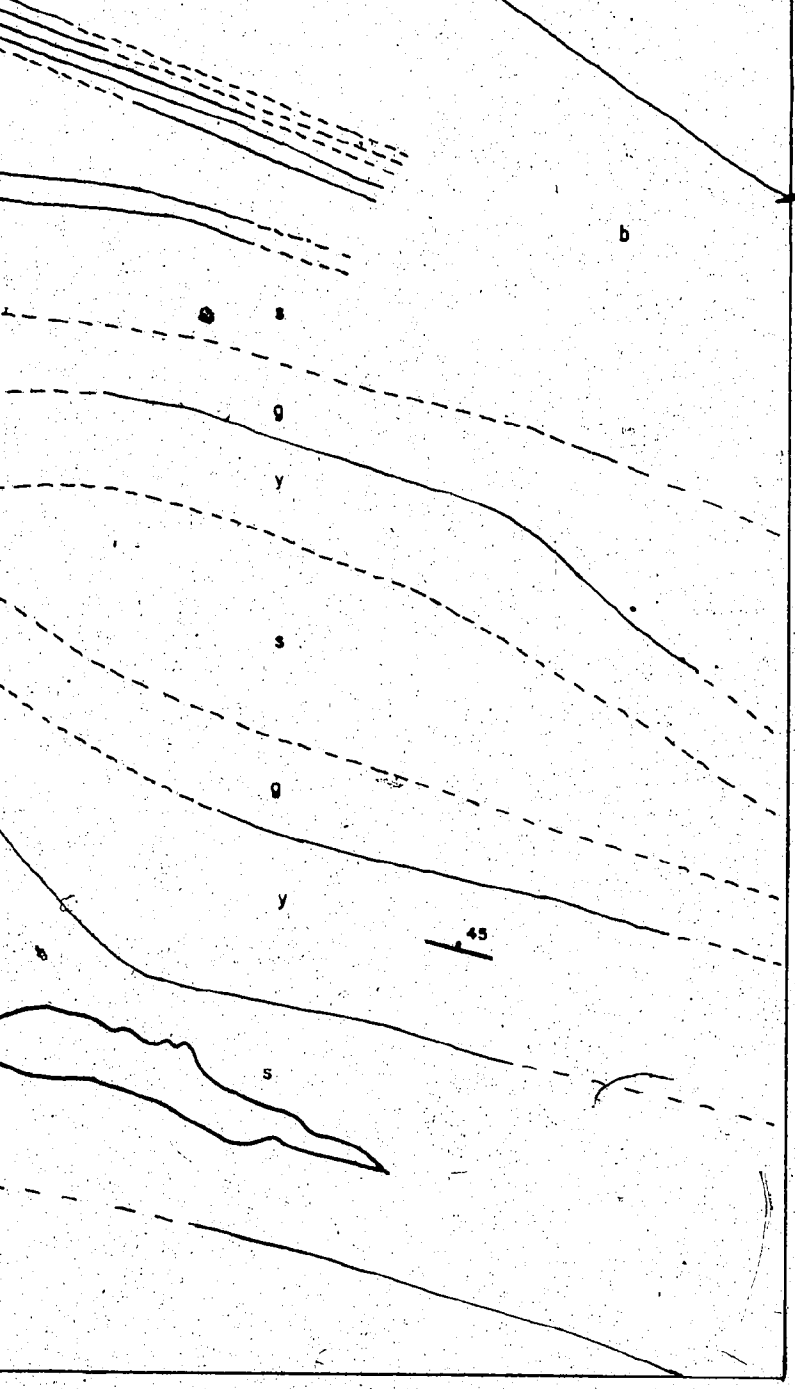

fault

scale

0 500m

Topography based on enlargment of air photograph A-16208-182 of the Department of Energy, Mines and Resources, Ottawa, (uncorrected).

NTS 35 H/10E

Location shown on geological map Wakeham River E.

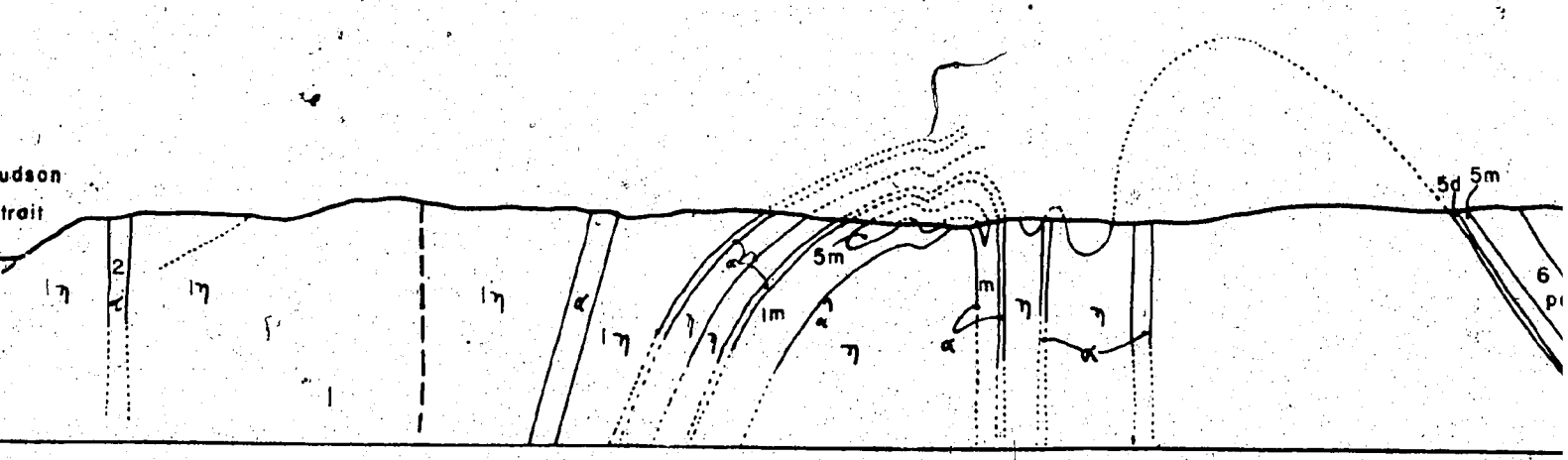
udson
trait
2
1η
1m
5m
5d
6

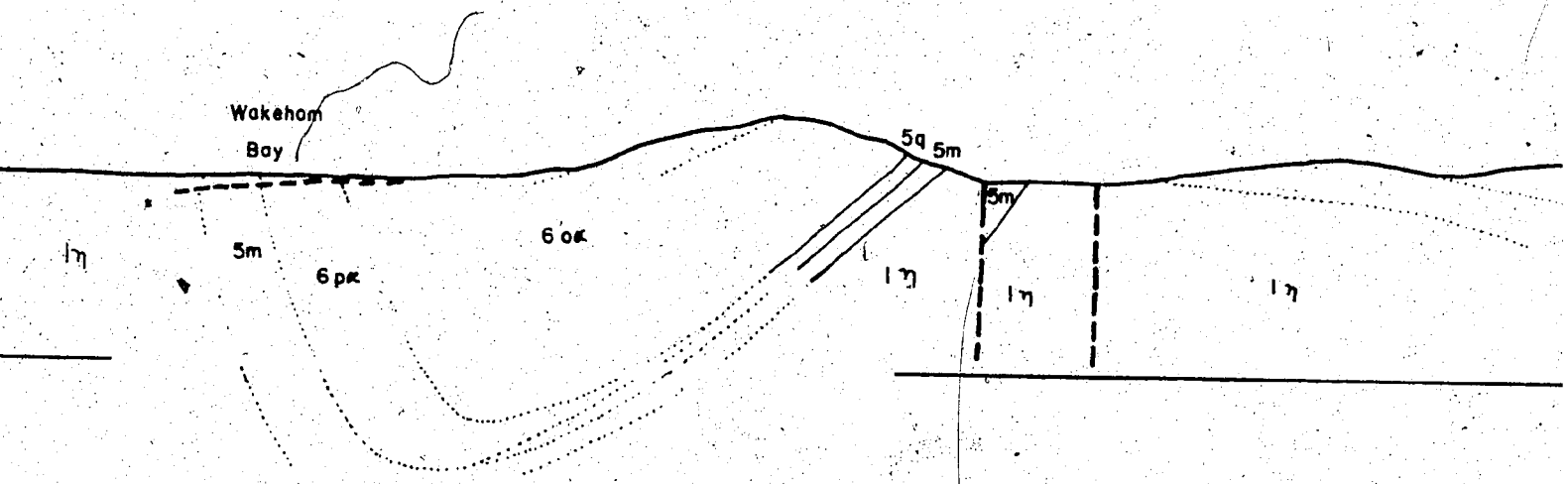
Wakeham
Bay
5q
5m
6 oα
6 pα
1η

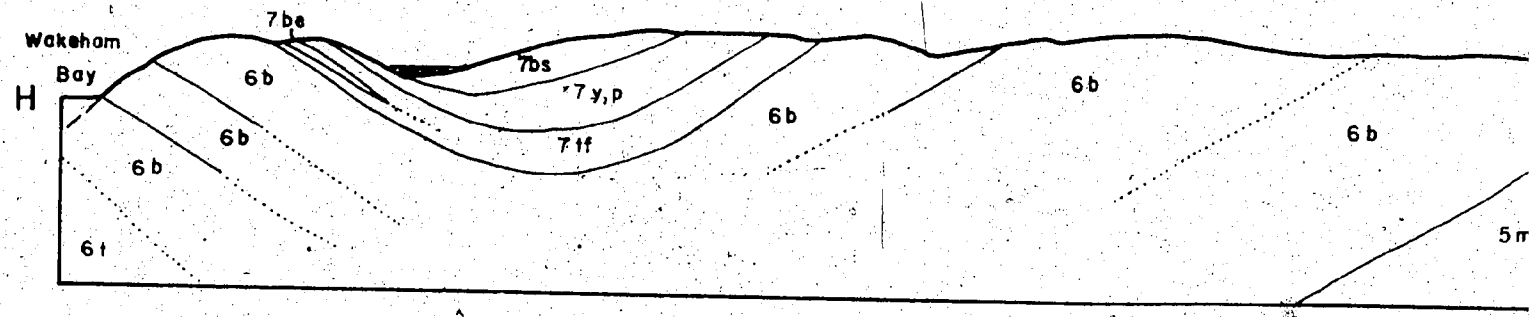
H
Wakeham
Bay
7be
7bs
7 y,p
7 tf
6 b
6 t
5m

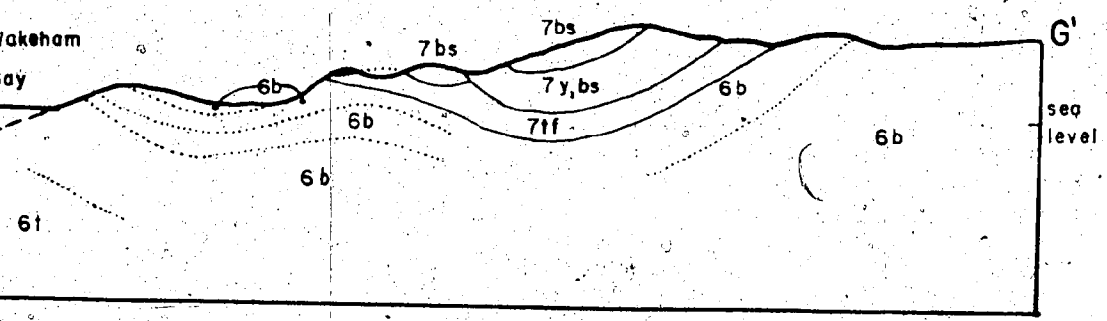
Wakeham
ay
7bs
7bs
6b
7 y,bs
6b
6b
7tf
6b
6b
6t
G'
sea
level

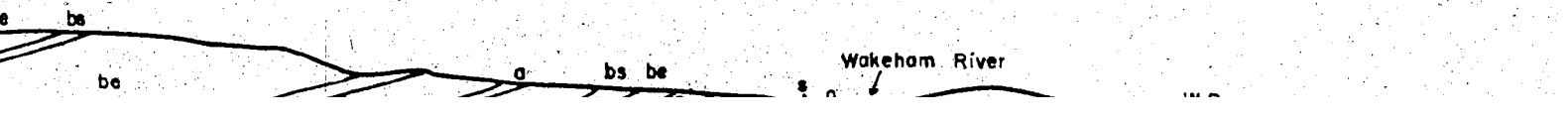
e
be
be
bs
be
Wakeham River

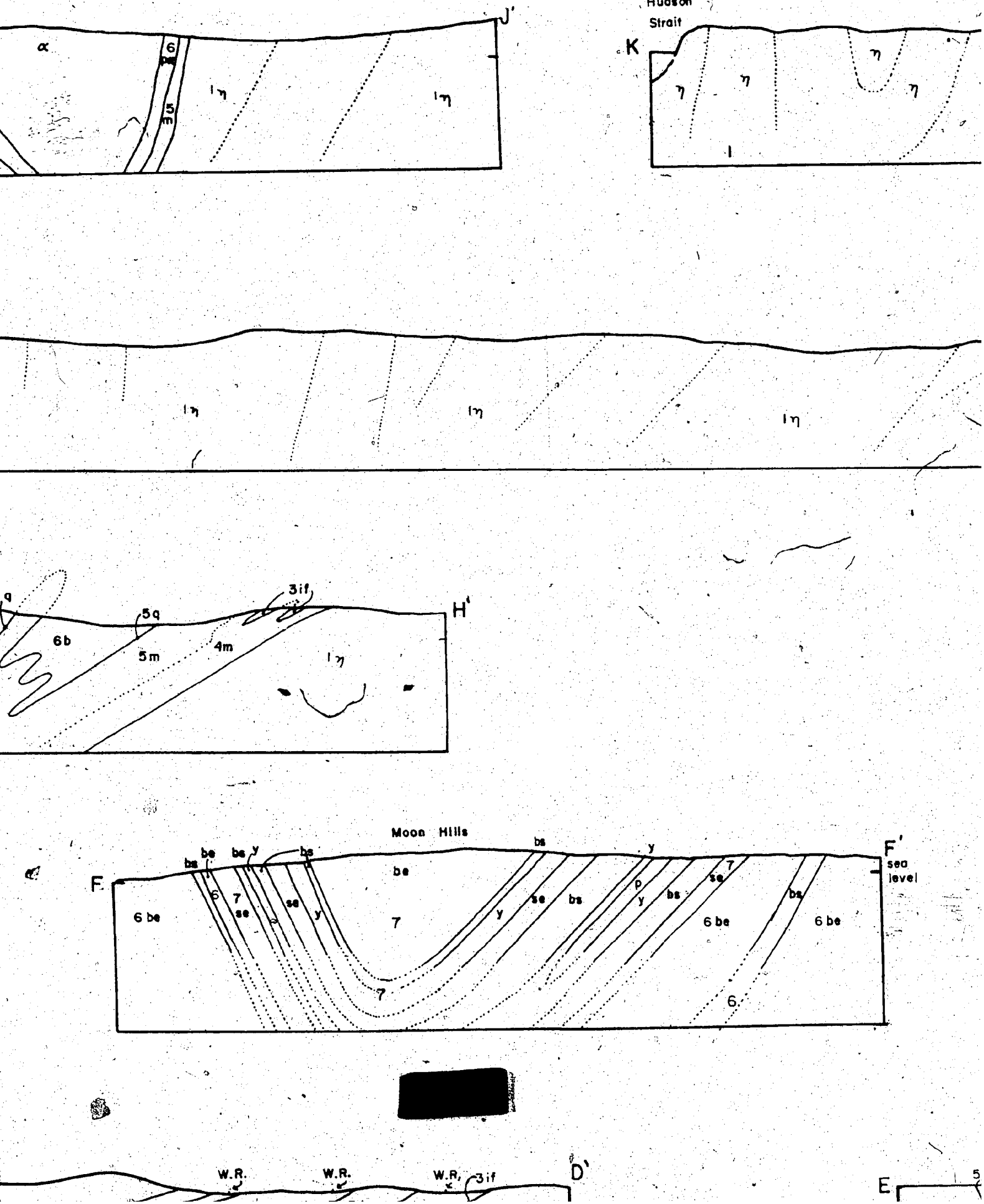
J'
α
6
5
1η
1η
Hudson
Strait
K
η
η
η
η
1
1η
1η
1η
q
3if
5q
H'
6b
5m
4m
1η
Moon Hills
F
F'
sea
level
be
bs
y
6 be
7
se
p
6
6 be
6 be
W.R.
W.R.
W.R.
3if
D'
E
5

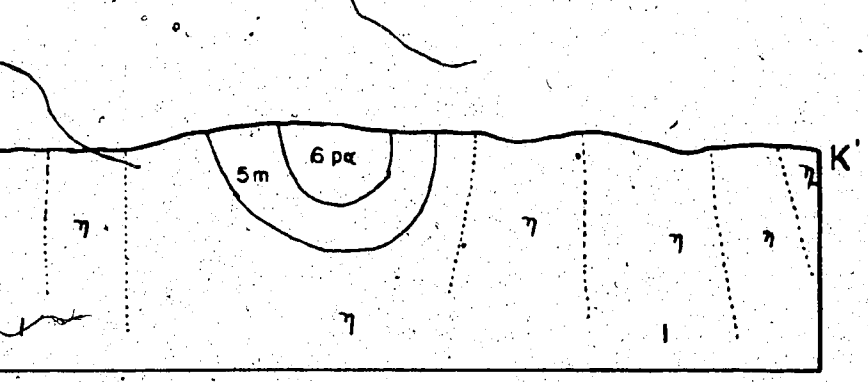

Vertical and horizontal sc

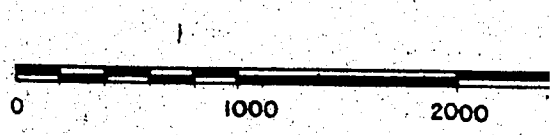

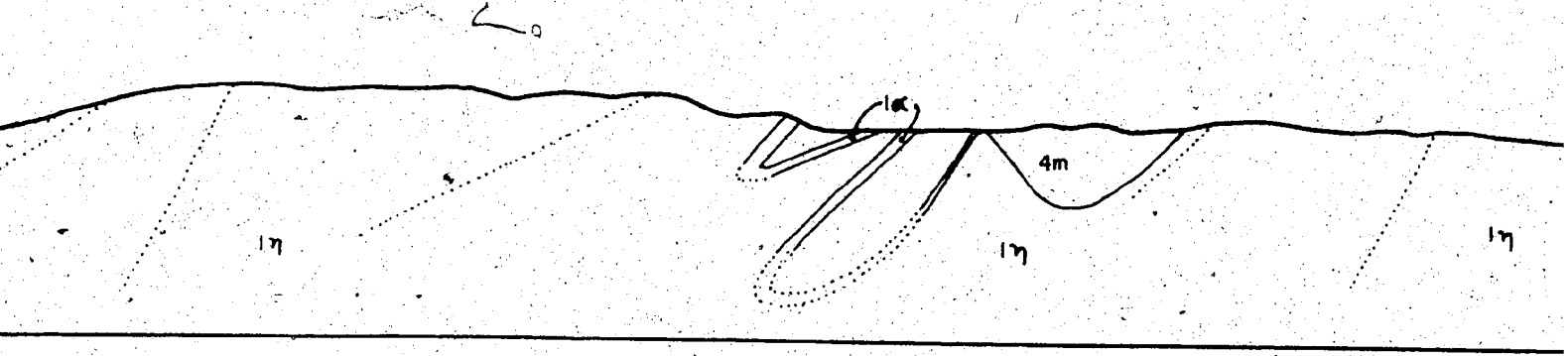

Sketch of East slope of Qinquaq, seen from the valley bottom.

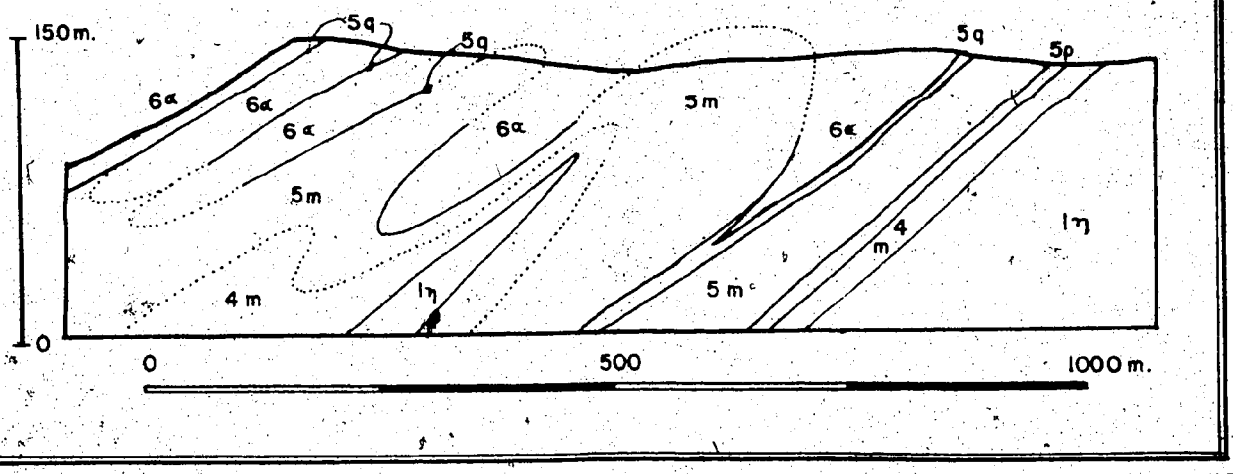

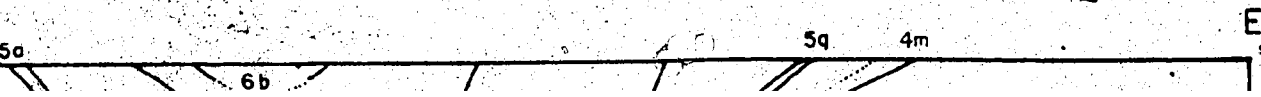

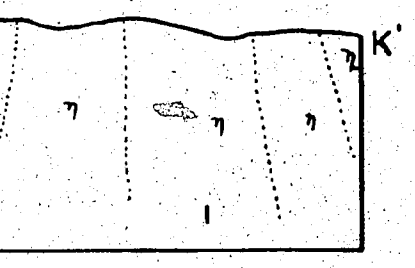

Vertical and horizontal scale

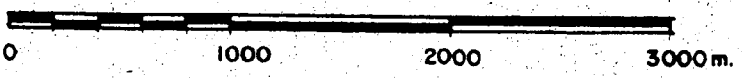

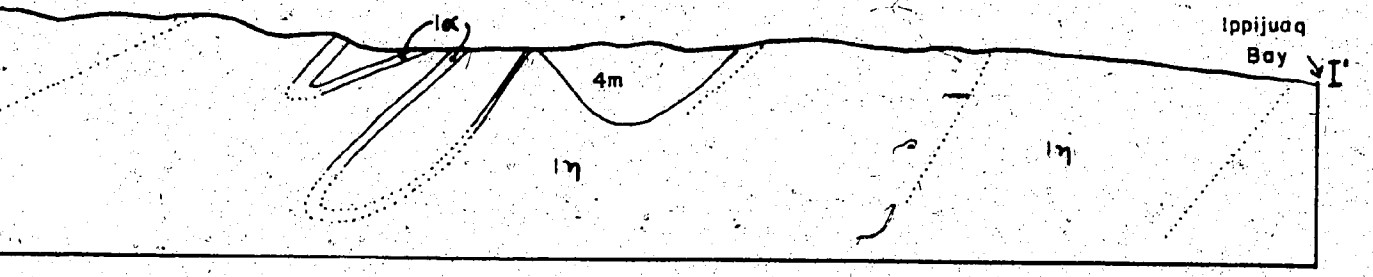

inquaq, seen from the valley bottom.

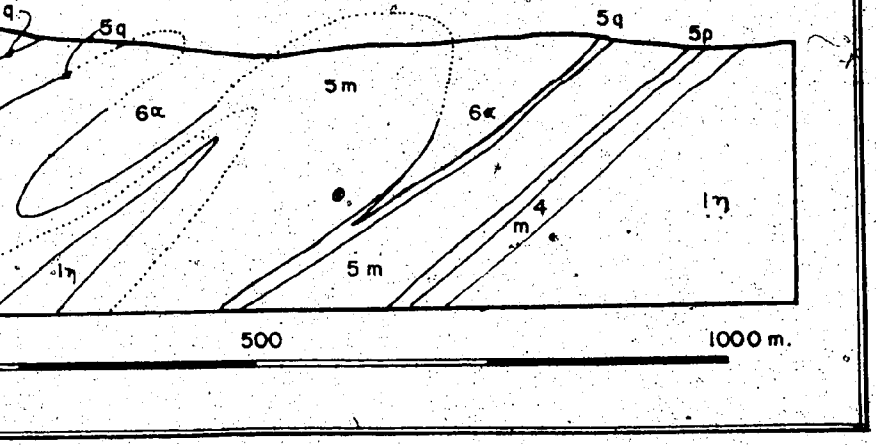

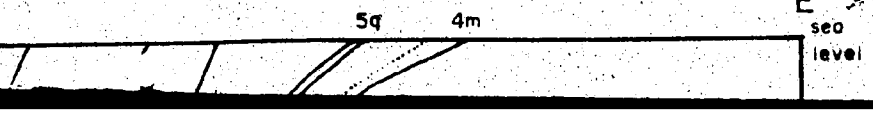

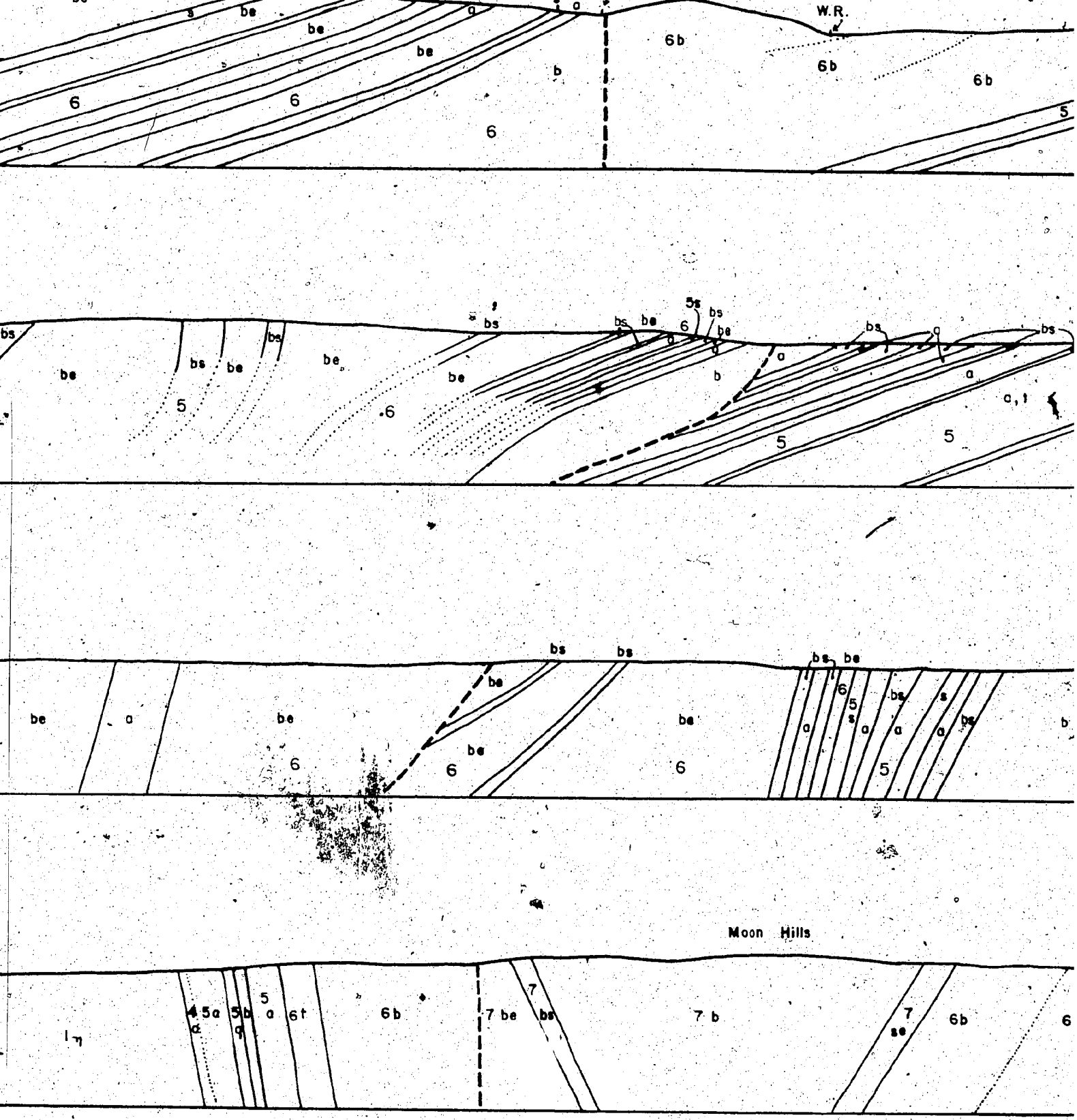

Fig. 15. Tectonic profiles accross the Cape Smith Wakeham Bay belt, between 73°00'

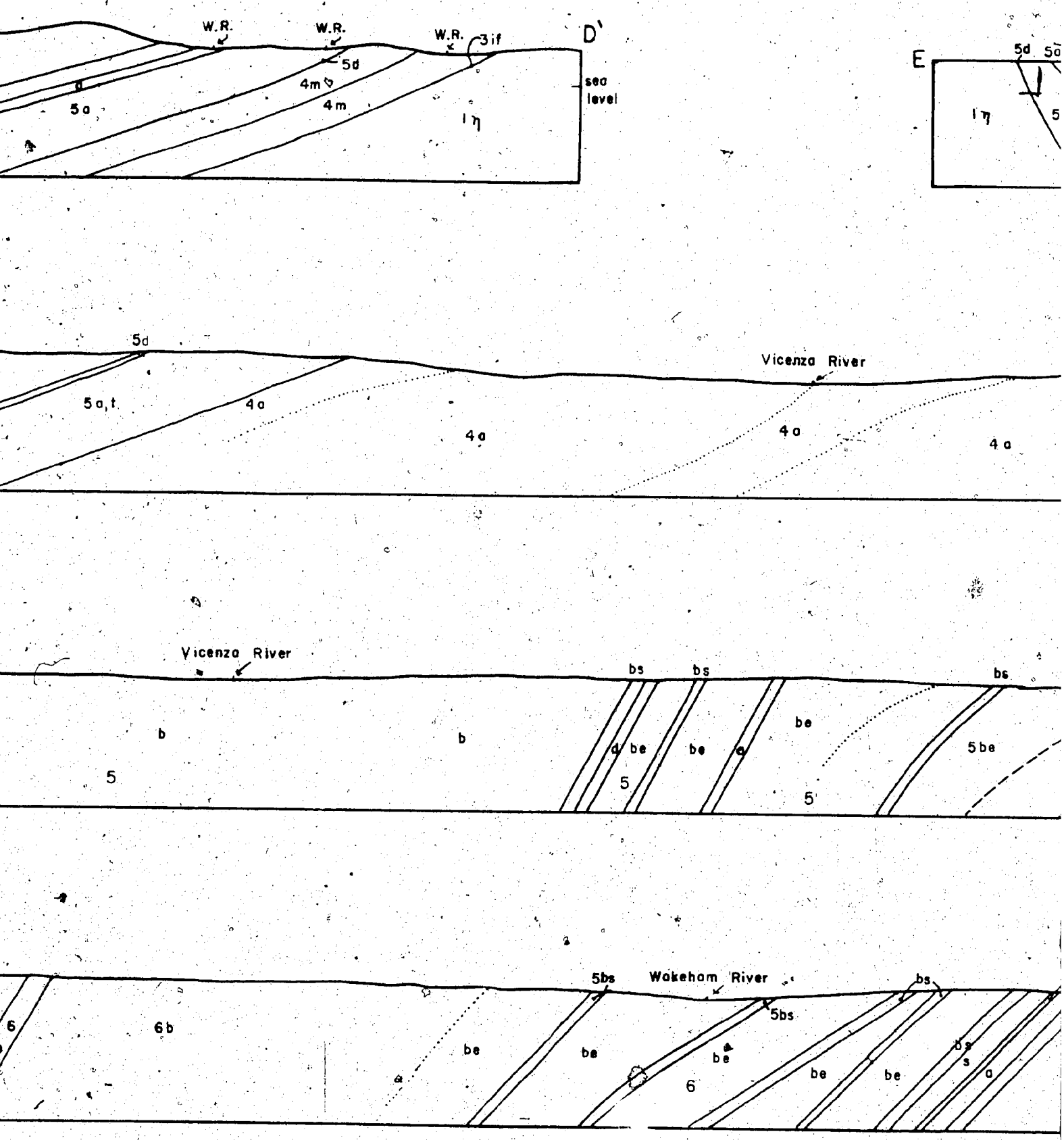

d 71°30'W (locations shown on Fig. 18).

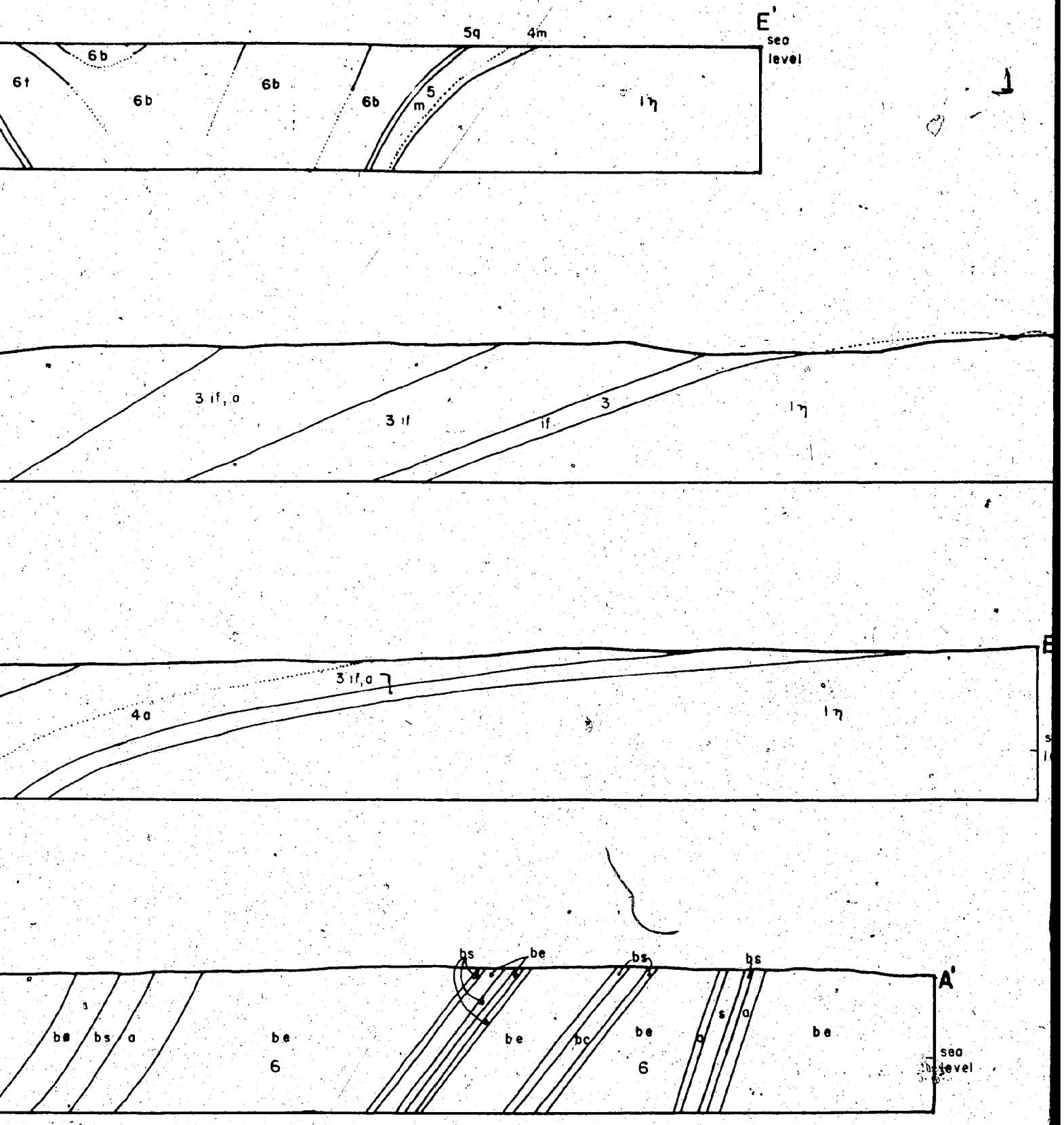
E'
sea level
5q
4m
6t
6b
6b
6b
6b
5
m
1η
3 if, a
3 if
if
3
1η
B
3 if, a
4a
1η
bs
be
bs
bs
A'
be
bs
a
be
be
be
be
s
a
be
6
6
sea level
30/I/77

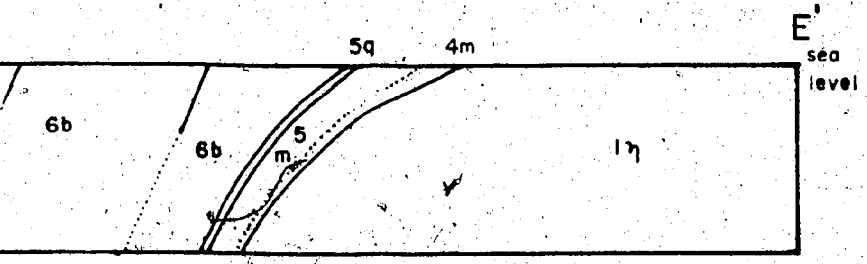
E'
sea level
5q
4m
6b
6b
5
m
1η

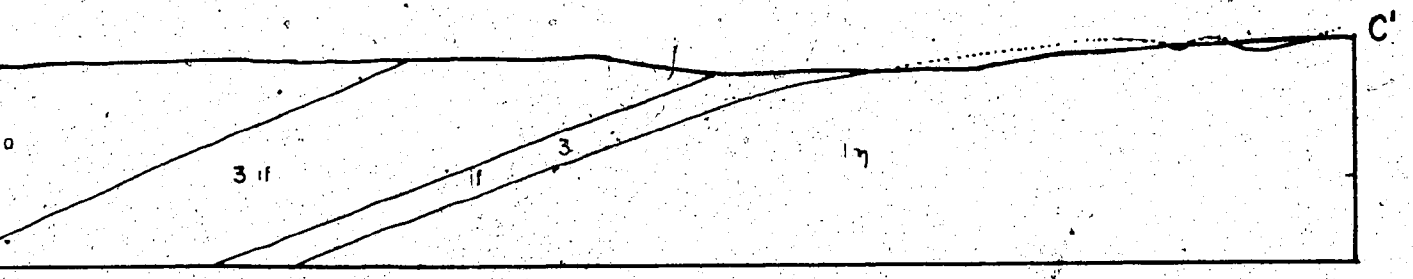
C'
3 if
if
3
1η

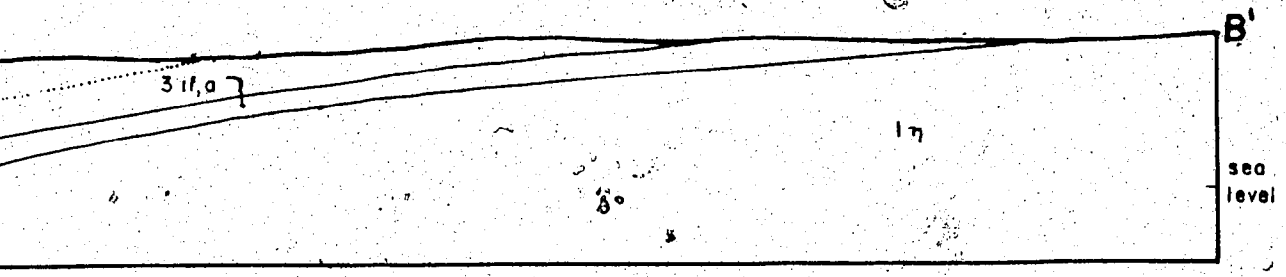
B'
3 if, a
1η
sea level

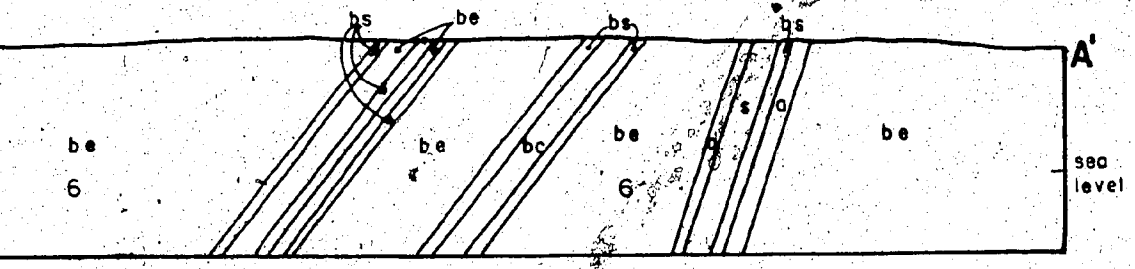
bs
be
bs
bs
A'
be
6
be
bc
be
6
s
o
be
sea level

30/I/77

Fig. 16. Lineament map of the Wakeham Bay area, New Quebec.

[redacted]

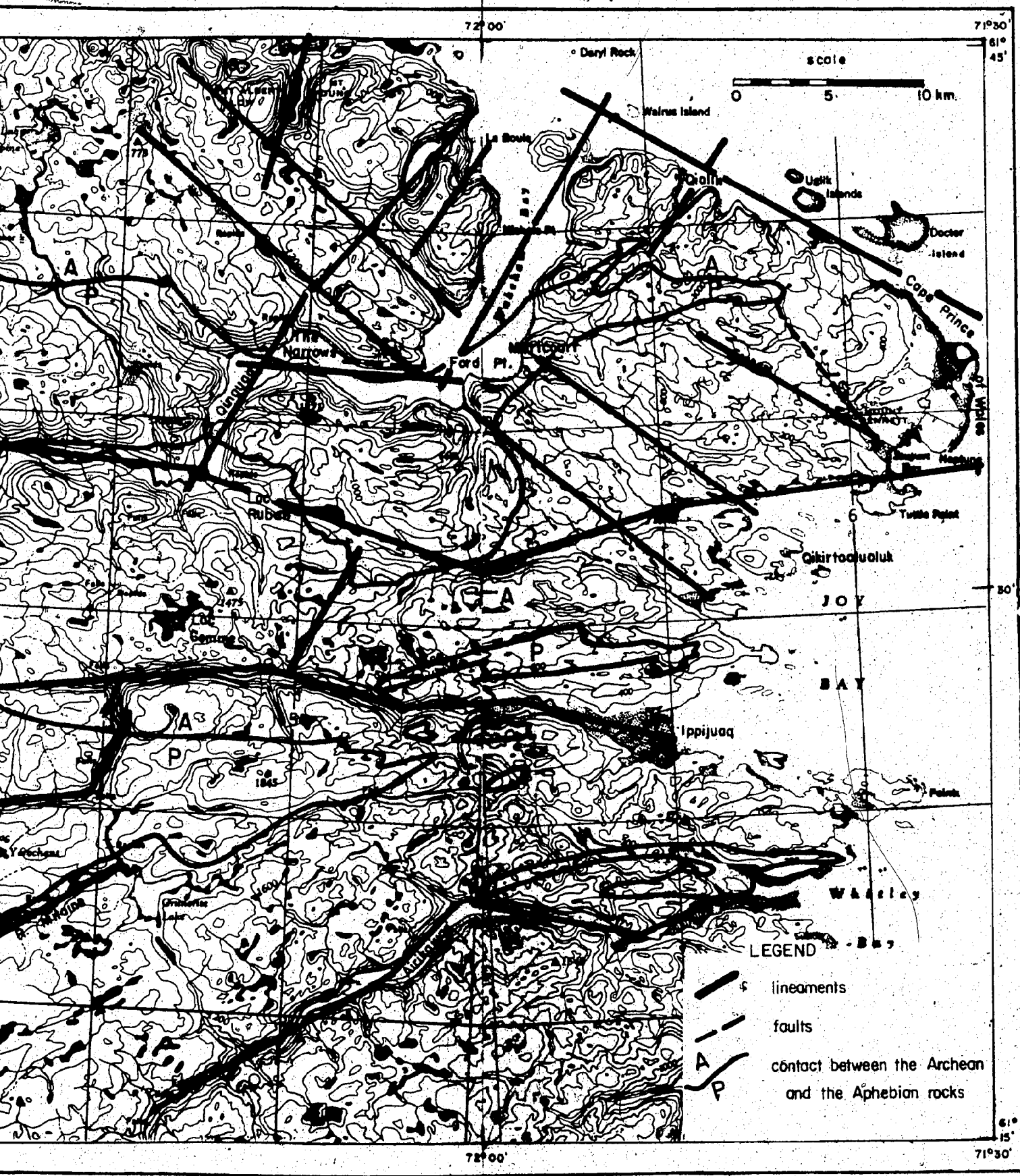
72°00'
71°30'
61° 45'
61° 15'
Daryl Rock
scale
0 5 10 km.
Walrus Island
La Boule
Qialik
Uglit Islands
Docker Island
Cape Prince
The Narrows
Ford Pt.
Qinguaq
Lac Rubeis
Turtle Point
Qikirtaalualuk
JOY
BAY
Ippijuaq
Points
LEGEND
lineaments
faults
contact between the Archean and the Aphebian rocks

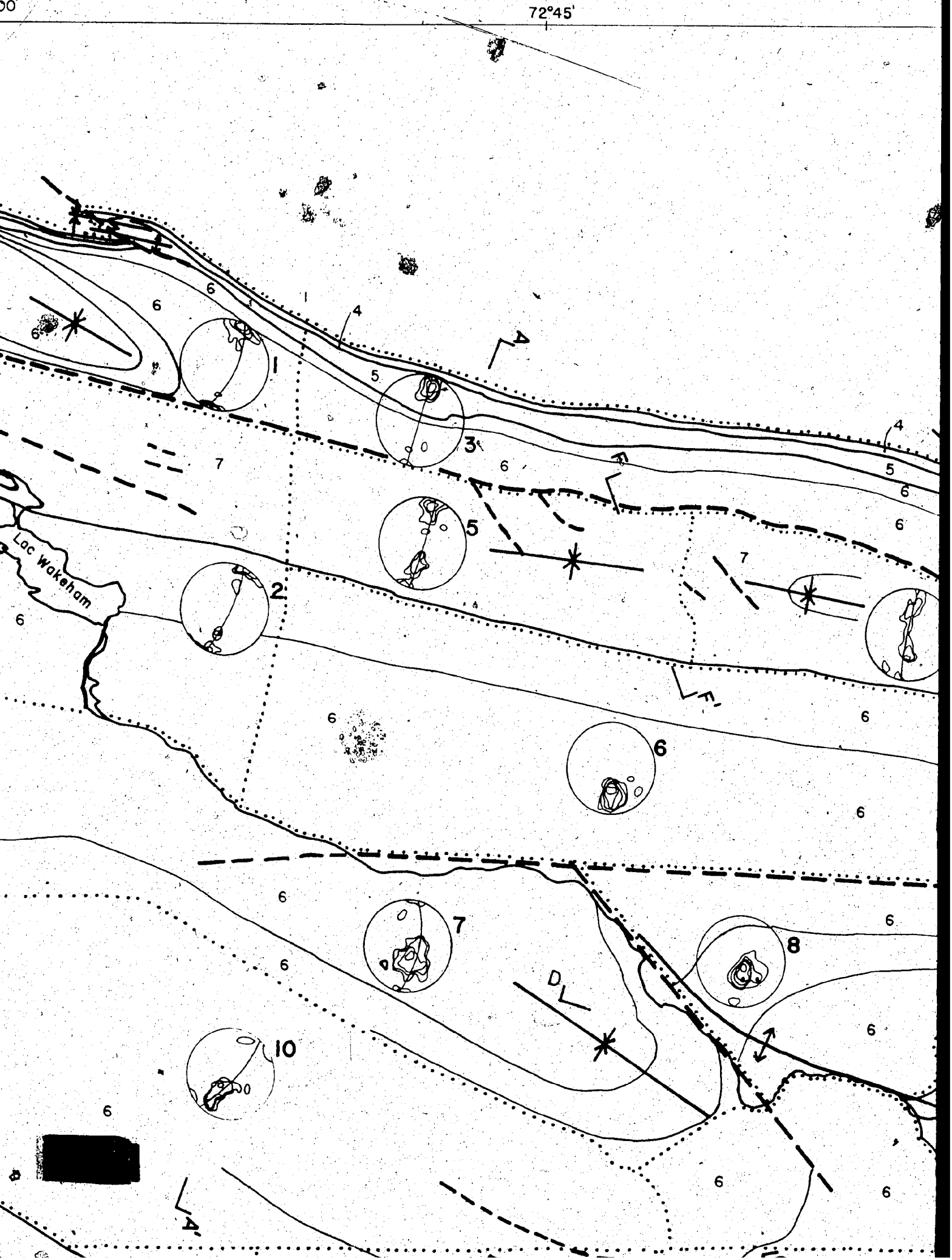
72°45'
Lac Wakeham
1
2
3
4
5
6
7
8
10
A
B
C
D

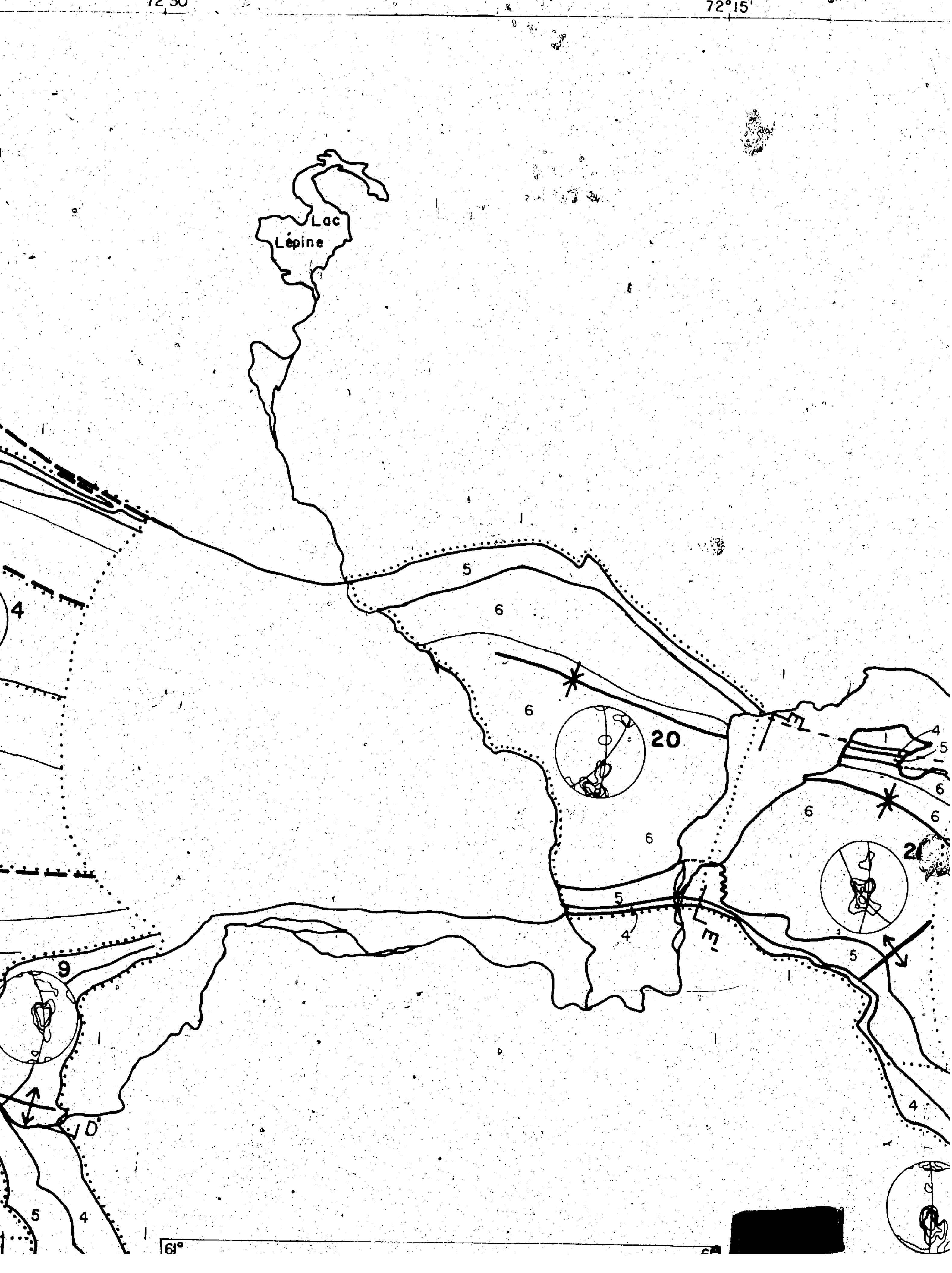

72°15'
Lac
Lépine
20
9
4
61°

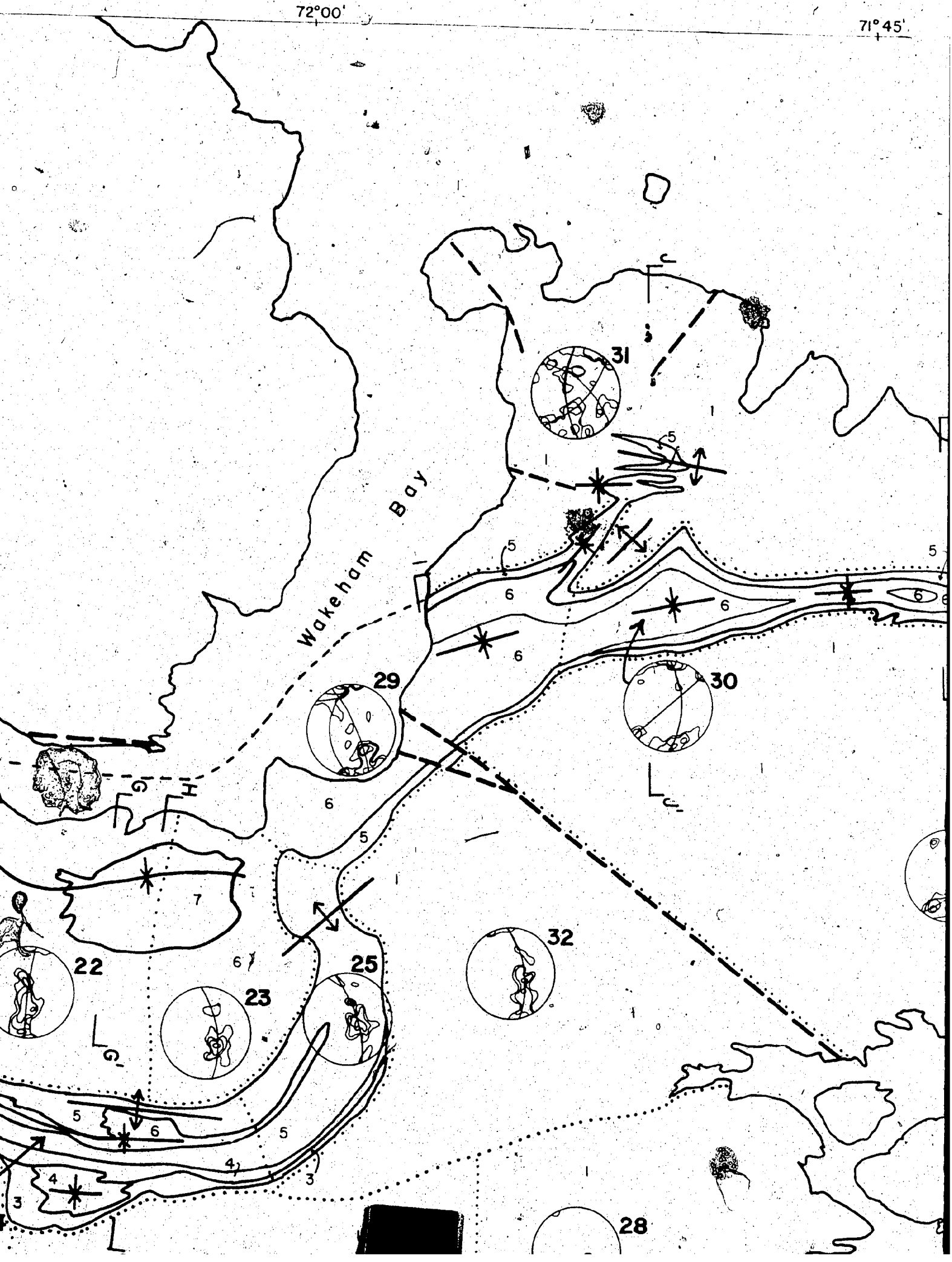
72°00'
71°45'
Wakeham Bay
31
29
30
32
25
22
23
28
C
G
H
L
5
6
7
4
3

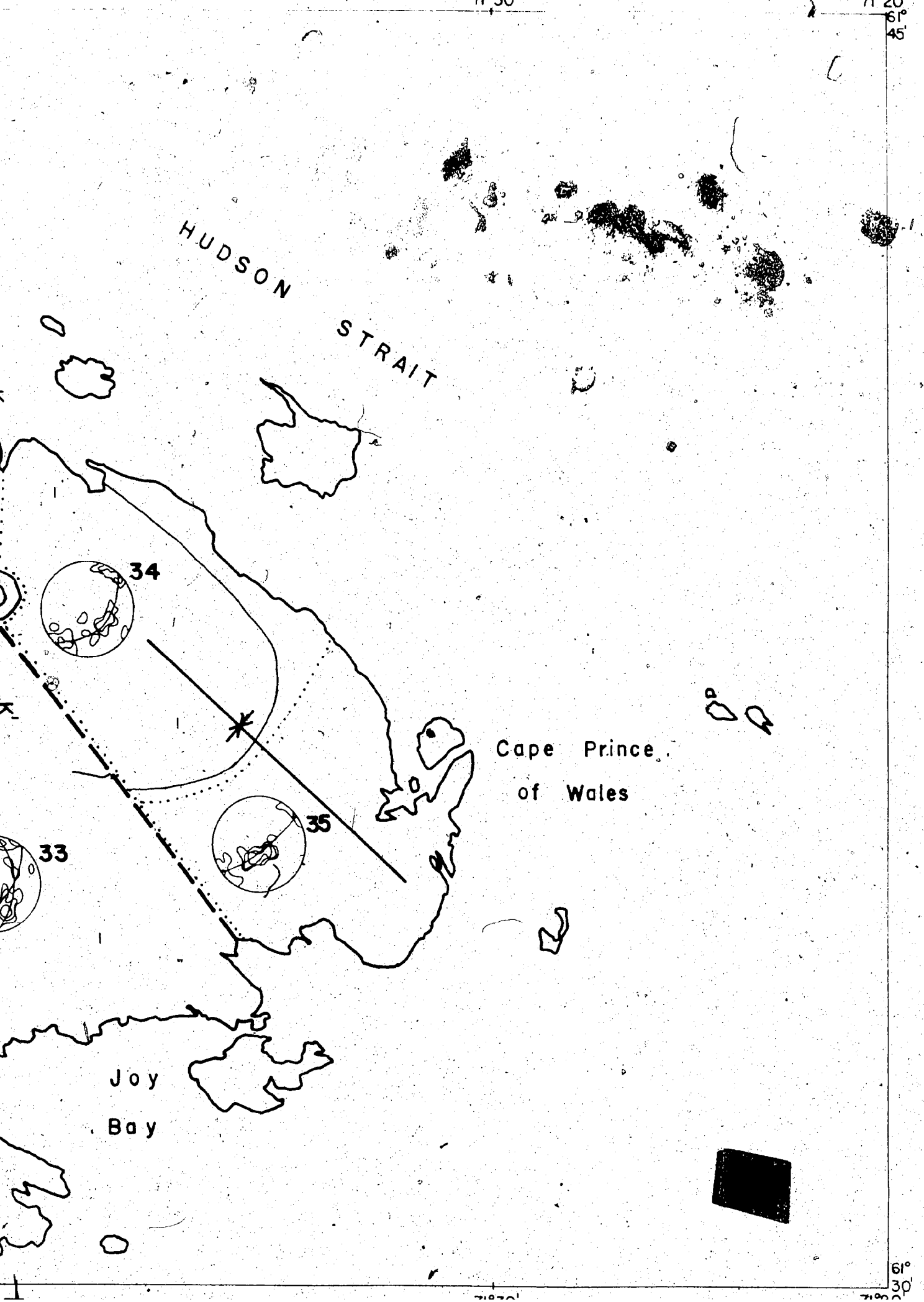
HUDSON STRAIT
34
35
33
Cape Prince of Wales
Joy Bay

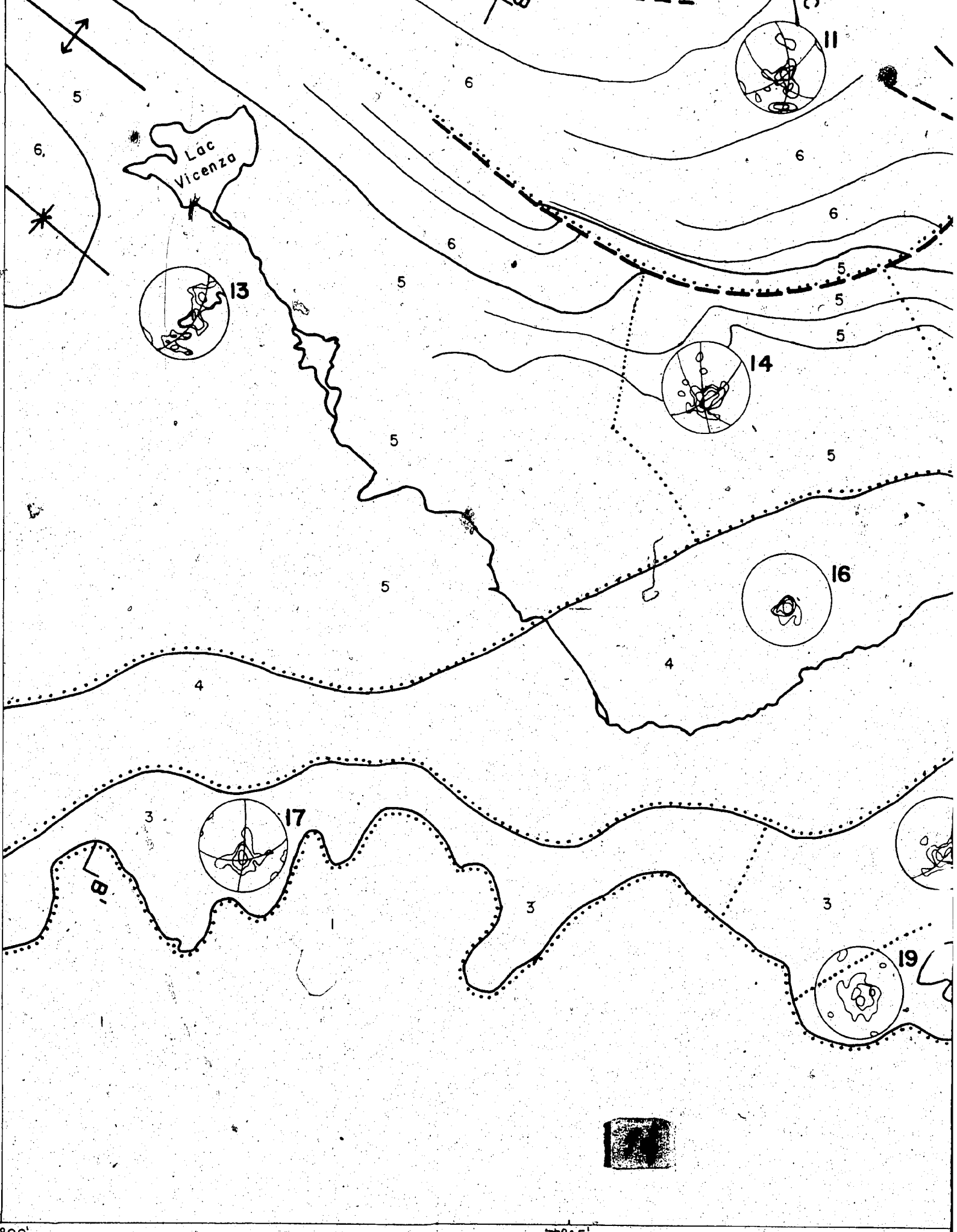
Lac
Vicenza
11
13
14
16
17
19
5
6
4
3
1
8'
72°45'

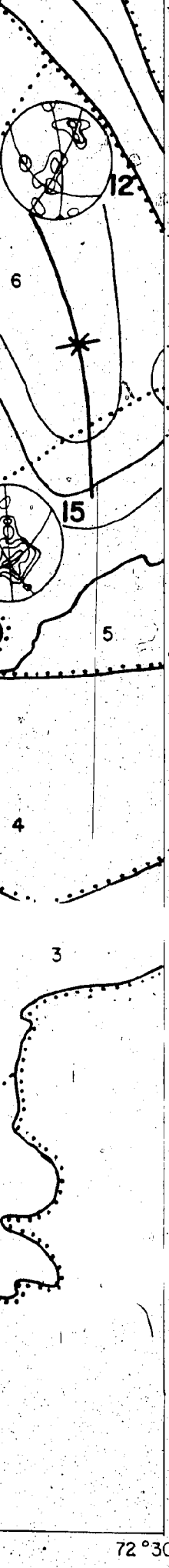

Scale

1:100 000

0 1 2 3 4 5km

Base-map assembled from topographic maps published at a scale of 1:50 000 by the Department of Energy, Mines, and Resources, Ottawa.

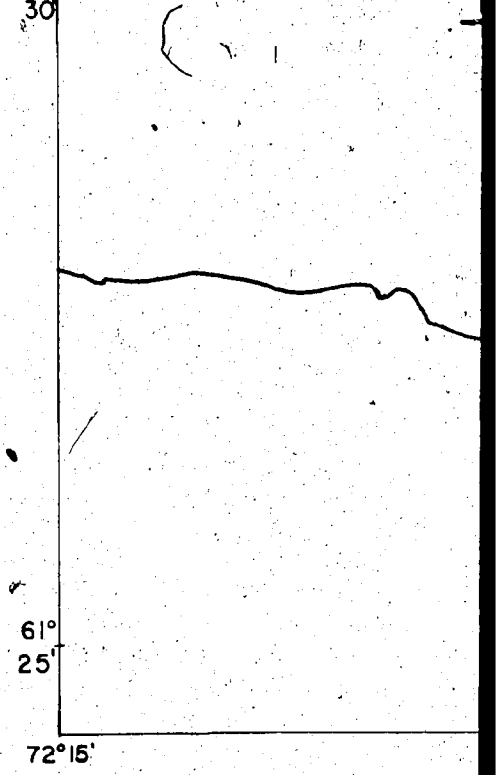

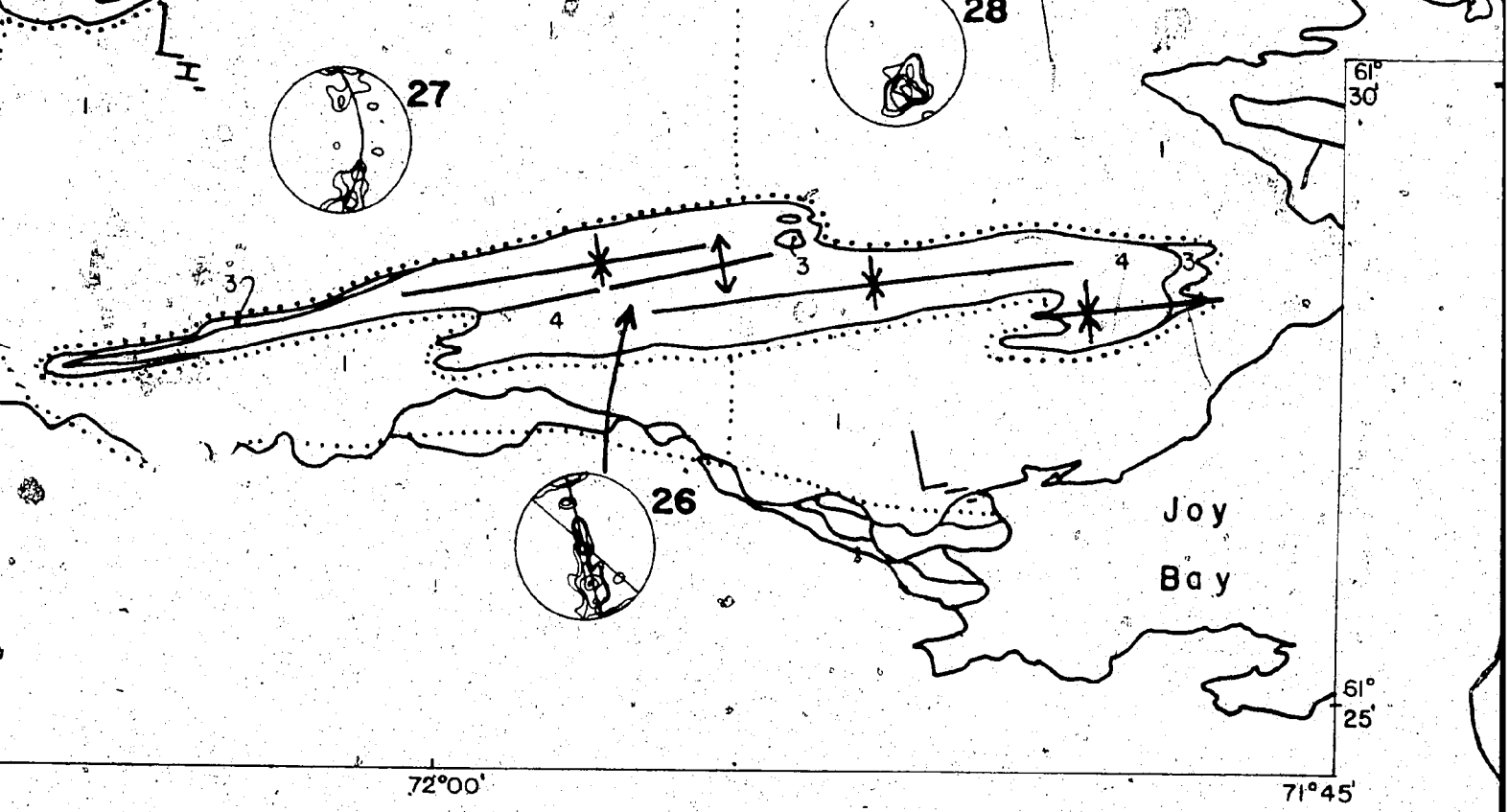

8. Structural map of the Wakeham Bay area

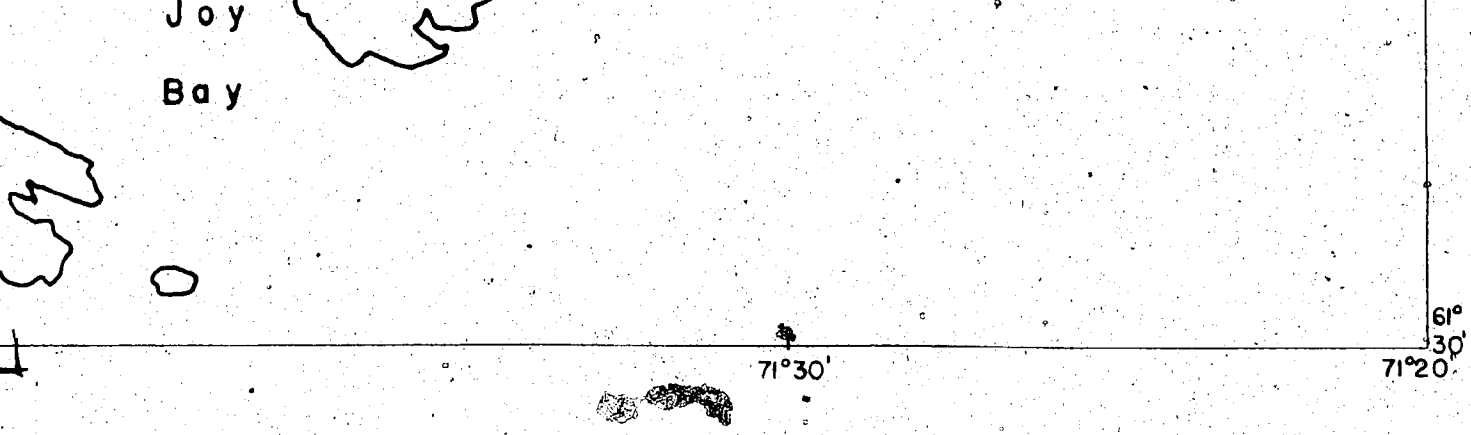

LEGEND

Aphebian rocks

7 Upper Volcanic Group

6 Lower Volcanic Group

5 Volcano Sedimentary Group

4 Pelitic Group

3 Iron Group

2 Early Aphebian (not shown here)

1 Archean rocks

contact

marker horizon (to illustrate the structure)

fault

anticline (trace of axial surface)

syncline (trace of axial surface)

domain boundary

domain number with equal-area lower hemisphere projection of foliations

F F' tectonic profile